Trans-bis(alkynyl) ruthenium complexes: synthesis, structure and reactivity

EAVES, SAMANTHA,GRACE

Trans-bis(alkynyl) ruthenium complexes:

synthesis, structure and reactivity

Samantha Grace Eaves MChem (Dunelm)

PhD Thesis

2015

Department of Chemistry

Durham University

and

School of Chemistry and Biochemistry

The University of Western Australia

This Thesis is presented in partial fulfillment of the requirements for the **Doctor of Philosophy – Cotutelle Degree** between Durham University (UK) and The University of Western Australia

THE UNIVERSITY OF WESTERN AUSTRALIA

DECLARATION FOR THESES CONTAINING PUBLISHED WORK AND / OR WORK PREPARED FOR PUBLICATION

This Thesis contains published work and work prepared for publication at the time of writing, some of which has been co-authored. The bibliographical details of the work, where it appears in the Thesis and percentage contributions of the authors are outlined below.

CHAPTER 2: S. G. Eaves, D. S. Yufit, B. W. Skelton, J. M. Lynam and P. J. Low, *Dalton Trans.*, **2015**, *44*, 21016. *SGE (60 %), DSY (5 %), BWS (5 %), JML (20 %), PJL (10 %).*

CHAPTER 3: S. G. Eaves, S. Hart, A. C. Whitwood, D. S. Yufit, P. J. Low and J. M. Lynam, *Chem. Commun.*, **2014**, *51*, 9362. *SGE (55 %), SH (5 %), ACW (5 %), DSY (5 %), PJL (15 %), JML (15 %).*

CHAPTER 5: S. Bock, **S. G. Eaves**, O. A. Al-Owaedi, D. Costa-Milan, B. W. Skelton, H. M. Osorio, R. J. Nichols, S. J. Higgins, P. Cea, S. Martín, C. J. Lambert and Paul J. Low, *manuscript in preparation. SB (15 %), SGE (10 %), OAA-O (15 %), DC-M (15 %), BWS (5 %), HMO (10 %), RJN (5 %), SJH (5 %), PC (5 %), SM (5 %), CJL (5 %), PJL (5 %).*

We hereby declare that the individual authors, or corresponding authors, have granted permission to the candidate (Samantha G. Eaves) to use the results presented in the manuscripts above in this Thesis.

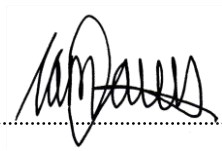

Samantha G. Eaves
(PhD Candidate)

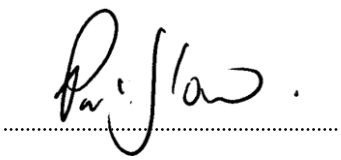

W / Prof. Paul J. Low
(Coordinating Supervisor)

Trans-bis(alkynyl) ruthenium complexes:

synthesis, structure and reactivity

Samantha Grace Eaves

This Thesis describes the synthesis and characterisation of a series of *trans*-bis(alkynyl) ruthenium complexes, *trans*-[Ru(C≡CR)$_2$(L)$_4$], to better understand how the variation of the metal ancillary ligands (L) affect electronic structure and spectroscopic properties, chemical reactivity, and behaviour in metal|molecule|metal junctions.

Reactions of *cis*-[RuCl$_2$(dppm)$_2$] with terminal alkyne HC≡CC$_6$H$_4$-4-R, in the presence of TlBF$_4$ and base, gives into *trans*-bis(alkynyl) complexes, *trans*-[Ru(C≡CC$_6$H$_4$-4-R)$_2$(dppm)$_2$], for electron withdrawing R groups or cationic η^3-butenynyl complexes, *E*-[Ru(η^3-{HC(C$_6$H$_4$-4-R)=CC≡C(C$_6$H$_4$-4-R)})(dppm)$_2$]$^+$ for electron donating R groups. Reactions of *cis*-[RuCl$_2$(dppm)$_2$] with di-terminal alkynes HC≡CC$_6$H$_4$-2,5-X$_2$-4-C≡CH, in the presence of TlBF$_4$ and [N^{n}Bu$_4$]Cl, gives *trans*-[RuCl(C≡CC$_6$H$_2$-2,5-X$_2$-4-CCl=CH$_2$)(dppm)$_2$], inferring a quinoidal cumulene intermediate.

Multi-metallic *trans*-bis(alkynyl) {Ru(dppe)$_2$} complexes, varying in binding groups and bridging ligands, have been prepared. Reversible oxidation processes, whilst corresponding to the number of integrated metal centres, exhibit a high degree of alkynyl character in all cases. The vibrational and electronic spectra of both neutral and oxidised complexes are complicated by the presence of numerous spectroscopically distinct rotamer conformations and redox isomers. For example in the case of *mono*-oxidised complexes, a principal low-energy (π-π*) NIR band is exhibited along with multiple higher energy (MLCT-type) NIR bands, which can be assigned by comparison with smaller model systems.

Finally, *trans*-bis(alkynyl) {Ru{P(OEt)$_3$}$_4$} complexes have been synthesised. As a result of the increased (*pseudo* D$_{4h}$) molecular symmetry and consequent fewer distinct rotamer conformations, a lesser number of NIR bands are exhibited for *trans*-[Ru(C≡CR)$_2$\{P(OEt)$_3$\}$_4$]$^+$ than *bis*-chelating dppm and dppe derivatives. Between *trans*-[Ru(C≡CR)$_2$(PP′)] (PP′ = (dppe)$_2$, {P(OEt)$_3$}$_4$) complexes, the {Ru(dppe)$_2$} derivatives give rise to conductance histograms with additional features. These features are attributed to contacts formed at or across the dppe-phenyl rings, leading to suggestions that phosphite complexes might be novel ‘insulated’ molecular wires.

DECLARATION

The material contained in this Thesis is, unless stated otherwise through cited reference, the result of the author's work conducted at both Durham University, Department of Chemistry and the University of Western Australia, School of Chemistry and Biochemistry between October 2012 and September 2015. This Thesis has been submitted to both Durham University and the University of Western Australia as part of a co-tutelle agreement.

STATEMENT OF COPYRIGHT

Publication List

S. Bock, **S. G. Eaves**, O. A. Al-Owaedi, D. Costa-Milan, B. W. Skelton, H. M. Osorio, R. J. Nichols, S. J. Higgins, P. Cea, S. Martín, C. J. Lambert and Paul J. Low, **2016**, manuscript in preparation. "*Single molecule conductance studies of organometallic complexes bearing 3-thienyl contacting groups"*.

S. G. Eaves, D. S. Yufit, B. W. Skelton, J. M. Lynam and P. J. Low, *Dalton Trans.*, **2015**, *44*, 21016. *"Reactions of alkynes with cis-*$RuCl_2(dppm)_2$*: exploring the interplay of vinylidene, alkynyl and* η^3*-butenynyl complexes"*.

S. G. Eaves, D. S. Yufit, B. W. Skelton, J. A. K. Howard and P. J. Low, *Dalton Trans.*, **2015**, *44*, 14341. *"Syntheses, structural characterisation and electronic structures of some simple acyclic amino carbene complexes"*.

S. G. Eaves, S. Hart, A. C. Whitwood, D. S. Yufit, P. J. Low and J. M. Lynam, *Chem. Commun.*, **2014**, *51*, 9362.*"Rapid Markovnikov addition of HCl to a pendant alkyne: evidence for a quinoidal cumulene"*.

J. B. G. Gluyas, A. J. Boden, **S. G. Eaves**, H. Yu and P. J. Low, *Dalton Trans.*, **2014**, *43*, 6291. *"Long range charge transfer in trimetallic mixed-valence iron complexes mediated by redox non-innocent cyanoacetylide ligands"*.

S. Bock, **S. G. Eaves**, M. Parthey, M. Kaupp, B. Le Guennic, J.-F. Halet, D. S. Yufit, J. A. K. Howard and P. J. Low, *Dalton Trans.*, **2013**, *42*, 4240. *"The preparation, characterisation and electronic structures of 2,4-pentadiynylnitrile (cyanobutadiynyl) complexes"*.

Conference list

S. G. Eaves, B. W. Skelton and P. J. Low; *"Synthesis and electronic structure of trans-[Ru(C≡CC$_6$H$_4$-4-R)$_2${P(OEt)$_3$}$_4$] complexes: From wire-like structures to 'inside-out' mixed-valency";* poster presentation at the 5th Asian Coordination Chemistry Conference (ACCC5), 12th – 16th July 2015, Hong Kong University, Hong Kong.

S. G. Eaves, D. Yufit, A. Whitwood, J. M. Lynam and P. J. Low; "*Synthesis, reactivity and electronic properties of [Ru(C≡CR)$_2$(dppx)$_2$] complexes*"; oral presentation at the 8th Australasian Organometallics Discussion Meeting (OZOM8), 22nd – 25th July 2014, James Cook University, Magnetic Island, Queensland, Australia.

S. G. Eaves, S. Marqués-González, D. Yufit and P. J. Low; *"Single molecules for molecular electronics"*; poster presentation at the Universities of Scotland Inorganic Conference (USIC), 25th – 26th July 2013, University of Edinburgh, Scotland. First prize.

For

Mum and Dad

who have given me everything,
yet have never asked me for anything.

"And so today my world it smiles
Your hand in mine, we'll walk the miles"
'Thank you'- Led Zeppelin

ACKNOWLEDGEMENTS

There is no '*me*' in Thesis….but there is an '*I*'. True, *I* have worked pretty hard for this Thesis and yes, *I* have flown across the world and back (and back again) for this Thesis. *I* have also worked at three different institutions for this Thesis…But *I* most certainly, definitely, absolutely and categorically could not have done any of it without the help of some pretty special people along the way…

Firstly, I thank my parents. You truly are two of the strongest, kindest, most humble and most patient people I have ever known. I have nothing but admiration for you both and I am so very proud to be your daughter. Even though I moved a little further away than you might have wanted (*the* furthest away…) home is wherever you two are and I love you both so very much. I must also thank my big sister, Jo / Joseph, who never fails to me smile and who I will always say is the nicer (slightly weirder) one of us both. I also take this opportunity to thank my Nana and Grandpa, Granny and Grampa for their limitless generosity, love and kindness given to me throughout my entire life.

Secondly, I thank my supervisor Paul. In the four years that I have worked for Paul, there was not a single day when I wished I did not. In fact, he mentioned he was moving to the other side of the world and my first thought was *"not without me he's not…"*. Of the spectrum of qualities that he has, I thank him in particular for his patience, intellect, benevolence and for being somebody truly inspirational to work for. I also have to thank Paul on behalf of anybody reading this Thesis, who now have a lot less to endure. Like myself, my work is the product of a 'carbs on carbs *on carbs*' diet.

For taking me in and putting up with me for five months, a huge thanks also goes to Jason. I could not have asked for a better surrogate-supervisor. I just hope the holiday (working, *of course…*) down under was at least some small payback. I also thank George, Mark and Andy for their support throughout the process and Allan for always giving his time generously (but mostly for sharing his crunchies).

Furthermore I would like to thank some of my colleagues turned friends over the years. I give thanks to: Dr. Phil for all the advice, Sören for knowing the only way to remove me from my desk is if you come bearing gifts of either tea, chocolate or bacon; Ross for

his (sparkly pink) donut generosity and friendship; Santiago 'the dppe king' Marqués-González; Marie for her 'French-ip'; Matthias for smashing the 'computational guy' stereotype; Campbell for his Hockey coaching; both Winnie and Kevin for not putting me off being a part of the PJL group in the first place and a very small (virtually non-existent) acknowledgement to Josef, who really hasn't helped me at all. I also thank members of the 'DP' lab group: Brad, Pete, Dave, Martina and Alex for their friendship; friends and colleagues at the University of Western Australia and members of the Lynam group, Lizzie and Lucy, for welcoming me into their group and above all else, teaching me how to procrastinate through knitting.

I would also like to give a separate thanks to Katie for being a good, honest friend; there is nobody better to share in this journey with and Emily / Vivian, one of my oldest friends, who I thank for understanding how bad I am at staying in touch but never being in doubt that you will be my friend always. Furthermore, I am so very thankful to Camille and Kat (go team Skam!) who have single-handedly managed my social life in Australia and with whom I will remain lifelong friends.

I gratefully acknowledge the analytical departments of Durham University and the University of York and the CMCA at the University of Western Australia. In particular to the crystallographers, Brian Skelton and Dimitry Yufit, who are deserving of credit given their way and to Lindsay Byrne for his generosity and unfailing assistance. Above all, I gratefully acknowledge Durham University for the funding of this Thesis through a Durham Doctoral Scholarship and the University of Western Australia for an Ad Hoc Scholarship.

And finally, for the permission to leave, and the love and support in the one and a half years away since, I cannot thank you enough Michael. I would have been so very lost without you.

"Well I'm half awake and half a world away,
All my past mistakes and every wasted day
I wouldn't have it any other way"
'*Gainsville Rock City*'- Less than Jake

LIST OF ABBREVIATIONS

°	degrees
°C	degrees Celcius
μm	micrometers
μ_q	the shear modulus
$^1\tau$	singlet lifetime
2D	two dimensional
3D	three dimensional
A	amperes *or* generic substituent *or* electrode area
Å	angstoms
a.u.	arbitrary units
Ac	acetyl
AFM	atomic force microscopy
AIBN	azo-diisobutyronitrile
amu	atomic mass unit
Anal.	analysis
Ar	aryl
ASAP	atmospheric pressure analysis probe mass spectroscopy
ATR	attenuated total reflection
avg	average
B	base *or* generic substituent
bpy	5-ethynyl-2,2′-bipyridine
br.	broad
BTD	benzothiodiazole
Bu	butyl
ca.	circa
Calc.	calculated
cat.	catalyst
carb	carbene
C_i	*ipso*-substituted carbon
cm	centimetre
C_m	*meta*-substituted carbon

C_o	*ortho*-substituted carbon
C_p	*para*-substituted carbon
CP-AFM	conducting probe atomic force microscope
CV	cyclic voltammetry
d	doublet *or* day(s)
DBU	1,8-diaazabicyclo[5.4.0]undec-7-ene
DCE	dichloroethane
depe	diethylphosphinoethane
DFT	density functional theory
dippe	diisopropylphosphinoethane
DMAP	4-dimethylaminopyridine
DMFC	decamethylferrocene
dmpe	dimethylphosphinoethane
DMSO	dimethylsulfoxide
DNT	dinitrotoluene
dpe	diphosphinoethane
dppe	diphenylphosphinoethane
dppm	diphenylphosphinomethane
DSSC	dye sensitiser solar cell
DTE	dithienylethene
e^-	electron
$E_{1/2}$	oxidation half potential
EC	electrochemical-chemical
E_f	Fermi level
ESCA	electron spectroscopy for chemical analysis
ESI	electrospray ionisation
Et	ethyl
etc.	etcetera
eV	electron volt
F	faraday constant
f_0	fundamental resonant frequency
Fc	ferrocene
FET	field effect transistor
FWHH	full width half height

g	grams
G	conductance
G_0	conductance quantum (77 480 nS)
g_e	free electron *g*-value
g_{iso}	isotropic *g*-value
GNI(s)	gold nano-island(s)
GNP(s)	gold nano-particle(s)
GPC	gel permeation chromatography
H	high conductance peak
HMBC	heteronuclear multiple bond correlation
HOCO	highest occupied crystal orbital
HOMO	highest occupied molecular orbital
HPLC	high performance liquid chromatography
Hz	Hertz
I	current
I(s)	current-distance STM technique
i.e.	*id est*
IL	intra-ligand
i_{pa}	anodic peak height
i_{pc}	cathodic peak height
^{i}Pr	isopropyl
IR	infrared
irrev.	irreversible
IVCT	intervalance charge transfer
J	coupling constant (Hz)
K	Kelvin
K_1	equilibrium constant
k_{app}	the rate of electron transfer from metal to surface bound molecule
K_c	disproportion constant
k_{ET}	rate of electron transfer
kJ	kilojoules
L	ligand (generic) *or* low conductance peak *or* molecular length
LCT	liquid chromatography time of flight
LFER	linear free energy plot

LMCT ligand to metal charge transfer

LL′CT ligand to ligand charge transfer

LUCO lowest unoccupied crystal orbital

LUMO lowest unoccupied molecular orbital

M metal (generic) *or* molarity

m mass *or* multiplet *or* medium

max maximum

MCU magnetic coupling unit

Me methyl

MHz mega-Hertz

MLCT metal to ligand charge transfer

MM′CT metal to metal charge transfer

MMOC multiple-metal organic compound

MOC metal organic compound

mol moles or molecules

MS mass spectrometry

M_w average molecular weight

N number of hopping sites

^{n}Bu n-butyl

NIR near-infrared

NLO(s) nonlinear optic(s)

nm nanometer

NMR nuclear magnetic resonance

NOESY nuclear overhauser effect spectroscopy

Nu nucleophile

OPEs oligo(phenylene)ethynylenes

OPVs oligo(phenylene)vinylenes

OTf trifluoromethanesulfonate

OTTLE optically transparent thin-layer electrode

OWL on-wire lithography

PCBM 6,6-phenyl-C_{61}-butyric acid methyl ester

Ph phenyl

por porphyrin

ppm parts per million

Pr	propyl
QCM	quartz crystal microbalance
quar.	quartet
quin.	quintet
r	atomic distance
R	gas constant *or* organic group (generic)
r.t.	room temperature
RAIRS	reflection-absorption infrared spectroscopy
red	reduction
rev.	reversible
s	sharp *or* second
SAM(s)	self-assembled monolayer(s)
sex.	sextet
SMM	single molecule magnet
SOMO	singly occupied molecular orbital
STM	scanning tunneling microscopy
T	temperature
t	triplet
TACN	1,4,7-triazacyclononane
TBAF	tetra-n-butylammonium fluoride
^{t}Bu	*tert*-butyl
TD-DFT	time dependant density functional theory
th	thiophene
THF	tetrahydrofuran
TIDOC	Thermally Induced Decomposition of an Organometallic Complex
TLC	thin-layer chromatography
TMEDA	tetramethylethylenediamine
TS	transition state
UV	ultraviolet
V	voltage
Vis	visible
vs.	*versus*
w	weak *or* week
X	generic group

XPS	X-ray photoelectron spectroscopy
X-wire	crossed-wire
z	charge
α^2	delocalisation parameter
β	tunneling attenuation factor
δ	chemical shift (ppm)
ΔE_{n-n+1}	potential separation between n^{th} and n^{th} + 1 redox events
ΔE_p	maximum current – minimum current
Δf	frequency variation before and after deposition of the monolayer
ΔG	Gibbs free energy ($kJmol^{-1}$)
ε	molar extinction coefficient
θ	angle (°)
λ	wavelength (nm)
ν	stretching mode *or* wavenumber (cm^{-1})
ρ_q	density of the quartz
σ_2	two photon absorption cross section value (cm^4s)
σ_{2eff}	effective two photon absorption cross section value (cm^4s)
σ_{para}	*para*-substituted Hammett parameter
υ	scan rate
ϕ	quantum yield of emission

TABLE OF CONTENTS

CHAPTER 1

Aspects of the chemistry of *trans*-bis(alkynyl) complexes

1.1. Introduction

The study of transition metal complexes bearing σ-acetylide ligands has been an area of intense interest for many decades. The nature of such complexes range from polymeric materials, encompassing a plethora of M-C≡C linkages (> 10 000), to smaller oligomeric systems, with a defined number of metallic and alkynyl fragments, through to monomeric molecular complexes with a single M-C≡C unit at the lowest level. Many such *mono*-alkynyl complexes are known, and serve as probes of metal-alkynyl bonding,[1] intermediates in the chemical transformations of alkynes,[2-6] and optoelectronic materials in their own right.[7-10] Interest in molecular *trans*-bis(alkynyl) metal complexes stems from the use of these compounds as models of metallopolymers,[11-13] but also as systems through which to study the efficient charge transfer process that can take place through unsaturated C≡C fragments, the fundamental concepts of delocalisation, the influence of integrating a metal centre within an organic π-conjugated system and the unique molecular and optoelectronic properties that such *d*-π systems may offer.

At the elementary level, for a single alkyne fragment, C≡C, the frontier orbitals can be described in terms of the overlap of two sets of perpendicular C(*p*) orbitals from each carbon to create a pair of orthogonal π bonding and π* antibonding molecular orbitals (Figure 1.1). Extending the organic fragment to oligomeric $-(C{\equiv}C)_n-$ systems results in overlap from two orthogonal sets of (2*n*) *p*-orbitals, each of which are comprised of *n* bonding and *n*-antibonding orbitals and populated by 2*n* electrons. With increasing *n*, these discrete molecular orbitals get closer and closer in energy, eventually forming continuous bands. The valence band is occupied by electrons, and facilitates the

transportation of holes whereas the conduction band is empty, and facilitates the transportation of electrons (Figure 1.1). Consequently, the electronic and physical properties of small molecules, such as acetylene, are vastly different from those of oligomeric (oligoyne) or polymeric (polyyne) materials, although the systems share a common electronic origin.

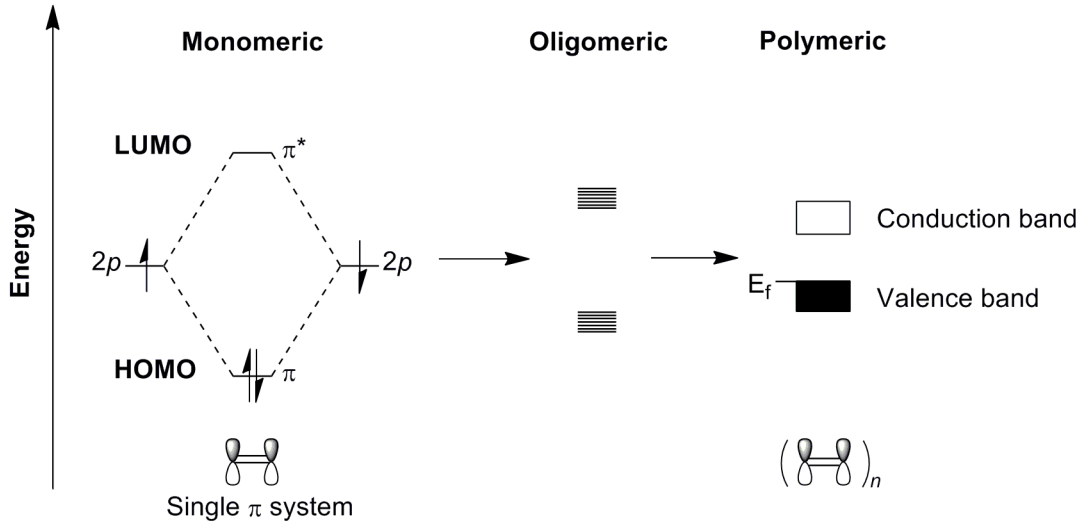

Figure 1.1: Schematic representation showing the evolution of delocalised band structures in highly conjugated -(C≡C)$_n$- π-systems.

Given that the extension of the π-electron system can also be achieved with the integration of alternative unsaturated fragments such as alkene (-CH=CH-) and phenylene (-C_6H_4-4-) moieties, carbon-rich oligo(phenylene)ethynylenes (OPEs), oligo(phenylene)vinylenes (OPVs) and related π-conjugated organic materials such as oligo(thiophenes) *etc.* appear frequently throughout the literature, particularly within the area of molecular electronics.[14-19] Metal centres offer *d*-orbitals that also have π-symmetry and complement these organic 'interpolating' π-fragments. This conceptual extension from molecules and materials in which the electronic structure is derived from 2*p*-2*p* orbital overlaps and broadens to organometallic systems in which *nd*-2*p* overlaps are introduced, leads to the fascination with metal σ-alkynyl systems and the prevalence of these systems in the organometallic literature. By careful design, the physical and optoelectronic properties of metal alkynyl complexes can be optimised for application. Obvious design elements to tune the energy and occupancy of the *d*-orbitals include the choice of metal, oxidation state and supporting ligands. For example, the frontier

orbitals of octahedral ruthenium(II) fragments bearing phosphine ligands are well matched in both symmetry and energy with the π-orbitals of the C≡C fragment, and hence a strong, Ru(*d*)-C≡C(*π*) π-type, filled-filled orbital interaction is favoured.[20] A smaller Ru(*d*)-C≡C(π*) backbonding interaction has also been established.[21] In contrast, square planar Pt(*d*) and Pd(*d*) orbitals are generally thought to be too low in energy to effectively overlap with C≡C(π); hence the Pt-C≡C bond is chiefly regarded as offering σ-character.[22]

Metal σ-alkynyl complexes are known for essentially every metallic element in the periodic table.[i] A number of broadly applicable synthetic routes for the preparation of M-C≡CR complexes are known, the most common of which can be generalised as:

(a) reaction of a nucleophilic acetylide with a metal centre bearing a suitable leaving group or vacant coordination site;[31-33]
(b) deprotonation of vinylidene complexes, M=C=CHR;[34-36]
(c) transmetallation reactions, typically involving Cu^{I},[37-39] Sn^{IV} [40-42] or Au^{I} [43] acetylides;
(d) functionalisation reactions of pre-formed metal acetylide complexes.[44-47]

The choice of synthetic methodology depends on both the alkyne reagent and the nature of the metal-ligand platform. For example, transmetallation reactions of Cu^{I}-acetylides, formed *in situ* from terminal alkynes in the presence of amine and catalytic CuI, are particularly useful in the formation of group 10 acetylide complexes from MX_2L_2 (X = halide) systems. Alternatively, Stille-type reactions of stannylalkynes in the presence of amine and catalytic CuI are effective for both group 8 and group 9 complexes with relatively electron-withdrawing ligands. For more electron-donating systems, the destabilisation of π-bound metal alkyne and preferential rearrangement to vinylidenes makes vinylidene intermediates particularly useful entry points to metal acetylides in this case.

[i] Metal complexes and clusters in which the alkyne π-system is involved in the bonding to the metal centre defines a separate class of compound, which is not considered further here. The interested reader is referred to the numerous reference works that describe these complexes.[23-30]

Throughout this Chapter, a chronological approach to the description of the field of metal σ-acetylide complexes has been adopted. The Chapter begins with an outline of the synthetic developments that were centred on the early examples of metallopolymers, and briefly presents details of the electronic structures of these pioneering materials. A broader discussion of synthetic methods associated with well-defined small molecule metal acetylide complexes follows. A survey of current applications of *trans*-bis(alkynyl) complexes in materials science then completes this review.

1.2. Metallopolymers

1.2.1. Introduction

Metallopolymers can be defined as polymers containing metal fragments within the repeating monomer unit. Combining the processing properties of polymers with the functionality of metal centres has been conceptually appealing to scientists since the 1950s.[48] There are several advantages arising from the incorporation of metals within a π-conjugated polymer framework, and the volume of work in the area has lead to many reviews.[49-53] For example, both physical (*e.g.* solubility) and electronic properties of a metal-organic hybrid polymer can be effectively tuned through variation of the metal centre and ancillary ligands, as well as the organic component. Exploiting the photophysical and photochemical properties of metal complexes has meant metallopolymers have been extensively explored as luminescent materials[54-60] and as light harvesting layers in solar cells,[61] whilst exploration of the unique binding affinities of metal centres has lead to applications in chemical sensing.[62-65] From the addition of redox-active metals, able to exist in multiple stable oxidation states, metallopolymers have found application in catalysis,[66-71] where the metal centres provide efficient sites for reaction, and molecular electronics,[72-74] allowing for either redox-mediated changes in conductivity or serving as thermodynamic sinks that may trap / localise charges depending on frontier orbital energies. The incorporation of spin-active nuclei has also lead to applications in data storage.[75-77] Although the addition of metal fragments significantly promotes functionality, the classical processing possibilities associated with purely organic polymers such as spin coating, extrusion, inkjet printing, compounding and film blowing are preserved.[53]

The conjugated metallopolymer framework is commonly based on combinations of C≡C triple bonds, C=C double bonds and / or aryl rings, and incorporates metals from across the periodic table. Metallopolymers containing transition metals such as Cu,[54-56, 63, 72, 78-81] Os,[64, 74] Zn,[72, 78, 82] Fe,[75, 76, 83, 84] Ru,[64, 68, 70] Co,[78] Ag,[81] Pt[58, 61, 73] and Pd[58, 71] in addition to those based on main group metals, such as Pb,[85, 86] are common. Complexes containing lanthanide metal ions, such as Eu[59, 60, 77] and Tb,[60] are also known. Additionally, the metal centre can either be integrated within the polymer backbone (main chain metallopolymers),[87] or located within a pendant side chain off the polymer backbone (side chain metallopolymers) (Figure 1.2a, 1.2b).[88] The three dimensional metallopolymer structures may be linear, star-shaped or dendritic (Figure 1.2c, 1.2d, 1.2e). Furthermore, the interaction between the metallic and organic fragments may either be *via* irreversible inert covalent bonds or reversible 'dynamic' labile or non-covalent bonds, such as π-π stacking or hydrogen bonding interactions.[82, 89-91]

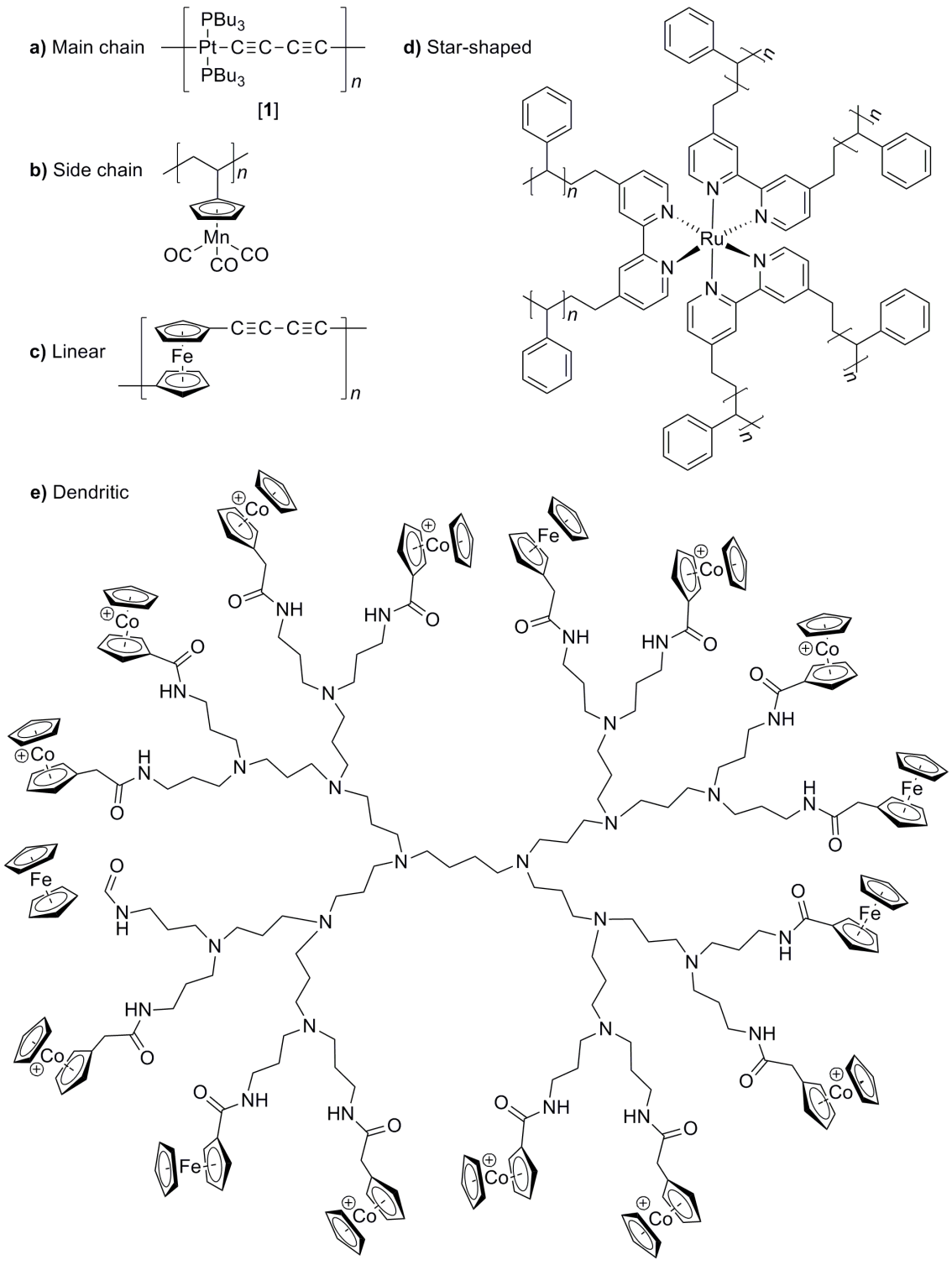

Figure 1.2: Representative examples showing the two methods of metal integration within metallopolymer structures (a, b) and the variety of three-dimensional metallopolymer structures (c, d, e).

Considering the vast structural diversity of metallopolymers, for the purpose of this review (and to align with work in this Thesis), the primary focus of discussion will be the chemistry of linear, main chain metallopolymers comprised of static metal-organic linkages, with a view to exploring and understanding highly conjugated, high molecular weight architectures for molecular electronics applications.

1.2.2. Early metallopolymers

The first metallopolymer reported in the literature is attributed to Arimoto and Haven in 1956 and was based on a ferrocene substructure integrated into a side chain.[48] Vinyl ferrocene, [Fe(η^5-C_5H_5){η^5-C_5(CH=CH_2)H_4}], was obtained in a low yield (21 %) *via* pyrolysis (200 °C) of [Fe(η^5-C_5H_5){η^5-C_5(CHMeOH)H_4}]. Subsequent thermolysis of vinyl ferrocene for 2 – 6 hours in the presence of a catalyst (85 % H_3PO_4, potassium persulfate or azo-diisobutyronitrile (AIBN)) achieved homo-polymerisation, although product characterisations were limited to melting point determinations (280 − 285 °C), which were significantly higher than the starting material (48 – 49 °C) (Scheme 1.1). Alternatively, co-polymerisation was achieved by thermolysis of vinyl ferrocene in the presence of a catalyst (potassium persulfate or azodiisobutyronitrile) and co-monomer (methyl methacrylate, styrene or 2-chlorobuta-1,3-diene), where the observed increase in product melting points (165 – 210 °C) was once again taken to indicate polymer formation (Scheme 1.1).

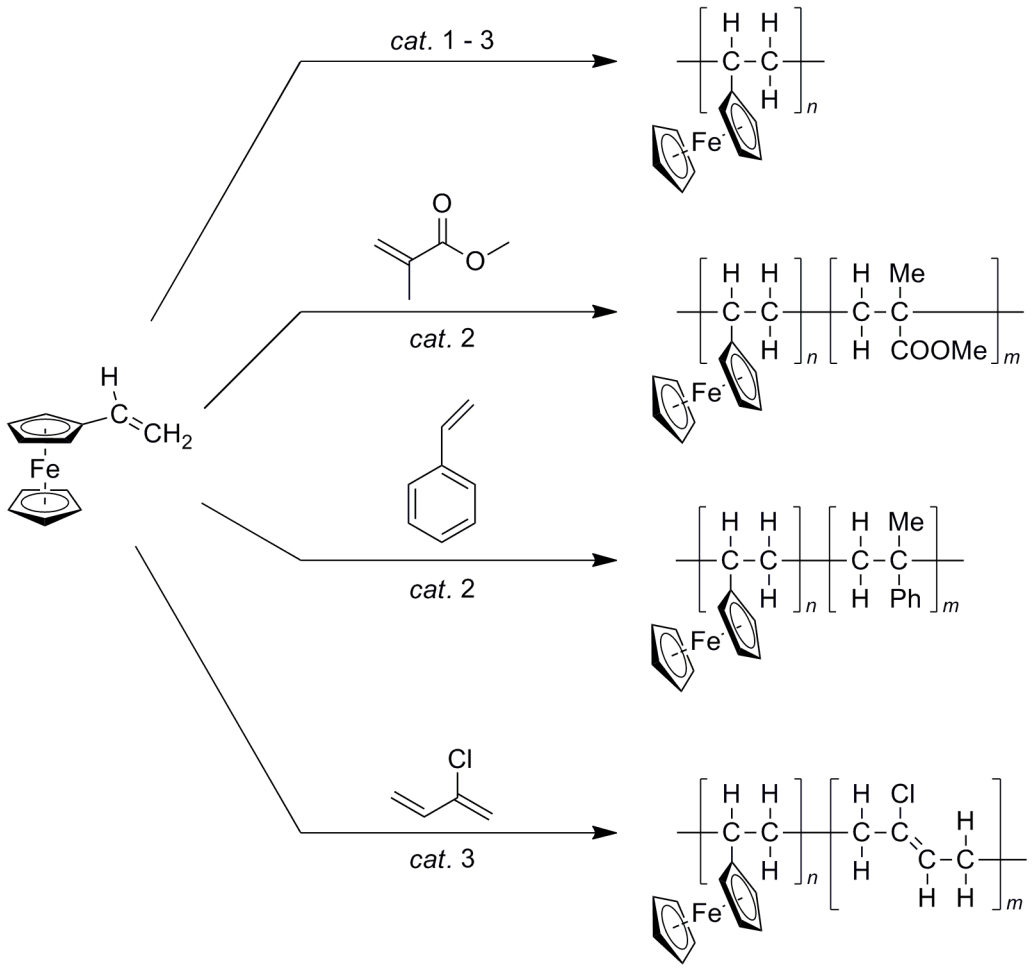

Scheme 1.1: Syntheses of the first reported metallopolymers, where *cat.* 1 = phosphoric acid; *cat.* 2 = AIBN and *cat.* 3 = potassium persulfate.[48]

Following this initial report, several groups claimed formations of metallopolymers, predominantly based on ferrocene sub-units,[92-96] although convincing characterisation data were not provided or available.[97] In their 1970 review of metallocene polymers, Neuse and Rosenberg concluded that *"progress* [within this field] *has been very modest indeed. Many of the structural assignments given, obviously, are hypothetical and need rigorous analytical verification, and the description of experimental procedures and polymer properties more often than not has been superficial or lacking altogether."*[97] The main hindrance to characterisation of metallopolymers at this time was the general insolubility of these materials in the solvents commonly required for techniques such as NMR spectroscopy for speciation and structural characterisation, and gel permeation chromatography (GPC) for molecular weight determinations. Furthermore, purification difficulties were often encountered due to uncontrolled side reactions and the lack of

readily available starting materials (with which to try to overcome these issues) merely compounded these problems.[53, 98]

The first readily-soluble metallopolymers of appreciable molecular weight to be isolated and thoroughly characterised (IR, NMR, UV and Mössbauer spectroscopy in addition to kinetic studies and elemental analyses) were reported by Patterson and co-workers in 1970.[98] Isolations of poly(ferrocenylmethy1)acrylate and poly(ferrocenylmethy1)methacrylate were achieved by reacting the monomers, ferrocenylmethy1acrylate and ferrocenylmethy1methacrylate (respectively), with the initiator AIBN in solutions of benzene at 0 °C, followed by precipitation with 40 − 60 °C petroleum ether. In 1974, Patterson extended the series of well characterised metallopolymers to include three novel linear poly(siloxanes) containing ferrocene units, prepared through reactions of 1,1-*bis*-(dimethylaminodimethylsilyl)ferrocene with dihydroxydiphenylsilane, 1-4-*bis*(hydroxydimethylsilyl)benzene or 4,4-*bis*(hydroxydimethylsilyl)biphenyl.[99]

1.2.3. σ-bonded main chain group 10 metallopolymers

In 1977, several years after the syntheses of original ferrocene-based metallopolymers were described, Sonogashira, Takahashi and Hagihara successfully prepared *trans*-$[(PBu_3)_2Pt(\mu\text{-}C{\equiv}CC{\equiv}C)]_n$, [**1**], as the first linear polymer to contain a σ-bonded transition metal in the main chain. The complex [**1**] was obtained in a high yield (96 %) from the reaction of $[Pt(C{\equiv}CC{\equiv}CH)_2(PBu_3)_2]$, [**2**], with $[PtCl_2(PBu_3)_2]$, [**3**], (1 equiv.) and catalytic CuI (2 mol %) in diethylamine (Scheme 1.2).[100]

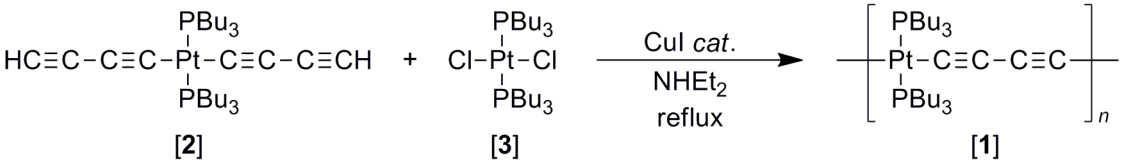

Scheme 1.2: Synthesis of the first σ-bonded transition metal (platinum) main chain metallopolymer, as reported by Sonogashira, Takahashi and Hagihara.[100]

The high solubility of [**1**] in aprotic organic solvents such as dichloromethane, diethylamine, benzene, toluene, THF and even *n*-hexane (assumed to be a direct result of the bulky, but flexible, *n*-butyl chains on the ancillary phosphine ligands preventing intermolecular interactions) allowed complete characterisation of the polymer.[101] In particular the *trans*-arrangement of the phosphine co-ligands around the square planar platinum centre, which leads to the proposed 'rod-like' structure, was confirmed by ^{31}P NMR spectroscopy (s, $\delta - 4.2$ ppm) while polymerisation was inferred by IR spectroscopy with the absence of ν(≡C-H) bands near 3300 cm^{-1}. The 'rod-like' structure was further supported by formation of anisotropic phases from concentrated CH_2Cl_2 solutions of the polymer observed under a polarised microscope,[102] leading to suggestions of potential application as liquid crystals.[103,104] However, additional NMR spectroscopy and viscosity experiments revealed a higher degree of flexibility than initially thought, with the polymer better described as a 'worm-like' chain.[105]

In order to form platinum metallopolymers with high average molecular weights (M_w), the presence of catalytic CuI (or CuBr or CuCl) was found to be integral,[102] although at the time of the original reports the precise mechanistic role of the catalyst was not fully determined. Moreover, strongly basic amines such as diethylamine or piperidine, where the amine operates as both the base (to assist formation of the key copper acetylide intermediates) and reaction solvent, also gives rise to high molecular weight materials. The longer the growing polymer is kept in solution, the higher the M_w, as the reaction continues until the product polymer precipitates from solution, evincing living polymerisation. As a clear demonstration, [**1**] was formed with an M_w of 70 000 $gmol^{-1}$ (determined by GPC analysis) after the month-long, room temperature reaction of [**2**] with [**3**] (1 equiv.) and catalytic CuI (2 mol %) in diethylamine whereas the reaction of 1,4-diethynylbenzene with [**3**] (1 equiv.) under analogous conditions yielded *trans*-$[(PBu_3)_2Pt(\mu\text{-}C{\equiv}CC_6H_4\text{-}4\text{-}C{\equiv}C)]_n$, [**4**], with a maximum M_w of only 8 000 $gmol^{-1}$, the differences being a direct consequence of polymer solubility. Upon conducting the latter reaction at reflux, a higher maximum M_w of 55 000 $gmol^{-1}$ was obtained.

The molar ratio of the two reactants is also shown to affect M_w, with a 1 : 1 ratio proving optimum. Furthermore, the presence of oxygen in these reaction schemes is an important consideration. For example, in order to form [**1**], the condensation

polymerisation reaction of [**2**] with [**3**] should be conducted under inert, oxygen-free conditions. If not, and in the presence of tetramethylethylenediamine (TMEDA) and a copper halide catalyst, oxidative coupling of the 1,4-butadiynediyl units occurs, giving competing formation of *trans*-$[(PBu_3)_2Pt(\mu\text{-}C{\equiv}CC{\equiv}CC{\equiv}CC{\equiv}C)]_n$ with octa-tetrayne links in the growing polymer chain. The homo-coupling does, however, establish an alternative route to σ-bonded platinum (and palladium) metallopolymers based on longer oligoyne fragments.[39, 106]

In 1978, Sonogashira, Kataoka and Hagihara increased the complexity of linear main chain metallopolymers through the introduction of two alternating metals, Pt and Pd, within the monomer unit in order to determine novel physical properties for potential applications in catalysis.[101] Air stable complexes of the type *trans-trans*-$[(PBu_3)_2M(\mu\text{-}C{\equiv}CC{\equiv}C)M'(PBu_3)_2(\mu\text{-}C{\equiv}CC{\equiv}C)]_{n/2}$ ([**5**]: M = Pt, M′ = Pd; [**6**]: M = Pd, M′ = Pt) were formed through reactions of *trans*-$[M(C{\equiv}CC{\equiv}CH)_2(PBu_3)_2]$ with *trans*-$[M'Cl_2(PBu_3)_2]$ (1 equiv.) and catalytic CuI (1 – 2 %), or CuBr or CuCl,[102] in solutions of diethylamine (M, M′ = Pt, Pd; Scheme 1.3).

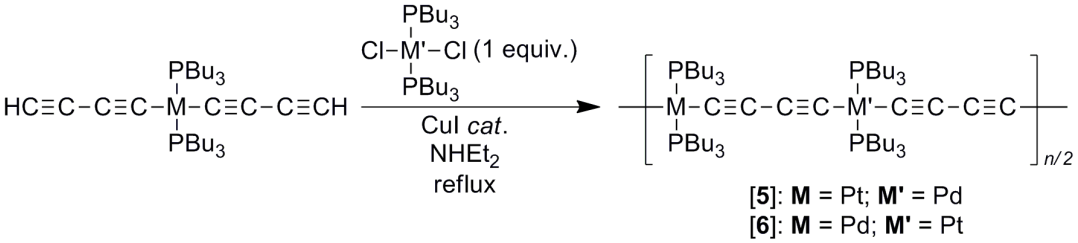

Scheme 1.3: Synthesis of the first σ-bonded main chain metallopolymers to contain two different metal fragments within the monomer, as reported by Sonogashira, Kataoka and Hagihara.[101]

Electron spectroscopy for chemical analysis (ESCA) and ^{31}P NMR spectroscopy confirmed the 1 : 1 ratio of Pd^{II} and Pt^{II} units in the polymer and *trans*-configuration at both metal centres. Interestingly, [**5**] (with M = Pt and M′ = Pd) was obtained as a higher M_w polymer (26 000 $gmol^{-1}$) with a higher melting point (194 °C) in a 95 % yield after a 20 hour room temperature reaction, than the inverse complex [**6**] (M = Pd and M′ = Pt), which was formed with a lower M_w (7 000 $gmol^{-1}$) and melting point (173 °C) in a 90 % yield after 6 hours in refluxing solvent (56 °C), highlighting the

importance of synthetic sequence and reaction conditions in governing metallopolymer product outcome.

A subsequent depolymerisation reaction of the higher M_w polymer [**5**] (26 000 $gmol^{-1}$) with [**3**] in the presence of catalytic CuI, yielded the trimetallic complex *trans-trans*-[{$(PBu_3)_2Pt$}{(μ-C≡CC≡C)$Pd(PBu_3)_2Cl$}$_2$], selectively in a high yield (75 %), evincing the strict alternating metal sequence of this metallopolymer. The analogous reaction with the lower M_w polymer [**6**] (7 000 $gmol^{-1}$) instead yielded a series of mixed-metal oligomers, indicating irregularity in the original metallopolymer.

Hagihara and co-workers have further explored the synthesis of platinum metallopolymers bearing alternating conjugation lengths between metal fragments.[107] Based on established methods,[100-102] reactions of *trans*-[{$Cl(PBu_3)_2Pt$}$_2${μ-C≡C(C_6H_4-4-)$_m$C≡C}] (m = 0, 1) with HC≡CXC≡CH (X = C_6H_4-4-, C_6H_4-4-C_6H_4-4-, C≡C$Pt(PBu_3)_2$C≡C) and catalytic CuI (1 %) in solutions of diethylamine resulted in the formations of *trans-trans*-[{$(PBu_3)_2Pt$}{μ-C≡C(C_6H_4-4-)$_m$C≡C}{$Pt(PBu_3)_2$(μ-C≡CXC≡C)}]$_n$ as yellow solids in high yields (95 − 97 %; Scheme 1.4).

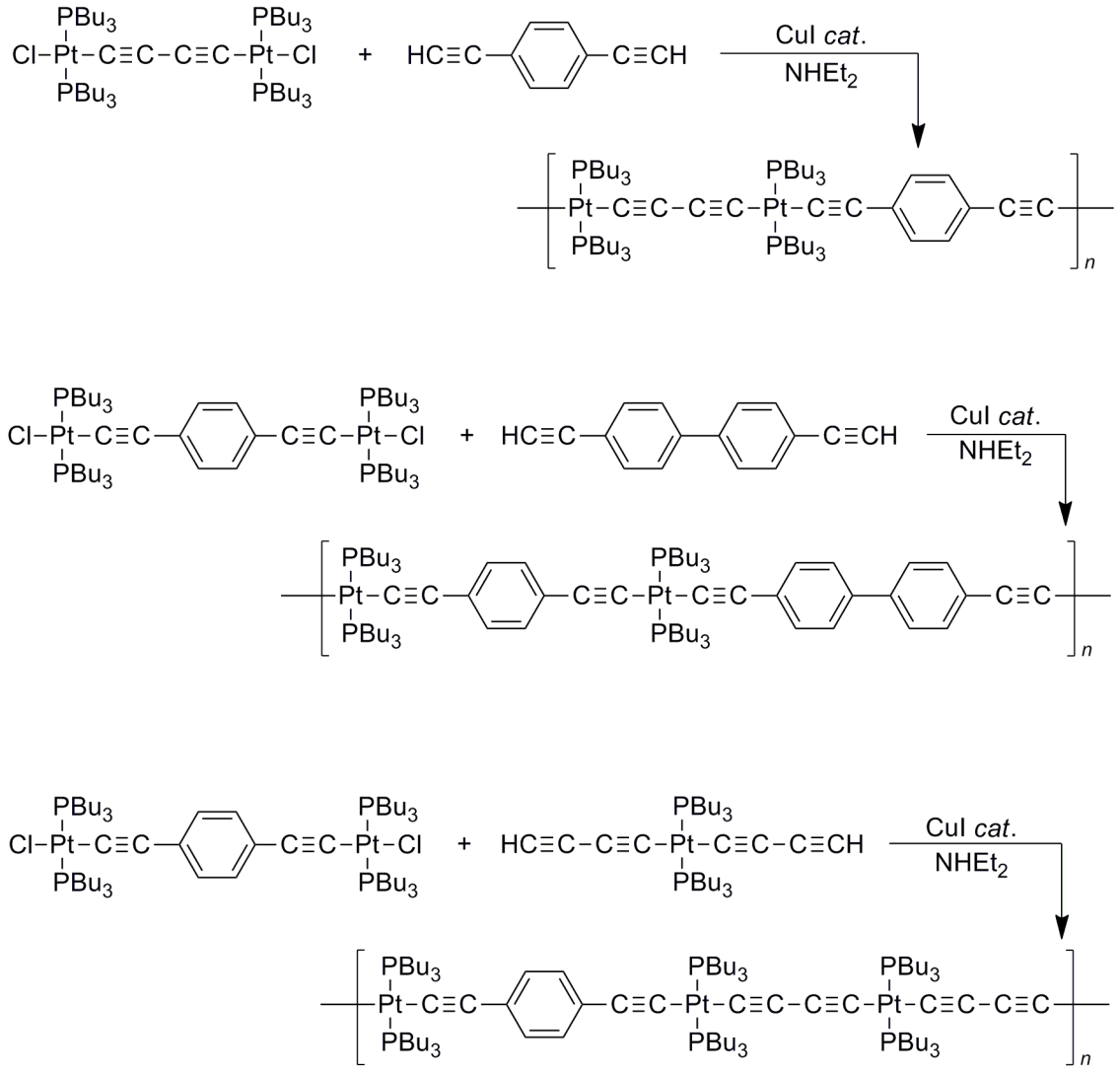

Scheme 1.4: Synthetic routes to platinum metallopolymers containing organic linker units of variable lengths between metal fragments, as reported by Hagihara and co-workers.[107]

The degree of regularity in these mixed linker-length polymers was confirmed by ^{31}P NMR spectroscopy and comparison of the spectra of hetero-coupled polymers with those of previously obtained homo-coupled polymers. In order to achieve extensive alternating regularity, the reaction was best conducted at room temperature, despite an extensive reaction length (12 days). Under reflux conditions, depolymerisation reactions are favoured (especially in the presence of the copper halide catalyst and amine solvent) resulting in continuous breaking and reforming of M-C bonds, leading to random metallopolymers with irregularities in conjugation lengths between metal centres.

In 1980, Hagihara reported metallopolymers containing nickel, completing the group 10 triad.[39] As a first row metal, the metal-carbon overlap with nickel is greater than the heavier members of the group, through better mixing of frontier orbital fragments of similar energy, simultaneously increasing the degree of metal-carbon *d*-π forward / backbonding interactions and lability of the PBu_3 units.[39] Formation of *trans*-$[(PBu_3)_2Ni(\mu\text{-}C{\equiv}CXC{\equiv}C)]_n$ (X = none; C_6H_4-4-, [**7**]; $C{\equiv}CPt(PBu_3)_2C{\equiv}C$ and C_6H_4-4-$C{\equiv}CPt(PBu_3)_2C{\equiv}CC_6H_4$-4-) was achieved in high yields (85 – 95 %) from reactions of *trans*-$[Ni(C{\equiv}CH)_2(PBu_3)_2]$ in diethylamine with $HC{\equiv}CXC{\equiv}CH$ (1 equiv.), catalytic CuI (1 %) and PBu_3 (required in order to circumvent metal phosphine dissociation leading to decomposition). These reactions represent the first examples of acetylide ligand displacement by more activated acetylene complexes. The electronic spectra of *trans*-$[(PBu_3)_2M(\mu\text{-}C{\equiv}CC{\equiv}C)]_n$ (M = Ni; Pd; Pt, [**1**]), revealed that the maximum wavelength (λ_{max}) of the lowest energy MLCT transition increased down the group, from Ni (414 nm) to Pd (382 nm) to Pt (342 nm), reflecting the larger HOMO-LUMO gaps and lower energy M(*d*) associated with the heavier metals.

As an alternative route to group 10 metallopolymers, Lewis explored the use of trimethylstannyl reagents as alkynyl-transfer (or transmetallation) agents,[42, 108-111] based on the original success of Lappert in forming M-C σ-bonds through this method.[112] Complexes *trans*-$[(PBu_3)_2Pt\{\mu\text{-}C{\equiv}C(C{\equiv}C)_mC{\equiv}C\}]_n$ ([**1**]: m = 0; [**8**]: m = 1), which includes the first triynediyl-containing platinum metallopolymer ([**8**]), and *trans*-$[(XBu_3)_2M(\mu\text{-}C{\equiv}CRC{\equiv}C)]_n$ ([**4**]: M = Pt, X = P, R = C_6H_4-4-; [**7**]: M = Ni, X = P, R = C_6H_4-4-; [**9**]: M = Pd, X = P, R = C_6H_4-4-; M = Pt, X = As, R = C_6H_2-2,5-Me_2) were obtained in high yields (88 – 92 %) from reactions of $[MCl_2(XBu_3)_2]$ with $Me_3SnC{\equiv}C\{R / (C{\equiv}C)_m\}C{\equiv}CSnMe_3$ (1 equiv.) and catalytic CuI (2 − 4 %) in toluene over various temperatures (30 – 50 °C) and lengths (1 – 12 hours). Adventitiously, this route favours the formation of high M_w metallopolymers, presumably due to the increased solubility of the growing polymer chains in toluene rather than amine solvents. Under these conditions the original platinum metallopolymer, [**1**], was obtained with an increased M_w of 130 000 $gmol^{-1}$ (*vs.* the previous M_w maximum of 70 000 $gmol^{-1}$ determined by Hagihara and co-workers).[102] Furthermore, *trans*-$[(PBu_3)_2Pd(\mu\text{-}C{\equiv}CC_6H_4\text{-}4\text{-}C{\equiv}C)]_n$, [**9**], was obtained with a higher M_w of 30 000 $gmol^{-1}$ (*vs.* M_w 22 000 $gmol^{-1}$ from previous methods).[113] During optimisation of

reaction conditions, Lewis and co-workers found that the specific 1 : 1 ratio of metal dihalide ([$MCl_2(PBu_3)_2$]) to *bis*-trimethylstannyl reagent ($Me_3SnC{\equiv}CRC{\equiv}CSnMe_3$), in addition with a CuI catalyst, were vital for yielding polymeric complexes (Scheme 1.5). At 1 : 2, metal dihalide : *bis*-trimethylstannyl, reagent ratios, monomeric complexes *trans*-[$M(C{\equiv}CRC{\equiv}CSnMe_3)_2(PBu_3)_2$] were obtained, which readily destannylated on alumina forming *trans*-[$M(C{\equiv}CRC{\equiv}CH)_2(PBu_3)_2$] in 85 − 90 % yields (Scheme 1.5). Conversely, if a 2 : 1 ratio is employed, oligomeric complexes are obtained in 85 − 90 % yields (Scheme 1.5).

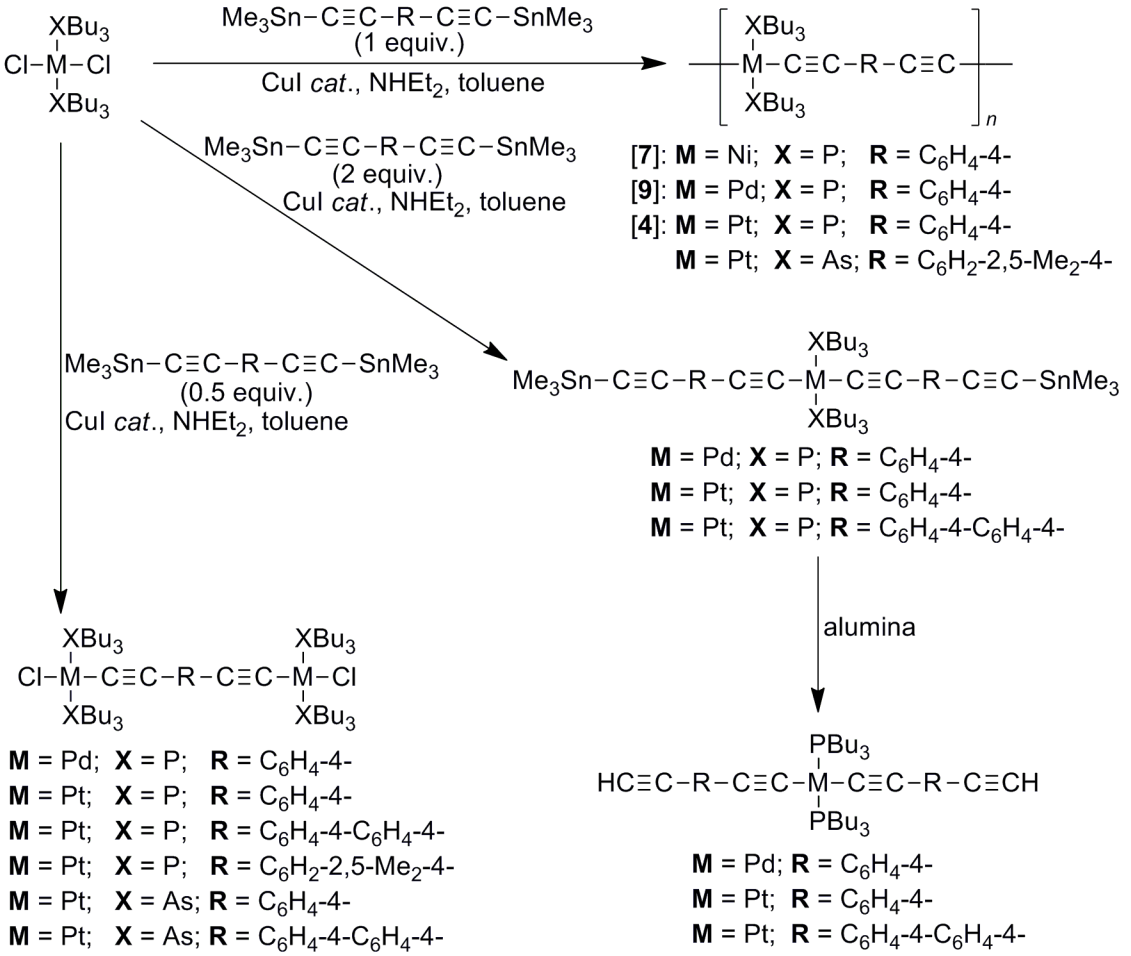

Scheme 1.5: Formations of polymeric, oligomeric and monomeric group 10 complexes as a result of varying reaction conditions, as reported by Lewis and co-workers.[42]

The optical absorption spectra of [**1**] and [**8**] displayed several bands between 2.8 − 5.4 eV. In each case, the lowest energy bands (also the most intense) were ascribed to correspond to the polymer band gap. As such, a smaller band gap was found

for [**8**] (3.12 eV) than [**1**] (3.23 eV),[114] a result of increased conjugation length, where the platinum centres are not expected to significantly hinder delocalisation.[115, 116] Insertion of a phenyl fragment, as in [**4**], or pyridine fragment within the polymer backbone, *trans*-[(P^nBu_3)$_2$Pt(μ-C≡C-3-C_5H_3N-6-C≡C)]$_n$, was shown to marginally reduce π-conjugation and increase this band gap (3.26 eV, 3.24 eV respectively).[114] In contrast, the addition of quaternarised pyridine units, *trans*-[(P^nBu_3)$_2$Pt{μ-C≡C-3-C_5H_3N(MeI)-6-C≡C}]$_n$, achieved by reacting [**3**] with Me_3SiC≡C-3-C_5H_3N(MeI)-6-C≡C$SiMe_3$ and a catalytic amount of CuI, increased π-conjugation (2.36 eV).[116] Similarly, the incorporation of anthracene units, *trans*-[(P^nBu_3)$_2$Pt(μ-C≡C-C_6H_4-4-C≡C$C_{14}H_8$-8-C≡CC_6H_4-4-C≡C)]$_n$, results in more highly conjugated complexes (with a comparable band gap of 2.48 eV), than structurally related metallopolymers containing arene and thiophene units, *trans*-[(P^nBu_3)$_2$Pt(μ-C≡C-C_6H_4-4-C≡CC_6H_4-4-C≡CC_6H_4-4-C≡C)]$_n$ (3.11 eV) and *trans*-[(P^nBu_3)$_2$Pt(μ-C≡C-C_6H_4-4-C≡C-2-C_4H_2S-5-C≡CC_6H_4-4-C≡C)]$_n$ (2.70 eV).[117] As the band gaps for these complexes are all around 3 eV, such systems can be classified as weak conductors or wide-band gap semi-conductors.[11] For the interested reader, a thorough analysis of the vibrational spectra (IR and Raman) of platinum metallopolymers, determining the relationship between structure and extent of π-conjugation, has been given by Lewis.[118]

As complexes anticipated to display increased thermal and mechanical stability, Lewis prepared cross-linked metallopolymers of the type *trans*-[1,3,5-{(XBu_3)$_2$PtC≡C-}$_3C_6H_3$]$_n$ (X = P, As; Scheme 1.6) *via* CuI catalysed (13 %) reactions of 1,3,5-triethynylbenzene with [$PtCl_2(XBu_3)_2$] (1.5 equiv) in solutions of diethylamine.[119] Though high yielding (92 – 95 %), products were "*virtually insoluble in common organic solvents*".[119] To increase solubility, branch-points based on the 1,3,5-triethylbenzene motif were included into an established rigid-rod platinum polymer. Reactions of HC≡CC_6H_2-2,5-Me_2-4-C≡CH and 1,3,5-triethynylbenzene (in molar ratio equivalents of 1 : 10; 1 : 50 and 1 : 100) with [$PtCl_2(XBu_3)_2$] (1 equiv.) resulted in formation of branched chain and cross-linked polymers, [(XBu_3)$_2$Pt(C≡CC_6H_2-2,5-Me_2-4-C≡C)]$_n$[1,3,5-{(XBu_3)$_2$PtC≡C-}$_3C_6H_3$]$_m$, in high yields (77 – 89 %; Scheme 1.6). Although the more highly cross-linked polymer (1 : 10 molar ratio) remained insoluble, the solubility of the other polymers (1 : 50 and 1 : 75 molar ratio) in toluene, THF and CH_2Cl_2 meant that the M_w values could be determined as 58 000 $gmol^{-1}$ and

27 000 $gmol^{-1}$ respectively, where analytical data obtained was consistent with compositions of *n* and *m* reflecting the molar ratios of the reagents employed.

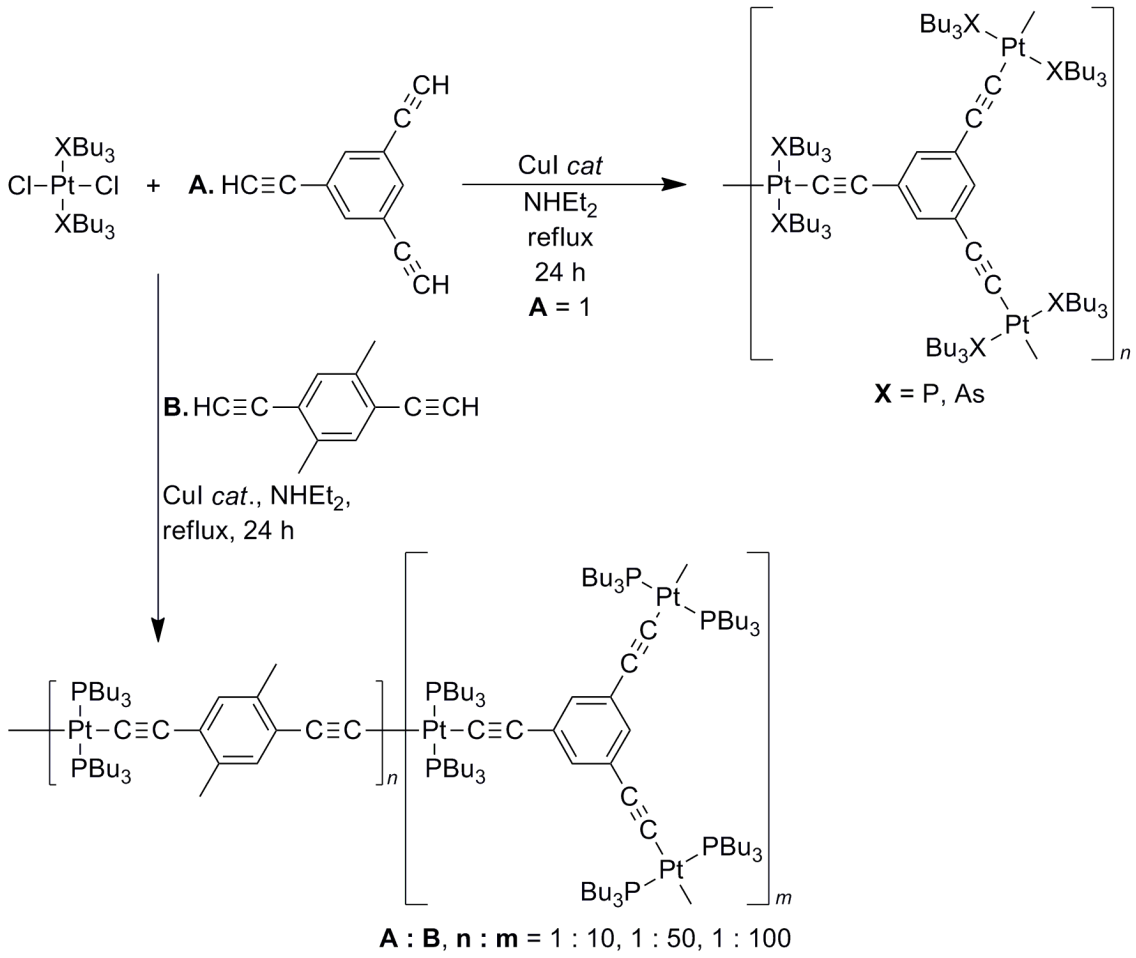

Scheme 1.6: Synthesis of cross-linked platinum metallopolymers, as reported by Lewis.[119]

1.2.4. σ-bonded main chain group 9 metallopolymers

Although copper halide-catalysed reactions of metal dihalides with alkynes in amine solvents is a highly successful route to forming metallopolymers, the synthesis is limited to group 10 metal complexes due to the instability of other metal dihalides in the amine solvents, prompting the derivation of alternative routes.[41, 42] In 1991, the first rhodium metallopolymers, *mer-trans*-$[(PX_3)_3(H)Rh(\mu\text{-}C{\equiv}CRC{\equiv}C)]_n$ (X = Me, ^{n}Bu; R= C_6H_4-4-, C_6H_4-4-C_6H_4-4-; Scheme 1.7) were prepared by Marder from C-H activation reactions of diynes and Rh-phosphine complexes.[120]

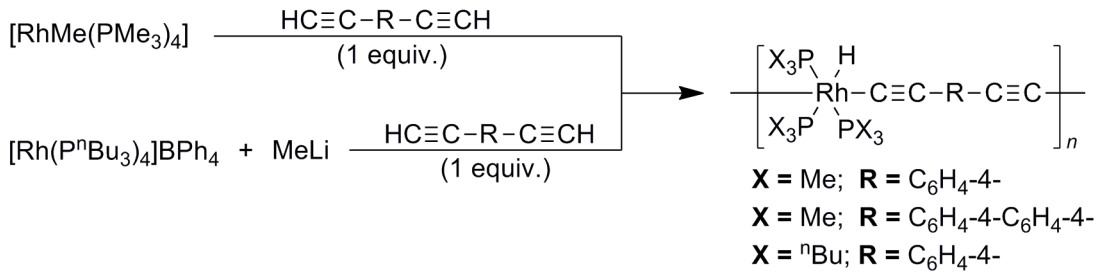

Scheme 1.7: The first reported syntheses of rhodium metallopolymers, as reported by Marder.[120]

Alkynylstannanes, pioneered in use for the formation of *trans*-bis(alkynyl) metal complexes by the Lewis group, have also been used in the formation of rhodium metallopolymers. Reactions of $[RhCl(PPh_3)_3]$ or $[RhCl(PMe_3)_4]$ with $Me_3SnC{\equiv}CC_6H_4$-4-C_6H_4-4-C≡CSnMe_3 (1 equiv.) in toluene or THF gave *trans*-$[(Me_3Sn)(PPh_3)_2Rh(\mu$-$C{\equiv}CC_6H_4$-4-C_6H_4-4-$C{\equiv}C)]_n$ and *trans*-$[(Me_3Sn)(PMe_3)_3Rh(\mu$-$C{\equiv}CC_6H_4$-4-C_6H_4-4-$C{\equiv}C)]_n$ in high yields (77 % and 72 % respectively) after oxidative addition accompanied by loss of both chloride and phosphine ligands, the product structure being confirmed by IR and mass spectrometry in addition to elemental analyses. The limited solubility of these polymers in all common organic solvents precluded further characterisation. Notably, varying the molar quantities of reagents in this case had no effect on the product outcome, with excess reagents being recovered.

Alkynylstannanes were also used in the formation of the first Co^{III}-containing metallopolymer, *trans*-$[(N')_4Co(\mu$-$C{\equiv}CC_6H_4$-4-$C{\equiv}C)]_n$; isolated as a soluble, air-stable and high M_w (15 800 $gmol^{-1}$) species (where $(N')_4$ = 3,3'-(1,3-propanediyldinitrilo)-*bis*(2-butanone)dioximato(1-)-*N*,*N*',*N*'',*N*''', otherwise known as 3,9-dimethyl-4,8-diazaundecane-2,10-dione dioxime; Scheme 1.8).[121]

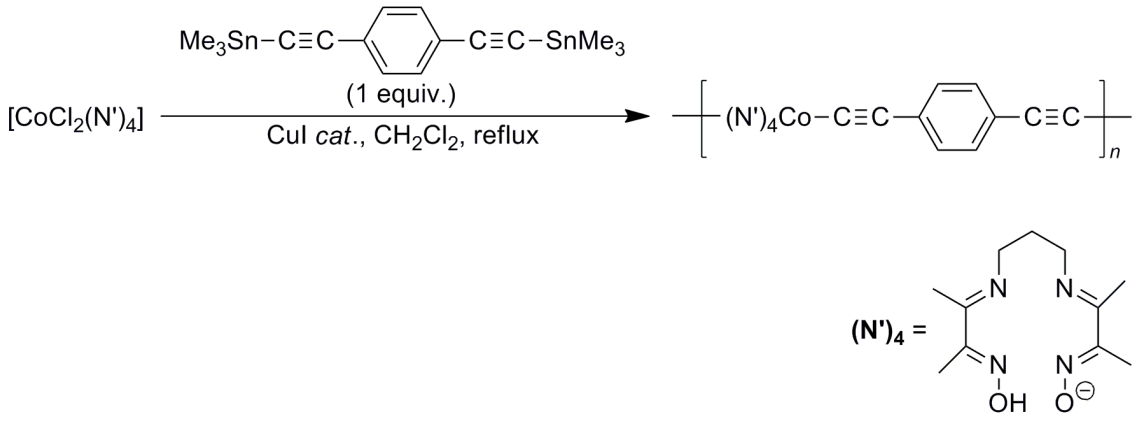

Scheme 1.8: Synthesis of the first Co^{III}-containing metallopolymer, as reported by Lewis.[121]

The *trans*-bis(alkynyl) configuration of the Co^{III}-containing metallopolymer was confirmed by IR spectroscopy (showing a single ν(C≡C) band at 2103 cm^{-1}) with further structural information inferred from single crystal diffraction studies on the related mononuclear complex *trans*-[CoI(C≡CSiMe$_3$)N′$_4$].[122] The lowest energy (and most strongly absorbing) bands in the UV-Vis-NIR spectrum were assigned as π-π* transitions. In comparison to the free ligand HC≡CC$_6$H$_4$-4-C≡CH, the π-π* band energy (and by inference the π-π* energy gap) was 0.28 eV lower for the polymeric complex, evincing extended conjugation through the Co^{III} metal fragments.

1.2.5. σ-bonded main chain group 8 metallopolymers

In 1991, in a preliminary communication, the Lewis group described the first linear main chain metallopolymers containing a group 8 metal. The iron-based polymers, *trans*-[Fe(depe)$_2$(C≡CRC≡C)]$_n$ (R = C$_6$H$_4$-4-, [**10**]; C$_6$H$_2$-2,5-Me$_2$-4-) were prepared from CuI catalysed reactions of [FeCl$_2$(depe)$_2$] with Me$_3$SnC≡CRC≡CSnMe$_3$ (1 equiv.) in toluene.[123] Notably, conducting the reactions in diethylamine, required in the formation of group 10 metallopolymers, was found to result in the instantaneous decomposition of the dichloride starting material.

Following this initial report, in 1993, the full group 8 triad of soluble metallopolymers, *trans*-[(PP′)$_2$M(μ-C≡CRC≡C)]$_n$ ([**10**]: M = Fe, PP′ = depe, R = C$_6$H$_4$-4-; [**11**]: M = Ru, PP′ = depe, R = C$_6$H$_4$-4-; M = Ru, PP′ = depe, R = C$_6$H$_2$-2,5-Me$_2$-4-; M = Ru, PP′ =

depe, R = C_6H_4-4-C_6H_4-4; [**12**]: M = Os, PP′ = dppm, R = C_6H_4-4-; M = Os, PP′ = dppm, R = C_6H_2-2,5-Me_2-4-; M = Os, PP′ = dppm, R = C_6H_4-4-C_6H_4-4-), were prepared from CuI-catalysed (13 %) reactions of $[MCl_2(PP')_2]$ with $Me_3SnC{\equiv}CRC{\equiv}CSnMe_3$ (1 equiv.) in refluxing toluene solutions, in moderate to high yields (45 − 70 %).[41] Even at this time, the authors stated that "*the role of CuI in such reactions is not yet very well understood.*"[41] Several years later, in 2002, Sonogashira also reported that *"the role of the CuI catalyst remain*[s] *obscure"*.[124] The group 8 metallopolymers were readily characterised by various spectroscopic methods (IR, ^{1}H NMR and $^{31}P\{^1H\}$ NMR), supporting a *trans*-arrangement of the alkyne ligands about the metal centre, in addition to elemental analyses and GPC, which indicated a high degree of polymerisation (M_w = 18 486 – 170 000 gmol^{-1}). The paper also included the first structural characterisation of a *trans*-bis(alkynyl) Ru^{II} complex supported by two chelating *bis*-phosphine ligands, *trans*-$[Ru(C{\equiv}CC_6H_5)_2(dppe)_2]$, [**13**], confirming the *trans*-arrangement of alkynyl ligands about the octahedral metal centre.

As a means to exploring the extent of π-conjugation in group 8 metallopolymers, Lewis prepared polymeric complexes *trans*-$[Ru(CO)_2(P^nBu_3)_2(\mu\text{-}C{\equiv}CRC{\equiv}C)]_n$ (R = C_6H_4-4-, [**14**]; C_6H_2-2,5-Me_2-4-, [**15**]) in high yields (81 %) from CuI catalysed (27 %) reactions of *trans*-$[RuCl_2(CO)_2(P^nBu_3)_2]$ and $Me_3SnC{\equiv}CRC{\equiv}CSnMe_3$ (1 equiv.) in CH_2Cl_2 solutions (reflux, 24 hours) in addition to the model bimetallic ruthenium complex, *trans*-$[\{Cl(P^nBu_3)_2(CO)_2Ru\}_2(\mu\text{-}C{\equiv}CC_6H_4\text{-}4\text{-}C_6H_4\text{-}4\text{-}C{\equiv}C)]$ (84 %), [**16**], through an analogous reaction in a THF solution using half an equivalent of $Me_3SnC{\equiv}CC_6H_4$-4-C_6H_4-4-$C{\equiv}CSnMe_3$.[12] On comparison between the polymers [**14, 15**] and bimetallic model complex [**16**], it was found that [**14, 15**] have experimentally determined band gaps (3.50, 3.51 eV) and ν(C≡C) frequencies (2084, 2085 cm^{-1}) of lower energy than [**16**] (4.40 eV, 2106 cm^{-1}) as a result of increased π-conjugation through the group 8 metal centres, consistent with previously published data.[109, 110, 115] In elucidating the effect of ancillary ligands on the underlying electronic structure, [**14**], bearing mixed carbonyl and phosphine ligands, has a larger optical band gap (3.51 eV) and a higher ν(C≡C) frequency (2084 cm^{-1}) than *bis*-depe supported [**11**] (3.19 eV, 2046 cm^{-1}),[41] containing all phosphine ligands, suggesting that electron donating ancillary ligands give rise to more highly conjugated polymeric materials.

In seeking to determine the effect of the metal on the electronic structure of metallopolymers, the vibrational spectra of *mono*-metallic model complexes were examined. The ν(C≡C) frequencies of first row group 8 complexes, *trans*-[Fe(C≡CC_6H_5)$_2$(depe)$_2$] (2035 cm^{-1})[125] and *trans*-[Fe(C≡CC_6H_5)$_2$(dmpe)$_2$] (2037cm^{-1})[125] were lower than closely related second row complexes *trans*-[Ru(C≡CC_6H_5)$_2$(PMe_3)$_4$] [**17**], (2055 cm^{-1}),[111] [**13**] (2061 cm^{-1})[41] and *trans*-[Ru(C≡CC_6H_5)$_2$(depe)$_2$] (2054 cm^{-1}),[41] which are in turn lower than third row group 10 complexes *trans*-[Pt(C≡CC_6H_5)$_2$(PMe_2Ph)$_2$] (2100 cm^{-1})[126] and [Pt(C≡CC_6H_5)$_2$(dppe)] (2110 cm^{-1}).[126] A similar trend is observed for ν(C≡C) frequencies in polymeric complexes, with *trans*-[(dppe)$_2$Ru(μ-C≡CC_6H_4-4-C≡C)]$_n$, (2056 cm^{-1}),[40] *trans*-[(dppm)$_2$Ru(μ-C≡CC_6H_4-4-C≡C)]$_n$ (2065 cm^{-1})[40] and [**12**] (2064 cm^{-1}),[41] having lower frequency ν(C≡C) bands than the related group 10 metallopolymers, [**7**] (2075 cm^{-1})[42] and [**9**] (2096 cm^{-1}).[42] Of course, such analyses ignore the role of kinematic effects in vibrational spectroscopy, but may give a first order approximation of the degree of conjugation (increasing conjugation being correlated with decreasing alkyne / C≡C character and hence decreased ν(C≡C) frequency).

Using extended Hückel theory, Frapper and Kertesz investigated the electronic structures of metallopolymers of the type *trans*-[(L)$_x$M(C≡CRC≡C)]$_n$ (where M = *e.g.* Mo, Fe, Pt, Hg; L = *e.g.* CO, PH_3; R = *e.g.* C≡C, C_6H_4-4-), in order to account for experimental observations.[11] The highest occupied crystal orbitals (HOCOs) and lowest unoccupied crystal orbitals (LOCOs) of the polymeric complexes show similar nodal properties to the HOMOs and LUMOs of the *mono*-metallic fragments, *trans*-[(L)$_x$M(C≡CRC≡CH)$_2$], but have reduced band gaps due to the increasing number of conjugated alkyne units (Figure 1.3), consistent with the experimental observation of smaller optical band gaps for polymers.

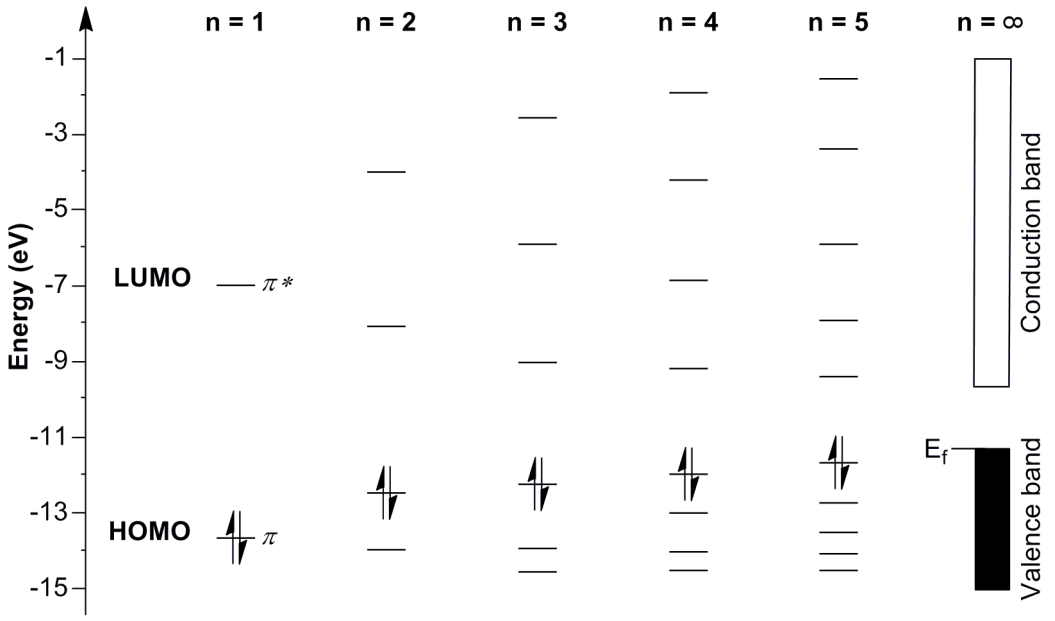

Figure 1.3: Schematic molecular orbital diagram, showing the stabilisation of the LUMO in $H(C{\equiv}C)_nH$ complexes, as a representative example, with increasing number of alkyne fragments (n). The additional stabilisation is minor after n = 4 or 5.

The HOMOs / HOCOs are predominantly more metal / ancillary ligand, $M(L)_x$, in character whereas the LUMOs / LUCOs are more acetylenic, C≡C, supported by density of states calculations. Therefore altering the nature of the metal ancillary ligands, L, will perturb the HOMOs / HOCOs more strongly than the LUMOs / LUCOs. Complexes containing strongly π-accepting carbonyl ancillary ligands stabilise the HOMO / HOCO to a greater extent than those containing phosphine ancillary ligands, due to the additional interaction between CO(π, π*) with M(*d*) (of correct symmetry),[12] systematically lowering the energies of the $M(L)_x$ fragment orbitals. Consequently, the HOMO-LUMO (HOCO-LUCO) gap is increased as the LUMO / LUCO remains largely unaffected, also accounting for trends in the experimentally determined optical band gaps. In contrast, with more electron releasing ancillary ligands (demonstrated for the case where L = PMe_3 *vs.* PH_3)[12] the HOMO is more destabilised, leading to smaller HOMO-LUMO (HOCO-LUCO) gaps. Furthermore, Friend and Lewis have found that the Mulliken charges on the metals are more positive with carbonyl (more accepting) ancillary ligands rather than phosphine (less accepting, more donating) ligands.[12] The energies of the HOMOs / HOCOs also strongly correlate with M(*d*) energies. Therefore higher energy *d*-orbitals, *i.e.* of first row metals compared with second row metals, will

destabilise the HOMO / HOCO, evincing smaller HOMO-LUMO (HOCO-LUCO) gaps (as the LUMO / LUCO again remains largely unaffected), consistent with experimental observations (Figure 1.4). By way of example, *trans*-$[(PH_3)_4Fe(\mu\text{-}C{\equiv}CC_6H_4\text{-}4\text{-}C{\equiv}C)]_n$ has a smaller computed band gap (2.82 eV) than *trans*-$[(PH_3)_4Ru(\mu\text{-}C{\equiv}CC_6H_4\text{-}4\text{-}C{\equiv}C)]_n$ (3.10 eV).

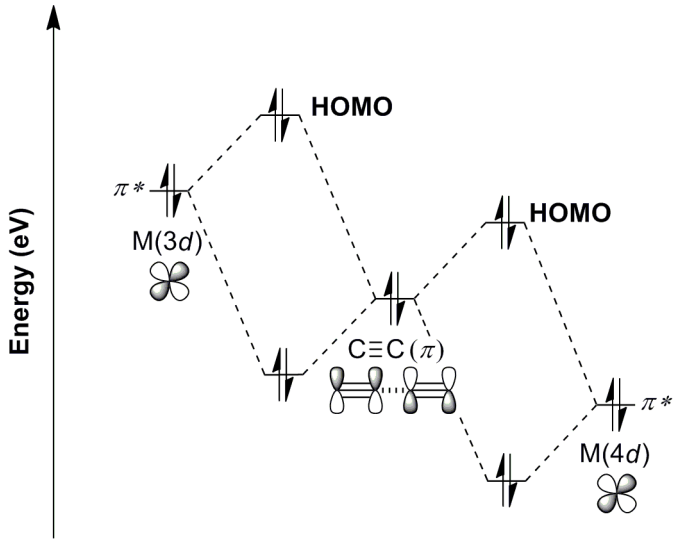

Figure 1.4: Schematic molecular orbital diagram showing the greater destabilisation of the HOMO in representative complexes, *trans*-$[M(C{\equiv}CR)_2(L)_x]$, with higher energy first row metals (M = *e.g.* Fe, left) than lower energy second row metals (M = *e.g.* Ru, right).

Turning to comparisons between group 8 and group 10 systems, the calculated energies of the LUMOs / LUCOs are lower for systems based on square planar group 10 fragments, of the type *trans*-$[(PH_3)_2M(\mu\text{-}C{\equiv}CC_6H_4\text{-}4\text{-}C{\equiv}C)]_n$ (M = Ni, Pd, Pt), by $0.2 - 0.3$ eV than octahedral group 8 systems, such as *trans*-$[(PH_3)_4M(\mu\text{-}C{\equiv}CC_6H_4\text{-}4\text{-}C{\equiv}C)]_n$ (M = Fe, Ru), as a result of stabilising M(π_y) interactions.[11] Therefore smaller HOCO-LUCO gaps might be expected for group 10 metallopolymers, although this does not account for the experimental observations of Friend and Lewis.[12] The calculated HOMO / HOCO energies of such complexes are instead found to be a result of several competing factors, depending not only on the M(*d*) energies, but also how diffuse the HOMO / HOCOs are and the degree of antibonding interaction between the metal and organic chain (forming the HOMO / HOCO), in addition with the M-C bond

length. Therefore a higher M(*d*) energy (such as for Ru *vs.* Pt) combined with a more diffuse HOMO / HOCO and shorter M-C bond length (where Ru-C < Pt-C as Ru(*d*) is better matched energetically with C≡C(π) than Pt(*d*)) will increase the energy of the HOMO / HOCO, leading to reduced HOMO-LUMO (HOCO-LUCO) gaps for the group 8 octahedral complexes,[11] accounting for experimental observations. Most unsurprisingly, variation of the metal identity in addition with the ancillary ligands will have a combined effect on the resultant band gap, and hence the π-conjugation. As a clear example, the optical band gap of the platinum metallopolymer [**4**] (3.26 eV)[110] is between that of the two ruthenium polymers: [**11**] (3.19 eV)[41] and [**14**] (3.51 eV).[12]

1.3. *Trans*-bis(alkynyl) complexes: deconstructing the metallopolymer

1.3.1. Introduction

Although monomeric and oligomeric metal acetylide complexes have been synthesised in support of metallopolymer research, both as starting materials and in order to understand the underlying electronic structures of the highly conjugated systems, these deconstructed units are intriguing and important materials in their own right. The wider range of synthetic possibilities associated with smaller molecular systems, in contrast to metallopolymers, allows the formation of a truly vast array of unique molecular architectures with novel material properties derived from the common *trans*-$[M(C{\equiv}CR)_2L_n]$ fragment. As noted for metallopolymers, the integration of metal units within an unsaturated framework in a molecular system can tune the physical, optical and electronic properties, such as extent of conjugation, through variations in the nature of the metal (identity, oxidation state, coordination number, geometry, size *etc.*) and ancillary ligands (electronics, sterics *etc.*), and therefore complexes can be elegantly tailored to fit specific applications. Examples of useful material and optoelectronic properties of monomeric and oligomeric metal acetylide complexes include: non-linear optical response;[127-129] high through-molecule conductance, of importance to molecular electronics;[130-133] luminescent properties;[134-136] liquid crystalline behaviour;[137, 138] and strong visible absorbance that leads to applications as photo-sensitisers.[139, 140]

In 1984, Bruce noted, at that time, that the chemistry of monomeric and oligomeric metal acetylide complexes chiefly encircled group 10 metal complexes, due to the stagnation of synthetic developments required for other metallic groups.[37] For example, the formation of group 8 acetylide complexes was inhibited by the sensitivity of complexes towards acids, water, alcohols or amines, resulting instead in the formation of alkyl, acyl or carbene complexes. The main routes to *trans*-bis(alkynyl) complexes at this time closely related to those used in the formation of metallopolymers, including: reactions of metal halide complexes with terminal alkynes in an ammonia or amine solution;[38, 101, 141, 142] reactions of metal halide complexes with alkynyl-tin reagents[143, 144] or reactions of metal halide complexes with alkynyl-lithium reagents.[145-147] In the 30 years since these comments, there has been a huge effort to address these synthetic shortcomings leading to remarkable development in the area, with the number of papers relating to the chemistry of monomeric and oligomeric metal acetylide complexes surpassing 20 000 by 2003.[148] Whilst the area now defies comprehensive review, there are several excellent summaries of aspects of this chemistry available.[148-150]

Although ancillary ligands supporting ruthenium acetylide complexes are known to include macrocyclic amines,[151] terpyridines[152] and carbonyls,[13, 153] the most commonly reported examples are based on ruthenium phosphine fragments.[36, 154-158] This is presumably due to the availability of *mono*- and *bi*-dentate phosphine ligands in addition to the gamut of electronic and steric properties that can be engineered with such ligands.[159] The following discussion will therefore concentrate on the synthesis and applications of *trans*-bis(alkynyl) complexes of ruthenium bearing phosphine ligands, which are most relevant to the topic and content of this Thesis.

1.3.2. Ruthenium *trans*-bis(alkynyl) complexes featuring *tetrakis*-phosphine ligands

Conceptually, the simplest *trans*-bis(alkynyl) ruthenium complexes to consider are those bearing four equivalent *mono*-dentate phosphine ligands, *i.e.* *trans*-[Ru(C≡CR)$_2$(PR$_3$)$_4$]. The first *trans*-bis(alkynyl) complex to contain the {Ru(PMe$_3$)$_4$} motif was reported by Werner in 1985 through the initial reduction of *trans*-[RuCl$_2$(PMe$_3$)$_4$] with sodium amalgam, yielding [Ru(H)(η^2-CH$_2$PMe$_2$)(PMe$_3$)$_3$] (82 %), followed by reaction with two equivalents of HC≡CC$_6$H$_5$, which gave *trans*-

$[Ru(C{\equiv}CC_6H_5)_2(PMe_3)_4]$, [**17**], (Scheme 1.9).[160] Formation of *trans*-[**17**] is thought to proceed *via* initial formation of *cis*-[**17**], before rapid isomerisation in the benzene solvent.

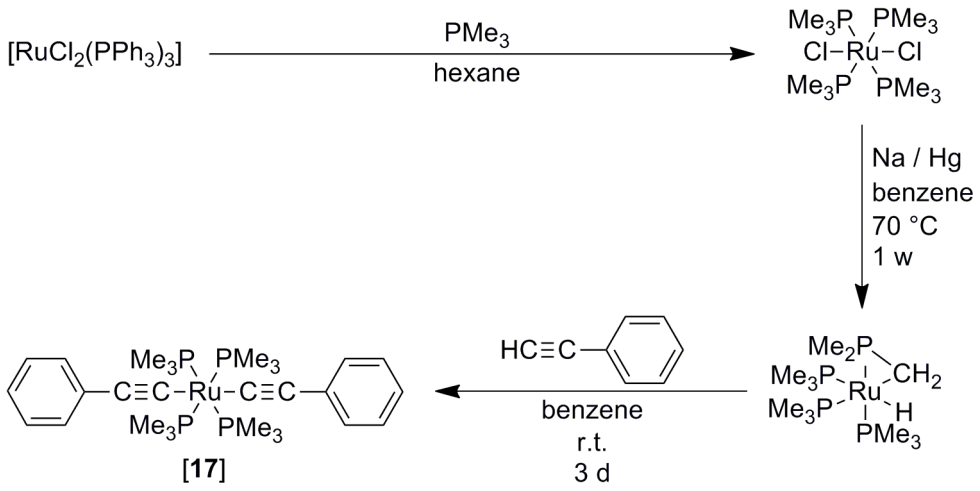

Scheme 1.9: Synthesis of the first *trans*-bis(alkynyl) *tetrakis*-trimethylphosphine ruthenium complex, [**17**], as reported by Werner.[160]

Although the reactivity of [**17**] was not discussed at this time, the intermediate complex $[Ru(H)(\eta^2\text{-}CH_2PMe_2)(PMe_3)_3]$ was reported to be air-sensitive, which, coupled with the use of Na / Hg amalgam and the long duration of the reaction to produce it, has limited the wider applications of this compound as a reagent. Several years later, in 1991, Lewis revised the synthesis of [**17**] by reaction of *trans*-$[RuCl_2(PMe_3)_4]$ with $Me_3SnC{\equiv}CC_6H_5$ (excess) in refluxing THF, although a reaction time was not given (Scheme 1.10).[111] Despite the synthetic challenges presented with the use of highly toxic trimethylstannyl reagents, the complex is obtained in a quantitative yield, albeit as air-sensitive yellow crystals. The extended complex, *trans*-$[Ru(C{\equiv}CC_6H_4\text{-}4\text{-}C_6H_4\text{-}4\text{-}C{\equiv}CSnMe_3)_2(PMe_3)_4]$, was also obtained in an analogous procedure (Scheme 1.10).[111]

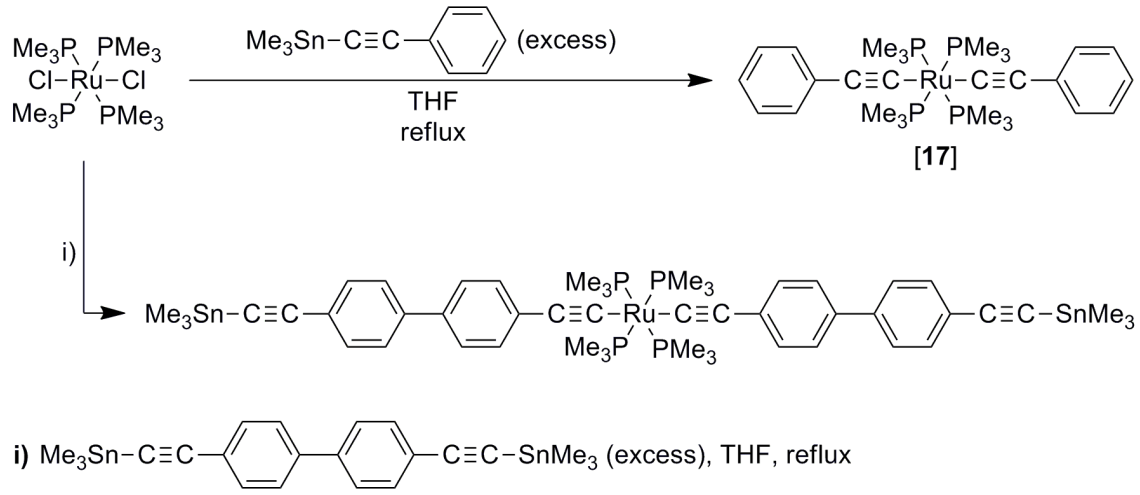

Scheme 1.10: Syntheses of *trans*-[Ru(C≡CR)$_2$(PMe$_3$)$_4$] complexes using trimethylstannyl reagents, as reported by Lewis.[111]

In 1994, Rappert and Yamamoto again amended the synthesis of [**17**] through the reaction of *cis*-[Ru(H)$_2$(PMe$_3$)$_4$] with phenylacetylene in acetone (two hours, 60 °C).[161] Similar complexes obtained by this method include *trans*-[Ru(C≡CSiMe$_3$)$_2$(PMe$_3$)$_4$] and *trans*-[Ru(C≡CCOOMe)$_2$(PMe$_3$)$_4$]. Despite the lower yields obtained (21 – 65 %), the wide availability of terminal alkynes and ease of work-up (where products are obtained cleanly after filtration from the reaction medium) is synthetically appealing. However, the preparation of the starting material, *cis*-[Ru(H)$_2$(PMe$_3$)$_4$], requires the use of sodium amalgam[162] or lithium reagents.[163]

The most facile synthesis of *trans*-[Ru(C≡CR)$_2$(PMe$_3$)$_4$] (R = C$_6$H$_5$, [**17**]; C$_6$H$_4$-4-OMe, C$_6$H$_4$-4-Me, ^{t}Bu, Me, SiMe$_3$, H) to date was devised by Field.[164] The *trans*-bis(alkynyl) compounds are obtained as moderately air-stable solids in average to good yields (38 − 75 %) *via* σ-bond metathesis reactions of *cis*-[RuMe$_2$(PMe$_3$)$_4$][164, 165] with terminal alkynes, HC≡CR, in either acetone or THF (Scheme 1.11). However, the products are invariably obtained as isomeric mixtures (*cis*- and *trans*-), with separation only possible by fractional crystallisation. A higher concentration of the *cis*-isomer is found for all cases, except when R = SiMe$_3$.

In a separate report, the sensitivity of both *cis*- and *trans*-[Ru(C≡CR)$_2$(PMe$_3$)$_4$] (R = C$_6$H$_5$, [**17**]; C$_6$H$_4$-4-OMe, C$_6$H$_4$-4-Me, ^{t}Bu, Me, SiMe$_3$, H) complexes towards

acids was explored. Reactions of the isomeric mixtures with either $HBF_4.Et_2O$ or 2,6-lutidinium tetrafluoroborate yielded stable, cationic η^3-butenynyl complexes, $[Ru\{\eta^3\text{-}HC(R)=CC\equiv CR\}(PMe_3)_4]^+$ in average to good yields (50 – 80 %), *via* the *in situ* formation of mixed alkynyl-vinylidene complexes (Scheme 1.11).[166] This work also included the first structurally characterised alkynyl-vinylidene complex containing unsubstituted alkynyl and vinylidene fragments; *trans*-$[Ru(C\equiv CH)(=C=CH_2)(PMe_3)_4]^+$. The Field group further explored the chemistry of $\{Ru(PMe_3)_4\}$ complexes with the formation of cyclometalated ruthenaindenes, $[Ru\{HC(C_6H_3\text{-}4\text{-}R')=CC\equiv CC_6H_4\text{-}4\text{-}R'\}(PMe_3)_4]$ (R′ = ^{t}Bu, Me, H; 49 – 64 % yields), through the reaction of η^3-butenynyl complexes with Me_2Mg in THF (Scheme 1.11).[167]

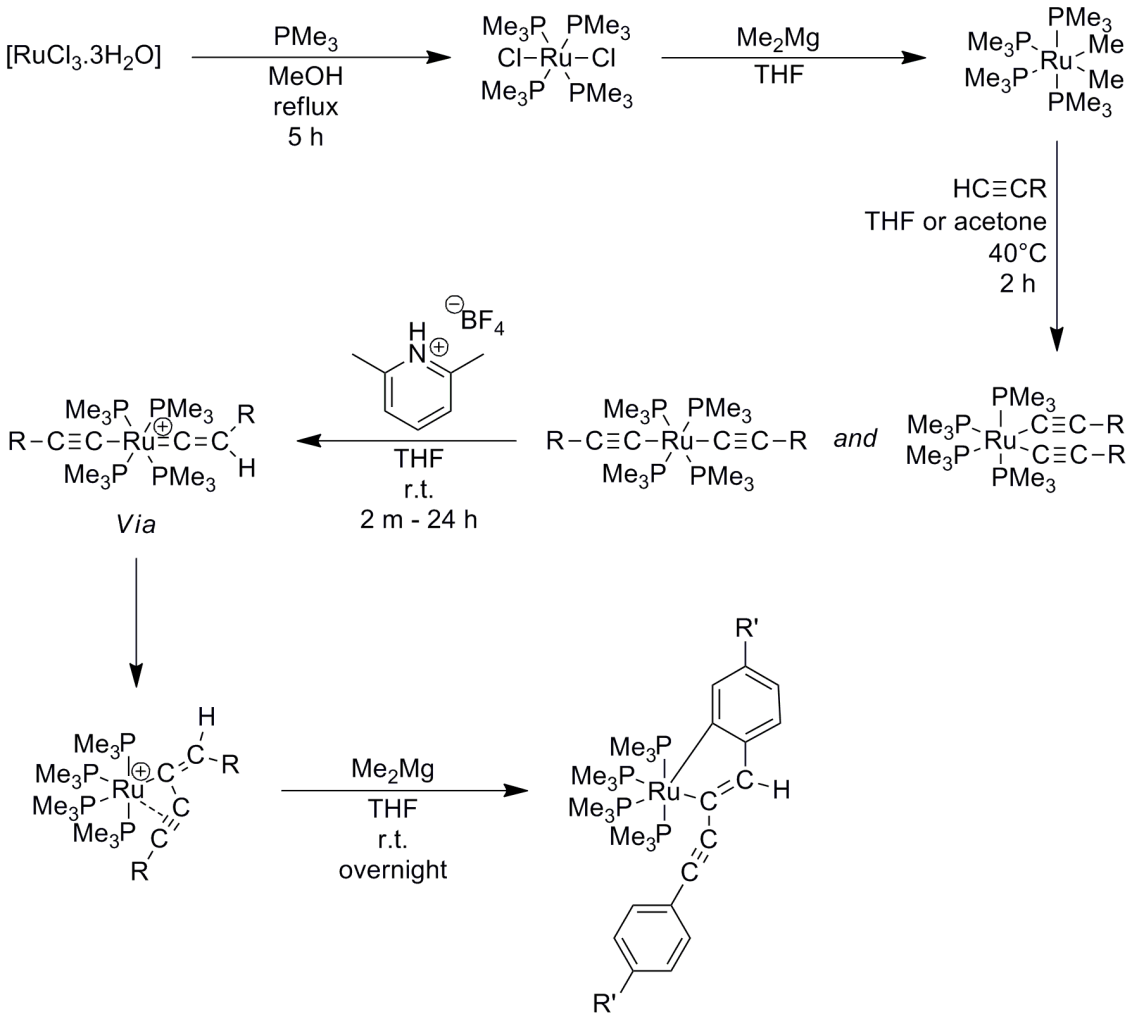

Scheme 1.11: General synthesis of *trans*-$[Ru(C\equiv CR)_2(PMe_3)_4]$ and related complexes from *cis*-$[RuMe_2(PMe_3)_4]$ where R = C_6H_5, C_6H_4-4-OMe, C_6H_4-4-Me, ^{t}Bu, Me, $SiMe_3$, H and R′ = ^{t}Bu, Me, H, as reported by the Field group.[164, 166, 167]

Although several *trans*-bis(alkynyl) *tetrakis*-trimethylphosphine ruthenium complexes have been prepared, research within this area is limited by the generally low to moderate stability of these species in air, their acid sensitivity (forming η^3-butenynyl complexes) and difficulty in obtaining isomerically pure material from the most facile preparative sequences. To date, no *mono*- or *trans*-bis(alkynyl) complexes containing the related $\{Ru(PEt_3)_4\}$ motif, a simple alkyl extension to the phosphine ligands, are known.

Ruthenium *trans*-bis(alkynyl) *tetrakis*-trimethyl and *tetrakis*-triethylphosphite complexes, *trans*-$[Ru(C{\equiv}CR)_2\{P(OMe)_3\}_4]$ and *trans*-$[Ru(C{\equiv}CR)_2\{P(OEt)_3\}_4]$, [**18**], are known, although this area remains largely unexplored. Of the few reports available,[33, 168, 169] such compounds are air stable[33] and are prepared from the easily accessible, stable starting materials *trans*-$[RuCl_2\{P(OMe)_3\}_4]$[33] and *trans*-$[RuCl_2\{P(OEt)_3\}_4]$, [**19**].[170] The only synthesis of *trans*-$[Ru(C{\equiv}CR)_2\{P(OX)_3\}_4]$ complexes (X = Me: R = C_6H_5, ^{t}Bu, C_6H_4-4-Me; X = Et: R = C_6H_5 [**18c**],[ii] ^{t}Bu, C_6H_4-4-Me) of which we are aware, involves the reaction of *trans*-$[RuCl_2\{P(OX)_3\}_4]$ with excess lithium acetylide, LiC≡CR, in solutions of THF.[33] The reaction is thought to proceed step-wise *via* the *mono*-alkynyl complex, *trans*-$[RuCl(C{\equiv}CR)\{P(OX)_3\}_4]$. Although the reaction time is rapid (15 minutes) and workup is synthetically simple (trituration from either methanol or ethanol), the reaction is low yielding (~ 35 %) and requires the use of sensitive alkynyl-lithium reagents. Further reactions of the *trans*-bis(alkynyl) complexes with electrophillic reagents ($HBF_4.Et_2O$, CF_3SO_3Me, I_2, $C_6H_5N_2^+$ and $ClSC_6H_3$-2,4-$(NO_2)_2$), in solutions of either diethyl ether or CH_2Cl_2, yielded alkynyl-vinylidene complexes, *trans*-$[Ru(C{\equiv}CR)(=C=CRR')\{P(OX)_3\}_4]^+$ (R′ = H, Me, I, N=NC_6H_5, SC_6H_3-2,4-$(NO_2)_2$) within ~ 1 − 2 hours in moderate to good yields (55 – 80 %; Scheme 1.12).

[ii] The numbering scheme for specific complexes of the type $[Ru(C{\equiv}CR)_2\{P(OEt)_3\}_4]$, [**18**], is expanded in Chapter 5

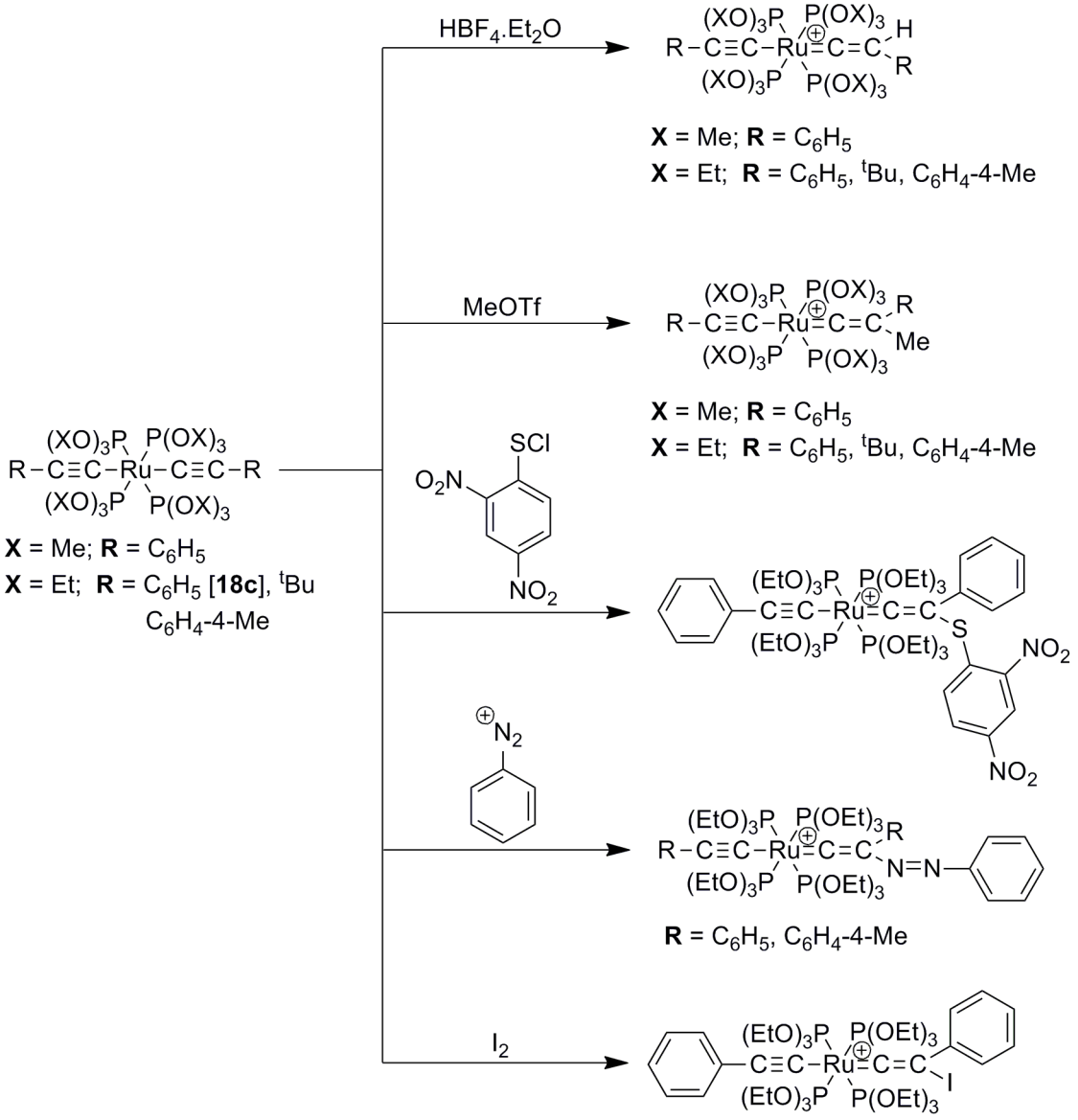

Scheme 1.12: Synthetic routes to alkynyl-vinylidene complexes bearing the *tetrakis*-trialkylphosphite motif.[33]

Substituted mixed alkynyl-vinylidene complexes, *trans*-$[Ru(C{\equiv}CR)\{=C=C(\mathbf{R'})R\}\{P(OX)_3\}_4]^+$ (Scheme 1.12) are stable to further ligand substitution reactions. In contrast, although isolable, the unsubstituted mixed alkynyl-vinylidene complex *trans*-$[Ru(C{\equiv}CC_6H_5)\{=C=C(\mathbf{H})C_6H_5\}\{P(OEt)_3\}_4]^+$ rearranges in a CH_2Cl_2 solution to give the η^3-butenynyl complex $[Ru\{\eta^3\text{-}HC(C_6H_5)=CC{\equiv}CC_6H_5\}\{P(OEt)_3\}_4]^+$ after two hours (85 %; Scheme 1.13). Upon incorporation of excess of $HC{\equiv}C^tBu$ into the initial CH_2Cl_2 solution, the mixed η^3-butenynyl complex $[Ru\{\eta^3\text{-}HC(^tBu)=CC{\equiv}CC_6H_5\}(P(OEt)_3)_4]^+$ was instead formed in a

high yield (> 80 %) after 90 minutes (Scheme 1.13). The reaction is proposed to proceed from *trans*-[Ru(C≡CC_6H_5){=C=C(**H**)C_6H_5}{P(OEt)$_3$}$_4$]$^+$ *via* a η^2-HC≡CC_6H_5 complex, *trans*-[Ru(C≡CC_6H_5)(η^2-HC≡CC_6H_5){P(OEt)$_3$}$_4$]$^+$, to the five-coordinate complex, [Ru(C≡CC_6H_5){P(OEt)$_3$}$_4$]$^+$, which may then react with excess introduced terminal alkyne, HC≡C^{t}Bu (Scheme 1.13).

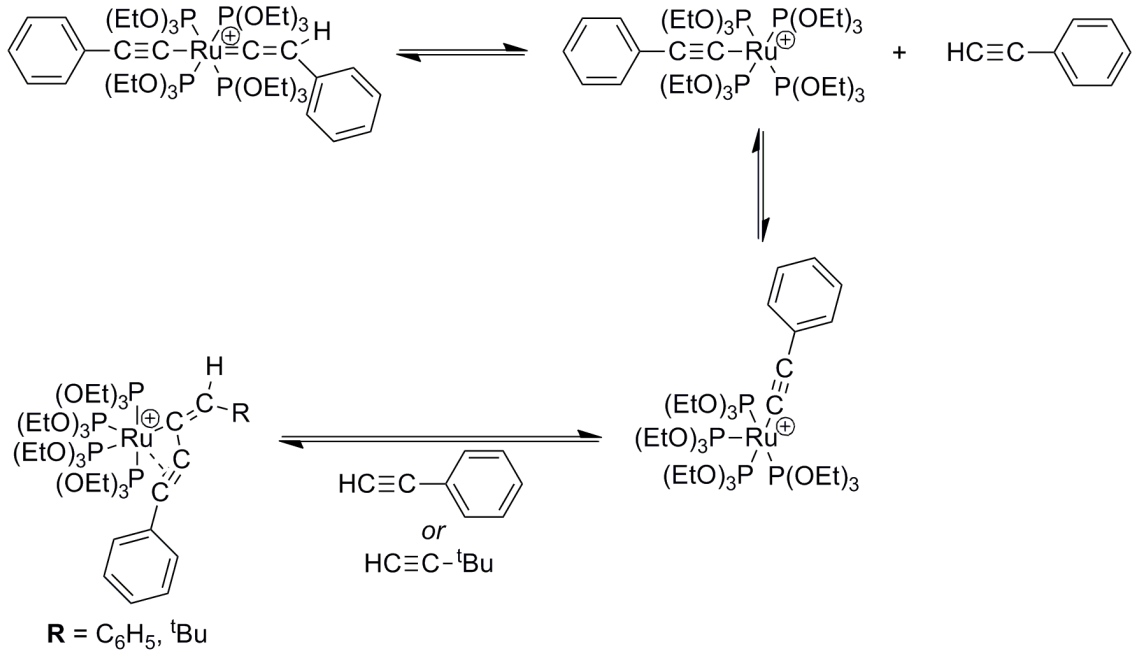

Scheme 1.13: Proposed formation of 'asymmetric' η^3-butenynyl complexes from unsubstituted alkynyl-vinylidene phosphite complexes.[33]

Alternatively, η^3-butenynyl complexes bearing the {Ru{P(OEt)$_3$}$_4$} motif have been prepared from initial reactions of [RuH_2P(OEt)$_3$}$_4$] with HBF_4.Et_2O (1 equiv.) at − 30 °C in diethyl ether, yielding *cis*-[RuH(η^2-H_2){P(OEt)$_3$}$_4$]BF_4 as a white precipitate, followed by the room temperature reaction with HC≡CR (6 equiv.) in mixed diethyl ether / CH_2Cl_2 solutions, forming [Ru{η^3-HC(R)=CC≡CR}{P(OEt)$_3$}$_4$]$^+$ (R = C_6H_4-4-Me; ^{t}Bu) as white powders in moderate yields (> 55 %).[168] Presumably alkynyl-vinylidene intermediates were also involved in this reaction sequence.

The synthesis of *mono*-alkynyl *tetrakis*-trialkylphosphite complexes of the type *trans*-[RuCl(C≡CR){P(OX)$_3$}$_4$] has been achieved through reactions of *trans*-[RuCl_2P(OX)$_3$}$_4$] with HC≡CR (10 equiv.) in THF solutions in the presence of

NEt_3 (10 equiv; Scheme 1.14).[169] Despite the modest yield (30 – 40 %) and excess reagents required, the route circumvents the use of alkynyl-lithium reagents. The reaction is thought to proceed *via* a η^2-alkyne complex subsequently followed by a 1,2-hydrogen shift to give the vinylidene *trans*-$[RuCl(=C=CHR)\{P(OEt)_3\}_4]^+$, which, upon deprotonation by the amine, then gives the acetylide product.

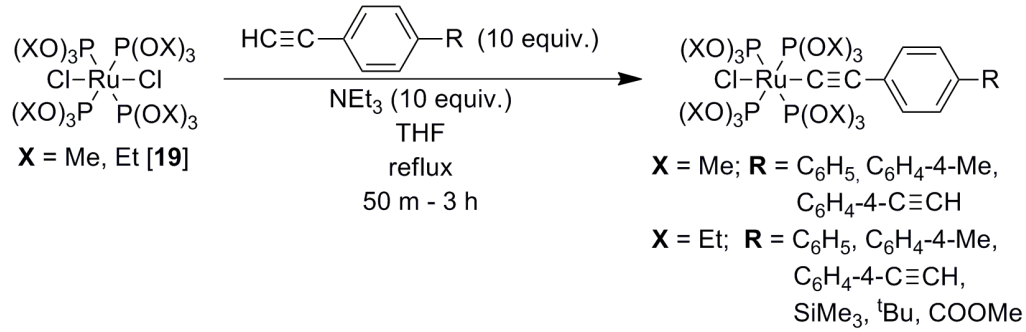

Scheme 1.14: Formation of *mono*-alkynyl *tetrakis*-trialkylphosphite complexes, *trans*-$[RuCl(C{\equiv}CR)\{P(OX)_3\}_4]$.

Synthetic routes to bimetallic alkynyl-bridged complexes bearing *tetrakis*-trialkylphosphite ligands have also been considered.[169] Although, the reactions of *trans*-$[RuCl(C{\equiv}CC_6H_4\text{-}4\text{-}C{\equiv}CH)\{P(OMe)_3\}_4]$ and *trans*-$[RuCl(C{\equiv}CC_6H_4\text{-}4\text{-}C{\equiv}CH)\{P(OEt)_3\}_4]$ with *trans*-$[RuCl_2\{P(OMe)_3\}_4]$ and [**19**], respectively, in mixed THF / NEt_3 solutions were unsuccessful, yielding intractable mixtures of products, the reaction of [**19**] with $HC{\equiv}CC_6H_4\text{-}4\text{-}C{\equiv}CH$ (0.5 equiv.) in a THF / NEt_3 solution in the presence of a halide abstracting agent, $NaPF_6$ (3 equiv.), unexpectedly yielded a *pentakis*-triethylphosphite complex, *trans*-$[\{Ru\{P(OEt)_3\}_5\}_2(\mu\text{-}C{\equiv}CC_6H_4\text{-}4\text{-}C{\equiv}C)][PF_6]_2$ (30 %; Scheme 1.15). The complex was characterised by the observation of two AB_4 multiplets in the $^{31}P\{^1H\}$ NMR spectrum and is inert to further substitution reactions with alkynes.

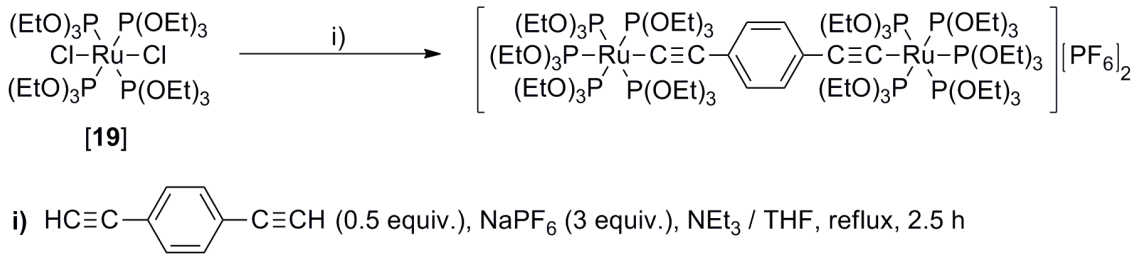

Scheme 1.15: Formation of a binuclear *pentakis*-triethylphosphite complex, as reported by Albertin.[169]

1.3.3. Ruthenium *trans*-bis(alkynyl) complexes featuring *bis*-chelating phosphine ligands

As noted earlier, *trans*-bis(alkynyl) complexes bearing chelating *bis*-phosphine ligands are prominent throughout the literature. The combination of the *trans*-geometry and electron donating ancillary ligands is expected to facilitate delocalisation along the RC≡C-M-C≡CR backbone.[171-173]

1.3.3.1. [$RuCl_2(dppm)_2$]

In 1984, Chaudret and Commenges reported that *cis*-[$RuCl_2(dppm)_2$], *cis*-[**20**], is selectively obtained (~ 100 % yield) as the thermodynamic product from the reaction between [$RuCl_2(DMSO)_4$], [**21**], and 1,2-*bis*-diphenylphosphinomethane (dppm; 2 equiv.) in toluene (80 °C, 15 hours).[174] Alternatively, *trans*-[**20**] is obtained (75 %) from the addition of [$RuCl_3.3H_2O$], dissolved in water, to an EtOH solution of dppm (2.5 equiv.) followed by heating for two hours under reflux.[175] In chlorinated solvents, isomerisation of *trans*-[**20**] to *cis*-[**20**] occurs by thermolysis over ten hours, whereas the reverse process (*cis*-[**20**] to *trans*-[**20**]) occurs photochemically, albeit over several days.[176] As a result of the *trans*-effect, previously observed by Chatt and Hayter in 1961,[175] the *cis*-positioned chlorides of *cis*-[**20**] opposite strongly donating phosphine ligands, are more labile, hence are more easily substituted, than those of *trans*-[**20**]. For this reason, *cis*-[**20**] is the commonly preferred starting material in chloride substitution reactions.

1.3.3.2. Mono and trans-bis(alkynyl) complexes featuring the {Ru(dppm)$_2$} fragment

Dixneuf and co-workers have described the highest cited and arguably most efficient route to *mono*-vinylidene, *mono*- and *trans*-bis(alkynyl) ruthenium complexes bearing the {Ru(dppm)$_2$} motif from *cis*-[**20**] (Scheme 1.16) during their exploration of novel unsaturated organometallic complexes for catalytic applications.[35, 154] The route, based on earlier work with half-sandwich complexes,[177, 178] relies on the step-wise abstraction of chloride ligands from *cis*-[**20**] by $NaPF_6$ in CH_2Cl_2 solutions to generate a reactive, five-coordinate, 16e$^-$ Ru^{II} species *in situ*. This species reacts with alkynes in the usual fashion *via* an initial π-complex which then rearranges to give vinylidene complexes of the type, *trans*-[RuCl(=C=CHR)(dppm)$_2$]$^+$.[179]

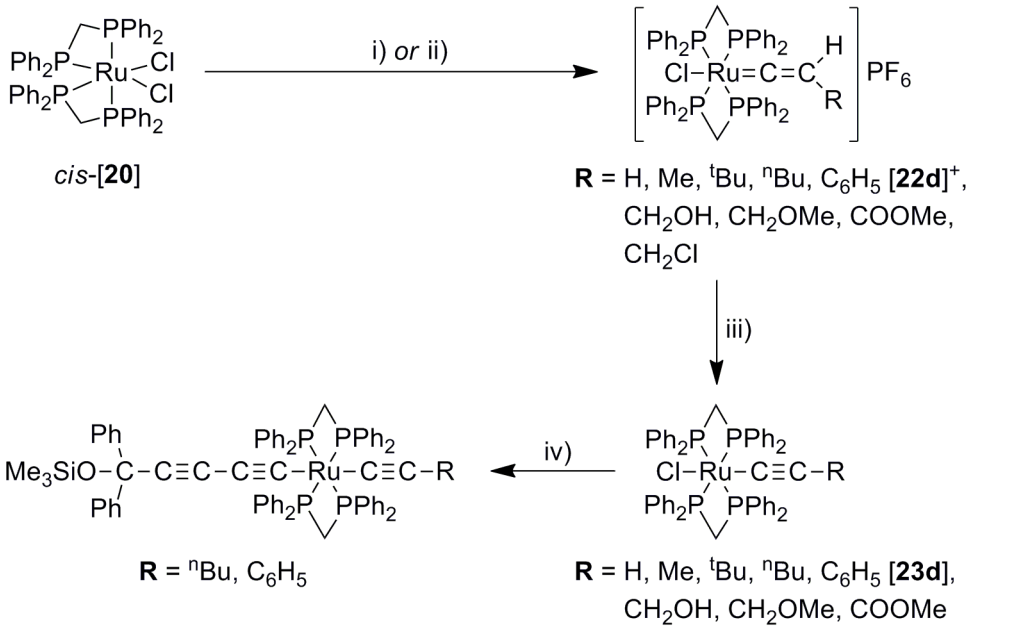

Scheme 1.16: Formation of *mono*- and *trans*-bis(alkynyl) {Ru(dppm)$_2$} complexes, as reported by Dixneuf and co-workers.[35, 154]

The strongly electron withdrawing character of the vinylidene ligand prevents further abstraction of the *trans*-chloride allowing isolation of *mono*-vinylidene complexes,

trans-[RuCl(=C=CHR)(dppm)$_2$]PF$_6$ (R = H, Me, ^{t}Bu, ^{n}Bu, C_6H_5 [**22d**]$^+$, [iii] CH_2OH, CH_2OMe, COOMe, CH_2Cl), in high yields (72 – 97 %). Addition of base yields the *mono*-alkynyl complexes, *trans*-[RuCl(C≡CR)(dppm)$_2$] (R = H, Me, ^{t}Bu, ^{n}Bu, C_6H_5 [**23d**],[iv] CH_2OH, CH_2OMe, COOMe), in 47 – 65 % isolated yields. The preparation of these *mono*-alkynyl {Ru(dppm)$_2$} complexes is solvent dependant.[154] For example, the formation of [**23d**] was less selective in CH_2Cl_2, with trace amounts of the 'symmetric' *trans*-bis(alkynyl) complex, *trans*-[Ru(C≡CC_6H_5)$_2$(dppm)$_2$], [**24d**], [v] being formed evincing a degree of Ru-Cl bond polarisation in CH_2Cl_2 (leading to chloride labilisation and abstraction), than in THF. Similarly, the use of alkynyl ligands with more electron-donating (R) substituents in *trans*-[RuCl(C≡CR)(dppm)$_2$] complexes allows more facile abstraction of the *trans*-chloride (stronger σ-donation and hence *trans*-influence), demonstrated in this case by the formation of 'asymmetric' *trans*-bis(alkynyl) complexes, *trans*-[Ru(C≡CR)(C≡CC≡C(C_6H_5)$_2$OSiMe_3)(dppm)$_2$] (R = ^{n}Bu, C_6H_5), albeit in low yields (25 – 28 %). As further evidence of this, Humphrey found that the 'asymmetric' *trans*-bis(alkynyl) complex, *trans*-[Ru(C≡CC_6H_5)(C≡CC_6H_4-4-NO_2)(dppm)$_2$] was only obtained (under similar conditions to those described by Dixneuf) from reactions of [**23d**] with HC≡CC_6H_4-NO_2 (albeit in a low yield (30 %)) and not from the reverse reaction, between *trans*-[RuCl(C≡CC_6H_4-4-NO_2)(dppm)$_2$], [**23a**],[iv] and HC≡CC_6H_5 (Scheme 1.17).[180]

[iii] The numbering scheme for specific complexes of the type [RuCl(=C=CHC_6H_4-4-R)(dppm)$_2$]$^+$, [**22**]$^+$, is expanded in Chapter 2.
[iv] The numbering scheme for specific complexes of the type [RuCl(C≡CC_6H_4-4-R)(dppm)$_2$], [**23**], is expanded in Chapter 2.
[v] The numbering scheme for specific complexes of the type [Ru(C≡CC_6H_4-4-R)$_2$(dppm)$_2$], [**24**], is expanded in Chapter 2

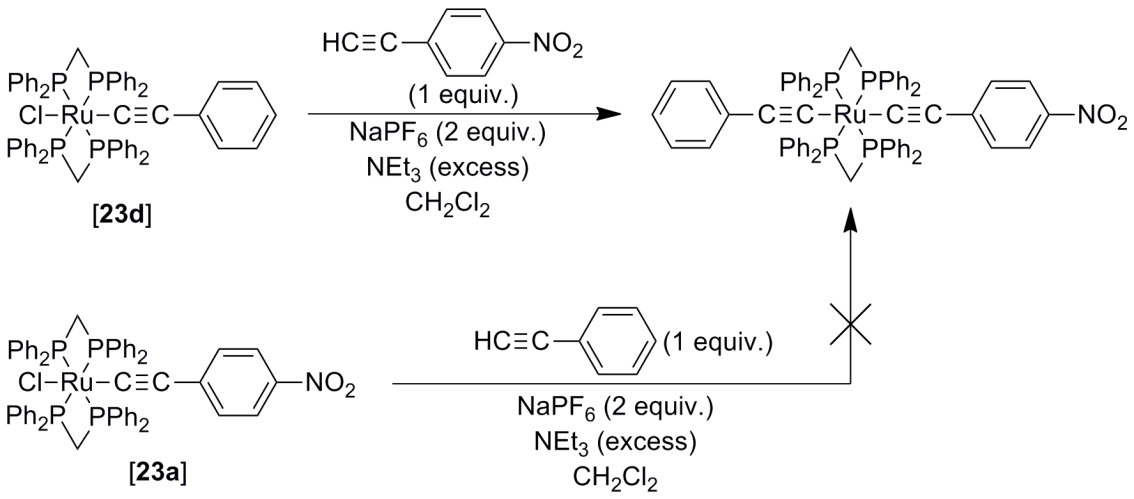

Scheme 1.17: The synthesis of *trans*-[Ru(C≡CC_6H_5)(C≡CC_6H_4-4-NO_2)(dppm)$_2$] depends on the electronics of the *mono*-alkynyl complex governing *trans*-chloride labilisation.[180]

In both reaction schemes shown in Scheme 1.17, small quantities of the 'symmetric' *trans*-bis(alkynyl) complex, *trans*-[Ru(C≡CC_6H_4-4-NO_2)$_2$(dppm)$_2$], [**24a**], were obtained, evincing ligand scrambling effects (Scheme 1.18). Formation of the second 'symmetric' *trans*-bis(alkynyl) product, [**24d**], was however not reported, which might infer complex instability.

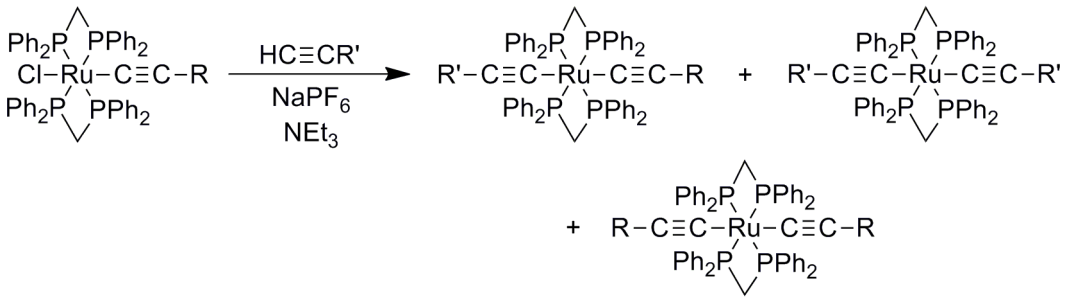

Scheme 1.18: Anticipated product distribution as a result of ligand scrambling effects.

'Symmetric' *trans*-bis(alkynyl) complexes of the type *trans*-[Ru(C≡CC_6H_4-4-R)$_2$(dppm)$_2$] have been prepared in low to good yields (16 – 62 %) from reactions of *cis*-[**20**] with HC≡CC_6H_4-4-R (2 equiv.) in the presence of $NaPF_6$ (2 equiv.) and

NEt_3 (5 equiv.) in either refluxing ([**24a**]: R = NO_2; 16 hours) or stirred (R = C_6H_4-4-NO_2; $CH{=}CHC_6H_4$-4-NO_2; four hours) CH_2Cl_2 solutions.[180]

Bimetallic complexes of the type *trans*-[{Cl(dppm)$_2$M}$_2$(μ-C≡CRC≡C)] (M = Ru, Os; R = C_6H_4-4-, C_6H_4-3-, C_6H_2-2,5-Me_2-4-, -3-C_5H_3N-6-, -2-C_4H_2S-5-) have similarly been prepared, in moderate yields (25 – 50 %), *via* the step-wise reactions of *cis*-[MCl_2(dppm)$_2$] with HC≡CRC≡CH (0.5 equiv.) and $NaPF_6$ (2 equiv.) in CH_2Cl_2 (stir eight hours), followed by the addition of DBU (1 equiv.; stir two hours).[181] In the 'mixed-valence' state, Long found that ν([C≡C]$^+$) values (1961 – 1984 cm^{-1}) were comparable with ν(C=C) of related allenylidene complexes, *trans*-[Cl(dppm)$_2$M(=C=C=CHC_6H_5)]$^+$ (M = Ru, Os; 1900 – 1940 cm^{-1}), evincing an extended, delocalised cumulenic structure (Scheme 1.19).[181]

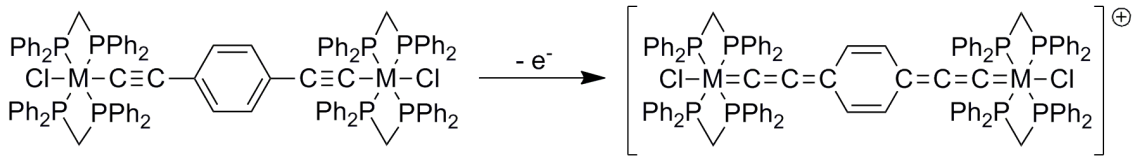

Scheme 1.19: Single oxidation of the polynynyl complex, *trans*-[{Cl(dppm)$_2$M}$_2$(μ-C≡CC_6H_4-4-C≡C)] (left) is thought to yield the cumulenic complex, *trans*-[{Cl(dppm)$_2$M}$_2${μ-(=C=CC_6H_4-4-=C=C=)}]$^+$ (right).[181]

Despite this, spectroelectrochemical studies revealed that these 'mixed-valence' bimetallic complexes exhibited Class II behaviour, according to the Robin and Day classification scheme.[182] As determined by delocalisation parameter values (α^2),[vi] for the *mono*-oxidised ruthenium series, the thiophene bridge (R = -2-C_4H_2S-5) was found to facilitate the strongest interaction between metal centres (8.9×10^3), followed by the xylene bridge (R = C_6H_2-2,5-Me_2-4-; 6.5×10^3), then pyridine (R = -3-C_5H_3N-6-; 4.9×10^3) and finally benzene (R = C_6H_4-4-; 4.4×10^3).

The Lewis group have also reported the formation of mixed-metal bimetallic complexes, *trans-trans*-[{Cl(dppm)$_2$Ru}(μ-C≡CC_6H_4-4-C≡C){ML_n}] (ML_n =

[vi] $\alpha^2 = \frac{(4.2 \times 10^{-4}) \varepsilon \Delta \nu_{1/2}}{\nu_{max} r^2}$
Where: ε is the molar absorptivity (M^{-1}cm^{-1}); $\Delta\nu_{1/2}$ is the full width at half height (nm); ν_{max} is the maximum absorption wavelength (nm) and r is the atomic distance between metals (Å).

$OsCl(dppm)_2$, [**25**]; $Pt(PEt_3)_2Ph$, [**26**]), as a means to optimise electronic communication between metal centres *via* a π-conjugated pathway using metal-based donor and acceptor termini.[183] Complexes were prepared *via* the initial reaction of *cis*-[**20**] with $NaPF_6$ (2 equiv.) and *trans*-[{L_nM}($C{\equiv}CC_6H_4$-4-$C{\equiv}CH$)] (1 equiv.) in CH_2Cl_2 (four hours, r.t.) followed by a subsequent reaction with DBU (three hours, r.t.). Although high yielding (85 %), in the formation of [**26**], minor quantities of the trimetallic complex *trans-trans*-[{$(dppm)_2Ru$}{μ-($C{\equiv}CC_6H_4$-4-$C{\equiv}C$)$Pt(PEt_3)_2Ph$}$_2$] were also obtained. The electrochemistry of [**25**] revealed two, reversible one-electron oxidation events at − 0.48 and − 0.12 V (referenced to internal ferrocene at 0.50 V *vs.* Ag / AgCl), attributed to the sequential generations of the redox couples [Os^{II}] / [Os^{III}] and [Ru^{II}] / [Ru^{III}]. As the *mono*-alkynyl complex *trans*-[$OsCl(C{\equiv}CC_6H_4$-4-$C{\equiv}CH)(dppm)_2$] has a higher (less negative) first oxidation potential than that in [**25**] (− 0.16 V *vs.* − 0.48 V), the {$Cl(dppm)_2Ru(\mu$-$C{\equiv}CC_6H_4$-4-$C{\equiv}C)$} fragment in [**25**] is shown to exhibit electron releasing character. Curiously, the first oxidation of *trans*-[$RuCl(C{\equiv}CC_6H_4$-4-$C{\equiv}CH)(dppm)_2$], [**27a**],[vii] is also higher than the corresponding redox event in [**25**] (0.00 V *vs.* − 0.12 V). Formation of the cumulenic structure in the *mono*-oxidised bimetallic complex, [**25**]$^+$, was proposed to account for the unexpected electrochemical behaviour, although now is more likely described in terms of the significant ligand character in these redox events.[149] More recent investigations have shown that 1,4-diethynylbenzene bridged bimetallic complexes and associated radical cations derived by one-electron oxidation exist in solution as a dynamic distribution of molecular conformers, with electronic character ranging from strongly localised to delocalised depending on the details of the molecular geometry.[184, 185]

In contrast to the Dixneuf reactions in CH_2Cl_2, Lynam found that the reaction of *cis*-[**20**] with $NaPF_6$ (2.1 equiv.) and $HC{\equiv}CC_6H_5$ (2.1 equiv.) in MeOH did not give the anticipated vinylidene complex, [**22d**]$^+$.[186] Instead, over a period of 48 hours, complex mixtures of products were produced, from which the η^3-butenynyl complex *E*-[$Ru(\eta^3$-{$HC(C_6H_5){=}CC{\equiv}CC_6H_5$}$)(dppm)_2]^+$, [**28d**]$^+$,[viii] was isolated. By increasing the alkyne equivalent to a 10 − 50 fold excess, a series of η^3-butenynyl complexes *E*-[$Ru(\eta^3$-$HCR{=}CC{\equiv}CR)(dppm)_2]PF_6$ (R = C_6H_5, [**28d**]PF_6; ^{t}Bu, [**29**]PF_6; ^{n}Pr, [**30**]PF_6;

[vii] The numbering scheme for specific complexes of the type *trans*-[$RuCl(C{\equiv}CC_6H_2$-2,5-R_2-4-$C{\equiv}CH)(dppm)_2$], [**27**], is expanded in Chapter 3.
[viii] The numbering scheme for specific complexes of the type: *E*-[$Ru(HC(C_6H_4$-4-$R){=}CC{\equiv}CC_6H_4$-4-$R)(dppm)_2]^+$, [**28**]$^+$, is expanded in Chapter 2.

Figure 1.5) were obtained in high yields (60 − 76 %). The *E : Z* selectivity ratio was highest when R = C_6H_5 ([**28d**]$^+$) as a consequence of increased steric interactions between the aryl alkynyl fragment and bulky dppm ancillary ligands. Bond angles and lengths, from single crystal diffraction data, are consistent with the general structure for η^3-butenynyl complexes for [**28d, 29**]$^+$ (Figure 1.5). However, for [**30**]$^+$, the Ru-C_a and C_b-C_c bond lengths (see Figure 1.5 for atom labelling scheme) are comparatively shorter (by ~ 0.142 and 0.027 Å, respectively) whereas C_a-C_b and Ru-C_c bond lengths are longer (by ~ 0.049 and 0.025 Å, respectively). To account for such structural differences, when R = ^{n}Pr ([**30**]$^+$), a higher contribution of the resonance form where the organic fragment is bound as a triene (Figure 1.5), is thought to be present in the structure.

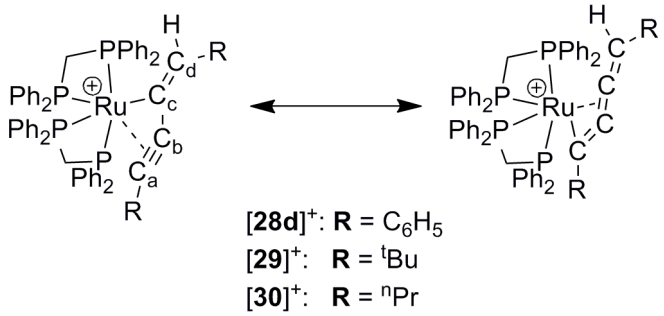

Figure 1.5: The general structure of η^3-butenynyl complexes of the type *E*-[Ru(η^3-HCR=CC≡CR)(dppm)$_2$]$^+$ (left), [**28d, 29, 30**]$^+$, and proposed 'triene' resonance form (right).

Despite some early success (Scheme 1.16), in 1997, Dixnuef stated that it was *"not found possible or easily feasible to directly introduce two alkynyl groups on the Ru(dppm)$_2$ moiety from the complex RuCl$_2$(dppm)$_2$" via* iterative chloride ligand abstractions using $NaPF_6$.[36] Consequently, alternative routes to *trans*-[Ru(C≡CR)(C≡CR/R′)(dppm)$_2$] complexes were sought. Lewis found 'symmetric' *trans*-bis(alkynyl) complexes bearing the {Ru(dppm)$_2$} motif could be obtained using trimethylstannyl reagents, successfully preparing [**24d**] from the reaction of *trans*-[**20**] with $Me_3SnC{\equiv}CC_6H_5$ (2.5 equiv.) in the presence of catalytic CuI in a CH_2Cl_2 solution (reflux, 48 hours; Scheme 1.20).[40]

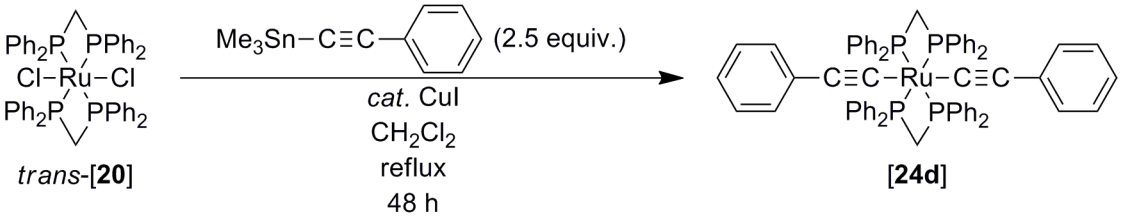

Scheme 1.20: Synthesis of [**24d**] using alkylstannyl reagents, as reported by Lewis.[40]

However, this route fails in the formation of *mono*-alkynyl complexes, for which *cis*-[**20**] / $NaPF_6$ works efficiently. Rather, reactions of *trans*-[**20**] with one equivalent of $Me_3SnC{\equiv}CC_6H_5$, in the presence of catalytic CuI, yielded a mixture of the dichloride starting material ([**20**]) and [**24d**].[40] Notably, in the absence of CuI, no reaction occurs. 'Asymmetric' *trans*-bis(alkynyl) complexes, *trans*-[M(C≡CC_6H_4-4-R)(C≡CC_6H_4-4-R′)$(dppm)_2$] (M = Ru, Os; R = H, Me; R′ = NO_2, H) have been obtained from reactions of *mono*-alkynyl complexes *trans*-[MCl(C≡CC_6H_4-4-R)$(dppm)_2$] with tin acetylides (1 equiv.) and a CuI catalyst (8 − 13 %) over 3 – 20 hours (Scheme 1.21).[187]

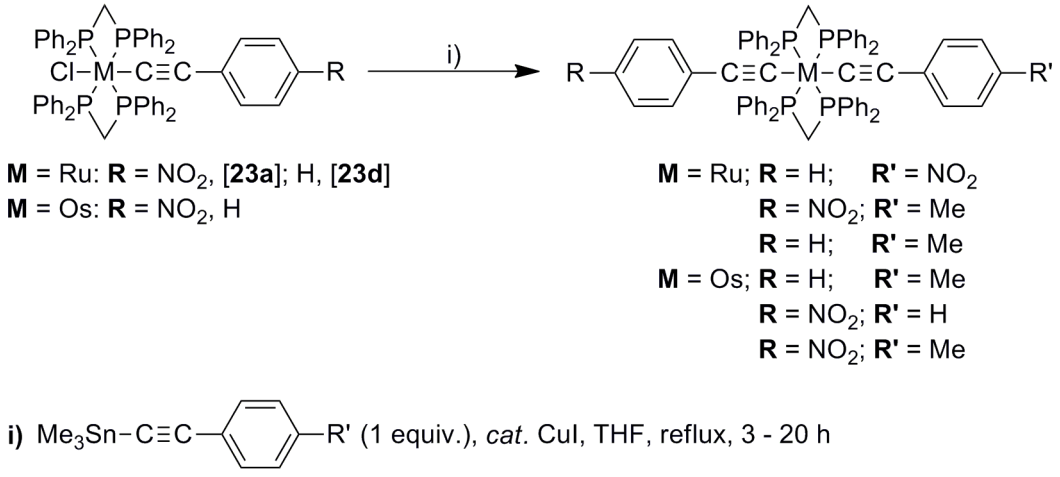

Scheme 1.21: Synthesis of 'asymmetric' *trans*-bis(alkynyl) {Ru$(dppm)_2$} complexes using alkynyl tin reagents.[187]

Reactions shown in Scheme 1.21 are marginally higher yielding (27 − 49 %) than *via* the Dixneuf route shown in Scheme 1.16,[180] though ligand scrambling effects for the ruthenium series are still apparent. For example, the reaction of [**23a**] with two equivalents of $Me_3SnC{\equiv}CC_6H_5$ in the presence of catalytic CuI (8 %) in solutions of

THF (reflux, 2 hours), gave both *trans*-[Ru(C≡CC_6H_5)(C≡CC_6H_4-4-NO_2)(dppm)$_2$] and the 'symmetric' *trans*-bis(alkynyl) complex [**24a**], in yields of 49 % and 17 % respectively, following chromatographic separation of the reaction mixture on alumina. If the same reaction was repeated with one equivalent of Me_3SnC≡CC_6H_4-4-Me, the distribution of ligand scrambling products is less weighted towards [**24a**] (8 %), compared with the 'asymmetric' complex *trans*-[Ru(C≡CC_6H_4-4-NO_2)(C≡CC_6H_4-4-Me)(dppm)$_2$] (45 %), although it is uncertain as to whether this is a result of reaction stoichiometry or the electronic properties of the incoming alkyne. Curiously, the second 'symmetric' complex, *trans*-[Ru(C≡CC_6H_4-4-R)$_2$(dppm)$_2$] (where R = H, [**24d**]; Me, [**24e**]), is not observed in either of these reactions. Alternatively, the reaction of [**23d**] with Me_3SnC≡CC_6H_4-4-Me (2 equiv.) in the presence of catalytic CuI (13 %) in a solution of THF (reflux, 2 hours) is reported to yield *trans*-[Ru(C≡CC_6H_5)(C≡CC_6H_4-4-Me)(dppm)$_2$] as the only *trans*-bis(alkynyl) product. However, as the reaction yield (46 %), is similar to those described above in analogous reaction schemes (45 %, 49 %), ligand scrambling effects are still likely to be in effect even if the full distribution of products were not isolated.

A key step in the activation of [**20**] within reaction sequences leading to *mono*- and *bis*-substituted products is the abstraction of the chloride ligands in a controlled fashion. To this end, silver(I) salts have been proposed. Winter and Scheiring found that the most efficient route to di-substituted {Ru(dppm)$_2$} complexes containing nitrile-bound ligands, of the type [Ru(N≡CR)$_2$(dppm)$_2$]$^{2+}$, is *via* reactions of *cis*-[**20**] with $AgBF_4$ in the presence of excess free ligand, N≡CR.[188] The *bis*-acetonitrile complex *cis*-[Ru(N≡CMe)$_2$(dppm)$_2$][BF_4]$_2$ was obtained selectively through this method, with product geometry governed by the steric influence of the phosphine ligands. However, attempts to form *mono*-acetonitrile complexes in this way failed, consistently producing inseparable mixtures of *mono*- and *di*-substituted products. Instead, complexes *cis*-[RuCl(N≡CR)(dppm)$_2$]BF_4 (R = Me, Et, ^{t}Bu, C_6H_5) have been obtained from reactions of *cis*-[**20**] with N≡CR in the presence of four equivalents of either $NaPF_6$ (R = Me, Et) or $NaSbF_6$ (R = C_6H_5) in 62 – 93 % yields. Alternatively, ligand substitution reactions of *cis*-[RuCl(N≡CMe)(dppm)$_2$]BF_4 with N≡CEt, N≡C^{t}Bu, C_5H_4N or 4-DMAP give the nitrile exchange products in 77 – 95 % yields after 4 – 15 hours. The use of labile nitrile

complexes as precursors to acetylide complexes does not seem to have been explored or reported.

In an attempt to isolate the active five-coordinate complex $[RuCl(dppm)_2]^+$, $[\mathbf{31}]^+$, Higgins has explored reactions of *trans*-[**20**] with AgOTf or $AgBF_4$ (1 equiv.) in solutions of 1,2-dichloroethane.[189-192] However the reaction course, monitored by $^{31}P\{^1H\}$ NMR spectroscopy, was quite unusual. After stirring at room temperature for one hour, the initial singlet at $\delta - 7.2$ ppm, which characterises *trans*-[**20**], was replaced by another singlet resonance ($\delta - 14.9$ ppm); assigned as the chloride bridged adduct, *trans*-$[\{Cl(dppm)_2Ru\}(\mu\text{-}Cl)\{Ag\}]^+$ (*trans*-$[\mathbf{32}]^+$, Scheme 1.22) on the basis of mass spectrometry and elemental analysis and by analogy with the crystallographically characterised complex, *cis*-$[\{(dppm)_2Ru(\mu\text{-}Cl)_2\}_2Cu][CuCl_2]$.[193] Upon heating the solution containing *trans*-$[\mathbf{32}]^+$ at reflux for 10 minutes, three pairs of second order triplets were observed in the $^{31}P\{^1H\}$ NMR spectrum at $\delta \sim 0.4$ and -24.8, ~ 0.4 and -26.0, ~ 0.4 and -27.5 ppm (showing a mutual coupling between triplet resonances of 75 Hz). As the solution did not contain precipitated AgCl, the isomerisation of *trans*-$[\mathbf{32}]^+$ to both *cis*-$[\mathbf{32}]^+$ and *cis*-$[\{(dppm)_2Ru\}_2(\mu\text{-}Cl)_4\{Ag\}]^+$ (*cis*-$[\mathbf{33}]^+$, Scheme 1.22), was proposed to occur. Though the exact structures of $[\mathbf{32, 33}]^+$ are unknown, further evidence to support these compositions was given by mass spectrometry.

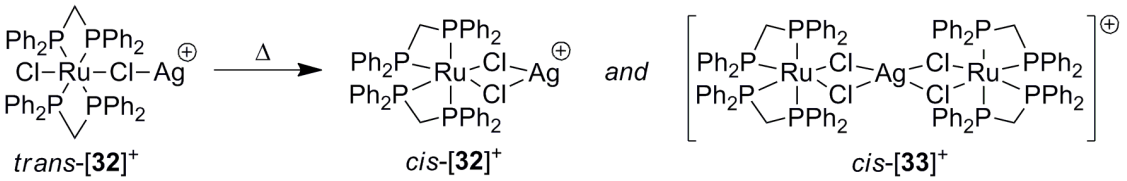

trans-$[\mathbf{32}]^+$ *cis*-$[\mathbf{32}]^+$ *cis*-$[\mathbf{33}]^+$

Scheme 1.22: Isomerisation of Ru / Ag bridging chloride complexes observed by Higgins, following reactions of *trans*-[**20**] with Ag^I salts.[191]

Upon heating mixtures of *cis*-$[\mathbf{32}]^+$ and *cis*-$[\mathbf{33}]^+$ (Scheme 1.22) for a further 30 minutes, precipitation of AgCl was observed. The resultant deep red colour of the solution, in addition to observation of a further set of second order triplets in the $^{31}P\{^1H\}$ NMR spectrum (δ 6.2 and -20.6 ppm; 70 Hz), suggested formation of $[\mathbf{31}]^+$, however this five-coordinate complex could not be separated from residual *cis*-[**20**] in solution. Notably, alternative reactions of the isomer *cis*-[**20**] with $AgBF_4$ or AgOTf in

solutions of 1,2-dichloroethane did increase the percentage formation of [**31**]$^+$ (adjudged from $^{31}P\{^1H\}$ NMR spectroscopy), although the final product remained contaminated by the dichloride starting material (*cis*-[**20**]). Evidence for the formation of [**31**]$^+$ was also demonstrated through further reactions of the reaction mixture with coordinating ligands, MeC≡N and CO, forming [RuCl(N≡CMe)(dppm)$_2$]OTf (72 − 87 %) and [RuCl(CO)(dppm)$_2$]OTf ([**34**]OTf; 78 − 79 %) respectively, where resultant *cis* / *trans* geometries of the products depend on the order of reagent addition.

The reaction of AgOTf (2 equiv.) with *trans*-[**20**] in 1,2-dichloroethane (reflux, 40 minutes) has been reported to give [Ru(dppm)$_2$][OTf]$_2$, although a full procedure was not given.[189] Further reactions of [Ru(dppm)$_2$][OTf]$_2$ with nucleophillic reagents (NH_4I, MeC≡N, ethylenediamine), readily yield disubstituted products [RuL$_2$(dppm)$_2$]$^{n+}$ (L = I (n = 0), MeCN (n = 2) or L$_2$ = ethylenediamine (n = 2)) in good to high yields (52 – 87 %).[192]

Koutsantonis has demonstrated the use of Ag^I salts in the preparation of *trans*-[RuCl{C≡C(bpy)}(dppm)$_2$] bearing an electron donating 5-ethynyl-2,2′-bipyridine (bpy) ligand.[194] The preliminary 15 hour reaction of *cis*-[**20**] with $AgPF_6$ (7 equiv.) in a CH_2Cl_2 solution in the absence of light is thought to give the five coordinate complex [**31**]$^+$. Although not isolated or characterised, this step-wise approach allows removal of Ag^I salts by filtration before the subsequent addition of HC≡C(bpy) (1.3 equiv.) and DBU, forming *trans*-[RuCl{C≡C(bpy)}(dppm)$_2$] in a 69 % yield after 2 hours.[194] If Ag^I salts are not removed, further chloride abstraction can occur, yielding trace amounts of *trans*-[Ru{C≡C(bpy)}$_2$(dppm)$_2$] which is arduous to separate. For this reason, the use of $NaPF_6$ as a halide abstracting agent was less successful given the partial solubility of Na^I salts in CH_2Cl_2 which prevents complete removal after activation of the ruthenium complex and prompting formation of mixtures of *mono*- and *trans*-bis(alkynyl) products. Furthermore, attempts to isolate the *mono*-vinylidene complex *trans*-[RuCl{=C=CH(bpy)}(dppm)$_2$]$^+$ *via* reactions of *cis*-[**20**] with $NaPF_6$ in CH_2Cl_2 solutions with a single equivalent of HC≡C(bpy) were also unsuccessful. This is due to the basicity of the bipyridene ligand, which readily deprotonates the vinylidene *in situ*, forming *trans*-[RuCl{C≡C(bpyH)}(dppm)$_2$]$^+$. As the *mono*-alkynyl ligand (albeit protonated at bpy) is much more electron donating than the *mono*-vinylidene, the *trans*-

chloride is labile, and undergoes further reactions with Na^{I} / HC≡C(bpy) to give inseparable mixtures of *mono*-vinylidene, *mono*-alkynyl and *trans*-bis(alkynyl) complexes, in addition to the dichloride starting material ([**20**]).

Although *trans*-[Ru{C≡C(bpy)}$_2$(dppm)$_2$] has been observed as a by-product in the reactions described above, neither Ag^{I} or Na^{I} salts under a variety of similar conditions (Na_2CO_3 / CH_2Cl_2; $NaPF_6$ / CH_2Cl_2; NaOMe / MeOH-CH_2Cl_2; $AgPF_6$ / THF-CH_2Cl_2) or alternative conditions (SnO_2 / CH_2Cl_2; KO^tBu / THF-CH_2Cl_2) gave complete conversion to the *trans*-bis(alkynyl) from either *cis*-[**20**] or *trans*-[RuCl{C≡C(bpy)}(dppm)$_2$]. Attempts to drive reactions further through prolonged reaction times or increased reaction temperature led only to decomposition. Furthermore, attempts to form the 'asymmetric' complex, *trans*-[Ru(C≡CC_6H_5){C≡C(bpy)}(dppm)$_2$], through reactions of [**23d**] with HC≡C(bpy) in the presence of $NaPF_6$ and NEt_3 in solutions of CH_2Cl_2, were complicated by ligand scrambling effects. However, for the first time, all possible *trans*-bis(alkynyl) ligand scrambling combinations, including the previously elusive complex [**24d**], were observed in this work.[194]

Riera and co-workers have noted that reactions of *trans*-[RuCl(C≡NR)(dppm)$_2$]PF_6 with silver salts, conducted in order to form *trans*-[Ru(C≡NR)$_2$(dppm)$_2$]PF_6, will induce ring opening of the chelating dppm ligands, producing complex mixtures of products.[195] Notably, in the same report, the efficiency of $TlPF_6$ as a strong, non-oxidising halide abstractor was demonstrated in the formation of *trans*-[Ru(C≡N^{t}Bu)$_2$(dppm){η^2-κ-(P,O)-P(C_6H_5)$_2$$CH_2$P($C_6H_5$)$_2$O}][$PF_6$]$_2$ (89 %) from the 24 hour reaction between *trans*-[RuCl(C≡N^{t}Bu)$_2$(dppm){η^1-P(C_6H_5)$_2$$CH_2$P=O($C_6H_5$)$_2$}]$PF_6$ and $TlPF_6$ (2 equiv.) in a CH_2Cl_2 solution (Scheme 1.23).

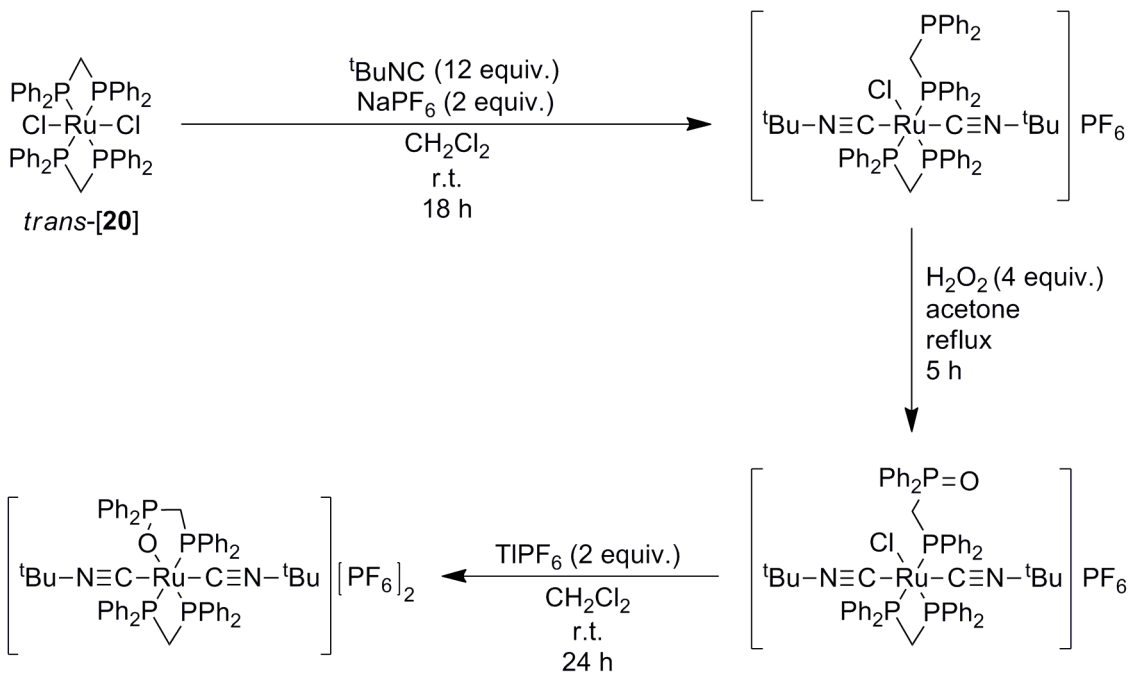

Scheme 1.23: Ring extension reactions of the {Ru(dppm)$_2$} fragment, facilitated by Tl^I salts, as reported by Riera.[195]

Winter and Hornung have explored the relative reactivities of halide abstracting agents, based on Na^I, Ag^I and Tl^I salts, at the {Ru(dppm)$_2$} centre during their studies of butatrienylidene complexes, *trans*-[RuCl(=C=C=C=CH$_2$)(dppm)$_2$]$^+$. Room temperature reactions of *cis*-[**20**] in CH_2Cl_2 or chlorobenzene with HC≡CC≡CH (excess) in the presence of either $NaPF_6$ or $NaSbF_6$ (4 equiv.; 40 minutes) followed by the addition of NR_2R' (NR_2R' = NEt_3, NPr_3, NEt{$(C_2H_4)_2O$}, $Me_2NCH_2C_6H_5$, $Me_2NCH_2C_6H_4$-3-OMe, Me_3TACN; 5 – 6 equiv.) gave the *mono*-alkynyl complexes *trans*-[RuCl{C≡CC(=CH$_2$)NR_2R'}(dppm)$_2$]$^+$ in variable yields (14 – 80 %) after 24 hours, evincing formation of the butatrienylidene intermediate, *trans*-[RuCl(=C=C=C=CH$_2$)(dppm)$_2$]$^+$ (IR: 1891 cm^{-1}, ν(C=C)).[196] Although reaction times are shortened if silver or thallium salts were employed, the reaction selectivity is reduced, increasing the difficulty of work-up procedures, ultimately leading to lower yields. The coordination of the Tl^I or Ag^I cations to the alkyne C≡C fragments was proposed to account for these observations.

Though there have been several further {Ru(dppm)$_2$} complexes reported bearing *mono*-alkynyl,[197-200] *trans*-bis(alkynyl)[201, 202] and cumulenic[203-205] ligands, especially

within the areas of non-linear optics[198, 206-208] and molecular electronics,[201, 209] work with alkynyl complexes of the {Ru(dppm)$_2$} fragment has gradually declined, no doubt a consequence of the synthetic challenges outlined above.

1.3.3.3. [RuCl$_2$(dppe)$_2$]

Sequential abstraction of chloride ligands from *cis*-[RuCl$_2$(dppe)$_2$], *cis*-[**35**], is facile in comparison with both the *trans*-isomer (*trans*-[**35**]), as a result of the *trans*-effect, and *cis*-[**20**]. Hence *cis*-[**35**] is an attractive starting material for the preparation of *mono*- and *trans*-bis(alkynyl) complexes.

The preparation of *cis*-[**35**] has been referenced[187, 207] to a 1961 paper by Chatt and Hayter that reports the synthesis of *trans*-[**35**].[175] In this report, *trans*-[**35**] is prepared either *via* the reaction of RuCl$_3$.3H$_2$O with 1,2-*bis*-diphenylphosphinoethane (dppe; 2.5 equiv.) in the absence of a solvent at 230 °C for 24 hours (25 % yield), or (in a method analogous to the preparation of *trans*-[**20**]) through the addition of RuCl$_3$.3H$_2$O, dissolved in water, to an EtOH solution of dppe (2.5 equiv.), followed by heating at reflux for 2 hours (66 % yield). The preparation of *cis*-[**35**] is also commonly referenced[36, 158, 210-216] to the 1984 method of Chaudret and Commenges, which describes the formation of *cis*-[**20**] from the reaction of [**21**] with dppm (2 equiv.) in toluene at 80 °C.[174] However the Low group reported that with dppe, this procedure only yields pure *trans*-[**35**] as the thermodynamic product,[210] corroborating an earlier procedure by Winter and Klinkhammer where *trans*-[**35**] was formed (88 %) from an analogous method after a seven hour reflux in xylene.[203] To clarify these issues, Humphrey has described the reaction of [**21**] with dppe (2 equiv.) in detail, with *cis*-[**35**] being formed (90%) after one hour in refluxing toluene.[217]

In contrast, the reaction of [**21**] and dppe (2 equiv.) in the alternative solvent CH$_2$Cl$_2$ at room temperature yielded a mixture of *cis*- and *trans*-[**35**], in an approximate 3 : 1 ratio, after one hour.[218] Although recrystallisation from a concentrated CH$_2$Cl$_2$ / hexane mixture was sufficient to isolate *cis*-[**35**] cleanly in a good yield (60 %), isomerisation to the thermodynamically preferred *trans*-[**35**] is accelerated in the presence of light and in chlorinated solvents.[219] For example, *cis*-[**35**] will isomerise into a 1 : 1, *cis* : *trans*

mixture after 24 hours at room temperature in $CDCl_3$ (monitored by $^{31}P\{^1H\}$ NMR spectroscopy) or a 3 : 1 ratio after 48 hours in CH_2Cl_2.[219] Hence, recrystallisation in the dark from non-chlorinated solvents is advised for optimum results. Even though *cis*-[**35**] can evidently be, and has been, isolated cleanly, Lewis and co-workers have noted (on two separate occasions) the experimental challenges associated with obtaining pure *cis*-[**35**] free from the less reactive *trans*-[**35**] isomer by these methods.[40, 220]

Recently, in a soon to be published report,[221] Humphrey has revealed that the key to obtaining *cis*-[**35**] cleanly is the isomeric purity of the starting material, *cis*-[**21**]. Initially, *cis* / *trans* isomeric mixtures of [**21**] are obtained after one hour from the reaction of $RuCl_3.3.H_2O$ in dimethyl sulfoxide with ascorbic acid (4 equiv.). The ascorbic acid facilitates the reduction of ruthenium, allowing the reaction to be conducted at room temperature. In order to then convert the *trans*-isomer (*trans*-[**21**]) to the desired *cis*-product (*cis*-[**21**]), the isomeric mixture is heated (150 °C) in dimethyl sulfoxide for two minutes before selective precipitation with acetone to yield *cis*-[**21**] (80 %). Any of the more soluble *trans*-isomer remains in solution. Subsequent reaction of *cis*-[**21**] with dppe (2.2 equiv.) in toluene (reflux / 1.5 hours), followed by a rapid hot filtration and washing the collected yellow solid with boiling toluene, affords the target complex *cis*-[**35**] (90 %). Although not mentioned in the paper, this unusual work-up procedure is necessary to remove traces of *trans*-[**35**], which is slightly more soluble than *cis*-[**35**] in toluene.[222]

The dissociation of a chloride ligand from *cis*-[**35**] is facile in the presence of various sodium salts to yield the reactive five-coordinate species $[RuCl(dppe)_2]^+$, $[\mathbf{36}]^+$. In the first instance, Morris reported that the overnight reaction of *cis*-[**35**] with $NaPF_6$ (5 equiv.) in a mixed EtOH / THF solution readily forms $[RuCl(THF)(dppe)_2]PF_6$ as a yellow precipitate which, on recrystallisation from solutions of CH_2Cl_2 and Et_2O, forms [**36**]PF_6 as red crystals in a near quantitative yield (99 %).[223] In a later paper, Touchard and Dixneuf obtained [**36**]PF_6 cleanly, in a reduced time (after six hours), upon reacting *cis*-[**35**] with $NaPF_6$ (quantity not given) in CH_2Cl_2, albeit in a lower yield (63 %).[224] Following this, Hidai extended the series of five coordinate complexes, through reactions of *cis*-[**35**] with 1.2 equivalents of NaX (where X = OTf, BAr_4, BPh_4) in EtOH (and in some cases THF) solutions forming [**36**]X complexes after 12 hours in 64 − 77 % yields.[225]

Morris has stated that in contrast to *cis*-[**35**], "*trans-$RuCl_2(dppe)_2$ does not react with reagents such as $NaPF_6$ or $NaBF_4$, or $NaBPh_4$ that precipitate NaCl*".[223] However Humphrey found that [**36**]PF_6 can be formed from *trans*-[**35**] (the more readily accessible isomer)[219] under similar conditions to those used from *cis*-[**35**] ($NaPF_6$ (3 equiv.) / CH_2Cl_2 / 16 hours), although the full synthetic account was not given in detail.[221] Alternatively, Higgins obtained [**36**]BF_4 (56 %) from the 40 minute reaction of *trans*-[**35**] with $AgBF_4$ (1 equiv.) in refluxing CH_2Cl_2.[191] Although reactions with AgOTf in 1,2-DCE were reported to proceed similarly, detailed experimental conditions were not given until several years later when Low described the formation of [**36**]OTf (85 %) from the room temperature (one hour) reaction of *trans*-[**35**] and AgOTf (1 equiv) in CH_2Cl_2.[219] Reactions of MeOTf with mixtures of *cis*- and *trans*-[**35**] in CH_2Cl_2 solutions will also give [**36**]OTf (90 %) selectively after two hours.[226]

The five coordinate complex [**36**]$^+$ is a useful entry point to substituted complexes $[RuCl(X)(dppe)_2]^{(n)}$. Based on the preliminary account by Morris,[223] the addition of [**36**]OTf to LiCl (10 equiv.) in methanol was shown to yield *cis*-[**35**] (84 %) as a pure precipitate after 15 minutes.[219] The use of [**36**]$^+$ salts as reagents for the preparation of acetylide complexes are described in more detail below.

1.3.3.4. Mono and trans-bis(alkynyl) complexes featuring the {Ru(dppe)$_2$} fragment

One of the earliest descriptions of alkynyl complexes featuring the $\{Ru(dppe)_2\}$ fragment was given in 1994 by the Dixneuf group who explored vinylidene and alkynyl complexes as intermediates in various catalytic transformations of alkynes.[227] In this account, *mono*-vinylidene complexes *trans*-$[RuCl(=C=CHR)(dppe)_2]PF_6$ (R = H, C_6H_5, ^nBu, $SiMe_3$) were obtained in high yields (85 − 90 %) after reactions of *cis*-[**35**] with terminal alkyne, HC≡CR (2 equiv.), and $NaPF_6$ (2 equiv.) for 4 hours in CH_2Cl_2. Upon subsequent addition of base (pulverised K_2CO_3), *mono*-alkynyl complexes *trans*-$[RuCl(C{\equiv}CR)(dppe)_2]$ (R = H, C_6H_5 [**37**], ^nBu, $SiMe_3$ [**38c**][ix]) were formed in high yields (70 − 75 %). In striking contrast to the dppm series, 'symmetric' *trans*-bis(alkynyl), *trans*-$[Ru(C{\equiv}CR)_2(dppe)_2]$ (R = C_6H_5 [**13**], ^nBu, $SiMe_3$ [**39**]) were

[ix] The numbering scheme for specific complexes of the type *trans*-$[RuCl(C{\equiv}CR)(dppe)_2]$, [**38**], is expanded in Chapter 4.

obtained in good yields (60 – 67 %) through facile one-pot reactions of *cis*-[**35**] with HC≡CR (3 equiv.), NEt_3 (6 equiv.) and $NaPF_6$ (3 equiv.) in CH_2Cl_2, though reaction times were not specified. Addition of NH_4PF_6 (2 equiv.) to CH_2Cl_2 solutions of the *trans*-bis(alkynyl) complexes resulted in the formation of the first mixed *trans*-ammine alkynyl complexes, *trans*-$[Ru(NH_3)(C{\equiv}CR)(dppe)_2]PF_6$ (R = C_6H_5, ^nBu, $SiMe_3$) in good yields (67 – 73 %) after 24 hours. In the absence of a ligand (*i.e.* NH_3) capable of replacing the labile vinylidene / π-alkyne complexes formed from reactions of *trans*-$[Ru(C{\equiv}CR)_2(dppe)_2]$ with acid, decomposition took place. The *trans*-ammine alkynyl complexes can also be obtained *via* analogous reactions from *mono*-alkynyl starting materials, following initial abstraction of the *trans*-chloride by NH_4^+, though the reaction time is extended (72 hours). Such complexes serve as alternative, convenient starting materials in the preparation of 'asymmetric' *trans*-bis(alkynyl) $\{Ru(dppe)_2\}$ complexes, due to the ready substitution of the ammonia ligand by incoming alkyne ligands.[228] Notably, equivalent one-pot reactions to form *trans*-ammine alkynyl complexes bearing the $\{Ru(dppm)_2\}$ fragment were unsuccessful, highlighting the importance of the ancillary ligands in molecular design. Several years later, in 1997, Dixenuf released the full synthetic account for the formation of *mono*-vinylidene, *mono*- and *trans*-bis(alkynyl) complexes bearing the $\{Ru(dppe)_2\}$ motif (Scheme 1.24).[36]

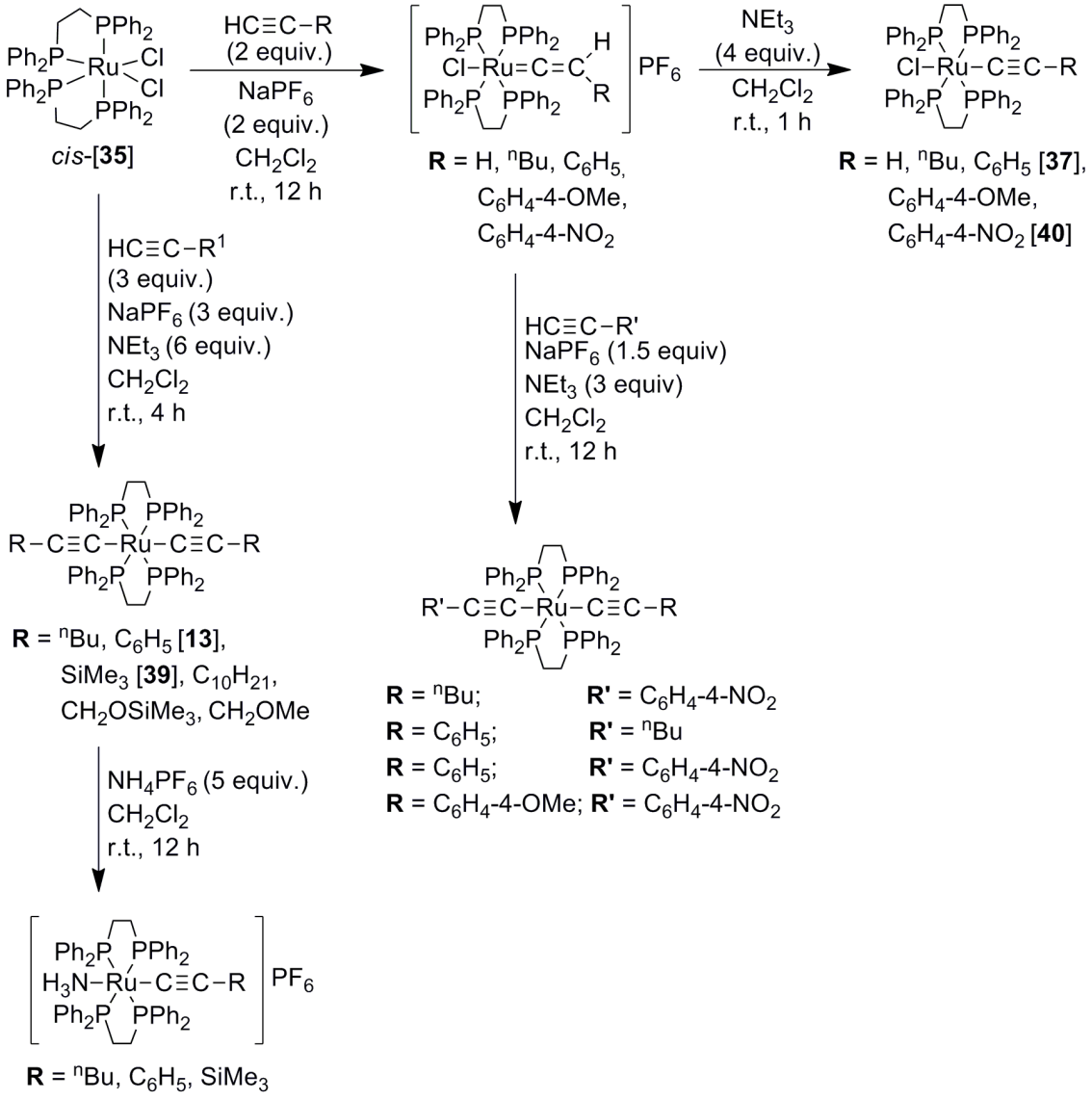

Scheme 1.24: Formation of *mono*-vinylidene, *mono*- and *trans*-bis(alkynyl) complexes bearing the {Ru(dppe)$_2$} motif, as reported by Dixneuf.[36]

The ability of $NaPF_6$ to promote the abstraction of either one or both chloride ligands is found to be essential in reactions of *cis*-[**35**] with alkynes; where these reactions do not proceed in its absence. The efficacy of the halide abstracting agent is demonstrated here by the relatively rapid formations (4 – 12 hours) of both 'symmetric' and 'asymmetric' *trans*-bis(alkynyl) complexes, *trans*-[Ru(C≡CR)(C≡CR′)(dppe)$_2$], which necessitate the non-trivial removal of a *trans*-chloride from precursor *mono*-alkynyl complexes, *trans*-[RuCl(C≡CR)(dppe)$_2$]. Although there was no explicit discussion at the time of the original report,[36] it is notable that the *trans*-bis(alkynyl) complexes formed generally

contain all electron donating substituents (in the case of 'symmetric' *trans*-bis(alkynyl) complexes) or are formed from *mono*-vinylidene complexes bearing electron donating substituents (in the case of 'asymmetric' *trans*-bis(alkynyl) complexes). Recently, Low found that reactions of [**36**]OTf in concentrated CH_2Cl_2 solutions with $HC{\equiv}CC_6H_4$-4-R (2.2 equiv.), where R is a strongly electron donating group (NH_2 or OMe), formed *trans*-[$Ru(C{\equiv}CC_6H_4$-4-$R)_2(dppe)_2$] in 44 − 48 % yields as pure precipitates in solution after seven days in the absence of any halide abstracting agent, where isolations of the products are achieved by a simple filtration.[229] In contrast, reactions with terminal alkynes bearing less electron donating or electron withdrawing substituents through this method failed to produce useable quantities of the *trans*-bis(alkynyl) complex, clearly demonstrating the electronic influence of the *para*-aryl alkynyl substituent in the activation (labilisation) of the *trans*-chloride within intermediate *mono*-alkynyl complexes in such reaction schemes.

Despite extensive use of the reactions described in Scheme 1.24, most notably by the Humphrey[198, 208, 216, 230, 231] and Rigaut groups,[211, 212, 232, 233] both of whom have mastered the preparation of *cis*-[**35**], Lewis stated that reactions of *cis*-[**35**] with $NaPF_6$, terminal alkyne and base "*was not a good route for formation of the Ru(dppe)$_2$* [acetylide complexes]. *This is because, despite our efforts, cis-[(dppe)$_2$RuCl$_2$] could not be synthesised in a pure form (it being contaminated with trans-[(dppe)$_2$RuCl$_2$]).*"[187] Instead, Lewis carried out reactions of the less-active *trans*-[**35**] with alkyne and $NaPF_6$ to generate *mono*-alkynyl complexes, *trans*-[$RuCl(C{\equiv}CR)(dppe)_2$] (R = C_6H_4-4-Me, C_6H_4-4-C_6H_5, C_6H_4-4-NO_2, [**40**]; C_6H_3-2-Me-4-NO_2). Despite extended reaction times (5 – 7 days), complexes were obtained in 67 – 76 % yields. In the same paper, the UV-Vis spectra of *mono*-alkynyl complexes bearing {$Ru(dppe)_2$} and {$Ru(dppm)_2$} fragments were not found to be significantly different, indicating similar underlying electronic structures.

Synthetic routes to *mono*-polyynyl {$Ru(dppe)_2$} complexes bearing long unsaturated carbon chains, developed as building blocks for higher molecular architectures, have been reported by the collaboration of Rigaut and Dixneuf.[211] Overnight reactions of *cis*-[**35**] in THF with a slight excess of $Li(C{\equiv}C)_nSiMe_3$ (n = 1 – 4), formed *in situ* by the

reaction of MeLi with $Me_3Si(C{\equiv}C)_nSiMe_3$ at – 78 °C, yielded *trans*-$[RuCl\{(C{\equiv}C)_nSiMe_3\}(dppe)_2]$ complexes in 20 – 70 % yields (Scheme 1.25).

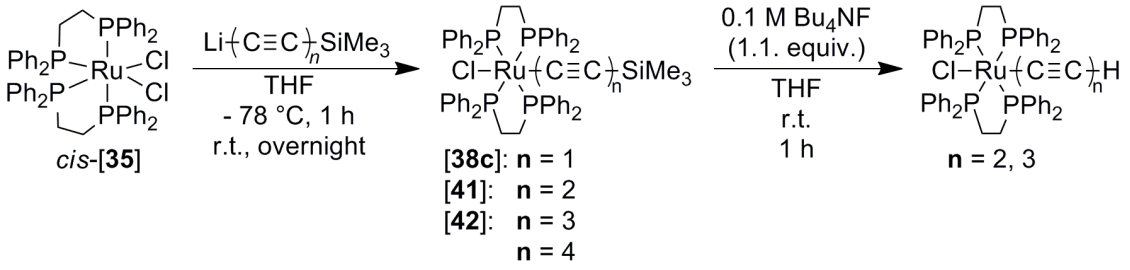

Scheme 1.25: Formation of *mono*-alkynyl $\{Ru(dppe)_2\}$ complexes using alkynyl-lithium reagents.[211]

Removal of the silyl group from *trans*-$[RuCl\{(C{\equiv}C)_nSiMe_3\}(dppe)_2]$ was only successful for [**41, 42**] (in 90 – 95 % yields; Scheme 1.25). For [**38c**], neither a large excess of Bu_4NF or solutions of KOH or K_2CO_3 in methanol were sufficient to induce a reaction, evincing the strong σ-donation of the $\{RuCl(dppe)_2\}^+$ fragment towards the silicon atom; extensive hyperconjugation along the Ru-C≡C-Si chain[13] and / or the steric hindrance of the dppe ligands.[211] Therefore the Dixneuf route shown in Scheme 1.24 remains the most effective way of accessing *trans*-$[RuCl(C{\equiv}CH)(dppe)_2]$, where desilylation precedes metal-alkynyl formation.[36]

Reactions of *cis*-[**35**] with even a large addition of the lithium acetylide reagent were unsuccessful in the preparation of 'symmetric' *trans*-bis(alkynyl) complexes.[211] Instead, *trans*-$[Ru(C{\equiv}CC{\equiv}CSiMe_3)_2(dppe)_2]$ (77 %) was prepared analogously to [**39**],[36] through the one-pot reaction of *cis*-[**35**] with $HC{\equiv}CC{\equiv}CSiMe_3$ (4 equiv.), $NaPF_6$ (4 equiv.) and NEt_3 (8 equiv.) in CH_2Cl_2. Although *trans*-$[Ru(C{\equiv}CC{\equiv}CSiMe_3)_2(dppe)_2]$ reacted readily with Bu_4NF (1M, 3 equiv.) in THF to form *trans*-$[Ru(C{\equiv}CC{\equiv}CH)_2(dppe)_2]$ in a near quantitative yield (97 %), *trans*-$[Ru(C{\equiv}CSiMe_3)_2(dppe)_2]$ ([**39**]) was inert to desilyation. Instead, *trans*-$[Ru(C{\equiv}CH)_2(dppe)_2]$ can be accessed *via* the reaction of *cis*-[**35**] with $NaPF_6$ (3 equiv.) and $HC{\equiv}CSnBu_3$ (3 equiv.) in the presence of NEt_3 (excess) in CH_2Cl_2.[36]

In 2009, Low published a facile, high-yielding (~ 70 − 80 %) and rapid (one hour) route to *mono*-aryl alkynyl complexes, *trans*-[RuCl(C≡CC_6H_4-4-R)(dppe)$_2$], *via* the step-wise reactions of the active five coordinate species, [**36**]OTf, with HC≡CC_6H_4-4-R (1 equiv.; R = H [**37**], OMe, NO_2 [**40**], Me, C_5H_{11}, COOMe) followed by addition of K_2CO_3 (excess).[219] Crucially, the method relies on the initial isolation of the crude *mono*-vinylidene (not characterised) and removal of any excess alkyne (*via* a thorough hexane wash) in order to prevent *trans*-chloride abstraction and subsequent *bis*-alkynyl complex formation. Although widely applicable, the route fails in the isolation of *trans*-[RuCl(C≡CC_6H_4-4-NH_2)(dppe)$_2$] as accumulation of the vinylidene is circumvented on account of the basicity of the aniline fragment. Instead, equilibrium concentrations of *trans*-[RuCl(C≡CC_6H_4-4-NH_2)(dppe)$_2$] are formed, which, in the presence of excess HC≡CC_6H_4-4-NH_2, reacts further to yield *trans*-[Ru(C≡CC_6H_4-4-NH_2)$_2$(dppe)$_2$], though the full procedure was not given until five years later.[229] Furthermore, reactions of [**36**]OTf with HC≡CC_6H_4-4-C≡N are complicated, due to presence of the coordinative and nucleophillic nitrile moiety which competitively binds to the ruthenium centre.[219]

Although reactions of *trans*-[RuCl(C≡CR)(dppe)$_2$] ([**38**]) to form *trans*-bis(alkynyl) complexes commonly use $NaPF_6$, first developed by Dixneuf[36] and perfected by Humphrey[207, 208, 216, 234, 235] and Rigaut,[173, 233] alternative halide abstracting agents have been reported. Of particular note, several groups have utilised NH_4PF_6[236-239] and KPF_6.[215, 240-245] Chloride abstraction from *trans*-[RuCl(C≡CR)(dppe)$_2$] by Ag^I salts and subsequent formation of *trans*-bis(alkynyl) complexes remains unreported. In perhaps the most closely related chemistry to date, Puerta found that the reaction of the related *mono*-alkynyl complex *trans*-[RuCl(C≡CC_6H_5)(dippe)$_2$] (dippe = diisopropylphosphinoethane) with AgOTf (1 equiv.) and HC≡CC_6H_5 (excess) in a THF solution resulted in two distinct products following the addition of $NaBPh_4$ in EtOH and work-up.[246] The first product, an insoluble grey solid with a ν(C≡C) stretch of 2048 cm^{-1}, was tentatively assigned as a metal-alkyne polymer, whilst the second, a yellow, crystalline substance soluble in polar solvents, was characterised as the novel *tetra*-nuclear complex, [{(dippe)$_2$Ru}$_2$(μ-Cl)$_3$(σ,η^2-C≡CC_6H_5)$_2$}{Ag_2(μ-dippe)}][BPh_4] (Figure 1.6), following single crystal X-ray diffraction studies. Formation of the *tetra*-metallic (Ru_2Ag_2) complex serves to demonstrate the propensity of alternative reaction pathways (and subsequent reaction products formed) to dominate between metal-

alkynyl complexes, *bis*-phosphines, and Ag^{I} salts and provides reasoning for the scarcity of such protocols in the literature.

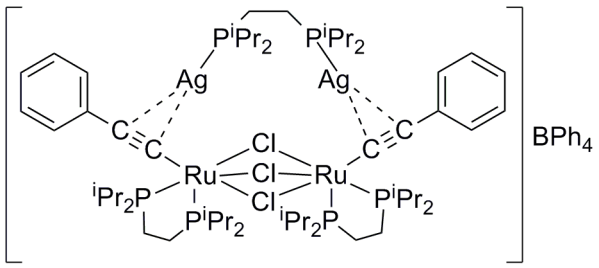

Figure 1.6: Product formed from the reaction of *trans*-[RuCl(C≡CC_6H_5)(dippe)$_2$] with AgOTf, HC≡CC_6H_5 and $NaBPh_4$.[246]

The factors influencing the lability of the *trans*-chloride of *mono*-alkynyl complexes, *trans*-[RuCl(C≡CR)(dppe)$_2$], and role in the formation of 'symmetric' *trans*-bis(alkynyl) complexes have been explored recently.[229] The effectiveness of Tl^{I} salts in subsequent halide abstraction reactions, where ligand scrambling pathways observed in analogous reaction schemes with Na^{I} salts are avoided, has been demonstrated. Addition of $TlBF_4$ (1 equiv.) to concentrated CH_2Cl_2 solutions of [**36**]OTf and HC≡CC_6H_4-4-R (2.2 equiv.) in the presence of DBU generated 'symmetric' *trans*-bis(alkynyl) complexes, *trans*-[Ru(C≡CC_6H_4-4-R)$_2$(dppe)$_2$] (R = Me, C_5H_{11}, OMe, COOMe, NO_2, C≡C$SiMe_3$ [**43a**],[x] C≡C^{t}Bu) in good yields (52 – 83 %), except for when R = NO_2 (14 %). In this case, the reaction was not complete even after 48 hours, with persistent mixtures of *mono*-([**40**]) and *trans*-bis(alkynyl) complexes being obtained. Clearly, the strongly electron-withdrawing nature of the NO_2 group limits the lability of the *trans*-chloride. Furthermore, the poor solubility of the product impeded facile purification.

The reaction protocol was also found to extend to 'asymmetric' *trans*-bis(alkynyl) complexes, where reactions of *trans*-[RuCl(C≡CC_6H_4-4-R)(dppe)$_2$] with HC≡CC_6H_4-4-R′ (1.1 equiv.) in the presence of $TlBF_4$ (1 equiv.) and DBU (excess) in concentrated CH_2Cl_2 solutions were successful in the rapid (30 minute) formations of *trans*-[Ru(C≡CC_6H_4-4-R)(C≡CC_6H_4-4-R′)(dppe)$_2$] complexes (R = C≡C$SiMe_3$, COOMe; R′ = NH_2, OMe) in 47 – 87 % yields in high purity (confirmed by elemental analyses). The

[x] The numbering scheme for specific complexes of the type *trans*-[Ru(C≡CR)$_2$(dppe)$_2$], [**43**], is expanded in Chapter 4.

importance of the strong, non-nucleophillic base DBU as a measure to prevent vexatious ligand scrambling effects by avoiding accumulation of the vinylidene intermediate is thought to be crucial for this reaction scheme, in addition to the presence of the halide abstracting agent $TlBF_4$, ensuing rapid reactions.

In the pursuit of higher molecular weight architectures with novel properties, Dixneuf has prepared the bimetallic complex, *trans*-[{Cl(dppe)$_2$Ru}$_2$(μ-C≡CC_6H_4-4-C≡C)], [**44**], in a 58 % yield.[210] In the initial step, the reaction of *cis*-[**35**] in THF with HC≡CC_6H_4-4-C≡CH (0.5 equiv.) and $NaPF_6$ (2 equiv.) yielded the bimetallic vinylidene complex, *trans*-[{Cl(dppe)$_2$Ru}$_2${μ-(=C=CHC_6H_4-4-CH=C=)}][PF_6]$_2$, as a pale green solid. Subsequent deprotonation (NEt_3) gave [**44**] after 16 hours (Scheme 1.26). Similarly, reactions of *cis*-[**35**] in CH_2Cl_2 with $NaPF_6$ (1 equiv.) and the *mono*-protected diethynyl benzene HC≡CC_6H_4-4-C≡CSi^{i}Pr$_3$ (2 equiv.), formed *trans*-[RuCl(=C=CHC_6H_4-4-C≡CSi^{i}Pr$_3$)(dppe)$_2$]PF_6 after 15 hours, where subsequent treatment with excess NEt_3 in THF afforded the *mono*-metallic complex *trans*-[RuCl(C≡CC_6H_4-4-C≡CSi^{i}Pr$_3$)(dppe)$_2$] in an 81 % yield (Scheme 1.26). Deprotection of the triisopropylsilyl group is then achieved by reaction (30 minutes, r.t.) with Bu_4NF (0.5 equiv.) in THF, giving *trans*-[RuCl(C≡CC_6H_4-4-C≡CH)(dppe)$_2$], [**45**] (93 %; Scheme 1.26). Exposure of the terminal alkyne allows ready access to novel oligomeric complexes. For example, the mixed ruthenium-palladium trimetallic complex *trans-trans*-[{(P^{n}Bu$_3$)$_2$Pd}{μ-(C≡CC_6H_4-4-C≡C)Ru(dppe)$_2$Cl}$_2$] (53 %) was prepared by reaction of [**45**] with [**3**] (0.5 equiv.) and $NHEt_2$ (excess) in the presence of catalytic CuI (0.9 %) for 20 hours in THF (Scheme 1.26). Such complexes bear obvious relationships to the multi-metallic dppm analogues described above (see section 1.3.3.2).[181, 183]

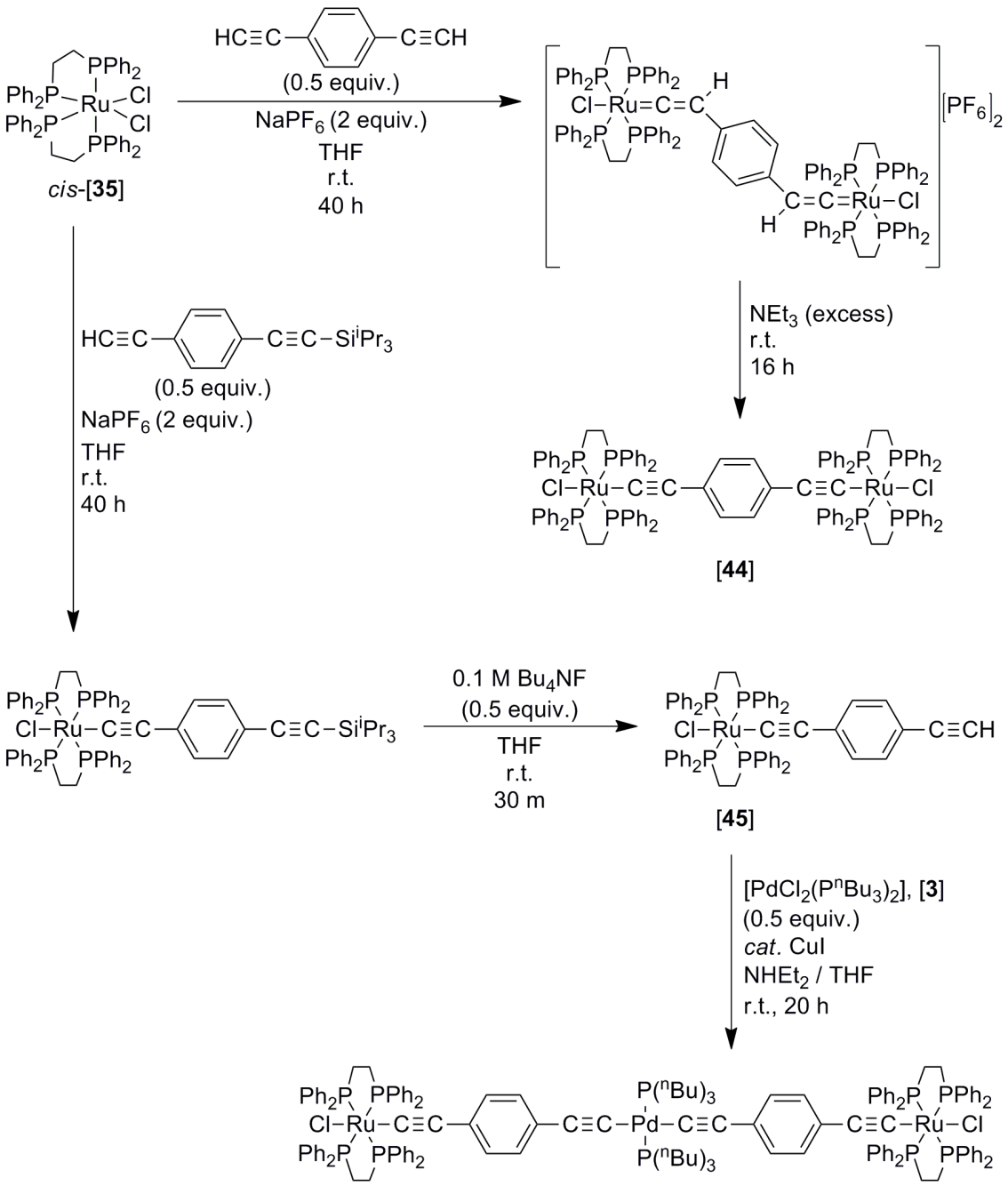

Scheme 1.26: Formation of bimetallic and trimetallic *mono*-alkynyl complexes containing the {Ru(dppe)$_2$} motif, as reported by Dixneuf.[210]

The bimetallic complex [**44**] displays two, reversible, one-electron oxidation events ($E_{1/2}(1)$ = 0.15 V; $E_{1/2}(2)$ = 0.55 V), initially attributed to the step-wise oxidations of the metal centres, and described as revealing an appreciable degree of electronic communication between the metal termini, permissible through the 1,4-ethynylbenzene bridge. However, it should be noted that oxidation events of ruthenium acetylide

complexes have a large degree of ligand character and interpretations of 'metal-metal' communication are somewhat over simplified.[149] The trimetallic complex *trans-trans*-[{(P^nBu_3)$_2$Pd}{μ-(C≡CC_6H_4-4-C≡C)Ru(dppe)$_2$Cl}$_2$] instead exhibited a single, reversible two-electron oxidation ($E_{1/2}(1)$ = 0.33 V) and two further, one-electron, irreversible oxidations at higher potentials ($E_{1/2}(2)$ = 1.14 V; $E_{1/2}(3)$ = 1.38 V). The first oxidation is attributed to the simultaneous oxidations of both ruthenium metal centres (or ruthenium-diethynylbenzene fragments), with the two-electron nature being confirmed by voltammetry with a rotating Pt electrode (2000 rpm). Consequently, the platinum fragment can be described as an insulator in this case, inhibiting electron communication between the (metal-alkynyl) termini.

The effectiveness of {Ru(dppe)$_2$} fragments as through-charge transport mediators has been demonstrated through electrochemical investigations of the mixed-metal trimetallic complex, *trans*-[{(dppe)$_2$Ru}{μ-(C≡C(η^5-C_5H_4))Fe(η^5-C_5H_5)}$_2$],[158] which exhibits three, one-electron oxidations ($E_{1/2}(1)$ = − 0.36 V; $E_{1/2}(2)$ = − 0.16 V; $E_{1/2}(3)$ = 0.53 V). The first two, attributed to the sequential [Fe^{II}] / [Fe^{III}] redox couples occur at lower potentials than ferrocene (0 V), evincing the electron releasing nature of the {RuCl(C≡C-)(dppe)$_2$} fragment, which has been found to behave electronically similarly to a methoxy or amino group.[243] The closely related trimetallic complex *trans*-[{(dppe)$_2$Ru}{{μ-(C≡CC≡C(η^5-C_5H_4))Fe(η^5-C_5H_5)}$_2$] with extended C≡CC≡C bridges behaves similarly.[158]

Rigaut and co-workers have demonstrated the use of the *mono*-alkynyl complexes *trans*-[RuCl{(C≡C)$_n$R}(dppe)$_2$] (R = H, $SiMe_3$) as starting materials in the formation of multiple metal systems in pursuit of redox-active molecular wires.[211, 247, 248] For example, the reaction of *trans*-[RuCl(C≡CC≡CC≡CH)(dppe)$_2$] with Cu(OAc)$_2$ (1 equiv.) and DBU (1 equiv.) in pyridine resulted in the formation of a rare, twelve carbon bridged compound, *trans*-[{Cl(dppe)$_2$Ru}$_2$(μ-C≡CC≡CC≡CC≡CC≡CC≡C)] (90 %).[211] Alternatively, room temperature reactions of [**41**] (n = 2; R = $SiMe_3$) in THF with ferrocenium hexafluorophosphate (0.5 equiv.) yielded a diruthenium complex uniquely featuring an odd numbered carbon bridge in a 75 % yield after eight hours, *via* a [2+2] coupling reaction following cation radical formation ([**46**]$^+$; Scheme 1.27).[247, 248] Furthermore, the slow addition of [**41**] (or *trans*-[RuCl(C≡CC≡CH)(dppe)$_2$]), over three

days, to a single equivalent of *trans*-[RuCl(=C=C=CRCH$_2$R′)(dppe)$_2$]BF$_4$ (R = Me, C$_6$H$_5$; R′ = H, Me) in a room temperature CH_2Cl_2 solution, generated bimetallic complexes *trans*-[{Cl(dppe)$_2$Ru}$_2${μ-C≡CC(Me)=C(R′)C(R)=C=C=}]BF$_4$, [**47 – 49**]$^+$ (Scheme 1.27), in good yields (79 – 85 %), which feature novel alkynyl-allenylidene bridges with an odd number of carbon atoms.[248, 249] Desilyation of the starting material [**41**] occurs spontaneously *in situ* therefore preliminary deprotection reactions are not necessary. The 'W' structure of [**47 – 49**]$^+$ is implied from spectroscopic analysis, where a 2D NOESY cross peak is not observed between the methyl group and R′ on the bridge fragment, in addition to single crystal X-ray diffraction data (for [**47**]$^+$) and supporting quantum chemical calculations.[248] The analogous reaction of [**42**] with *trans*-[RuCl(=C=C=CMe$_2$)(dppe)$_2$]OTf produced the first bimetallic complex to be bridged by nine conjugated carbon atoms (in a 49 % yield); though the reaction time is greatly increased (19 days).[248]

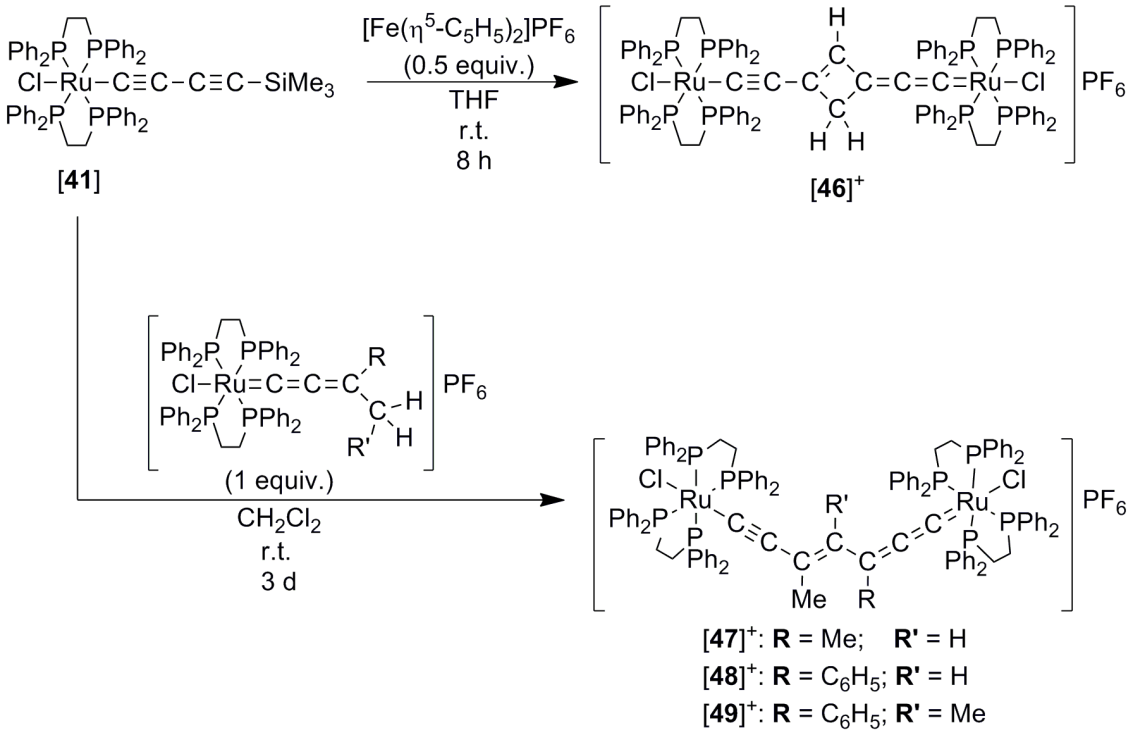

Scheme 1.27: Formation of novel diruthenium bimetallic complexes from [**41**] featuring odd numbered carbon bridges, as reported by Rigaut .[211, 247, 248]

Both types of C$_7$ bridged bimetallic complexes, [**46**]$^+$ and [**47 − 49**]$^+$ shown in Scheme 1.27, exhibit three redox events; two, one-electron oxidations (one reversible, one

partially reversible) and a single, one-electron reversible reduction.[248] The two oxidation processes correspond to the separate formations of (formally) $[Ru^{II}] / [Ru^{III}]$ couples (although considerable carbon-ligand character is likely), while the reduction is assigned to population of virtual orbitals on the organic linker. The potential separation between oxidations ($\Delta E_{1\text{-}2}$ ~ 0.65 V; $K_c = 1.50 \times 10^{11}$) [xi] demonstrates the thermodynamic stability of the *mono*-oxidised species with respect to disproportionation. Although K_c is often used as a proxy measure of the extent to which such conjugated bridges facilitate charge delocalisation between metal centres, care is needed in such interpretations.[250, 251]

Electron paramagnetic resonance (EPR) spectroscopy has been used as a means to quantify the extent of electron distribution over the metal and / or ligand fragments in the open shell bimetallic complexes by assessments of isotropic g-values (g_{iso}) and corresponding de*via*tions from the free electron case ($g_e = 2.0023$).[252] The *mono*-reduced derivatives (*i.e.* [**46** − **49**]) display g_{iso} values of ~ 2.0047, which are close to the free electron case, confirming electron population at the (organic) bridging ligand. Upon oxidation, forming $[\mathbf{46} - \mathbf{49}]^{2+}$, g_{iso} values are only slightly increased (~ 2.024), implying admixtures of metal and ligand character to describe the cation radical. Although increasing the conjugation of the bridge might be expected to lower g_{iso} in the corresponding *mono*-oxidised forms, g_{iso} for the *mono*-oxidised allenylidene bridged bimetallic complex, *trans*-[{Cl(dppe)$_2$Ru}$_2${μ-(=C=C=C(C$_6$H$_5$)C$_6$H$_4$-4-C(C$_6$H$_5$)=C=C=)}][OTf]$_2$,[253] is comparable (2.0244) with the shorter derivates.

In a later paper, two alkynyl-allenylidene bridged bimetallic complexes were successfully linked *via* the central organic fragment, as a means to resourcefully increase complex dimensionality.[254] The *tetra*-metallic complex $[\mathbf{50}]^{2+}$ (Scheme 1.28) bearing two 'W-shaped' units, was formed in a high yield (72 %) as stable green crystals after [**41**] (2 equiv.) was added to a room temperature CH_2Cl_2 solution of *trans*-[{Cl(dppe)$_2$Ru}$_2${μ-(=C=C=C(Me)C$_6$H$_4$-4-C$_6$H$_4$-4-C(Me)=C=C=)}][OTf]$_2$ over three days. Data obtained from electrochemical and spectroscopic investigations are near-identical with the related alkynyl-allenylidene bimetallic complex $[\mathbf{48}]^{+}$, evincing the

[xi] $K_c = exp(\frac{\Delta E_{1-2}\mathrm{F}}{\mathrm{RT}})$
Where: K_c = disproportionation constant; $\Delta E_{1\text{-}2}$ = potential difference between first and second oxidations; F = faraday constant and R = gas constant; T = temperature (298 K).

lack of communication between linked chains due to the central biphenyl fragment, which is assumed to be rotated out of the plane of conjugation on steric grounds.

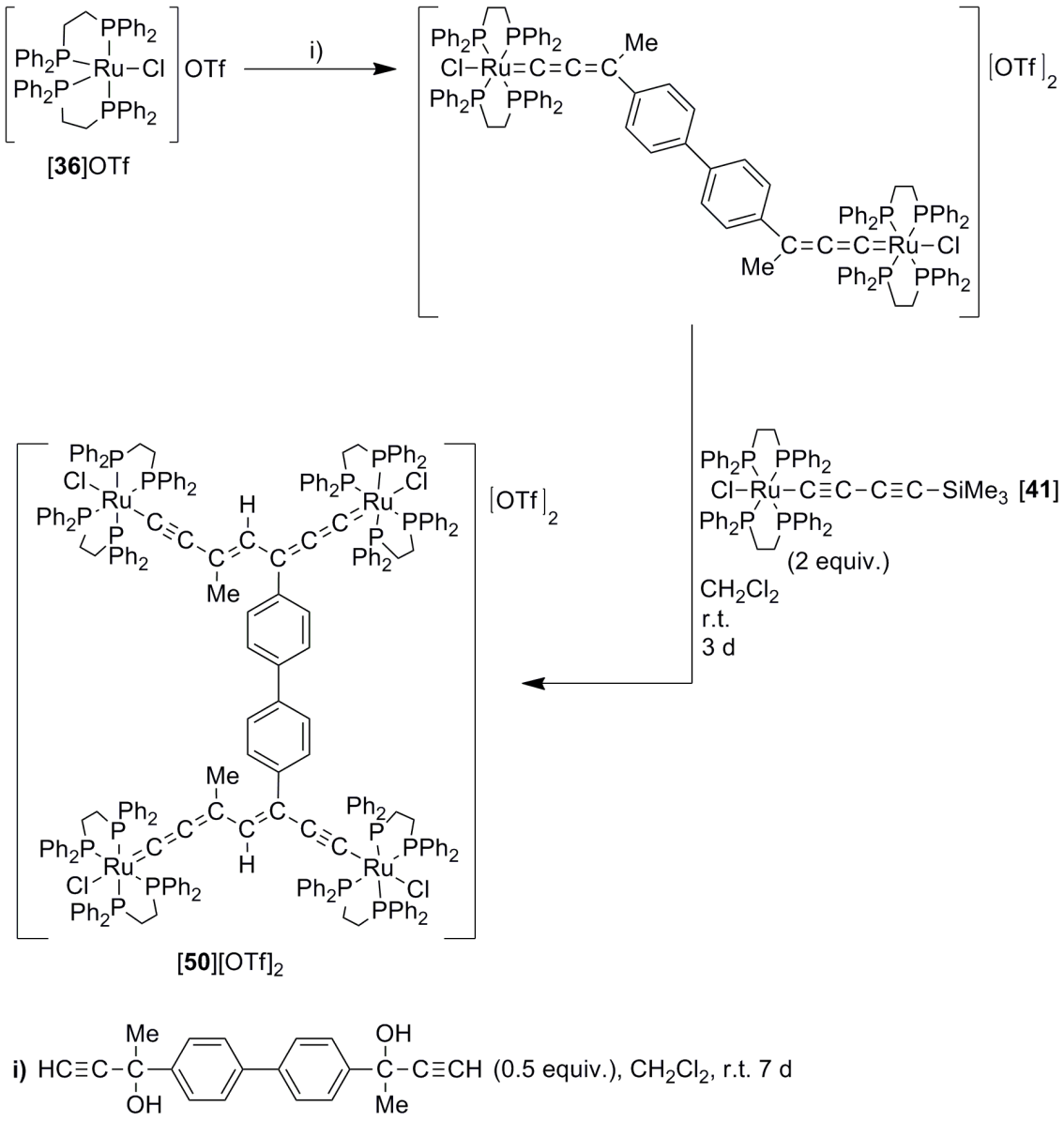

Scheme 1.28: Formation of a bridging alkynyl-allenylidene *tetra*-ruthenium complex, [**50**][OTf]$_2$, as reported by Rigaut.[254]

1.4. Current applications of *trans*-bis(alkynyl) ruthenium complexes, *trans*-[Ru(C≡CR)$_2$L$_4$]

Given the development of facile and high yielding synthetic protocols over the past two decades or so, it is unsurprising to find that the number of potential applications of *trans*-bis(alkynyl) complexes of ruthenium has increased. Herein is described some of these main research areas.

1.4.1. Molecular electronics

With a backdrop of rich redox chemistry and evidence of extensive delocalisation along the {C≡C}-[Ru]-{C≡C} backbone, in addition to established synthetic foundations, *trans*-bis(alkynyl) complexes bearing {Ru(dppe)$_2$} fragments are emerging as an important class of compounds within the area of molecular electronics.[22, 255]

Wang has investigated factors governing the charge transport through single molecules of *trans*-[Ru(C≡CC$_6$H$_4$-4-SAc)$_2$(dppm)$_2$], [**51**], and AcSC$_6$H$_4$-4-C≡CC$_6$H$_4$-4-C≡CC$_6$H$_4$-4-SAc, [**52**], in Au|molecule|Au junctions *via* scanning tunnelling microscopy (STM) and conducting-probe atomic force microscopy (CP-AFM) measurements.[209] Although topographical images revealed a lower surface coverage of [**51**] than [**52**], due to the steric demands of the bulky ancillary ligands, the calculated electronic decay constant (β)[xii] of [**51**] (1.01 ± 0.25 Å^{-1}) is comparable with [**52**] (1.11 ± 0.18 Å^{-1}) and alkane-thiols of similar lengths (1.07 − 1.2 Å^{-1}).[258-260] In accordance, STM break junction[261] measurements revealed a higher conductance value for [**51**] (2.45 ± 0.90 × 10^{-4} G$_0$) than [**52**] (0.46 ± 0.26 × 10^{-4} G$_0$) (Figure 1.7). The second, higher (H) conductance peak in the histogram may be attributed to alternative sulphur-gold contact geometries[262, 263] or the presence of two (or more) molecules within the junction.[264]

[xii] Values are calculated via the STM apparent height method.[256] Conductance G as a function of molecular length, l, is given by $G \propto e^{-\beta l}$.[257]

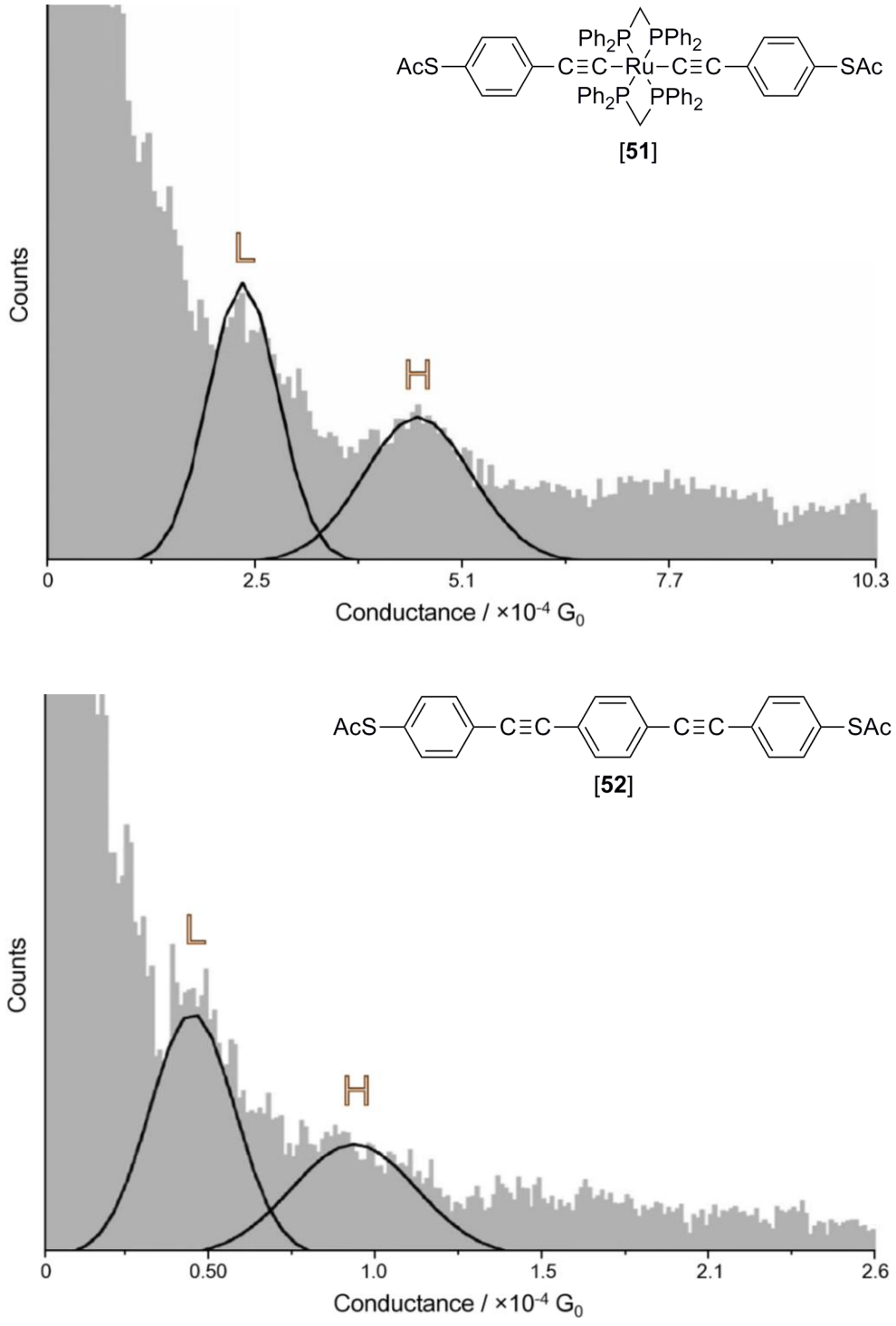

Figure 1.7: Conductance histograms of [**51**] (top) and [**52**] (bottom), obtained by the STM break junction method[261] where L and H refer to low and high conductance respectively. (Adapted with permission from ref[209]. Copyright 2008 American Chemical Society).

Although the molecular length of [**51**] (1.88 nm) is shorter than [**52**] (2.01 nm), undoubtedly contributing somewhat to the higher conductance value obtained for the metal complex, UV-Vis spectroscopy experiments indicated a lower HOMO-LUMO band gap for [**51**] (355 nm, 3.46 eV) than [**52**] (334 nm, 3.69 eV). Furthermore, DFT calculations on [**51**] revealed that the energy of the HOMO, which spans the entire length of the molecular backbone, is comparable with the gold Fermi level and would indicate that a low tunnelling barrier to conductance through the HOMO of [**51**] exists within Au|[**51**]|Au junctions. The integration of ruthenium fragments within conjugated wire backbones is therefore an advantageous design element to optimise through-charge transfer. In contrast, as square-planar Pt(*d*) and Pd(*d*) orbitals are too low in energy to effectively overlap with C≡C(π) orbitals[22] (hence the Pt / Pd-C≡C bond is chiefly regarded as offering σ-character), resultant molecules should display insulating properties (at least for hole-based, HOMO-mediated conduction mechanisms), to which Mayor and co-workers have found is true for $[Pt(C{\equiv}CC_6H_4\text{-}4\text{-}SAc)_2(PPh_3)_2]$.[265]

A parallel series of neutral, redox-active molecular wires of varying lengths (2.4 to 4.9 nm), containing 1,4-diethynylbenzene linker units and isocyanide binding groups has been prepared by Rigaut in order to elucidate trends between charge transport and length within organometallic wires ([**53** − **55**]; Figure 1.8).[233, 257]

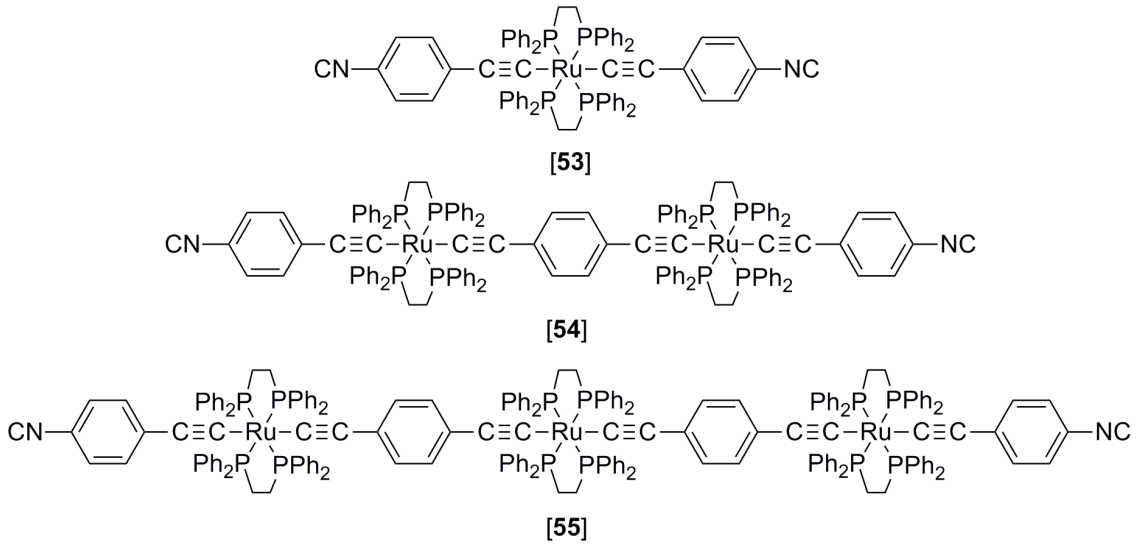

Figure 1.8: Organometallic molecular wires [**53** − **55**] of growing lengths, featuring the $\{Ru(dppe)_2\}$ fragment.[233, 257]

Broad, low energy, highly absorbing bands in the UV-Vis spectra of complexes [**53** − **55**] are assigned to overlapping MLCT (Ru($d\pi$) to C≡C(π^*)) and intra-ligand (IL) (C≡C(π to π^*)) transitions. On increasing molecular length ([**53**] to [**54**] to [**55**]), a bathochromic shift in the apparent maximum wavelength (λ_{max}) is observed, consistent with an increased degree of conjugation and reduction in the HOMO-LUMO gap. The 'wire-like' properties of [**53** − **55**] have been assessed using cyclic voltammetry, with the separation of redox events (attributed to the metal centres) taken as a proxy measure of conductance. Although voltammograms are broadened as a result of the competitive and fluxional binding of the terminal isocyanide groups to the electrode surface, the number of reversible redox events is consistent with the number of integrated metals for the series. The first oxidation potentials of [**54**] (− 0.20 V) and [**55**] (− 0.20 V) are both less positive than [**53**] (0.12 V), as a result of increased conjugation length. For [**55**], the second and third oxidations appear coincident (0.10 V), though are believed to be two overlapping, independent processes rather than a genuine two-electron event. All three complexes [**53** − **55**] form loosely packed self-assembled monolayers (SAMs) on gold surfaces, each with a surface coverage of $1 – 2 \times 10^{13}$ molecules / cm^2 (estimated from surface cyclic voltammetry studies), where maximum coverage is calculated as 4×10^{13} molecules / cm^2.[257] Ellipsometry and X-ray photoelectron spectroscopy (XPS) studies reveal SAM thickness, although increasing linearly, is shorter than the estimated molecular lengths by 0.1 – 0.6 nm, suggesting a tilted arrangement of molecules at the electrode surface. Reflection-absorption infrared spectroscopy (RAIRS) showed that although ν(C≡N) of the free molecules are ~ 50 cm^{-1} lower in energy than ν(C≡N) of molecules bound to gold surfaces, band intensities are unchanged, indicating a lack of physisorbed multi-layers on the SAMs.

Complexes [**53** − **55**] were integrated within Au|monolayer|Au junctions by both conducting-probe atomic force microscopy (CP-AFM) and crossed-wire (X-wire) methods and exhibited sigmoidal current-voltage curves at room temperature, characteristic of molecular conductance. For this series of complexes, based on three points, these authors report a β value of 0.09 $Å^{-1}$,[257, xiii] which is lower than purely organic systems of comparable lengths such as oligoacenes bearing thiol

[xiii] It is however noted that for the series of complexes, [**53** − **55**], a change in charge transport mechanism upon extending the molecular length was observed. Such charge transport mechanisms are discussed further in section 4.2. of Chapter 4.

($\beta = 0.49$ Å^{-1})[218] and isocyanide ($\beta = 0.50$ Å^{-1})[218] binding groups, thiol capped OPVs ($\beta = 0.53 - 0.99$ Å^{-1})[215] and thiol capped OPEs ($0.94 - 0.99$ Å^{-1}),[266] reflecting the superior frontier orbital matching between the organometallic wires and gold Fermi levels.

Rigaut has also reported the synthesis and electronic characterisation of a further series of molecular wires bearing thioacetate-protected thiol binding groups: *trans*-[Ru(C≡CC_6H_4-4-R)$_2$(dppe)$_2$] ([**56**]: R = CH_2SAc; [**59**]: O$(CH_2)_6$SAc); *trans*-[{(RC_6H_4-4-C≡C)(dppe)$_2$Ru}$_2$(μ-C≡CC_6H_4-4-C≡C)] ([**57**]: R = CH_2SAc; [**60**]: O$(CH_2)_6$SAc); and *trans-trans*-[{(dppe)$_2$Ru}{μ-(C≡CC_6H_4-4-C≡C)Ru(dppe)$_2$(C≡CC_6H_4-4-R)}$_2$] ([**58**]: R = CH_2SAc; [**61**]: O$(CH_2)_6$SAc).[212] Results obtained from cyclic voltammetry and UV-Vis spectroscopy experiments of [**56** − **61**] are comparable with the isocyanide series of complexes [**53** − **55**].[233, 257] Within Au|monolayer|Au junctions (achieved by CP-AFM), a smaller β value (0.10 Å^{-1}) was obtained for the series of complexes bearing shorter terminal groups ([**56** − **58**]) than longer terminal groups ([**59** − **61**]; 0.16 Å^{-1}),[xiv] evincing increased resistance (tunneling barriers) in complexes [**59** − **61**] as a consequence of integrating (more extended) non-conjugated fragments.[267]

Based on their earlier synthetic work,[172] the collaboration of Winter and Rigaut have investigated the electronic effect of introducing ethynylvinyl(phenylene) bridges into molecular wires.[268] Complexes of the type, *trans*-[{(dppe)$_2$Ru}{μ-(C≡CC_6H_4-4-CH=CH){Ru(CO)(P^{i}Pr$_3$)$_2$R}}$_2$] (R = Cl, η^2-$O_2CC_6H_4$-4-SAc), exhibited four reversible, one-electron redox events at low potentials (between − 0.31 and 0.63 V). Altering the coordination number of the terminal metal fragments from 5 to 6 (from R = Cl to η^2-$O_2CC_6H_4$-4-SAc) was found to lower all oxidation potentials by ~ 0.09 V. Most remarkably, IR-spectroelectrochemical investigations (for R = Cl), supported by quantum chemical calculations, revealed that the charge(s) are fully delocalised over the 21-atom conjugated wire backbone, advantageous for efficient charge transport. When R = η^2-$O_2CC_6H_4$-4-SAc, ν(C=O) stretches of the benzoate ligands are largely unaffected upon oxidation, establishing a disconnection between the Ru-Ru-Ru conjugation path and terminal electrode binding fragment.

[xiv] The tunnelling decay parameters given for the series of complexes [**56** − **58**] and [**59** − **61**] were each calculated based on three points. Notably, for both series, a change in charge transport mechanism upon extending the molecular length was observed. Such charge transport mechanisms are discussed further in section 4.2. of Chapter 4.

The Rigaut group have also demonstrated the capacity of bimetallic ruthenium complexes, containing dithienylethene bridges, to operate as photo- and electro-chromic molecular switches (Figure 1.9).[173]

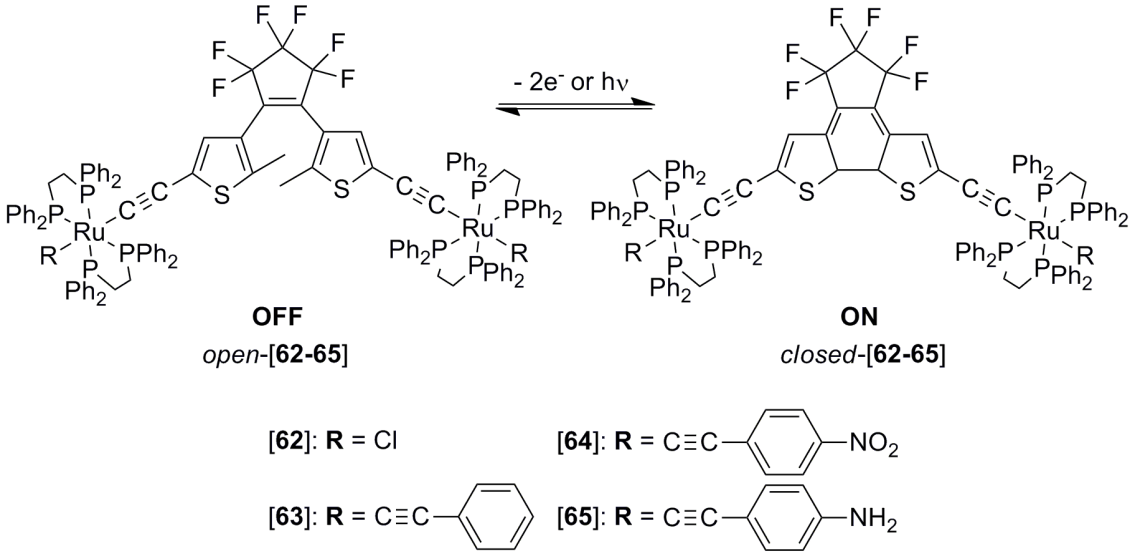

Figure 1.9: Photo- and electrochemical switching observed in bimetallic ruthenium complexes [**62** − **65**] bridged by dithienylethene (DTE) units.[173]

The UV-Vis spectra of neutral *open*-[**62** − **64**] complexes, display intense absorption bands within the range 340 – 344 nm, with large molar absorptivity coefficients (ε) between 28 280 – 50 200 $M^{-1}cm^{-1}$, assigned to intra-ligand (IL) transitions of the central DTE unit. Broadening of the absorption bands in the spectra arises due to the plethora of electronic transitions occurring on account of the presence of rotamers in solutions. Upon exposure to UV light (λ_{max} = 350 nm), these optical absorption bands are replaced by a broad absorption band centred between 714 – 718 nm (ε = 25 767 − 47 553 $M^{-1}cm^{-1}$) and a higher energy shoulder band between 660 – 688 nm (ε = 23 750 – 44 524 $M^{-1}cm^{-1}$), indicating ring closure and formation of *closed*-[**62** − **64**].

Quantum chemical calculations (for [**62**]) revealed that the first excited state of the open form (*open*-[**62**]$^{+}$) reflects a mixed MLCT / IL, {RuC≡C}(d / π) to DTE(π*), HOMO-LUMO transition, whereby sufficient electron density is deposited onto the two methyl substituents of the DTE bridge to photochemically induce ring closure, hence increasing the conjugation of the system and systematically turning the switch 'on'. The

first excited state of the closed form (*closed*-[**62**]$^{+}$) also exhibits a mixed MLCT / IL, {RuC≡C}(d / π)DTE(π) to {RuC≡C}(d / π)DTE(π*), HOMO-LUMO transition, which in contrast to the situation described above, removes electron density from the central DTE fragment leading to ring opening as a result of photochemically induced bond breaking, subsequently turning the switch 'off'. Consequently, upon systematic exposure of the *closed*-[**62 − 64**] to visible light, the original optical spectrum (of *open*-[**62 − 64**]) is recovered with minimal intensity loss, indicating efficient reversibility of the bimetallic DTE switch.

Cyclic voltammetry (CV) based investigations of complexes [**62 − 64**] revealed that an electrochemical stimulus can also induce ring closure.[173] At moderate scan rates (5 Vs^{-1}), *open*-[**62 − 64**] complexes exhibit a single, broad, two-electron, reversible wave between 0.36 – 0.58 V arising from simultaneous, one-electron oxidations of the two independent, non-conjugated ruthenium centres. At slow scan rates (0.2 Vs^{-1}), the original single oxidation event loses reversibility and on the reverse scan, two new redox events are observed at lower potentials with a potential separation ($\Delta E_{1\text{-}2}$) of ~ 0.12 V, interpreted as evincing electronic communication between the metal centres, and in turn suggesting that generation of the more conjugated form, *closed*-[**62 − 64**], occurs on the CV timescale. Compared with purely organic DTE-based systems and alternative bridging-DTE bimetallic (Ru, Os, Fe, Co) systems featuring terpyridine ancillary ligands,[269, 270] the oxidative ring closing mechanism favourably occurs at lower potentials with the integration of {Ru(dppe)$_2$} units. Unfortunately incorporation of an amine group into the molecular structure ([**65**]), to serve as a surface binding group to assemble the organometallic molecular switch within a molecular junction, was found to perturb the underlying electronic structure to such as degree as to render electrochemical stimuli ineffective.

The ring closing process is thought to proceed *via* a bi-radical mechanism after generation of the di-oxidised open form, *open*-[**62 − 65**]$^{2+}$, provided the thiophene fragments are in an anti-parallel conformation (favoured on the basis of steric arguments). For complexes [**62 − 64**], the di-oxidised closed form, *closed*-[**62 − 64**]$^{2+}$, is lower in energy by 0.026 – 0.477 eV than *open*-[**62 − 64**]$^{2+}$, favouring cyclisation by intramolecular radical coupling. However for [**65**], *closed*-[**65**]$^{2+}$ is higher in energy by

0.011 eV than *open*-[**65**]$^{2+}$, disfavouring the process. Moreover, the magnitude of atomic spin densities calculated for the two methyl substituents of the central DTE bridge are lower for *open*-[**65**]$^{2+}$ (0.04) than *open*-[**62 − 64**]$^{2+}$ (0.10 – 0.18), despite comparable Me-Me distances (between 3.655 – 3.745 Å for all complexes), which are within range for cyclisation.[271] Although an electrochemical stimulus is insufficient to control the molecular switching properties for [**65**], UV-Vis measurements reveal that photo-chemical switching still remains an option.

Chen and Rigaut have successfully fabricated Au|molecule|Au molecular transport junctions of *trans*-[{(AcSC$_6$H$_4$-4-C≡C)(dppe)$_2$Ru}$_2$(μ-DTE)], [**66**] (*c.f.* R = C≡CC$_6$H$_4$-4-SAc in Figure 1.9),[272] using on-wire lithography (OWL).[273] Quantum chemical calculations in the free (unbound) state show that the open form, *open*-[**66**], has a distance between the sulphur anchor atoms of 33.1 Å, while the closed form, *closed*-[**66**], is longer by 1.1 Å, reflecting the more 'rod-like' nature of the closed form. This is especially true given that the determined angle between internal {RuC≡C} alkynyl fragments (calculated using projected straight lines) is wider in *closed*-[**66**] (~ 158 °) than *open*-[**66**] (~ 135 °). Constraining the length of *open*-[**66**] to mimic that of *closed*-[**66**] requires an energetic constraint of only 0.03 eV, therefore geometric transformations between *open*- and *closed*-[**66**] in a junction are anticipated to occur without necessitating molecule-electrode detachment. Base deprotection of the thioacetate groups by ammonia exposed thiol groups to give [**66′**], which could be assembled in a junction. The closed form, *closed*-[**66′**], exhibited a sigmoidal current-voltage (I-V) curve, with the experiment conducted in the dark, under vacuum and at low bias (≤ 1 V; Figure 1.10).

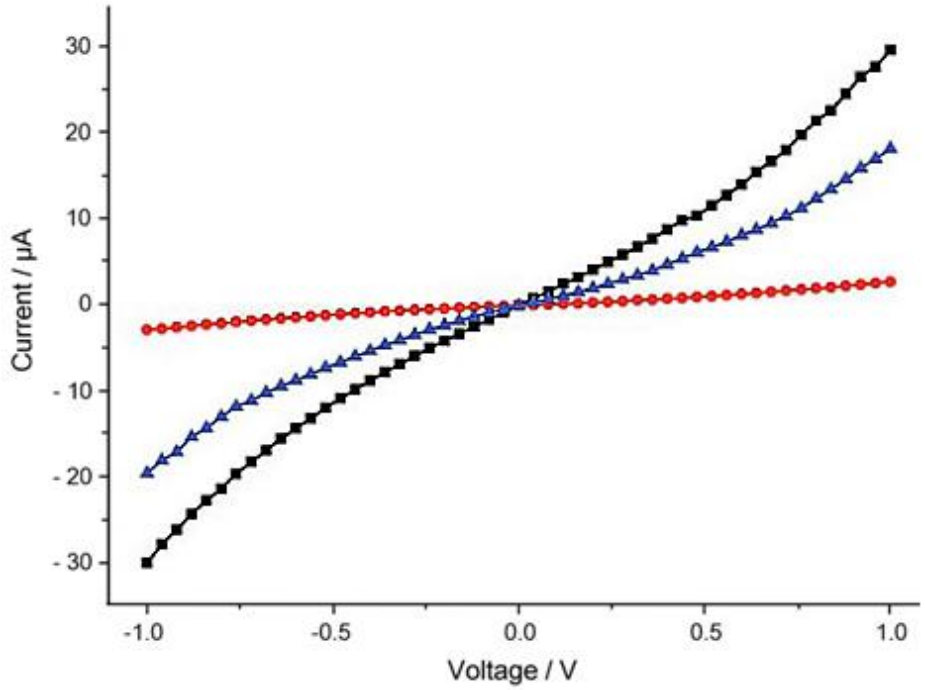

Figure 1.10: Resultant I-V curves of [**66**] within an OWL generated nano-device (forming [**66′**]); initially as the *closed*-[**66′**] complex (black squares) and then after systematic exposure to visible light (700 nm; red dots) for 150 minutes, forming *open*-[**66′**], and then UV light (365 nm; blue triangles) for 30 minutes, reforming *closed*-[**66′**]. (Reproduced from ref[272] with permission from The Royal Society of Chemistry.)

After visible light irradiation (λ_{max} = 700 nm) for 150 minutes (Figure 1.10), photo-chemically generating *open*-[**66′**], the current decreased considerably. Further irradiation with UV light (λ = 365 nm) for 30 minutes prompted the reformation of the original sigmoidal I-V curve of *closed*-[**66′**] (Figure 1.10), albeit with lower maximum current values, demonstrating the applicability of [**66**] / [**66′**] to operate as a molecular switch. Attempts to fabricate devices using *open*-[**66′**] initially were less successful. The less linear-like geometry of *open*-[**66′**] was thought to circumvent successful junction formations in this case. Although the 'on / off' switching mechanism of [**66**] within junctions ([**66′**]) is somewhat stable for several cycles, the reversibility declines over time. These authors have proposed several reasons for the observed phenomenon, which are: the stochastic behaviour of thiols on gold, promoting molecule-substrate desorption; the ductility of gold substrates, especially during the ring opening transformation, potentially rendering new thiol-gold contacts less favourable or the

decomposition of molecules over time by UV irradiation. The 'open / closed' ('off / on') switching process of [**66**] within junctions ([**66′**]) can also be controlled by electrochemical stimuli.[274] As such, these molecules are the first to display multi-mode switching conductivity as a result of both electrochemical and photochemical stimuli, hence further supporting application of [**66**] as a resettable electronic logic gate.

In the pursuit of more complex molecular architectures for molecular electronics, anticipated to display novel properties, the trimetallic complex, *trans-trans*-[{(dppe)$_2$Ru}{μ-(DTE)Ru(dppe)$_2$(C≡CC$_6$H$_4$-4-SAc)}$_2$] has also been investigated.[274] Conversion from the stable *open-open*-form (displaying an absorption maximum, λ_{max}, at 357 nm) to the stable *closed-closed*-complex (λ_{max} = 733 nm), occurs facilely under both photochemical and electrochemical control. Notably, UV-Vis spectroscopy and CV experiments tracking the switching processes of the trimetallic complex, in addition with I-V curves obtained following integration within a junction, exhibit very similar characteristics to the bimetallic analogue, [**66**] / [**66′**].

The data output (displayed as histograms) obtained from single molecule conductance measurements represent a range of values, reflecting variations in (but not limited to): molecular tilt-angle;[262] the number of molecules confined within a junction;[264] the nature of molecule-surface contact and site of binding, such as on flat terraces (type A, Figure 1.11), near step edges [263] or adjacent adatoms[17] on one (type B, Figure 1.11) or both (type C, Figure 1.11) contacts.[275] Hence, changes in the both chemical composition of the binding groups and surface roughness are expected to influence the conductance profiles. Whilst thiolate-on-gold contacts have been widely used for conductance studies of both organic[276-278] and organometallic[209, 265, 267, 279] compounds, there has been an increasing body of work in recent years exploring alternative molecule-surface contacts.[275, 278, 280-282]

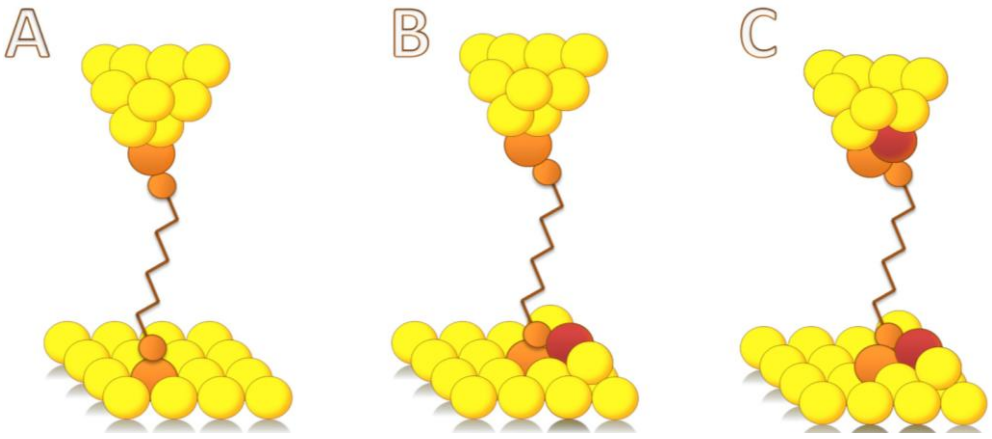

Figure 1.11: Contact modes A, B and C observed in Au|molecule|Au junctions are expected to contribute to the number of bands observed in resultant conductance profiles. Higher conductance values are obtained with increasing surface roughness (*i.e.* from A → B → C). Orange and red colour coding represents molecule-metal contact.

Ethynyl trimethylsilane, -C≡CSiMe$_3$, has been identified as a potential surface binding group by Fichou,[283-285] Aso[286] and Watcharinyanon[287] in addition to the Cea, Low and Nichols collaboration.[275, 288] In contrast to the multiple conductance signatures exhibited by, for example, thiolate contacted compounds (Figure 1.7), conductance profiles of *trans*-[Ru(C≡CC$_6$H$_4$-4-C≡CSiMe$_3$)$_2$(dppe)$_2$], [**43a**], and Me$_3$SiC≡CC$_6$H$_4$-4-C≡CC$_6$H$_4$-4-C≡CC$_6$H$_4$-4-C≡CSiMe$_3$, [**67**], (obtained *via* the I(s) method)[261] showed only a single conductance peak. Whilst a detailed model of the contact is currently being reviewed, it is clear that the -C≡CSiMe$_3$ contact permits a more precise, single value description of the conductance through the linear Au|molecule|Au array. The organometallic complex [**43a**] displays a higher conductance value ($5.10 \pm 0.99\ 10^{-5}\ G_0$) than [**67**] ($2.75 \pm 0.56\ 10^{-5}\ G_0$). Even though [**43a**] is expected to be slightly shorter than [**67**], the difference in conductance values is thought to better reflect the more superior alignment of frontier orbital energies of [**43a**] with the gold Fermi level.

Recently, in 2014, Fabre and Humphrey have reported the covalent attachment of redox active Ru / Fe molecular wires, bearing {Ru(dppe)$_2$} fragments, to hydrogen terminated Si(111) surfaces in order to generate rapid charge storage materials (Scheme 1.29).[289] The approach also has merit in looking ahead towards a hybrid silicon-molecular electronics technology.[290] In the unbound state, *trans*-[Ru(C≡CFc)(C≡CC$_6$H$_4$-4-

C≡CH)(dppe)$_2$], [**68**], and *trans*-[Ru(C≡CC$_6$H$_5$)(C≡CFcC≡CH)(dppe)$_2$], [**69**], (where Fc = ferrocenyl or -diyl) display two, reversible, single-electron oxidations, corresponding to [Fe^{II}] / [Fe^{III}] and (formally) [Ru^{II}] / [Ru^{III}] couples, in addition to a single-electron, irreversible oxidation event at higher potentials, thought to correspond to (formally) [Ru^{III}] / [Ru^{IV}]. On comparing between [**68, 69**], binding a second ethynyl fragment to ferrocene (in [**69**]) was found to increase $E_{1/2}(1)$ by 0.10 V, while $E_{1/2}(2)$ and $E_{1/2}(3)$ are similar.

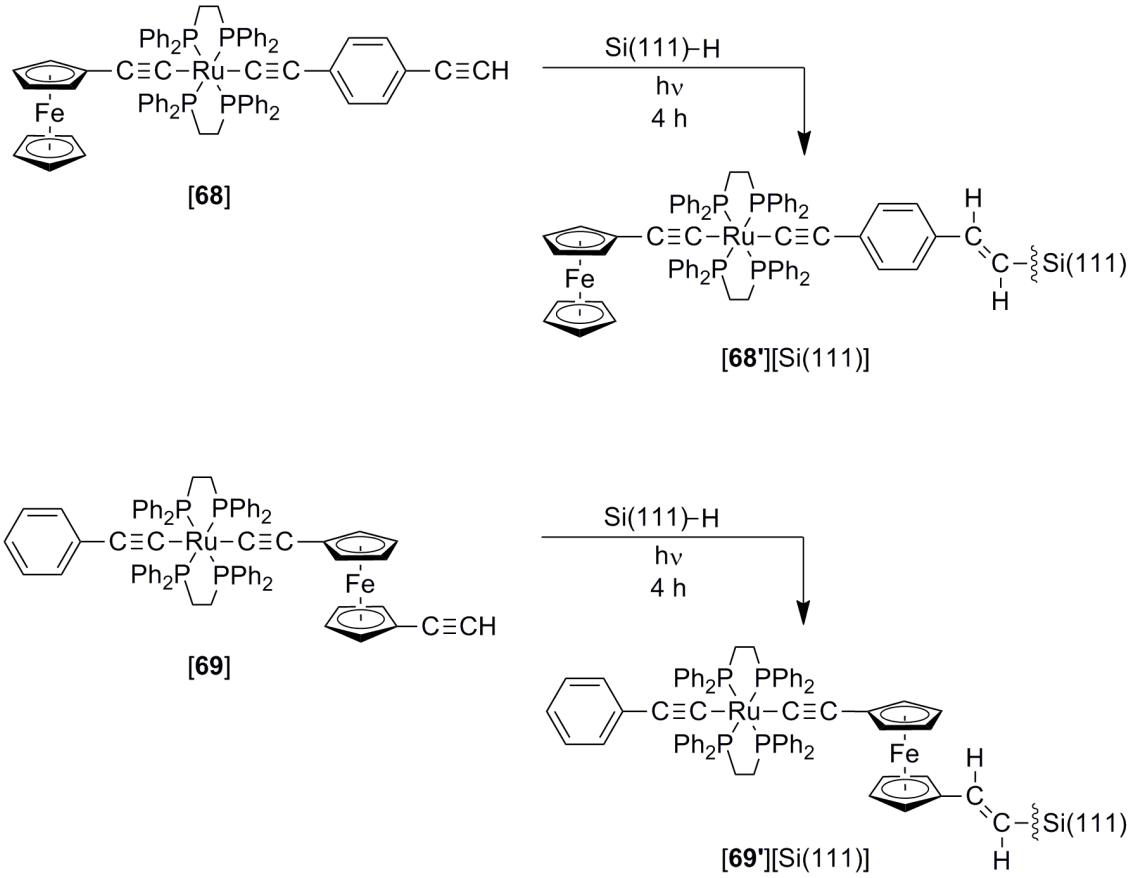

Scheme 1.29: Redox active Ru / Fe molecular wires [**68, 69**] covalently bound to hydrogen terminated Si(111) surfaces, forming [**68′, 69′**][Si(111)], as reported by Fabre and Humphrey.[289]

Grafting the molecules [**68, 69**] to a Si(111) surface was achieved following exposure to UV light (λ_{max} = 254 nm) for four hours in the presence of Si(111)-H surfaces, forming [**68′, 69′**][Si(111)] (Scheme 1.29), with the resulting surface assemblies characterised by XPS. The lower molecular surface coverage of [**69′**][Si(111)]

($1.1 \pm 0.1 \times 10^{-10}$ mol cm^{-2}) compared with [**68′**][Si(111)] ($1.3 \pm 0.1 \times 10^{-10}$ mol cm^{-2}) results from the free rotation of the cyclopentadieneyl ligands about the iron centre, which is more significant in [**69′**][Si(111)], being closer to the Si(111) surface, preventing a systematic and optimised molecular surface alignment. Quantum chemical calculations do not show significant differences in the bond distances and atomic spin densities comprising the central (chemically unchanged) portion between *mono*-cationic surface-bound and *mono*-cationic unbound structures.

Surface CV experiments on [**68′**][Si(111)] arrays reveal two, one-electron oxidation events. On comparison with data obtained for the free molecule, [**68**], $E_{1/2}(1)$ values are similar, suggesting a surface-confined redox species however $E_{1/2}(2)$ values are comparatively lower in [**68′**][Si(111)] (by ~ 0.2 V), to which Fabre and Humphrey have assigned to the increased stability of $[Ru^{II}]$ / $[Ru^{III}]$ as a result of the strong ion pairing between the electrolyte counter ions (ClO_4^-) and dicationic molecular state. If the electrode potential is increased further than the second redox event of [**68′**][Si(111)], the first $[Fe^{II}]$ / $[Fe^{III}]$ event diminishes whilst the second $[Ru^{II}]$ / $[Ru^{III}]$ event remains unaffected. For the first $[Fe^{II}]$ / $[Fe^{III}]$ and second (formally) $[Ru^{II}]$ / $[Ru^{III}]$ events, rate constants for electron transfer from the metal to the surface (k_{app}) of [**68′**][Si(111)] were calculated as 560 ± 60 and 320 ± 80 s^{-1}, respectively, which are on average higher than k_{app} values reported previously (140 ± 60 s^{-1} to 350 ± 150 s^{-1}) for half-sandwich iron complexes, [Fe(C≡CR)(dppe)(η^5-C_5Me_5)] (R = C_6H_4-4-C≡CH, C_6H_4-3-C≡CH, C_6H_4-4-C≡CC_6H_4-4-C≡CH) also bound to Si(111) surfaces.[291] Surface CV experiments of [**69′**][Si(111)] arrays reveal a single, one-electron oxidation within the expected region for the first $[Fe^{II}]$ / $[Fe^{III}]$ redox process occurring in [**69**], at comparatively identical values ($k_{app} = 640 \pm 80$ s^{-1}). However, if the potential window is increased, the expected second $[Ru^{II}]$ / $[Ru^{III}]$ event is revealed in the first scan, yet is absent from subsequent cycles whereas the first $[Fe^{II}]$ / $[Fe^{III}]$ event still remains, but is shifted to higher potentials (by 0.18 V).

The fragility of [**68′, 69′**][Si(111)] molecules at higher oxidations was in part attributed to reactions of trace oxygen at the ruthenium-alkynyl radical, severing the molecule-surface assembly and forming electrochemically silent (within the observed electrochemical window) ruthenium carbonyl complexes.[289] Alternatively, protonation

of the dication, *via* reactions with residual solvent or unreacted Si-H may have occurred, forming electrochemically silent (within the observed electrochemical window) ruthenium vinylidenes complexes. The increased spin density found on the *mono*-oxidised ferrocenyl terminus compared with *mono*-oxidised ruthenium units in the triplet state dications was further proposed as a contributing factor to rationalise such observations.

The propensity of mixed ruthenium *trans*-bis(alkynyl) / dysprosium complexes to serve as prospective single molecule magnets (SMMs), within the area of molecular spintronics, has been investigated by Rigaut and co-workers.[292, 293] The incorporation of ruthenium fragments favourably increased the redox reversibility (enhancing the SMM properties), whilst providing design versatility. The group has also, very recently (2015), explored *trans*-bis(alkynyl) {Ru(dppe)$_2$} complexes as magnetic coupling units (MCUs) between remote radicals.[232] Notably, the antiferromagnetic coupling between two nitronyl nitroxide units was higher (-2.1 cm^{-1}) with a central {Ru(dppe)$_2$} fragment than a central {Pt(PPh$_3$)$_3$} fragment (-1.0 to -0.1 cm^{-1}),[294] the only other organometallic MCU complex to date.

The recent work of Berke and co-workers is also worth mentioning here in their investigation of related iron acetylide complexes, bearing the {Fe(depe)$_2$} motif (depe = diethylphosphinoethane), as molecular components.[130, 131, 295, 296] In particular, bimetallic complexes *trans*-[{R(depe)$_2$Fe}$_2$(μ-C≡CC≡C)] (R = SH, C≡N, N=C=S, N=C=Se, C≡CC≡CSnMe$_3$, C≡CSnMe$_3$) were synthesised with a view to elucidating the role of conjugated binding groups on molecular conductance.[130, 296] Binding groups that could form either covalent or coordinative bonds with gold electrodes were chosen to weight electron delocalisation towards the termini (leads), following frontier orbital reorganisation on molecular binding, in order to achieve high conductance values as the injection barrier height will be decreased. In the junction, complexes with direct C-Au coupling (R = C≡CC≡C-, C≡C-, established after cleavage of the SnMe$_3$ group) exhibited the highest current (6.0×10^{-7} to 7.2×10^{-7} A)[296] and conductance values (8.9×10^{-3} G_0);[130] three orders of magnitude higher than the analogous complex bearing the N=C=S group (1.5×10^{-10} to 2.2×10^{-10} A;[296] 7.9×10^{-6} G_0),[130] which must reflect the increased strength of molecule / Au molecular orbital hybridisations in C-Au

contacts. The complexes *trans*-[{($Me_3SnC{\equiv}C$)$(depe)_2Fe$}$_2$(μ-$C{\equiv}CC{\equiv}C$)] and *trans*-[{($Me_3SnC{\equiv}CC{\equiv}C$)$(depe)_2Fe$}($\mu$-$C{\equiv}CC{\equiv}C$)] are anticipated to outperform the best molecular wires to date (of comparable lengths), with smaller β values (4.4 nm^{-1}, determined from experimental values at 1 V bias, or 3.5 nm^{-1}, calculated from DFT at zero bias)[130] than purely organic polyphenylene complexes coupling to electrodes *via* Au-C bonds (4.0 – 6.0 nm^{-1}).[297]

1.4.2. Solar cells

Despite their capacity to form expansive molecular arrays with broad absorption profiles and vibrant redox chemistry, *trans*-bis(alkynyl) complexes bearing {$Ru(dppm)_2$} and {$Ru(dppe)_2$} fragments have received little attention for applications as dyes in solar cells. The first account of a ruthenium acetylide complex investigated for bulk hetero-junction application, as a novel donor material to function within solar cells, was reported only recently (2011) by the collaboration of Colombo, Falciola and Luzzati ([**70**]; Figure 1.12).[298]

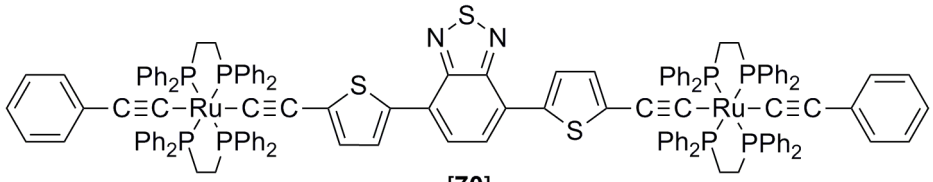

[**70**]

Figure 1.12: The *trans*-bis(alkynyl) di-ruthenium complex [**70**], featuring a benzothiodiazole and thiophene based bridging unit, was synthesised as a novel donor material to function within solar cells.[298]

The UV-Vis spectrum of [**70**] revealed two strong absorption bands: λ_{max} = 393 nm (ε = 35 011 $M^{-1}cm^{-1}$) and 633 nm (ε = 35 340 $M^{-1}cm^{-1}$). Compared with the individual organic bridge fragment, $HC{\equiv}C\text{-}2\text{-}C_4H_2S\text{-}5\text{-}C_6H_2N_2S\text{-}4\text{-}2\text{-}C_4H_2S\text{-}5\text{-}C{\equiv}CH$, ($\lambda_{max}$ = 322 nm; ε = 7592 $M^{-1}cm^{-1}$ and λ_{max} = 464 nm; ε = 6960 $M^{-1}cm^{-1}$), the organometallic bands of [**70**] are red shifted (therefore extending coverage of the solar spectrum) and are more intense, demonstrating the effectiveness of {$Ru(dppe)_2$} integration in the design of dyes. Platinum complexes are also emerging as effective donor molecules in

solar cells due to effective inter-system crossing from increased spin-orbit coupling of heavier elements.[299] On comparing the optical profile of [**70**] with the platinum analogue (λ_{max} = 372 nm; ε = 40 900 $M^{-1}cm^{-1}$ and λ_{max} = 549 nm; ε = 28 400 $M^{-1}cm^{-1}$),[299] substituting {Ru(dppe)$_2$} for {Pt(PBu_3)$_2$} in the complex shown in Figure 1.12, bands are of similar intensity, but are again red shifted for [**70**], which is deemed advantageous for broader solar spectrum coverage.

The effectiveness of electron transfer from the donor molecule [**70**] to an electron acceptor (6,6-phenyl-C_{61}-butric acid methyl ester, PCBM) was explored using cyclic voltammetry. The voltammogram of [**70**] displays a single, two-electron oxidation at − 0.06 V and a single, one-electron reduction at − 1.73 V (both chemically reversible and electrochemically *quasi*-reversible) in addition to a single, two-electron oxidation at 1.78 V (irreversible). The oxidation events have been assigned to the step-wise formations of [Ru^{II}] / [Ru^{III}] and [Ru^{III}] / [Ru^{IV}] redox couples for the two independent, non-conjugated metal centres (although the involvement of the ethynyl fragments should be considered), whereas the reduction is assigned to electron population at the organic bridge. PCBM displays three reversible, one-electron reductions at − 1.13 V, − 1.52 V and − 2.01 V. The anticipated donor-acceptor mechanism from [**70**] to PCBM was confirmed by fluorescence spectroscopy measurements where the fluorescence spectrum of [**70**] is quenched upon addition of PCBM. The charge separated state of [**70**][**PCBM**] was found to be lower in energy than the singlet state of [**70**] (by 0.5 eV), proving yet further evidence for *trans*-bis(alkynyl) ruthenium complexes to operate within this area; although the preliminary power conversion efficiency was low (0.1 %).

The first examples of ‘asymmetric’ *trans*-bis(alkynyl) {Ru(dppe)$_2$} complexes, featuring strong internal donor and acceptor fragments for a dynamic ‘push-pull’ mechanism, as photo-sensitisers in dye-sensitised solar cells (DSSCs) have also been prepared ([**71**]; Figure 1.13).[300]

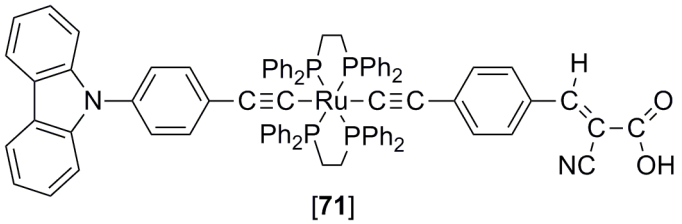

[**71**]

Figure 1.13: Complex [**71**] is proposed to operate as a photo-sensitiser in a DSSC, featuring a terminal carboxylic acid group for effective binding to TiO_2 surfaces.[300]

The UV-Vis spectrum of [**71**] revealed an intense broad absorption band at λ_{max} = 520 nm (ε = 30 600 $M^{-1}cm^{-1}$), corresponding to a HOMO-LUMO (MLCT-type) transition. Compared with the purely organic analogue (λ_{max} = 374 nm; ε = 12 300 $M^{-1}cm^{-1}$),[301] the electronic absorption profile is red-shifted and of higher intensity, endorsing the integration of {Ru(dppe)$_2$} units as a *via*ble design strategy. A single, reversible one-electron oxidation is found for [**71**] at 0.60 V. Consequently, the HOMO position is anticipated to favour effective redox-shuttle processes with iodine (where the $[I]^{3-}$ / $[I]^-$ couple is determined at ~ 0.45 V) during oxidised dye regeneration in the operational cell. The LUMO position (− 1.37 V), deduced from the HOMO position and optical band gap, is higher than the conduction band of TiO_2, permitting charge injection from the oxidised dye to the semi-conductor. After grafting molecules to thin TiO_2 films, forming [**71′**], UV-Vis bands are blue shifted by ~ 50 nm; attributed to either the deprotonation of the terminal carboxylic acid group or dye aggregation. Surface ATR-FTIR experiments on [**71′**] confirmed anchoring of ruthenium molecules *via* the carboxylic acid group, determined from the absence of ν(C=O) at 1713 cm^{-1}. The presence of $\nu(COO^-)$ at 1575 and 1360 cm^{-1}, indicated linkage through bidentate chelation (binding to one titanium atom) or bridging mode (binding to two titanium atoms). Following integration of [**71**] within a DSSC, a power conversion efficiency of 7.32 % was obtained; the highest value for an organometallic photo-sensitiser bearing alkynyl units to date.

Colombo and Biagini have also investigated 'asymmetric' *trans*-bis(alkynyl) {Ru(dppe)$_2$} complexes as candidates for photo-sensitisers within DSSCs ([**72, 73**]; Figure 1.14).[302] In contrast, power conversion efficiencies of [**72, 73**] (0.3 – 1.5 %) were significantly lower than the benchmark ruthenium dye, **N719** (8.1 %) as a result of

narrower absorption profiles and favorable charge-recombination processes, highlighting the importance of functional group selection.

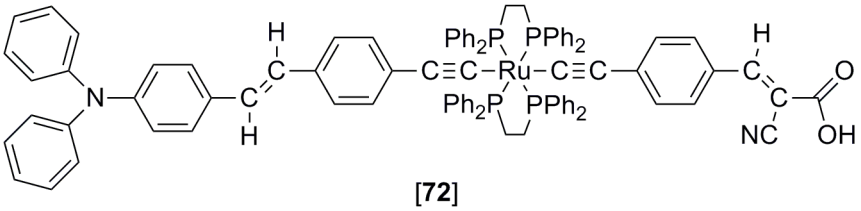

[**72**]

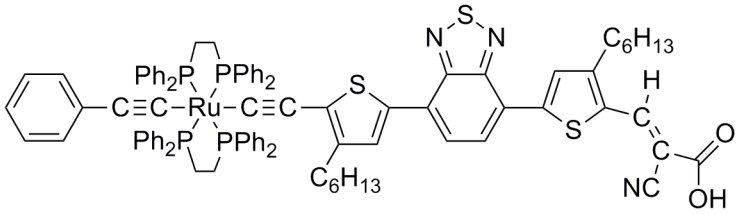

[**73**]

Figure 1.14: Complexes [**72, 73**] are proposed to operate as photo-sensitisers within DSSCs.[302]

1.4.3. Non-linear optics

As {ClRu(dppm)$_2$} and {ClRu(dppe)$_2$} are both good donor fragments and both {Ru(dppm)$_2$} and {Ru(dppe)$_2$} motifs readily facilitate the formation of highly conjugated / delocalised *trans*-bis(alkynyl) complexes, there has been much interest in the optical properties of such systems,[231, 303, 304] especially within the area of non-linear optics (NLOs). Given that Humphrey and co-workers have reviewed progress within this field extensively,[305-308] only selected examples will be discussed here for illustrative purposes.

In 1995, Lewis and co-workers found that *mono*-alkynyl {Ru(dppm)$_2$} complexes, *trans*-[RuCl(C≡CC_6H_4-4-R)(dppm)$_2$] containing an electron withdrawing nitro group, R = NO_2, [**23a**], exhibited lower energy ν(C≡C) bands than those bearing electron donating groups (R = H [**23d**], C_6H_5, Me [**23e**]), evincing a donor-acceptor relationship.[309] In the following year, Humphrey made a similar observation with *trans*-[RuCl(C≡CC_6H_4-4-R)(dppm)$_2$] (R = NO_2 [**23a**], H [**23d**], C_6H_4-4-NO_2, CH=CHC_6H_4-4-

NO_2) complexes.[156] Calculated quadratic optical non-linearities were found to be higher for *mono*-alkynyl complexes with electron withdrawing groups in addition with complexes bearing extended unsaturated ligands and where the relative orientation of the aryl fragment favours π-conjugation, hence establishing a design strategy for future molecules tailored for NLO application. Since these important discoveries, the optical properties of a plethora of linear, one-dimensional, metal acetylide complexes have been explored.[128, 216, 310-312]

Higher molecular architectures, such as dendritic molecules, have also received attention within this field, exhibiting strong NLO activity. Although *"the differences in optical nonlinearities on replacing bidentate diphosphine* [replacing {Ru(dppe)$_2$} with {Ru(dppm)$_2$}] *are minor"*,[313] {Ru(dppe)$_2$} is a more appropriate fragment to employ than {Ru(dppm)$_2$} on synthetic grounds, given the increased capacity for *trans*-chlorides to be substituted from *mono*-alkynyl complexes of the former than the latter.[207] NLO measurements (Z scan method; 800 nm laser) have been made with both first and second generation organometallic dendrimers, *trans*-[{($C_6H_5C{\equiv}C$)(dppe)$_2$Ru}$_3${μ-C≡CC_6H_4-4-C≡C-1,3,5-C_6H_3(C≡CC_6H_4-4-C≡C-)$_2$}] and *trans*-[{($C_6H_5C{\equiv}C$)(dppe)$_2$Ru(μ-C≡CC_6H_4-4-C≡C)Ru(dppe)}$_3${μ-C≡CC_6H_4-4-C≡C-1,3,5-C_6H_3(C≡CC_6H_4-4-C≡C-)$_2$}].[235] From the first to the second generation dendrimer, there is only a slight blue shift (8 nm) observed in the resultant UV-Vis spectra, hence optical transparency is favourably preserved with increasing dimensionality, while the molar absorptivity constant is increased 4-fold (from $11.6 \times 10^{-4}\ M^{-1}cm^{-1}$ to $4.2 \times 10^{-3}\ M^{-1}cm^{-1}$). Furthermore, a significant increase in the two-photon absorption cross-section value (σ_2) was observed (from $7.0 \pm 1.2 \times 10^{-48}\ cm^4s$ to $4.8 \pm 0.5 \times 10^{-47}\ cm^4s$) evincing the potential for higher molecular weight organometallic dendrimers as efficient two photon absorption complexes within the area of NLOs.

The development of wavelength-tunable lasers has allowed broad spectral range NLO studies (520 nm – 1600 nm; as opposed to single wavelength studies) of first and second generation dendrimers featuring *mono*- and *trans*-bis(alkynyl) {Ru(dppe)$_2$} fragments based on a 1,4-diethylbenzene-1,3,5-benzene core.[314] At wavelengths up to 1000 nm, these complexes are effective two-photon absorption materials ($\sigma_2 = 3.7 \pm 0.8 \times 10^{-48}\ cm^4s$ to $3.5 \pm 0.5 \times 10^{-47}\ cm^4s$). Above 1000 nm, large three-

photon absorption values are obtained (with effective two-photon absorption cross-section values, σ_{2eff}, = $6.5 \pm 2.0 \times 10^{-49}$ cm^4s to $1.4 \pm 0.4 \times 10^{-47}$ cm^4s). Further dendritic complexes studied for NLO activity, bearing $\{Ru(dppe)_2\}$ fragments, have included those based on 1,3,5-triazine;[315] tri(ethynylphenyl)amine[215] in addition to 1,3,5-substituted benzene cores.[234, 237, 240, 242, 316] Although significant progress has been made in this field, research is limited generally by the time-consuming syntheses of the dendrimers.[314]

The NLO activity of zinc tetraphenylporphyrin complexes bearing terminal *trans*-bis(alkynyl) ruthenium fragments, $[\{Zn_{por}\}\{\mu\text{-}(C{\equiv}CC_6H_4\text{-}4\text{-}C{\equiv}C)Ru(dppe)_2(C{\equiv}CC_6H_4\text{-}4\text{-}R)\}_4]$ (R = H [**74**], NO_2 [**75**], OMe [**76**]; Figure 1.15), has also been investigated.[230]

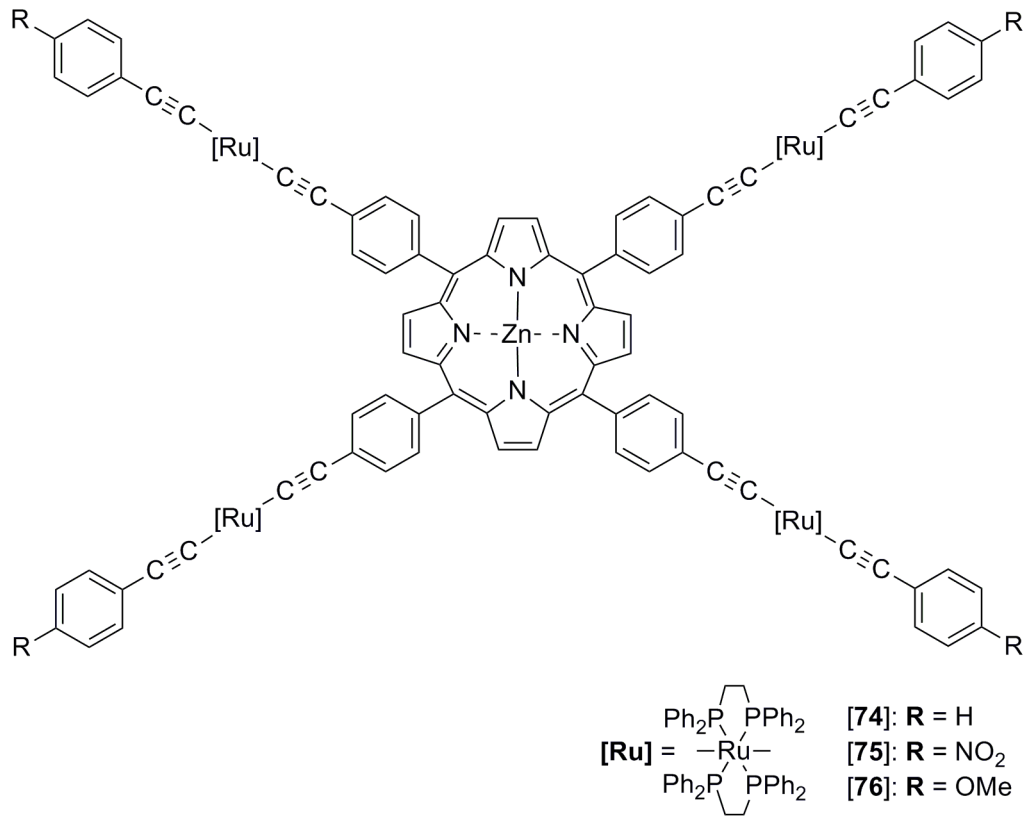

Figure 1.15: Zinc tetraphenylporphyrin complexes [**74** – **76**] bearing terminal *trans*-bis(alkynyl) ruthenium fragments are anticipated to display NLO properties.[230]

The multi-metallic complexes [**74** − **76**] exhibit three oxidations, at ~ 0.45, 0.86 and 1.21 V, in a 4 : 1 : 1 ratio, corresponding to the simultaneous oxidations of the four

independent ruthenium centres followed by sequential oxidations of the zinc-porphyrin core. Compared with [{Zn_{por}}($C{\equiv}CC_6H_4$-4-$C{\equiv}CH)_4$], oxidation of the zinc-porphyrin core, {Zn_{por}}, in [**74 − 76**] is lower (less positive) by ~ 0.05 V reflecting the weakly electron releasing nature of *trans*-bis(alkynyl) {$Ru(dppe)_2$} fragments. In the UV-Vis-NIR spectra, [**74 − 76**] exhibit several bands between 300 – 650 nm. Bands corresponding to the central zinc-porphyrin fragment {Zn_{Por}} are similar in maximum wavelength to [{Zn_{Por}}($C{\equiv}CC_6H_4$-4-$C{\equiv}CH)_4$], with additional bands observed near 330 nm, assigned to Ru(*d*) / C≡C(π*) MLCT transitions. Preliminary NLO measurements (Z scan method; 530 – 1600 nm), revealed that [**74 − 76**] are effective two-photon abortion materials around 1100 nm (σ_2 = 4.2 ± 0.5 × $10^{-47}$$cm^4$s to 6.0 ± 3.0 × $10^{-47}$$cm^4$s) and 710 nm ($\sigma_2$ = 1.3 ± 0.1 × $10^{-47}$$cm^4$s to 1.5 ± 0.5 $10^{-47}$$cm^4$s).

Humphrey has further demonstrated the capacity of *trans*-[$RuCl(C{\equiv}CC_6H_4$-4-R)$(dppe)_2$] (R = H, [**37**]; $C{\equiv}CC_6H_5$, [**77**]) and *trans*-[$Ru(C{\equiv}CC_6H_5)(C{\equiv}CC_6H_4$-4-R)$(dppe)_2$] (R = H, [**13**]; $C{\equiv}CC_6H_5$, [**78**]) complexes to operate as NLO electrochromic switches.[7, 313] Complexes [**13, 37, 77, 78**] exhibit a single reversible to *quasi*-reversible oxidation (i_{pa} / i_{pc} = 0.9 – 1.0) between 0.55 − 0.60 V, which was assigned to the [Ru^{II}] / [Ru^{III}] couple, although DFT calculations suggest an appreciable degree of Ru(*d*) / C≡C(π) mixing occurs in the oxidation event. In the UV-Vis-NIR spectra, neutral complexes, [**13, 37, 77, 78**], are featureless in the NIR region (< 20 000 cm^{-1}) whereas *mono*-oxidised complexes, [**13, 37, 77, 78**]$^+$, display intense bands (where ε is within the range 2 × 10^3 $M^{-1}cm^{-1}$ to 3.6 × 10^4 $M^{-1}cm^{-1}$), which have been assigned to the promotion of an electron from C≡C(π) to the partially occupied HOMO. As a result, optical transitions are 'switched-on' following oxidation at a low potential. NLO studies (Z scan method; 800 nm laser) show an increase in the two-photon absorption cross-section values (σ_2) from the neutral complexes ([**77**]: σ_2 = − 5.4 ± 2 ×10^{-48} cm^4s and [**78**]: σ_2 = − 3.0 ± 0.7 ×10^{-48} cm^4s) to the *mono*-oxidised complexes ([**77**]$^+$: σ_2 = 1.1 ± 0.5 ×10^{-48} cm^4s and [**78**]$^+$: 3.1 ± 0.7 ×10^{-48} cm^4s). Several further examples of NLO switches have been reported by Humphrey and co-workers.[217, 242, 317]

1.4.4. Sensors

The superior frontier orbital matching between Ru(*d*) / C≡C(π) fragments results in efficient through-charge transfer between remote groups and the metal, forming highly conjugated molecules. Consequently, optical profiles of ruthenium acetylide complexes are highly sensitive to changes on both electronic and geometric grounds, leading to application as sensors. Furthermore, optical spectra of organometallic complexes commonly extend into the useful visible spectral region, allowing for rapid naked-eye detection. As the area is still in its infancy there are only few reports in the literature, especially bearing the {Ru(dppe)$_2$} motif.

In 2005, Fillaut reported the first instance of a {Ru(dppe)$_2$} acetylide complex to show sensory application, through colorimetric recognition.[318] The optical spectra of complexes bearing fragments based on thiazolidinedione, rhodanine and 6-hydroxyuracil moieties ([**79** − **81**]; Figure 1.16) were changed after exposure to low analyte concentrations of fluoride (F^-), acetate ($[OAc]^-$) and phosphate ($[H_2PO_4]^-$) anions. Guests are bound to the host through H-bonding interactions.

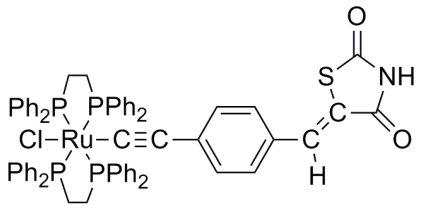

[**79**]

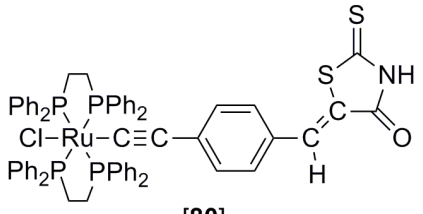

[**80**]

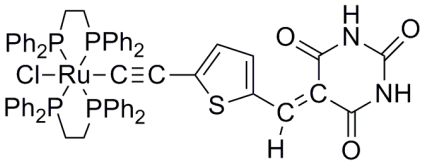

[**81**]

Figure 1.16: Complexes [**79** − **81**] studied for anion recognition.[318]

Complex [**79**] (λ_{max} = 490 nm, $\varepsilon = 2.5 \times 10^4$ $M^{-1}cm^{-1}$) underwent an identical colour change (λ_{max} = 415 nm, $\varepsilon = 2.3 \times 10^4$ $M^{-1}cm^{-1}$) upon addition of either $[F]^-$ (6 equiv.) or $[OAc]^-$ (10 equiv.). Similarly, [**80**] (λ_{max} = 550 nm, $\varepsilon = 2.6 \times 10^4$ $M^{-1}cm^{-1}$) does not show selectivity between these two anions, although does display heightened sensitivity as a lower anion equivalent (2 equiv.) is required to complete the colour change (λ_{max} = 465 nm, $\varepsilon = 2.2 \times 10^4$ $M^{-1}cm^{-1}$). In contrast, [**81**] (λ_{max} = 590 nm, $\varepsilon = 4.0 \times 10^4$ $M^{-1}cm^{-1}$) displays both high selectivity and sensitivity towards F^-, exhibiting a full colour change (λ_{max} = 480 nm, $\varepsilon = 2.6 \times 10^4$ $M^{-1}cm^{-1}$) after only a four-fold addition of the anion, whereas $[AcO]^-$ and $[H_2PO_4]^-$ required significantly larger concentrations (260 and 1000 equiv. respectively) to achieve the same effect. Complex [**81**] has two potential (-NH) binding sites. Calculated equilibrium constants for initial anion binding with [**81**] were comparable (log $K_1 \approx 4$) for all three anions, however were notably different for binding the second, indicating that the observed differences of [**81**] (*vs.* [**79, 80**]) are a result of electronic changes imposed after initial complexation. Binding a second $[AcO]^-$ or $[H_2PO_4]^-$ molecule is disfavoured by electrostatic interactions and instead favoured for F^- forming strong H-bond interactions with the available -NH binding site. Displacement of the bound anion can be achieved with the addition of water in all three cases, and the original spectra recovered. A more detailed study of these complexes was given by the authors several years later.[319]

Fillaut has also reported a *mono*-alkynyl {$Ru(dppe)_2$} complex bearing a hydroxyflavone unit as a potential sensor for heavy metals ions ([**82**]$^+$; Figure 1.17).[320]

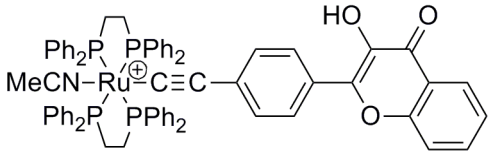

[**82**]$^+$

Figure 1.17: Complex [**82**]$^+$ studied for heavy metal ion recognition, as reported by Fillaut.[320]

The UV-Vis-NIR spectrum of [**82**]$^+$ reveals a strong MLCT band (λ_{max} = 405 nm, $\varepsilon = 2.9 \times 10^4$ $M^{-1}cm^{-1}$). After excitation of [**82**]$^+$ (at 400 nm), luminescence is observed (λ_{max} = 560 nm, ϕ = quantum yield of emission = 0.016, $^1\tau$ = singlet lifetime = 2.1 ns).

The fluorescence emission arises from a singlet state of the flavonol fragment, which is decoupled from the metal centre in the excited state. Given that the addition of M^{n+} (Li^{+}, Na^{+}, Ba^{2+}, Ca^{2+}, Cd^{2+}, Mg^{2+}, Co^{2+}, Cr^{2+}, Ni^{2+}, Zn^{2+} and Pb^{2+} as perchlorate salts) to acetonitrile solutions of [**82**]$^{+}$ had no noticeable effect on the original absorption spectrum, the optical effect following UV irradiation (λ_{max} = 365 nm) of the M^{n+} containing solutions was investigated. In general, the resultant absorption and emission spectra were unchanged from standard [**82**]$^{+}$ solutions. However, for Pd^{2+} containing solutions, both the absorption (λ_{max} = 465 nm) and florescence (λ_{max} = 605 nm, ϕ = 0.0083, $^{1}\tau$ = < 1 ns) spectra were notably different; hence [**82**]$^{+}$ shows strong potential as an efficient Pd^{2+} sensor. The Pd^{2+} ion is bound in a 1 : 1 stoichiometry to the terminal hydroxyl of the flavone unit.

The capacity for a supramolecular, *mono*-alkynyl {$Ru(dppe)_2$} complex to operate as a sensor for nitroaromatics ([**83** / **84** / **83**]; Scheme 1.30) has also been described.[245]

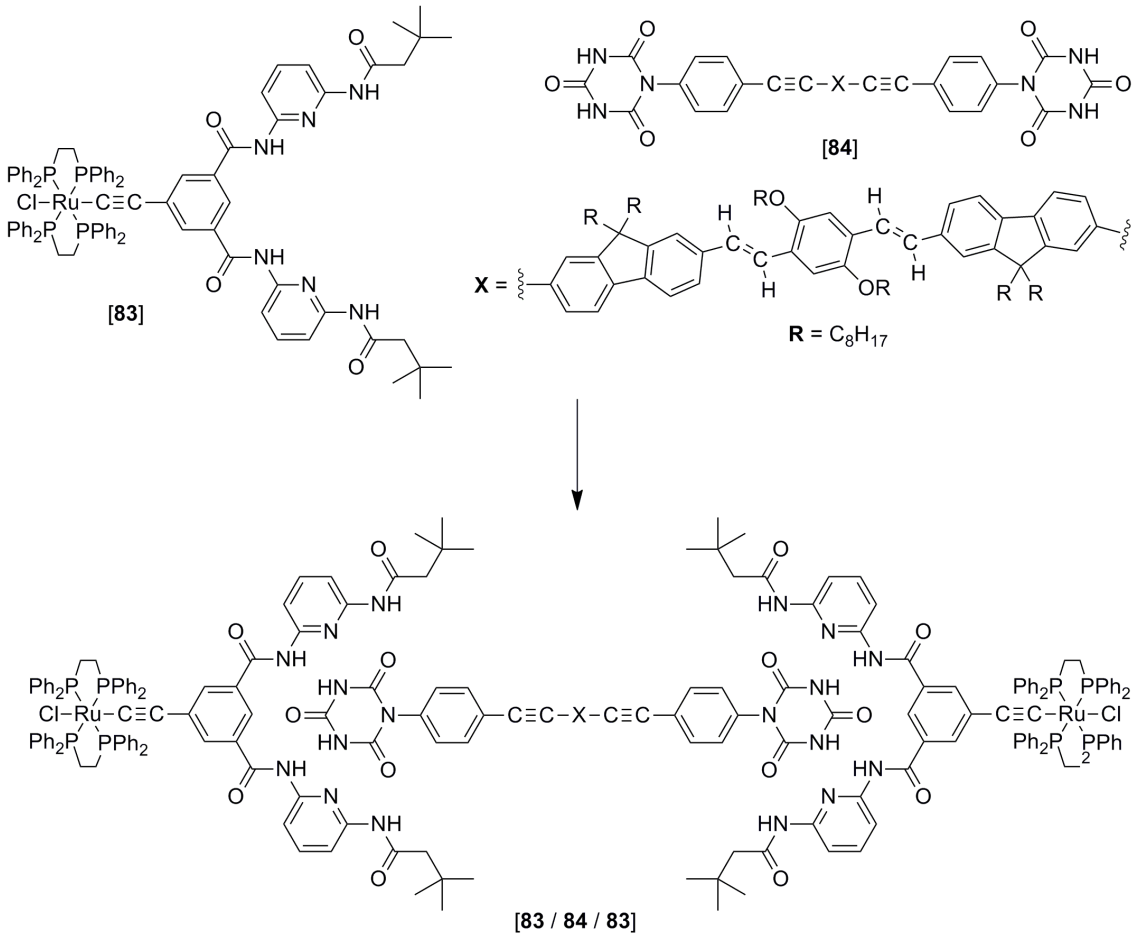

Scheme 1.30: The responsiveness of the supramolecular complex, [**83** / **84** / **83**], towards nitroaromatics has been studied by Fillaut.[245]

Between [**83** / **84** / **83**], and the free organic fluorophore [**84**], selectivity towards the detection of general aromatic and aliphatic complexes is similar. In addition, the efficiency of fluorescence quenching by (responsiveness towards) nitroaromatics, such as 2,4-dinitrotoluene (DNT), is similar, as determined from Stern-Volmer plots. Consequently, complexation of terminal ruthenium [**83**] fragments to the organic fluorophore [**84**] (*i.e.* formation of [**83** / **84** / **83**]) is not shown to affect the π-π interaction between the electron-deficient nitroaromatic and electron rich [**84**].

1.4.5. Nanocars

Molecular architectures featuring the {Ru(dppe)$_2$} motif also include the formation of a whimsical molecular 'Nanocar' ([**85**]; Figure 1.18). Vives and Tour have proposed the

conceptually appealing model that the bulky phosphine ancillary ligands can potentially serve as surrogate molecular tyres, when bound to a rigid organic core (chassis), where the rolling motion of the molecular car along a surface (as opposed to sliding) depends on the low rotation barrier of the alkyne to metal bond and good physisorption to the surface.[321] The proposal for rotation of the *trans*-bis(alkynyl) {Ru(dppe)$_2$} 'tyres' resonates with previous discussions concerning the spectroscopically observed distribution of conformers in solution.

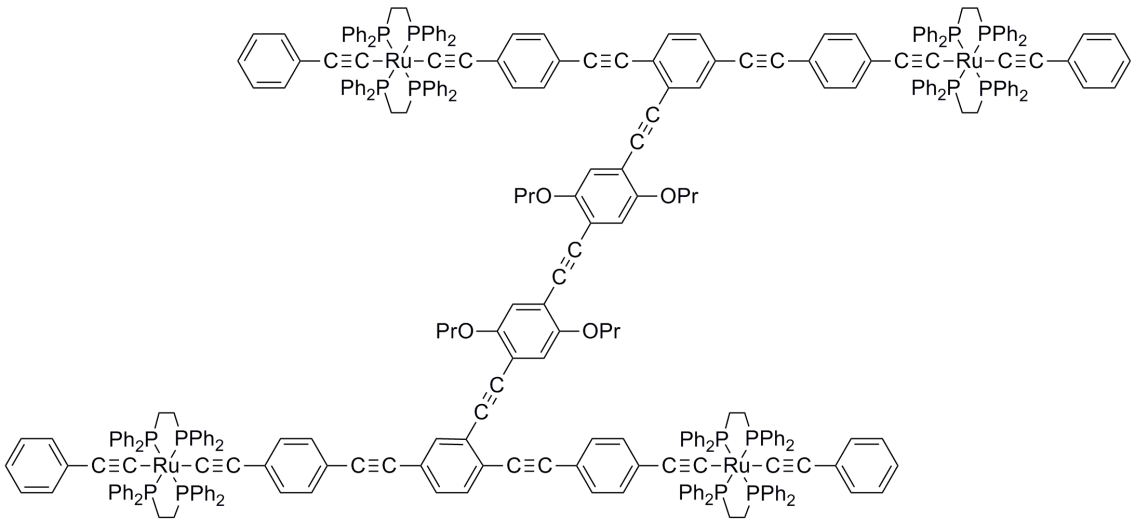

[**85**]

Figure 1.18: Formation of a Nanocar, [**85**], featuring {Ru(dppe)$_2$} fragments as molecular tyres.[321]

1.5. Summary and Thesis outlook

The catalyst for the plethora of research on *trans*-bis(alkynyl) complexes can be attributed to the initial discovery of highly conjugated, rigid and *soluble* platinum polymers, by Hagihara and co-workers in 1977.[100] From this point, after overcoming many synthetic challenges, several further linear main chain metallopolymers with structural modifications were developed, where changes in the metal centre, ancillary ligands and linker fragments provided strong foundations to understand the role of these fragments on electronic transport. In turn, research of metallopolymers then migrated towards the study of the *mono*- and multi-metallic comprising fragments, offering much more by way of molecular design and as such, the anticipated material properties. Great efforts are being made by the scientific community to exploit such novel properties, with the corresponding number of current and potential applications growing, serving to highlight the importance of continued research within this area. However, formation of intricate architectures is not without synthetic obstacles. Although many have been circumvented or overcome, several are still evident.

The overarching focus for this Thesis is to explore the role of the ancillary ligands (specifically $(dppm)_2$, $(dppe)_2$ and $\{P(OEt)_3\}_4$) with regards to the synthesis, electronic structure and charge transfer (in both solution and solid state) of *trans*-bis(alkynyl) ruthenium complexes. The following body of work will commence by highlighting, addressing, and in some cases overcoming, a few of the major synthetic challenges encountered with *trans*-bis(alkynyl) $\{Ru(dppm)_2\}$ complexes, which have contributed to their declining prevalence within this field (Chapters 2 – 3). Subsequently, the effect of multiple-metal integration along a conjugated wire backbone on the underlying electronic structure will be investigated for related *trans*-bis(alkynyl) $\{Ru(dppe)_2\}$ complexes (Chapter 4). Finally, this Thesis will investigate relatively unexplored *trans*-bis(alkynyl) *tetrakis*-triethylphosphite complexes, and their capacity to operate as superior organometallic wires (Chapter 5). The experimental techniques of spectroscopy, single crystal X-ray diffractometry, cyclic voltammetry and spectroelectrochemistry are relied upon heavily in order to explore and optimise synthetic transformations and investigate the underlying electronic structures of *trans*-bis(alkynyl) ruthenium complexes, with support from quantum chemical calculations.

1.6. References

1. J. Manna, K. D. John and M. D. Hopkins, *Adv. Organomet. Chem.*, **1995**, *38*, 79.
2. Y. Wakatsuki, H. Yamazaki, N. Kumegawa, T. Satoh and J. Y. Satoh, *J. Am. Chem. Soc.*, **1991**, *113*, 9604.
3. I. de los Ríos, M. J. Tenorio, M. C. Puerta and P. Valerga, *J. Am. Chem. Soc.*, **1997**, *119*, 6529.
4. E. Peréz-Carreño, P. Paoli, A. Ienco and C. Mealli, *Eur. J. Inorg. Chem.*, **1999**, *1999*, 1315.
5. C. Bianchini, M. Peruzzini, F. Zanobini, P. Frediani and A. Albinati, *J. Am. Chem. Soc.*, **1991**, *113*, 5453.
6. C. Bianchini, P. Frediani, D. Masi, M. Peruzzini and F. Zanobini, *Organometallics*, **1994**, *13*, 4616.
7. C. E. Powell, M. P. Cifuentes, J. P. Morrall, R. Stranger, M. G. Humphrey, M. Samoc, B. Luther-Davies and G. A. Heath, *J. Am. Chem. Soc.*, **2003**, *125*, 602.
8. I. R. Whittall, M. G. Humphrey, M. Samoc, B. Luther-Davies and D. C. R. Hockless, *J. Organomet. Chem.*, **1997**, *544*, 189.
9. C. E. Powell, M. P. Cifuentes, A. M. McDonagh, S. K. Hurst, N. T. Lucas, C. D. Delfs, R. Stranger, M. G. Humphrey, S. Houbrechts, I. Asselberghs, A. Persoons and D. C. R. Hockless, *Inorg. Chim. Acta*, **2003**, *352*, 9.
10. S. K. Hurst, M. P. Cifuentes, J. P. L. Morrall, N. T. Lucas, I. R. Whittall, M. G. Humphrey, I. Asselberghs, A. Persoons, M. Samoc, B. Luther-Davies and A. C. Willis, *Organometallics*, **2001**, *20*, 4664.
11. G. Frapper and M. Kertesz, *Inorg. Chem.*, **1993**, *32*, 732.
12. M. S. Khan, A. K. Kakkar, S. L. Ingham, P. R. Raithby, J. Lewis, B. Spencer, F. Wittmann and R. H. Friend, *J. Organomet. Chem.*, **1994**, *472*, 247.
13. Y. Sun, N. J. Taylor and A. J. Carty, *Organometallics*, **1992**, *11*, 4293.
14. S. Kubatkin, A. Danilov, M. Hjort, J. Cornil, J. L. Bredas, N. Stuhr-Hansen, P. Hedegard and T. Bjornholm, *Nature*, **2003**, *425*, 698.
15. H. D. Sikes, J. F. Smalley, S. P. Dudek, A. R. Cook, M. D. Newton, C. E. D. Chidsey and S. W. Feldberg, *Science*, **2001**, *291*, 1519.
16. M. T. González, X. Zhao, D. Z. Manrique, D. Miguel, E. Leary, M. Gulcur, A. S. Batsanov, G. Rubio-Bollinger, C. J. Lambert, M. R. Bryce and N. Agraït, *J. Phys. Chem. C*, **2014**, *118*, 21655.
17. C. Wang, A. S. Batsanov, M. R. Bryce, S. Martín, R. J. Nichols, S. J. Higgins, V. M. García-Suárez and C. J. Lambert, *J. Am. Chem. Soc.*, **2009**, *131*, 15647.
18. T. Otsubo, Y. Aso and K. Takimiya, *J. Mater. Chem.*, **2002**, *12*, 2565.
19. E. A. Weiss, M. J. Ahrens, L. E. Sinks, A. V. Gusev, M. A. Ratner and M. R. Wasielewski, *J. Am. Chem. Soc.*, **2004**, *126*, 5577.
20. M. I. Bruce, P. J. Low, K. Costuas, J.-F. Halet, S. P. Best and G. A. Heath, *J. Am. Chem. Soc.*, **2000**, *122*, 1949.
21. J. E. McGrady, T. Lovell, R. Stranger and M. G. Humphrey, *Organometallics*, **1997**, *16*, 4004.
22. P. J. Low, *Dalton Trans.*, **2005**, 2821.
23. R. Nast, *Coord. Chem. Rev.*, **1982**, *47*, 89.
24. M. Akita and Y. Morooka, *B. Chem. Soc. Jpn.*, **1995**, *68*, 420.
25. M. Akita, A. Sakurai, M.-C. Chung and Y. Morooka, *J. Organomet. Chem.*, **2003**, *670*, 2.

26. C. S. Griffith, G. A. Koutsantonis, B. W. Skelton and A. H. White, *J. Organomet. Chem.*, **2003**, *670*, 198.
27. U. Rosenthal, *Angew. Chem. Int. Ed. Engl.*, **2003**, *42*, 1794.
28. C. S. Griffith, G. A. Koutsantonis, B. W. Skelton and A. H. White, *Chem. Commun.*, **2002**, 2174.
29. M. Akita, M.-C. Chung, M. Terada, M. Miyauti, M. Tanaka and Y. Morooka, *J. Organomet. Chem.*, **1998**, *565*, 49.
30. J. Becica, A. B. Jackson, W. G. Dougherty, W. S. Kassel and N. M. West, *Dalton Trans.*, **2014**, *43*, 8738.
31. O. Schuster, R.-Y. Liau, A. Schier and H. Schmidbaur, *Inorg. Chim. Acta*, **2005**, *358*, 1429.
32. H. Werner, M. Meyer, M. A. Esteruelas, E. Sola and L. A. Oro, *J. Organomet. Chem.*, **1989**, *366*, 187.
33. G. Albertin, S. Autoniutti, E. Bordignon, F. Cazzaro, S. Ianelli and G. Pelizzi, *Organometallics*, **1995**, *14*, 4114.
34. M. I. Bruce and R. C. Wallis, *J. Organomet. Chem.*, **1978**, *161*, C1.
35. P. Haquette, N. Pirio, D. Touchard, L. Toupet and P. H. Dixneuf, *J. Chem. Soc., Chem. Commun.*, **1993**, 163.
36. D. Touchard, P. Haquette, S. Guesmi, L. Le Pichon, A. Daridor, L. Toupet and P. H. Dixneuf, *Organometallics*, **1997**, *16*, 3640.
37. M. I. Bruce, M. G. Humphrey, J. G. Matisons, S. K. Roy and A. G. Swincer, *Aust. J. Chem.*, **1984**, *37*, 1955.
38. K. Sonogashira, Y. Fujikura, T. Yatake, N. Toyoshima, S. Takahashi and N. Hagihara, *J. Organomet. Chem.*, **1978**, *145*, 101.
39. K. Sonogashira, K. Ohga, S. Takahashi and N. Hagihara, *J. Organomet. Chem.*, **1980**, *188*, 237.
40. C. W. Faulkner, S. L. Ingham, M. S. Khan, J. Lewis, N. J. Long and P. R. Raithby, *J. Organomet. Chem.*, **1994**, *482*, 139.
41. Z. Atherton, C. W. Faulkner, S. L. Ingham, A. K. Kakkar, M. S. Khan, J. Lewis, N. J. Long and P. R. Raithby, *J. Organomet. Chem.*, **1993**, *462*, 265.
42. M. S. Khan, S. J. Davies, A. K. Kakkar, D. Schwartz, B. Lin, B. F. G. Johnson and J. Lewis, *J. Organomet. Chem.*, **1992**, *424*, 87.
43. W. M. Khairul, M. A. Fox, N. N. Zaitseva, M. Gaudio, D. S. Yufit, B. W. Skelton, A. H. White, J. A. K. Howard, M. I. Bruce and P. J. Low, *Dalton Trans.*, **2009**, 610.
44. M. I. Bruce, N. Scoleri and B. W. Skelton, *J. Organomet. Chem.*, **2011**, *696*, 3473.
45. R. L. Cordiner, D. Corcoran, D. S. Yufit, A. E. Goeta, J. A. K. Howard and P. J. Low, *Dalton Trans.*, **2003**, 3541.
46. F. Paul, B. G. Ellis, M. I. Bruce, L. Toupet, T. Roisnel, K. Costuas, J.-F. Halet and C. Lapinte, *Organometallics*, **2006**, *25*, 649.
47. R. Denis, L. Toupet, F. Paul and C. Lapinte, *Organometallics*, **2000**, *19*, 4240.
48. F. S. Arimoto and A. C. Haven, *J. Am. Chem. Soc.*, **1955**, *77*, 6295.
49. E. M. Natanson and T. B. Mikhail, *Russ. Chem. Rev.*, **1972**, *41*, 671.
50. J.-C. Eloi, L. Chabanne, G. R. Whittell and I. Manners, *Mater. Today*, **2008**, *11*, 28.
51. J. M. Stanley and B. J. Holliday, *Coord. Chem. Rev.*, **2012**, *256*, 1520.
52. B. J. Holliday and T. M. Swager, *Chem. Commun.*, **2005**, 23.
53. G. R. Whittell, M. D. Hager, U. S. Schubert and I. Manners, *Nat. Mater.*, **2011**, *10*, 176.

54. D. Asil, J. A. Foster, A. Patra, X. de Hatten, J. del Barrio, O. A. Scherman, J. R. Nitschke and R. H. Friend, *Angew. Chem. Int. Ed. Engl.*, **2014**, *53*, 8388.
55. X. de Hatten, D. Asil, R. H. Friend and J. R. Nitschke, *J. Am. Chem. Soc.*, **2012**, *134*, 19170.
56. X. de Hatten, N. Bell, N. Yufa, G. Christmann and J. R. Nitschke, *J. Am. Chem. Soc.*, **2011**, *133*, 3158.
57. B. E. R. Schilling, R. Hoffmann and D. L. Lichtenberger, *J. Am. Chem. Soc.*, **1979**, *101*, 585.
58. A. Ionescu, R. Lento, T. F. Mastropietro, I. Aiello, R. Termine, A. Golemme, M. Ghedini, N. Bellec, E. Pini, I. Rimoldi and N. Godbert, *ACS Appl. Mater. Inter.*, **2015**, *7*, 4019.
59. X.-Y. Chen, X. Yang and B. J. Holliday, *J. Am. Chem. Soc.*, **2008**, *130*, 1546.
60. D. Wang, J. Zhang, Q. Lin, L. Fu, H. Zhang and B. Yang, *J. Mater. Chem.*, **2003**, *13*, 2279.
61. L. Li, W.-C. Chow, W.-Y. Wong, C.-H. Chui and R. S.-M. Wong, *J. Organomet. Chem.*, **2011**, *696*, 1189.
62. A. G. Tennyson, L. Do, R. C. Smith and S. J. Lippard, *Polyhedron*, **2007**, *26*, 4625.
63. R. C. Smith, A. G. Tennyson, A. C. Won and S. J. Lippard, *Inorg. Chem.*, **2006**, *45*, 9367.
64. J. F. Rusling and R. J. Forster, *J. Colloid Interf. Sci.*, **2003**, *262*, 1.
65. L. Zhou and J. F. Rusling, *Anal. Chem.*, **2001**, *73*, 4780.
66. P. Scrimin, P. Tecilla and U. Tonellato, *Eur. J. Org. Chem.*, **1998**, *1998*, 1143.
67. J. F. Rusling, E. G. Hvastkovs, D. O. Hull and J. B. Schenkman, *Chem. Commun.*, **2008**, 141.
68. L. Dennany, R. J. Forster and J. F. Rusling, *J. Am. Chem. Soc.*, **2003**, *125*, 5213.
69. A. I. Hanafy, V. Lykourinou-Tibbs, K. S. Bisht and L.-J. Ming, *Inorg. Chim. Acta*, **2005**, *358*, 1247.
70. B. Wang, S. Brown and J. F. Rusling, *Electroanal.*, **2005**, *17*, 1601.
71. K. R. Edelman, K. J. Stevenson and B. J. Holliday, *Macromol. Rapid Commun.*, **2012**, *33*, 610.
72. S. S. Zhu and T. M. Swager, *J. Am. Chem. Soc.*, **1997**, *119*, 12568.
73. L. Yan, Y. Zhao, X. Wang, X.-Z. Wang, W.-Y. Wong, Y. Liu, W. Wu, Q. Xiao, G. Wang, X. Zhou, W. Zeng, C. Li, X. Wang and H. Wu, *Macromol. Rapid Commun.*, **2012**, *33*, 603.
74. J. Hjelm, R. W. Handel, A. Hagfeldt, E. C. Constable, C. E. Housecroft and R. J. Forster, *Electrochem. Commun.*, **2004**, *6*, 193.
75. Q. Dong, G. Li, C.-L. Ho, C.-W. Leung, P. W.-T. Pong, I. Manners and W.-Y. Wong, *Adv. Funct. Mater.*, **2014**, *24*, 857.
76. T.-L. Choi, K.-H. Lee, W.-J. Joo, S. Lee, T.-W. Lee and M. Y. Chae, *J. Am. Chem. Soc.*, **2007**, *129*, 9842.
77. Q. Ling, Y. Song, S. J. Ding, C. Zhu, D. S. H. Chan, D. L. Kwong, E. T. Kang and K. G. Neoh, *Adv. Mater.*, **2005**, *17*, 455.
78. A. C. Jackson, F. L. Beyer, S. C. Price, B. C. Rinderspacher and R. H. Lambeth, *Macromol.*, **2013**, *46*, 5416.
79. Y.-T. Li, W. Sun, Z.-Y. Wu, Y.-J. Zheng and C.-W. Yan, *J. Inorg. Organomet. Polym. Mater.*, **2010**, *20*, 586.
80. M. S. A. Begum, U. Flörke and G. Henkel, *Inorg. Chim. Acta*, **2010**, *363*, 2144.
81. C. M. Fitchett and P. J. Steel, *New J. Chem.*, **2000**, *24*, 945.

82. M. Burnworth, L. Tang, J. R. Kumpfer, A. J. Duncan, F. L. Beyer, G. L. Fiore, S. J. Rowan and C. Weder, *Nature*, **2011**, *472*, 334.
83. F. Pammer, R. A. Lalancette and F. Jäkle, *Chem. Eur. J.*, **2011**, *17*, 11280.
84. B. Djukic, T. Seda, S. I. Gorelsky, A. J. Lough and M. T. Lemaire, *Inorg. Chem.*, **2011**, *50*, 7334.
85. S. Taheri, A. Mojidov and A. Morsali, *Z. Anorg. Allg. Chem.*, **2007**, *633*, 1949.
86. L. Hashemi, A. Morsali and S. W. Joo, *Dalton Trans.*, **2014**, *43*, 1489.
87. P. Nguyen, P. Gómez-Elipe and I. Manners, *Chem. Rev.*, **1999**, *99*, 1515.
88. C. G. Hardy, J. Zhang, Y. Yan, L. Ren and C. Tang, *Prog. Polym. Sci.*, **2014**, *39*, 1742.
89. D. G. Kurth and M. Higuchi, *Soft Matter*, **2006**, *2*, 915.
90. D. Knapton, S. J. Rowan and C. Weder, *Macromol.*, **2006**, *39*, 651.
91. C.-F. Chow, S. Fujii and J.-M. Lehn, *Angew. Chem. Int. Edit.*, **2007**, *119*, 5095.
92. E. W. Neuse, *Nature*, **1964**, *204*, 179.
93. E. W. Neuse and K. Koda, *J. Organomet. Chem.*, **1965**, *4*, 475.
94. E. W. Neuse and K. Koda, *B. Chem. Soc. Jpn.*, **1966**, *39*, 1502.
95. C. U. Pittman, *J. Polym. Sci. A Polym. Chem.*, **1967**, *5*, 2927.
96. S. L. Sosin, V. P. Alexeeva and V. V. Korshak, *Dokl. Akad. Nauk SSSR*, **1963**, *149*, 327.
97. E. W. Neuse and H. Rosenberg, *J. Macromol. Sci. C*, **1970**, *4*, 1.
98. C. U. Pittman, J. C. Lai, D. P. Vanderpool, M. Good and R. Prado, *Macromol.*, **1970**, *3*, 746.
99. W. J. Patterson, S. P. McManus and C. U. Pittman, *J. Polym. Sci. A Polym. Chem.*, **1974**, *12*, 837.
100. K. Sonogashira, S. Takahashi and N. Hagihara, *Macromol.*, **1977**, *10*, 879.
101. K. Sonogashira, S. Kataoka, S. Takahashi and N. Hagihara, *J. Organomet. Chem.*, **1978**, *160*, 319.
102. S. Takahashi, M. Kariya, T. Yatake, K. Sonogashira and N. Hagihara, *Macromol.*, **1978**, *11*, 1063.
103. S. Guha, C. C. Frazier, P. L. Porter, K. Kang and S. E. Finberg, *Opt. Lett.*, **1989**, *14*, 952.
104. S. Takahashi, Y. Takai, H. Morimoto and K. Sonogashira, *J. Chem. Soc., Chem. Commun.*, **1984**, 3.
105. M. Motowoka, T. Norisuye, A. Teramoto and H. Fujita, *Polym. J.*, **1979**, *11*, 665.
106. S. Takahashi, E. Murata, K. Sonogashira and N. Hagihara, *J. Polym. Sci. A Polym. Chem.*, **1980**, *18*, 661.
107. S. Takahashi, Y. Ohyama, E. Murata, K. Sonogashira and N. Hagihara, *J. Polym. Sci. A Polym. Chem.*, **1980**, *18*, 349.
108. S. J. Davies, B. F. G. Johnson, M. S. Khan and J. Lewis, *J. Chem. Soc., Chem. Commun.*, **1991**, 187.
109. B. F. G. Johnson, A. K. Kakkar, M. S. Khan, J. Lewis, A. E. Dray, R. H. Friend and F. Wittmann, *J. Mater. Chem.*, **1991**, *1*, 485.
110. J. Lewis, M. S. Khan, A. K. Kakkar, B. F. G. Johnson, T. B. Marder, H. B. Fyfe, F. Wittmann, R. H. Friend and A. E. Dray, *J. Organomet. Chem.*, **1992**, *425*, 165.
111. S. J. Davies, B. F. G. Johnson, J. Lewis and P. R. Raithby, *J. Organomet. Chem.*, **1991**, *414*, C51.
112. B. Cetinkaya, M. F. Lappert, J. McMeeking and D. E. Palmer, *J. Chem. Soc., Dalton Trans.*, **1973**, 1202.

113. S. Takahashi, H. Morimoto, E. Murata, S. Kataoka, K. Sonogashira and N. Hagihara, *J. Polym. Sci. A Polym. Chem.*, **1982**, *20*, 565.
114. J. Lewis, M. S. Khan, A. K. Kakkar, B. F. G. Johnson, T. B. Marder, H. B. Fyfe, F. Wittmann, R. H. Friend and A. E. Dray, *J. Organomet. Chem.*, **1992**, *425*, 165.
115. A. E. Dray, F. Wittmann, R. H. Friend, A. M. Donald, M. S. Khan, J. Lewis and B. F. G. Johnson, *Synth. Met.*, **1991**, *41*, 871.
116. K. A. Bunten and A. K. Kakkar, *J. Mater. Chem.*, **1995**, *5*, 2041.
117. M. S. Khan, A. K. Kakkar, N. J. Long, J. Lewis, P. Raithby, P. Nguyen, T. B. Marder, F. Wittmann and R. H. Friend, *J. Mater. Chem.*, **1994**, *4*, 1227.
118. R. D. Markwell, I. S. Butler, A. K. Kakkar, M. S. Khan, Z. H. Al-Zakwani and J. Lewis, *Organometallics*, **1996**, *15*, 2331.
119. M. S. Khan, D. J. Schwartz, N. A. Pasha, A. K. Kakkar, B. Lin, P. R. Raithby and J. Lewis, *Z. Anorg. Allg. Chem.*, **1992**, *616*, 121.
120. H. B. Fyfe, M. Mlekuz, D. Zargarian, N. J. Taylor and T. B. Marder, *J. Chem. Soc., Chem. Commun.*, **1991**, 188.
121. M. S. Khan, N. A. Pasha, A. K. Kakkar, P. R. Raithby, J. Lewis, K. Fuhrmann and R. H. Friend, *J. Mater. Chem.*, **1992**, *2*, 759.
122. B. Giese, M. Zehnder, M. Neuburger and F. Trach, *J. Organomet. Chem.*, **1991**, *412*, 415.
123. B. F. G. Johnson, A. K. Kakkar, M. S. Khan and J. Lewis, *J. Organomet. Chem.*, **1991**, *409*, C12.
124. K. Sonogashira, *J. Organomet. Chem.*, **2002**, *653*, 46.
125. L. D. Field, A. V. George, E. Y. Malouf, I. H. M. Slip and T. W. Hambley, *Organometallics*, **1991**, *10*, 3842.
126. J. F. Almeida and A. Pidcock, *J. Organomet. Chem.*, **1981**, *209*, 415.
127. A. Barlow, B. Babgi, M. Samoc, T. C. Corkery, S. van Cleuvenbergen, I. Asselberghs, K. Clays, M. P. Cifuentes and M. G. Humphrey, *Aust. J. Chem.*, **2012**, *65*, 834.
128. S. K. Hurst, N. T. Lucas, M. G. Humphrey, I. Asselberghs, R. V. Boxel and A. Persoons, *Aust. J. Chem.*, **2001**, *54*, 447.
129. P. Xie, L. Wang, Z. Huang, F. Guo and Q. Jin, *Eur. J. Inorg. Chem.*, **2014**, *2014*, 2544.
130. F. Schwarz, G. Kastlunger, F. Lissel, H. Riel, K. Venkatesan, H. Berke, R. Stadler and E. Lörtscher, *Nano Lett.*, **2014**, *14*, 5932.
131. F. Lissel, T. Fox, O. Blacque, W. Polit, R. F. Winter, K. Venkatesan and H. Berke, *J. Am. Chem. Soc.*, **2013**, *135*, 4051.
132. M. I. Bruce, B. Le Guennic, N. Scoleri, N. N. Zaitseva and J.-F. Halet, *Organometallics*, **2012**, *31*, 4701.
133. T. D. Cook, P. E. Fanwick and T. Ren, *Organometallics*, **2014**, *33*, 4621.
134. V. W.-W. Yam, *Acc. Chem. Res.*, **2002**, *35*, 555.
135. V. W.-W. Yam, V. C. Y. Lau and K.-K. Cheung, *Organometallics*, **1996**, *15*, 1740.
136. V. W.-W. Yam, K.-L. Yu, K. M.-C. Wong and K.-K. Cheung, *Organometallics*, **2001**, *20*, 721.
137. A. Abe, N. Kimura and S. Tabata, *Macromol.*, **1991**, *24*, 6238.
138. F. Camerel, R. Ziessel, B. Donnio, C. Bourgogne, D. Guillon, M. Schmutz, C. Iacovita and J.-P. Bucher, *Angew. Chem. Int. Edit.*, **2007**, *119*, 2713.
139. W. Wu, J. Zhao, J. Sun, L. Huang and X. Yi, *J. Mater. Chem.*, **2013**, *1*, 705.

140. L. Liu, S. Guo, J. Ma, K. Xu, J. Zhao and T. Zhang, *Chem. Eur. J.*, **2014**, *20*, 14282.
141. K. Sonogashira, T. Yatake, Y. Tohda, S. Takahashi and N. Hagihara, *J. Chem. Soc., Chem. Commun.*, **1977**, 291.
142. Y. Fujikura, K. Sonogashira and N. Hagihara, *Chem. Lett.*, **1975**, 1067.
143. A. Sebald, C. Stader, B. Wrackmeyer and W. Bensch, *J. Organomet. Chem.*, **1986**, *311*, 233.
144. G. K. Anderson and G. J. Lumetta, *J. Organomet. Chem.*, **1985**, *295*, 257.
145. M. Suzuki, Y. Kimura and S. Terashima, *Chem. Pharm. Bull.*, **1986**, *34*, 1531.
146. B. Wrackmeyer, *J. Organomet. Chem.*, **1986**, *310*, 151.
147. E.-i. Negishi, K. Akiyoshi and T. Takahashi, *J. Chem. Soc., Chem. Commun.*, **1987**, 477.
148. N. J. Long and C. K. Williams, *Angew. Chem. Int. Edit.*, **2003**, *42*, 2586.
149. K. Costuas and S. Rigaut, *Dalton Trans.*, **2011**, *40*, 5643.
150. P. J. Low, *Coord. Chem. Rev.*, **2013**, *257*, 1507.
151. C.-Y. Wong, C.-M. Che, M. C. W. Chan, J. Han, K.-H. Leung, D. L. Phillips, K.-Y. Wong and N. Zhu, *J. Am. Chem. Soc.*, **2005**, *127*, 13997.
152. H.-M. Wen, Y. Yang, X.-S. Zhou, J.-Y. Liu, D.-B. Zhang, Z.-B. Chen, J.-Y. Wang, Z.-N. Chen and Z.-Q. Tian, *J. Chem. Sci.*, **2013**, *4*, 2471.
153. Y. Sun, N. J. Taylor and A. J. Carty, *J. Organomet. Chem.*, **1992**, *423*, C43.
154. D. Touchard, P. Haquette, N. Pirio, L. Toupet and P. H. Dixneuf, *Organometallics*, **1993**, *12*, 3132.
155. L. D. Field, A. V. George, G. R. Purches and A. H. White, *J. Chem. Soc., Dalton Trans.*, **1996**, 2011.
156. A. M. McDonagh, I. R. Whittall, M. G. Humphrey, B. W. Skelton and A. H. White, *J. Organomet. Chem.*, **1996**, *519*, 229.
157. J. B. G. Gluyas, A. J. Boden, S. G. Eaves, H. Yu and P. J. Low, *Dalton Trans.*, **2014**, *43*, 6291.
158. C. Lebreton, D. Touchard, L. Le Pichon, A. Daridor, L. Toupet and P. H. Dixneuf, *Inorg. Chim. Acta*, **1998**, *272*, 188.
159. C. A. Tolman, *Chem. Rev.*, **1977**, *77*, 313.
160. J. Gotzig, R. Werner and H. Werner, *J. Organomet. Chem.*, **1985**, *290*, 99.
161. T. Rappert and A. Yamamoto, *Organometallics*, **1994**, *13*, 4984.
162. R. A. Jones, G. Wilkinson, I. J. Colquohoun, W. McFarlane, A. M. R. Galas and M. B. Hursthouse, *J. Chem. Soc., Dalton Trans.*, **1980**, 2480.
163. J. F. Hartwig, R. A. Andersen and R. G. Bergman, *J. Am. Chem. Soc.*, **1991**, *113*, 6492.
164. L. D. Field, A. M. Magill, S. J. Dalgarno and P. Jensen, *Eur. J. Inorg. Chem.*, **2008**, 4248.
165. K. McNeill, R. A. Andersen and R. G. Bergman, *J. Am. Chem. Soc.*, **1997**, *119*, 11244.
166. L. D. Field, A. M. Magill and P. Jensen, *Organometallics*, **2008**, *27*, 6539.
167. L. D. Field, A. M. Magill, M. M. Bhadbhade and S. J. Dalgarno, *Organometallics*, **2009**, *28*, 5514.
168. G. Albertin, P. Amendola, S. Antoniutti, S. Ianelli, G. Pelizzi and E. Bordignon, *Organometallics*, **1991**, *10*, 2876.
169. G. Albertin, S. Antoniutti, E. Bordignon and M. Granzotto, *J. Organomet. Chem.*, **1999**, *585*, 83.
170. W. G. Peet, D. H. Gerlach and D. D. Titus, *Inorg. Synth.*, **2007**, *15*, 38.

171. S. Rigaut, K. Costuas, D. Touchard, J.-Y. Saillard, S. Golhen and P. H. Dixneuf, *J. Am. Chem. Soc.*, **2004**, *126*, 4072.
172. E. Wuttke, F. Pevny, Y.-M. Hervault, L. Norel, M. Drescher, R. F. Winter and S. Rigaut, *Inorg. Chem.*, **2012**, *51*, 1902.
173. Y. Liu, C. M. Ndiaye, C. Lagrost, K. Costuas, S. Choua, P. Turek, L. Norel and S. Rigaut, *Inorg. Chem.*, **2014**, *53*, 8172.
174. B. Chaudret, G. Commenges and R. Poilblanc, *J. Chem. Soc., Dalton Trans.*, **1984**, 1635.
175. J. Chatt and R. G. Hayter, *J. Chem. Soc.*, **1961**, 896.
176. B. P. Sullivan and T. J. Meyer, *Inorg. Chem.*, **1982**, *21*, 1037.
177. K. Ouzzine, H. Lebozec and P. H. Dixneuf, *J. Organomet. Chem.*, **1986**, *317*, C25.
178. M. I. Bruce, *Chem. Rev.*, **1998**, *98*, 2797.
179. J. M. Lynam, *Chem. Eur. J.*, **2010**, *16*, 8238.
180. A. M. McDonagh, I. R. Whittall, M. G. Humphrey, D. C. R. Hockless, B. W. Skelton and A. H. White, *J. Organomet. Chem.*, **1996**, *523*, 33.
181. M. C. B. Colbert, J. Lewis, N. J. Long, P. R. Raithby, M. Younus, A. J. P. White, D. J. Williams, N. N. Payne, L. Yellowlees, D. Beljonne, N. Chawdhury and R. H. Friend, *Organometallics*, **1998**, *17*, 3034.
182. M. B. Robin and P. Day, *Adv. Inorg. Chem. Radiochem.*, **1968**, *10*, 422.
183. M. Younus, N. J. Long, P. R. Raithby and J. Lewis, *J. Organomet. Chem.*, **1998**, *570*, 55.
184. M. Parthey, J. B. G. Gluyas, M. A. Fox, P. J. Low and M. Kaupp, *Chem. Eur. J.*, **2014**, *20*, 6895.
185. E. Kulasekera, S. Petrie, R. Stranger, M. P. Cifuentes and M. G. Humphrey, *J. Organomet. Chem.*, **2013**, *748*, 21.
186. J. M. Lynam, T. D. Nixon and A. C. Whitwood, *J. Organomet. Chem.*, **2008**, *693*, 3103.
187. M. Younus, N. J. Long, P. R. Raithby, J. Lewis, N. A. Page, A. J. P. White, D. J. Williams, M. C. B. Colbert, A. J. Hodge, M. S. Khan and D. G. Parker, *J. Organomet. Chem.*, **1999**, *578*, 198.
188. R. F. Winter and T. Scheiring, *Z. Anorg. Allg. Chem.*, **2000**, *626*, 1196.
189. J. F. Bickley, S. J. Higgins, C. A. Stuart and A. Steiner, *Inorg. Chem. Commun.*, **2000**, *3*, 211.
190. S. J. Higgins, C. A. Stuart and A. Mills, *Inorg. Chem. Commun.*, **2000**, *3*, 208.
191. S. J. Higgins, A. La Pensée, C. A. Stuart and J. M. Charnock, *J. Chem. Soc., Dalton Trans.*, **2001**, 902.
192. J. F. Bickley, A. A. La Pensée, S. J. Higgins and C. A. Stuart, *Dalton Trans.*, **2003**, 4663.
193. Y. B. Zhu, M. O. Wolf and G. P. A. Yap, *Inorg. Chem.*, **1997**, *36*, 5483.
194. G. A. Koutsantonis, G. I. Jenkins, P. A. Schauer, B. Szczepaniak, B. W. Skelton, C. Tan and A. H. White, *Organometallics*, **2009**, *28*, 2195.
195. J. Ruiz, M. E. G. Mosquera and V. Riera, *J. Organomet. Chem.*, **1997**, *527*, 35.
196. R. F. Winter and F. M. Hornung, *Organometallics*, **1999**, *18*, 4005.
197. G. A. Koutsantonis, P. J. Low, C. F. R. Mackenzie, B. W. Skelton and D. S. Yufit, *Organometallics*, **2014**, *33*, 4911.
198. L. Rigamonti, B. Babgi, M. P. Cifuentes, R. L. Roberts, S. Petrie, R. Stranger, S. Righetto, A. Teshome, I. Asselberghs, K. Clays and M. G. Humphrey, *Inorg. Chem.*, **2009**, *48*, 3562.

199. N. J. Long, A. J. Martin, F. F. de Biani and P. Zanello, *J. Chem. Soc., Dalton Trans.*, **1998**, 2017.
200. Q. Ge and T. S. A. Hor, *Dalton Trans.*, **2008**, 2929.
201. M. C. B. Colbert, J. Lewis, N. J. Long, P. R. Raithby, A. J. P. White and D. J. Williams, *J. Chem. Soc., Dalton Trans.*, **1997**, 99.
202. K. Johno, Y. Tanaka, T. Koike and M. Akita, *Dalton Trans.*, **2011**, *40*, 8089.
203. R. F. Winter, K.-W. Klinkhammer and S. Záliš, *Organometallics*, **2001**, *20*, 1317.
204. M. P. Cifuentes, M. G. Humphrey, G. A. Koutsantonis, N. A. Lengkeek, S. Petrie, V. Sanford, P. A. Schauer, B. W. Skelton, R. Stranger and A. H. White, *Organometallics*, **2008**, *27*, 1716.
205. G. A. Koutsantonis, P. A. Schauer and B. W. Skelton, *Organometallics*, **2011**, *30*, 2680.
206. I. R. Whittall, M. G. Humphrey, S. Houbrechts, J. Maes, A. Persoons, S. Schmid and D. C. R. Hockless, *J. Organomet. Chem.*, **1997**, *544*, 277.
207. A. M. McDonagh, C. E. Powell, J. P. Morrall, M. P. Cifuentes and M. G. Humphrey, *Organometallics*, **2003**, *22*, 1402.
208. G. T. Dalton, M. P. Cifuentes, L. A. Watson, S. Petrie, R. Stranger, M. Samoc and M. G. Humphrey, *Inorg. Chem.*, **2009**, *48*, 6534.
209. K. Liu, X. Wang and F. Wang, *ACS Nano*, **2008**, *2*, 2315.
210. O. Lavastre, J. Plass, P. Bachmann, S. Guesmi, C. Moinet and P. H. Dixneuf, *Organometallics*, **1997**, *16*, 184.
211. S. Rigaut, J. Perruchon, L. Le Pichon, D. Touchard and P. H. Dixneuf, *J. Organomet. Chem.*, **2003**, *670*, 37.
212. A. Benameur, P. Brignou, E. Di Piazza, Y.-M. Hervault, L. Norel and S. Rigaut, *New J. Chem.*, **2011**, *35*, 2105.
213. H. Qi, A. Gupta, B. C. Noll, G. L. Snider, Y. H. Lu, C. Lent and T. P. Fehlner, *J. Am. Chem. Soc.*, **2005**, *127*, 15218.
214. P. Haquette, D. Touchard, L. Toupet and P. Dixneuf, *J. Organomet. Chem.*, **1998**, *565*, 63.
215. K. Onitsuka, N. Ohara, F. Takei and S. Takahashi, *Dalton Trans.*, **2006**, 3693.
216. S. K. Hurst, M. P. Cifuentes, A. M. McDonagh, M. G. Humphrey, M. Samoc, B. Luther-Davies, I. Asselberghs and A. Persoons, *J. Organomet. Chem.*, **2002**, *642*, 259.
217. K. A. Green, M. P. Cifuentes, T. C. Corkery, M. Samoc and M. G. Humphrey, *Angew. Chem. Int. Ed. Engl.*, **2009**, *48*, 7867.
218. M. T. Bautista, E. P. Cappellani, S. D. Drouin, R. H. Morris, C. T. Schweitzer, A. Sella and J. Zubkowski, *J. Am. Chem. Soc.*, **1991**, *113*, 4876.
219. M. A. Fox, J. E. Harris, S. Heider, V. Pérez-Gregorio, M. E. Zakrzewska, J. D. Farmer, D. S. Yufit, J. A. K. Howard and P. J. Low, *J. Organomet. Chem.*, **2009**, *694*, 2350.
220. M. Younus, N. J. Long, P. R. Raithby, J. Lewis, N. A. Page, A. J. P. White, D. J. Williams, M. C. B. Colbert, A. J. Hodge, M. S. Khan and D. G. Parker, *J. Organomet. Chem.*, **1999**, *578*, 198.
221. M. Morshedi, P. V. Simpson, B. Babgi, K. Green, G. J. Moxey, M. S. Jennaway, M. P. Cifuentes and M. G. Humphrey, Checked By: S. G. Eaves and P. J. Low, *unpublished work*, Australian National University, **2015**.
222. M. G. Humphrey, *personal communication*, **2015**.
223. B. Chin, A. J. Lough, R. H. Morris, C. T. Schweitzer and C. D'Agostino, *Inorg. Chem.*, **1994**, *33*, 6278.

224. S. Guesmi, D. Touchard and P. H. Dixneuf, *Chem. Commun.*, **1996**, 2773.
225. Y. Nishibayashi, S. Takemoto, S. Iwai and M. Hidai, *Inorg. Chem.*, **2000**, *39*, 5946.
226. N. Mantovani, M. Brugnati, L. Gonsalvi, E. Grigiotti, F. Laschi, L. Marvelli, M. Peruzzini, G. Reginato, R. Rossi and P. Zanello, *Organometallics*, **2005**, *24*, 405.
227. D. Touchard, C. Morice, V. Cadierno, P. Haquette, L. Toupet and P. H. Dixneuf, *J. Chem. Soc., Chem. Commun.*, **1994**, 859.
228. D. Touchard, S. Guesmi, L. Le Pichon, A. Daridor and P. H. Dixneuf, *Inorg. Chim. Acta*, **1998**, *280*, 118.
229. S. Marqués-González, M. Parthey, D. S. Yufit, J. A. K. Howard, M. Kaupp and P. J. Low, *Organometallics*, **2014**, *33*, 4947.
230. S. Drouet, A. Merhi, D. Yao, M. P. Cifuentes, M. G. Humphrey, M. Wielgus, J. Olesiak-Banska, K. Matczyszyn, M. Samoc, F. Paul and C. O. Paul-Roth, *Tetrahedron*, **2012**, *68*, 10351.
231. P. J. West, T. Schwich, M. P. Cifuentes and M. G. Humphrey, *J. Organomet. Chem.*, **2011**, *696*, 2886.
232. E. Di Piazza, A. Merhi, L. Norel, S. Choua, P. Turek and S. Rigaut, *Inorg. Chem.*, **2015**.
233. C. Olivier, B. Kim, D. Touchard and S. Rigaut, *Organometallics*, **2008**, *27*, 509.
234. A. M. McDonagh, M. G. Humphrey, M. Samoc, B. Luther-Davies, S. Houbrechts, T. Wada, H. Sasabe and A. Persoons, *J. Am. Chem. Soc.*, **1999**, *121*, 1405.
235. A. M. McDonagh, M. G. Humphrey, M. Samoc and B. Luther-Davies, *Organometallics*, **1999**, *18*, 5195.
236. J. P. L. Morrall, M. P. Cifuentes, M. G. Humphrey, R. Kellens, E. Robijns, I. Asselberghs, K. Clays, A. Persoons, M. Samoc and A. C. Willis, *Inorg. Chim. Acta*, **2006**, *359*, 998.
237. S. K. Hurst, M. P. Cifuentes and M. G. Humphrey, *Organometallics*, **2002**, *21*, 2353.
238. C. E. Powell, S. K. Hurst, J. P. Morrall, M. P. Cifuentes, R. L. Roberts, M. Samoc and M. G. Humphrey, *Organometallics*, **2007**, *26*, 4456.
239. S. K. Hurst, M. G. Humphrey, T. Isoshima, K. Wostyn, I. Asselberghs, K. Clays, A. Persoons, M. Samoc and B. Luther-Davies, *Organometallics*, **2002**, *21*, 2024.
240. M. Uno and P. H. Dixneuf, *Angew. Chem. Int. Edit.*, **1998**, *37*, 1714.
241. K. Onitsuka, N. Ohara, F. Takei and S. Takahashi, *Organometallics*, **2008**, *27*, 25.
242. N. Gauthier, G. Argouarch, F. Paul, L. Toupet, A. Ladjarafi, K. Costuas, J.-F. Halet, M. Samoc, M. P. Cifuentes, T. C. Corkery and M. G. Humphrey, *Chem. Eur. J.*, **2011**, *17*, 5561.
243. N. Gauthier, C. Olivier, S. Rigaut, D. Touchard, T. Roisnel, M. G. Humphrey and F. Paul, *Organometallics*, **2008**, *27*, 1063.
244. S. Zhang, Y. Sheng, G. Wei, Y. Quan, Y. Cheng and C. Zhu, *J. Polym. Sci. A Polym. Chem.*, **2014**, *52*, 1686.
245. R. Gatri, I. Ouerfelli, M. L. Efrit, F. Serein-Spirau, J. P. Lere-Porte, P. Valvin, T. Roisnel, S. Bivaud, H. Akdas-Kilig and J. L. Fillaut, *Organometallics*, **2014**, *33*, 665.
246. I. de los Rios, M. J. Tenorio, M. C. Puerta and P. Valerga, *Organometallics*, **1998**, *17*, 3356.

247. S. Rigaut, L. Le Pichon, J. C. Daran, D. Touchard and P. H. Dixneuf, *Chem. Commun.*, **2001**, 1206.
248. S. Rigaut, C. Olivier, K. Costuas, S. Choua, O. Fadhel, J. Massue, P. Turek, J.-Y. Saillard, P. H. Dixneuf and D. Touchard, *J. Am. Chem. Soc.*, **2006**, *128*, 5859.
249. S. Rigaut, J. Massue, D. Touchard, J. L. Fillaut, S. Golhen and P. H. Dixneuf, *Angew. Chem. Int. Edit.*, **2002**, *41*, 4513.
250. P. Low and N. Brown, *J. Clust. Sci.*, **2010**, *21*, 235.
251. D. M. D'Alessandro and F. R. Keene, *Chem. Soc. Rev.*, **2006**, *35*, 424.
252. W. Kaim, S. Ernst and V. Kasack, *J. Am. Chem. Soc.*, **1990**, *112*, 173.
253. S. Rigaut, J. Perruchon, S. Guesmi, C. Fave, D. Touchard and P. H. Dixneuf, *Eur. J. Inorg. Chem.*, **2005**, *2005*, 447.
254. A. Vacher, A. Benameur, C. M. Ndiaye, D. Touchard and S. Rigaut, *Organometallics*, **2009**, *28*, 6096.
255. S. Rigaut, *Dalton Trans.*, **2013**, *42*, 15859.
256. L. A. Bumm, J. J. Arnold, T. D. Dunbar, D. L. Allara and P. S. Weiss, *J. Phys. Chem. A*, **1999**, *103*, 8122.
257. B. Kim, J. M. Beebe, C. Olivier, S. Rigaut, D. Touchard, J. G. Kushmerick, X. Y. Zhu and C. D. Frisbie, *J. Phys. Chem. C*, **2007**, *111*, 7521.
258. K. Slowinski, R. V. Chamberlain, R. Bilewicz and M. Majda, *J. Am. Chem. Soc.*, **1996**, *118*, 4709.
259. X. Li, J. He, J. Hihath, B. Xu, S. M. Lindsay and N. Tao, *J. Am. Chem. Soc.*, **2006**, *128*, 2135.
260. D. J. Wold and C. D. Frisbie, *J. Am. Chem. Soc.*, **2001**, *123*, 5549.
261. R. J. Nichols, W. Haiss, S. J. Higgins, E. Leary, S. Martín and D. Bethell, *Phys. Chem. Chem. Phys.*, **2010**, *12*, 2801.
262. W. Haiss, C. S. Wang, I. Grace, A. S. Batsanov, D. J. Schiffrin, S. J. Higgins, M. R. Bryce, C. J. Lambert and R. J. Nichols, *Nat. Mater.*, **2006**, *5*, 995.
263. W. Haiss, S. Martin, E. Leary, H. van Zalinge, S. J. Higgins, L. Bouffier and R. J. Nichols, *J. Phys. Chem. C*, **2009**, *113*, 5823.
264. B. Xu and N. J. Tao, *Science*, **2003**, *301*, 1221.
265. M. Mayor, C. von Hanisch, H. B. Weber, J. Reichert and D. Beckmann, *Angew. Chem. Int. Edit.*, **2002**, *41*, 1183.
266. K. Moth-Poulsen, L. Patrone, N. Stuhr-Hansen, J. B. Christensen, J.-P. Bourgoin and T. Bjornholm, *Nano Lett.*, **2005**, *5*, 783.
267. L. Luo, A. Benameur, P. Brignou, S. H. Choi, S. Rigaut and C. D. Frisbie, *J. Phys. Chem. C*, **2011**, *115*, 19955.
268. E. Wuttke, Y.-M. Hervault, W. Polit, M. Linseis, P. Erler, S. Rigaut and R. F. Winter, *Organometallics*, **2014**, *33*, 4672.
269. Y.-W. Zhong, N. Vila, J. C. Henderson, S. Flores-Torres and H. D. Abruna, *Inorg. Chem.*, **2007**, *46*, 10470.
270. Y.-W. Zhong, N. Vila, J. C. Henderson and H. D. Abruna, *Inorg. Chem.*, **2009**, *48*, 991.
271. S. Kobatake, K. Uchida, E. Tsuchida and M. Irie, *Chem. Commun.*, **2002**, 2804.
272. F. Meng, Y.-M. Hervault, L. Norel, K. Costuas, C. Van Dyck, V. Geskin, J. Cornil, H. H. Hng, S. Rigaut and X. Chen, *J. Chem. Sci.*, **2012**, *3*, 3113.
273. L. Qin, S. Park, L. Huang and C. A. Mirkin, *Science*, **2005**, *309*, 113.
274. F. Meng, Y.-M. Hervault, Q. Shao, B. Hu, L. Norel, S. Rigaut and X. Chen, *Nat. Commun.*, **2014**, *5*, 1.

275. S. Marqués-González, D. S. Yufit, J. A. K. Howard, S. Martín, H. M. Osorio, V. M. García-Suárez, R. J. Nichols, S. J. Higgins, P. Cea and P. J. Low, *Dalton Trans.*, **2013**, *42*, 338.
276. F. Chen, X. L. Li, J. Hihath, Z. F. Huang and N. J. Tao, *J. Am. Chem. Soc.*, **2006**, *128*, 15874.
277. C.-H. Ko, M.-J. Huang, M.-D. Fu and C.-h. Chen, *J. Am. Chem. Soc.*, **2010**, *132*, 756.
278. S. N. Yaliraki, M. Kemp and M. A. Ratner, *J. Am. Chem. Soc.*, **1999**, *121*, 3428.
279. A. Mulas, Y.-M. Hervault, X. He, E. Di Piazza, L. Norel, S. Rigaut and C. Lagrost, *Langmuir*, **2015**, *31*, 7138.
280. W. Hong, D. Z. Manrique, P. Moreno-García, M. Gulcur, A. Mishchenko, C. J. Lambert, M. R. Bryce and T. Wandlowski, *J. Am. Chem. Soc.*, **2012**, *134*, 2292.
281. Z. L. Cheng, R. Skouta, H. Vázquez, J. R. Widawsky, S. Schneebeli, W. Chen, M. S. Hybertsen, R. Breslow and L. Venkataraman, *Nat. Nano.*, **2011**, *6*, 353.
282. F. Lissel, F. Schwarz, O. Blacque, H. Riel, E. Lörtscher, K. Venkatesan and H. Berke, *J. Am. Chem. Soc.*, **2014**, *136*, 14560.
283. A. Marchenko, N. Katsonis, D. Fichou, C. Aubert and M. Malacria, *J. Am. Chem. Soc.*, **2002**, *124*, 9998.
284. N. Katsonis, A. Marchenko, D. Fichou and N. Barrett, *Surf. Sci.*, **2008**, *602*, 9.
285. N. Katsonis, A. Marchenko, S. Taillemite, D. Fichou, G. Chouraqui, C. Aubert and M. Malacria, *Chem. Eur. J.*, **2003**, *9*, 2574.
286. M. Endou, Y. Ie, T. Kaneda and Y. Aso, *J. Org. Chem.*, **2007**, *72*, 2659.
287. S. Watcharinyanon, D. Nilsson, E. Moons, A. Shaporenko, M. Zharnikov, B. Albinsson, J. Martensson and L. S. O. Johansson, *Phys. Chem. Chem. Phys.*, **2008**, *10*, 5264.
288. G. Pera, S. Martín, L. M. Ballesteros, A. J. Hope, P. J. Low, R. J. Nichols and P. Cea, *Chem. Eur. J.*, **2010**, *16*, 13398.
289. G. Grelaud, N. Gauthier, Y. Luo, F. Paul, B. Fabre, F. Barrière, S. Ababou-Girard, T. Roisnel and M. G. Humphrey, *J. Phys. Chem. C*, **2014**, *118*, 3680.
290. G. P. Lopinski, D. D. M. Wayner and R. A. Wolkow, *Nature*, **2000**, *406*, 48.
291. K. Green, N. Gauthier, H. Sahnoune, J.-F. Halet, F. Paul and B. Fabre, *Organometallics*, **2013**, *32*, 5333.
292. L. Norel, K. Bernot, M. Feng, T. Roisnel, A. Caneschi, R. Sessoli and S. Rigaut, *Chem. Commun.*, **2012**, *48*, 3948.
293. L. Norel, M. Feng, K. Bernot, T. Roisnel, T. Guizouarn, K. Costuas and S. Rigaut, *Inorg. Chem.*, **2014**, *53*, 2361.
294. C. Stroh, M. Mayor, C. von Hanisch and P. Turek, *Chem. Commun.*, **2004**, 2050.
295. F. Lissel, O. Blacque, K. Venkatesan and H. Berke, *Organometallics*, **2015**, *34*, 408.
296. F. Lissel, F. Schwarz, O. Blacque, H. Riel, E. Loertscher, K. Venkatesan and H. Berke, *J. Am. Chem. Soc.*, **2014**, *136*, 14560.
297. W. Chen, J. R. Widawsky, H. Vázquez, S. T. Schneebeli, M. S. Hybertsen, R. Breslow and L. Venkataraman, *J. Am. Chem. Soc.*, **2011**, *133*, 17160.
298. A. Colombo, C. Dragonetti, D. Roberto, R. Ugo, L. Falciola, S. Luzzati and D. Kotowski, *Organometallics*, **2011**, *30*, 1279.
299. J. Mei, K. Ogawa, Y.-G. Kim, N. C. Heston, D. J. Arenas, Z. Nasrollahi, T. D. McCarley, D. B. Tanner, J. R. Reynolds and K. S. Schanze, *ACS Appl. Mater. Inter.*, **2009**, *1*, 150.
300. S. De Sousa, L. Ducasse, B. Kauffmann, T. Toupance and C. Olivier, *Chem. Eur. J.*, **2014**, *20*, 7017.

301. C. Teng, X. Yang, S. Li, M. Cheng, A. Hagfeldt, L.-Z. Wu and L. Sun, *Chem. Eur. J.*, **2010**, *16*, 13127.
302. F. Nisic, A. Colombo, C. Dragonetti, E. Garoni, D. Marinotto, S. Righetto, F. De Angelis, M. G. Lobello, P. Salvatori, P. Biagini and F. Melchiorre, *Organometallics*, **2015**, *34*, 94.
303. K. N. Gherab, R. Gatri, Z. Hank, B. Dick, R.-J. Kutta, R. Winter, J. Luc, B. Sahraoui and J.-L. Fillaut, *J. Mater. Chem.*, **2010**, *20*, 2858.
304. L. Norel, E. Di Piazza, M. Feng, A. Vacher, X. He, T. Roisnel, O. Maury and S. Rigaut, *Organometallics*, **2014**, *33*, 4824.
305. I. R. Whittall, A. M. McDonagh, M. G. Humphrey and M. Samoc, *Adv. Organomet. Chem.*, **1998**, *42*, 291.
306. C. E. Powell and M. G. Humphrey, *Coord. Chem. Rev.*, **2004**, *248*, 725.
307. I. R. Whittall, A. M. McDonagh, M. G. Humphrey and M. Samoc, in *Adv. Organomet. Chem.*, Academic Press, **1999**, vol. 43, pp. 349-405.
308. M. P. Cifuentes and M. G. Humphrey, *J. Organomet. Chem.*, **2004**, *689*, 3968.
309. A. J. Hodge, S. L. Ingham, A. K. Kakkar, M. S. Khan, J. Lewis, N. J. Long, D. G. Parker and P. R. Raithby, *J. Organomet. Chem.*, **1995**, *488*, 205.
310. G. Grelaud, M. P. Cifuentes, T. Schwich, G. Argouarch, S. Petrie, R. Stranger, F. Paul and M. G. Humphrey, *Eur. J. Inorg. Chem.*, **2012**, 65.
311. B. Babgi, L. Rigamonti, M. P. Cifuentes, T. C. Corkery, M. D. Randles, T. Schwich, S. Petrie, R. Stranger, A. Teshome, I. Asselberghs, K. Clays, M. Samoc and M. G. Humphrey, *J. Am. Chem. Soc.*, **2009**, *131*, 10293.
312. J. Niziol, J.-L. Fillaut, M. Sniechowski, F. Khammar and B. Sahraoui, *Opt. Mater.*, **2012**, *34*, 1670.
313. C. E. Powell, M. P. Cifuentes, J. P. Morrall, R. Stranger, M. G. Humphrey, M. Samoc, B. Luther-Davies and G. A. Heath, *J. Am. Chem. Soc.*, **2002**, *125*, 602.
314. M. Samoc, T. C. Corkery, A. M. McDonagh, M. P. Cifuentes and M. G. Humphrey, *Aust. J. Chem.*, **2011**, *64*, 1269.
315. Q. Y. Hu, W. X. Lu, H. D. Tang, H. H. Y. Sung, T. B. Wen, I. D. Williams, G. K. L. Wong, Z. Lin and G. Jia, *Organometallics*, **2005**, *24*, 3966.
316. K. A. Green, P. V. Simpson, T. C. Corkery, M. P. Cifuentes, M. Samoc and M. G. Humphrey, *Macromol. Rapid Commun.*, **2012**, *33*, 573.
317. M. P. Cifuentes, C. E. Powell, M. G. Humphrey, G. A. Heath, M. Samoc and B. Luther-Davies, *J. Phys. Chem. A*, **2001**, *105*, 9625.
318. J.-L. Fillaut, J. Andriès, L. Toupet and J.-P. Desvergne, *Chem. Commun.*, **2005**, 2924.
319. J.-L. Fillaut, J. Andriès, J. Perruchon, J.-P. Desvergne, L. Toupet, L. Fadel, B. Zouchoune and J.-Y. Saillard, *Inorg. Chem.*, **2007**, *46*, 5922.
320. J.-L. Fillaut, J. Andriès, R. D. Marwaha, P.-H. Lanoë, O. Lohio, L. Toupet and J. A. G. Williams, *J. Organomet. Chem.*, **2008**, *693*, 228.
321. G. Vives and J. M. Tour, *Tetrahedron Lett.*, **2009**, *50*, 1427.

CHAPTER 2

Reactions of alkynes with *cis*-[$RuCl_2(dppm)_2$]: exploring the interplay of vinylidene, alkynyl and η^3-butenynyl complexes

2.1. Abstract

Reactions of *cis*-[$RuCl_2(dppm)_2$], *cis*-[**20**], with various terminal alkynes of the type HC≡CC_6H_4-4-R in the presence of $TlBF_4$ have resulted in formation of cationic vinylidene complexes, *trans*-[RuCl(=C=CHC_6H_4-4-R)$(dppm)_2]^+$ (R = NO_2, [**22a**]$^+$; COOMe, [**22b**]$^+$; C≡C$SiMe_3$, [**22c**]$^+$; H, [**22d**]$^+$; Me, [**22e**]$^+$; OMe, [**22f**]$^+$). These complexes can be isolated as the respective tetrafluoroborate salts or treated *in situ* with a suitable base (Proton Sponge, 1,8-*bis*-dimethylaminonapthalene) to yield the *mono*-alkynyl complexes, *trans*-[RuCl(C≡CC_6H_4-4-R)$(dppm)_2$] (R = NO_2, [**23a**]; COOMe, [**23b**]; C≡C$SiMe_3$, [**23c**]; H, [**23d**]; Me, [**23e**]; OMe, [**23f**]). Through similar reactions of *cis*-[**20**] with two equivalents of alkyne, $TlBF_4$ and base, *trans*-bis(alkynyl) complexes, *trans*-[Ru(C≡CC_6H_4-4-R$)_2(dppm)_2$], can be isolated when R is an electron withdrawing substituent (R = NO_2, [**24a**]; COOMe, [**24b**]; C≡C$SiMe_3$, [**24c**]), whereas reactions with alkynes bearing electron donating substituents form cationic η^3-butenynyl complexes, *E*-[Ru{η^3-HC(C_6H_4-4-R)=CC≡CC_6H_4-4-R}$(dppm)_2]^+$ (R = Me, [**28e**]$^+$; OMe, [**28f**]$^+$). The molecular structures of [**23b** – **f**], [**24b**] and [**28e**]BF_4, together with those of *trans*-[RuCl(CO)$(dppm)_2]BF_4$, [**34**]BF_4, and *trans*-[Ru(C≡C$SiMe_3)_2(dppm)_2$], [**86**], are reported and discussed, making comparisons with previously reported, closely related structures where appropriate. Electrochemical studies show that complexes [**22**]BF_4, [**23**] and [**24**] generally display a single, *quasi*-reversible, one-electron ligand-centred oxidation and a single, irreversible, one-electron metal-centred oxidation. Vinylidene complexes [**22**]$^+$ also exhibit a further one-electron reduction associated with the vinylidene ligand. This work highlights the importance of the electronic character of the alkyne in governing product outcome upon reaction with *cis*-[**20**],

which contrasts with the more uniform behaviour of *cis*-[$RuCl_2(dppe)_2$], *cis*-[**35**], and [$RuCl(dppe)_2$]OTf, [**36**]OTf, with similar reagents. Aspects of this work have been published,[1] and further details are given here.

2.2. Introduction

Moore's law, describing the pace of silicon technology development, states that roughly every two years transistor densities on an integrated circuit will double; increasing device functionality and performance with a systematic decrease in device size.[2] In accordance with this technological forecast, current state of the art devices featuring scaled silicon transistor sizes of 22 nm (first generation tri-gate transistor; Intel Ivy-Bridge and Haswell chips) and 14 nm (second generation tri-gate transistor featuring taller, thinner fins; Intel Broadwell chips) have been realised. However this trend is nearing the physical limits of solid materials, with effects such as interconnect delays and quantum tunnelling (caused as a result of gate oxide unreliability associated with the very thin features) leading to excessive heat and power dissipation, collectively inhibiting optimised performances.[3] Whilst improved device design, such as Intel's 3D 'fin' based transistors (finFET), can alleviate some of these problems in the short to medium term, prohibitive fabrication costs, as described in Moore's Second Law,[4] motivates the exploration of entirely new paradigms for future technologies. As a result, current research is now focussed towards replacing some conventional solid state circuit components with molecules operating as self-contained electronics; hence the advent of *molecular electronics*, of which the journal *Science* named, perhaps rather optimistically, *"the breakthrough of the year"* in 2001.[5]

In principle, molecules which act as self-contained electronic devices or components could make a step change in the Moore's Law progression given typical molecular sizes of ~ 2 − 4 nm and high packing densities achieved in well-ordered molecular films. Molecules provide rich structural and electronic variety, in addition to controlled and large-scale uniform production through chemical syntheses (a 'bottom-up' approach). Therefore, tailoring both the physical and chemical properties is achievable at a fraction of the cost (by utilising spin-coating or simple self-assembly production techniques)[4] with minimal structural defects.[6]

The most basic component of a molecular circuit is the *molecular wire*, which can be described as a molecule able to facilitate charge transport between two (or more) internal reservoirs *via* a (typically) π-conjugated pathway. The term was first coined by Lehn in his description of charge transport through a caroviologen molecule (Figure 2.1).[7] This internal charge transport mechanism is far superior in speed and efficiency than through-space electron transport, thus allowing for longer ranges, and faster rates, of electron transfer.

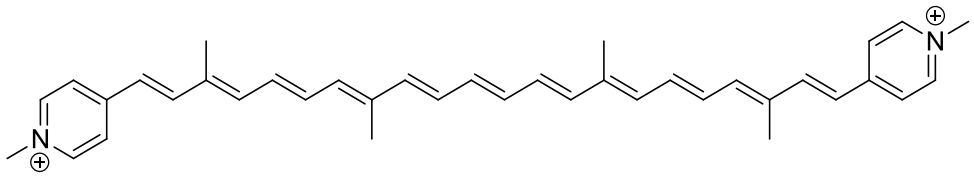

Figure 2.1: The first reported molecular wire, as described by Lehn.[7]

The electronic properties of individual molecular wires can be probed by physically inserting the single molecule between two macroscopic electrodes,[8] forming metal|molecule|metal junctions. Whilst the great majority of work within this area has been directed towards understanding the 'wire-like' properties of organic molecules (*organic molecular wires*), the incorporation of metal fragments within a conjugated π-system (*organometallic molecular wires*) allows further fine tuning of the frontier orbital energies to better match electrode Fermi levels, whilst also introducing redox-active hopping sites, both of which potentially lead to higher conduction values.[9-16] As a clear demonstration, Wang and co-workers showed that the conductance of oligo(phenylene)ethynylene (OPE) complexes, of varying lengths, is enhanced with the incorporation of ferrocene units.[17] In contrast, integrating Pd^{II}, Pt^{II}, Au^{II} or Hg^{II} metals into a π-conjugated wire backbone results in an inefficient 'wire' performance as a direct result of poorly matched M(*d*)-C≡C(*π*) frontier orbital energies, consequently impeding ground state electron transfer between termini through the introduction of additional tunnelling barriers.[14] For example, the Pt^{II} containing complex *trans*-$[Pt(C{\equiv}CC_6H_4\text{-}4\text{-}SAc)_2(PPh_3)_2]$ displays insulating properties when measured in a junction[18] whilst the Ru^{II} containing complex *trans*-$[Ru(C{\equiv}CC_6H_4\text{-}4\text{-}SAc)_2(dppm)_2]$, [**51**], with a more conjugated M(*d*)-C≡C(π) electronic structure and higher lying HOMO, displays much more significant conductance behaviour.[12]

The introduction of redox-active metals within a 'wire-like' framework can be used as a design strategy to accomplish a prototypical molecular transistor. In this case, the internal metal operates as a 'dopable' semiconductor, regulating through-charge transfer from the source to the drain in response to the potential applied by a third gate electrode. Consequently, a variety of current-voltage (I-V) traces are possible as a function of the gate potential. As a further advantage, organometallic derivatives are more synthetically diverse than their organic counterparts, and variation of metal ancillary ligands presents as a facile method for system modification in terms of physical properties, such as solubility, and electronic properties. The presence of electron releasing ligands, such as pyridine or tributylphosphine, are expected to help facilitate (and hence improve) internal charge-transfer, whereas the reverse is true for electron accepting ligands, such as carbonyls, as has been demonstrated in the investigation of electron transportation between terminal ferrocene units in *trans*-$[Ru(C{\equiv}CFc)_2(L)_4]$ complexes.[19] However, such trends have not yet been explored within a molecular junction.

Despite decades of research, the field of molecular electronics is still in its infancy and considerable progress is needed before this technology can be exploited. As an active topic of study within this field, several groups have explored the influence of the nature and length of the alkynyl fragments and surface binding groups on the extent of conjugation in *mono*- and multi-metallic group 8 complexes bearing acetylide fragments.[11, 20-26] However, given the importance the metal supporting ligands might play in tuning solubility, redox potentials and chemical stability, optimisation of the metal ligand sphere should also be an important consideration in the molecular design.

Ruthenium *trans*-bis(alkynyl) complexes of the type *trans*-$[Ru(C{\equiv}CR')_2(dppe)_2]$, bearing *bis*-chelating diphenylphosphinoethane (dppe) ligands, have been widely discussed as potential components in the area of molecular electronics,[24, 25, 27-31] due to the extensive Ru(*d*)-C≡C(π) frontier orbital mixing,[15] 'wire-like' behaviour,[23-25, 32, 33] and facile synthesis from *cis*-[**35**][34, 35] or five-coordinate [**36**]X (X = PF_6, OTf).[36-38] In contrast, *trans*-$[Ru(C{\equiv}CR')_2(dppm)_2]$ complexes, bearing related *bis*-chelating diphenylphosphinomethane (dppm) ligands with a reduced P-Ru-P bite angle, are less commonly encountered.

As described in Chapter 1, earlier reports have described the preparation of *trans*-[Ru(C≡CR′)$_2$(dppm)$_2$] complexes from *cis*-[**20**], or the intermediate *mono*-alkynyl complexes *trans*-[RuCl(C≡CR′)(dppm)$_2$], and terminal alkynes in the presence of $NaPF_6$ and various bases in reactions that take place over 12 − 24 hours. However, yields of these complexes are often low (< 30%).[39-41] Trimethylstannylalkynes have also been used in related transformations employing a CuI catalyst.[42-44] Furthermore, reactions of *cis*-[**20**] with more than one equivalent of alkyl or phenyl acetylenes and $NaPF_6$ in methanol can be intercepted by the formation of η^3-butenynyl products.[45] The hemi-lability of the dppm ligands, contributing to the convolution of the reaction medium, has also been observed.[45, 46]

In seeking to explore the influence of supporting ligands on the molecular electronic properties of *trans*-bis(alkynyl) complexes of ruthenium, as a complementary study of *trans*-[Ru(C≡CR′)$_2$(dppe)$_2$] complexes, this Chapter will focus attention on *trans*-[Ru(C≡CR′)$_2$(dppm)$_2$] complexes. Within this Chapter, simple synthetic protocols for the preparations of *trans*-[RuCl(=C=CHC$_6$H$_4$-4-R)$_2$(dppm)$_2$]$^+$ (R = NO_2, [**22a**]$^+$; COOMe, [**22b**]$^+$; C≡CSiMe$_3$, [**22c**]$^+$; H, [**22d**]$^+$; Me, [**22e**]$^+$; OMe, [**22f**]$^+$), *trans*-[RuCl(C≡CC$_6$H$_4$-4-R)(dppm)$_2$] (R = NO_2, [**23a**]; COOMe, [**23b**]; C≡CSiMe$_3$, [**23c**]; H, [**23d**]; Me, [**23e**]; OMe, [**23f**]), *trans*-[Ru(C≡CC$_6$H$_4$-4-R)$_2$(dppm)$_2$] (R = NO_2, [**24a**]; COOMe, [**24b**]; C≡CSiMe$_3$, [**24c**]) and *E*-[Ru{η^3-HC(C$_6$H$_4$-4-R)=CC≡CC$_6$H$_4$-4-R}(dppm)$_2$]$^+$ (R = Me, [**28e**]$^+$; OMe, [**28f**]$^+$) complexes are reported from reactions of *cis*-[**20**] with HC≡CC$_6$H$_4$-4-R in the presence of $TlBF_4$ and a suitable base (Proton Sponge, 1,8-*bis*-dimethylaminonaphthalene) in CH_2Cl_2 solutions. Moreover, the role played by the electronic character of the alkynyl substituents, in directing the product distribution between *trans*-bis(alkynyl) and η^3-butenynyl complexes, is explored.

2.3. Results

2.3.1. Synthesis of vinylidene complexes: *trans*-[RuCl(=C=CHC$_6$H$_4$-4-R)(dppm)$_2$]BF$_4$

The use of $TlBF_4$ as a halide abstracting agent in the facile formation of *trans*-bis(alkynyl) ruthenium complexes from *trans*-[RuCl(C≡CR′)(dppe)$_2$] has recently been demonstrated.[25] This method has now been applied to *cis*-[**20**] in order to circumvent synthetic problems described by others in the reactions of *cis*-[**20**] and terminal alkynes with alternative halide abstracting agents (*eg.* Ag^I and Na^I salts),[45, 47, 48] as described in Chapter 1.[45, 47, 48] Reactions of CH_2Cl_2 solutions of *cis*-[**20**] with various terminal alkynes of the type HC≡CC$_6$H$_4$-4-R (1 equiv.), in the presence of $TlBF_4$ (1. equiv), have resulted in the formation of vinylidene complexes, [**22**]BF_4, in moderate to high yields (66 – 83 %; R = NO_2, [**22a**]BF_4; COOMe, [**22b**]BF_4; C≡CSiMe$_3$, [**22c**]BF_4; H, [**22d**]BF_4; Me, [**22e**]BF_4 and OMe [**22f**]BF_4) after 1 – 2 hours (Scheme 2.1).

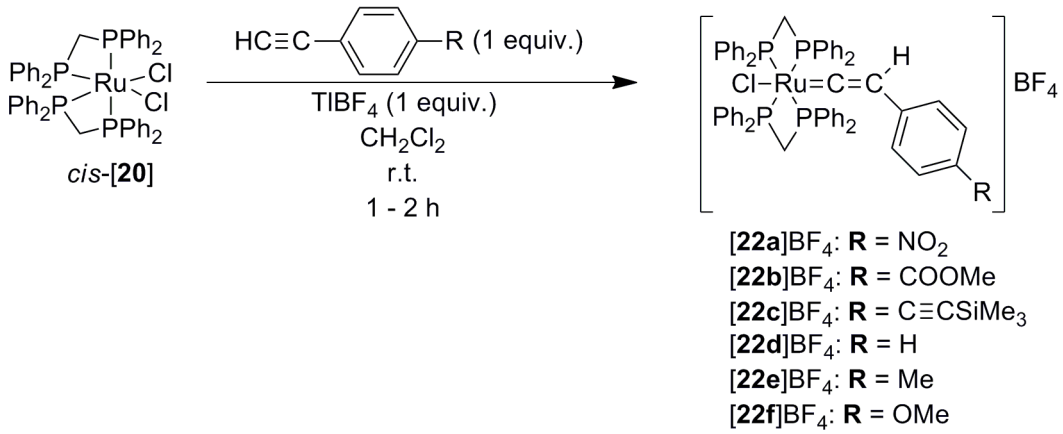

Scheme 2.1: Synthesis of complexes [**22a – f**]BF_4.

Evidence for the formation of the vinylidene cations [**22**]$^+$ is found in the ^{1}H NMR spectra where quintet (or unresolved multiplet) resonances for the vinylidene protons were observed between δ 2.94 – 3.36 ppm, with a $^4J_{PH}$ coupling of 3 Hz. In the $^{13}C\{^1H\}$ NMR spectra, low field multiplet resonances for the carbene-like Ru=*C* carbon nuclei (δ 352.7 – 360.9 ppm; Table 2.1), coupling to the four *cis*-phosphines, and singlet resonances for the Ru=C=*C* carbon nuclei (δ 109.4 – 111.1 ppm) confirmed the

presence of the vinylidene ligand. In the IR spectra, ν(Ru=C=C) bands ($1605 - 1653\ cm^{-1}$) further support vinylidene functionality. The purities of [**22a**, **b**, **d − f**]BF_4 have been confirmed by elemental analyses. However, despite spectroscopic evidence for the formation of [**22c**]BF_4, this complex failed to give an acceptable analysis (Anal. Found: C, 56.12; H, 4.08; Calc. for $C_{63}H_{58}BClF_4P_4RuSi$: C, 63.52; H, 4.91).

Table 2.1: Selected $^{13}C\{^1H\}$ NMR spectroscopic data (ppm), as reported in the experimental section, for {Ru(dppm)$_2$} vinylidene, [**22**]$^+$, (CD_2Cl_2) and *mono*-alkynyl complexes, [**23**], ($CDCl_3$).

		[**22**]$^+$		[**23**]	
Complex	**R**	**C_α / ppm**	**$^2J_{CP}$ / Hz**	**C_α / ppm**	**$^2J_{CP}$ / Hz**
a	NO_2	352.5	14	147.6	16
b	COOMe	355.4	14	144.8^m	-
c	C≡C$SiMe_3$	356.0^m	-	130.8	15
d	H	358.2	13	123.0	15
e	Me	359.5	15	120.4	15
f	OMe	362.5^m	-	118.2	15

m-multiplet

Although complexes [**22**]BF_4 are relatively stable in solution short-term, over prolonged periods of time (~ 16 – 24 hours), reaction with adventitious water results in the formation of the carbonyl complex, *trans*-[RuCl(CO)(dppm)$_2$]BF_4, [**34**]BF_4. The crystallographically determined structure of [**34**]$^+$ is shown in Figure 2.2 (determined from the tetrafluoroborate salt), and does not differ significantly from that previously published.[49]

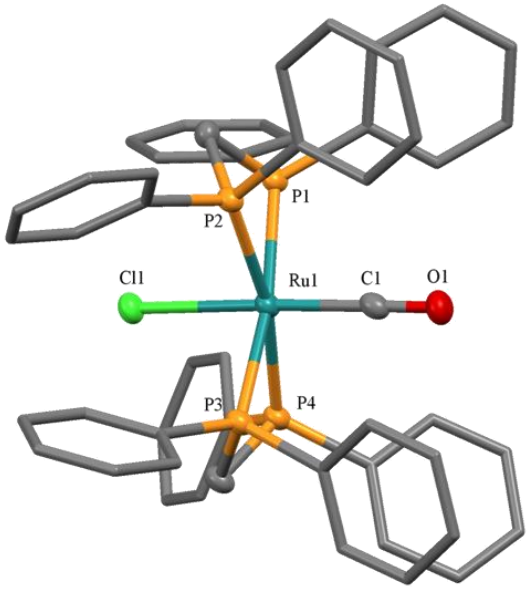

Figure 2.2: Solid state structure of [**34**]$^{+}$, with counter ion (BF_4^-) and hydrogen atoms removed for clarity. Ellipsoids for key atoms are drawn at the 50 % probability level. Selected bond lengths / Å: Ru(1)-Cl(1) 2.441(1), Ru(1)-C(1) 1.863(5), Ru(1)-P(1) 2.410(1), Ru(1)-P(2) 2.385(1), Ru(1)-P(3) 2.374(1), Ru(1)-P(4) 2.394(1), C(1)-O(1) 1.125(6). Selected bond angles / °: Cl(1)-Ru(1)-C(1) 174.1(2), Ru(1)-C(1)-O(1) 178.2(4), P(1)-Ru(1)-P(2) 69.50(4), P(3)-Ru(1)-P(4) 69.79(4), P(1)-Ru(1)-P(3) 171.13(4), P(2)-Ru(1)-P(4) 168.40(4).

2.3.2. Synthesis of *mono*-alkynyl complexes: *trans*-[RuCl(C≡CC_6H_4-4-R)(dppm)$_2$]

Following formation of [**22**]BF_4 *in situ*, filtration to remove the precipitated Tl^I salts and subsequent addition of Proton Sponge immediately generates the *mono*-alkynyl complexes, *trans*-[RuCl(C≡CC_6H_4-4-R)(dppm)$_2$], [**23**], in high yields (74 – 92 %; R = NO_2, [**23a**]; COOMe, [**23b**]; C≡C$SiMe_3$, [**23c**]; H, [**23d**]; Me, [**23e**]; OMe [**23f**]; Scheme 2.2). Proton Sponge was chosen as the base for practical reasons, simplifying the work-up procedure with a facile filtration to remove precipitated salts (including the conjugate acid of Proton Sponge) followed by precipitation of [**23**] from the filtrates by addition of hexanes generally proving sufficient to give the complexes in good yield and purity.

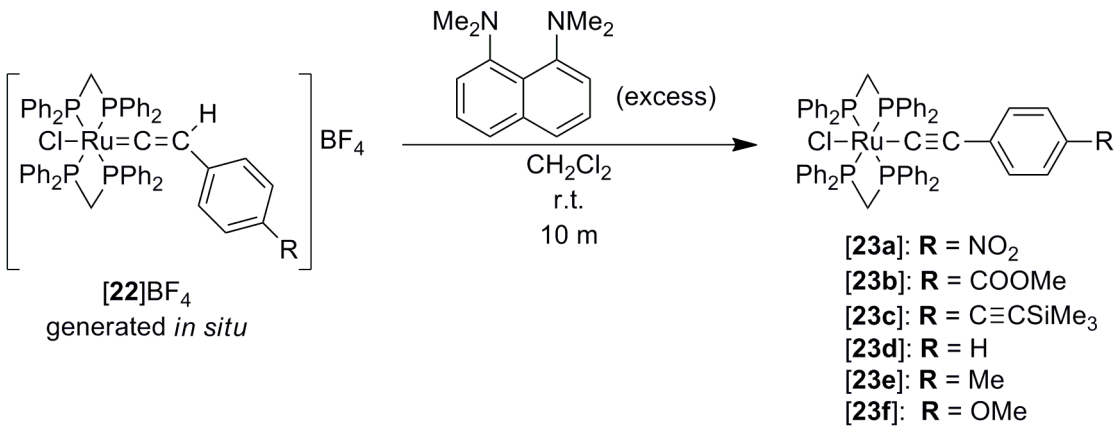

Scheme 2.2: Synthesis of complexes [**23a – f**].

Due to the strongly π-accepting nature of the vinylidene ligand, abstraction of the *trans*-chloride from $[\mathbf{22}]^+$ (the preliminary step in forming *bis*-alkynyl complexes, *vide infra*) is slow, allowing selective formation of the *mono*-vinylidene ($[\mathbf{22}]^+$) *in situ* and subsequent *mono*-alkynyl products ([**23**]). However, failure to control the 1 : 1 : 1, *cis*-[**20**] : $TlBF_4$: alkyne, stoichiometry or failure to allow complete formation of the *mono*-vinylidene before addition of the base, results in contamination of the product by the *trans*-bis(alkynyl) complexes *trans*-$[Ru(C{\equiv}CC_6H_4\text{-}4\text{-}R)_2(dppm)_2]$, [**24**], which are difficult to separate from the desired products.

Evidence for the formation of [**23**] is found in the $^{13}C\{^1H\}$ NMR spectra, where quintet (or unresolved multiplet) resonances for the Ru-*C* carbon nuclei (δ 118.2 – 147.6 ppm; Table 2.1), coupling to the four phosphines, and singlet resonances for the Ru-C≡*C* carbon nuclei (δ 111.9 – 117.0 ppm) confirmed the presence of the alkynyl ligand. In the IR spectra ν(RuC≡C) bands, observed within the range 2058 – 2083 cm^{-1}, further support the acetylide nature of the products. The purities of [**23a**, **b**, **c**] have been confirmed by elemental analyses. The elemental analysis obtained for [**23e**] (Anal. Found: C, 67.87; H, 4.78. Calc. for $C_{59}H_{51}ClP_4Ru$: C, 69.40; H, 5.04.) likely reflects partial desolvation of the crystalline sample (Calc. for $C_{59}H_{51}ClP_4Ru \times 0.5\ CH_2Cl_2$: C, 67.22; H, 4.93), which has been structurally determined with one CH_2Cl_2 solvate molecule (see section 2.3.4.) whilst the elemental analysis obtained for [**23f**] (Anal. Found: C, 64.53; H, 4.22. Calc. for $C_{59}H_{51}ClOP_4Ru$: C, 68.33; H, 4.96) better reflects the solvated crystalline sample (Calc. for $C_{59}H_{51}ClOP_4Ru \times CH_2Cl_2$: C, 64.23; H, 4.77),

which has been structurally determined with one CH_2Cl_2 solvate molecule (see section 2.3.4.). Finally, the structures of [**23b – f**] have been determined by single crystal X-ray diffraction studies (see section 2.3.4.), the structure of [**23a**] having been previously reported,[50] which confirmed the structural assignments based on NMR and IR spectroscopies.

2.3.3. Synthesis of *trans*-bis(alkynyl) complexes: *trans*-[Ru(C≡CC_6H_4-4-R)$_2$(dppm)$_2$] and η^3-butenynyl complexes: *E*-[Ru(η^3-{HC(C_6H_4-4-R)=CC≡CC_6H_4-4-R})(dppm)$_2$]BF_4

One-pot reactions of *cis*-[**20**] with $TlBF_4$ (2 equiv.), HC≡CC_6H_4-4-R (2.2 equiv) bearing electron withdrawing substituents (R = NO_2, [**24a**]; COOMe, [**24b**]; C≡C$SiMe_3$, [**24c**]) and Proton Sponge (excess) in CH_2Cl_2 solutions allowed the isolation of *trans*-bis(alkynyl) complexes *trans*-[Ru(C≡CC_6H_4-4-R)$_2$(dppm)$_2$], [**24**], in moderate to good yields (48 – 80 %) after prolonged reaction times (16 hours – 3.5 days; Scheme 2.3). Evidence for the formation of [**24**] is found in the $^{13}C\{^1H\}$ NMR spectra with multiplet (unresolved quintet) resonances for the Ru-*C* carbon nuclei (δ 136.7 – 150.1 ppm), coupling to the four mutually *cis*-phosphines, and singlet resonances for the Ru-C≡*C* carbon nuclei (δ 116.2 – 119.0 ppm). In the IR spectra ν(RuC≡C) bands observed within the range 2053 – 2062 cm^{-1} confirmed the presence of the alkynyl ligands. The purities of [**24a**, **b**] have been confirmed by elemental analyses. The structure of [**24b**] has also been determined by single crystal X-ray diffraction (see section 2.3.4.), the structure of [**24a**] having been previously reported.[51]

In contrast, analogous one-pot reactions of *cis*-[**20**] with more electron-rich alkynes HC≡CC_6H_4-4-R (2.2 equiv; R = Me, [**28e**]$^+$; OMe, [**28f**]$^+$) yielded cationic η^3-butenynyl complexes *E*-[Ru(η^3-{HC(C_6H_4-4-R)=CC≡CC_6H_4-4-R})(dppm)$_2$]BF_4, [**28**]$^+$ (Scheme 2.3).

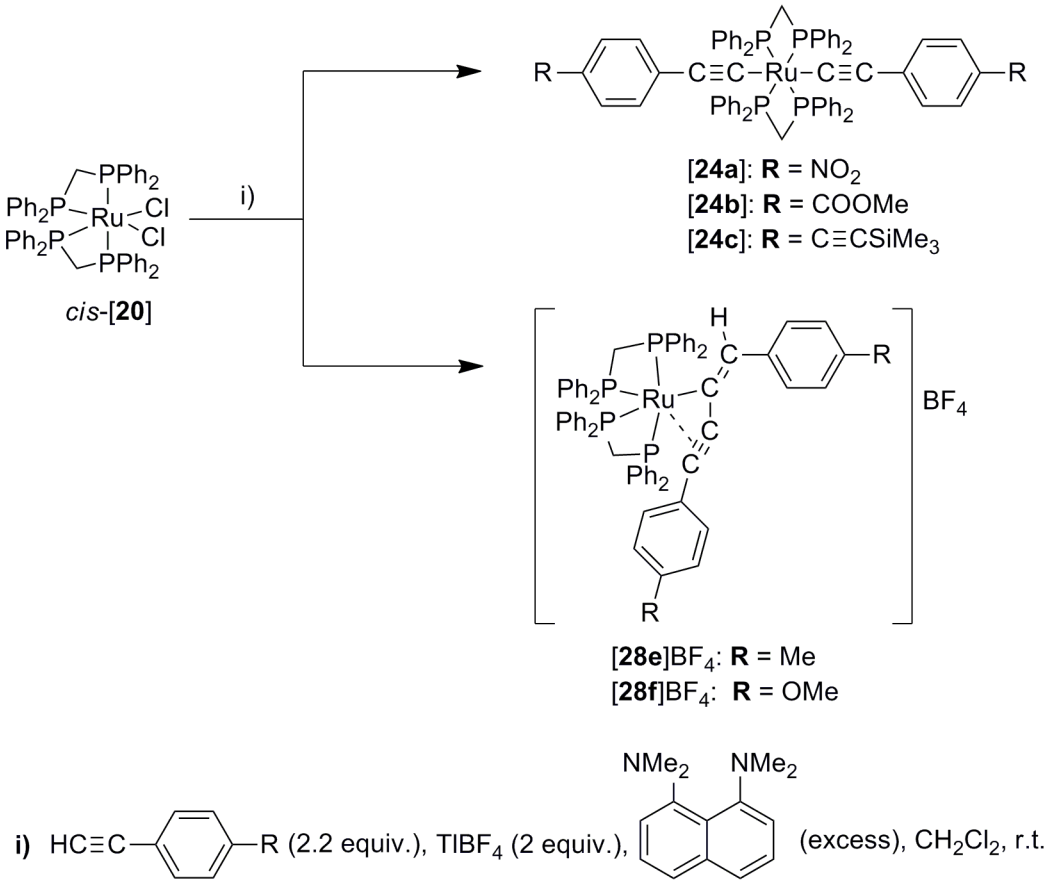

Scheme 2.3: Synthesis of complexes [**24a − c**] and [**28e − f**]$^+$.

Evidence for the formation of [**28**]$^+$ includes the observation of four doublet of doublet of doublet (ddd) resonances in the $^{31}P\{^1H\}$ NMR spectra from the four inequivalent phosphorus atoms, two of which are in a mutually *trans*-arrangement and show a large $^2J_{PP}$ coupling constant (318 Hz, [**28e**]$^+$; 322 Hz, [**28f**]$^+$), consistent with previously published data.[45] In the ^1H NMR spectra, singlet resonances for the R group methyl protons were observed at δ 2.34 ([**28e**]$^+$) and δ 3.81 ppm ([**28f**]$^+$), while doublet resonances for the vinyl protons were observed at δ 5.55 ([**28e**]$^+$) and δ 5.53 ppm ([**28f**]$^+$), with a $^4J_{PH}$ coupling of 5 Hz. The inequivalence of the four dppm protons in the ^1H NMR spectra also supported their asymmetric arrangement within this structure. The coordination of the alkyne group to the metal centre was confirmed by doublet resonances at δ 108.7 ([**28e**]$^+$) and δ 108.5 ppm ([**28f**]$^+$) in the $^{13}C\{^1H\}$ NMR spectra for C^1 (where [Ru(η^3-{$HC^4(R')=C^3C^2{\equiv}C^1R'$})$(dppm)_2$]$BF_4$), with a $^2J_{CP}$ coupling of 22 Hz. The purity of [**28e**]BF_4 has been confirmed by elemental analysis. Furthermore, the structure of [**28e**]$^+$ (Figure 2.13) has been determined by a single crystal X-ray

diffraction study (see section 2.3.4.), which confirmed the structural assignments made on the basis of the spectroscopic data.

In an attempt to isolate *trans*-bis(alkynyl) complexes containing electron donating groups, *cis*-[**20**] was reacted with HC≡CC_6H_4-4-Me (excess) and $TlBF_4$ (2 equiv.) in NH^iPr_2 (excess) and THF. Although unsuccessful in this case, an analogous test reaction with HC≡C$SiMe_3$ allowed the formation of *trans*-[Ru(C≡C$SiMe_3)_2(dppm)_2$], [**86**], in a high yield (80 %).

As discussed in Chapter 1, Dixneuf has previously reported the formation of 'asymmetric' *trans*-bis(alkynyl) {$Ru(dppm)_2$} complexes of the type *trans*-[Ru(C≡CR)(C≡CR′)$(dppm)_2$] bearing electron donating R / R′ groups (R = C_6H_5, ^nBu; R′ = C≡C$(C_6H_5)_2OSiMe_3$) in low yields (25 – 28 %).[39] More recently, Low has demonstrated the efficacy of Tl^I salts in the higher yielding (47 – 87 %) preparation of 'asymmetric' *trans*-bis(alkynyl) complexes of the type *trans*-[Ru(C≡CC_6H_4-4-R)(C≡CC_6H_4-4-R′)$(dppe)_2$] (R = COOMe, C≡C$SiMe_3$; R′ = NH_2, OMe) bearing electron withdrawing groups.[25] With a view to accessing 'asymmetric' *trans*-bis(alkynyl) complexes based on the *trans*-{$Ru(dppm)_2$} fragment, a CH_2Cl_2 solution of [**23a**] was reacted with $TlBF_4$ (2 equiv.), in the presence of HC≡CC_6H_4-4-COOMe (1 equiv.) and Proton Sponge (excess), and the course of the reaction monitored by *in situ* $^{31}P\{^1H\}$ NMR spectroscopy (Figure 2.3).

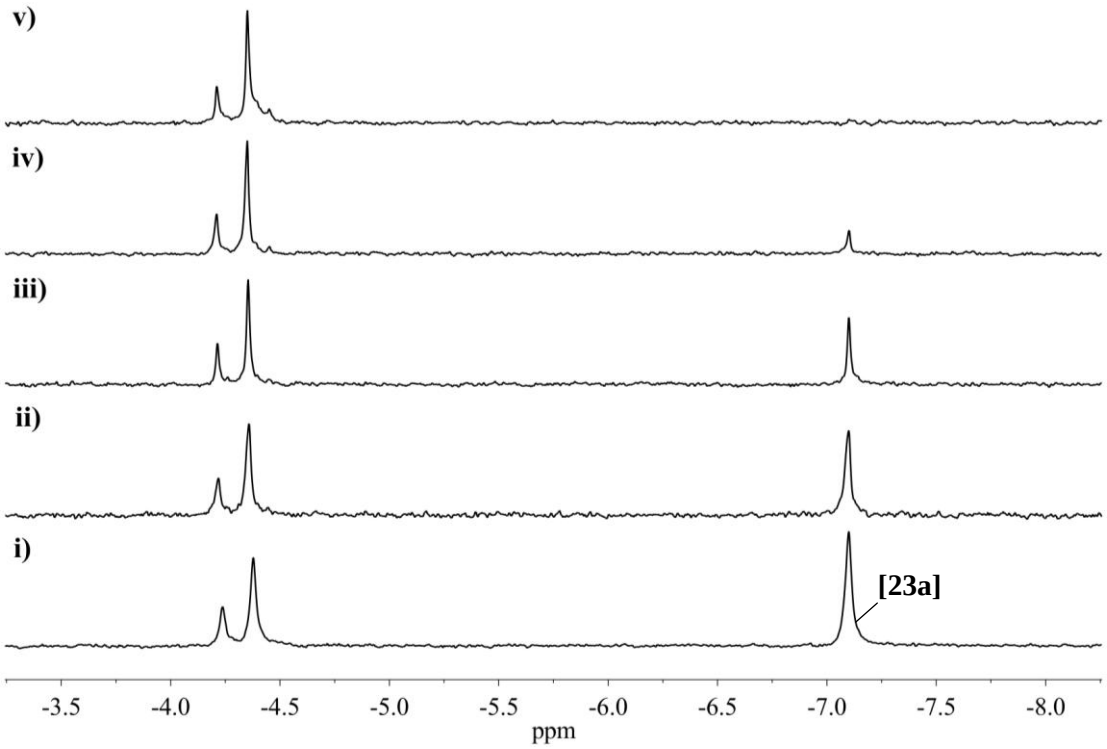

Figure 2.3: *In situ* unlocked $^{31}P\{^{1}H\}$ NMR (300 MHz) solution spectroscopy monitoring of the reaction between [**23a**], $TlBF_4$ (2 equiv.), $HC{\equiv}CC_6H_4$-4-COOMe (1 equiv.) and Proton Sponge (excess) in CH_2Cl_2 after i) stirring at room temperature for 3 days, and then subsequently heating the solution at reflux for ii) 2 hours; iii) 6 hours; iv) 16 hours and v) 48 hours.

With reference to the $^{31}P\{^{1}H\}$ NMR spectra shown in Figure 2.3, as the reaction progressed, the starting material [**23a**] (s, δ – 7.1 ppm) wholly transformed into two new products giving singlet signals at δ – 4.2 and – 4.4 ppm, consistent with the formation of multiple *trans*-bis(alkynyl) complexes. Purification was limited to precipitation with an anti-solvent (hexanes) by the general instability of *trans*-bis(alkynyl) {$Ru(dppm)_2$} complexes on chromatographic medium and as such, no pure complexes were isolated from the reaction mixture. However, the mass spectrum (MALDI from methanol solutions) taken of the crude mixture indicated formation of [**24b**] ($[M + H]^+$: 1189 *m/z*) whilst the IR spectrum (CH_2Cl_2) revealed a broad band at 2055 cm^{-1} with a shoulder at 2075 cm^{-1}, consistent with multiple ν(RuC≡C) environments. Ligand scrambling effects have previously been observed at the {$Ru(dppm)_2$} centre,[44, 48, 51] and are likely complicating the reaction profile here as well as accounting for the low yields obtained by Dixneuf.[39]

2.3.4. Single crystal X-ray diffraction studies

Single crystal X-ray structure determinations have been carried out for the complexes *trans*-[RuCl(C≡CC_6H_4-4-COOMe)(dppm)$_2$], [**23b**] as a CH_2Cl_2 solvate (Figure 2.4); *trans*-[RuCl(C≡CC_6H_4-4-C≡C$SiMe_3$)(dppm)$_2$], [**23c**] as a CH_2Cl_2 solvate (Figure 2.5); *trans*-[RuCl(C≡CC_6H_5)(dppm)$_2$], [**23d**] (Figure 2.6); *trans*-[RuCl(C≡CC_6H_4-4-Me)(dppm)$_2$], [**23e**] as a CH_2Cl_2 solvate (Figure 2.7); *trans*-[RuCl(C≡CC_6H_4-4-OMe)(dppm)$_2$], [**23f**] as a CH_2Cl_2 solvate (Figure 2.8) and *trans*-[Ru(C≡CC_6H_4-4-COOMe)$_2$(dppm)$_2$], [**24b**] as a $CHCl_3$ solvate (Figure 2.9). The atom labelling scheme and representation of the torsion angle θ are given in Figures 2.10 and 2.11, respectively, to clarify important bond lengths and angles of complexes [**23b – f, 24b**] which have been summarised in Tables 2.2 and 2.3, together with those of literature complexes *trans*-[RuCl(C≡CC_6H_4-4-NO_2)(dppm)$_2$], [**23a**],[50] and *trans*-[Ru(C≡CC_6H_4-4-NO_2)$_2$(dppm)$_2$], [**24a**][51] for comparison.

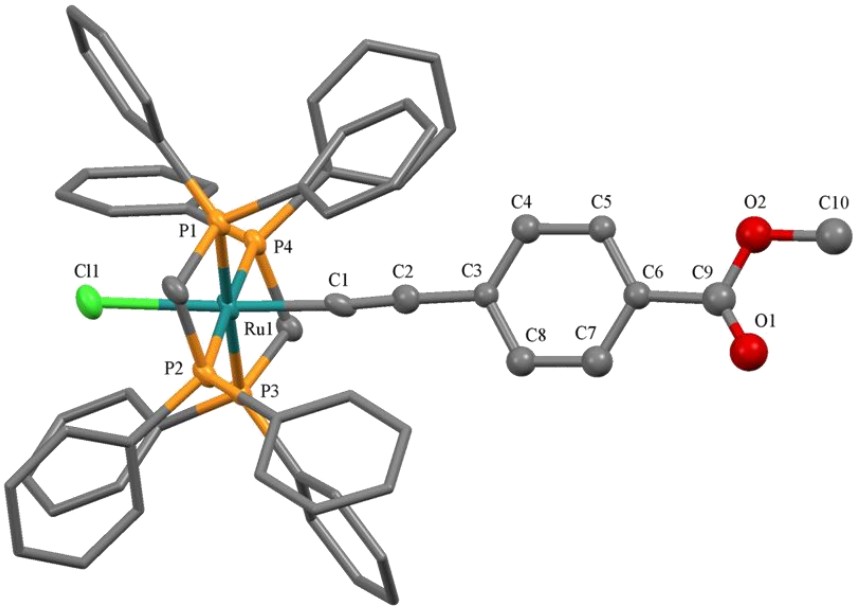

Figure 2.4: A plot of a molecule of [**23b**], with solvent of crystallisation (1 × CH_2Cl_2) and hydrogen atoms removed for clarity. Ellipsoids for key atoms are drawn at the 50 % probability level.

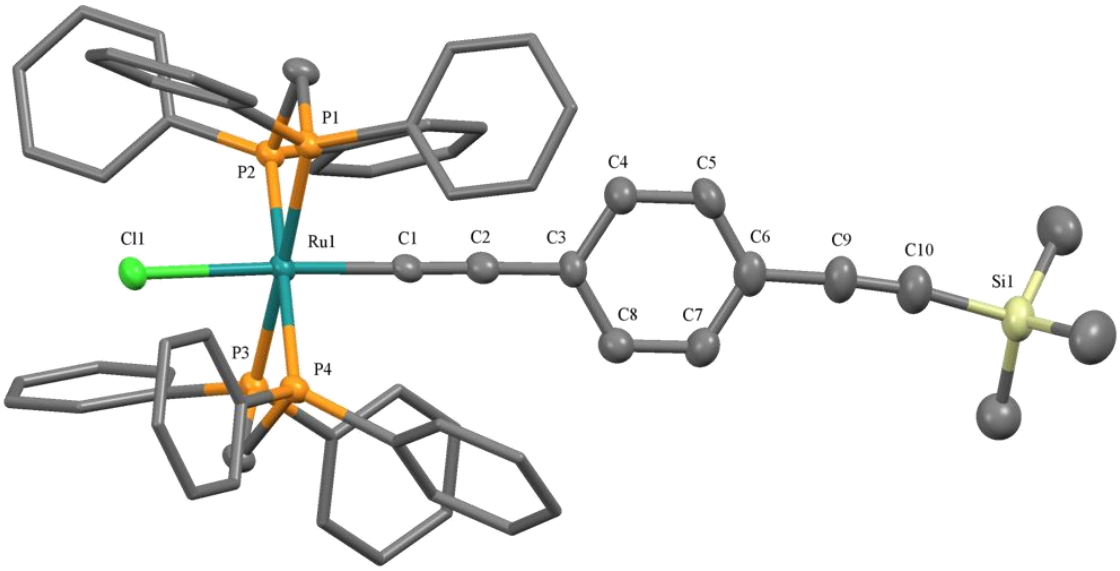

Figure 2.5: A plot of a molecule of [**23c**], with solvent of crystallisation (1 × CH_2Cl_2) and hydrogen atoms removed for clarity. Ellipsoids for key atoms are drawn at the 50 % probability level.

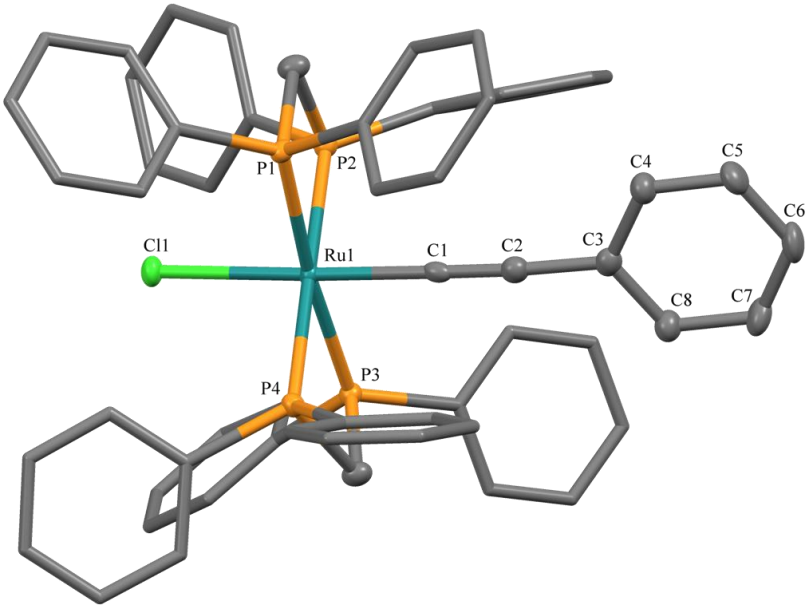

Figure 2.6: A plot of a molecule of [**23d**], with hydrogen atoms removed for clarity. Ellipsoids for key atoms are drawn at the 50 % probability level.

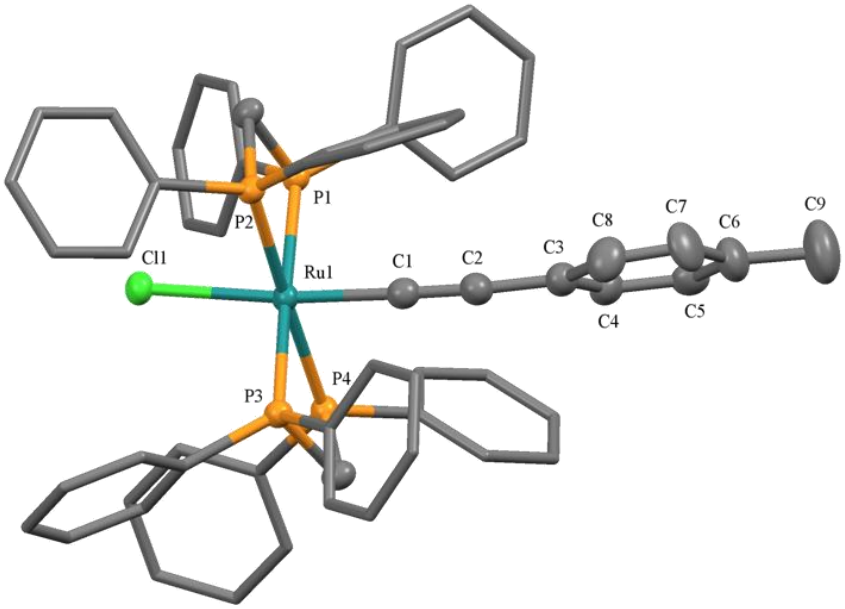

Figure 2.7: A plot of a molecule of [**23e**], with solvent of crystallisation (1 × CH_2Cl_2) and hydrogen atoms removed for clarity. Ellipsoids for key atoms are drawn at the 50 % probability level.

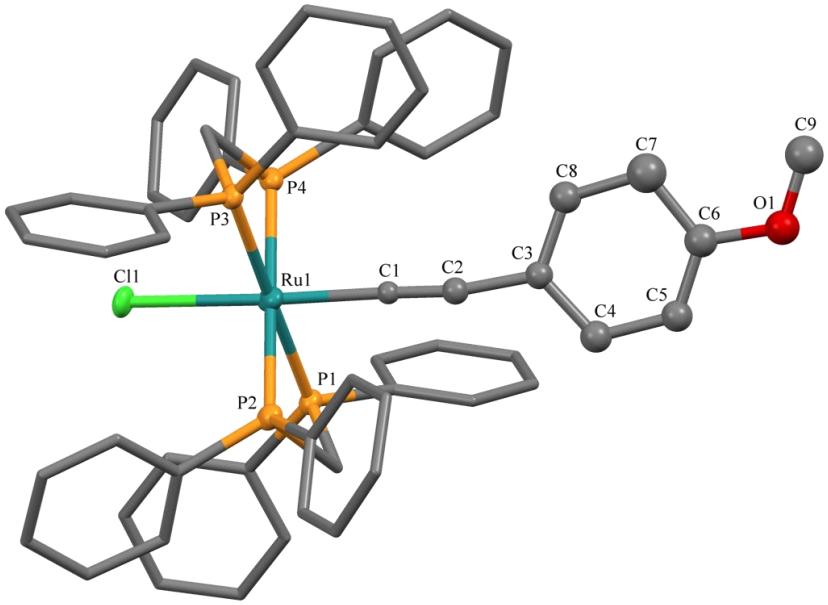

Figure 2.8: A plot of a molecule of [**23f**], with solvent of crystallisation (1 × CH_2Cl_2) and hydrogen atoms removed for clarity. Ellipsoids for key atoms are drawn at the 50 % probability level.

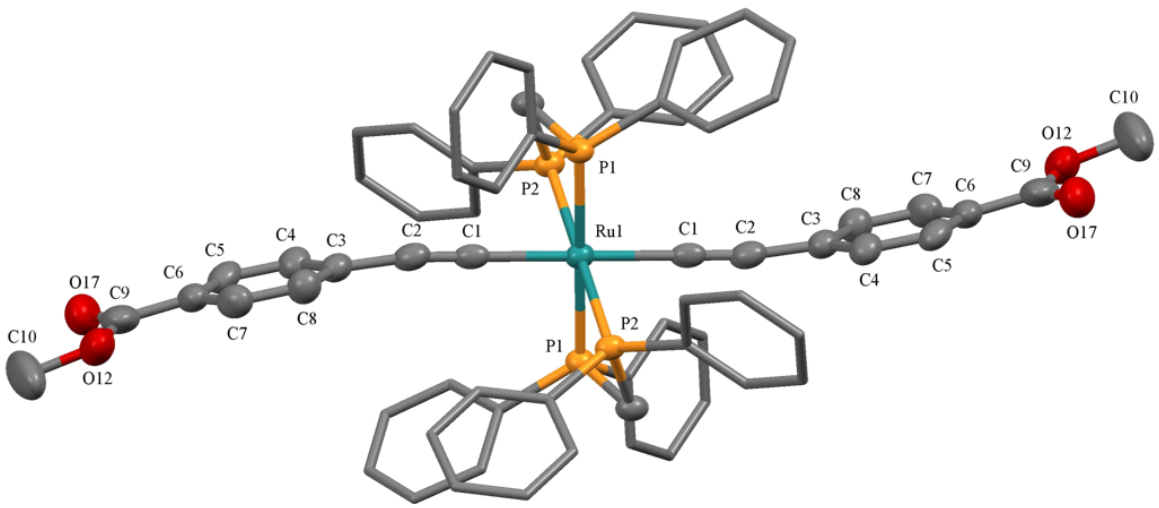

Figure 2.9: A plot of a molecule of [**24b**], with solvent of crystallisation (1 × $CHCl_3$) and hydrogen atoms removed for clarity. Ellipsoids for key atoms are drawn at the 50 % probability level.

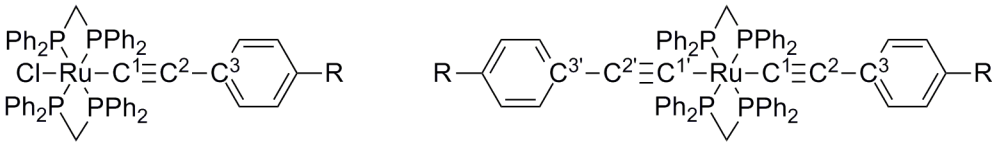

[23] **[24]**

Figure 2.10: The atom labelling schemes of complexes [**23**] and [**24**] used in Tables 2.2 and 2.3.

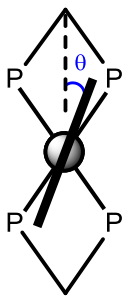

Figure 2.11: Representation of angle θ in *trans*-[RuCl(C≡CC_6H_4-4-R)(dppm)$_2$], [**23**], and *trans*-[Ru(C≡CC_6H_4-4-R)$_2$(dppm)$_2$], [**24**], complexes.

Table 2.2: Selected bond distances (Å) and torsion angles (θ / °) for: *trans*-[RuCl(C≡CC_6H_4-4-COOMe)(dppm)$_2$], [**23b**]; *trans*-[RuCl(C≡CC_6H_4-4-C≡C$SiMe_3$)(dppm)$_2$], [**23c**]; *trans*-[RuCl(C≡CC_6H_5)(dppm)$_2$], [**23d**]; *trans*-[RuCl(C≡CC_6H_4-4-Me)(dppm)$_2$], [**23e**]; *trans*-[RuCl(C≡CC_6H_4-4-OMe)(dppm)$_2$], [**23f**] and *trans*-[Ru(C≡CC_6H_4-4-COOMe)$_2$(dppm)$_2$], [**24b**] (this work) together with *trans*-[RuCl(C≡CC_6H_4-4-NO_2)(dppm)$_2$], [**23a**][50] and *trans*-[Ru(C≡CC_6H_4-4-NO_2)$_2$(dppm)$_2$], [**24a**].[51]

Complex	**Ru-C^1**	**C^1≡C^2**	**C^2-C^3**	**Ru-Cl**	**Ru-P$^{1-4}$**	θ
[**23a**]	1.998(7)	1.190(8)	1.428(8)	2.483(2)	2.332(2), 2.379(2), 2.332(2), 2.358(2)	84.1
[**23b**]	2.019(3)	1.181(4)	1.464(4)	2.4862(7)	2.3427(7), 2.3692(7), 2.3247(7), 2.3678(6)	92.5
[**23c**]	2.010(3)	1.187(4)	1.432(4)	2.4629(8)	2.3404(7), 2.3138(8), 2.3302(7), 2.3593(8)	9.1
[**23d**]	2.004(1)	1.201(3)	1.436(3)	2.4511(4)	2.3445(5), 2.3454(5), 2.3557(5), 2.3205(5)	25.3
[**23e**]	1.999(4)	1.221(5)	1.427(5)	2.4938(9)	2.3487(8), 2.3358(8), 2.3312(8), 2.3744(8)	82.3
[**23f**]	2.014(9)	1.15(1)	1.45(1)	2.558(2)	2.338(2), 2.315(2), 2.348(2), 2.347(2)	2.7
[**24a**]	2.051(3)	1.207(4)	1.427(5)	-	2.344(1), 2.344(1), 2.3341(9), 2.3341(9)	13.8
[**24b**]	2.085(6)	1.150(7)	1.457(8)	-	2.331(2), 2.360(1), 2.331(1), 2.360(1)	80.3

Table 2.3: Selected bond angles (º) for: *trans*-[RuCl(C≡CC_6H_4-4-COOMe)(dppm)$_2$], [**23b**]; *trans*-[RuCl(C≡CC_6H_4-4-C≡C$SiMe_3$)(dppm)$_2$], [**23c**]; *trans*-[RuCl(C≡CC_6H_5)(dppm)$_2$], [**23d**]; *trans*-[RuCl(C≡CC_6H_4-4-Me)(dppm)$_2$], [**23e**]; *trans*-[RuCl(C≡CC_6H_4-4-OMe)(dppm)$_2$], [**23f**] and *trans*-[Ru(C≡CC_6H_4-4-COOMe)$_2$(dppm)$_2$], [**24b**] (this work) together with *trans*-[RuCl(C≡CC_6H_4-4-NO_2)(dppm)$_2$], [**23a**][50] and *trans*-[Ru(C≡CC_6H_4-4-NO_2)$_2$(dppm)$_2$], [**24a**].[51]

Complex	Cl-Ru-C^1	Ru-C^1≡C^2	C^1≡C^2-C^3	P^1-Ru-P^4	P^2-Ru-P^3	P^1-Ru-P^2	P^3-Ru-P^4
[**23a**]	177.7(2)	176.8(5)	168.4(7)	177.9(1)	177.2(1)	70.2(1)	71.0(1)
[**23b**]	175.3(1)	175.5(2)	172.9(3)	178.0(1)	177.7(1)	71.1(1)	70.9(1)
[**23c**]	173.8(1)	173.9(3)	177.7(4)	177.1(1)	176.3(1)	72.0(1)	71.6(1)
[**23d**]	177.9(1)	177.4(2)	175.2(2)	174.4(1)	178.9(1)	72.2(1)	71.8(1)
[**23e**]	173.9(1)	175.5(3)	172.5(4)	177.0(1)	177.3(1)	71.7(1)	71.4(1)
[**23f**]	174.7(2)	177.8(8)	169.1(1)	179.1(1)	179.9(1)	70.8(1)	71.2(1)
[**24a**]	180[a]	178.3(3)	173.9(4)	180	180	70.8	70.8
[**24b**]	180[a]	177.7(5)	172.0(6)	180	180	71.0(1)	71.0(0)

[a] *for Cl read C(1')*

The complexes [**23b**], [**23e**] and [**23d**] all crystallise in the triclinic space group $P\bar{1}$, whilst [**23c**], [**23f**] and [**24b**] crystallise in the monoclinic space groups $P2_1/n$, $P2_1$ and $C2/c$ space groups, respectively. The P-Ru-P bond angles between *cis*-phosphines (~ 70 °) and those between *trans*-phosphines (~ 178 °) and Cl / C(1′)-Ru-C(1)≡ angles (173.8 – 180 º), indicate approximate octahedral geometry about the ruthenium centre, in agreement with the previously reported structures of [**23a**] and [**24a**].[50, 51] The bond angles along the 5-atom Cl-Ru-C(1)≡C(2)-C(3)- and –C(1′)-Ru-C(1)≡C(2)-C(3)- chains are close to 180 °, confirming a rod-type structure, with slight deviations that may be attributed to molecular packing and steric effects.

McGrady has analysed the electronic structures of [Ru(C≡CR′)$(PH_3)_2(\eta^5$-$C_5Me_5)$] and *trans*-[RuCl(C≡CR′)$(PH_3)_4$] complexes (where R′ = H, C_6H_5, C_6H_4-4-NO_2), and found that electronic variation of the alkynyl fragment will synergistically affect both the σ-forward and π-backbonding effects between C≡C(π) and M(*d*), therefore interpretations of Ru-C≡C bond length perturbations cannot be based solely on backbonding interactions.[52] Further to this, Low has shown that the orientation adopted

by the phenylene ring system relative to the RuP_4 fragment determines the effectiveness of M(*d*) / C≡C(π) orbital overlaps, and hence the extent to which the π-donor or acceptor properties of the remote substituent can be inferred from solid-state structural parameters.[25]

The angle θ (Figure 2.11) provides a convenient proxy measure for the alignment of the aryl (Ar) π-system with M(*d*) on geometric grounds. Angles close to 0° or 90° give rise to the most effective overlaps and hence greatest correlation of structural and electronic properties.[25] For complexes [**23a**] and [**23b**] bearing electron withdrawing R groups, the Ru-Cl distances cluster at the shorter end of the range, whilst those from [**23e**] and [**23f**] bearing the more electron-rich tolyl and anisole rings are significantly longer. These complexes adopt conformations in the solid state with θ angles close to the idealised values. However, less clear trends in Ru-Cl bond lengths with nature of the aryl substituent are observed for [**23c**] (θ = 10°) and [**23d**] (θ = 25°). Similarly, [**23e**] and [**23f**] have, on average, shorter Ru-P bond lengths than [**23a**] and [**23b**] (by ~ 0.01 Å) consistent with increased Ru-P backbonding arising from the increased σ-donation to the metal from the alkynyl fragments.

The Ru-C(1) bond length appears insensitive to the electronic nature of the R substituent for *mono*-alkynyl complexes [**23a – f**] (determined within the narrow range of 1.998(7) – 2.019(3) Å). Humphrey similarly found that introduction of a strongly withdrawing *para*-substituent (R = NO_2, C_6H_4-4-NO_2) had little effect on the Ru-C(1) bond length, comparing *trans*-[RuCl(C≡CC_6H_4-4-C_6H_4-4-NO_2)(dppm)$_2$] (1.994(4) Å) and [**23a**] (1.998(7) Å)[50] with *trans*-[RuCl(C≡CC_6H_5)(dppe)$_2$], [**37**] (2.007(5) Å),[42] although the electronic effect due to different ancillary ligands, nor the alignment of Ar(π) / M(*d*), was discussed.[51] In contrast, the Ru-C(1) bond lengths vary significantly between *trans*-bis(alkynyl) complexes [**24a**] (2.051(3) Å)[2] and [**24b**] (2.085(6) Å) reflecting the differences in σ-donor / π-acceptor strengths of the phenylene fragments compared with the chloride of *mono*-alkynyl complexes.

In seeking to understand the influence of the dppm and dppe ligands on molecular structure, comparable complexes featuring these ligands were sought. The search is compounded by the range of θ values adopted in these complexes. Following a

systematic survey of *mono*-alkynyl {Ru(dppe)$_2$} complexes,[25] only the pairing of *trans*-[RuCl(C≡CC$_6$H$_4$-4-COOMe)(dppe)$_2$][36] and the dppm analogue [**23b**] (this work) are found with similar optimised θ values (close to 90 °) and thus may be directly compared. All bond lengths and angles are similar except for the longer Ru-Cl bond length (by 0.056 Å) and shorter average Ru-P bond lengths (by 0.017 Å) of [**23b**] reflecting the increased σ-donor / π-acceptor strength of the dppm ligands compared with dppe.

During the exploration of *trans*-bis(alkynyl) {Ru(dppm)$_2$} complexes, the *bis*(trimethylsilyl)ethynyl complex [**86**] was also structurally characterised (Figure 2.12). Given that such complexes are not affected by θ values, direct comparisons can be made with similar systems bearing alternative ancillary ligands.

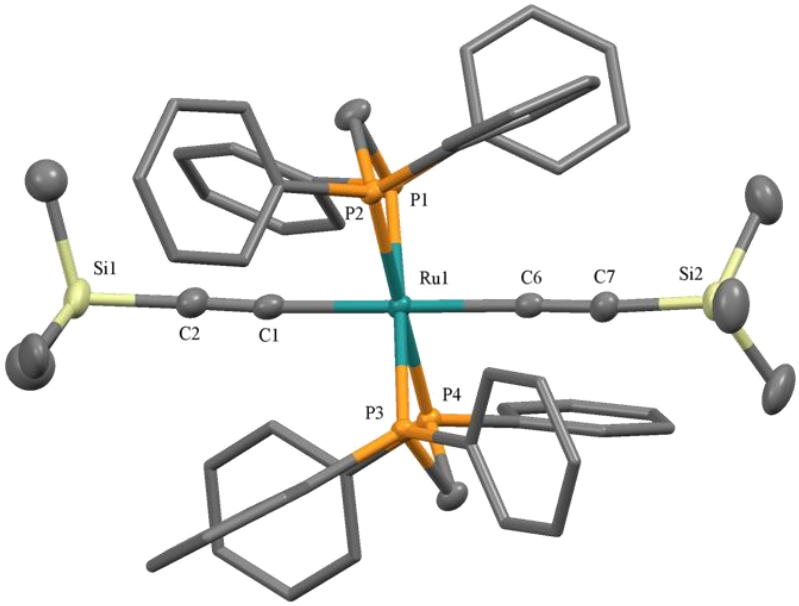

Figure 2.12: Solid state structure of one molecule of [**86**], with solvate (0.25 × CH_2Cl_2) atoms and hydrogen atoms removed for clarity. Ellipsoids for key atoms are drawn at the 50 % probability level. Selected bond lengths / Å; molecule 1: Ru(1)-C(1) 2.057(5), Ru(1)-C(6) 2.060(5), Ru(1)-P(1) 2.314(1), Ru(1)-P(2) 2.317(1), Ru(1)-P(3) 2.319(1), Ru(1)-P(4) 2.326(1), C(1)-C(2) 1.203(7), C(6)-C(7) 1.219(7); molecule 2: Ru(1)-C(1) 2.067(5) Ru(1)-C(6) 2.050(5) Ru(1)-P(1) 2.317(1), Ru(1)-P(2) 2.319(1), Ru(1)-P(3) 2.330(1), Ru(1)-P(4) 2.320(1), C(1)-C(2) 1.214(7), C(6)-C(7) 1.200(7). Selected bond angles / °; molecule 1: C(1)-Ru(1)-C(6) 174.5(2), Ru-C(1)-C(2) 174.4(4), Ru-C(6)-C(7) 176.1(4), P(1)-Ru(1)-P(2) 72.65(4), P(3)-Ru(1)-P(4) 72.14(4), P(1)-Ru(1)-P(3) 177.07(4), P(2)-Ru(1)-P(4) 178.93(4); molecule 2: C(1)-Ru(1)-C(6) 174.2(2), Ru-C(1)-C(2) 173.4(4), Ru-C(6)-C(7) 175.5(4), P(1)-Ru(1)-P(2) 72.46(4), P(3)-Ru(1)-P(4) 72.25(4), P(1)-Ru(1)-P(3) 178.22(4), P(2)-Ru(1)-P(4) 177.82(4).

The complex [**86**] is found to crystallise in a triclinic crystal system containing two independent molecules, with a $P\bar{1}$ space group. The P-Ru-P bond angles between *cis*-phosphines (~ 72 °) and those between *trans*-phosphines (~ 176 °) in addition to the C(1)-Ru-C(6) angle (~ 174 °), indicates octahedral geometry about the ruthenium centre supported by the chelating dppm ligands and two trimethylsilyl-ethynyl ligands, consistent with the {$Ru(dppm)_2$} series presented here. Few crystallographically determined *bis*(trimethylsilyl)ethynyl ruthenium complexes exist.[53-55] Within this family of complexes (*trans*-[$Ru(C{\equiv}CSiMe_3)_2(dmpe)_2$],[53] *trans*-[$Ru(C{\equiv}CSiMe_3)_2(CO)_2(PEt_3)_2$][54]

and *trans*-[Ru(C≡CSiMe$_3$)$_2$(PMe$_3$)$_4$][55]), Ru-C(1/6) and C(1/6)≡C(2/7) bond lengths (see Figure 2.12 for labelling scheme) are similar. However, the average Ru-P bond length (Ru-P$_{avg}$) of [**86**] (2.319 Å) is shorter than *trans*-[Ru(C≡CSiMe$_3$)$_2$(PMe$_3$)$_4$] (2.335 Å), yet longer than *trans*-[Ru(C≡CSiMe$_3$)$_2$(dmpe)$_2$] (2.305 Å), establishing that the σ-donor / π-acceptor properties of the dppm ligands are increased compared with PMe$_3$ in the former and decreased compared with dmpe in the latter. The longer Ru-P$_{avg}$ length of *trans*-[Ru(C≡CSiMe$_3$)$_2$(CO)$_2$(PEt$_3$)$_2$] (2.369 Å) is reflective of the strong π-accepting nature of the carbonyl ligands, which limits backbonding to the phosphines.

A molecule of *E*-[Ru(η^3-{HC(C$_6$H$_4$-4-Me)=CC≡CC$_6$H$_4$-4-Me})(dppm)$_2$]BF$_4$, [**28e**]$^+$, is shown in Figure 2.13.

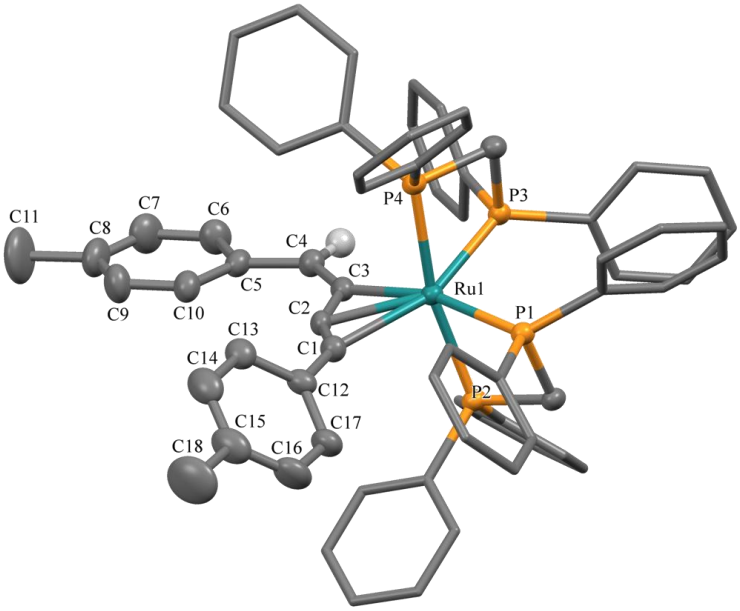

Figure 2.13: A plot of the cation [**28e**]$^+$, with solvate (0.5 × C$_3$H$_6$O), counter ion ([BF$_4$]$^-$) and selected hydrogen atoms removed for clarity. Ellipsoids for key atoms are drawn at the 50 % probability level. Selected bond lengths / Å: Ru(1)-C(1) 2.386(4), Ru(1)-C(2) 2.208(4), Ru(1)-C(3) 2.136(4), Ru(1)-P(1) 2.372(1), Ru(1)-P(2) 2.3496(9), Ru(1)-P(3) 2.3127(7), Ru(1)-P(4) 2.3684(9), C(1)-C(2) 1.259(5), C(2)-C(3) 1.367(5), C(3)-C(4) 1.343(6). Selected bond angles / °: C(1)-Ru(1)-C(3) 68.1(1), C(1)-C(2)-C(3) 150.9(4), C(2)-C(1)-C(12) 144.1(4), C(2)-C(3)-C(4) 135.7(4), P(1)-Ru(1)-P(2) 70.90(3), P(3)-Ru(1)-P(4) 70.47(4), P(1)-Ru(1)-P(3) 94.70(3), P(2)-Ru(1)-P(4) 167.75(3).

The complex [**28e**]BF_4 is found in an orthorhombic crystal system and a *Pca*2_1 space group. The chelating dppm ligands adopt a mutually *cis*-position with the η^3-butenynyl ligand, exhibiting *E*-stereochemistry, occupying the remaining two coordination sites in the equatorial plane around the approximately octahedral cationic ruthenium centre. Structures of this type are not uncommon.[45, 56-58] Albertin and Bordignon have structurally characterised *E*-[Ru(η^3-{HC(C_6H_4-4-Me)=CC≡CC_6H_4-4-Me})$\{P(OEt)_2Ph\}_4$]BF_4, thus allowing the role of the ancillary ligands in these complexes to be explored.[59] The Ru$\{P(OEt)_2Ph\}_4$ complex has a shorter Ru-P_{avg} bond length (2.329 *vs.* 2.351 Å) reflecting the stronger σ-donor / π-acceptor strength of the $P(OEt)_2Ph$ ancillary ligands, compared with dppm. Although Ru-C(3) and C(3)=C(4) bond lengths are comparable between the two complexes (see Figure 2.13 for atom labelling scheme), in the Ru$\{P(OEt)_2Ph\}_4$ derivative, both the Ru-C(2) (2.244 Å) and C(2)-C(3) (1.39(2) Å) bond lengths are longer, whilst the C(1)≡C(2) (1.23(2) Å) length is shorter. As the structures of η^3-butenynyl complexes have been previously described with a fractional contribution of triene resonance form (Figure 2.14),[45] the data might indicate that complexes bearing less strongly σ-donating / π-accepting ligands (such as dppm *vs.* $P(OEt)_2Ph$) will contain a higher proportion of the triene to account for these differences.

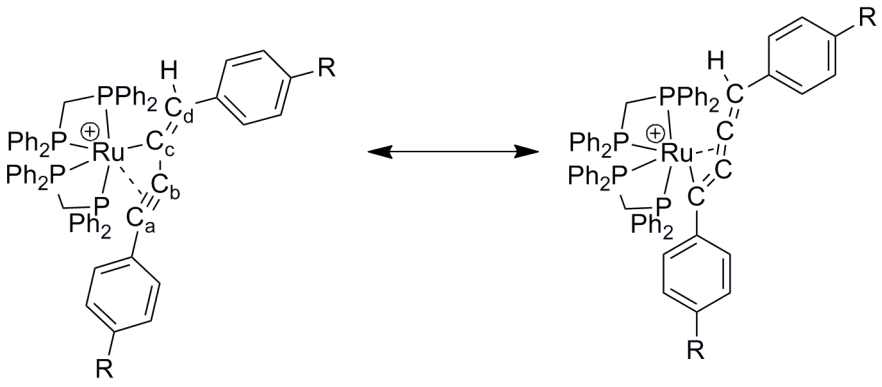

Figure 2.14: Resonance forms of η^3-butenynyl complexes of the type, *E*-[Ru(η^3-{HC(C_6H_4-4R)=CC≡CC_6H_4-4-R})$(dppm)_2$]$^+$ with the generally accepted structure on the left and the proposed triene structure on the right.

In order to suitably explore the role of the R substituent in such complexes, [**28e**]$^+$ (this work) can be compared with *E*-[Ru(η^3-{HC(C_6H_5)=CC≡CC_6H_5})$(dppm)_2$]BF_4, [**28d**]$^+$.[45]

Between the structures, Ru-P_{avg}, C(1)≡C(2), C(2)-C(3) and C(3)=C(4) bond distances are similar (see Figure 2.13 for atom labelling scheme). However, for [**28d**]$^+$, the Ru-C(1) (2.404(4) Å), Ru-C(2) (2.230(4) Å) and Ru-C(3) (2.156(4) Å) bond lengths are collectively longer, reflecting the increased σ-donor character of the tolyl substituent. Interestingly, in the same paper by Lynam,[45] *E*-[Ru(η^3-{HC(^{n}Pr)=CC≡C^{n}Pr})(dppm)$_2$]BF_4, [**30**]$^+$, was structurally characterised with the shortest average Ru-C(1/2/3) bond length (2.226 Å) of their series (*E*-[Ru(η^3-{HCR′=CC≡CR′})(dppm)$_2$]BF_4: R′ = C_6H_5, [**28d**]$^+$; ^{n}Bu, [**29**]$^+$; ^{n}Pr, [**30**]$^+$) in addition to very similar C(1)≡C(2) (1.301(6) Å), C(2)-C(3) (1.345(6) Å) and C(3)=C(4) (1.369(6) Å) bond lengths implicating a higher proportion of the triene resonance structure for the saturated R′ group (R′ = ^{n}Pr, [**30**]$^+$), compared with aryl-containing R′ groups (R′ = C_6H_5, [**28d**]$^+$; C_6H_4-4-Me, [**28e**]$^+$), hence further elucidating the role of the R substituent.

2.3.5. Electrochemistry

The electrochemical responses of complexes [**22**]BF_4, [**23**] and [**24**] were examined by cyclic voltammetry (CV) in 0.1 M tetra-butylammonium hexafluorophosphate ([N^{n}Bu$_4$]PF_6) CH_2Cl_2 solutions. Potentials are quoted against ferrocene using an internal decamethylferrocene / decamethylferrocenium reference ([Fe(η^5-C_5Me_5)$_2$] / [Fe(η^5-C_5Me_5)$_2$]$^+$ = – 0.48 V *vs.* [Fe(η^5-C_5H_5)$_2$] / [Fe(η^5-C_5H_5)$_2$]$^+$) (Table 2.4).[60] In all cases, the first oxidation process of complexes [**22**]$^+$, [**23**] and [**24**] displayed *quasi*-reversible electrochemical behaviour at the electrode interface, with ΔE_p ($E_{pc} - E_{pa}$) values being close to that of the internal standard at slow scan rates, but increasing with increasing scan rate. At room temperature there was evidence of electrochemical-chemical (EC) behaviour, with $i_{pc} > i_{pa}$, but with improvement to the chemical reversibility evident at reduced temperatures (dry ice / acetone bath), where current ratios approach unity.

Table 2.4: Selected electrochemical data (V) of vinylidene [**22**]$^+$, *mono*-alkynyl [**23**] and *trans*-bis(alkynyl) [**24**] {Ru(dppm)$_2$} complexes where: $E_{1/2}(n)$ = half-wave potential of nth oxidation; $E_{1/2}(red)$ = half-wave potential of reduction; ΔE_{1-2} = potential difference between first and second oxidations and ΔE_{red-1} = potential difference between first oxidation and reduction.

Complex	$E_{1/2}(1)$	$E_{1/2}(2)$	$E_{1/2}(red)$	ΔE_{1-2}	ΔE_{red-1}
[**22a**]$^+$	1.07	1.35	− 1.79	0.28	2.44
			− 1.37		
[**22b**]$^+$	1.04	1.33	− 1.13	0.29	2.17
[**22c**]$^+$	0.91	1.28	− 1.09	0.37	2.19
[**22d**]$^+$	0.92	1.26	− 1.04	0.34	1.96
[**22e**]$^+$	0.84	1.27	− 1.09	0.43	1.93
[**22f**]$^+$	0.72	1.02	− 1.17	0.30	1.89
[**23a**]	0.23	1.19	− 1.76	0.96	1.97
[**23b**]	0.13	1.18	-	1.05	-
[**23c**]	0.06	1.07	-	1.00	-
[**23d**]	0.03	1.08	-	1.06	-
[**23e**]	0.00	1.03	-	1.03	-
[**23f**]	− 0.08	0.79	-	0.87	-
[**24a**]	0.24	0.94	− 1.69	0.70	1.93
[**24b**]	0.13	0.96	-	0.83	-
[**24c**]	0.06	1.06	-	1.00	-

The vinylidene complexes ([**22**]BF_4) all display two, one-electron oxidation events (the first *quasi*-reversible, the second irreversible; except [**22f**]BF_4 where both are *quasi*-reversible) and a single, one-electron, irreversible reduction event. The trend in $E_{1/2}(1)$, which span some 0.35 V, follows the electronic properties of the alkynyl ligand, leading to the assignment of these events as oxidation largely of the phenylene fragment. In turn, $E_{1/2}(2)$ is, with the exception of [**22f**]BF_4, less sensitive to the nature of the R group and is therefore assigned to a more metal-centred, [Ru^{II}] / [Ru^{III}], oxidation. In the case of [**22f**]BF_4, the combination of the strongly electron-donating OMe group and {Ru(dppm)$_2$} fragment may lead to greater stabilisation of the second oxidation product. The reduction, $E_{1/2}(red)$, can be attributed to reduction of the vinylidene ligand

(population of the singlet carbene-like C(*p*) orbital at C_α).[61] For [**22a**]BF_4, R = NO_2, the vinylidene reduction overlaps the reduction of the terminal NO_2 group, indicated by the doubly higher peak current and slightly larger ΔE_p value (90 mV) versus the internal standard (70 mV).

The *mono*-[**23**] and *bis*-[**24**] alkynyl complexes display two, one-electron oxidation events (the first *quasi*-reversible, the second irreversible; except [**23f**] where both oxidations are *quasi*-reversible). For [**23a**], a one-electron reduction of the nitro group is also observed. In the case of [**24a**], the two nitro aromatic reductions are overlapped, as evidenced by the larger apparent ΔE_p value (190 mV) compared with the internal standard (80 mV) and larger peak current.

For [**23**], higher $E_{1/2}(1)$ values are found for complexes containing electron withdrawing R groups ([**23a** − **c**]) than those bearing electron donating R groups ([**23e** − **f**]) (Figure 2.15).

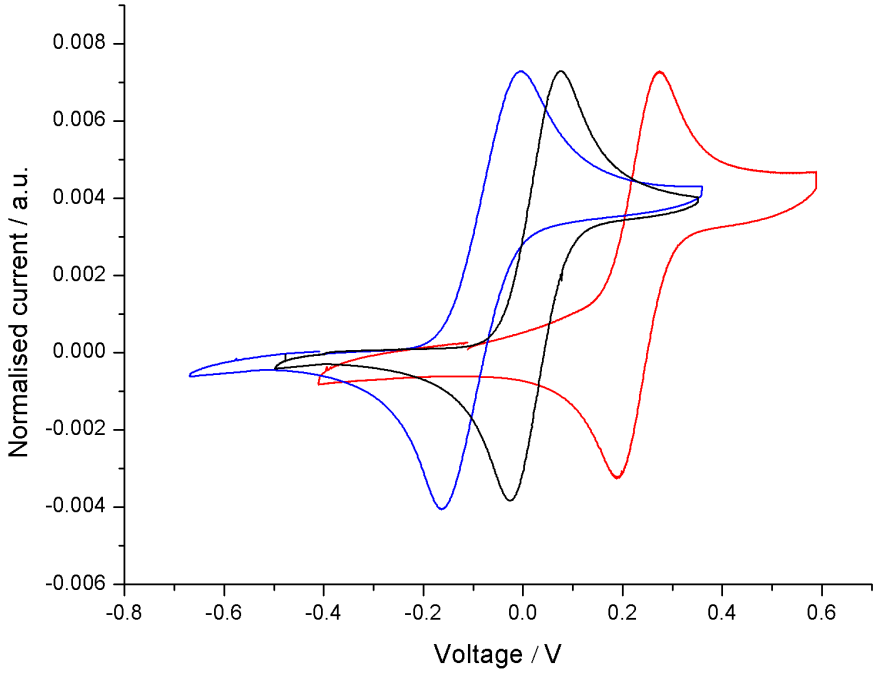

Figure 2.15: Cyclic voltammograms of representative *trans*-[RuCl(C≡CC_6H_4-4-R)$(dppm)_2$] complexes where R = NO_2, [**23a**] (red line); H, [**23d**] (black line) and OMe, [**23f**], (blue line) showing the electronic dependence of the *para*-substituent on first oxidation potential. Scans were recorded in 0.1M $[N^nBu_4]PF_6$ CH_2Cl_2 solutions in an acetone / dry ice bath at rates of 100 mVs^{-1} and have been normalised to the maximum current of [**23b**].

For related *mono*-alkynyl *trans*-[RuCl(C≡CC_6H_4-4-R)$(dppe)_2$] complexes, Humphrey and co-workers have determined a near-perfect positive, linear free-energy relationship (LFER) exists between the Hammett electronic substituent parameter of the *para*-substituted R group (σ_{para}) and $E_{1/2}(1)$,[62] which is consistent with observations made here in the {$Ru(dppm)_2$} series, reflecting a strong electronic origin for this phenomenon. As the first oxidation potentials ($E_{1/2}(1)$) of [**23**] track the electronic properties of the alkynyl ligand, the event likely arises from depopulation of an orbital with considerable ligand character whereas the second oxidations likely have more metal character, which is in keeping with the [**22**]BF_4 series and previous assignments based on the electrochemical responses of ruthenium(II) alkynyl complexes.[25]

2.4. Discussion

The formation, isolation and characterisation of the vinylidene complexes [**22**]BF_4 and *mono*-alkynyl complexes [**23**] allowed the sequence of events leading to the formation of *trans*-bis(alkynyl) complexes [**24**] *vs.* the η^3-butenynyl complexes [**28**]$^+$ to be followed by *in situ* (unlocked) $^{31}P\{^1H\}$ NMR spectroscopy (Figures 2.16 and 2.17). From a mixture of *cis*-[**20**], $TlBF_4$ (2 equiv.), HC≡CC_6H_4-4-R (2.2 equiv.) and Proton Sponge (excess) in a CH_2Cl_2 solution, the *mono*-alkynyl complexes [**23**] (s, ~ δ − 7.0 ppm) begin to form within 5 minutes. As the reaction proceeds, [**23**] reacts further to give the *trans*-bis(alkynyl) complexes [**24**] (s, ~ δ – 4.0 ppm). For cases when the R substituent is electron withdrawing (Figure 2.16), [**24**] was ultimately formed without any appreciable by-products. However, when the R substituent is electron donating (Figure 2.17), before complete conversion of [**23**] to [**24**], the η^3-butenynyl complex [**28**]$^+$ is observed as four new $^{31}P\{^1H\}$ NMR resonances in a characteristic ABMX coupling pattern.[45] As the reaction proceeds, the product distribution shifts to give the η^3-butenynyl species cleanly without any appreciable by-products, implying the intermediacy of [**24**] in the formation of [**28**]$^+$.

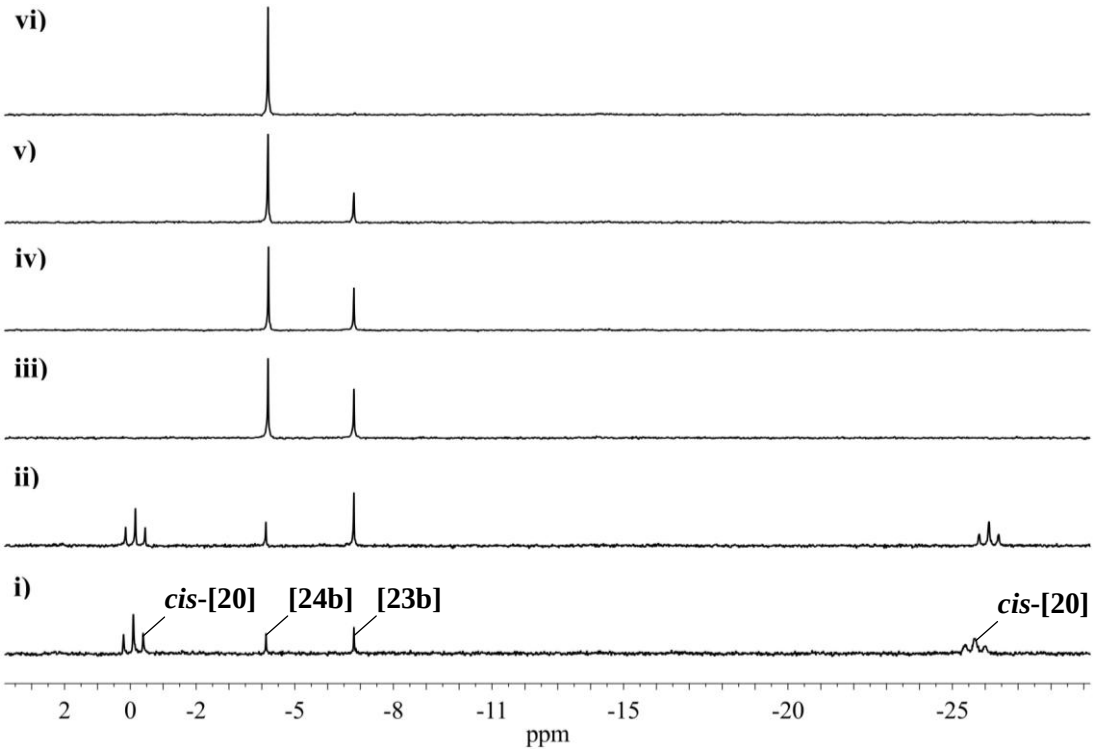

Figure 2.16: *In situ* unlocked $^{31}P\{^{1}H\}$ NMR (400 MHz) solution spectroscopy monitoring of *cis*-[**20**], $TlBF_4$ (2 equiv.), $HC{\equiv}CC_6H_4$-4-COOMe (2.2 equiv.) and Proton Sponge (excess) in CH_2Cl_2 at room temperature after: i) 5 minutes; ii) 20 minutes; iii) 1 hour; iv) 3 hours; v) 7 hours and vi) 30 hours.

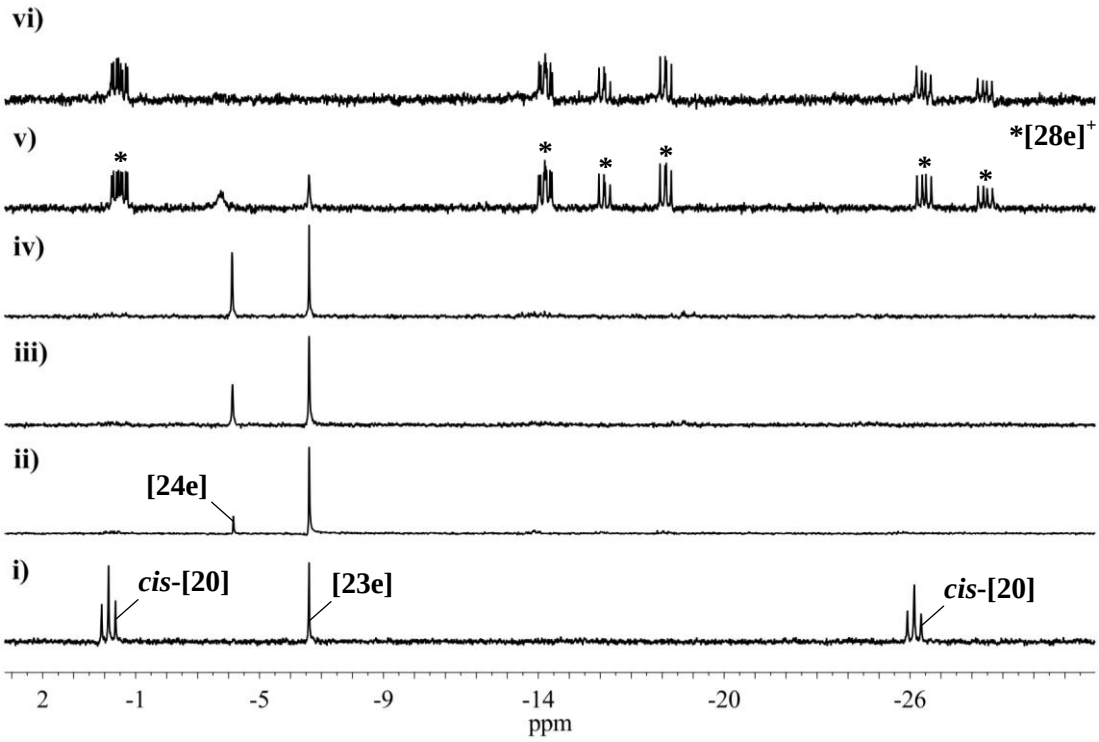

Figure 2.17: *In situ* unlocked $^{31}P\{^{1}H\}$ NMR (400 MHz) solution spectroscopy of *cis*-[**20**], $TlBF_4$ (2 equiv.), $HC{\equiv}CC_6H_4$-4-Me (2.2 equiv.) and Proton Sponge (excess) in CH_2Cl_2 at room temperature after: i) 5 minutes; ii) 75 minutes; iii) 2 hours; iv) 3 hours; v) 24 hours and vi) 48 hours.

In the cases where R is an electron donating group, attempts were made to purify the reaction mixture at intermediate times and isolate the spectroscopically-observed intermediate *trans*-bis(alkynyl) complexes, though these were unsuccessful; yielding only the η^3-butenynyl complex, [**28**]BF_4; suggesting further reaction on work-up (indicating the acid-sensitivity of [**24**] and / or the instability of [**24**] containing electron donating substituents). Interestingly, upon extending the reaction time leading to the formation of *trans*-$[Ru(C{\equiv}CC_6H_4\text{-}4\text{-}COOMe)_2(dppm)_2]$ ([**24b**]) from 30 to 48 hours (Figure 2.18), minor amounts of the corresponding η^3-butenynyl complex ([**28b**]$^+$) were observed in solution.

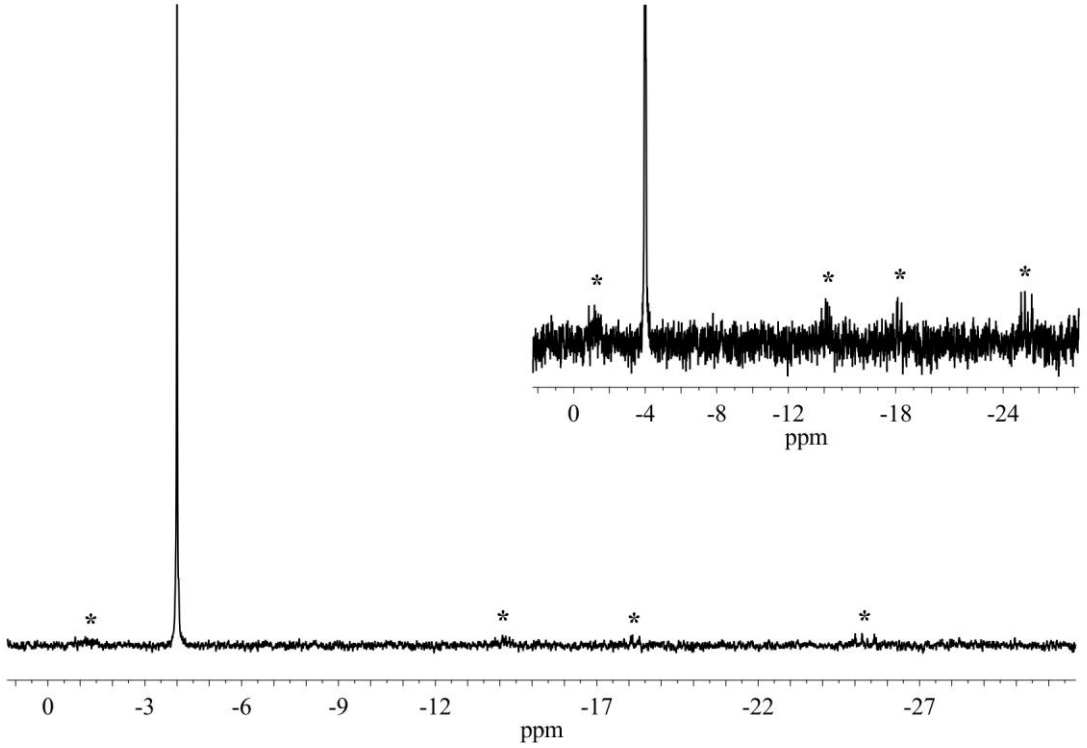

Figure 2.18: *In situ* (unlocked) $^{31}P\{^{1}H\}$ NMR (400 MHz, $CDCl_3$) spectrum following the reaction of *cis*-[**20**], $TlBF_4$ (2 equiv.), $HC{\equiv}CC_6H_4$-4-COOMe (2.2 equiv.) and Proton Sponge (excess) in CH_2Cl_2 at room temperature after 48 hours. Resonances corresponding to the proposed formation of [**28b**]$^+$ are indicated with asterisks, while the resonance at δ – 4.0 ppm corresponds to [**24b**].

This implies that the nature of the R group determines the rate of η^3-butenynyl complex formation, where vinylidene, [**22**]$^+$, *mono*-alkynyl, [**23**], and *trans*-bis(alkynyl) complexes, [**24**], are formed as intermediates in the overall transformation from *cis*-[**20**] to [**28**]$^+$. Though the formations of complexes of the general type [**23**],[39-42, 50, 63-67] [**24**][12, 42, 51, 68-70] and [**28**]$^+$ [71-75] are not uncommon, the role of the incoming alkyne in the transformations to these complexes has not yet been explored.

A proposed mechanism for the formation of {$Ru(dppm)_2$} η^3-butenynyl complexes from reactions of *cis*-[**20**] in methanol solutions with $HC{\equiv}CC_6H_5$ in the presence of $NaPF_6$ and base has been previously reported (Scheme 2.4).[45]

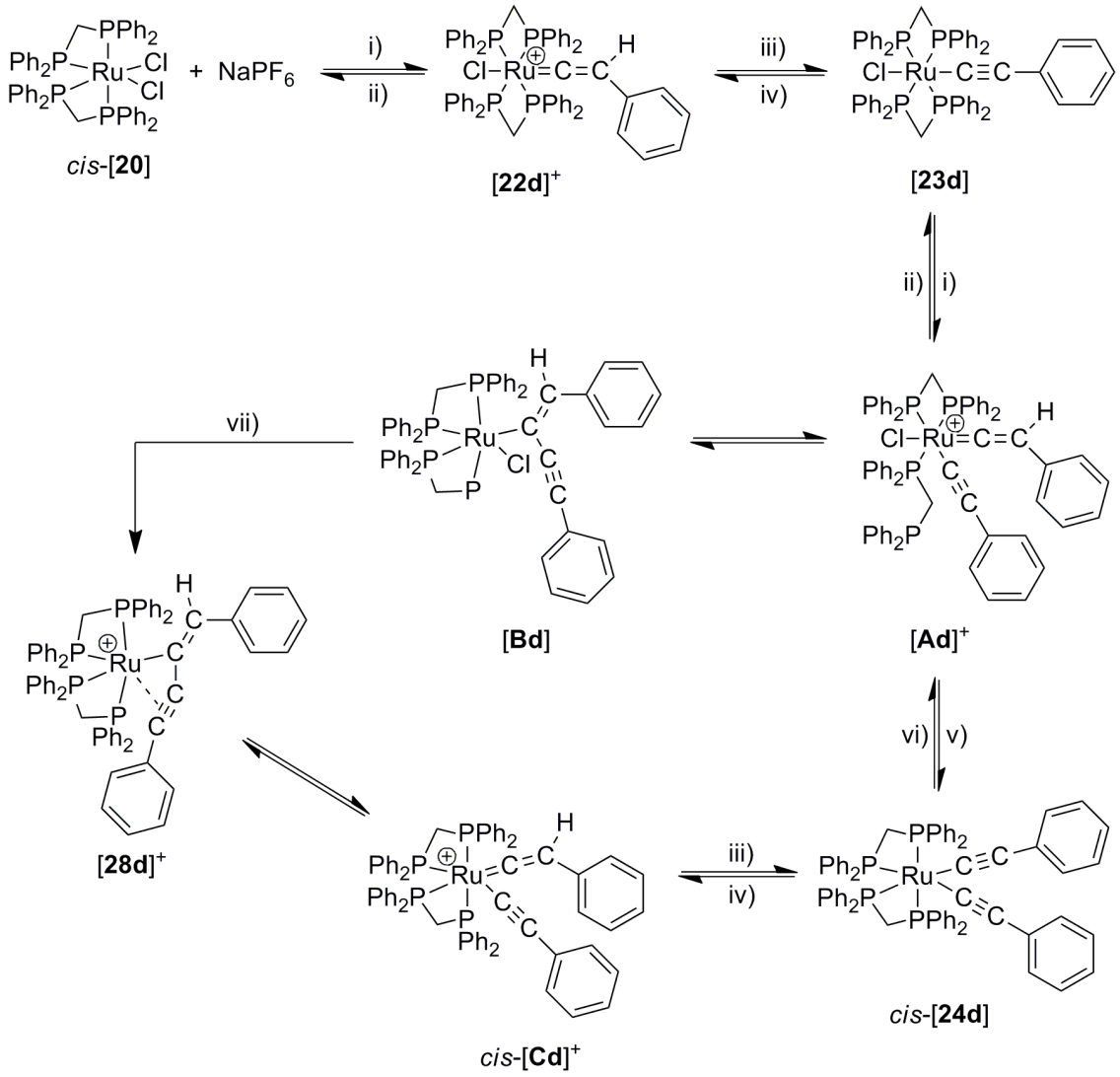

Scheme 2.4: Proposed mechanism for the reaction between *cis*-[**20**], $NaPF_6$, $HC{\equiv}CC_6H_5$ and base in methanol, where: i) + $HC{\equiv}CC_6H_5$; ii) − $HC{\equiv}CC_6H_5$; iii) − H^+; iv) + H^+; v) − HCl; vi) + HCl; vii) − Cl.[45]

In the mechanism described above, initial reaction of *cis*-[**20**] with $NaPF_6$ is thought to form the active five coordinate complex, $[RuCl(dppm)_2]^+$ ([**31**]$^+$; not shown in Scheme 2.4). Subsequent addition of the terminal alkyne, $HC{\equiv}CC_6H_5$, yields the *mono*-vinylidene complex [**22d**]$^+$ which is then rapidly transformed into [**23d**] upon deprotonation.[39] The formation of the neutral complex [**Bd**] and the cationic η^3-butenynyl complex [**28d**]$^+$ was confirmed *via* $^{31}P\{^1H\}$ NMR spectroscopy. The additional intermediate complexes [**Ad**]$^+$, *cis*-[**24d**] and *cis*-[**Cd**]$^+$ were not unambiguously defined, but were proposed on the basis of *in situ* NMR monitoring of

^{13}C-labelled experiments. During the reaction between *trans*-[RuCl(=C^{13}=CHC$_6$H$_5$)(dppm)$_2$]$^+$ with HC≡CC$_6$H$_5$, an intermediate low field quartet resonance in the ^{13}C{^{1}H} spectrum (δ 363.1 ppm, $^2J_{PC}$ = 15.5 Hz) was observed, implicating the presence of the intermediate complex [**Ad**]$^+$ bearing a vinylidene ligand *cis*- to only three phosphines, with the fourth not bound to the ruthenium centre. Notably, the hemi-lability of dppm ancillary ligands has been observed previously and is not a novel characteristic.[46] After a prolonged reaction time, mixtures of *E*-[Ru(η^3-{HC(C$_6$H$_5$)=C^{13}C≡CC$_6$H$_5$})(dppm)$_2$]$^+$ and *E*-[Ru(η^3-{HC(C$_6$H$_5$)=CC^{13}≡CC$_6$H$_5$})(dppm)$_2$]$^+$ were obtained in approximately equal quantities. In order to account for the uptake of C^{13} at both C^2 and C^3, the 'symmetric' complex *cis*-[**24d**] was proposed, establishing an alternative mechanistic route from [**23d**] to the η^3-butenynyl complex [**28d**]$^+$ with *cis*-[**Cd**]$^+$ having been included to account for the propensity of alkynyl ligands to be protonated. Interestingly, {Ru(dppe)$_2$} η^3-butenynyl complexes have not been observed in analogous reaction schemes.[45] Hence the unique formations of {Ru(dppm)$_2$} η^3-butenynyl complexes are thought to arise as a consequence of the comparatively more strained phosphine bite angle, which no doubt contributes to Ru-P dissociation and the hemi-lability of dppm ligands (*c.f.* [**Ad**]$^+$, Scheme 2.4).

In the cases of reactions reported here, which differ from the Lynam work with the inclusion of TlBF$_4$ in the reaction mixture and reactions instead conducted in CH$_2$Cl$_2$ (*vs.* NaPF$_6$ / MeOH), no spectroscopic evidence for either [**A**]$^+$ or [**B**] could be obtained (Figures 2.16 and 2.17). Rather, deprotonation of vinylidene complexes [**22**]$^+$ affords *mono*-alkynyl complexes, [**23**] and a subsequent reaction with the efficient halide abstracting agent TlBF$_4$ presumably then forms the five coordinate species [**D**]$^+$, which, in the presence of a terminal alkyne and excess Proton Sponge, gives *trans*-[**24**], which is likely to occur *via* the intermediate alkynyl-vinylidene species *trans*-[**C**]$^+$ (Scheme 2.5).

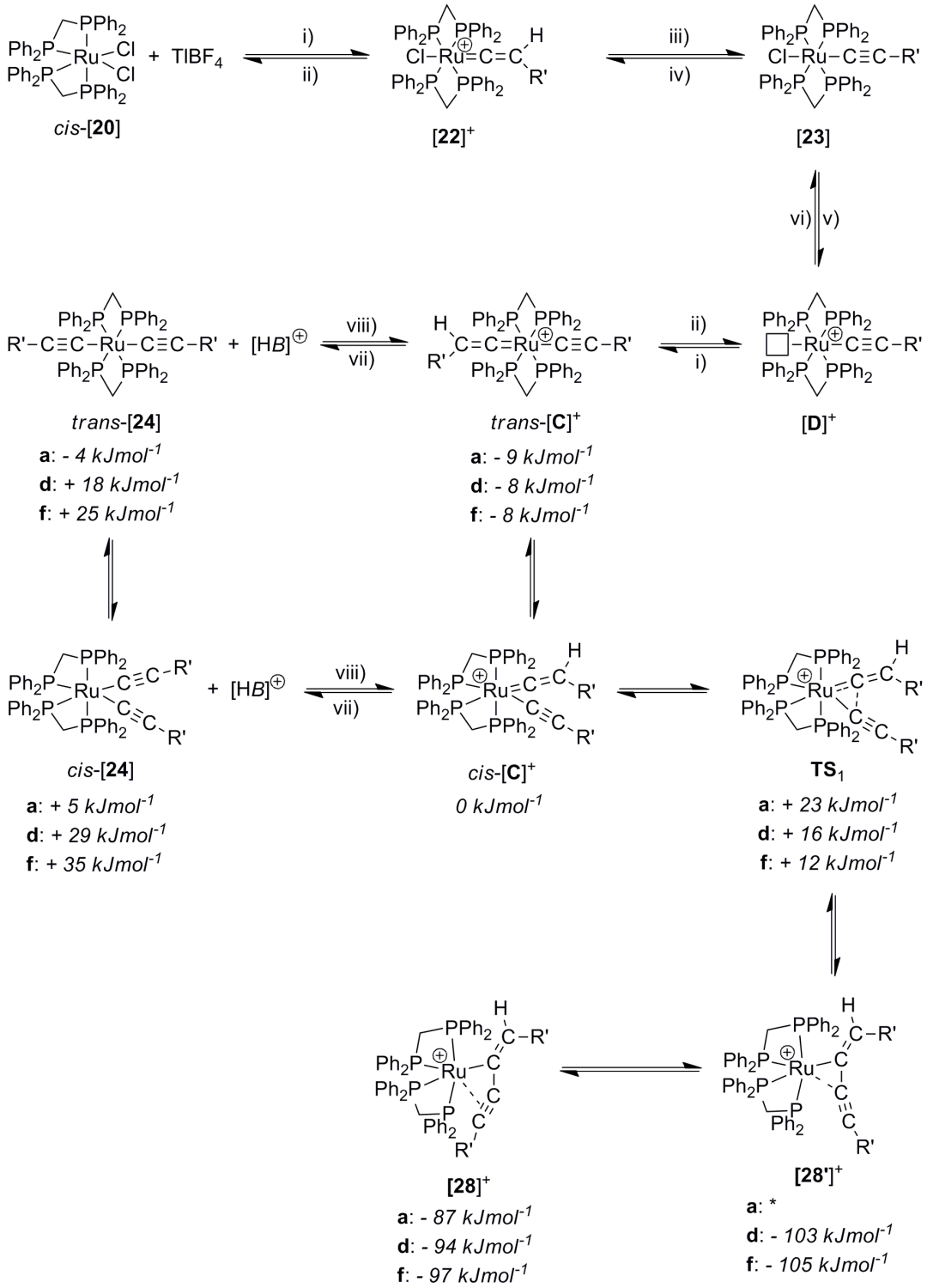

Scheme 2.5: Proposed mechanism for the reaction of *cis*-[**20**], $TlBF_4$, $HC{\equiv}CC_6H_4$-4-R and base in CH_2Cl_2, where: i) + HC≡CR′; ii) – HC≡CR′; iii) − H; iv) + H; v) – Cl; vi) + Cl; vii) + base (*B*); viii) – base (*B*); R′ = C_6H_4-4-R (**a**: R = NO_2; **d**: R = H and **f**: R = OMe). Quantum chemically calculated free energies for the case where B = pyridine are shown in italics. *geometry optimisation resulted in [**28a**]$^+$.

From *trans*-[**24**] (Scheme 2.5), it is possible to envisage two alternate routes to [**28**]$^+$, either *via* the reverse reaction to give *trans*-[**C**]$^+$ and isomerisation to the key *cis*-alkynyl vinylidene *cis*-[**C**]$^+$ or through initial isomerisation to the *cis*-bis(alkynyl) complex (*cis*-[**24**]) prior to protonation to give *cis*-[**C**]$^+$. On the one hand, the route *trans*-[**24**] → *trans*-[**C**]$^+$ → *cis*-[**C**]$^+$ → [**28**]$^+$ is similar to that proposed by Rappert and Yamamoto to account for the formation of η^3-butenynyl complexes from *trans*-[Ru(C≡CC_6H_5)$_2$(PMe_3)$_4$], [**17**].[76] On the other hand, the formation of η^3-butenynyl complexes from *cis*-[**24**] (Schemes 2.4 and 2.5) is similar to the formation of η^3-butenynyl complexes from reactions of *cis*-[Ru(C≡CC_6H_5)$_2${P($CH_2CH_2PPh_2$)$_3$}] with weak acids (pK_a(NH_4^+)= 9; pK_a(EtOH) = 18; *c.f.* pK_a(Proton Sponge) = 12.1 (in water)[77] − 18.62 (in NCMe)[78] observed by Bianchini and colleagues.[79]

The rate of formation of intermediate *cis*-[**24**] (Scheme 2.5) might be enhanced by the more favourable *trans*-effects in the case of reactions with alkynes bearing electron-withdrawing substituents, but the lower basicity of the alkynyl ligands will limit equilibrium concentrations of both *cis*- and *trans*-[**C**]$^+$ (Scheme 2.5) as well as reducing the nucleophilicity of the alkynyl C_α in *cis*-[**C**]$^+$. In contrast, electron-donating substituents will destabilise *cis*-[**24**] but stabilise the vinylidene intermediates *cis*- and *trans*-[**C**]$^+$.

In order to gain further insight into these different mechanistic possibilities and also to rationalise the observed substituent effects, the potential energy surface for the formation of [**28**]$^+$ (in Scheme 2.5) was examined using DFT at the PBE0-D3/def2-TZVPP//BP86/SV(P) level with solvation corrections applied in CH_2Cl_2. All calculations were conducted by Dr J. M. Lynam at the University of York and details of the computational methods employed have been included in the experimental section (see section 2.6.1.). All energies are Gibbs energies at 298.15 K. Complexes bearing three different R substituents (**a**: R = NO_2; **d**: R = H and **f**: R = OMe; where R′ = C_6H_4-4-R in Scheme 2.5.) were examined and in each case, the alkynyl-vinylidene complex *cis*-[**C**]$^+$ was taken as the reference point.

The calculations indicate that in the cases of [**24**] and [**C**]$^+$, the *trans*-isomers are more thermodynamically favourable than the corresponding *cis*-arrangement of ligands,

although the differences are relatively small (~ 10 kJmol^{-1}). The isomerism of *trans*-[**C**]$^+$ to *cis*-[**C**]$^+$ and *trans*-[**24**] to *cis*-[**24**] was not modelled but is thought to proceed *via* a five-coordinate intermediate with a κ^1-bound dppm ligand. In order to assess the differences in acidity of the vinylidene ligands, deprotonation of the cationic complexes [**C**]$^+$ by pyridine (*B* = pyridine in Scheme 2.5), to give a pyridinium cation and [**24**], was modelled. The data indicate that in all cases, except [**24a**], deprotonation of the alkynyl vinylidenes ([**C**]$^+$) by pyridine is thermodynamically unfavourable. There is a pronounced substituent effect with the greatest difference in energy between the (less favourable) *bis*-alkynyl complexes ([**24**]) and the alkynyl-vinylidene species ([**C**]$^+$) arising when two OMe substituents (**f**) are present (33 – 35 kJmol^{-1}). The energy difference is much smaller in the NO_2-containing case (**a**; 5 kJmol^{-1}). This trend may simply represent the increased basicity of the alkynyl ligands in the presence of the OMe group.

The formation of the η^3-butenynyl ligand from intermediate *cis*-[**C**]$^+$ proceeds through a low energy transition state, **TS**$_1$ (Scheme 2.5). There is a small substituent effect in this case with the barrier to C-C bond formation being lowest in the case of the OMe-substituted complex (**f**; ΔG = + 12 kJ mol^{-1}) and greatest in the case of the NO_2-derviative (**a**; ΔG = + 23 kJ mol^{-1}). This is consistent with the relative nucleophilicity of the alkynyl ligands coupling with the electrophilic metal-bound carbon of the vinylidene. However, given that the barriers are very small, the calculations predict that the C-C bond formation step from *cis*-[**C**]$^+$ will be extremely rapid at 298 K, regardless of the substituent employed. The observed experimental substituent effect, where the presence of electron donating groups favour the formation of the η^3-butenynyl complexes, may be more readily explained on the basis of the protonation states of the complexes. The presence of the more basic (OMe-containing) alkynyl ligand (**f**) will increase the proportion of alkynyl-vinylidene complexes [**C**]$^+$ thus promoting the formation of the η^3-butenynyl complex [**28**]$^+$, whereas in the case of the NO_2-containing species (**a**), the proportion of these intermediate complexes [**C**]$^+$ will be lower, hence a much slower formation of the η^3-butenynyl complex [**28**]$^+$ is exhibited.

One additional aspect of the calculations is that a dynamic reaction coordinate analysis of $\mathbf{TS}_1$ (and also the corresponding *Z*-isomer, *c.f.* $\mathbf{TS}_2$ shown in Scheme 2.6) reveals that the transition state does not directly connect *cis*-[**C**]$^+$ to [**28**]$^+$, but to an isomeric complex, [**28′**]$^+$ in which the butenynyl ligand is bound in an η^1-fashion. At all levels of theory employed, [**28′**]$^+$ is at lower energy than [**28**]$^+$ for the hydrogen- and methoxy-substituted complexes, by 9 and 8 kJmol^{-1} respectively, where geometry optimisation of the corresponding NO_2-substituted species resulted in generation of [**28a**]$^+$. Although the energy differences here are small and so care should be taken in interpreting such data, the calculations would indicate that [**28**]$^+$ and [**28′**]$^+$ should both be in equilibrium in solution. This is consistent with the fact that the alkyne functionality in η^3-butenynyl ligands is labile and may be readily replaced by donor ligands such as CO.[56]

These calculations also explain the stereochemical outcome of the reaction as the *E*-substituted η^3-butenynyl ligand is obtained. As shown in Scheme 2.6, the calculations indicate that the intermediates and transition states which lead to complex *Z*-[**28d**]$^+$ (*cis*-*Z*-[**Cd**]$^+$ and $\mathbf{TS}_2$) are only slightly higher in energy than the corresponding complexes that lead to the experimentally observed *E*-isomer (by 9 and 6 kJmol^{-1} respectively). However, *Z*-[**28d**]$^+$ is far higher in energy than the *E*-isomer, *E*-[**28d**]$^+$ (− 47 kJmol^{-1} compared to − 94 kJmol^{-1}), as is *Z*-[**28d′**]$^+$ (− 62 kJmol^{-1} *vs.* − 103 kJmol^{-1} for *E*-[**28d′**]$^+$). This indicates that the reverse reaction from *Z*-[**28d′**]$^+$ to *cis*-*Z*-[**Cd**]$^+$ has a barrier of 84 kJmol^{-1} and may be reversible at 298 K, implying that the reaction is under thermodynamic control.

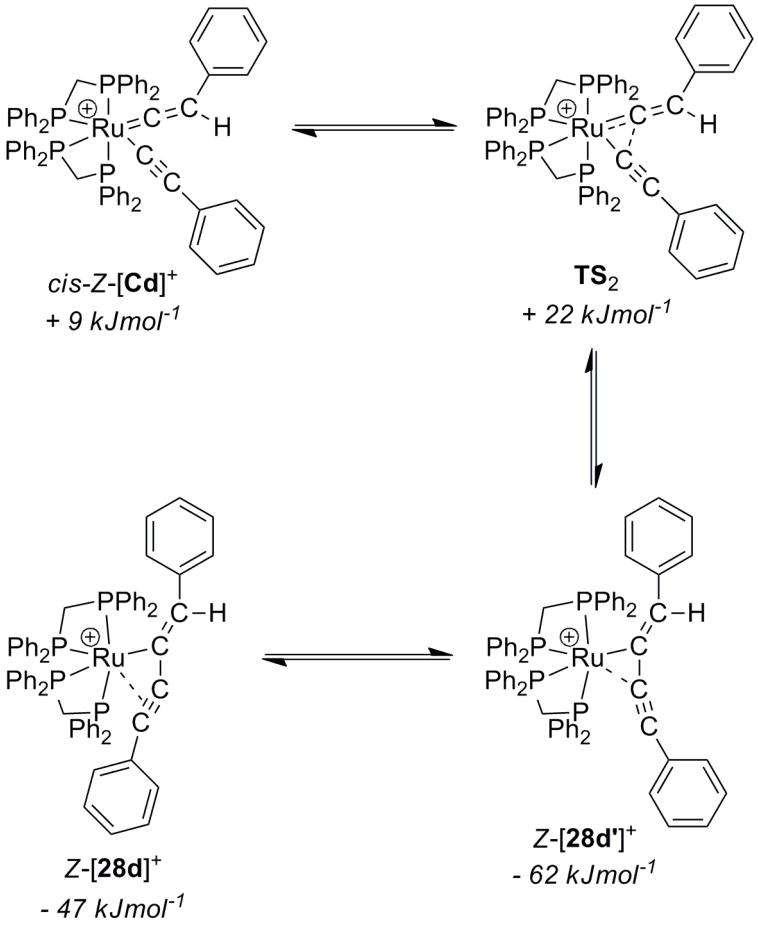

Scheme 2.6: Proposed mechanism for the formation of the *Z*-isomer of the η^3-butenynyl complex, *Z*-[**28d**]$^+$. Quantum chemically calculated free energies are shown in italics.

2.5. Conclusions

In summary, $TlBF_4$ has been shown to be a reliable and efficient halide abstracting agent in the transformation of *cis*-[**20**] into *mono*-vinylidene and *mono*-alkynyl complexes. Although *trans*-bis(alkynyl) complexes, *trans*-[Ru(C≡CC_6H_4-4-R)$_2$(dppm)$_2$], can be obtained from terminal alkynes HC≡CC_6H_4-4-R containing electron withdrawing R substituents, terminal alkynes containing electron donating R substituents promote further reaction to give cationic η^3-butenynyl complexes *E*-[Ru(η^3-{HC(C_6H_4-4-R)=CC≡CC_6H_4-4-R})(dppm)$_2$]BF_4. Although electron donating R substituents increase the nucleophilicity of C^1 in the incoming alkyne, (HC^1≡C^2C_6H_4-4-R), which increases the nucleophilicity and electrophilicity of the alkynyl and vinylidene C_α carbons (respectively) in the

intermediate alkynyl-vinylidene complexes, it appears that it is the control of the protonation state by raising the energy of the *bis*-alkynyl complex that promotes the formation of the η^3-butenynyl complexes. Such experimental observations are assumed to be a direct and unique result of the decreased phosphine bite angle in the $\{Ru(dppm)_2\}$ motif when compared with the $\{Ru(dppe)_2\}$ fragment, where analogous results are not observed. Ultimately, this work is evidence that the ancillary ligands *are* an important consideration in effective molecular engineering.

2.6. Experimental

2.6.1. General considerations

All reactions were carried out under an atmosphere of dry nitrogen using standard Schlenk techniques. Dichloromethane was dried over CaH_2, all other solvents were standard reagent grade and used as received. No special precautions were taken to exclude air or moisture during workup. The compounds *cis*-[**20**];[80] $HC{\equiv}CC_6H_4$-4-NO_2;[81] $HC{\equiv}CC_6H_4$-4-COOMe;[81] $HC{\equiv}CC_6H_4$-4-$C{\equiv}CSiMe_3$[25] and $TlBF_4$[82] were synthesised by literature methods. All other reagents were commercially available and used as received.

Safety spectacles and gloves were worn at all times, and all experiments conducted in an efficient fume hood, following completion of appropriate COSHH assessments. Relatively non-toxic solvents were disposed of in the appropriate waste solvent container (chlorinated / non-chlorinated). Given the extremely toxicity of $TlBF_4$, the reagent was separately weighed in a sealed container in a fumehood. The solid was transferred to the reaction flask using a disposable paper funnel. The paper funnel was discarded immediately after use into a thallium-containing solid waste receptacle. For larger scale reactions, a secondary containment flask was utilised during the reaction period. Reactions reported below involving $TlBF_4$, (generally) produce equimolar amounts of TlCl, which is similarly extremely toxic. After completion of the reaction, following isolation of TlCl / residual $TlBF_4$ by the work-up procedures reported, the salts were either disposed of by i) dissolving in HNO_3 (aq.) and transferring into a

thallium-containing solvent waste container or ii) in a thallium-containing solid waste container (along with the chromatographic medium, celite *etc.*).

NMR spectra were recorded at 25 ºC either on a Varian Inova 300 (^{1}H, 300.2 MHz; ^{31}P, 121.5 MHz), Jeol 400 (^{1}H, 399.78 MHz; ^{13}C, 100.53 MHz; ^{19}F, 376.17 MHz; ^{11}B, 128.27 MHz), Varian Mercury-400 (^{1}H, 399.97 MHz; ^{31}P, 161.10 MHz), Bruker AV500 (^{1}H, 500.23 MHz; ^{31}P, 202.50 MHz; ^{13}C, 125.77 MHz), Bruker Avance 600 (^{1}H, 600.1 MHz; ^{13}C, 150.9 MHz; ^{19}F, 564.6 MHz; ^{31}P, 242.9 MHz) or a Varian VNMRS-700 (^{1}H, 699.73 MHz; ^{13}C, 175.95 MHz ; ^{31}P, 279.89 MHz) spectrometer using $CDCl_3$ or CD_2Cl_2 as the solvent. Chemical shifts were determined relative to internal residual solvent signals (^{1}H, δ = 7.26 ppm, 5.32 ppm; ^{13}C, δ = 77.2 ppm, 54.2 ppm) or external 85% H_3PO_4 (^{31}P, δ = 0.0 ppm).[83] FT-IR spectra were measured on an Agilent Technologies Cary 660 spectrometer or a Nicolet Avatar 360 spectrometer from solutions in CH_2Cl_2 in a thin-layer cell fitted with CaF_2 windows. ESI-MS and APCI-MS were recorded on a Waters LCT Premier XE mass spectrometer in positive or negative ion mode from solutions in methanol. MALDI-MS were recorded using an Autoflex II TOF / TOF mass spectrometer (Bruker Daltonik, GmbH) equipped with a 337 nm laser. Cyclic voltammetry was carried out using Autolab PGSTAT 30 or Princeton Applied Research Versastat 3 potentiostats, with a platinum disc working electrode, a platinum wire counter electrode and a platinum wire pseudo-reference electrode from solutions in CH_2Cl_2 containing 0.1 M $[N^nBu_4]PF_6$ as the electrolyte. Potentials are reported *vs.* ferrocene / ferrocenium ($[Fe(\eta^5\text{-}C_5H_5)_2]$ / $[Fe(\eta^5\text{-}C_5H_5)_2]^+$ = 0 V)[60] using a decamethylferrocene / decamethylferrocenium internal standard ($[Fe(\eta^5\text{-}C_5Me_5)_2]$ / $[Fe(\eta^5\text{-}C_5Me_5)_2]^+$ = – 0.48 V).

For quantum chemical calculations, initial optimisations were performed at the (RI-)BP86/SV(P) level, followed by frequency calculations at the same level. Transition states were located by initially performing a constrained minimisation (by freezing the internal coordinates that change most during the reaction) of a structure close to the anticipated transition state. This was followed by a frequency calculation to identify the transition vector to follow during a subsequent transition state optimisation. A final frequency calculation was then performed on the optimised transition state structure. All minima were confirmed as such by the absence of imaginary frequencies and all

transition states were identified by the presence of only one imaginary frequency. Single-point calculations on the (RI-)BP86/SV(P) optimised geometries were performed using the hybrid PBE0 functional and the flexible def2-TZVPP basis set. The (RI-)PBE0/def2-TZVPP SCF energies were corrected for their zero point energies, thermal energies and entropies (obtained from the (RI-)BP86/SV(P)-level frequency calculations). In all calculations, a 28 electron quasi-relativistic ECP replaced the core electrons of Ru and Rh. No symmetry constraints were applied during optimisations. Solvent corrections were applied with the COSMO dielectric continuum model[84] and dispersion effects modeled with Grimme's D3 method.[85, 86] All calculations were performed using the TURBOMOLE V6.4 package using the resolution of identity (RI) approximation.[87-95]

2.6.2. Syntheses and characterisations of *mono*-vinylidene complexes

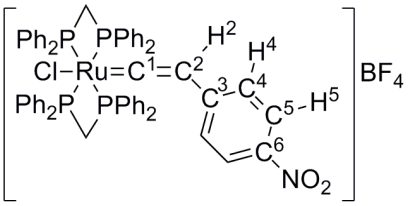

*Synthesis of trans-[RuCl(=C=CHC$_6$H$_4$-4-NO$_2$)(dppm)$_2$]BF$_4$, [**22a**]BF$_4$*

A mixture of *cis*-[**20**] (0.050 g, 0.05 mmol), TlBF$_4$ (0.016 g, 0.05 mmol) and HC≡CC$_6$H$_4$-4-NO$_2$ (0.0082 g, 0.05 mmol) in CH$_2$Cl$_2$ (5 ml) was stirred under N$_2$ for two hours. The solution colour changed from yellow to red and a white solid (TlCl) precipitated. The TlCl was removed by filtration through a HPLC Teflon filter (20 µm pores) and the filtrate concentrated to ~ 1 ml by rotary evaporation. Excess diethyl ether was then added to the red solution, resulting in the instantaneous precipitation of a red solid which was collected by filtration, washed with diethyl ether (3 × 10 ml) and hexanes (3 × 10 ml) and then air dried (0.049 g, 80 %).

IR (CH$_2$Cl$_2$, cm^{-1}): 1635 ν(Ru=C=C), 1550 ν(N=O), 1340 ν(N-O). ^{1}H NMR (CDCl$_3$, 400 MHz) δ / ppm: 3.36 (quin., J = 3 Hz, 1H, H^2), 5.21 (dt, J = 16, 5 Hz, 2H, CH$_2$, dppm), 5.42 (dt, J = 16, 5 Hz, 2H, CH$_2$, dppm), 5.65 (apparent doublet, splitting = 8 Hz, 2H, H^4), 7.23 (t, J = 8 Hz, 8H, H$_m$, dppm), 7.25 (t, J = 8 Hz, 8H, H$_m$, dppm), 7.31 – 7.38 (m, 8H, H$_o$, dppm), 7.42 (t, J = 8 Hz, 4H, H$_p$, dppm), 7.45 (apparent doublet,

splitting = 8 Hz, 2H, H^5), 7.44 – 7.50 (m, 12H, H_o and H_p, dppm). $^{31}P\{^1H\}$ NMR ($CDCl_3$, 400 MHz) δ / ppm: − 17.3 (s, Ru(dppm)$_2$). ^{19}F NMR ($CDCl_3$, 400 MHz) δ / ppm: − 155.3 (s, BF_4). $^{13}C\{^1H\}$ NMR (CD_2Cl_2, 400 MHz) δ / ppm: 46.2 (t, J = 12 Hz, CH_2, dppm), 110.4 (s, C^2), 124.2 (s, C^5), 127.2 (s, C^4), 128.8 (s, C_m, dppm), 129.4 (s, C_m, dppm), 131.6 (s, C_p, dppm), 131.8 (s, C_p, dppm), 132.4 (quin., J = 13 Hz, C_i, dppm), 132.7 (s, C_o, dppm), 133.5 (quin., J = 13 Hz, C_i, dppm), 133.6 (s, C_o, dppm), 136.2 (s, C^3), 145.8 (s, C^6), 352.5 (quin., J = 14 Hz, C^1). ASAP (+)-MS (*m/z*): 1052 $[RuCl(=C=CHC_6H_4\text{-}4\text{-}NO_2)(dppm)_2]^+$. Anal. Found: C, 60.94; H, 4.28; N, 1.34. Calc. for $C_{58}H_{49}BClF_4NO_2P_4Ru$: C, 61.10; H, 4.34; N, 1.23.

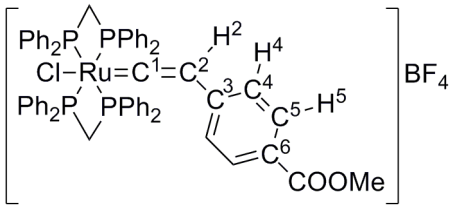

*Synthesis of trans-[RuCl(=C=CHC$_6$H$_4$-4-COOMe)(dppm)$_2$]BF$_4$, [**22b**]BF$_4$*

A mixture of *cis*-[**20**] (0.050 g, 0.05 mmol), $TlBF_4$ (0.016 g, 0.05 mmol) and HC≡CC_6H_4-4-COOMe (0.0087 g, 0.05 mmol) in CH_2Cl_2 (5 ml) was stirred under N_2 for one hour. The solution colour changed from yellow to orange / brown and a white solid (TlCl) precipitated. The TlCl was removed by filtration through a HPLC Teflon filter (20 µm pores) and the filtrate concentrated to ~ 1 ml by rotary evaporation. Excess diethyl ether was then added to the orange / brown solution, resulting in the instantaneous precipitation of a pale brown solid which was collected by filtration, washed with diethyl ether (3 × 10 ml) and hexanes (3 × 10 ml) and then air dried (0.046 g, 75 %).

IR (CH_2Cl_2, cm^{-1}): 1717 ν(C=O), 1635 ν(Ru=C=C). ^1H NMR (CD_2Cl_2, 700 MHz) δ / ppm: 3.13 (quin., J = 3 Hz, 1H, H^2), 3.90 (s, 3H, CH_3), 5.14 (dt, J = 15, 5 Hz, 2H, CH_2, dppm), 5.36 (dt, J = 15, 5 Hz, 2H, CH_2, dppm), 5.58 (apparent doublet, splitting = 8 Hz, 2H, H^4), 7.25 (t, J = 7 Hz, 16H, H_m, dppm), 7.31 – 7.36 (m, 8H, H_o, dppm), 7.40 – 7.46 (m, 16H, H_o and H_p, dppm), 7.41 (apparent doublet, splitting = 8 Hz, 2H, H^5). ^{11}B NMR (CD_2Cl_2, 500 MHz) δ / ppm: – 2.0 (s, BF_4). ^{19}F NMR (CD_2Cl_2, 500 MHz) δ / ppm: – 152.5 (s, BF_4). $^{31}P\{^1H\}$ NMR ($CDCl_3$, 700 MHz) δ / ppm: – 16.6 (s, Ru(dppm)$_2$). $^{13}C\{^1H\}$ NMR (CD_2Cl_2, 500 MHz) δ / ppm: 46.4 (t, J = 13 Hz, CH_2,

dppm), 52.6 (s, CH_3), 110.7 (s, C^2), 127.2 (s, C^4), 128.2 (s, C^3), 129.1 (t, J = 3 Hz, C_m, dppm), 129.7 (t, J = 3 Hz, C_m, dppm), 129.8 (quin., J = 12 Hz, C_i, dppm), 130.2 (s, C^5), 131.3 (quin., J = 12 Hz, C_i, dppm), 132.0 (s, C_p, dppm), 132.3 (s, C_p, dppm), 132.6 (s, C^6), 132.9 (quin., J = 3 Hz, C_o, dppm), 133.9 (quin., J = 3 Hz, C_o, dppm), 166.9 (s, C=O), 355.4 (quin., J = 14 Hz, C^1). ASAP (+)-MS (*m/z*): 1065 [RuCl(=C=CHC_6H_4-4-COOMe)$(dppm)_2]^+$, 521 [RuCl(dppm)]$^+$. Anal. Found: C, 61.04; H, 4.08. Calc. for $C_{60}H_{52}BClF_4O_2P_4Ru$: C, 62.49; H, 4.55.

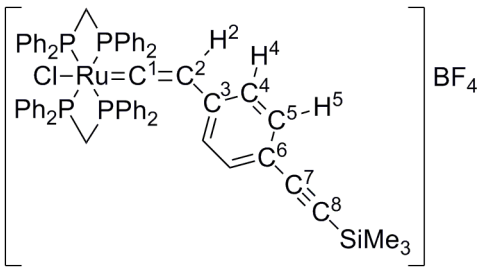

*Synthesis of trans-[RuCl(=C=CHC_6H_4-4-C≡C$SiMe_3$)$(dppm)_2$]BF_4, [**22c**]BF_4*

A mixture of *cis*-[**20**] (0.049 g, 0.05 mmol), $TlBF_4$ (0.016 g, 0.06 mmol) and HC≡CC_6H_4-4-C≡C$SiMe_3$ (0.011 g, 0.06 mmol) in CH_2Cl_2 (5 ml) was stirred under N_2 for two hours. The solution colour changed from yellow to brown and a white solid (TlCl) precipitated. The TlCl was removed by filtration through a HPLC Teflon filter (20 μm pores) and the filtrate concentrated to ~ 1 ml by rotary evaporation. Excess diethyl ether was then added to the brown solution, resulting in the instantaneous precipitation of a brown solid which was collected by filtration, washed with diethyl ether (3 × 10 ml) and hexanes (3 × 10 ml) and then air dried (0.041 g, 66 %).

IR (CH_2Cl_2, cm^{-1}): 1605 ν(Ru=C=C). ^{1}H NMR ($CDCl_3$, 600 MHz) δ / ppm: 0.25 (s, 9H, $SiMe_3$), 3.00 (quin., J = 3 Hz, 1H, H^2), 5.14 (dt, J = 15, 4 Hz, 2H, CH_2, dppm), 5.42 (dt, J = 15, 4 Hz, 2H, CH_2, dppm), 5.43 (apparent doublet, splitting = 8 Hz, 2H, H^4), 6.82 (apparent doublet, splitting = 8 Hz, 2H, H^5), 7.21 (t, J = 8 Hz, 8H, H_m, dppm), 7.22 (t, J = 8 Hz, 8H, H_m, dppm), 7.32 – 7.35 (m, 8H, H_o, dppm), 7.35 (t, J = 8 Hz, 4H, H_p, dppm), 7.38 – 7.44 (m, 12H, H_o and H_p, dppm). $^{31}P\{^1H\}$ NMR ($CDCl_3$, 600 MHz) δ / ppm: – 16.3 (s, Ru$(dppm)_2$). $^{13}C\{^1H\}$ NMR ($CDCl_3$, 600 MHz) δ / ppm: 0.19 (s, $SiMe_3$), 46.2 (quin., J = 13 Hz, CH_2, dppm), 94.6 (s, C^8), 105.0 (s, C^7), 110.1 (s, C^2), 120.5 (s, C^3), 126.9 (s, C^4), 127.7 (s, C^6), 128.7 (s, C_m, dppm), 129.3 (s, C_m, dppm), 129.6 (quin., J = 13 Hz, C_i, dppm), 131.1 (quin., J = 13 Hz, C_i, dppm), 131.4 (s, C_p,

dppm), 131.7 (s, C_p, dppm), 132.1 (s, C^5), 132.7 (s, C_o, dppm), 133.6 (s, C_o, dppm), 355.9 – 356.1 (m, C^1). ESI (+)-MS (*m/z*): 1103 [RuCl(=C=CHC_6H_4-4-C≡C$SiMe_3$)(dppm)$_2$]$^+$, 905 [Ru(dppm)$_2$]$^+$.

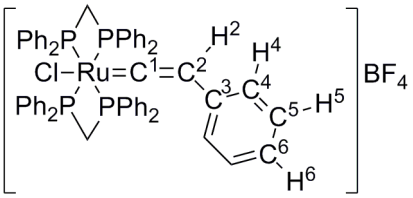

*Synthesis of trans-[RuCl(=C=CHC_6H_5)(dppm)$_2$]BF_4, [**22d**]BF_4*

A mixture of *cis*-[**20**] (0.050 g, 0.05 mmol), $TlBF_4$ (0.016 g, 0.05 mmol) and HC≡CC_6H_5 (6 µL, 0.06 mmol) in CH_2Cl_2 (5 ml) was stirred under N_2 for one hour. The solution colour changed from yellow to orange and a white solid (TlCl) precipitated. The TlCl was removed by filtration through a HPLC Teflon filter (20 µm pores) and the filtrate concentrated to ~ 1 ml by rotary evaporation. Excess diethyl ether was then added to the orange / brown solution, resulting in the instantaneous precipitation of a pale yellow / brown solid which was collected by filtration, washed with diethyl ether (3 × 10 ml) and hexanes (3 × 10 ml) and then air dried (0.047 g, 82 %).

IR (CH_2Cl_2, cm^{-1}): 1605 ν(Ru=C=C). ^{1}H NMR (CD_2Cl_2, 400 MHz) δ / ppm: 3.10 (quin., J = 3 Hz, 1H, H^2), 5.03 – 5.10 (m, 2H, CH_2, dppm), 5.11 – 5.18 (m, 2H, CH_2, dppm), 5.56 (d, J = 8 Hz, 2H, H^4), 6.79 (t, J = 8 Hz, 2H, H^5), 6.92 (t, J = 8 Hz, 1H, H^6), 7.22 – 7.32 (m, 16H, H_m, dppm), 7.32 – 7.42 (m, 16H, H_o, dppm), 7.48 (t, J = 8 Hz, 8H, H_p, dppm). ^{19}F NMR (CD_2Cl_2, 400 MHz) δ / ppm: – 152.8 (s, BF_4). ^{31}P{^{1}H} NMR (CD_2Cl_2, 400 MHz) δ / ppm: – 15.4 (s, Ru(dppm)$_2$). ^{13}C{^{1}H} NMR (CD_2Cl_2, 400 MHz) δ / ppm: 46.7 (t, J = 12 Hz, CH_2, dppm), 111.1 (s, C^2), 126.9 (s, C^3), 127.9 (s, C^4), 129.5 (s, C_m, dppm), 130.0 (s, C_m, dppm), 131.3 – 131.8 (m, C_i, dppm), 132.14 (s, C^6), 132.4 (s, C^5), 132.3 (s, C_p, dppm), 132.7 (s, C_p, dppm), 132.9 (s, C_o, dppm), 134.0 (s, C_o, dppm), 358.2 (quin., J = 13 Hz, C^1). ESI (+)-MS (*m/z*): 1007 [RuCl(=C=CHC_6H_5)(dppm)$_2$]$^+$. ESI (–)-MS (*m/z*): 87 [BF_4]$^-$. Anal. Found: C, 63.01; H, 4.55. Calc. for $C_{58}H_{50}BClF_4P_4Ru$: C, 63.67; H, 4.52.

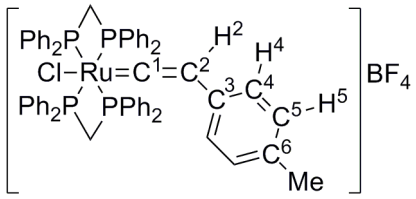

*Synthesis of trans-[RuCl(=C=CHC$_6$H$_4$-4-Me)(dppm)$_2$]BF$_4$, [**22e**]BF$_4$*

A mixture of *cis*-[**20**] (0.047 g, 0.05 mmol), TlBF$_4$ (0.015 g, 0.05 mmol) and HC≡CC$_6$H$_4$-4-Me (7 µL, 0.06 mmol) in CH_2Cl_2 (5 ml) was stirred under N_2 for one hour. The solution colour changed from yellow to orange and a white solid (TlCl) precipitated. The TlCl was removed by filtration through a HPLC Teflon filter (20 µm pores) and the filtrate concentrated to ~ 1 ml by rotary evaporation. Excess diethyl ether was then added to the orange / brown solution, resulting in the instantaneous precipitation of a pale orange / brown solid, which was collected by filtration, washed with diethyl ether (3 × 10 ml) and hexanes (3 × 10 ml) and then air dried (0.046 g, 83 %).

IR (CH_2Cl_2, cm^{-1}): 1646 ν(Ru=C=C). ^{1}H NMR ($CDCl_3$, 400 MHz) δ / ppm: 2.16 (s, 3H, CH_3), 2.94 (quin., J = 3 Hz, 1H, C=CH), 5.11 (dt, J = 15, 5 Hz, 2H, CH_2, dppm), 5.41 (dt, J = 15, 5 Hz, 2H, CH_2, dppm), 5.36 (apparent doublet, splitting = 8 Hz, 2H, H^4), 6.50 (apparent doublet, splitting = 8 Hz, 2H, H^5), 7.12 – 7.26 (m, 16H, H$_m$, dppm), 7.26 – 7.37 (m, 16H, H$_o$, dppm), 7.37 – 7.45 (m, 8H, H$_p$, dppm). ^{19}F NMR ($CDCl_3$, 400 MHz) δ / ppm: –152.4 (s, BF_4). ^{31}P{^{1}H} NMR ($CDCl_3$, 400 MHz) δ / ppm: – 15.9 (s, Ru(dppm)$_2$). ^{13}C{^{1}H} NMR (CD_2Cl_2, 500 MHz) δ / ppm: 21.2 (s, CH_3), 46.5 (t, J = 12 Hz, CH_2, dppm), 110.6 (s, C^2), 123.8 (s, C^3), 127.6 (s, C^4), 129.2 (t, J = 3 Hz, C$_m$, dppm), 129.8 (t, J = 3 Hz, C$_m$, dppm), 129.6 (s, C^5), 130.4 (quin., J = 13 Hz, C$_i$, dppm), 131.6 (quin., J = 13 Hz, C$_i$, dppm), 132.0 (s, C$_p$, dppm), 132.3 (s, C$_p$, dppm), 133.2 (quin., J = 3 Hz, C$_o$, dppm), 134.1 (quin., J = 3 Hz, C$_o$, dppm), 136.6 (s, C^6), 359.5 (quin., J = 15 Hz, C^1). ASAP (+)-MS (m/z): 1021 [RuCl(=C=CHC$_6$H$_4$-4-Me)(dppm)$_2$]$^+$. Anal. Found: C, 62.65; H, 4.28. Calc. for $C_{59}H_{52}BClF_4P_4Ru$: C, 63.89; H, 4.73.

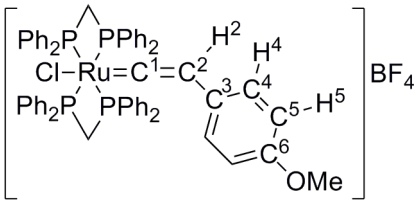

*Synthesis of trans-[RuCl(=C=CHC$_6$H$_4$-4-OMe)(dppm)$_2$]BF$_4$, [**22f**]BF$_4$*

A mixture of *cis*-[**20**] (0.050 g, 0.05 mmol), TlBF$_4$ (0.016 g, 0.05 mmol) and HC≡CC$_6$H$_4$-4-OMe (7 µL, 0.05 mmol) in CH_2Cl_2 (5 ml) was stirred under N_2 for one hour. The solution colour changed from yellow to orange and a white solid (TlCl) precipitated. The TlCl was removed by filtration through a HPLC Teflon filter (20 µm pores) and the filtrate concentrated to ~ 1 ml by rotary evaporation. Excess diethyl ether was then added to the orange / brown solution, resulting in the instantaneous precipitation of a pale yellow / brown solid that was collected by filtration, washed with diethyl ether (3 × 10 ml) and hexanes (3 × 10 ml) and then air dried (0.050 g, 83 %).

IR (CH_2Cl_2, cm^{-1}): 1653 ν(Ru=C=C). ^{1}H NMR (CD_2Cl_2, 500 MHz) δ / ppm: 3.05 – 3.12 (m, 1H, H^2), 3.71 (s, 3H, CH_3), 5.09 (dt, J = 16, 4 Hz, 2H, CH_2, dppm), 5.16 (dt, J = 16, 4 Hz, 2H, CH_2, dppm), 5.49 (apparent doublet, splitting = 8 Hz, 2H, H^4), 6.35 (apparent doublet, splitting = 8 Hz, 2H, H^5), 7.24 – 7.32 (m, 16H, H$_m$, dppm), 7.33 – 7.41 (m, 16H, H$_o$, dppm), 7.45 – 8.41 (m, 8H, H$_p$, dppm). ^{11}B NMR (CD_2Cl_2, 400 MHz) δ / ppm: – 2.0 (s, BF_4). ^{19}F NMR (CD_2Cl_2, 400 MHz) δ / ppm: – 152.6 (s, BF_4). ^{31}P{^{1}H} NMR (CD_2Cl_2, 500 MHz) δ / ppm: – 15.9 (s, Ru(dppm)$_2$). ^{13}C{^{1}H} NMR (CD_2Cl_2, 500 MHz) δ / ppm: 46.7 (t, J = 13 Hz, CH_2, dppm), 56.0 (s, CH_3), 110.5 (s, C^2), 114.7 (s, C^5), 118.7 (s, C^3), 129.2 (s, C^4), 129.6 (t, J = 3 Hz, C$_m$, dppm), 130.2 (t, J = 3 Hz, C$_m$, dppm), 130.8 (quin., J = 13 Hz, C$_i$, dppm), 132.2 (quin., J = 13 Hz C$_i$, dppm), 132.7 (s, C$_p$, dppm), 133.0 (s, C$_p$, dppm), 133.6 (quin., J = 3 Hz, C$_o$, dppm), 134.5 (quin., J = 3 Hz, C$_o$, dppm), 158.8 (s, C^6), 362.5 – 362.6 (m, C^1). ASAP (+)-MS (*m/z*): 1037 [RuCl(=C=CHC$_6$H$_4$-4-OMe)(dppm)$_2$]$^+$. Anal. Found: C, 62.90; H, 4.57. Calc. for $C_{59}H_{52}BClF_4OP_4Ru$: C, 62.98; H, 4.66.

2.6.3. Syntheses and characterisations of *mono*-alkynyl complexes

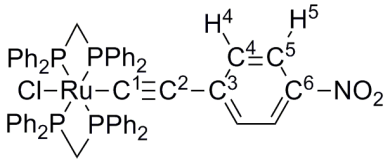

*Synthesis of trans-[RuCl(C≡CC$_6$H$_4$-4-NO$_2$)(dppm)$_2$], **[23a]***

A mixture of *cis*-[**20**] (0.050 g, 0.05 mmol), $TlBF_4$ (0.016 g, 0.05 mmol) and HC≡CC$_6$H$_4$-4-NO$_2$ (0.0083 g, 0.05 mmol) in CH_2Cl_2 (5 ml) was stirred under N_2 for two hours. The solution colour changed from yellow to red and a white solid (TlCl) precipitated. The solution was then transferred, *via* cannular filtration (– TlCl), into a separate dry, degassed flask containing 1,8-*bis*-dimethylaminonapthalene (Proton Sponge) (0.046 g, 0.21 mmol) in CH_2Cl_2 (2 ml), where the red solution colour darkened instantly. The solution was stirred for a further ten minutes, then filtered through celite to remove reaction salts. The red filtrate is concentrated to ~ 0.5 ml by rotary evaporation then excess hexanes added, resulting in the instantaneous precipitation of a red solid. The solid was collected by filtration, washed with hexanes (3 × 20 ml) and air dried (0.049 g, 88 %). Crystals of the complex were obtained from a CH_2Cl_2 / hexanes layer diffusion.

IR (CH_2Cl_2, cm^{-1}): 2058 ν(RuC≡C), 1579 ν(N=O), 1322 ν(N-O). ^{1}H NMR ($CDCl_3$, 400 MHz) δ / ppm: 4.86 – 5.05 (m, 4H, CH_2, dppm), 5.95 (apparent doublet, splitting = 8 Hz, 2H, H^4), 7.09 (t, J = 8 Hz, 8H, H$_m$, dppm), 7.18 (t, J = 8 Hz, 8H, H$_m$, dppm), 7.26 (t, J = 8 Hz, 4H, H$_p$, dppm), 7.31 (t, J = 8 Hz, 4H, H$_p$, dppm), 7.36 – 7.41 (m, 8H, H$_o$, dppm), 7.42 – 7.46 (m, 8H, H$_o$, dppm), 7.78 (apparent doublet, splitting = 8 Hz, 2H, H^5). ^{31}P{^{1}H} NMR ($CDCl_3$, 400 MHz) δ / ppm: – 7.1 (s, Ru(dppm)$_2$). ^{13}C{^{1}H} NMR ($CDCl_3$, 500 MHz) δ / ppm: 50.2, (t, J = 11 Hz, CH_2, dppm), 115.8 (s, C^2), 122.9 (s, C^5), 127.7 (s, C$_m$, dppm), 127.8 (s, C$_m$, dppm), 129.5 (s, C$_p$, dppm) 129.7 (s, C$_p$, dppm), 129.8 (s, C^4), 133.3 (t, J = 3 Hz, C$_o$, dppm) 133.8 (t, J = 3 Hz, C$_o$, dppm), 133.9 (quin., J = 11 Hz, C$_i$, dppm), 134.7 (quin., J = 11 Hz, C$_i$, dppm), 137.6 (s, C^3), 141.9 (s, C^6), 147.6 (quin., J = 16 Hz, C^1). MALDI (+)-MS (*m/z*): 1051 [RuCl(C≡CC$_6$H$_4$-4-NO$_2$)(dppm)$_2$ + H]$^+$, 870 [Ru(dppm)$_2$]$^+$. Anal. Found: C, 66.30; H, 4.48; N, 1.39. Calc. for $C_{58}H_{48}ClNO_2P_4Ru$: C, 66.21; H, 4.60; N, 1.33.

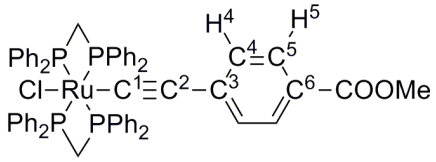

*Synthesis of trans-[RuCl(C≡CC$_6$H$_4$-4-COOMe)(dppm)$_2$], [**23b**]*

A mixture of *cis*-[**20**] (0.050 g, 0.05 mmol), $TlBF_4$ (0.017 g, 0.06 mmol) and HC≡CC$_6$H$_4$-4-COOMe (0.0086 g, 0.05 mmol) in CH_2Cl_2 (5 ml) was stirred under N_2 for one hour. The solution colour changed from yellow to orange and a white solid (TlCl) precipitated. The solution was then transferred, *via* cannular filtration (– TlCl), into a separate dry, degassed flask containing 1,8-*bis*-dimethylaminonapthalene (Proton Sponge) (0.045 g, 0.21 mmol) in CH_2Cl_2 (2 ml), where solution colour immediately changed from orange to yellow. The solution was stirred for a further ten minutes, then filtered through celite to remove reaction salts. The yellow filtrate is concentrated to ~ 0.5 ml by rotary evaporation then excess hexanes added; resulting in the instantaneous precipitation of a yellow solid. The solid was collected by filtration, washed with hexanes (3 × 20 ml) and air dried (0.048 g, 86 %). Crystals of the complex were obtained from a CH_2Cl_2 / pentane layer diffusion.

IR (CH_2Cl_2, cm^{-1}): 2073 ν(RuC≡C), 1705 ν(C=O), 1590 ν(C-O). ^{1}H NMR ($CDCl_3$, 400 MHz) δ / ppm: 3.84 (s, 3H, CH_3), 4.86 – 4.95 (m, 4H, CH_2, dppm), 6.00 (apparent doublet, splitting = 8 Hz, 2H, H^4), 7.06 (t, J = 8 Hz, 8H, H_m, dppm), 7.72 (t, J = 8 Hz, 8H, H_m, dppm), 7.23 (t, J = 8 Hz, 4H, H_p, dppm), 7.29 (t, J = 8 Hz, 4H, H_p, dppm), 7.37 – 7.43 (m, 8H, H_o, dppm), 7.43 – 7.49 (m, 8H, H_o, dppm), 7.48 (apparent doublet, splitting = 8 Hz, 2H, H^5). ^{31}P{^{1}H} NMR ($CDCl_3$, 400 MHz) δ / ppm: – 6.8 (s, Ru(dppm)$_2$). ^{13}C{^{1}H} NMR ($CDCl_3$, 600 MHz) δ / ppm: 50.4 (quin., J = 10 Hz, CH_2, dppm), 51.8 (s, CH_3), 113.9 (s, C^2), 123.2 (s, C^3), 127.7 (s, C_m, dppm), 128.5 (s, C^5), 129.3 (s, C_p, dppm), 129.5 (s, C_p, dppm), 129.9 (s, C^4), 133.5 (s, C_o, dppm), 133.8 (s, C_o, dppm), 134.2 (quin., J = 10 Hz, C_i, dppm), 134.9 (quin., J = 10 Hz, C_i, dppm), 135.6 (s, C^6), 144.7 – 145.0 (m, C^1), 167.8 (s, C=O). MALDI (+)-MS (*m/z*): 1189 [RuCl(C≡CC$_6$H$_4$-4-COOMe)(dppm)$_2$ + H]$^+$, 870 [Ru(dppm)$_2$]$^+$. Anal. Found: C, 62.96; H, 4.67. Calc. for $C_{60}H_{51}ClO_2P_4Ru \times CH_2Cl_2$: C, 63.76; H, 4.65.

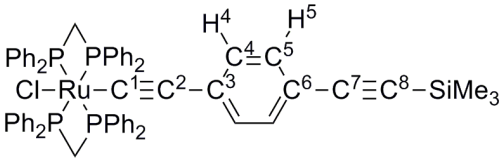

*Synthesis of trans-[RuCl(C≡CC$_6$H$_4$C≡CSiMe$_3$)(dppm)$_2$], [**23c**]*

A mixture of *cis*-[**20**] (0.11 g, 0.12 mmol), $TlBF_4$ (0.035 g, 0.12 mmol) and HC≡CC$_6$H$_4$-4-C≡CSiMe$_3$ (0.035 g, 0.12 mmol) in CH_2Cl_2 (5 ml) was stirred under N_2 for 75 minutes. The solution colour changed from yellow to orange and a white solid (TlCl) precipitated. The solution was then transferred, *via* cannular filtration (– TlCl), into a separate dry degassed flask containing 1,8-*bis*-dimethylaminonapthalene (Proton Sponge) (0.088 g, 0.48 mmol) in CH_2Cl_2 (2 ml), where solution colour immediately changed from orange to yellow. The solution was stirred for a further ten minutes, then filtered through celite to remove reaction salts. The yellow filtrate is concentrated to ~ 0.5 ml by rotary evaporation then excess hexanes added; resulting in the instantaneous precipitation of a yellow solid. The solid was collected by filtration, washed with hexanes (3 × 20 ml) and air dried (0.11 g, 80 %). Crystals of the complex were obtained from a CH_2Cl_2 / MeOH layer diffusion.

IR (CH_2Cl_2, cm^{-1}): 2146 ν(C≡CSiMe$_3$), 2073 ν(RuC≡C). ^{1}H NMR (CD_2Cl_2, 700 MHz) δ / ppm: 0.23 (s, 9H, SiMe$_3$), 4.88 – 4.98 (m, 4H, CH_2, dppm), 5.95 (apparent doublet, splitting = 8 Hz, 2H, H^4), 6.96 (apparent doublet, splitting = 8 Hz, 2H, H^5), 7.04 (t, J = 8 Hz, 8H, H$_m$, dppm), 7.17 (t, J = 8 Hz, 8H, H$_m$, dppm), 7.21 (t, J = 8 Hz, 4H, H$_p$, dppm), 7.28 (t, J = 8 Hz, 4H, H$_p$, dppm), 7.36 – 7.44 (m, 8H, H$_o$, dppm), 7.44 – 7.50 (m, 8H, H$_o$, dppm). ^{31}P{^{1}H} NMR ($CDCl_3$, 400 MHz) δ / ppm: – 6.6 ppm (s, Ru(dppm)$_2$). ^{13}C{^{1}H} NMR (CD_2Cl_2, 700 MHz) δ / ppm: – 0.3 (s, SiMe$_3$), 49.8 (t, J = 10 Hz, CH_2, dppm), 93.2 (s, C^8), 106.0 (s, C^7), 112.9 (s, C^2), 116.0 (s, C^3), 128.3 (t, J = 3 Hz, C$_m$, dppm), 128.4 (t, J = 3Hz, C$_m$, dppm), 129.9 (s, C$_p$, dppm), 130.1 (s, C$_p$, dppm), 130.4 (s, C^4), 130.8 (quin., J = 15 Hz, C^1), 131.1 (s, C^5), 131.4 (s, C^6), 134.0 (t, J = 3 Hz, C$_o$, dppm), 134.3 (t, J = 3 Hz, C$_o$, dppm), 135.4 (quin., J = 11 Hz, C$_i$, dppm), 135.9 (quin., J = 11 Hz, C$_i$, dppm). MALDI (+)-MS (*m*/*z*): 1102 [RuCl(C≡CC$_6$H$_4$-4-C≡CSiMe$_3$)(dppm)$_2$]$^+$, 933 [RuCl(dppm)$_2$ + C$_2$H$_4$]$^+$. Anal. Found: C, 68.51; H, 5.35. Calc. for C$_{63}$H$_{57}$ClP$_4$RuSi: C, 68.59; H, 5.21.

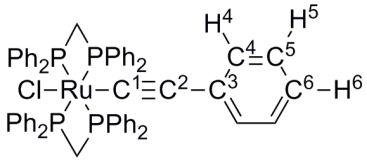

*Synthesis of trans-[RuCl(C≡CC$_6$H$_5$)(dppm)$_2$], **[23d]***

A mixture of *cis*-[**20**] (0.049 g, 0.05 mmol), $TlBF_4$ (0.016 g, 0.05 mmol) and $HC{\equiv}CC_6H_5$ (6 µL, 0.06 mmol) in CH_2Cl_2 (5 ml) was stirred under N_2 for one hour. The solution colour changed from yellow to orange and a white solid (TlCl) precipitated. The solution was then transferred, *via* cannular filtration (– TlCl), into a separate dry degassed flask containing 1,8-*bis*-dimethylaminonapthalene (Proton Sponge) (0.041 g, 0.19 mmol) in CH_2Cl_2 (2 ml), where solution colour immediately changed from orange to yellow. The solution was stirred for a further ten minutes, then filtered through celite to remove reaction salts. The yellow filtrate is concentrated to ~ 0.5 ml by rotary evaporation then excess hexanes added, resulting in the instantaneous precipitation of a yellow solid. The solid was collected by filtration, washed with hexanes (3 × 20 ml) and air dried (0.047 g, 90 %). Crystals suitable for single crystal X-ray diffraction were grown from a CH_2Cl_2 / hexanes layer diffusion.

IR (CH_2Cl_2, cm^{-1}): 2081 ν(RuC≡C). ^{1}H NMR ($CDCl_3$, 600 MHz) δ / ppm: 4.89 – 4.93 (m, 4H, CH_2, dppm), 6.11 (d, J = 7 Hz, 2H, H^4), 6.83 (t, J = 7 Hz, 1H, H^6), 6.89 (t, J = 7 Hz, 2H, H^5), 7.07 (t, J = 8 Hz, 8H, H_m, dppm), 7.17 (t, J = 8 Hz, 8H, H_m, dppm), 7.23 (t, J = 8 Hz, 4H, H_p, dppm), 7.28 (t, J = 8 Hz, 4H, H_p, dppm), 7.43 – 7.54 (m, 16H, H_o, dppm). ^{31}P{^{1}H} NMR ($CDCl_3$, 300 MHz) δ / ppm: – 5.2 (s, Ru(dppm)$_2$). ^{13}C{^{1}H} NMR ($CDCl_3$, 600 MHz) δ / ppm: 50.4 (t, J = 10 Hz, CH_2, dppm), 112.5 (s, C^2), 122.4 (s, C^6), 123.0 (quin., J = 15 Hz, C^1), 126.9 (s, C^5), 127.6 – 127.7 (m, C_m, dppm), 129.2 (s, C_p, dppm), 129.4 (s, C_p, dppm), 130.3 (s, C^4), 130.8 (s, C^3), 133.6 (t, J = 3 Hz, C_o, dppm), 133.9 (t, J = 3 Hz, C_o, dppm), 134.5 (quin., J = 11 Hz, C_i, dppm), 135.3 (quin., J = 11 Hz, C_i, dppm). ESI (+)-MS (*m/z*): 1032 [RuCl(C≡CC$_6$H$_5$)(dppm)$_2$ + MeOH]$^+$, 1007 [RuCl(C≡CC$_6$H$_5$)(dppm)$_2$ + H]$^+$, 933 [RuCl(dppm)$_2$ + C_2H_4]$^+$.

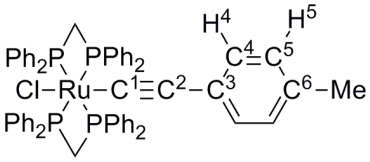

*Synthesis of trans-[RuCl(C≡CC$_6$H$_4$-4-Me)(dppm)$_2$], [**23e**]*

A mixture of *cis*-[**20**] (0.050 g, 0.05 mmol), $TlBF_4$ (0.016 g, 0.05 mmol) and HC≡CC$_6$H$_4$-4-Me (7.5 µL, 0.06 mmol) in CH_2Cl_2 (7 ml) was stirred under N_2 for one hour. The solution colour changed from yellow to orange and a white solid (TlCl) precipitated. The solution was then transferred, *via* cannular filtration (– TlCl), into a separate dry, degassed flask containing 1,8-*bis*-dimethylaminonapthalene (Proton Sponge) (0.045 g, 0.21 mmol) in CH_2Cl_2 (2 ml), where solution colour immediately changed from orange to yellow. The solution was stirred for a further ten minutes, then filtered through celite to remove reaction salts. The yellow filtrate is concentrated to ~ 0.5 ml by rotary evaporation then excess hexanes added, resulting in the instantaneous precipitation of a bright yellow solid. The solid was collected by filtration, washed with hexanes (3 × 20 ml) and air dried (0.050 g, 92 %). Crystals suitable for single crystal X-ray diffraction were grown from a CH_2Cl_2 / pentane layer diffusion.

IR (CH_2Cl_2, cm^{-1}): 2082 ν(RuC≡C). ^{1}H NMR ($CDCl_3$, 400 MHz) δ / ppm: 2.20 (s, 3H, CH_3), 4.86 – 4.93 (m, 4H, CH_2, dppm), 6.03 (apparent doublet, splitting = 8 Hz, 2H, H^4), 6.71 (apparent doublet, splitting = 8 Hz, 2H, H^5), 7.07 (t, J = 8 Hz, 8H, H_m, dppm), 7.17 (t, J = 8 Hz, 8H, H_m, dppm), 7.23 (t, J = 8 Hz, 4H, H_p, dppm), 7.27 (t, J = 8 Hz, 4H, H_p, dppm), 7.42 – 7.54 (m, 16H, H_o, dppm). ^{31}P{^{1}H} NMR ($CDCl_3$, 400 MHz) δ / ppm: – 6.6 (s, Ru(dppm)$_2$). ^{13}C{^{1}H} NMR ($CDCl_3$, 500 MHz) δ / ppm: 21.1 (s, CH_3), 50.2 (t, J = 10 Hz, CH_2, dppm), 111.9 (s, C^2), 120.4 (quin., J = 15 Hz, C^1), 127.2 – 127.7 (m, C_m, dppm), 127.6 (s, C^5), 128.8 (s, C^3), 129.1 (s, C_p, dppm), 129.3 (s, C_p, dppm), 130.0 (s, C^4), 131.5 (s, C^6), 133.6 (s, C_o, dppm), 133.9 (s, C_o, dppm), 134.6 (quin., J = 10 Hz, C_i, dppm), 135.4 (quin., J = 10 Hz, C_i, dppm). MALDI (+)-MS (*m/z*): 1020 [RuCl(C≡CC$_6$H$_4$-4-Me)(dppm)$_2$]$^+$, 933 [RuCl(dppm)$_2$ + C_2H_4]$^+$, 905 [RuCl(dppm)$_2$]$^+$, 870 [Ru(dppm)$_2$]$^+$. Anal. Found: C, 67.87; H, 4.78. Calc. for $C_{59}H_{51}ClP_4Ru$ × 0.5 CH_2Cl_2: C, 67.22; H, 4.93.

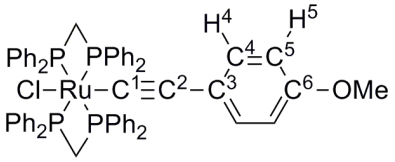

*Synthesis of trans-[RuCl(C≡CC$_6$H$_4$-4-OMe)(dppm)$_2$], [**23f**]*

A mixture of *cis*-[**20**] (0.050 g, 0.05 mmol), $TlBF_4$ (0.017 g, 0.06 mmol) and HC≡CC$_6$H$_4$-4-OMe (7 µL, 0.05 mmol) in CH_2Cl_2 (5 ml) was stirred under N_2 for one hour. The solution colour changed from yellow to orange and a white solid (TlCl) precipitated. The solution was then transferred, *via* cannular filtration (– TlCl), into a separate dry degassed flask containing 1,8-*bis*-dimethylaminonapthalene (Proton Sponge) (0.045 g, 0.21 mmol) in CH_2Cl_2 (2 ml), where solution colour immediately changed from orange to yellow. The solution was stirred for a further ten minutes, then filtered through celite to remove reaction salts. The yellow filtrate is concentrated to ~ 0.5 ml by rotary evaporation then excess hexanes added, resulting in the instantaneous precipitation of a yellow solid. The solid was collected by filtration, washed with hexanes (3 × 20 ml) and air dried (0.041 g, 74 %). Crystals suitable for single crystal X-ray diffraction were grown from a CH_2Cl_2 / diisopropylether layer diffusion.

IR (CH_2Cl_2, cm^{-1}): 2083 ν(RuC≡C). ^{1}H NMR ($CDCl_3$, 400 MHz) δ / ppm: 3.72 (s, 3H, CH_3), 4.85 – 4.96 (m, 4H, CH_2, dppm), 6.04 (apparent doublet, splitting = 8 Hz, 2H, H^4), 6.40 (apparent doublet, splitting = 8 Hz, 2H, H^5), 7.06 (t, J = 8 Hz, 8H, H_m, dppm), 7.16 (t, J = 8 Hz, 8H, H_m, dppm), 7.23 (t, J = 8 Hz, 4H, H_p, dppm), 7.27 (t, J = 8 Hz, 4H, H_p, dppm), 7.42 – 7.52 (m, 16H, H_o, dppm). ^{31}P{^{1}H} NMR ($CDCl_3$, 400 MHz) δ / ppm: – 6.6 (s, Ru(dppm)$_2$). ^{13}C{^{1}H} NMR ($CDCl_3$, 600 MHz) δ / ppm: 55.3 (s, CH_3), 50.5 (t, J = 11 Hz, CH_2, dppm), 111.4 (s, C^2), 112.6 (s, C^5), 118.2 (quin., J = 15 Hz, C^1), 123.8 (s, C^3), 127.6 (s, C_m, dppm), 127.8 (s, C_m, dppm), 129.1 (s, C_p, dppm), 129.4 (s, C_p, dppm), 131.1 (s, C^4), 133.6 – 133.7 (m, C_o, dppm), 133.8 – 133.9 (m, C_o, dppm), 134.6 (quin., J = 10 Hz, C_i, dppm), 135.4 (quin., J = 10 Hz, C_i, dppm), 155.5 (s, C^6). MALDI (+)-MS *(m/z)*: 1036 [RuCl(C≡CC$_6$H$_4$-4-OMe)(dppm)$_2$]$^+$, 933 [RuCl(dppm)$_2$ + C_2H_4]$^+$, 905 [RuCl(dppm)$_2$]$^+$, 870 [Ru(dppm)$_2$]$^+$. Anal. Found: C, 64.53; H, 4.22. Calc. for $C_{59}H_{51}ClOP_4Ru \times CH_2Cl_2$: C, 64.28; H, 4.77.

2.6.4. Syntheses and characterisations of *trans*-bis(alkynyl) complexes

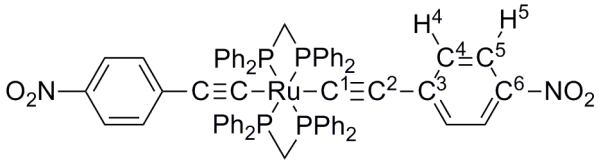

*Synthesis of trans-[Ru(C≡CC$_6$H$_4$NO$_2$)$_2$(dppm)$_2$], **[24a]***

A mixture of *cis*-[**20**] (0.049 g, 0.05 mmol), $TlBF_4$ (0.032 g, 0.10 mmol), HC≡CC$_6$H$_4$-4-NO_2 (0.016 g, 0.11 mmol) and 1,8-*bis*-dimethylaminonapthalene (Proton Sponge) (0.068 g, 0.32 mmol) in CH_2Cl_2 (5 ml) was stirred under N_2 for 3.5 days. The red solution colour darkened over the reaction period and a white solid (TlCl) precipitated. The solution is then carefully concentrated to ~ 3 ml under high vacuum and filtered through celite to remove TlCl and reaction salts. The red filtrate was concentrated to dryness by rotary evaporation and purified by column chromatography on alumina (basic, oven-dried; 30 : 70 40 – 60 petroleum ether : CH_2Cl_2). The first red band was collected, concentrated to ~ 0.5 ml by rotary evaporation then excess hexanes added; resulting in the instantaneous precipitation of a dark red solid. The solid was collected by filtration, washed with hexanes (3 × 10 ml) and then air dried (0.048 g, 80 %).

IR (CH_2Cl_2, cm^{-1}): 2053 ν(RuC≡C), 1581 ν(N=O), 1322 ν(N-O). ^{1}H NMR ($CDCl_3$, 400 MHz) δ / ppm: 4.83 – 4.90 (m, 4H, CH_2, dppm), 6.16 (apparent doublet, splitting = 8 Hz, 4H, H^4), 7.12 (t, J = 8 Hz, 16H H_m, dppm), 7.30 (t, J = 8 Hz, 8H, H_p, dppm), 7.35 – 7.45 (m, 16H, H_o, dppm), 7.83 (apparent doublet, splitting = 8 Hz, 4H, H^5). ^{31}P{^{1}H} NMR ($CDCl_3$, 400 MHz) δ / ppm: – 4.1 (s, Ru(dppm)$_2$). ^{13}C{^{1}H} NMR ($CDCl_3$) δ / ppm: 52.3 (t, J = 11 Hz, CH_2, dppm), 119.0 (s, C^2), 123.2 (s, C^5), 127.8 (s, C_m, dppm), 129.6 (s, C_p, dppm), 130.0 (s, C^4), 133.4 (s, C_o, dppm), 135.2 (quin., J = 11 Hz, C_i, dppm), 137.7 (s, C^6), 142.7 (s, C^3), 150.1 (quin., J = 15 Hz, C^1). MALDI (+)-MS (*m/z*): 1162 [Ru(C≡CC$_6$H$_4$NO$_2$)$_2$(dppm)$_2$]$^+$, 870 [Ru(dppm)$_2$]$^+$. Anal. Found: C, 68.27; H, 4.50; N, 2.37. Calc. for $C_{66}H_{52}N_2O_4P_4Ru$: C, 68.15; H, 4.51; N, 2.41.

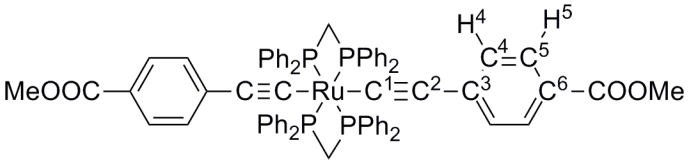

*Synthesis of trans-[Ru(C≡CC$_6$H$_4$-4-COOMe)$_2$(dppm)$_2$], **[24b]***

A mixture of *cis*-[**20**] (0.051 g, 0.05 mmol), $TlBF_4$ (0.032 g, 0.10 mmol), HC≡CC$_6$H$_4$-4-COOMe (0.019 g, 0.12 mmol) and 1,8-*bis*-dimethylaminonapthalene (Proton Sponge) (0.069 g, 0.32 mmol) in CH_2Cl_2 (5 ml) was stirred under N_2 for 36 hours. The yellow solution colour darkened over the reaction period and a white solid (TlCl) precipitated. The solution is then carefully concentrated to ~ 1 ml under high vacuum and then filtered through a short pad of alumina (basic, oven-dried) to remove TlCl and reaction salts. The first yellow fraction is collected, concentrated to *ca* 0.5 ml by rotary evaporation then excess hexanes added, resulting in the instantaneous precipitation of a bright yellow solid. The solid was collected by filtration, washed with hexanes (3 × 10 ml) and diethyl ether (3 × 5 ml) then air dried (0.038 g, 60 %). Crystals suitable for single crystal X-ray diffraction were grown from a $CDCl_3$ / 40 – 60 petroleum ether layer diffusion.

IR (CH_2Cl_2, cm^{-1}): 2062 ν(RuC≡C), 1705 ν(C=O). ^{1}H NMR ($CDCl_3$, 400 MHz) δ / ppm: 3.79 (s, 6H, CH_3), 4.74 – 4.80 (m, 4H, CH_2, dppm), 6.15 (apparent doublet, splitting = 8 Hz, 4H, H^4), 7.02 (t, J = 8 Hz, 16H H_m, dppm), 7.18 (t, J = 8 Hz, 8H, H_p, dppm), 7.34 – 7.48 (m, 16H, H_o, dppm), 7.55 (apparent doublet, splitting = 8 Hz, 4H, H^5). ^{31}P{^{1}H} NMR ($CDCl_3$, 400 MHz) δ / ppm: – 4.0 (s, Ru(dppm)$_2$). ^{13}C{^{1}H} NMR ($CDCl_3$) δ / ppm: 51.8 (s, CH_3), 52.4 (t, J = 10 Hz, CH_2, dppm), 117.3 (s, C^2), 123.5 (s, C^3), 127.7 (s, C_m, dppm), 128.7 (s, C^5), 129.3 (s, C_p, dppm), 129.8 (s, C^4), 133.5 (s, C_o, dppm), 135.6 (quin., J = 11 Hz, C_i, dppm), 135.8 (s, C^6), 141.1 (quin., J = 15 Hz, C^1), 167.8 (s, C=O). MALDI (+)-MS (*m/z*): 1189 [Ru(C≡CC$_6$H$_4$-4-COOMe)$_2$(dppm)$_2$ + H]$^+$, 870 [Ru(dppm)$_2$]$^+$. Anal. Found: C, 70.62; H, 5.05. Calc. for $C_{70}H_{58}O_4P_4Ru$: C, 70.69; H, 4.92.

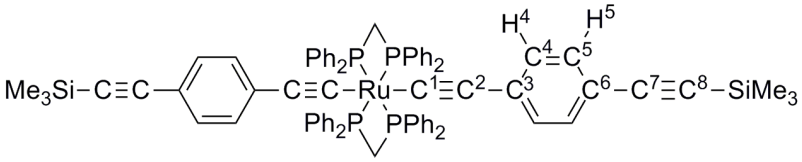

*Synthesis of trans-[Ru(C≡CC$_6$H$_4$-4-C≡CSiMe$_3$)$_2$(dppm)$_2$], [**24c**]*

A mixture of *cis*-[**20**] (0.051 g, 0.05 mmol), $TlBF_4$ (0.032 g, 0.10 mmol), HC≡CC$_6$H$_4$-4-C≡CSiMe$_3$ (0.022 g, 0.11 mmol) and 1,8-*bis*-dimethylaminonapthalene (Proton Sponge) (0.073 g, 0.34 mmol) in CH_2Cl_2 (5 ml) was stirred under N_2 for 16 hours. The yellow solution colour darkened over the reaction period and a white solid (TlCl) precipitated. The solution is then carefully concentrated to ~ 3 ml under high vacuum and then filtered through celite to remove TlCl and reaction salts. The yellow filtrate is concentrated again to ~ 1 ml by rotary evaporation then excess diethyl ether added (~ 10 ml); resulting in the instantaneous precipitation of a yellow solid. The mixture is left in the fridge for several hours to aid precipitation before filtering. The collected yellow solid was washed with cold diethyl ether (1 × 5 ml) and hexanes (3 × 15 ml) and then air dried (0.033 g, 48 %).

IR (CH_2Cl_2, cm^{-1}): 2149 ν(C≡CSiMe$_3$), 2058 ν(RuC≡C). ^{1}H NMR ($CDCl_3$, 400 MHz) δ / ppm: 0.26 (s, 18H, SiMe$_3$), 4.80 – 4.89 (m, 4H, CH_2, dppm), 6.15 (apparent doublet, splitting = 8 Hz, 4H, H^4), 7.07 (apparent doublet, J = 8 Hz, 4H, H^5), 7.09 (t, J = 8 Hz, 16H, H$_m$, dppm), 7.25 (t, J = 8 Hz, 8H, H$_p$, dppm) 7.41 – 7.55 (m, 16H, H$_o$, dppm). ^{31}P{^{1}H} NMR ($CDCl_3$, 400 MHz) δ / ppm: – 3.8 ppm (s, Ru(dppm)$_2$). ^{13}C{^{1}H} NMR ($CDCl_3$, 600 MHz) δ / ppm: 0.3 (s, SiMe$_3$), 52.4 (t, J = 11 Hz, CH_2, dppm), 93.3 (s, C^8), 106.9 (s, C^7), 116.2 (s, C^2), 129.4 (s, C^3), 127.6 (s, C$_m$, dppm), 129.2 (s, C$_p$, dppm), 129.9 (s, C^4), 131.0 (s, C^5), 131.5 (s, C^6), 133.4 – 133.6 (m, C$_o$, dppm), 135.8 (quin., J = 10 Hz, C$_i$, dppm), 136.7 – 137.0 (m, C^1). ASAP (+)-MS (*m*/*z*): 1265 [Ru(C≡CC$_6$H$_4$-4-C≡CSiMe$_3$)$_2$(dppm)$_2$ + H]$^+$, 1264 [Ru(C≡CC$_6$H$_4$-4-C≡CSiMe$_3$)$_2$(dppm)$_2$]$^+$, 1067 [Ru(C≡CC$_6$H$_4$-4-C≡CSiMe$_3$)(dppm)$_2$]$^+$, 870 [Ru(dppm)$_2$]$^+$.

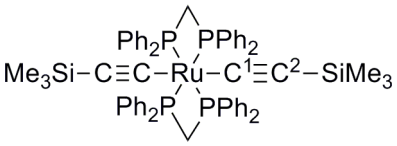

*Synthesis of trans-[Ru(C≡CSiMe$_3$)$_2$(dppm)$_2$], [**86**]*

A mixture of *cis*-[**20**] (0.11 g, 0.11 mmol) HC≡CSiMe$_3$ (0.17 ml, 1.23 mmol) and TlBF$_4$ (0.072 g, 0.29 mmol) in NH^{i}Pr$_2$ (4 ml) and CH$_2$Cl$_2$ (2 ml) was heated under a gentle reflux (30 °C) under N$_2$ for 24 hours. The yellow solution colour lightened over time and a white solid (TlCl) precipitated. The solution was then filtered through celite to remove TlCl and reaction salts and filtrate concentrated to dryness by rotary evaporation. The brown residue was extracted with minimum CH$_2$Cl$_2$, layered with MeOH (1 : 6) and left in the freezer for several hours, forming a bright yellow precipitate. The precipitate was collected by filtration, washed with MeOH (1 × 20 ml) and hexanes (2 × 20 ml) then air dried (0.11 g, 80 %). Crystals suitable for single crystal X-ray diffraction were grown from a CH$_2$Cl$_2$ / hexanes layer diffusion.

IR (CH$_2$Cl$_2$, cm^{-1}): 1997 ν(C≡C). ^{1}H NMR (CDCl$_3$, 600 MHz) δ / ppm: – 0.49 (s, 18 H, SiMe$_3$), 4.80 – 4.87 (m, 4H, CH$_2$, dppm), 7.13 (t, J = 8 Hz, 16H, H$_m$, dppm), 7.24 (t, J = 8 Hz, 8H, H$_p$, dppm), 7.56 – 7.64 (m, 16H, H$_o$, dppm). ^{31}P{^{1}H} NMR (CDCl$_3$, 400 MHz) δ / ppm: – 3.6 (s, Ru(dppm)$_2$). ^{13}C{^{1}H} NMR (CDCl$_3$) δ / ppm: 1.17 (s, SiMe$_3$), 51.7 (t, J = 10 Hz, CH$_2$, dppm), 118.7 (s, C^2), 127.4 (s, C$_m$, dppm), 129.0 (s, C$_p$, dppm), 133.8 (s, C$_o$, dppm), 136.5 (quin., J = 11 Hz, C$_i$, dppm), 152.1 (quin., J = 14 Hz, C^1). MALDI (+)-MS (*m/z*): 967 [Ru(C≡CSiMe$_3$)(dppm)$_2$]$^+$, 870 [Ru(dppm)$_2$]$^+$. Anal. Found: C, 67.73; H, 5.73. Calc. for C$_{60}$H$_{62}$P$_4$RuSi$_2$: C, 67.65; H, 5.87.

2.6.5. Syntheses and characterisations of η^3-butenynyl complexes

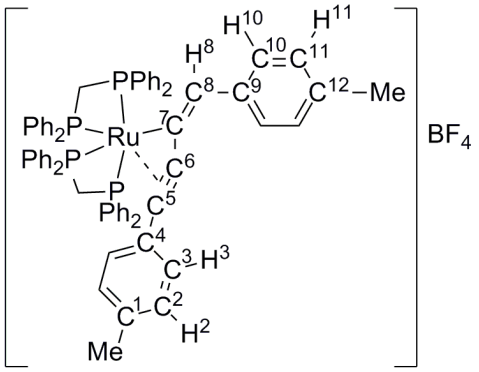

*Synthesis of E-[Ru(η^3-{HC(C_6H_4-4-Me)=CC≡CC_6H_4-4-Me})(dppm)$_2$]BF_4, [**28e**]BF_4*

A mixture of *cis*-[**20**] (0.049 g, 0.05 mmol), $TlBF_4$ (0.032 g, 0.11 mmol), HC≡CC_6H_4-4-Me (14.5 µL, 0.11 mmol) and 1,8-*bis*-dimethylaminonapthalene (Proton Sponge) (0.066 g, 0.31 mmol) in CH_2Cl_2 (8 ml) was stirred under N_2 for 40 hours. A white solid (TlCl) precipitated from the yellow solution over the reaction period. The yellow solution is concentrated carefully to half volume under high vacuum then filtered through a HPLC Teflon filter (20 µm pores) to remove TlCl and reaction salts. To the yellow filtrate, CH_2Cl_2 (~ 5 ml) and diethyl ether (~ 30 ml) are then added and solution left in the fridge overnight, where large yellow crystals formed round the flask. The solvent is decanted, crystals washed with diethyl ether (3 × 10 ml) and hexanes (3 × 10 ml) then air dried before collection (0.042 g, 56 %). Crystals suitable for single crystal X-ray diffraction were grown from an acetone / pentane layer diffusion.

IR (CH_2Cl_2, cm^{-1}): 1967 ν(C≡C), 1606 ν(C=C). ^1H NMR (CD_2Cl_2, 400 MHz) δ / ppm: 2.34 (s, 6H, CH_3), 4.20 (dt, J = 15, 11 Hz, 1H, CH_2, dppm), 4.50 (dt, J = 15, 11 Hz, 1H, CH_2, dppm), 4.93 – 5.07 (m, 2H, CH_2, dppm), 5.55 (d, J = 5 Hz, 1H, H^8), 6.18 (apparent doublet, splitting = 8 Hz, 2H, H^3), 6.36 – 7.76 (m, 40H, Ph, dppm), 6.85 (apparent doublet, splitting = 8 Hz, 2H, H^2), 7.14 (apparent doublet, splitting = 8 Hz, 2H, H^{11}), 7.29 (apparent doublet, splitting = 8 Hz, 2H, H^{10}). ^{11}B NMR (CD_2Cl_2, 400 MHz) δ / ppm: – 2.1 (s, BF_4). ^{19}F NMR (CD_2Cl_2, 400 MHz) δ / ppm: – 149.9 (s, BF_4). $^{31}P\{^1H\}$ NMR ($CDCl_3$, 400 MHz) δ / ppm: – 27.2 (ddd, J = 318, 49, 26 Hz, dppm), – 16.9 (ddd, J = 318, 40, 26 Hz, dppm), – 14.0 (ddd, J = 40, 26, 10 Hz, dppm), – 0.2 (ddd, J = 49, 26, 10 Hz, dppm). $^{13}C\{^1H\}$ NMR (CD_2Cl_2, 400 MHz) δ / ppm: 21.7 (s, CH_3), 22.0 (s, CH_3), 42.0 (t, J = 24 Hz, CH_2, dppm), 45.2 (t, J = 24 Hz, CH_2, dppm), 108.7 (d, J = 22 Hz, C^5),

126.7 (s, C^9), 128.9 – 139.9 (m, Ph, dppm), 129.7 (s, C^2), 130.2 (s, C^1 or C^{12}), 130.4 (s, C^8), 131.0 (s, C^3), 138.9 (s, C^1 or C^{12}), 139.8 (s, C^4). ESI (+)-MS (*m/z*): 1101 [Ru(η^3-{HC(C_6H_4-4-Me)=CC≡CC_6H_4-4-Me})$(dppm)_2]^+$. Anal. Found: C, 68.59; H, 4.68. Calc. for $C_{68}H_{59}BF_4P_4Ru$: C, 68.67; H, 5.00.

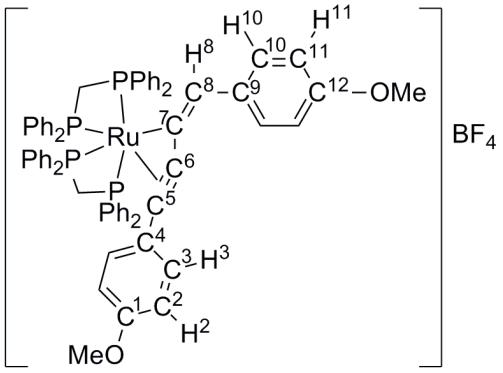

*Synthesis of E-[Ru(η^3-{HC(C_6H_4-4-OMe)=CC≡CC_6H_4-4-OMe})$(dppm)_2]BF_4$, **[28f]**BF_4*

A mixture of *cis*-[**20**] (0.10 g, 0.11 mmol), $TlBF_4$ (0.065 g, 0.22 mmol), HC≡CC_6H_4-4-OMe (30 µL, 0.23 mmol) and 1,8-*bis*-dimethylaminonapthalene (Proton Sponge) (0.078 g, 0.43 mmol) in CH_2Cl_2 (20 ml) was stirred under N_2 overnight. A white solid (TlCl) precipitated from the yellow solution over the reaction period. The solution was then filtered through celite to remove TlCl and reaction salts and the yellow filtrate concentrated to half volume. To the yellow solution, diethyl ether (~ 30 ml) is then added and left for several days, where large yellow crystals formed round the flask. The solvent was then decanted, crystals collected by filtration, washed with diethyl ether (3 × 10 ml) and hexanes (3 × 10 ml), then air dried (0.066 g, 50 %).

IR (CH_2Cl_2, cm^{-1}): 1870 ν(C≡C), 1602 ν(C=C). ^{1}H NMR (CD_2Cl_2, 400 MHz) δ / ppm: 3.81 (s, 3H, CH_3), 3.81 (s, 3H, CH_3), 4.21 (dt, J = 15, 11 Hz, 1H, CH_2, dppm), 4.49 (dt, J = 15, 11 Hz, 1H, CH_2, dppm), 4.93 – 5.03 (m, 2H, CH_2, dppm), 5.53 (d, J = 5 Hz, 1H, H^8), 6.23 (apparent doublet, splitting = 8 Hz, 2H, H^3), 6.36 – 7.74 (m, 40H, Ph, dppm), 6.56 (apparent doublet, splitting = 8 Hz, 2H, H^2), 6.87 (apparent doublet, splitting = 8 Hz, 2H, H^{11}), 7.29 (apparent doublet, splitting = 8 Hz, 2H, H^{10}). ^{11}B NMR (CD_2Cl_2, 400 MHz) δ / ppm: – 2.1 (s, BF_4). ^{19}F NMR (CD_2Cl_2, 400 MHz) δ / ppm: – 153.1 (s, BF_4). $^{31}P\{^1H\}$ NMR (CD_2Cl_2, 400 MHz) δ / ppm: – 25.4 (ddd, J = 322, 48, 26 Hz, dppm), – 16.4 (ddd, J = 322, 35, 26 Hz, dppm), – 13.2 (ddd, J = 35, 26, 9 Hz, dppm), 0.69 (ddd, J = 48, 26, 9 Hz, dppm). $^{13}C\{^1H\}$ NMR (CD_2Cl_2, 400 MHz) δ / ppm: 42.2 (t,

J = 26 Hz, CH_2, dppm), 45.4 (t, J = 26 Hz, CH_2, dppm), 56.1 (s, CH_3), 56.3 (s, CH_3), 108.5 (d, J = 22 Hz, C^5), 114.8 (s, C^2 or C^{11}), 114.9 (s, C^2 or C^{11}), 127.7 – 133.2 (m, Ph), 130.3 (s, C^8), 132.8 (s, C^3), 159.8 (s, C^{12}), 160.8 (s, C^1). ESI (+)-MS (*m/z*): 1133 [Ru(η^3-{HC(C_6H_4-4-OMe)=CC≡CC_6H_4-4-OMe})$(dppm)_2$]$^+$.

2.7. References

1. S. G. Eaves, D. S. Yufit, B. W. Skelton, J. M. Lynam and P. J. Low, *Dalton Trans.*, **2015**, *44*, 21016.
2. G. E. Moore, *Electronics*, **1965**, *38*, 114.
3. D. J. Frank, R. H. Dennard, E. Nowak, P. M. Solomon, Y. Taur and H. S. P. Wong, *P. IEEE*, **2001**, *89*, 259.
4. R. R. Schaller, *IEEE Spectrum*, **1997**, *34*, 52.
5. R. F. Service, *Science*, **2001**, *294*, 2442.
6. Y. Wada, *Pure Appl. Chem*, **1999**, *71*, 2055.
7. J. M. Lehn, *Angew. Chem. Int. Ed. Eng.*, **1988**, *27*, 89.
8. R. J. Nichols, W. Haiss, S. J. Higgins, E. Leary, S. Martín and D. Bethell, *Phys. Chem. Chem. Phys.*, **2010**, *12*, 2801.
9. P. J. Low, *Coord. Chem. Rev.*, **2013**, *257*, 1507.
10. N. Tuccitto, V. Ferri, M. Cavazzini, S. Quici, G. Zhavnerko, A. Licciardello and M. A. Rampi, *Nat. Mater.*, **2009**, *8*, 41.
11. F. Schwarz, G. Kastlunger, F. Lissel, H. Riel, K. Venkatesan, H. Berke, R. Stadler and E. Lörtscher, *Nano Lett.*, **2014**, *14*, 5932.
12. K. Liu, X. Wang and F. Wang, *ACS Nano*, **2008**, *2*, 2315.
13. F. Lissel, F. Schwarz, O. Blacque, H. Riel, E. Loertscher, K. Venkatesan and H. Berke, *J. Am. Chem. Soc.*, **2014**, *136*, 14560.
14. P. J. Low, *Dalton Trans.*, **2005**, 2821.
15. K. Costuas and S. Rigaut, *Dalton Trans.*, **2011**, *40*, 5643.
16. F. Paul and C. Lapinte, *Coord. Chem. Rev.*, **1998**, *178*, 431.
17. Q. Lu, C. Yao, X. Wang and F. Wang, *J. Phys. Chem. C*, **2012**, *116*, 17853.
18. M. Mayor, C. von Hanisch, H. B. Weber, J. Reichert and D. Beckmann, *Angew. Chem. Int. Edit.*, **2002**, *41*, 1183.
19. Y. B. Zhu, O. Clot, M. O. Wolf and G. P. A. Yap, *J. Am. Chem. Soc.*, **1998**, *120*, 1812.
20. F. Lissel, F. Schwarz, O. Blacque, H. Riel, E. Lörtscher, K. Venkatesan and H. Berke, *J. Am. Chem. Soc.*, **2014**, *136*, 14560.
21. Z. Cao, B. Xi, D. S. Jodoin, L. Zhang, S. P. Cummings, Y. Gao, S. F. Tyler, P. E. Fanwick, R. J. Crutchley and T. Ren, *J. Am. Chem. Soc.*, **2014**, *136*, 12174.
22. S. Marqués-González, D. S. Yufit, J. A. K. Howard, S. Martín, H. M. Osorio, V. M. García-Suárez, R. J. Nichols, S. J. Higgins, P. Cea and P. J. Low, *Dalton Trans.*, **2013**, *42*, 338.
23. B. Kim, J. M. Beebe, C. Olivier, S. Rigaut, D. Touchard, J. G. Kushmerick, X. Y. Zhu and C. D. Frisbie, *J. Phys. Chem. C*, **2007**, *111*, 7521.
24. L. Luo, A. Benameur, P. Brignou, S. H. Choi, S. Rigaut and C. D. Frisbie, *J. Phys. Chem. C*, **2011**, *115*, 19955.

25. S. Marqués-González, M. Parthey, D. S. Yufit, J. A. K. Howard, M. Kaupp and P. J. Low, *Organometallics*, **2014**, *33*, 4947.
26. G. Kastlunger and R. Stadler, *Phys. Rev. B*, **2014**, *89*, 115412.
27. Y. Liu, C. M. Ndiaye, C. Lagrost, K. Costuas, S. Choua, P. Turek, L. Norel and S. Rigaut, *Inorg. Chem.*, **2014**, *53*, 8172.
28. E. Wuttke, Y.-M. Hervault, W. Polit, M. Linseis, P. Erler, S. Rigaut and R. F. Winter, *Organometallics*, **2014**, *33*, 4672.
29. G. Grelaud, N. Gauthier, Y. Luo, F. Paul, B. Fabre, F. Barrière, S. Ababou-Girard, T. Roisnel and M. G. Humphrey, *J. Phys. Chem. C*, **2014**, *118*, 3680.
30. A. Vacher, F. Barrière and D. Lorcy, *Organometallics*, **2013**, *32*, 6130.
31. E. Wuttke, F. Pevny, Y.-M. Hervault, L. Norel, M. Drescher, R. F. Winter and S. Rigaut, *Inorg. Chem.*, **2012**, *51*, 1902.
32. C. Olivier, B. Kim, D. Touchard and S. Rigaut, *Organometallics*, **2008**, *27*, 509.
33. J.-W. Ying, Z. Cao, C. Campana, Y. Song, J.-L. Zuo, S. F. Tyler and T. Ren, *Polyhedron*, **2015**, *86*, 76.
34. D. Touchard, C. Morice, V. Cadierno, P. Haquette, L. Toupet and P. H. Dixneuf, *J. Chem. Soc., Chem. Commun.*, **1994**, 859.
35. D. Touchard, P. Haquette, A. Daridor, A. Romero and P. H. Dixneuf, *Organometallics*, **1998**, *17*, 3844.
36. M. A. Fox, J. E. Harris, S. Heider, V. Pérez-Gregorio, M. E. Zakrzewska, J. D. Farmer, D. S. Yufit, J. A. K. Howard and P. J. Low, *J. Organomet. Chem.*, **2009**, *694*, 2350.
37. S. Guesmi, D. Touchard and P. H. Dixneuf, *Chem. Commun.*, **1996**, 2773.
38. B. Chin, A. J. Lough, R. H. Morris, C. T. Schweitzer and C. D'Agostino, *Inorg. Chem.*, **1994**, *33*, 6278.
39. D. Touchard, P. Haquette, N. Pirio, L. Toupet and P. H. Dixneuf, *Organometallics*, **1993**, *12*, 3132.
40. P. Haquette, N. Pirio, D. Touchard, L. Toupet and P. H. Dixneuf, *J. Chem. Soc., Chem. Commun.*, **1993**, 163.
41. M. C. B. Colbert, J. Lewis, N. J. Long, P. R. Raithby, M. Younus, A. J. P. White, D. J. Williams, N. N. Payne, L. Yellowlees, D. Beljonne, N. Chawdhury and R. H. Friend, *Organometallics*, **1998**, *17*, 3034.
42. C. W. Faulkner, S. L. Ingham, M. S. Khan, J. Lewis, N. J. Long and P. R. Raithby, *J. Organomet. Chem.*, **1994**, *482*, 139.
43. Z. Atherton, C. W. Faulkner, S. L. Ingham, A. K. Kakkar, M. S. Khan, J. Lewis, N. J. Long and P. R. Raithby, *J. Organomet. Chem.*, **1993**, *462*, 265.
44. M. Younus, N. J. Long, P. R. Raithby, J. Lewis, N. A. Page, A. J. P. White, D. J. Williams, M. C. B. Colbert, A. J. Hodge, M. S. Khan and D. G. Parker, *J. Organomet. Chem.*, **1999**, *578*, 198.
45. J. M. Lynam, T. D. Nixon and A. C. Whitwood, *J. Organomet. Chem.*, **2008**, *693*, 3103.
46. J. Ruiz, M. E. G. Mosquera and V. Riera, *J. Organomet. Chem.*, **1997**, *527*, 35.
47. S. J. Higgins, A. La Pensée, C. A. Stuart and J. M. Charnock, *J. Chem. Soc., Dalton Trans.*, **2001**, 902.
48. G. A. Koutsantonis, G. I. Jenkins, P. A. Schauer, B. Szczepaniak, B. W. Skelton, C. Tan and A. H. White, *Organometallics*, **2009**, *28*, 2195.
49. L. F. Szczepura, J. Giambra, R. F. See, H. Lawson, T. S. Janik, A. J. Jircitano, M. R. Churchill and K. J. Takeuchi, *Inorg. Chim. Acta*, **1995**, *239*, 77.
50. A. J. Hodge, S. L. Ingham, A. K. Kakkar, M. S. Khan, J. Lewis, N. J. Long, D. G. Parker and P. R. Raithby, *J. Organomet. Chem.*, **1995**, *488*, 205.

51. A. M. McDonagh, I. R. Whittall, M. G. Humphrey, D. C. R. Hockless, B. W. Skelton and A. H. White, *J. Organomet. Chem.*, **1996**, *523*, 33.
52. J. E. McGrady, T. Lovell, R. Stranger and M. G. Humphrey, *Organometallics*, **1997**, *16*, 4004.
53. L. D. Field, A. M. Magill, T. K. Shearer, S. J. Dalgarno and M. M. Bhadbhade, *Eur. J. Inorg. Chem.*, **2011**, *2011*, 3503.
54. Y. Sun, N. J. Taylor and A. J. Carty, *Organometallics*, **1992**, *11*, 4293.
55. L. D. Field, A. M. Magill, S. J. Dalgarno and P. Jensen, *Eur. J. Inorg. Chem.*, **2008**, 4248.
56. C. Bianchini, M. Peruzzini, F. Zanobini, P. Frediani and A. Albinati, *J. Am. Chem. Soc.*, **1991**, *113*, 5453.
57. G. Jia, A. L. Rheingold and D. W. Meek, *Organometallics*, **1989**, *8*, 1378.
58. C. Bianchini, P. Innocenti, M. Peruzzini, A. Romerosa and F. Zanobini, *Organometallics*, **1996**, *15*, 272.
59. G. Albertin, P. Amendola, S. Antoniutti, S. Ianelli, G. Pelizzi and E. Bordignon, *Organometallics*, **1991**, *10*, 2876.
60. N. G. Connelly and W. E. Geiger, *Chem. Rev.*, **1996**, *96*, 877.
61. E. M. Long, N. J. Brown, W. Y. Man, M. A. Fox, D. S. Yufit, J. A. K. Howard and P. J. Low, *Inorg. Chim. Acta*, **2012**, *380*, 358.
62. N. Gauthier, N. Tchouar, F. Justaud, G. Argouarch, M. P. Cifuentes, L. Toupet, D. Touchard, J.-F. Halet, S. Rigaut, M. G. Humphrey, K. Costuas and F. Paul, *Organometallics*, **2009**, *28*, 2253.
63. A. M. McDonagh, I. R. Whittall, M. G. Humphrey, B. W. Skelton and A. H. White, *J. Organomet. Chem.*, **1996**, *519*, 229.
64. N. J. Long, A. J. Martin, F. F. de Biani and P. Zanello, *J. Chem. Soc., Dalton Trans.*, **1998**, 2017.
65. A. M. McDonagh, N. T. Lucas, M. P. Cifuentes, M. G. Humphrey, S. Houbrechts and A. Persoons, *J. Organomet. Chem.*, **2000**, *605*, 193.
66. S. K. Hurst, M. P. Cifuentes, J. P. L. Morrall, N. T. Lucas, I. R. Whittall, M. G. Humphrey, I. Asselberghs, A. Persoons, M. Samoc, B. Luther-Davies and A. C. Willis, *Organometallics*, **2001**, *20*, 4664.
67. B. Babgi, L. Rigamonti, M. P. Cifuentes, T. C. Corkery, M. D. Randles, T. Schwich, S. Petrie, R. Stranger, A. Teshome, I. Asselberghs, K. Clays, M. Samoc and M. G. Humphrey, *J. Am. Chem. Soc.*, **2009**, *131*, 10293.
68. M. Younus, N. J. Long, P. R. Raithby, J. Lewis, N. A. Page, A. J. P. White, D. J. Williams, M. C. B. Colbert, A. J. Hodge, M. S. Khan and D. G. Parker, *J. Organomet. Chem.*, **1999**, *578*, 198.
69. A. M. McDonagh, M. P. Cifuentes, I. R. Whittall, M. G. Humphrey, M. Samoc, B. Luther-Davies and D. C. R. Hockless, *J. Organomet. Chem.*, **1996**, *526*, 99.
70. H. W. Lin, X. H. Wang, X. J. Zhao, J. Li and F. S. Wang, *Synth. Met.*, **2003**, *135–136*, 239.
71. G. C. Jia, J. C. Gallucci, A. L. Rheingold, B. S. Haggerty and D. W. Meek, *Organometallics*, **1991**, *10*, 3459.
72. G. Albertin, P. Amendola, S. Antoniutti, S. Ianelli, G. Pelizzi and E. Bordignon, *Organometallics*, **1991**, *10*, 2876.
73. A. Dobson, D. S. Moore, S. D. Robinson, M. B. Hursthouse and L. New, *Polyhedron*, **1985**, *4*, 1119.
74. G. Albertin, S. Autoniutti, E. Bordignon, F. Cazzaro, S. Ianelli and G. Pelizzi, *Organometallics*, **1995**, *14*, 4114.

75. L. D. Field, A. V. George, G. R. Purches and I. H. M. Slip, *Organometallics*, **1992**, *11*, 3019.
76. T. Rappert and A. Yamamoto, *Organometallics*, **1994**, *13*, 4984.
77. D. Banerjee, Z. Hu and J. Li, *Dalton Trans.*, **2014**, *43*, 10668.
78. I. Kaljurand, A. Kütt, L. Sooväli, T. Rodima, V. Mäemets, I. Leito and I. A. Koppel, *J. Org. Chem.*, **2005**, *70*, 1019.
79. C. Bianchini, P. Frediani, D. Masi, M. Peruzzini and F. Zanobini, *Organometallics*, **1994**, *13*, 4616.
80. B. Chaudret, G. Commenges and R. Poilblanc, *J. Chem. Soc., Dalton Trans.*, **1984**, 1635.
81. S. Takahashi, Y. Kuroyama, K. Sonogashira and N. Hagihara, *Synthesis-Stuttgart*, **1980**, 627.
82. F. J. Arnaiz, *J. Chem. Educ.*, **1997**, *74*, 1332.
83. H. E. Gottlieb, V. Kotlyar and A. Nudelman, *J. Org. Chem.*, **1997**, *62*, 7512.
84. A. Klamt and G. Schuurmann, *J. Chem. Soc., Perkin Trans. 2*, **1993**, 799.
85. S. Grimme, J. Antony, S. Ehrlich and H. Krieg, *J. Chem. Phys.*, **2010**, *132*, 154104.
86. S. Grimme, S. Ehrlich and L. Goerigk, *J. Comput. Chem.*, **2011**, *32*, 1456.
87. P. Csaszar and P. Pulay, *J. Mol. Struct.*, **1984**, *114*, 31.
88. R. Ahlrichs, M. Bar, M. Haser, H. Horn and C. Kolmel, *Chem. Phys. Lett.*, **1989**, *162*, 165.
89. K. Eichkorn, O. Treutler, H. Ohm, M. Haser and R. Ahlrichs, *Chem. Phys. Lett.*, **1995**, *240*, 283.
90. O. Treutler and R. Ahlrichs, *J. Chem. Phys.*, **1995**, *102*, 346.
91. K. Eichkorn, F. Weigend, O. Treutler and R. Ahlrichs, *Theor. Chem. Acc.*, **1997**, *97*, 119.
92. M. von Arnim and R. Ahlrichs, *J. Chem. Phys.*, **1999**, *111*, 9183.
93. P. Deglmann and F. Furche, *J. Chem. Phys.*, **2002**, *117*, 9535.
94. P. Deglmann, F. Furche and R. Ahlrichs, *Chem. Phys. Lett.*, **2002**, *362*, 511.
95. P. Deglmann, K. May, F. Furche and R. Ahlrichs, *Chem. Phys. Lett.*, **2004**, *384*, 103.

CHAPTER 3

Rapid Markovnikov addition of HCl to a pendant alkyne: evidence for a quinoidal cumulene

3.1. Abstract

Reactions of *cis*-[$RuCl_2(dppm)_2$], *cis*-[**20**], with $TlBF_4$ and 1,4-diethynylbenzenes result in the formation of the vinylidene cations *trans*-[$RuCl(=C=CHC_6H_2\text{-}2,5\text{-}R_2\text{-}4\text{-}C{\equiv}CH)(dppm)_2]^+$, [**87**]$^+$, (R = H, [**87a**]$^+$; Me, [**87b**]$^+$). Subsequent reactions with [N^nBu_4]Cl result in nucleophilic attack by chloride at the coordinated organic ligand, but not at the expected metal-bound (C_α) carbon atom. Instead, complexes *trans*-[$RuCl(C{\equiv}CC_6H_2\text{-}2,5\text{-}R_2\text{-}4\text{-}CCl=CH_2)(dppm)_2$], [**89**], (R = H, [**89a**]; Me, [**89b**]) were isolated which, when coupled with quantum calculations carried out by Dr. J. M. Lynam of the University of York, provides evidence for an intermediate quinoidal cumulene complex of the type, *trans*-[$RuCl(=C=C=C_6H_2\text{-}2,5\text{-}R_2\text{-}4\text{-}=C=CH_2)(dppm)_2]^+$, [**88**]$^+$. Aspects of this work have been published,[1] and further details are given here.

3.2. Introduction

Metallocumulene complexes, $[L_mM=C=(C)_n=CRR']^{x+}$, have attracted appreciable interest over the past few decades.[2-6] Donation of the carbene-like **:**C(σ) lone pair to an empty M(*d*) and synergistic π backbonding interactions from a filled M(*d*) orbital to an empty C(*p* or π*) orbital, forms a strong M=C bond, effectively stabilising highly reactive, free cumulenylidene compounds, **:**$C(=C)_n=CRR'$.[7] The use of metallocumulenes in molecular electronics[8-10] and non-linear optics[11] has been anticipated stemming from the extensive conjugation along the metallocumulene

chain,[12] allowing electronic communication between remote sites through an established π framework. Alternating electrophilic / nucleophilic character along the carbon backbone has also lead to applications of metallocumulenes as reagents in catalysis.[13-16]

The simplest members of the M=C family are transition metal carbenes, *i.e.* $[L_mM{=}CAB]^{x+}$, where A, B = alkyl, H, OR, NR_2, X *etc*.. Such complexes have been widely studied,[17-19] especially within the area of catalysis.[20-24] This is no doubt a consequence of the fact that substituents A and B effectively govern the electronic ground state configuration of the free carbene fragment and hence the nature of the M=C bond upon complexation, systematically altering the reactivity of the metal-carbene. Two main types of transition metal carbene complexes exist: Fischer carbenes and Schrock carbenes. In Fischer carbenes, bonding of the singlet carbene carbon (C_{carb}) to the metal (M) (where A and / or B are heteroatoms in this case) follows traditional σ forward / π backbonding descriptions (Figure 3.1).[25] In Schrock carbenes, bonding of the triplet carbene carbon (C_{carb}) to the metal (M) (where A and B are now alkyl substituents) is alternatively described as electron sharing between singly occupied $C_{carb}(sp^2)$ and $C_{carb}(p_z)$, which are of similar energy, with two singly occupied M(*d*) (Figure 3.1).[25]

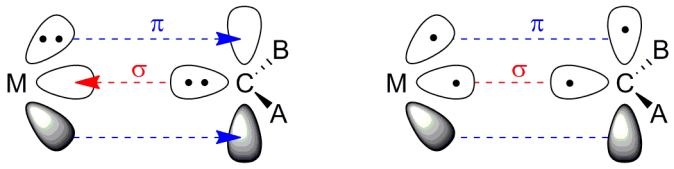

Figure 3.1: Bonding descriptions of Fischer (left) and Schrock (right) carbenes.

Fischer carbenes are typically formed at electron-rich, low oxidation state metal centres containing π-acceptor ligands, *e.g.* $[W(CO)_5]^+$,[26] and react as electrophiles.[27] Alternatively, Schrock carbenes are generally formed at electron-deficient, high oxidation state metal centres containing π-donating ligands, *e.g.* $[Ta(\eta^5\text{-}C_5H_5)_2]^{3+}$,[28] and generally react as nucleophiles, therefore are commonly regarded as transition metal ylides (*c.f.* the Wittig reaction).[29]

Transition metal vinylidenes, the simplest unsaturated carbene complexes, are found as important intermediates and key precursor molecules in numerous catalytic processes;[30-32] including the dimerisation,[33] polymerisation[34] and cycloaromatisation[35] reactions of alkynes. Many synthetic routes to vinylidene complexes are known.[36-41] Of these, the reaction of half-sandwich metal chloride complexes with terminal alkynes, HC≡CR, in the presence of a halide abstracting agent is one of the most facile and highest yielding routes to half-sandwich vinylidenes.[36] Such a route has proven especially versatile, serving as the synthetic foundation for Dixneuf and co-workers to access *trans*-diopic ruthenium vinylidenes bearing chelating phosphine ligands.[42-44] The relative stability of vinylidene complexes parallels the degree of electron density at the metal centre; hence electron donating ancillary ligands are optimal.[2, 45] The mechanisms for vinylidene formation have been extensively reviewed by Lynam.[46] Notably, rates of formation are increased in the presence of electron releasing alkynes.[47, 48] Metal vinylidenes offer both an electrophillic C_α and a nucleophillic C_β hence the scope for further reactions is vast, and as such, this reaction chemistry has been reviewed extensively.[3, 49-51]

Allenylidene, [L_nM=C=C=CRR′] complexes, serving as single carbon extensions to transition metal vinylidenes, are also well documented in the literature.[9, 52-55] Formation of the first metal allenylidene complexes, [M{=C=C=C(C_6H_5)(NMe_2)}$(CO)_5$] (M = Cr, W), was reported by Fischer in 1976 from the step-wise reactions of [M{=C(OEt)CH=C(C_6H_5)(NMe_2)}$(CO)_5$] with either BF_3 or $AlEt_3$ (1 equiv.) in CH_2Cl_2, followed by addition of THF as a weak base.[56] Single crystal X-ray diffraction studies of [Cr{=C=C=C(C_6H_5)(NMe_2)}$(CO)_5$] revealed a Cr-C_α bond length of 2.015(15) Å, falling between the lengths of a single M-C and double M=C bond, and very short C_α-C_β (1.236(22) Å) and C_γ-N (1.372(21) Å) bond lengths, which collectively indicated a significant contribution of the mesomeric alkynyl form (Scheme 3.1) to the overall structure.

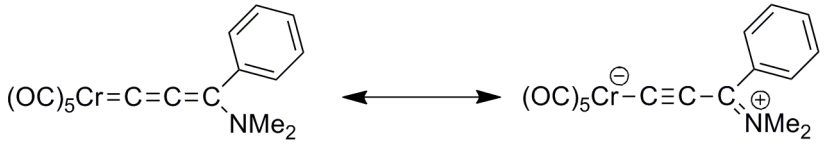

Scheme 3.1: Both the cumulenic (left) and mesomeric (right) resonance forms are said to account for the solid-state structure of $[Cr\{=C=C=C(C_6H_5)(NMe_2)\}(CO)_5]$.[56]

This initial discovery did not however galvanise interest in the field and only a few reports of metal allenylidene complexes followed,[57, 58] until 1982 when Selegue discovered that the room temperature reaction of $[RuCl(PMe_3)_2(\eta^5\text{-}C_5H_5)]$ with $HC{\equiv}CC(C_6H_5)_2OH$ and NH_4PF_6 (reagent quantities not reported) in an ethanol solution generated $[Ru\{=C=C=C(C_6H_5)_2\}(PMe_3)_2(\eta^5\text{-}C_5H_5)]^+$, in a 76 % yield after 27 hours, evincing the high acidity of C_β in the intermediate hydroxyl-vinylidene complex, $[Ru\{=C=CHC(C_6H_5)_2OH\}(PMe_3)_2(\eta^5\text{-}C_5H_5)]^+$ which favours rapid dehydration (Scheme 3.2).[52] This concept formed the basis for a general synthesis of metal allenylidene complexes. The chemistry of allenylidenes, including the more unusual synthetic routes, has been reviewed by Bruce,[4] Gimeno[59] and Selegue.[3, 52]

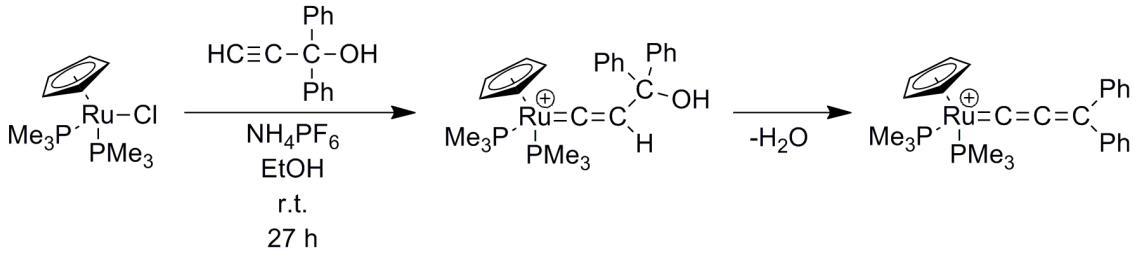

Scheme 3.2: Synthesis of metal allenylidene complexes, as initially reported by Selegue.[52]

It follows from the alternating charge density of the carbon atoms along the allenylidene chain and contributions to the HOMO and LUMO that electrophiles will generally add to C_β. For example, the room temperature reactions of $[Mn(=C=C=CR_2)(CO)_2(\eta^5\text{-}C_5H_5)]$ ($R = {}^tBu$, C_6H_5) with HX (excess; X = CF_3COO, Cl, BF_4) in diethyl ether or CH_2Cl_2 generate $[Mn(\equiv CCH=CR_2)(CO)_2(\eta^5\text{-}C_5H_5)]X$ complexes in 33 – 93 % yields.[53] In contrast, nucleophiles will attack at either C_α or C_γ,

depending on the electronic and steric demands of the ancillary ligands and nature of the metal. By way of example, $[Os\{=C=C=C(C_6H_5)_2\}(CO)(P^iPr_3)(\eta^5\text{-}C_5H_5)]PF_6$ in methanol will slowly (12 hours) transform to $[Os\{=C(OMe)CH=C(C_6H_5)_2\}(CO)(P^iPr_3)(\eta^5\text{-}C_5H_5)]^+$ (90 %; Scheme 3.3),[60] whereas the reaction of *trans*-$[RuCl\{=C=C=C(C_6H_5)_2\}(dppm)_2]BF_4$, bearing more sterically demanding and electron donating ancillary ligands, reacts with NaOMe (10 equiv.) in methanol to yield *trans*-$[RuCl\{C\equiv CC(C_6H_5)_2(OMe)\}(dppm)_2]$ (55 %) after only 2 hours (Scheme 3.3).[55]

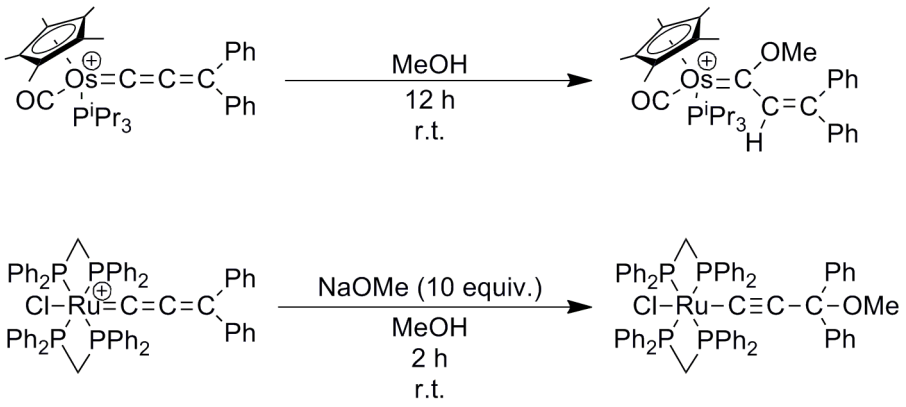

Scheme 3.3: Nucleophilic attack (here: methoxy) of metal allenylidene complexes is possible at both C_α (top) and C_γ (bottom) depending on the nature of the metal endcaps.

Butatrienylidene complexes, $[L_nM=C=C=C=CRR']$, are more reactive than transition metal allenylidenes, hence are more difficult to prepare, with earlier reports only inferring existence from analysis of reaction products.[61-64] The first stable butatrienylidene complex to be isolated and fully characterised, both by spectroscopic methods and a single crystal X-ray diffraction study, was reported by Ilg and Werner.[65] The low temperature reaction of $[Ir(H)_2Cl(P^iPr_3)_2]$ with NEt_3 (1 equiv.) and $HC\equiv CC(OTf)=C(C_6H_5)_2$ (1 equiv.) in solutions of hexane yielded $[IrCl\{=C=C=C=C(C_6H_5)_2\}(P^iPr_3)_2]$ (77 %) as an olive green solid. The numerous further reactions reported for this butatrienylidene complex,[6, 66] showed that electrophiles (such as CF_3CO_2H) will, in general, add across the $C_\beta=C_\gamma$ bond (forming $[Ir\{=C=CHC(OC=OCF_3)=C(C_6H_5)_2\}(P^iPr_3)_2]$). Alternatively, Bruce demonstrated that nucleophillic attack of butatrienylidenes will occur at C_γ, as reactions of the unsubstituted butatrienylidene intermediate, $[Ru(=C=C=C=CH_2)(PPh_3)_2(\eta^5\text{-}C_5H_5)]^+$

(formed *in situ* at low temperature from the reaction of $[Ru(THF)(PPh_3)_2(\eta^5\text{-}C_5H_5)]PF_6$ with HC≡CC≡CH) with various nucleophiles generated products of the type $[Ru\{=C=C=C(MeNu)\}(PPh_3)_2(\eta^5\text{-}C_5H_5)]^+$ (Nu = NPh_2, N-methylpyrrole) or $[Ru\{C\equiv CC(Nu)=CH_2\}(PPh_3)_2(\eta^5\text{-}C_5H_5)]^+$ (Nu = PPh_3). [67]

Examples of longer metallocumulenes are rare,[4, 68, 69] and for reasons of synthetic convenience, extended cumulene ligands of odd chain lengths are more readily accessible using Selegue-type synthetic strategies, than those with an even number of carbon atoms in the cumulated chain, which require higher order poly-ynes or synthons. For example, Dixneuf and co-workers successfully synthesised and characterised the stable pentatetraenylidene complex, *trans*-$[RuCl\{=C=C=C=C(C_6H_5)_2\}(dppe)_2]PF_6$ (Scheme 3.4), six years prior to the isolation of the first butatrienylidene.[70] Moreover, whilst a heptahexaenylidene[71] complex has been isolated (albeit stabilised with two dimethylamino-substituents), the existence of a hexapentaenylidene complex has only been inferred from the isolation and characterisation of addition products.[72]

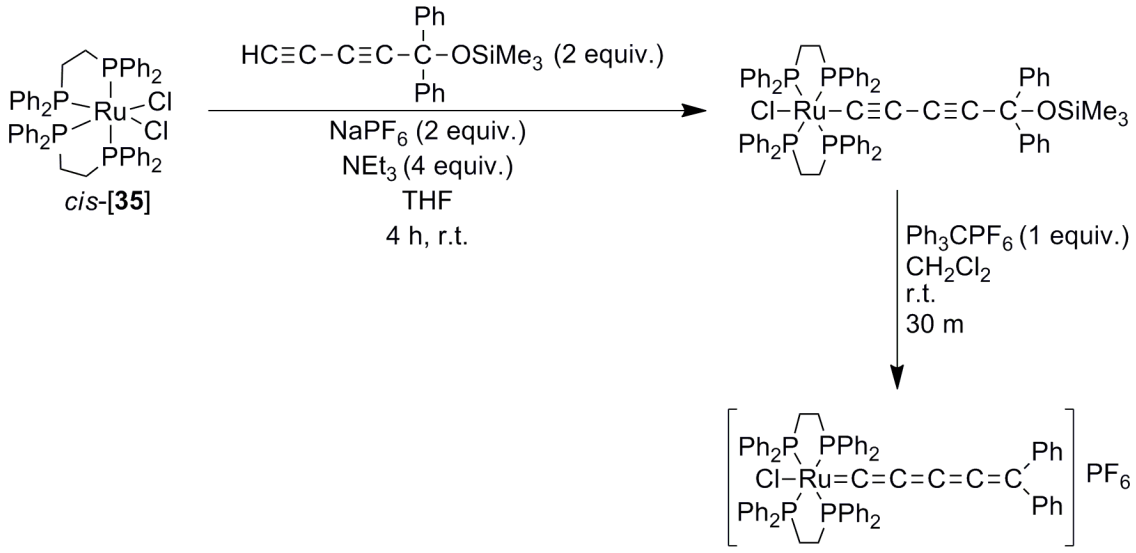

Scheme 3.4: Synthesis of the first pentatetraenylidene complex, as reported by Dixneuf.[70]

Through computational investigations of *trans*-$[RuCl\{(=C)_nCH_2\}(PH_3)_4]$ and $[Cr\{(=C)_nCH_2\}(CO)_5]$ (n = 1 − 9) complexes, Nazzareno found that odd-membered metallocumulenes (n = 2, 4, 6, 8) have polarised polyyne-like character with alternating

C-C / C≡C bonds along the carbon backbone,[7] while even-membered metallocumulenes (n = 1, 3, 5, 7, 9) are better described as organic cumulenes.[73] A lack of a thermodynamic upper limit upon increasing cumulene chain length indicated that synthetic difficulties in accessing even metallocumulenes are an unlikely factor of inherent stability, but more a consequence of the increased reactivity of the exposed carbon chain. Furthermore, as the cumulene backbone does not display significant polarisation (from Mulliken charge calculations) the observed reactivities of metallocumulenes towards nucleophiles and electrophiles is likely determined by frontier orbital considerations rather than charge distributions. The composition of the calculated orbitals further supports this finding as the HOMO has more metal character with significant contributions from even numbered carbons whereas the LUMO shows more organic ligand character with higher contributions from odd numbered carbons. As a result, nucleophillic attack (LUMO population) of metallocumulenes is expected at odd numbered carbons while electrophillic attack (HOMO depopulation) is anticipated at even numbered carbons, consistent with experimental observations. The metal centre is not expected to significantly influence the underlying electronic structure, and hence reactivity, of metallocumulenes.[7, 74]

In 2009, Nazzareno proposed that the butadiyne to butatrienylidene isomerisation of $[Ru(HC{\equiv}CC{\equiv}CH)(PMe_3)_2(\eta^5\text{-}C_5H_5)]^+$ occurs initially *via* a 1,2-hydrogen shift (analogous to simpler alkyne rearrangements for d^6 metal complexes),[46] forming an ethynyl-vinyl intermediate, $[Ru(=C=CHC{\equiv}CH)(PMe_3)_2(\eta^5\text{-}C_5H_5)]^+$ (Scheme 3.5).[75] Following this, a deprotonation / protonation process (*i.e.* a proton migration from C_β to C_δ) then occurs forming the more stable butatrienylidene product, $[Ru(=C=C=C=CH_2)(PMe_3)_2(\eta^5\text{-}C_5H_5)]^+$, *via* an intermediate buta-1,3-diynyl species (Scheme 3.5).

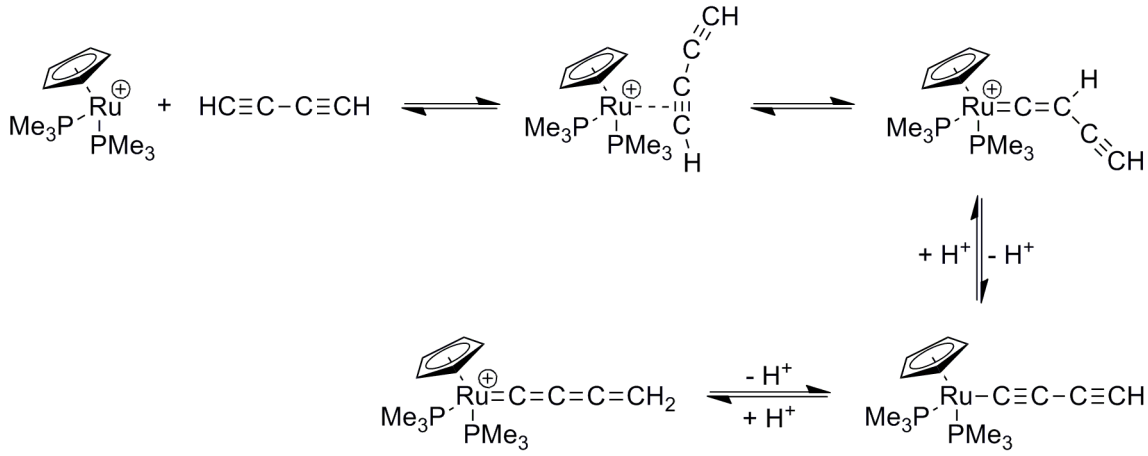

Scheme 3.5: Accepted mechanism for the ethynyl-vinyl to butatrienylidene isomerisation supported by the $[Ru(PMe_3)_2(\eta^5\text{-}C_5H_5)]^+$ centre.[75]

We speculated that this might be a general route to preparing metallocumulenes containing cumulated quinoidal fragments in which the integration of a phenylene fragment serves as a method to stabilise (and therefore access) higher chain cumulenes (Scheme 3.6).

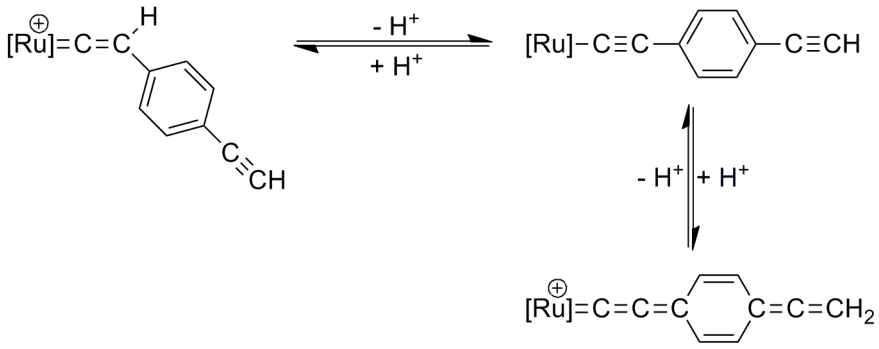

Scheme 3.6: Proposed (general) route to higher chain metallocummulenes containing quinoidal fragments.

Although 4-ethynylphenyl vinylidenes are known, with ground state structures lying firmly to the phenylvinylidene isomer,[76-84] preliminary calculations carried out by Dr. J. M. Lynam (University of York) on the isomeric vinylidene and quinoidal cumulene complexes, *trans*-$[RuCl(=C=CHC_6H_4\text{-}4\text{-}C{\equiv}CH)(dppm)_2]^+$ ([**87a**]$^+$) and *trans*-$[RuCl(=C=C=C_6H_4\text{-}4\text{-}=C=CH_2)(dppm)_2]^+$ ([**88a**]$^+$), revealed the quinoidal form to

lie only some 41 kJmol^{-1} higher in energy, and was therefore identified as a potential target for investigation.

In this Chapter, a rapid synthetic protocol for the preparation of *trans*-[RuCl(C≡CC_6H_2-2,5-R_2-4-CCl=CH_2)(dppm)$_2$], [**89**], is reported from reactions of cationic vinylidene complexes *trans*-[RuCl(=C=CHC_6H_2-2,5-R_2-4-C≡CH)(dppm)$_2$]$^+$, [**87**]$^+$, with [N^{n}Bu$_4$]Cl in CH_2Cl_2 solutions, indicating the intermediacy of the quinoidal cumulene, *trans*-[RuCl(=C=C=C_6H_2-2,5-R_2-4-=C=CH_2)(dppm)$_2$]$^+$, [**88**]$^+$.

3.3. Results

3.3.1. Synthesis of *trans*-[RuCl(=C=CHC_6H_2-2,5-R_2-4-C≡CH)(dppm)$_2$]$^+$ complexes

As an initial step towards accessing metallocumulene complexes, *trans*-[RuCl(=C=C=C_6H_2-2,5-R_2-4-=C=CH_2)(dppm)$_2$]$^+$, [**88**]$^+$, the synthesis of related vinylidene complexes, *trans*-[RuCl(=C=CHC_6H_2-2,5-R_2-4-C≡CH)(dppm)$_2$]$^+$ (R = H, [**87a**]$^+$; Me, [**87b**]$^+$) was explored. Room temperature reactions of *cis*-[**20**] with $TlBF_4$ (1 equiv.) and an excess of either 1,4-diethynyl benzene ([**87a**]$^+$) or 1,4-diethynyl-2,5-dimethylbenzene ([**87b**]$^+$) in CH_2Cl_2, gave the anticipated vinylidene complexes [**87a**]$^+$ (87 %) and [**87b**]$^+$ (67 %) after 80 minutes (Scheme 3.7).

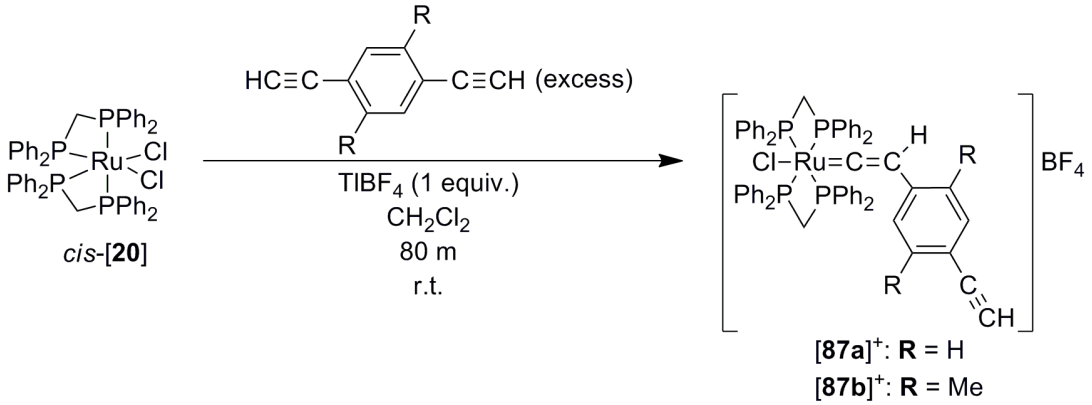

Scheme 3.7: Synthesis of complexes [**87**]BF_4.

The ^{1}H NMR spectra of [**87**]BF_4 supports the formation of the vinylidene complexes with singlet resonances (integrating to one proton) observed at δ 3.04 ([**87a**]$^{+}$) and δ 3.18 ppm ([**87b**]$^{+}$), corresponding the terminal alkyne protons, in addition to quintet resonances (also integrating to one proton) observed at δ 3.07 ([**87a**]$^{+}$) and δ 3.46 ppm ([**87b**]$^{+}$), corresponding to the vinylidene protons, showing a $^{4}J_{HP}$ coupling of 3 Hz to the four mutually *cis*-phosphorus atoms. Low field resonances at δ 356.2 ([**87a**]$^{+}$) and δ 354.7 ppm ([**87b**]$^{+}$) in the $^{13}C\{^{1}H\}$ NMR spectra confirmed the presence of the carbene-like C_α carbon of the vinylidene ligand, showing unresolved coupling to the four phosphorus atoms. Formation of [**87**]$^{+}$ was also confirmed by mass spectrometry, where molecular ion peaks ([**87a**]$^{+}$, 1031 *m/z*; [**87b**]$^{+}$, 1059 *m/z*) were observed, and by IR spectroscopy confirming a terminal alkyne with ν(C≡C) stretches at 2074 cm^{-1} and 2099 cm^{-1} for [**87a**]$^{+}$ and [**87b**]$^{+}$, respectively. The purities of the [**87**]BF_4 salts have been confirmed by elemental analyses.

The vinylidene cations [**87**]$^{+}$ appeared to be stable in solution. No spectroscopic (^{1}H NMR, $^{31}P\{^{1}H\}$ NMR, IR) evidence for a formal 1,7-hydrogen migration to [**88**]$^{+}$ was found. In light of this, the possibility of trapping the putative quinoidal cumulene by addition of nucleophillic chloride was explored. The weakly-basic properties of chloride avoids deprotonation of the vinylidene (and subsequent formation of *trans*-[RuCl(C≡CC_6H_2-2,5-R_2-4-C≡CH)$(dppm)_2$], [**27**]), whilst competitive ligand substitution reactions at the metal centre are rendered inconsequential.

3.3.2. Synthesis of *trans*-[RuCl(C≡CC_6H_2-2,5-R_2-4-CCl=CH_2)$(dppm)_2$] complexes

Addition of [N^{n}Bu_4]Cl (1.2 equiv.) to [**87**]BF_4 in room temperature CH_2Cl_2 solutions resulted in the rapid (one hour) formation of a single new compound identified as *trans*-[RuCl(C≡CC_6H_2-2,5-R_2-4-CCl=CH_2)$(dppm)_2$], [**89**], (R = H, [**89a**]; Me, [**89b**]) in high yields (74 and 92 % respectively; Scheme 3.8).

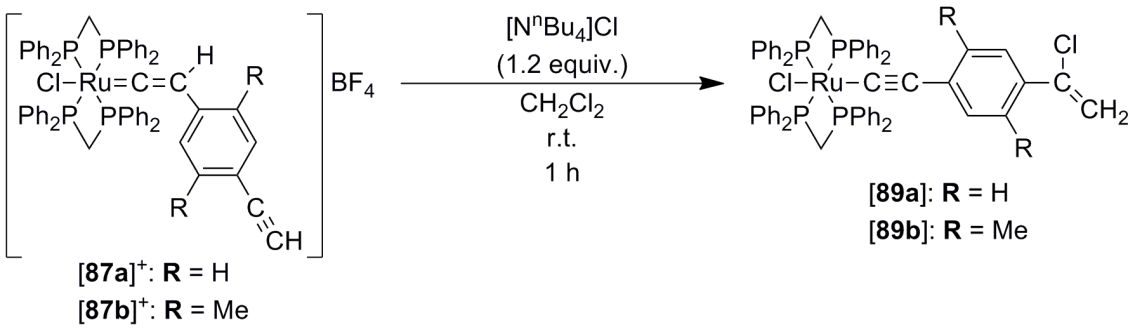

Scheme 3.8: Synthesis of complexes [**89**].

The formation of [**89**] is evidenced spectroscopically. The ^{1}H NMR spectra display two doublet resonances for the geminal protons on the terminal alkene (δ 5.33 and δ 5.60 ppm ([**89a**]) and δ 5.23 and δ 5.52 ppm ([**89b**])) with a mutual $^2J_{HH}$ coupling of 1.5 Hz. The presence of the alkene group was confirmed by resonances at δ 110.0 and δ 140.7 ppm ([**89a**]) and δ 114.2 and δ 139.4 ppm ([**89b**]) in the ^{13}C{^{1}H} NMR spectra, the latter showing cross peaks in a ^{1}H-^{13}C HMBC experiment to the two geminal protons described above in each case. The peak intensities of quaternary carbons are often low, especially those showing coupling to other nuclei. To this end, although Ru-*C* can be resolved in the ^{13}C{^{1}H} NMR spectrum of [**89b**] (as a quintet at δ 146.8 ppm with a $^2J_{CP}$ coupling of 19 Hz), this feature is undetected in the analogous spectrum of [**89a**]. The observation of ν(RuC≡C) bands at 2074 cm^{-1} ([**89a**]) and 2065 cm^{-1} ([**89b**]) in the IR spectra instead confirmed the presence of the alkynyl functionality while the observation of ν(C=C) bands at 1591 cm^{-1} ([**89a**]) and 1597 cm^{-1} ([**89b**]) affirmed the terminal alkene functionality. The chloride addition is established from the observation of $[M + H]^+$ peaks, at 1067 ([**89a**]) and 1095 *m/z* ([**89b**]), in the mass spectra. The purity of [**89b**] has been confirmed by elemental analysis. The elemental analysis obtained for [**89a**] (Anal. Found: C, 65.97; H, 4.70. Calc. for $C_{60}H_{50}Cl_2P_4Ru$: C, 67.53; H, 4.73.), likely reflects partial desolvation of the crystalline sample (Calc. for $C_{60}H_{50}Cl_2P_4Ru \times 0.5\ CH_2Cl_2$: C, 65.51; H, 4.64), which has been structurally determined with two CH_2Cl_2 solvate molecules (see section 3.3.3).

The usual basicity of the alkynyl ligand in [**89**] has been demonstrated by the addition of $HBF_4.Et_2O$ to [**89b**], forming *trans*-[RuCl(=C=CHC$_6$H$_2$-2,5-Me$_2$-4-CCl=CH$_2$)(dppm)$_2$]BF$_4$ (85 %).

3.3.3. Single crystal X-ray diffraction studies

The structures of [**89a**] (Figure 3.2) and [**89b**] (Figure 3.3) have been elucidated by single crystal X-ray diffraction studies, which confirmed structural predictions made on the basis of spectroscopic evidence.

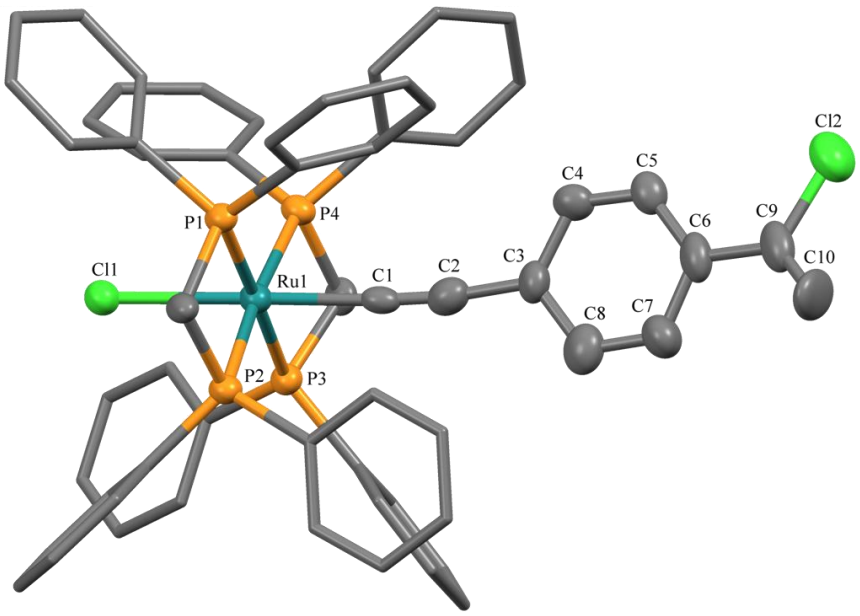

Figure 3.2: Solid state structure of [**89a**], with solvent of crystallisation ($2 \times CH_2Cl_2$) and hydrogen atoms removed for clarity. Ellipsoids of key atoms are drawn at the 50 % probability level. Selected bond lengths / Å: Ru(1)-Cl(1) 2.490(2), Ru(1)-C(1) 2.042(10), Ru(1)-P(1) 2.371(2), Ru(1)-P(2) 2.342(3), Ru(1)-P(3) 2.325(2), Ru(1)-P(4) 2.361(3), C(1)-C(2) 1.109(13), C(2)-C(3) 1.48(2), C(3)-C(4) 1.43(2), C(3)-C(8) 1.44(1), C(4)-C(5) 1.32(2), C(5)-C(6) 1.40(1), C(6)-C(7) 1.39(2), C(7)-C(8) 1.37(2), C(6)-C(9) 1.47(2), C(9)-C(10) 1.330(15), C(9)-Cl(2) 1.743(12). Selected bond angles / °: Cl(1)-Ru(1)-C(1) 177.3(2), Ru(1)-C(1)-C(2) 176.1(10), C(1)-C(2)-C(3) 169.3(12), C(6)-C(9)-Cl(2) 115.8(9), C(6)-C(9)-C(10) 128.5(12).

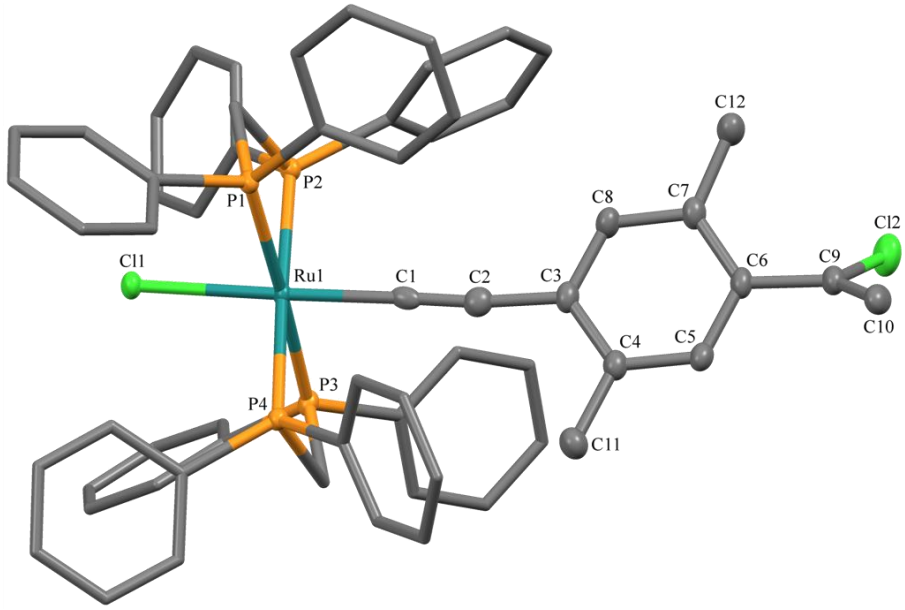

Figure 3.3: Solid state structure of [**89b**], with solvent of crystallisation (1.5 × CH_2Cl_2) and selected hydrogen atoms removed for clarity. Ellipsoids of key atoms are drawn at the 50 % probability level. Selected bond lengths / Å: Ru(1)-Cl(1) 2.4819(5), Ru(1)-C(1) 2.025(2), Ru(1)-P(1) 2.3738(5), Ru(1)-P(2) 2.3380(4), Ru(1)-P(3) 2.3330(5), Ru(1)-P(4) 2.3381(4), C(1)-C(2) 1.179(3), C(2)-C(3) 1.440(3), C(3)-C(4) 1.412(3), C(3)-C(10) 1.401(3), C(4)-C(5) 1.393(3), C(5)-C(6) 1.400(3), C(6)-C(9) 1.406(3), C(6)-C(7) 1.482(3), C(7)-C(8) 1.322(3), C(7)-Cl(2) 1.757(3), C(9)-C(10) 1.392(3). Selected bond angles / °: Cl(1)-Ru(1)-C(1) 177.86(5), Ru(1)-C(1)-C(2) 177.36(17), C(1)-C(2)-C(3) 172.7(2), C(6)-C(7)-Cl(2) 116.32(15), C(6)-C(7)-C(8) 125.6(2).

Both [**89a**] and [**89b**] crystallise in the triclinic space group $P\bar{1}$. The geometry about the ruthenium centre is approximately octahedral, defined by two chelating *bis*-phosphine ligands in addition to single alkynyl and chloride ligands in a mutually *trans*-disposition, with Cl(1)-Ru(1)-C(1)≡C(2)-C(3) bond angles close to 180 °. Slight deviations from ideal octahedral geometry may be attributed to the restricted bite angle of the dppm ligand, increasing steric interactions between the conjugated organic ligand and the bulky dppm ligands, and crystal packing effects.

The lower precision of the crystal structure determination of [**89a**] precludes a rigorous structural comparison here with [**89b**], though structures are expected to be similar. Between [**89a**] and [**89b**], all corresponding bond lengths except for C(1)≡C(2) are

equivalent within statistical error, confirming the anticipated similarities and demonstrating the comparable σ donor / π acceptor strengths of the two alkynyl ligands. The inconsistent C(1)≡C(2) bond length is longer in [**89b**] by 0.07 Å. This may indicate the cumulenic form (C=C) is favoured with the marginally more electron rich organic ligand of [**89b**], though the poorer crystal quality demands caution in interpretation when evaluated within the context of other values obtained. For both [**89a**] and [**89b**], bond lengths comprising the terminal C(Cl)=CH_2 motifs are in close agreement with analogous chloro-vinyl fragments found in similar organic compounds, supporting structural identity.[85, 86]

3.4. Discussion

3.4.1. Mechanistic considerations for the formation of *trans*-[RuCl(C≡CC_6H_2-2,5-R_2-4-CCl=CH_2)$(dppm)_2$] complexes

In organic chemistry, the Markovnikov rule is used to predict the product regiochemistry of HX addition (X = halogen) to unsymmetrical alkenes and terminal alkynes, where the halide will formally add to the most substituted carbon (Scheme 3.9). This is due to the increased stability of the carbocation in this position following the initial addition of the proton to the multiple bond. Anti-Markovnikov products do exist and are generally a feature of radical induced reactions (Scheme 3.9). Although the uncatalysed addition of HX to unsubstituted alkenes is slow, the uncatalysed addition of HX to terminal alkynes is even slower, despite both reactions being exothermic.[87]

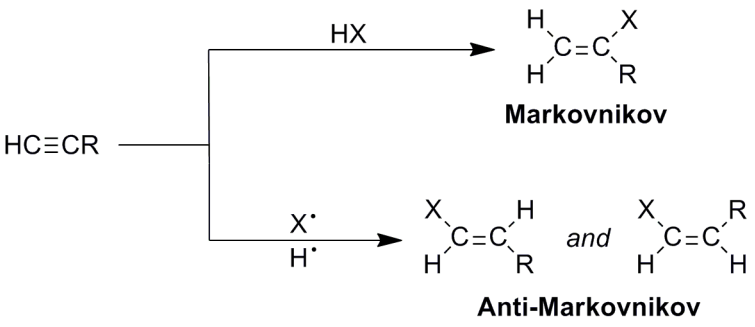

Scheme 3.9: Application of Markovnikov's rule to terminal alkynes.

Complexes [**89**] are formed as formal Markovnikov products following the addition of 'HCl' to the pendant alkyne of the vinylidene complexes [**87**]$^+$. The ease of the reaction (with products [**89**] formed within one hour) demonstrates the efficacy of metal fragments in such transformations.

In order to determine if the addition of the weakly-basic nucleophile, chloride to the terminal alkyne of the vinylidene isomer proceeds *via* a mechanism involving a quinoidal cumulene intermediate [**88**]$^+$, the mechanism of the transformation from [**87**]$^+$ to [**89**] has been considered in collaboration with Dr. J. M. Lynam (University of York) where competition between two potential pathways for nucleophilic attack by chloride at cationic complexes (Pathway A: Scheme 3.10 and Pathway B: Scheme 3.11) was examined.

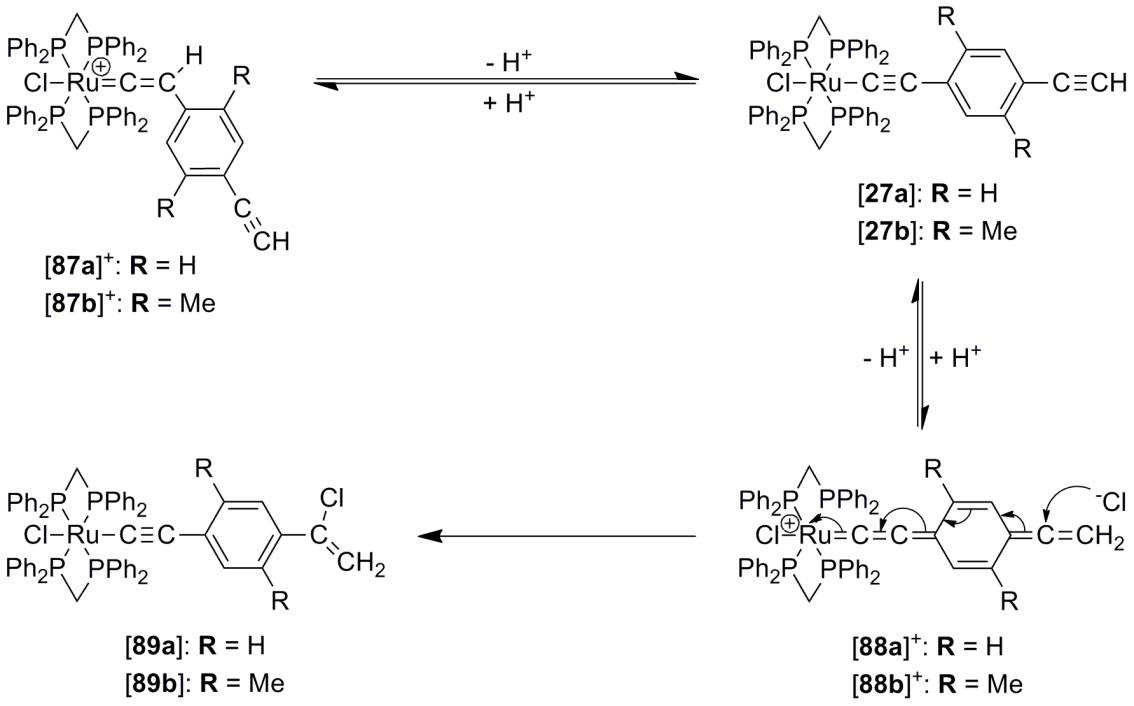

Scheme 3.10: First proposed mechanism for the reaction of [**87**]$^+$ with nucleophilic chloride: Pathway A.

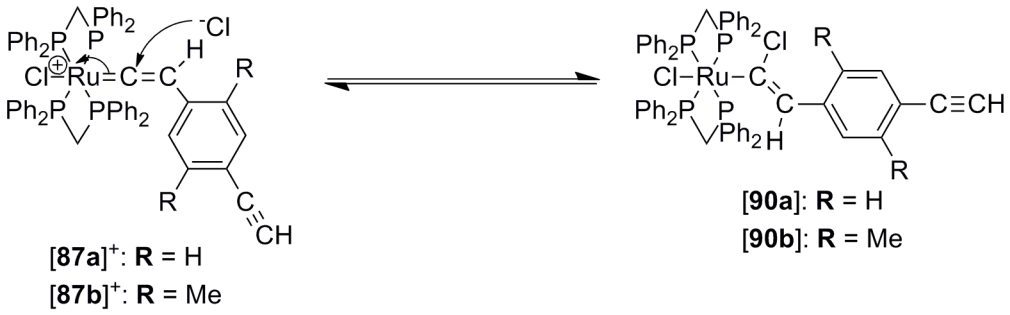

Scheme 3.11: Second proposed mechanism for the reaction of [**87**]$^+$ with nucleophilic chloride: Pathway B.

In the first case (Pathway A, Scheme 3.10), rearrangement of [**87**]$^+$ to give cumulene [**88**]$^+$ could occur *via* a deprotonation / reprotonation proton shift (*via* [**27**]). The cumulated system [**88**]$^+$ would then undergo direct nucleophilic attack at C^7 (where *trans*-[RuCl(=C^1=C^2=C_6H_2-2,5-R_2-4-=C^7=C^8H_2)(dppm)$_2$]) to give [**89**]. Metal-bound, carbene carbon atoms of vinylidene ligands are highly electrophilic,[69] and initial attack at C^1 of the vinylidene [**87**]$^+$ (where *trans*-[RuCl(=C^1=$C^2HC_6H_2$-2,5-R_2-4-C^7≡C^8H)(dppm)$_2$]) might have been rationally anticipated to give *trans*-[RuCl(CCl=CHC_6H_2-2,5-R_2-4-C≡CH)(dppm)$_2$], [**90**], (Pathway B, Scheme 3.11). The possibility of direct nucleophillic attack of the chloride at [**27**] was dismissed due to the lack of an observed reaction between [**27a**] (for synthesis see experimental section) and [N^nBu_4]Cl until the addition of HBF_4 (*i.e.* following *in situ* formation of the vinylidene [**87a**]$^+$) where [**89a**] is then formed. Both these Pathways (A and B, for when R = H) were evaluated through a quantum chemical investigation conducted by Dr. J. M. Lynam. Details of the computational methods employed have been included in the experimental section (see section 3.6.1.) for completeness.

In the case of Pathway A (Scheme 3.10) the calculations demonstrated that the quindoidal species [**88a**]$^+$, lies only 41 kJmol^{-1} higher in energy than the vinylidene [**87a**]$^+$ and, given that in the presence of even weak bases (such as acetate or chloride) low energy proton shuttle pathways become available for transition metal vinylidene complexes,[88, 89] rapid interconversion between [**87a**]$^+$ and [**88a**]$^+$ *via* [**27a**] is proposed. However, the difference in energy between the two isomers ([**87a**]$^+$ and [**88a**]$^+$) indicates that the equilibrium lies in favour of [**87a**]$^+$, as was noted spectroscopically. In

both Pathways A and B, linear transit scans were performed to model the approach of chloride to C^1 of [**87a**]$^+$ and C^7 of [**88a**]$^+$ (Figure 3.4).

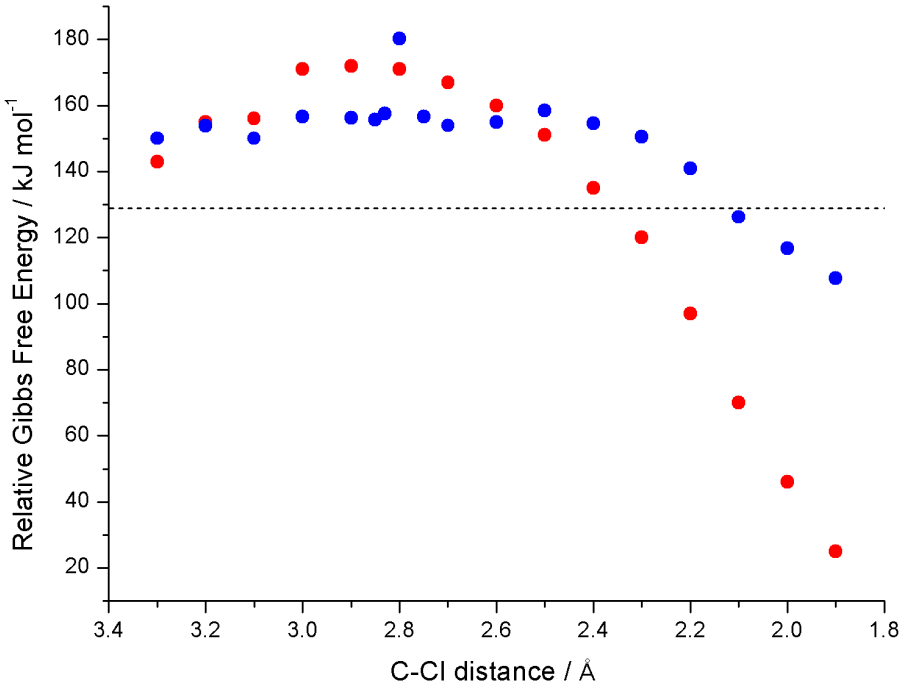

Figure 3.4: Linear transit scans for nucleophilic attack of chloride on complexes [**87a**]$^+$ (C^1 position, blue dots) and [**88a**]$^+$ (C^7 position, red dots). Free energies are at 298 K and relative to the optimised structure of [**89a**]. The dotted line shows the relative energy of [**87a**]$^+$ and free chloride.

The energy of a series of complexes with varied C-Cl distances were probed; those species exhibiting C-Cl bond lengths between 3.3 Å and 2.2 Å all exhibited single imaginary frequencies corresponding to C-Cl bond formation. To try to determine the origin of the outlier shown with a C-Cl distance of 2.8 Å, points were calculated either side in smaller increments (2.75 and 2.85 Å). However, such points were unsuccessful in providing an explanation for the anomalous result; hence the outlier is likely an artefact of the calculations. Although the kinetic barriers for attack by chloride at C^1 in [**87a**]$^+$ and C^7 in [**88a**]$^+$ appear to be broadly similar, and relatively low, it is clear that the formation of [**89a**] is thermodynamically preferred as this complex lies 129 kJmol^{-1} lower in energy than [**87a**]$^+$ with free chloride (shown as a dotted line in Figure 3.4), and 105 kJmol^{-1} lower in energy than [**90a**]. Indeed, the free energy of formation of [**90a**] is only favourable by 14 kJmol^{-1} when compared to [**87a**]$^+$ and free chloride.

Given that the transit scan shows that the greatest barrier to the reverse reaction would be 75 kJmol^{-1}, attack at C^1 is expected to be reversible and so the calculations provide an explanation as to why nucleophilic attack at this site is not observed, in addition to steric arguments. This is further evidenced by the lack of an experimentally-observed reaction between *trans*-[RuCl{=C=CH(C_6H_5)}(dppm)$_2$]$^+$, [**22d**]$^+$, and [N^{n}Bu$_4$]Cl. Therefore the DFT calculations not only indicate that [**88a**]$^+$ is accessible in solution, but that there is a significant thermodynamic preference for nucleophilic attack at the coordinated quinoidal cumulene ligand. The nature of the products obtained from these reactions support such assignments. Attack of nucleophillic chloride at C^7 of [**87**]$^+$ is shown to principally occur as products [**89**] are obtained in high yields (72 − 94 %) without significant formation of ^{31}P-containing side products. As discussed in the introduction, Nazzareno has reported that nucleophillic attack at straight chain metallocumulenes is expected to occur at odd numbered carbon sites.[7] In the proposed quinoidal cumulene intermediate, [**88**]$^+$, the attack site is odd numbered (C^7; if a linear counting sequence is adopted); supporting formation of a quinoidal cumulene.

In considering the scope of the vinylidene / cumulene rearrangement, it is interesting to note that Markovnikov addition of HBr to the pendant alkyne in [Mn(=C=CHC_6H_4-4-C≡CH)(CO)$_2$(η^5-C_5H_5)] has also been observed (forming [Mn(=C=CHC_6H_4-4-C(Br)=CH_2)(CO)$_2$(η^5-C_5H_5)]).[76] Although at that time, no quinoidal cumulene was implicated in the process.

3.4.2. Further reactions evincing quinoidal cumulene intermediates

In order to determine the generality of rapid Markovnikov additions of 'HCl' to metal supported pendant alkynes, evincing quinoidal cumulene intermediates, variations of the coordination sphere about the ruthenium metal centre were considered (Scheme 3.12).

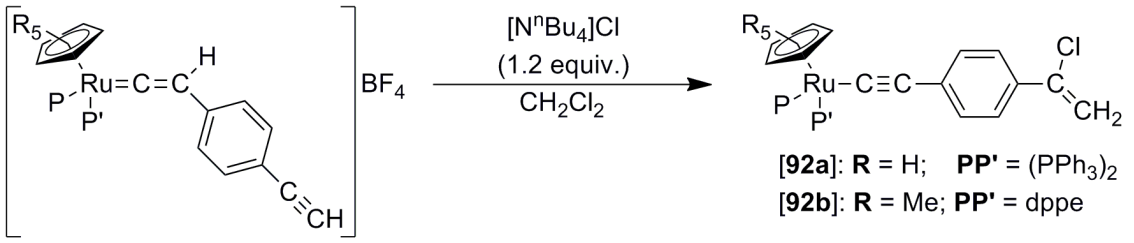

[**91a**]$^+$: **R** = H; **PP'** = $(PPh_3)_2$
[**91b**]$^+$: **R** = Me; **PP'** = dppe

[**92a**]: **R** = H; **PP'** = $(PPh_3)_2$
[**92b**]: **R** = Me; **PP'** = dppe

Scheme 3.12: Proposed reaction scheme to form half-sandwich 'HCl' addition products, [Ru(C≡CC_6H_4-4-CCl=CH_2)(PP′)(η^5-C_5R_5)], [**92**] from the respective vinylidene complex [Ru(=C=CHC_6H_4-4-C≡CH)(PP′)(η^5-C_5R_5)]$^+$, [**91**]$^+$.

In an attempt to initially isolate the vinylidene complexes [Ru(=C=CHC_6H_4-4-C≡CH)(PP′)(η^5-C_5R_5)]$^+$, [**91**]$^+$ ((PP′)(η^5-C_5R_5) = $(PPh_3)_2$(η^5-C_5H_5), [**91a**]$^+$; (dppe)(η^5-C_5Me_5), [**91b**]$^+$), metal-alkynyl complexes [Ru(C≡CC_6H_4-4-C≡CH)(PP′)(η^5-C_5R_5)], [**93**], were reacted at room temperature with HBF_4.Et_2O (1 equiv.) in solutions of CH_2Cl_2. However, such efforts proved unsuccessful, resulting only in significant decomposition, where analysis of the crude reaction mixtures by $^{31}P\{^1H\}$ NMR spectroscopy revealed formation of several unidentified ^{31}P-containing side products. The successful transformation from [Ru(C≡CC_6H_5)$(PPh_3)_2$(η^5-C_5H_5)] to [Ru(=C=CHC_6H_5)$(PPh_3)_2$(η^5-C_5H_5)]BF_4 in an analogous manner, as originally reported by Bruce,[90] discounted the unreliability of the acid reagent (HBF_4.Et_2O) and systematically inferred the sensitivity of [**91**]$^+$ towards strongly acidic reagents, prompting derivation of an alternative route. The synthesis of [**93**], including precursor complexes [Ru(C≡CC_6H_4-4-C≡C$SiMe_3$)(PP′)(η^5-C_5R_5)], where (PP′)(η^5-C_5R_5) = $(PPh_3)_2$(η^5-C_5H_5) and (dppe)(η^5-C_5Me_5), in addition to a modified synthesis of [Ru(C≡CC_6H_5)$(PPh_3)_2$(η^5-C_5H_5)], have been included in the experimental section.

Formation of [**91**]$^+$ was instead achieved upon reacting [RuCl(PP′)(η^5-C_5R_5)] ((PP′)(η^5-C_5R_5) = $(PPh_3)_2$(η^5-C_5H_5), [**91a**]$^+$; (dppe)(η^5-C_5Me_5), [**91b**]$^+$) with excess 1,4-diethynyl benzene at room temperature in the presence of NH_4PF_6 (2 equiv.) in dilute solutions of CH_2Cl_2. The ^{1}H NMR spectra of [**91**]$^+$ support the formation of the vinylidene isomers with single integration, singlet resonances observed at

δ 3.04 ([**91a**]$^+$) and δ 3.01 ppm ([**91b**]$^+$) for the terminal alkyne protons and single integration triplet (or unresolved multiplet) resonances observed at δ 5.39 ([**91a**]$^+$) and δ 4.37 ppm ([**91b**]$^+$) for the vinylidene protons, coupling to the two mutually *cis*-phosphorus atoms. Low field triplet (or unresolved multiplet) resonances at δ 354.2 ([**91a**]$^+$) and 352.8 ppm ([**91b**]$^+$) in the $^{13}C\{^1H\}$ NMR confirmed the presence of the vinylidene ligand (Ru=*C*), showing coupling to the two phosphorus atoms. Formation of [**91**]$^+$ was also confirmed by mass spectrometry, where both molecular ion peaks [**91a**]$^+$ (817 *m/z*) and [**91b**]$^+$ (761 *m/z*) were observed, and by IR spectroscopy confirming the preservation of the terminal alkyne, with ν(C≡C) stretches observed at 2107 cm^{-1} ([**91a**]$^+$) and 2106 cm^{-1} ([**91b**]$^+$).

The reaction progress between [**91a**]$^+$ and [N^{n}Bu$_4$]Cl (1.2 equiv.) in a CH_2Cl_2 solution was monitored by unlocked $^{31}P\{^1H\}$ NMR spectroscopy. After the complete consumption of [**91a**]$^+$ (16 hours), the crude reaction mixture was purified by column chromatography (basic alumina, CH_2Cl_2) and major species analysed using ^1H NMR spectroscopy (Figure 3.5).

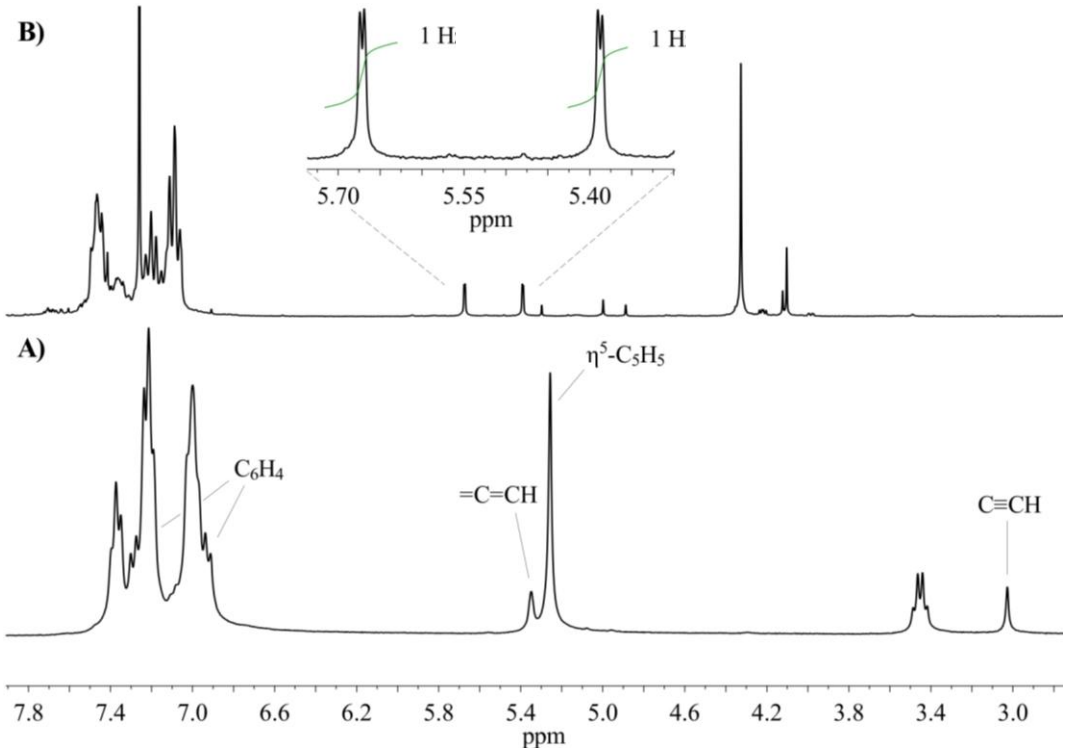

Figure 3.5: ^{1}H NMR ($CDCl_3$, 300 MHz) spectra of A) starting material, [**91a**]$^{+}$ and B) the major species obtained after the 16 hour room temperature reaction between [**91a**]$^{+}$ and [N^nBu_4]Cl in CH_2Cl_2 and subsequent purification by column chromatography.

The ^{1}H NMR spectrum of the major species obtained (B, Figure 3.5) contains a set of doublet resonances (δ 5.39, 5.67 ppm), each integrating to a single proton, with coupling constants of 1.5 Hz. Such resonances are characteristic of the geminal protons observed in [**89**], implying 'HCl' addition at pendant alkynes following formation of a quinoidal cumulene intermediate is possible for alternative coordination spheres of ruthenium. Although the proposed 'HCl' adduct, [Ru(C≡CC_6H_4-4-CCl=CH_2)(PPh_3)$_2$(η^5-C_5H_5)] ([**92a**]) could not be isolated cleanly from the crude reaction mixture, further evidence for the formation of [**92a**] was given by mass spectrometry (ESI) with the molecular ion peak, [**92a**]$^{+}$ (852 *m/z*), being observed.

In an analogous procedure, [**91b**]$^{+}$ was added to a solution of [N^nBu_4]Cl (1.2 equiv.) in CH_2Cl_2 and stirred overnight at room temperature. In this case, there was a lack of any reaction, adjudged by both ^{1}H and ^{31}P{^{1}H} NMR spectroscopy, even after an increased quantity of [N^nBu_4]Cl (to 3 equiv.). This contrast, to the behaviour of [**91a**]$^{+}$ under similar conditions, might reflect the steric bulk of [**91b**]$^{+}$ preventing base-assisted

proton migrations, as the more electron donating [**91b**]$^+$ (*vs.* [**91a**]$^+$) would be expected to support formation of the quinoidal structure more readily. Alternatively, an increased stabilisation of the vinylidene [**91b**]$^+$ relative to [**91a**]$^+$ may give rise to a greater energetic barrier to proton migration (vinylidene / cumulene interconversion) and subsequent 'HCl' addition for the {Ru(dppe)(η^5-C_5Me_5)} centre compared with {Ru(PPh_3)$_2$(η^5-C_5H_5)}. In an attempt to overcome this possible energy barrier, the reaction was repeated under reflux conditions. The crude reaction residue was then examined by ^{1}H NMR spectroscopy (Figure 3.6).

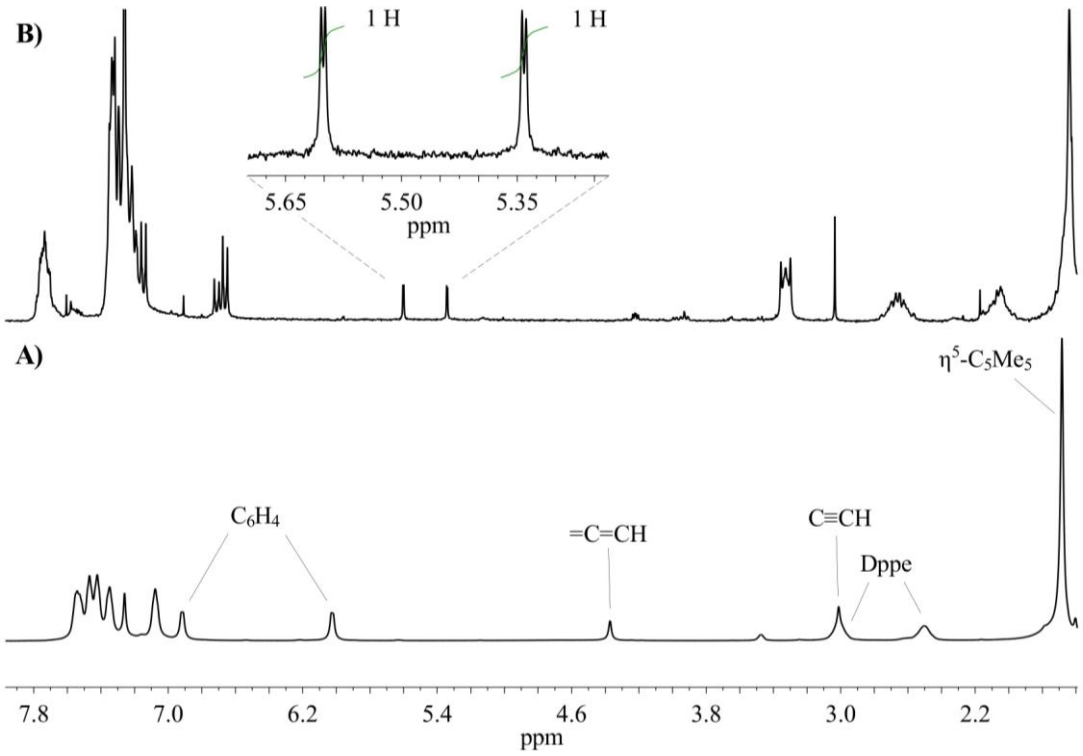

Figure 3.6: ^{1}H NMR ($CDCl_3$) spectra of A) starting material, [**91b**]$^+$ (600 MHz) and B) the major species obtained after the 16 hour reflux of [**91b**]$^+$ with [N^nBu_4]Cl in CH_2Cl_2 followed by removal of solvent, extraction with diethyl ether and subsequent filtration (300 MHz).

The presence of the two characteristic geminal doublet resonances (δ 5.34, 5.60 ppm) each integrating to a single proton with mutual $^2J_{HH}$ coupling constants of 1.5 Hz (B, Figure 3.6) suggests [**92b**] is the major product in the reaction of [**91b**]$^+$ with [N^nBu_4]Cl at elevated temperature. Further evidence for this assignment comes from mass spectrometry (ESI) of the crude sample, with the protonated molecular ion peak

[**92b** + H]$^+$ (797 *m/z*) observed, and IR spectroscopy, with a collection of ν(RuC≡C) bands observed within the range 2037 – 2064 cm^{-1}; implying metal-alkynyl functionality. The formation of [**92b**] under these conditions would confirm that an increased kinetic barrier to rearrangement from [**91b**]$^+$ to [**92b**] (*vs.* [**91a**]$^+$ to [**92a**]) exists.

The second major product formed in this reaction ([**91b**]$^+$ / [N^{n}Bu$_4$]Cl / reflux / 16 hours) is [Ru(C≡CC$_6$H$_4$-4-C≡CH)(dppe)(η^5-C$_5$Me$_5$)], [**93b**], formed by deprotonation of [**91b**]$^+$, confirmed by comparison with authentic spectra (see experimental section). Previous synthetic studies with the {Ru(dppm)$_2$} motif suggest deprotonation of the vinylidene to give the metal-alkynyl is a key step in the generation of the quinoidal cumulene complex and is likely observed as a product in this reaction due to the increased acidity of C$_\beta$ in [**91b**]$^+$, which contains electron releasing ancillary ligands.

3.5. Conclusions

Facile extension of cumulene length through the introduction of a phenyl fragment, yielding a quinoidal cumulene, was anticipated at a {Ru(dppm)$_2$} centre after quantum chemical calculations revealed the quinoidal complex to be energetically accessible by proton migration. The vinylidene complexes, [**87**]$^+$, did not show any evidence for formation of the cumulene [**88**]$^+$ in quantities detectable by solution state NMR spectroscopy, indicating any equilibrium is heavily weighted to the side of the vinylidene. Addition of the weak, non-basic nucleophile chloride to the vinylidene complexes [**87**]$^+$ resulted in the selective formation of 'HCl' addition products, [**89**], where the observed site of nucleophilic attack (C^7) is evidence for an intermediate quinoidal cumulene. No evidence was found for nucleophillic attack at the conventional C^1 position of [**87**]$^+$; an assumed consequence of the steric interference at the metal centre supported by bulky dppm ancillary ligands. Analogous transformations from half-sandwich vinylidenes, [**91**]$^+$, to the corresponding 'HCl' addition products, [**92**], have also been observed, supporting the generality of rapid Markovnikov addition reactions of 'HCl' to pendant alkynes operating *via* a quinoidal cumulene complex, at least in the case of ruthenium complexes. Further work in this area should look towards

exploring the effects of other aromatic and heterocyclic moieties as conjugated spacers to support extended cumulated ligand structures and investigate dipolar additions to these extended carbon-rich, unsaturated ligands.

3.6. Experimental

3.6.1. General considerations

All reactions were carried out under an atmosphere of dry nitrogen using standard Schlenk techniques. The reaction solvent CH_2Cl_2 was dried over CaH_2 whilst MeOH was dried over magnesium turnings and iodine. All other solvents were standard reagent grade and used as received. No special precautions were taken to exclude air or moisture during workup. The compounds: *cis*-[**20**],[91] $HC{\equiv}CC_6H_4$-4-$C{\equiv}CH$,[92] $HC{\equiv}CC_6H_4$-4-$C{\equiv}CSiMe_3$,[93] $Me_3SiC{\equiv}CC_6H_2$-2,5-Me_2-4-$C{\equiv}CSiMe_3$,[92] $[RuCl(PPh_3)_2(\eta^5\text{-}C_5H_5)]$,[90] $[RuCl(dppe)(\eta^5\text{-}C_5Me_5)]$[94] and $TlBF_4$[95] were synthesised by literature methods. All other reagents were commercially available and used as received.

Safety spectacles and gloves were worn at all times, and all experiments conducted in an efficient fume hood, following completion of appropriate COSHH assessments. Relatively non-toxic solvents were disposed of in the appropriate waste solvent container (chlorinated / non-chlorinated). Given the extremely toxicity of $TlBF_4$, the reagent was separately weighed in a sealed container in a fume hood. The solid was transferred to the reaction flask using a disposable paper funnel. The paper funnel was discarded immediately after use into a thallium-containing solid waste receptacle. For larger scale reactions, a secondary containment flask was utilised during the reaction period. Reactions reported below involving $TlBF_4$, (generally) produce equimolar amounts of TlCl, which is similarly extremely toxic. After completion of the reaction, following isolation of TlCl / residual $TlBF_4$ by the work-up procedures reported, the salts were either disposed of by i) dissolving in HNO_3 (aq.) and transferring into a thallium-containing solvent waste container or ii) in a thallium-containing solid waste container (along with the chromatographic medium, celite *etc.*).

NMR spectra were recorded at 25 ºC on Jeol 400 (^{1}H, 399.78 MHz; ^{13}C, 100.53 MHz; ^{19}F, 376.17 MHz), Bruker AV500 (^{1}H, 500.23 MHz; ^{31}P, 202.50 MHz; ^{13}C, 125.77 MHz), Bruker Avance 600 (^{1}H, 600.1 MHz; ^{13}C, 150.9 MHz; ^{19}F, 564.6 MHz; ^{31}P, 242.9 MHz) or a Varian Inova 300 (^{1}H, 300.2 MHz; ^{13}C, 75.5 MHz) spectrometers using $CDCl_3$ or CD_2Cl_2 as the solvent. Chemical shifts were determined relative to internal residual solvent signals (^{1}H, ^{13}C),[96] or external 85% H_3PO_4 (^{31}P δ = 0.0 ppm). FT-IR spectra were measured on an Agilent Technologies Cary 660 spectrometer or a Nicolet Avatar 360 spectrometer from CH_2Cl_2 solutions in a thin-layer cell fitted with CaF_2 windows. ESI-MS and APCI-MS were recorded on a Waters CT Premier XE mass spectrometer in positive or negative ion mode from solutions in methanol. Elemental analyses were performed at the London Metropolitan University.

Initial optimisations were performed at the (RI-)BP86/SV(P) level, followed by frequency calculations at the same level. Transition states were located by initially performing a constrained minimisation (by freezing internal coordinates that change most during the reaction) of a structure close to the anticipated transition state. This was followed by a frequency calculation to identify the transition vector to follow during a subsequent transition state optimisation. A final frequency calculation was then performed on the optimised transition state structure. All minima were confirmed as such by the absence of imaginary frequencies and all transition states were identified by the presence of only one imaginary frequency. Single-point calculations on the (RI−)BP86/SV(P) optimised geometries were performed using the hybrid PBE0 functional and the flexible def2-TZVPP basis set. The (RI-)PBE0/def2-TZVPP SCF energies were corrected for their zero point energies, thermal energies and entropies (obtained from the (RI-)BP86/SV(P)-level frequency calculations). In all calculations, a 28 electron quasi-relativistic ECP replaced the core electrons of Ru. No symmetry constraints were applied during optimisations. Solvent corrections were applied with the COSMO dielectric continuum model[97] and dispersion effects modelled with Grimme's D3 method.[98, 99] All calculations were performed using the TURBOMOLE V6.4 package using the resolution of identity (RI) approximation.[100-108]

3.6.2. Syntheses and characterisations of organic compounds

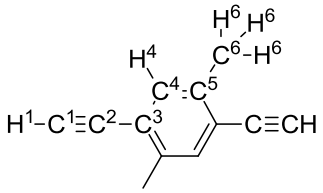

Synthesis of HC≡CC$_6$H$_2$-2,5-Me$_2$-4-C≡CH

A mixture of Me$_3$SiC≡CC$_6$H$_2$-2,5-Me$_2$-4-C≡CSiMe$_3$ (1.39 g, 4.7 mmol) and K_2CO_3 (2.05 g, 14.9 mmol) in MeOH (30 ml) and H_2O (4 ml) was stirred overnight. To quench the reaction, water (30 ml) and CH_2Cl_2 (30 ml) were then added to the mixture, forming two layers. The organic layer was washed three times with water and twice with brine before being dried over magnesium sulphate. The pale yellow solution was then filtered through filter paper and filtrate concentrated to dryness, where a white precipitate formed and was collected (0.67 g, 93 %).

IR (CH_2Cl_2, cm^{-1}): 2104 ν(C≡C). ^{1}H NMR ($CDCl_3$, 600 MHz) δ / ppm: 2.38 (s, 6H, H^6), 3.32 (s, 2H, H^1), 7.30 (s, 2H, H^4). ^{13}C NMR ($CDCl_3$, 300MHz) δ / ppm: 20.0 (s, C^6), 82.26 (s, C^1), 82.31 (s, C^2), 122.5 (s, C^3), 133.4 (s, C^4), 138.0 (s, C^5). ESI(+)-MS (*m/z*): 154 [HC≡CC$_6$H$_2$-2,5-Me$_2$-4-C≡CH]$^+$.

3.6.3. Syntheses and characterisations of *trans*-{Ru(dppm)$_2$} complexes

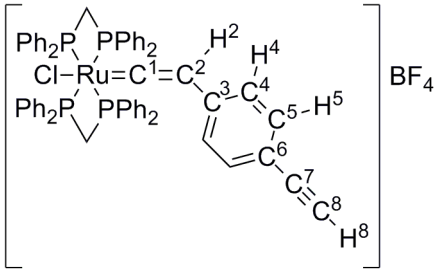

*Synthesis of trans-[RuCl(=C=CHC$_6$H$_4$-4-C≡CH)(dppm)$_2$]BF$_4$, [**87a**]BF$_4$*

A mixture of *cis*-[**20**] (0.11 g, 0.11 mmol), $TlBF_4$ (0.034 g, 0.12 mmol) and HC≡CC$_6$H$_4$-4-C≡CH (0.085 g, 0.67 mmol) in CH_2Cl_2 (6 ml) was stirred under N_2 for 80 minutes. The solution colour changed from clear yellow to dark orange and a white solid (TlCl) precipitated. The solution was then filtered through a HPLC teflon filter

(20 μm pores) to remove TlCl and the orange filtrate concentrated to ~ 2 ml by rotary evaporation. Excess diethyl ether (~ 15 ml) was then added to the filtrate, resulting in the instantaneous precipitation of a pale brown solid. The solid was collected by filtration, washed with diethyl ether (3 × 10 ml) and hexanes (2 × 10 ml) then air dried (0.11 g, 87 %).

IR (CH_2Cl_2, cm^{-1}): 3296 ν(CC-H), 2074 ν(C≡C), 1641 ν(Ru=C=C). ^{1}H NMR ($CDCl_3$, 600 MHz) δ / ppm: 3.04 (s, 1H, H^8), 3.07 (quin, J = 3 Hz, 1H, H^2), 5.38 (dm, J = 82 Hz, CH_2, dppm), 5.46 (apparent doublet, splitting = 8 Hz, 2H, H^4), 6.84 (apparent doublet, splitting = 8 Hz, 2H, H^5), 7.20 – 7.26 (m, 16H, H_m, dppm), 7.32 – 7.38 (m, 8H, H_p, dppm), 7.39 – 7.46 (m, 16H, H_o, dppm). ^{31}P{^{1}H} NMR ($CDCl_3$, 300 MHz) δ / ppm: − 15.3 (s, Ru(dppm)$_2$). ^{19}F NMR ($CDCl_3$, 400 MHz) δ / ppm: − 153.2 (s, BF_4). ^{13}C{^{1}H} NMR ($CDCl_3$, 600 MHz) δ / ppm: 46.5 (t, J = 13 Hz, CH_2, dppm), 83.6 (s, C^7), 110.1 (s, C^8), 112.5 (s, C^2), 119.3 (s, C^3), 127.9 (s, C^5), 126.9 (s, C^4), 128.8 (s, C_m, dppm), 129.4 (s, C_m, dppm), 131.5 (s, C_p, dppm), 132.0 (s, C_p, dppm), 130.7 – 131.3 (m, C_i, dppm), 131.9 (s, C^6), 132.4 (s, C_o, dppm), 133.5 (s, C_o, dppm), 355.9 – 356.4 (m, C^1). ESI(+)-MS (*m/z*): 1031 [RuCl(=C=CHC$_6$H$_4$-4-C≡CH)(dppm)$_2$]$^+$, 995 [Ru(=C=CHC$_6$H$_4$-4-C≡CH)(dppm)$_2$]$^+$, 906 [RuCl(dppm)$_2$ + H]$^+$. Anal. Found: C, 64.35; H, 4.58. Calc. for $C_{60}H_{50}BClF_4P_4Ru$: C, 64.39; H, 4.51.

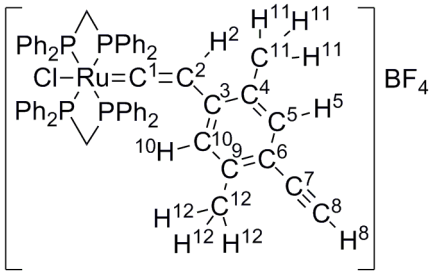

*Synthesis of trans-[RuCl(=C=CHC$_6$H$_2$-2,5-Me$_2$-4-C≡CH)(dppm)$_2$]BF$_4$, [**87b**]BF$_4$*

A mixture of *cis*-[**20**] (0.13 g, 0.13 mmol), $TlBF_4$ (0.040 g, 0.13 mmol) and HC≡CC$_6$H$_2$-2,5-Me$_2$-4-C≡CH (0.17 g, 1.1 mmol) in CH_2Cl_2 (6 ml) was stirred under N_2 for 80 minutes. The solution colour changed from clear yellow to dark orange and a white solid (TlCl) precipitated. The solution was then filtered through a HPLC teflon filter (20 μm pores) to remove TlCl and the orange filtrate concentrated to ~ 2 ml by rotary evaporation. Excess diethyl ether (~ 20 ml) was then added to the filtrate, resulting in the instantaneous precipitation of a pale brown solid. The solid was

collected by filtration, washed with diethyl ether (3 × 10 ml) and hexanes (2 × 10 ml) then air dried (0.10 g, 67 %).

IR (CH_2Cl_2, cm^{-1}): 3299 ν(CC-H), 2099 ν(C≡C), 1636 ν(Ru=C=C). ^1H NMR ($CDCl_3$, 600 MHz) δ / ppm: 1.32 (s, 3H, H^{11}), 1.75 (s, 3H, H^{12}), 3.18 (s, 1H, H^8), 3.46 (quin, J = 3 Hz, 1H, H^2), 5.26 (dm, J = 94 Hz, CH_2, dppm), 5.46 (s, 1H, H^{10}), 6.97 (s, 1H, H^5), 7.18 – 7.26 (m, 16H, H_m, dppm), 7.30 – 7.36 (m, 8H, H_o, dppm), 7.35 – 7.44 (m, 8H, H_p, dppm), 7.44 – 7.54 (m, 8H, H_o, dppm). $^{31}P\{^1H\}$ NMR ($CDCl_3$, 300 MHz) δ / ppm: − 14.4 (s, $Ru(dppm)_2$). $^{13}C\{^1H\}$ NMR ($CDCl_3$, 600 MHz) δ / ppm: 17.9 (s, C^{11}), 19.3 (s, C^{12}), 45.6 – 46.3 (m, CH_2, dppm), 81.5 (s, C^7), 105.0 (s, C^2), 106.5 (s, C^8), 118.6 (s, C^9), 125.0 (s, C^4), 128.2 – 129.6 (m, C_m, dppm), 128.7 (s, C^3), 130.4 – 132.2 (m, C_p, dppm), 130.9 (s, C^{10}), 133.0 (s, H_o, dppm), 133.2 (s, C^5), 134.0 (s, H_o, dppm), 354.3 – 355.1 (m, C^1). APCI(+)-MS (*m/z*): 1059 $[RuCl(=C=CHC_6H_2\text{-}2,5\text{-}Me_2\text{-}4\text{-}C{\equiv}CH)(dppm)_2]^+$, 1024 $[Ru(C{\equiv}CC_6H_2\text{-}2,5\text{-}Me_2\text{-}4\text{-}C{\equiv}CH)(dppm)_2]^+$, 905 $[RuCl(dppm)_2]^+$. Anal. Found: C, 64.93; H, 4.79. Calc. for $C_{62}H_{54}BClF_4P_4Ru$: C, 64.91; H, 4.75.

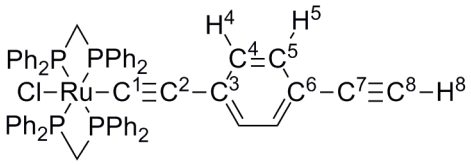

*Synthesis of trans-[RuCl(C≡CC$_6$H$_4$-4-C≡CH)(dppm)$_2$], **[27a]***

A mixture of [**87a**]BF_4 (0.070 g, 0.063 mmol) and 1,8-*bis*-dimethylaminonapthalene (Proton Sponge) (0.050 g, 0.20 mmol) in CH_2Cl_2 (3 ml) was stirred under N_2 for two hours. The orange solution colour lightened over time and a fine white solid precipitated. The solution was then concentrated (~ 0.5 ml) *via* rotary evaporation, filtered through a very short, basic alumina plug (oven-dried) to remove reaction salts, eluting with CH_2Cl_2, into vigorously stirred hexanes where a pale orange / brown solid precipitated instantly. The solid was collected by filtration and washed with hexanes (5 × 10 ml). The solid was then extracted with diethyl ether, filtered and filtrate concentrated to dryness, yielding a brown solid (0.056 g, 86 %).

IR (CH_2Cl_2, cm^{-1}): 2075 ν(RuC≡C), 2040 ν(C≡CH). ^1H NMR ($CDCl_3$, 300 MHz) δ / ppm: 3.05 (s, 1H, H^8), 4.91 (quin., J = 4 Hz, 4H, CH_2, dppm), 5.95 (apparent doublet, splitting = 8 Hz, 2H, H^4), 7.01 (apparent doublet, splitting = 8 Hz, 2H, H^5), 7.07, (t, J = 8 Hz, 8H, H_m, dppm), 7.17 (t, J = 8 Hz, 8H, H_m, dppm), 7.23 (t, J = 8 Hz,

4H, H_p, dppm), 7.28 (t, J = 8 Hz, 4H, H_p, dppm), 7.40 − 7.45 (m, 8H, H_o, dppm), 7.45 − 7.50 (m, 8H, H_o, dppm). $^{31}P\{^1H\}$ NMR ($CDCl_3$, 300 MHz) δ / ppm: − 5.4 ppm (s, Ru(dppm)$_2$). $^{13}C\{^1H\}$ NMR ($CDCl_3$, 600 MHz) δ / ppm: 50.5 (t, J = 10 Hz, CH_2, dppm), 85.2 (s, C^8), 113.1 (s, C^2), 115.0 (s, C^7), 127.7 (s, C_m, dppm), 129.3 (s, C_p, dppm), 129.5 (s, C_p, dppm), 130.1 (s, C^4), 131.0 (s, C^5), 131.4 (s, C^6), 133.5 (s, C_o, dppm), 133.9 (s, C_o, dppm), 134.3 (quin., J = 11 Hz, C_i, dppm), 135.1 (quin., J = 11 Hz, C_i, dppm). APCI(+)-MS (*m/z*): 1031 [RuCl(C≡CC_6H_4-4-C≡CH)(dppm)$_2$ + H]$^+$, 995 [Ru(C≡CC_6H_4-4-C≡CH)(dppm)$_2$]$^+$. Anal. Found: C, 69.87; H, 4.86. Calc. for $C_{60}H_{49}ClP_4Ru$: C, 69.90; H, 4.79.

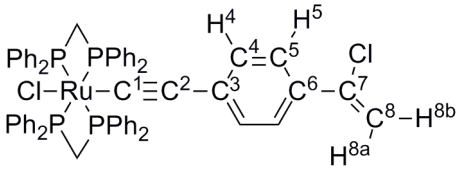

*Synthesis of trans-[RuCl(C≡CC_6H_4-4-CCl=CH_2)(dppm)$_2$], **[89a]***

A mixture of [**87a**]BF_4 (0.055 g, 0.049 mmol) and [N^{n}Bu$_4$]Cl (0.018 g, 0.063 mmol) in CH_2Cl_2 (4 ml) was stirred under N_2 for one hour. The orange solution colour lightened over the reaction period and a fine white solid precipitated. The solvent was then removed under high vacuum leaving a brown / orange residue. The residue was extracted with minimum CH_2Cl_2 and filtered through a short pad of alumina (basic, oven-dried) to remove reaction salts, eluting with CH_2Cl_2. The first orange band was collected and concentrated to dryness by rotary evaporation, yielding a brown residue. The residue was then re-extracted with diethyl ether and filtered, until extracts are colourless. The orange filtrate was then concentrated to dryness by rotary evaporation, yielding a red / orange solid, which was washed with minimum, cold MeOH (2 × 5 ml) and then vacuum dried (0.039 g, 74 %). Single crystals, suitable for X-ray crystallography, were grown by a CH_2Cl_2 / pentane layer diffusion.

IR (CH_2Cl_2, cm^{-1}): 2074 ν(RuC≡C), 1591 ν(C=C). ^1H NMR ($CDCl_3$, 300 MHz) δ / ppm: 4.89 (quin., J = 4 Hz, 4H, CH_2, dppm), 5.33 (d, J = 1.5 Hz, 1H, H^{8a}), 5.60 (d, J = 1.5 Hz, 1H, H^{8b}), 6.01 (apparent doublet, splitting = 8 Hz, 2H, H^4), 7.07 (t, J = 8 Hz, 8H, H_m, dppm), 7.17 (t, J = 8 Hz, 8H, H_m, dppm), 7.20 (apparent doublet, splitting = 8 Hz, 2H, H^5), 7.24 (t, J = 8 Hz, 8H, H_p, dppm), 7.28 (t, J = 8 Hz, 8H, H_p, dppm), 7.39 − 7.50 (m, 16H, H_o, dppm). $^{31}P\{^1H\}$ NMR ($CDCl_3$, 300 MHz) δ / ppm: − 5.4 ppm

(s, Ru(dppm)$_2$). $^{13}C\{^1H\}$ NMR ($CDCl_3$, 600 MHz) δ / ppm: 50.4 (t, J = 9 Hz, CH_2, dppm), 110.0 (s, C^8), 112.9 (s, C^2), 125.1 (s, C^5), 127.7 (s, C_m, dppm), 129.3 (s, C_p, dppm), 129.5 (s, C_p, dppm), 129.9 (s, C^4), 130.3 (s, C^6), 133.5 (s, C_o, dppm), 133.8 (s, C_o, dppm), 134.3 (quin., J = 12 Hz, C_i, dppm), 135.2 (quin., J = 12 Hz, C_i, dppm), 140.7 (s, C^7). APCI(+)-MS (*m/z*): 1067 $[RuCl(C{\equiv}CC_6H_4\text{-}4\text{-}CCl{=}CH_2)(dppm)_2 + H]^+$, 1031 $[Ru(C{\equiv}CC_6H_4\text{-}4\text{-}CCl{=}CH_2)(dppm)_2]^+$, 905 $[RuCl(dppm)_2]^+$. Anal. Found: C, 65.97; H, 4.70. Calc. for $C_{60}H_{50}Cl_2P_4Ru \times 0.5\ CH_2Cl_2$: C, 65.51; H, 4.64.

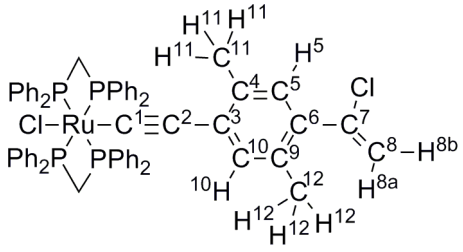

*Synthesis of trans-[RuCl(C≡CC$_6$H$_2$-2,5-Me$_2$-4-CCl=CH$_2$)(dppm)$_2$], [**89b**]*

A mixture of [**87b**]BF_4, (0.017 g, 0.015 mmol) and $[N^nBu_4]Cl$ (0.005 g, 0.018 mmol) in CH_2Cl_2 (5 ml) was stirred under N_2 for one hour. The orange solution colour lightened over the reaction period and a fine white solid precipitated. The solvent was then removed under high vacuum leaving an orange residue. The residue was extracted with diethyl ether and filtered through a short pad of alumina (basic, oven-dried) to remove reaction salts, eluting with diethyl ether until extracts are colourless. The yellow / orange filtrate was then concentrated to dryness by rotary evaporation, yielding a yellow / orange solid (0.015 g, 92 %). Single crystals, suitable for X-ray crystallography, were grown by a CH_2Cl_2 / hexane layer diffusion.

IR (CH_2Cl_2, cm^{-1}): 2065 ν(RuC≡C), 1597 ν(C=C). ^1H NMR (CD_2Cl_2, 400 MHz) δ / ppm: 1.24 (s, 3H, H^{11}), 2.10 (s, 3H, H^{12}), 4.89 – 5.08 (m, 4H, CH_2, dppm), 5.23 (d, J = 1.5 Hz, 1H, H^{8a}), 5.52 (d, J = 1.5 Hz, 1H, H^{8b}), 5.63 (s, 1H, H^{10}), 6.74 (s, 1H, H^5), 7.13 (t, J = 8 Hz, 8H, H_m, dppm), 7.21 (t, J = 8 Hz, 8H, H_m, dppm),7.28 (t, J = 8 Hz, 4H, H_p, dppm), 7.33 (t, J = 8 Hz, 4H, H_p, dppm), 7.48 – 7.54 (m, 8H, H_o, dppm), 7.56 – 7.62 (m, 8H, H_o, dppm). $^{31}P\{^1H\}$ NMR ($CDCl_3$, 400 MHz) δ / ppm: − 6.0 ppm (s, Ru(dppm)$_2$). $^{13}C\{^1H\}$ NMR (CD_2Cl_2, 400 MHz) δ / ppm: 17.9 (s, C^{12}), 18.2 (s, C^{11}), 48.6 (t, J = 11 Hz, CH_2, dppm), 111.9 (s, C^2), 114.2 (s, C^8), 126.5 (s, C_m, dppm), 126.7 (s, C_m, dppm), 128.3 (s, C_p, dppm), 129.3 (s, C^5), 131.0 (s, C^4), 131.4 (s, C^9), 132.3 (s, C_o, dppm), 132.4 (s, C_o, dppm), 132.7 (s, C^6), 133.8 (quin., J = 11 Hz, C_i, dppm), 134.3

(s, C^{10}), 134.6 (quin., J = 11 Hz, C_i, dppm), 135.3 (s, C^3), 139.4 (s, C^7), 146.8 (quin., J = 19 Hz, C^1). ESI(+)-MS (*m/z*): 1095 [RuCl(C≡CC_6H_2-2,5-Me_2-4-CCl=CH_2)(dppm)$_2$ + H]$^+$, 905 [RuCl(dppm)$_2$]$^+$, 871 [Ru(dppm)$_2$ + H]$^+$. Anal. Found: C, 68.10; H, 4.87. Calc. for $C_{62}H_{54}Cl_2P_4Ru$: C, 68.01; H, 4.94.

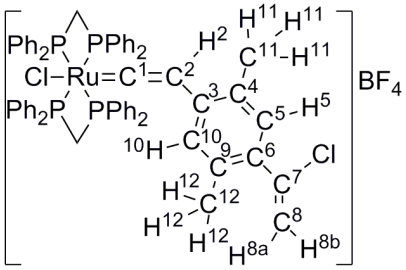

Synthesis of trans-[RuCl(=C=CHC_6H_2-2,5-Me_2-4-CCl=CH_2)(dppm)$_2$]BF_4

A mixture of [**89b**] (0.030 g, 0.028 mmol) and HBF_4.Et_2O (7 µL, 0.051 mmol) in CH_2Cl_2 (4 ml) was stirred under N_2 for 45 minutes. The solution colour changed from yellow to orange. The solution was then concentrated to ~ 0.5 ml under high vacuum and excess diethyl ether added, resulting in the instant precipitation of a pale orange / red solid. The solvent was decanted and solid washed a further three times with diethyl ether (2 × 10 ml) and hexanes (1 × 10 ml) and then vacuum dried (0.028 g, 86 %).

IR (CH_2Cl_2, cm^{-1}): 1604 ν(Ru=C=C). ^{1}H NMR (CD_2Cl_2, 400 MHz) δ / ppm: 1.38 (s, 3H, H^{11}), 1.70 (s, 3H, H^{12}), 3.56 (quin., J = 3 Hz, 1H, H^2), 5.27 (dm., J = 156 Hz 4H, CH_2, dppm), 5.21 (d, J = 1 Hz, 1H, H^{8a}), 5.49 (s, 1H, H^{10}), 5.57 (d, J = 1 Hz, 1H, H^{8b}), 6.83 (s, 1H, H^5), 7.24 – 7.50 (m, 40H, Ph, dppm). ^{31}P{^{1}H} NMR (CD_2Cl_2, 500 MHz) δ / ppm: − 15.89 (s, Ru(dppm)$_2$). ^{19}F NMR ($CDCl_3$, 400 MHz) δ / ppm: − 152.4 (s, BF_4). ^{13}C{^{1}H} NMR (CD_2Cl_2, 500 MHz) δ / ppm: 19.3 (s, C^{11}), 19.4 (s, C^{12}), 46.0 (t, J = 13 Hz, CH_2, dppm), 116.3 (s, C^8), 130.2 (s, C^5), 132.5 (s, C^{10}), 106.1 (s, C^2), 126.0 (s, C^4), 128.7 (s, C^3), 132.3 (s, C^9), 136.4 (s, C^6), 139.2 (s, C^7), 128.6 (t, J = 3 Hz, C_m, dppm), 129.3 (t, J = 3 Hz, C_m, dppm), 131.1 (s, C_p, dppm), 131.7 (s, C_p, dppm), 132.7 (t, J = 3 Hz, C_o, dppm), 133.6 (t, J = 3 Hz, C_o, dppm), 354.3 – 354.7 (m, C^1). ESI(+)-MS (*m/z*): 1095 [RuCl(=C=CHC_6H_2-2,5-Me_2-4-CCl=CH_2)(dppm)$_2$]$^+$, 905 [RuCl(dppm)$_2$]$^+$.

3.6.4. Syntheses and characterisations of half-sandwich complexes

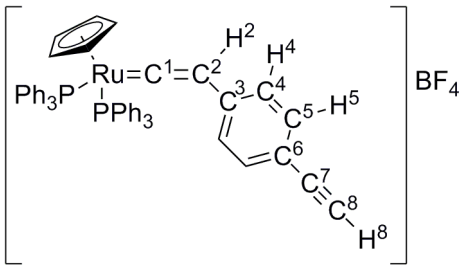

*Synthesis of [RuCl(=C=CHC$_6$H$_4$-4-C≡CH)(PPh$_3$)$_2$(η^5-C$_5$H$_5$)]PF$_6$, [**91a**]PF$_6$*[77]

A mixture of [RuCl(PPh$_3$)$_2$(η^5-C$_5$H$_5$)] (0.050 g, 0.07 mmol), NH_4PF_6 (0.022 g, 0.14 mmol) and HC≡CC$_6$H$_4$-4-C≡CH (0.081 g, 0.64 mmol) in CH_2Cl_2 (7 ml) was stirred under N_2 overnight. The orange solution colour changed to red / brown over the reaction period and a fine white solid precipitated. The solution was concentrated to ~ 3 ml under high vacuum before filtering through celite (to remove reaction salts) into rapidly stirred, ice cold, diethyl ether, resulting in the instant precipitation of a pale pink solid. The solid was collected by filtration, washed with cold diethyl ether (2 × 10 ml) and air dried (0.039 g, 60 %).

IR (CH_2Cl_2, cm^{-1}): 2107 ν(C≡C), 1635 ν(C=C), 1600 ν(C=C). ^{1}H NMR ($CDCl_3$, 600 MHz) δ / ppm: 3.04 (s, 1H, H^8), 5.27 (s, 5H, η^5-C$_5$H$_5$), 5.39 (t, J = 2 Hz, 1H, H^2), 6.95 (apparent doublet, splitting = 8 Hz, 2H, H^4), 7.00 – 7.05 (m, 12H, H$_o$, PPh$_3$), 7.23 (t, J = 7 Hz, 12H, H$_m$, PPh$_3$), 7.31 (apparent doublet, splitting = 8 Hz, 2H, H^5), 7.39 (t, J = 7 Hz, 6H, H$_p$, PPh$_3$). ^{31}P{^{1}H} NMR ($CDCl_3$, 300 MHz) δ / ppm: 43.1 (s, Ru(PPh$_3$)$_2$). ^{13}C{^{1}H} NMR ($CDCl_3$, 600 MHz) δ / ppm: 78.1 (s, C^8), 83.7 (s, C^7), 94.8 (s, η^5-C$_5$H$_5$), 119.0 (s, C^2), 127.5 (s, C^4), 128.4 (s, C$_m$, PPh$_3$), 130.7 (s, C^3), 130.8 (s, C$_p$, PPh$_3$), 131.9 (s, C^5), 132.2 (s, C^6), 133.5 (t, J = 8 Hz, C$_i$, PPh$_3$), 133.8 (s, C$_o$, PPh$_3$), 354.2 (t, J = 14 Hz, C^1). ESI(+)-MS (*m/z*): 817 [RuCl(=C=CHC$_6$H$_4$-4-C≡CH)(PPh$_3$)$_2$(η^5-C$_5$H$_5$)]$^+$, 732 [Ru(PPh$_3$)$_2$(η^5-C$_5$H$_5$) + MeCN]$^+$.

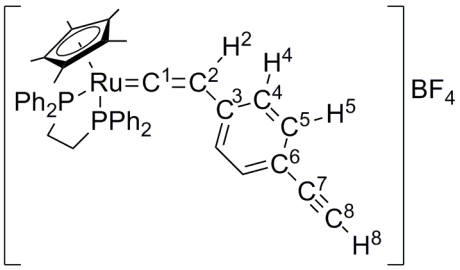

*Synthesis of [RuCl(=C=CHC$_6$H$_4$-4-C≡CH)(dppe)(η^5-C$_5$Me$_5$)]PF$_6$, **[91b]**PF$_6$*

A mixture of [RuCl(dppe)(η^5-C$_5$Me$_5$)] (0.069 g, 0.10 mmol), NH_4PF_6 (0.028 g, 0.17 mmol) and HC≡CC$_6$H$_4$-4-C≡CH (0.14 g, 1.1 mmol) in CH_2Cl_2 (25 ml) was stirred under N_2 overnight. The orange solution colour darkened over the reaction period and a fine white solid precipitated. The solution was concentrated to ~ 3 ml under high vacuum and filtered through a cotton wool pipette (to remove reaction salts) into rapidly stirred, ice cold, diethyl ether, resulting in the instantaneous precipitation of a pale pink solid. The solid was then collected by filtration, washed with cold diethyl ether (3 × 10 ml) and cold hexanes (3 × 10 ml) then air dried (0.072 g, 79 %).

IR (CH_2Cl_2, cm^{-1}): 2106 ν(C≡C), 1631 ν(C=C), 1606 ν(C=C), 1599 ν(C=C). ^{1}H NMR ($CDCl_3$, 600 MHz) δ / ppm: 1.68 (s, 15H, η^5-C$_5$Me$_5$), 2.41 – 2.60 (m, 2H, CH_2, dppe), 2.90 – 3.12 (m, 2H, CH_2, dppe), 3.01 (s, 1H, H^8), 4.35 – 4.39 (m, 1H, H^2), 6.02 (apparent doublet, splitting = 6 Hz, 2H, H^4), 6.92 (apparent doublet, splitting = 6 Hz, 2H, H^5), 7.08 (t, J = 8 Hz, 4H, H$_p$, dppe), 7.34 (t, J = 8 Hz, 4H, H$_o$, dppe), 7.42 (t, J = 8 Hz, 4H, H$_m$, dppe), 7.47 (t, J = 8 Hz, 4H, H$_m$, dppe), 7.50 – 7.58 (m, 4H, H$_o$, dppe). ^{31}P{^{1}H} NMR ($CDCl_3$, 600 MHz) δ / ppm: 71.8 (s, Ru(dppe)). ^{13}C{^{1}H} NMR ($CDCl_3$, 600 MHz) δ / ppm: 10.0 (s, η^5-C$_5$*Me*$_5$), 27.9 (t, J = 24 Hz, CH_2, dppe), 77.3 (s, C^8), 83.7 (s, C^7), 103.9 (s, η^5-*C*$_5$Me$_5$), 115.9 (s, C^2), 125.1 (s, C^4), 128.0 (s, C^3), 128.6 (s, C$_m$, dppe), 128.9 (s, C$_m$, dppe), 131.2 – 131.6 (m, C$_o$, dppe), 131.7 (s, C^5), 132.0 (s, C^6), 132.6 (s, C$_p$, dppe), 133.6 – 134.2 (m, C$_i$, dppe), 352.6 – 353.0 (m, C^1). ESI(+)-MS (*m/z*): 761 [RuCl(=C=CHC$_6$H$_4$-4-C≡CH)(dppe)(η^5-C$_5$Me$_5$)]$^+$, 667 [Ru(dppe)(η^5-C$_5$Me$_5$) + MeOH]$^+$, 635 [Ru(dppe)(η^5-C$_5$Me$_5$)]$^+$.

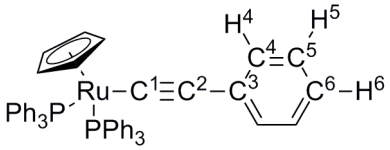

Synthesis of [Ru(C≡CC$_6$H$_5$)(PPh$_3$)$_2$(η^5-C$_5$H$_5$)][90]

A mixture of [RuCl(PPh$_3$)$_2$(η^5-C$_5$H$_5$)] (0.10 g, 0.14 mmol), NH_4PF_6 (0.023 g, 0.14 mmol) and HC≡CC$_6$H$_5$ (17 µL, 0.15 mmol) in MeOH (10 ml) was heated at reflux under N_2 for 30 minutes. The orange solution colour darkened over the reaction period. The orange solution was then cooled to room temperature before the addition of DBU (6 drops, excess), resulting in the immediate precipitation of a yellow solid. The solid was then collected by filtration, washed with MeOH (3 × 10 ml) and hexanes (2 × 10 ml), then air dried (0.078 g, 71 %).

IR (CH_2Cl_2, cm^{-1}): 2074 ν(RuC≡C), 1605 ν(C=C), 1591 ν(C=C). ^{1}H NMR ($CDCl_3$, 600 MHz) δ / ppm: 4.33 (s, 5H, η^5-C$_5$H$_5$), 6.99 – 7.01 (m, 1H, H^6), 7.09 (t, J = 7 Hz, 12H, H$_m$, PPh$_3$), 7.13 – 7.16 (m, 4H, H^4 and H^5), 7.19 (t, J = 7 Hz, 6H, H$_p$, PPh$_3$), 7.46 − 7.54 (m, 12H, H$_o$, PPh$_3$). ^{31}P{^{1}H} NMR ($CDCl_3$, 300 MHz) δ / ppm: 51.5 (s, Ru(PPh$_3$)$_2$). ^{13}C{^{1}H} NMR ($CDCl_3$, 600 MHz) δ / ppm: 85.3 (s, η^5-C$_5$H$_5$), 114.5 (s, C^2), 116.3 (t, J = 26 Hz, C^1), 123.1 (s, C^6), 127.4 (t, J = 5 Hz, C$_m$, PPh$_3$), 127.8 (s, C^4), 128.5 (s, C$_p$, PPh$_3$), 130.7 (s, C^5), 134.0 (t, J = 5 Hz, C$_o$, PPh$_3$), 139.0 (t, J = 21 Hz, C$_i$, PPh$_3$), 139.2 (t, J = 21 Hz, C$_i$, PPh$_3$). ESI(+)-MS (*m/z*): 792 [Ru(C≡CC$_6$H$_5$)(PPh$_3$)$_2$(η^5-C$_5$H$_5$)]$^+$, 691 [Ru(PPh$_3$)$_2$(η^5-C$_5$H$_5$)]$^+$.

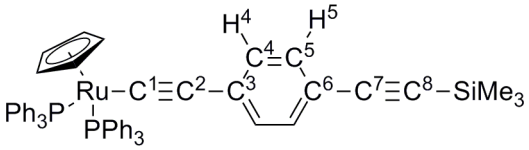

Synthesis of [Ru(C≡CC$_6$H$_4$-4-C≡CSiMe$_3$)(PPh$_3$)$_2$(η^5-C$_5$H$_5$)][109]

A mixture of [RuCl(PPh$_3$)$_2$(η^5-C$_5$H$_5$)] (0.10 g, 0.14 mmol), NH_4BF_4 (0.032 g, 0.30 mmol) and HC≡CC$_6$H$_4$-4-C≡CSiMe$_3$ (0.037 g, 0.19 mmol) in MeOH (10 ml) was refluxed under N_2 for 3.5 hours. The orange solution colour darkened over the reaction period. The solution was then cooled to room temperature before the addition of DBU (4 drops, excess), resulting in the instant precipitation of a yellow solid. The solid was

then collected by filtration, washed with MeOH (3 × 10 ml) and vacuum dried (0.070 g, 60 %).

IR (CH_2Cl_2, cm^{-1}): 2148 ν(C≡CSiMe$_3$), 2066 ν(RuC≡C), 1596 ν(C=C). ^{1}H NMR ($CDCl_3$, 300 MHz) δ / ppm: 0.24 (s, 9H, SiMe$_3$), 4.32 (s, 5H, η^5-C$_5$H$_5$), 6.98 (apparent doublet, splitting = 8 Hz, 2H, H^4), 7.07 (t, J = 7 Hz, 12H, H$_m$, PPh$_3$), 7.19 (t, J = 7 Hz, 6H, H$_p$, PPh$_3$), 7.24 (apparent doublet, splitting = 8 Hz, 2H, H^5), 7.39 – 7.51 (m, 12H, H$_o$, PPh$_3$). ^{31}P{^{1}H} NMR ($CDCl_3$, 300 MHz) δ / ppm: 51.3 (s, Ru(PPh$_3$)$_2$). ^{13}C{^{1}H} NMR ($CDCl_3$, 600 MHz) δ / ppm: 0.3 (s, SiMe$_3$), 85.4 (s, η^5-C$_5$H$_5$), 93.6 (s, C^8), 106.7 (s, C^7), 115.3 (s, C^2 or C^3), 117.0 (s, C^2 or C^3) 123.6 (t, J = 25 Hz, C^1), 127.4 (t, J = 4 Hz, C$_m$, PPh$_3$), 128.6 (s, C$_p$, PPh$_3$), 130.4 (s, C^4), 131.1 (s, C^6), 131.7 (s, C^5), 134.0 (t, J = 5 Hz, C$_o$, PPh$_3$), 138.8 (t, J = 21 Hz, C$_i$, PPh$_3$), 139.0 (t, J = 21 Hz, C$_i$, PPh$_3$). ESI(+)-MS (*m/z*): 889 [Ru(C≡CC$_6$H$_4$-4-C≡CSiMe$_3$)(PPh$_3$)$_2$(η^5-C$_5$H$_5$) + H]$^+$, 719 [Ru(PPh$_3$)$_2$(η^5-C$_5$H$_5$) + C$_2$H$_4$]$^+$.

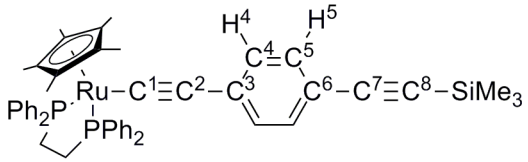

Synthesis of [Ru(C≡CC$_6$H$_4$-4-C≡CSiMe$_3$)(dppe)(η^5-C$_5$Me$_5$)][109]

A mixture of [RuCl(dppe)(η^5-C$_5$Me$_5$)] (0.12 g, 0.18 mmol), NH_4BF_4 (0.034 g, 0.32 mmol) and HC≡CC$_6$H$_4$-4-C≡CSiMe$_3$ (0.043 g, 0.22 mmol) in MeOH (10 ml) was refluxed under N_2 for 3.5 hours. The orange solution colour darkened over the reaction period. The solution was then cooled to room temperature before the addition of DBU (10 drops, excess), resulting in the instantaneous precipitation of a yellow solid. The yellow solid was then collected by filtration, washed with MeOH (3 × 10 ml) and air dried (0.10 g, 68 %).

IR (CH_2Cl_2, cm^{-1}): 2147 ν(C≡CSiMe$_3$), 2065 ν(RuC≡C), 1605 ν(C=C), 1595 ν(C=C). ^{1}H NMR ($CDCl_3$, 600 MHz) δ / ppm: 0.23 (s, 9H, SiMe$_3$), 1.56 (s, 15H, η^5-C$_5$Me$_5$), 2.00 – 2.14 (m, 2H, dppe), 2.59 – 2.73 (m, 2H, dppe), 6.64 (apparent doublet, splitting = 8 Hz, 2H, H^4), 7.12 (apparent doublet, splitting = 8 Hz, 2H, H^5), 7.19 – 7.32 (m, 12H, H$_m$ and H$_p$, dppe), 7.32 – 7.39 (m, 4H, H$_o$, dppe), 7.68 – 7.80 (m, 4H, H$_o$, dppe). ^{31}P{^{1}H} NMR ($CDCl_3$, 300 MHz) δ / ppm: 81.8 (s, Ru(dppe)). ^{13}C{^{1}H} NMR ($CDCl_3$, 600 MHz) δ / ppm: 0.3 (s, SiMe$_3$), 10.2 (s, η^5-C$_5$*Me*$_5$), 29.6 (t, J = 23 Hz, CH_2,

dppe), 92.9 (s, η^5-C_5Me_5), 93.2 (s, C^8), 106.9 (s, C^7), 111.1 (s, C^2), 116.3 (s, C^3), 127.4 (t, J = 4 Hz, C_m, dppe), 127.6 (t, J = 4 Hz, C_m, dppe), 129.0 (s, C_p, dppe), 129.1 (s, C_p, dppe), 130.0 (s, C^4), 131.4 (s, C^5), 131.6 (s, C^6), 133.4 (t, J = 4 Hz, C_o, dppe), 133.8 (t, J = 4 Hz, C_o, dppe), 136.0 (t, J = 25 Hz, C^1), 138.7 − 139.0 (m, C_i, dppe). ESI(+)-MS (*m/z*): 832 $[Ru(C{\equiv}CC_6H_4\text{-}4\text{-}C{\equiv}CSiMe_3)(dppe)(\eta^5\text{-}C_5Me_5) + H]^+$, 761 $[Ru(C{\equiv}CC_6H_4\text{-}4\text{-}C{\equiv}CH)(dppe)(\eta^5\text{-}C_5Me_5) + H]^+$, 663 $[Ru(dppe)(\eta^5\text{-}C_5Me_5) + C_2H_4]^+$.

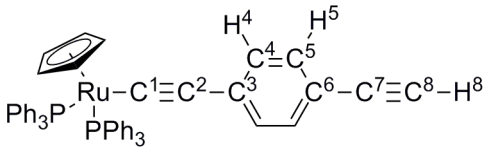

*Synthesis of [Ru(C≡CC$_6$H$_4$-4-C≡CH)(PPh$_3$)$_2$(η^5-C$_5$H$_5$)], [**93a**]*

A mixture of $[Ru(C{\equiv}CC_6H_4\text{-}4\text{-}C{\equiv}CSiMe_3)(PPh_3)_2(\eta^5\text{-}C_5H_5)]$ (0.11 g, 0.13 mmol) and TBAF.3H$_2$O (0.041 g, 0.13 mmol) in CH_2Cl_2 (6 ml) was stirred under N_2 overnight. The yellow solution colour darkened to brown over the reaction period. The solution was then concentrated to dryness under high vacuum, yielding a dark brown, oily residue. The subsequent addition of excess MeOH (~ 20 ml) to the residue resulted in the formation of a yellow / brown solid. The solid was then collected by filtration, washed with MeOH (3 × 10 ml) and air dried (0.088 g, 83 %).

IR (CH_2Cl_2, cm^{-1}): 2068 ν(RuC≡C), 2037 ν(C≡CH), 1607 ν(C=C), 1594 ν(C=C). ^{1}H NMR ($CDCl_3$, 300 MHz) δ / ppm: 3.07 (s, 1H, H^8), 4.32 (s, 5H, η^5-C_5H_5), 7.02 (apparent doublet, splitting = 8 Hz, 2H, H^4), 7.08 (t, J = 7 Hz, 12H, H_m, PPh_3), 7.20 (t, J = 7 Hz, 6H, H_p, PPh_3), 7.24 (apparent doublet, splitting = 8 Hz, 2H, H^5), 7.40 – 7.56 (m, 12H, H_o, PPh_3). ^{31}P{^{1}H} NMR ($CDCl_3$, 300 MHz) δ / ppm: 51.4 (s, $Ru(PPh_3)_2$). ^{13}C{^{1}H} NMR ($CDCl_3$, 600 MHz) δ / ppm: 85.1 (s, C^8), 85.4 (s, η^5-C_5H_5), 115.2 (s, C^7), 115.9 (s, C^2), 123.7 (t, J = 25 Hz, C^1), 127.4 (t, J = 4 Hz, C_m, PPh_3), 128.6 (s, C_p, PPh_3), 128.7 (s, C^3), 130.5 (s, C^4), 131.3 (s, C^6), 131.8 (s, C^5), 134.0 (t, J = 5 Hz, C_o, PPh_3), 138.8 (t, J = 21 Hz, C_i, PPh_3), 139.1 (t, J = 21 Hz, C_i, PPh_3). ESI(+)-MS (*m/z*): 817 $[Ru(C{\equiv}CC_6H_4\text{-}4\text{-}C{\equiv}CH)(PPh_3)_2(\eta^5\text{-}C_5H_5) + H]^+$, 719 $[Ru(PPh_3)_2(\eta^5\text{-}C_5H_5) + C_2H_4]^+$, 301 $[Ru(C{\equiv}CC_6H_4\text{-}4\text{-}C{\equiv}CH)(\eta^5\text{-}C_5H_5)]^+$.

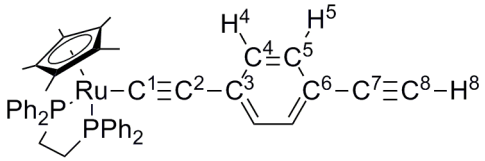

*Synthesis of [Ru(C≡CC$_6$H$_4$-4-C≡CH)(dppe)(η^5-C$_5$Me$_5$)], **[93b]***

A mixture of [Ru(C≡CC$_6$H$_4$-4-C≡CSiMe$_3$)(dppe)(η^5-C$_5$Me$_5$)] (0.079 g, 0.095 mmol) and TBAF.3H$_2$O (0.047 g, 0.15 mmol) in CH$_2$Cl$_2$ (6 ml) was stirred under N$_2$ overnight. The yellow solution colour darkened to brown over the reaction period. The solution was then concentrated to dryness under high vacuum, yielding a dark brown oily residue. The subsequent addition of excess MeOH (~ 20 ml) to the residue resulted in the formation of a yellow solid. The solid was collected by filtration, washed with MeOH (3 × 10 ml) then air dried (0.045 g, 62 %).

IR (CH$_2$Cl$_2$, cm^{-1}): 2065 ν(RuC≡C), 2036 ν(C≡CH), 1605 ν(C=C), 1595 ν(C=C). ^{1}H NMR (CDCl$_3$, 600 MHz) δ / ppm: 1.56 (s, 15H, η^5-C$_5$Me$_5$), 2.00 – 2.13 (m, 2H, dppe), 2.59 – 2.73 (m, 2H, dppe), 3.04 (s, 1H, H^8), 6.64 (apparent doublet, splitting = 6 Hz, 2H, H^4), 7.12 (apparent doublet, splitting = 6 Hz, 2H, H^5), 7.19 – 7.26 (m, 6H, H$_o$, dppe), 7.28 – 7.38 (m, 18H, H$_m$ and H$_p$, dppe), 7.68 – 7.77 (m, 6H, H$_o$, dppe). ^{31}P{^{1}H} NMR (CDCl$_3$, 600 MHz) δ / ppm: 80.7 (s, Ru(dppe)). ^{13}C{^{1}H} NMR (CDCl$_3$, 600 MHz) δ / ppm: 10.2 (s, η^5-C$_5$*Me*$_5$), 29.6 (t, J = 23 Hz, CH$_2$, dppe), 85.2 (s, C^8), 92.9 (s, η^5-*C*$_5$Me$_5$), 111.1 (s, C^2), 115.2 (s, C^7), 116.2 (s, C^3), 127.4 (t, J = 5 Hz, C$_m$, dppe), 127.6 (t, J = 5 Hz, C$_m$, dppe), 129.0 (s, C$_p$, dppe), 129.1 (s, C$_p$, dppe), 130.0 (s, C^4), 131.4 (s, C^5), 131.6 (s, C^6), 133.4 (t, J = 5 Hz, C$_o$, dppe), 133.8 (t, J = 5 Hz, C$_o$, dppe), 136.0 (t, J = 24 Hz, C^1), 138.6 – 139.1 (m, C$_i$, dppe). ESI(+)-MS (*m/z*): 761 [Ru(C≡CC$_6$H$_4$-4-C≡CH)(dppe)(η^5-C$_5$Me$_5$) + H]$^+$, 663 [Ru(dppe)(η^5-C$_5$Me$_5$) + C$_2$H$_4$]$^+$.

3.7. References

1. S. G. Eaves, S. Hart, A. C. Whitwood, D. S. Yufit, P. Low and J. Lynam, *Chem. Commun.*, **2015**, *51*, 9362.
2. S. Rigaut, D. Touchard and P. H. Dixneuf, *Coord. Chem. Rev.*, **2004**, *248*, 1585.
3. J. P. Selegue, *Coord. Chem. Rev.*, **2004**, *248*, 1543.
4. M. I. Bruce, *Chem. Rev.*, **1998**, *98*, 2797.
5. D. Touchard and P. H. Dixneuf, *Coord. Chem. Rev.*, **1998**, *178*, 409.
6. H. Werner, K. Ilg, R. Lass and J. Wolf, *J. Organomet. Chem.*, **2002**, *661*, 137.
7. C. Coletti, A. Marrone and N. Re, *Acc. Chem. Res.*, **2011**, *45*, 139.
8. S. Guesmi, D. Touchard and P. H. Dixneuf, *Chem. Commun.*, **1996**, 2773.

9. S. Rigaut, J. Perruchon, S. Guesmi, C. Fave, D. Touchard and P. H. Dixneuf, *Eur. J. Inorg. Chem.*, **2005**, *2005*, 447.
10. W. Skibar, H. Kopacka, K. Wurst, C. Salzmann, K. H. Ongania, F. F. de Biani, P. Zanello and B. Bildstein, *Organometallics*, **2004**, *23*, 1024.
11. G. Roth, H. Fischer, T. Meyer-Friedrichsen, J. Heck, S. Houbrechts and A. Persoons, *Organometallics*, **1998**, *17*, 1511.
12. G. Frapper and M. Kertesz, *Inorg. Chem.*, **1993**, *32*, 732.
13. Y. Miyake, S. Endo, T. Moriyama, K. Sakata and Y. Nishibayashi, *Angew. Chem. Int. Edit.*, **2013**, *52*, 1758.
14. D. A. Valyaev, M. G. Peterleitner, O. V. Semeikin, K. I. Utegenov, N. A. Ustynyuk, A. Sournia-Saquet, N. Lugan and G. Lavigne, *J. Organomet. Chem.*, **2007**, *692*, 3207.
15. R. F. Winter, K.-W. Klinkhammer and S. Záliš, *Organometallics*, **2001**, *20*, 1317.
16. A. Furstner, M. Liebl, C. W. Lehmann, M. Picquet, R. Kunz, C. Bruneau, D. Touchard and P. H. Dixneuf, *Chem. Eur. J.*, **2000**, *6*, 1847.
17. D. J. Cardin, Cetinkay.B and M. F. Lappert, *Chem. Rev.*, **1972**, *72*, 545.
18. P. de Frémont, N. Marion and S. P. Nolan, *Coord. Chem. Rev.*, **2009**, *253*, 862.
19. W. A. Herrmann, *Angew. Chem. Int. Ed. Engl.*, **2002**, *41*, 1290.
20. S. T. Nguyen, L. K. Johnson, R. H. Grubbs and J. W. Ziller, *J. Am. Chem. Soc.*, **1992**, *114*, 3974.
21. M. Scholl, S. Ding, C. W. Lee and R. H. Grubbs, *Org. Lett,*, **1999**, *1*, 953.
22. J. K. Huang, E. D. Stevens, S. P. Nolan and J. L. Petersen, *J. Am. Chem. Soc.*, **1999**, *121*, 2674.
23. L. Ackermann, A. Furstner, T. Weskamp, F. J. Kohl and W. A. Herrmann, *Tetrahedron Lett.*, **1999**, *40*, 4787.
24. T. M. Trnka and R. H. Grubbs, *Acc. Chem. Res.*, **2001**, *34*, 18.
25. N. Fey, M. F. Haddow, J. N. Harvey, C. L. McMullin and A. G. Orpen, *Dalton Trans.*, **2009**, 8183.
26. E. O. Fischer and A. Maasbol, *Angew. Chem. Int. Ed. Eng.*, **1964**, *3*, 580.
27. K. H. Dötz and J. Stendel, *Chem. Rev.*, **2009**, *109*, 3227.
28. R. R. Schrock and P. R. Sharp, *J. Am. Chem. Soc.*, **1978**, *100*, 2389.
29. D. Astruc, *Organometallic Chemistry and Catalysis*, Springer, Berlin Heidelberg New York, pp. 197-215, **2007**.
30. C. Bruneau and P. H. Dixneuf, *Acc. Chem. Res.*, **1999**, *32*, 311.
31. C. Bruneau and P. Dixneuf, *Metal Vinylidenes and Allenylidenes in Catalysis*, Wiley, Weinheim Germany, pp. 1-20, **2008**.
32. B. M. Trost and A. McClory, *Chem. Asian J.*, **2008**, *3*, 164.
33. C. Slugovc, K. Mereiter, E. Zobetz, R. Schmid and K. Kirchner, *Organometallics*, **1996**, *15*, 5275.
34. S. J. Landon, P. M. Shulman and G. L. Geoffroy, *J. Am. Chem. Soc.*, **1985**, *107*, 6739.
35. J. M. O'Connor, A. Closson, K. Hiibner, R. Merwin and P. Gantzel, *Organometallics*, **2001**, *20*, 3710.
36. M. I. Bruce and R. C. Wallis, *J. Organomet. Chem.*, **1978**, *161*, C1.
37. O. S. Mills and A. D. Redhouse, *Chem. Commun.*, **1966**, 444.
38. R. B. King and M. S. Saran, *J. Am. Chem. Soc.*, **1972**, *94*, 1784.
39. R. B. King and M. S. Saran, *J. Chem. Soc., Chem. Commun.*, **1972**, 1053.
40. A. Davison and J. P. Solar, *J. Organomet. Chem.*, **1978**, *155*, C8.
41. A. Davison and J. P. Selegue, *J. Am. Chem. Soc.*, **1978**, *100*, 7763.

42. D. Touchard, P. Haquette, N. Pirio, L. Toupet and P. H. Dixneuf, *Organometallics*, **1993**, *12*, 3132.
43. D. Touchard, P. Haquette, S. Guesmi, L. Le Pichon, A. Daridor, L. Toupet and P. H. Dixneuf, *Organometallics*, **1997**, *16*, 3640.
44. P. Haquette, N. Pirio, D. Touchard, L. Toupet and P. H. Dixneuf, *J. Chem. Soc., Chem. Commun.*, **1993**, 163.
45. M. I. Bruce and A. G. Swincer, *Adv. Organomet. Chem.*, **1983**, *22*, 59.
46. J. M. Lynam, *Chem. Eur. J.*, **2010**, *16*, 8238.
47. Y. Ikeda, T. Yamaguchi, K. Kanao, K. Kimura, S. Kamimura, Y. Mutoh, Y. Tanabe and Y. Ishii, *J. Am. Chem. Soc.*, **2008**, *130*, 16856.
48. M. Otsuka, N. Tsuchida, Y. Ikeda, Y. Kimura, Y. Mutoh, Y. Ishii and K. Takano, *J. Am. Chem. Soc.*, **2012**, *134*, 17746.
49. M. I. Bruce, *Pure Appl. Chem*, **1986**, *58*, 553.
50. M. C. Puerta and P. Valerga, *Coord. Chem. Rev.*, **1999**, *193-5*, 977.
51. D. A. Valyaev, O. V. Semeikin and N. A. Ustynyuk, *Coord. Chem. Rev.*, **2004**, *248*, 1679.
52. J. P. Selegue, *Organometallics*, **1982**, *1*, 217.
53. N. E. Kolobova, L. L. Ivanov, O. S. Zhvanko, O. M. Khitrova, A. S. Batsanov and Y. T. Struchkov, *J. Organomet. Chem.*, **1984**, *262*, 39.
54. N. Pirio, D. Touchard and P. H. Dixneuf, *J. Organomet. Chem.*, **1993**, *462*, C18.
55. D. Touchard, N. Pirio and P. H. Dixneuf, *Organometallics*, **1995**, *14*, 4920.
56. E. O. Fischer, H. J. Kalder, A. Frank, F. H. Kohler and G. Huttner, *Angew. Chem. Int. Ed. Eng.*, **1976**, *15*, 623.
57. P. J. Stang and T. E. Fisk, *J. Am. Chem. Soc.*, **1979**, *101*, 4772.
58. H. Berke, *J. Organomet. Chem.*, **1980**, *185*, 75.
59. V. Cadierno, P. Crochet and J. Gimeno, in *Metal Vinylidenes and Allenylidenes in Catalysis*, C. Bruneau and P. H. Dixneuf, Wiley, Weinheim Germany, **2008**, pp. 61-98.
60. A. Asensio, M. L. Buil, M. A. Esteruelas and E. Oñate, *Organometallics*, **2004**, *23*, 5787.
61. J. R. Lomprey and J. P. Selegue, *Organometallics*, **1993**, *12*, 616.
62. M. I. Bruce, P. Hinterding, E. R. T. Tiekink, B. W. Skelton and A. H. White, *J. Organomet. Chem.*, **1993**, *450*, 209.
63. R. F. Winter and F. M. Hornung, *Organometallics*, **1997**, *16*, 4248.
64. P. Haquette, D. Touchard, L. Toupet and P. Dixneuf, *J. Organomet. Chem.*, **1998**, *565*, 63.
65. K. Ilg and H. Werner, *Angew. Chem. Int. Ed. Engl.*, **2000**, *39*, 1632.
66. K. Ilg and H. Werner, *Chem. Eur. J.*, **2002**, *8*, 2812.
67. M. I. Bruce, P. Hinterding, P. J. Low, B. W. Skelton and A. H. White, *Chem. Commun.*, **1996**, 1009.
68. M. I. Bruce, *Coord. Chem. Rev.*, **2004**, *248*, 1603.
69. M. I. Bruce, *Chem. Rev.*, **1991**, *91*, 197.
70. D. Touchard, P. Haquette, A. Daridor, L. Toupet and P. H. Dixneuf, *J. Am. Chem. Soc.*, **1994**, *116*, 11157.
71. M. Dede, M. Drexler and H. Fischer, *Organometallics*, **2007**, *26*, 4294.
72. S. Rigaut, C. Olivier, K. Costuas, S. Choua, O. Fadhel, J. Massue, P. Turek, J.-Y. Saillard, P. H. Dixneuf and D. Touchard, *J. Am. Chem. Soc.*, **2006**, *128*, 5859.
73. H. Irngartinger and W. Gotzmann, *Angew. Chem. Int. Ed. Eng.*, **1986**, *25*, 340.
74. A. Marrone, C. Coletti and N. Re, *Organometallics*, **2004**, *23*, 4952.

75. F. Creati, C. Coletti and N. Re, *Organometallics*, **2009**, *28*, 6603.
76. N. E. Kolobova, O. S. Zhvanko, L. L. Ivanov, A. S. Batsanov and Y. T. Struchkov, *J. Organomet. Chem.*, **1986**, *302*, 235.
77. M. I. Bruce, B. C. Hall, P. J. Low, B. W. Skelton and A. H. White, *J. Organomet. Chem.*, **1999**, *592*, 74.
78. C. W. Faulkner, S. L. Ingham, M. S. Khan, J. Lewis, N. J. Long and P. R. Raithby, *J. Organomet. Chem.*, **1994**, *482*, 139.
79. H. Werner, A. Stark, P. Steinert, C. Grunwald and J. Wolf, *Chem. Ber.*, **1995**, *128*, 49.
80. C. Gauss, D. Veghini and H. Berke, *Chem. Ber. Recl.*, **1997**, *130*, 183.
81. G. Albertin, S. Antoniutti, E. Bordignon and M. Granzotto, *J. Organomet. Chem.*, **1999**, *585*, 83.
82. G. Albertin, S. Antoniutti, E. Bordignon and D. Bresolin, *J. Organomet. Chem.*, **2000**, *609*, 10.
83. H. Werner, P. Bachmann and M. Martin, *Can. J. Chem.*, **2001**, *79*, 519.
84. C. Olivier, B. Kim, D. Touchard and S. Rigaut, *Organometallics*, **2008**, *27*, 509.
85. T. Bekele, S. R. Brunette and M. A. Lipton, *J. Org. Chem.*, **2003**, *68*, 8471.
86. P. Prince, K. L. Evans, K. R. Boss, F. R. Fronczek and R. D. Gandour, *Acta Crystallogr., Sect. C*, **1990**, *46*, 1150.
87. F. A. Carey and R. J. Sundberg, *Advanced Organic Chemistry: Part A: Structure and Mechanisms*, Springer, New York, edn. 5, pp. 536-545, **2007**.
88. D. G. Johnson, J. M. Lynam, J. M. Slattery and C. E. Welby, *Dalton Trans.*, **2010**, *39*, 10432.
89. M. Jimenez-Tenorio, M. C. Puerta, P. Valerga, M. A. Ortuno, G. Ujaque and A. Lledos, *Inorg. Chem.*, **2013**, *52*, 8919.
90. M. I. Bruce, C. Hameister, A. G. Swincer and R. C. Wallis, *Inorg. Synth.*, **1982**, *21*, 78.
91. B. Chaudret, G. Commenges and R. Poilblanc, *J. Chem. Soc., Dalton Trans.*, **1984**, 1635.
92. S. Takahashi, Y. Kuroyama, K. Sonogashira and N. Hagihara, *Synthesis*, **1980**, 627.
93. S. Marqués-González, M. Parthey, D. S. Yufit, J. A. K. Howard, M. Kaupp and P. J. Low, *Organometallics*, **2014**, *33*, 4947.
94. M. I. Bruce, B. G. Ellis, P. J. Low, B. W. Skelton and A. H. White, *Organometallics*, **2003**, *22*, 3184.
95. P. Pascal, *P. Nouveau Traité de Chimie Minérale*, Masson-Paris, edn. 1961, vol. VI, pp. 92.
96. H. E. Gottlieb, V. Kotlyar and A. Nudelman, *J. Org. Chem.*, **1997**, *62*, 7512.
97. A. Klamt and G. Schuurmann, *J. Chem. Soc., Perkin Trans. 2*, **1993**, 799.
98. S. Grimme, J. Antony, S. Ehrlich and H. Krieg, *J. Chem. Phys.*, **2010**, *132*, 154104.
99. S. Grimme, S. Ehrlich and L. Goerigk, *J. Comput. Chem.*, **2011**, *32*, 1456.
100. P. Csaszar and P. Pulay, *J. Mol. Struct.*, **1984**, *114*, 31.
101. R. Ahlrichs, M. Bar, M. Haser, H. Horn and C. Kolmel, *Chem. Phys. Lett.*, **1989**, *162*, 165.
102. K. Eichkorn, O. Treutler, H. Ohm, M. Haser and R. Ahlrichs, *Chem. Phys. Lett.*, **1995**, *240*, 283.
103. O. Treutler and R. Ahlrichs, *J. Chem. Phys.*, **1995**, *102*, 346.
104. K. Eichkorn, F. Weigend, O. Treutler and R. Ahlrichs, *Theor. Chem. Acc.*, **1997**, *97*, 119.

105. M. von Arnim and R. Ahlrichs, *J. Chem. Phys.*, **1999**, *111*, 9183.
106. P. Deglmann and F. Furche, *J. Chem. Phys.*, **2002**, *117*, 9535.
107. P. Deglmann, F. Furche and R. Ahlrichs, *Chem. Phys. Lett.*, **2002**, *362*, 511.
108. P. Deglmann, K. May, F. Furche and R. Ahlrichs, *Chem. Phys. Lett.*, **2004**, *384*, 103.
109. W. M. Khairul, M. A. Fox, P. A. Schauer, D. Albesa-Jove, D. S. Yufit, J. A. K. Howard and P. J. Low, *Inorg. Chim. Acta*, **2011**, *374*, 461.

CHAPTER 4

Synthesis and electronic characterisation of multi-metallic 'wire-like' molecules containing *trans*-bis(alkynyl) {Ru(dppe)$_2$} fragments

4.1. Abstract

In this Chapter, mono- and multi-metallic complexes containing *trans*-bis(alkynyl) {Ru(dppe)$_2$} fragments have been prepared. The *mono*-metallic complexes *trans*-[Ru(C≡CR)$_2$(dppe)$_2$], [**43**] ([**43a**]: R = C$_6$H$_4$-4-C≡CSiMe$_3$; [**43b**]: R = 3-thiophene (3-*th*)) serve as reference materials for electrochemical and spectroscopic studies of the multi-metallic analogues. The 1,4-diethynylbenzene-bridged bimetallic complexes, *trans*-[{(RC≡C)(dppe)$_2$Ru}$_2$(μ-C≡CC$_6$H$_2$-2,5-X$_2$-4-C≡C)], [**94**] ([**94a**]: R = C$_6$H$_4$-4-C≡CSiMe$_3$, X = H; [**94a-Me**]: R = C$_6$H$_4$-4-C≡CSiMe$_3$, X = Me; [**94a-^{i}Pr**]: R = C$_6$H$_4$-4-C≡CSiMe$_3$, X = ^{i}Pr; [**94b**]: R = 3-*th*, X = H; [**94c-Me**]: R = C≡CSiMe$_3$, X = Me) were prepared in 44 – 84 % yields from reactions of *trans*-[RuCl(C≡CR)(dppe)$_2$] with half an equivalent of a 1,4-diethynylbenzene, HC≡CC$_6$H$_2$-2,5-X$_2$-4-C≡CH, in CH$_2$Cl$_2$ solutions in the presence of TlBF$_4$ and DBU. On reaction of [**94**] with one equivalent of FcPF$_6$ in CH$_2$Cl$_2$ solutions, *mono*-oxidised bimetallic complexes, [**94a**]PF$_6$, [**94a-Me**]PF$_6$ and [**94b**]PF$_6$, were obtained. The trimetallic complexes, *trans-trans*-[{Ru(dppe)$_2$}{μ-(C≡CC$_6$H$_4$-4-C≡C)Ru(dppe)$_2$(C≡CR)}$_2$], [**95**] ([**95a**]: R = C$_6$H$_4$-4-C≡CSiMe$_3$; [**95b**]: R = 3-*th*), were prepared similarly to [**94**], from reactions of *trans*-[RuCl(C≡CR)(dppe)$_2$] and *trans*-[Ru(C≡CC$_6$H$_4$-4-C≡CH)$_2$(dppe)$_2$], [**96**], (0.5 equiv.) in 43 – 66 % yields. Complexes [**43**], [**94**] and [**95**] coincidently exhibit the same number of reversible, one-electron oxidation events as integrated metals centres, although redox products likely involve significant alkynyl ligand character based on the significant (~ − 100 cm^{-1}) shift in key ν(C≡C) bands on oxidation. The *mono*-oxidation products [**94**]$^+$ and [**95a**]$^+$,

which may be described as organic 'mixed-valence' complexes, generally exhibit one principal NIR absorption band (of intra-ligand (π-π*) or organic intervalence charge transfer (IVCT) character), and several less intense NIR absorption bands (with metal-to-ligand charge transfer (MLCT) character) within the range 4000 – 16 000 cm^{-1}. For [**94**]$^{+}$, principal NIR bands are more intense and (generally) more asymmetric with increasing steric bulk of the bridge (indicating more delocalised character or Robin and Day Class III organic 'mixed-valence' complexes). Band profiles in the spectra of multi-metallic complexes (both neutral and oxidised) are complicated due the presence of rotamers. The molecular structures of *trans*-[RuCl(C≡CSiMe$_3$)(dppe)$_2$], [**38c**], *trans*-[Ru(C≡C-3-*th*)(C≡CC$_6$H$_4$-4-C≡CSiMe$_3$)(dppe)$_2$], [**97**], *trans*-[Ru(C≡CSiMe$_3$)(C≡CC$_6$H$_4$-4-C≡CSiMe$_3$)(dppe)$_2$], [**98**], and *trans*-[Ru(C≡CSiMe$_3$)(C≡CC$_6$H$_4$-4-C≡CH)(dppe)$_2$], [**99**], are reported and discussed. The heterobimetallic complex *trans*-[{(*th*-3-C≡C)(dppe)$_2$Ru}(μ-C≡CC$_6$H$_4$-4-C≡C){AuPPh$_3$}], [**100**], is also reported and used to form Au|molecule|Au junctions through the Thermally Induced Decomposition of Organometallic Complexes (TIDOC) method.

4.2. Introduction

In the design of molecular wires, incorporation of a single metal fragment along the conjugated wire backbone has been shown to exhibit several favourable properties such as increased solubility and facile tuning of both electronic and magnetic properties, in addition to versatile design strategies leading to more diverse molecular architectures, as described in previous Chapters. The incorporation of multiple metals and the advent of longer (> 4 nm) oligomeric *trans*-bis(alkynyl) metal complexes is therefore anticipated to be a figurative and literal extension of these studies. However, despite the possible range of properties that multi-metallic 'wire-like' complexes might offer, and their facile preparation *via* step-wise, modular synthetic schemes, such complexes have only been modestly explored in the literature. Although the longest single molecular wire to date is a rigid phenylethylene-based organic complex (Figure 4.1),[1] measuring 7 nm in length, similarly impressively long organometallic complexes are being developed, which predominantly feature polyynyl[2-5] backbones.

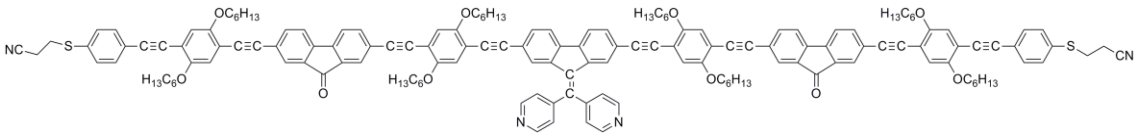

Figure 4.1: The longest organic molecular wire to be measured to date, featuring cyanoethyl-protected thiol groups that allow docking to gold surfaces and formation of Au|molecule|Au junctions following deprotection by NaOMe in THF solutions.[1]

The conductance of molecular wires decays upon increasing molecular length, either exponentially in the tunnelling regime ($G \propto e^{-\beta l}$), or geometrically in the case of hopping mechanisms ($G \propto \frac{1}{l}$).[6] The combination of multiple-metal fragments within a conjugated backbone can lead to surprisingly low tunneling decay constants (β). For example, Co^{II}-containing organometallic wires featuring terpyridine units exhibit an extremely low attenuation factor (β = 0.01 $Å^{-1}$),[7] where corresponding values for highly π-conjugated organic wires (featuring both aromatic and unsaturated fragments) are typically within the range 0.1 – 0.6 $Å^{-1}$.[8] Self assembly techniques were used to grow these Co^{II} wires directly on the electrode surface, with molecular lengths estimated to have reached up to 40 nm. For analogous Fe^{II} containing terpyridine wires, an increased resistance with molecular length (β = 0.28 $Å^{-1}$) was found, evincing the importance of metal identity on conductance. In addition, organometallic wires featuring Zn porphyrin units and thiol binding groups (reaching up to 5 nm in length) exhibit a very low attenuation factor (0.04 $Å^{-1}$)[6] as a result of the extensive π-conjugation in such systems.[9, 10]

Given the plethora of synthetic routes available for the preparation of conjugated, oligomeric, *trans*-bis(alkynyl) {$Ru(dppe)_2$} complexes (Chapter 1), it is unsurprising to find that these complexes have emerged as strong candidates as superior molecular wires. To this end, Frisbie and Rigaut have reported three series of organometallic wires containing one, two and three {$Ru(dppe)_2$} moieties within a conjugated phenylethynylene backbone featuring various surface binding groups (Figure 4.2).

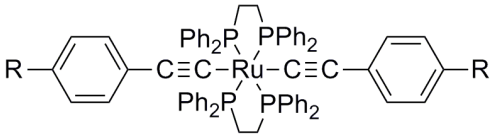

[**53**]: **R** = NC
[**56**]: **R** = CH_2SAc
[**59**]: **R** = $O(CH_2)_6SAc$

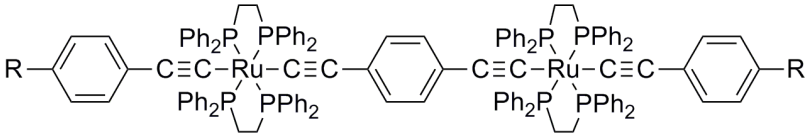

[**54**]: **R** = NC
[**57**]: **R** = CH_2SAc
[**60**]: **R** = $O(CH_2)_6SAc$

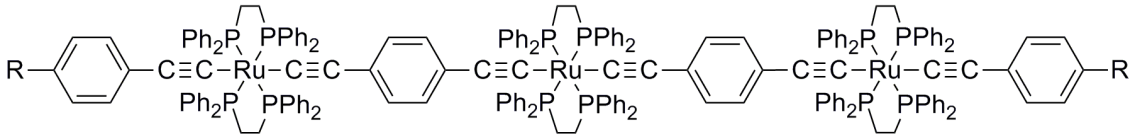

[**55**]: **R** = NC
[**58**]: **R** = CH_2SAc
[**61**]: **R** = $O(CH_2)_6SAc$

Figure 4.2: Organometallic molecular wires, [**53 – 61**], of increasing lengths featuring the {$Ru(dppe)_2$} fragment, as reported by Frisbie and Rigaut (R = NC,[11, 12] CH_2SAc[16, 17] or $O(CH_2)_6SAc$).[13, 14]

The mechanism by which charge travels from source to drain, *via* a molecular wire, in a molecular junction is dependent on molecular length. For shorter molecules such as *mono*-metallic *trans*-bis(alkynyl) complexes, where the continuum density of states of the two electrodes can span sufficiently far into the junction as to overlap and in effect be directly electronically coupled,[15] a direct electron tunnelling charge transport mechanism prevails. In this case, conductance decays exponentially with molecular length and is largely independent of temperature. For longer molecules, such as multi-metallic *trans*-bis(alkynyl) complexes, charge hopping (thermally permitted formal oxidations and / or reductions at discrete sites along the length of the molecular wire) is generally encountered. Contrastingly, this mechanism exhibits strong temperature dependence and evidence of this behaviour is the common diagnostic. Hopping mechanisms exhibit a much weaker molecular length dependence,[13] where $k_{ET} = \mathrm{N}^{-\eta}$ (k_{ET} = rate of electron transfer; N = number of hopping sites and the factor $\eta \approx 1 - 2$).[16] For example, within the series of mono-, bi- and trimetallic, redox-active molecular

wires shown in Figure 4.2 featuring {Ru(dppe)$_2$} units and thioacetate-protected thiol binding groups ([**59 – 61**]), the *mono*-metallic complex [**59**] (3.4 nm) exhibited one-step (metal to metal) direct tunneling behaviour, where conductance was independent over a range of temperatures (248 – 333 K), while both bimetallic [**60**] (4.6 nm) and trimetallic [**61**] complexes (5.8 nm) evinced the two-step (metal to molecule, molecule to metal) charge hopping regime, where conductance values were sensitive to changing temperature.[14] For the near-identical series of redox-active molecular wires contacted by isocyanide binding groups ([**53 – 55**]; Figure 4.2), both the *mono*-metallic [**53**] (2.4 nm) and bimetallic [**54**] (3.6 nm) complexes displayed tunneling behaviour.[12] This difference has been rationalised as a consequence of the particular binding group employed,[14] with the isocyanide anchor being directly conjugated within the 'wire-like' backbone whereas the alkyl-thiol groups (following deprotection) establish a molecule-electrode charge injection barrier. Curiously, the differences in molecular lengths were not considered. For the trimetallic complex [**55**] (4.9 nm), with isocyanide terminal fragments, Coulomb-blockade like behaviour was observed at low temperature.[12]

The crossover length between the tunnelling and hopping regimes for molecular wires of the type shown in Figure 4.2 has recently (2015) been determined as 6.48 nm (at zero bias and zero gate voltage) using a blend of computational and theoretical models.[17] Although this critical length is much higher than for OPEs (experimentally determined at ~ 2.75 nm),[18] the length at which the tunneling and hopping mechanisms crossover can be shifted upon application of external gate potential.

In this Chapter, a series of neutral, redox-active, *trans*-bis(alkynyl) {Ru(dppe)$_2$} complexes bearing both trimethylsilyl and thienyl binding groups (Figure 4.3) have been synthesised to further explore the effect of increasing the number of metal fragments within a conjugated wire backbone, supplementing previous studies in the literature of analogous complexes bearing isocyanide[11, 12] and thioacetate-protected thiol[13, 14] binding groups. The complexes shown in Figure 4.3 have been primarily studied by electrochemical and spectroelectrochemical methods as a means to elucidate the underlying electronic structures.

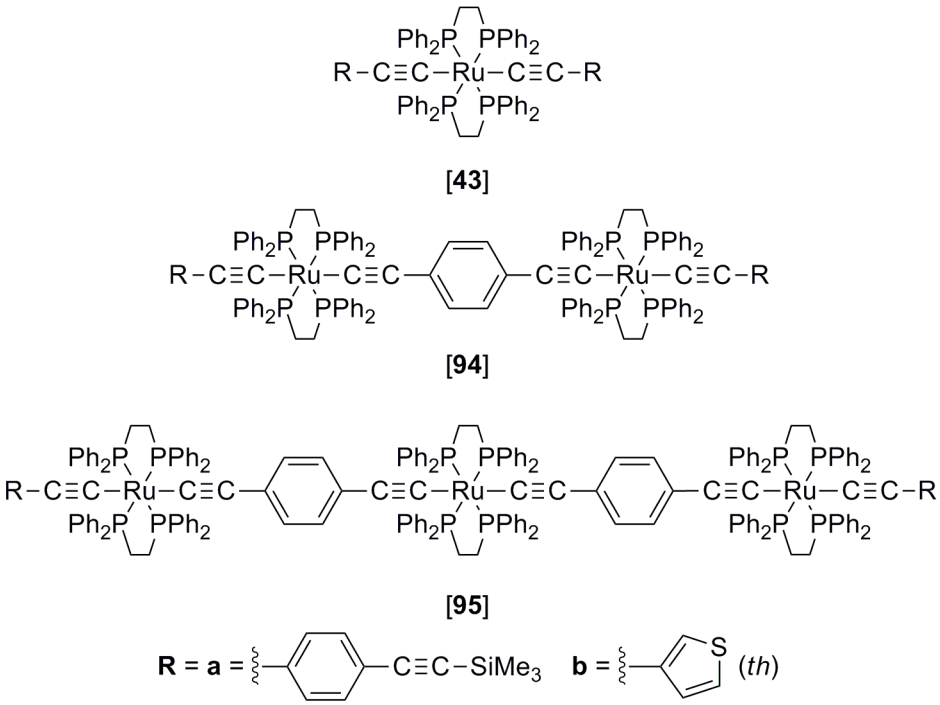

Figure 4.3: Series 1: complexes explored in this Chapter to determine the effect of i) changing the terminal fragment and ii) increasing the number of {Ru(dppe)$_2$} moieties on the underlying electronic structure.

The trimethylsilylethynyl and 3-thienyl terminal fragments in [**43, 94, 95**] were chosen with a view to allowing the study of these complexes within a molecular junction. However, such studies are time consuming and require specialised application of STM methods or nanofabricated junction methods. Alternatively, many studies have sought to gain a degree of information concerning 'wire-like' properties of linear molecular fragments by studying intramolecular electron transfer properties.[11, 13, 19, 20] In turn, these investigations are often conducted within the framework of 'mixed-valence' complexes,[xv] with analyses derived from the classical 'two-state' model developed by Hush[21] and Marcus,[22] and elaborated by others.[23, 24] Although reports describing the influence of the organic 'bridge' on electronic structure and charge transfer (or 'mixed-valence') characteristics in (-metal-bridge)$_n$- oligomers are common,[25-28] the influence of conformational freedom in the bridging component on the electronic structure of these complexes and hence their electron transfer behaviour, has hardly been considered. Interestingly, the 2-methyl fragment of the molecular structure of

[xv] A 'mixed-valence' state is conditioned if individual redox-active fragments within a molecule are present in different, stable states, with respect to disproportionation.

trans-[RuCl(C≡CC_6H_3-2-Me-4-NO_2)(dppe)$_2$][29] (Figure 4.4) lies within the pocket formed by the phenyl rings of one of dppe ligands.

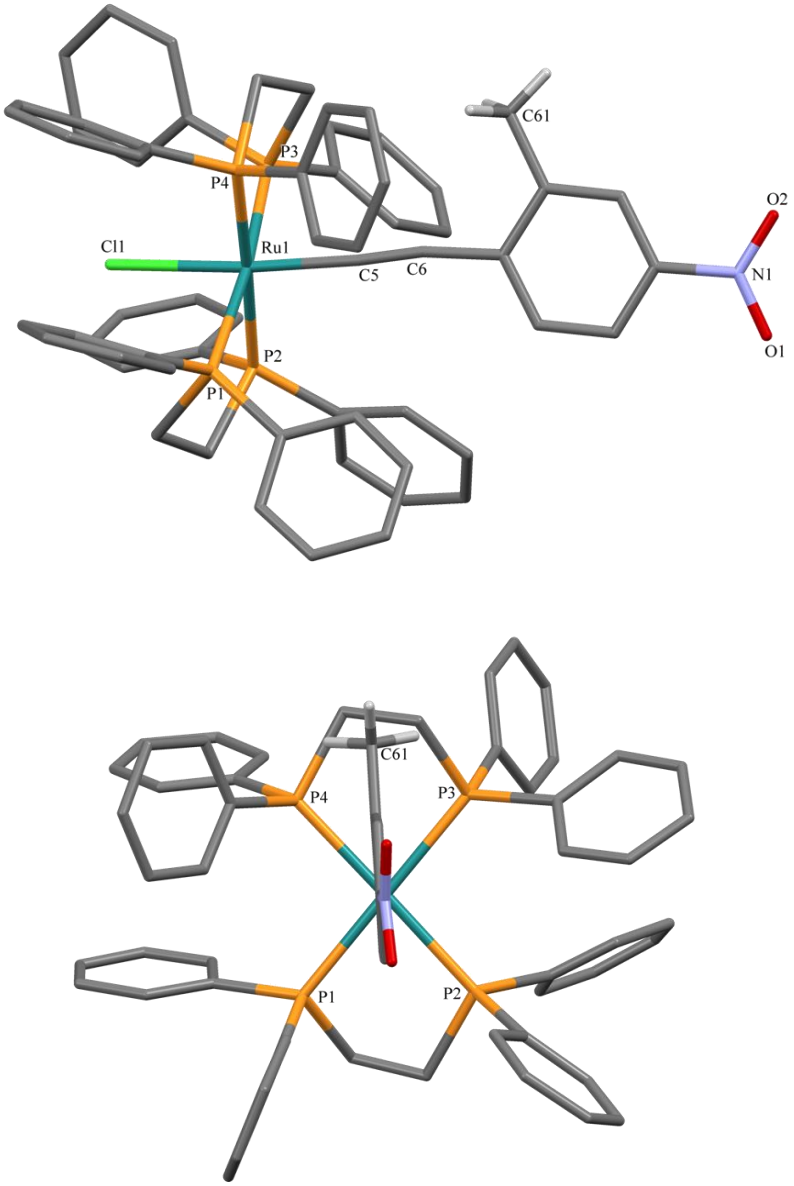

Figure 4.4: Solid state structure of *trans*-[RuCl(C≡CC_6H_3-2-Me-4-NO_2)(dppe)$_2$] viewed along (top) and down (bottom) the C≡C-Ru-Cl axis, labeled as reported, with selected hydrogens removed for clarity.[29]

This suggests that the rotational orientation of the nitrobenzene moiety can be sterically restricted hence limiting the range of available conformers or at least biasing the population distribution. The position of the nitrobenzene ring in the solid state structure

is such that conjugation of Ar(π) with the metal *d*-orbitals *via* the ethynyl fragment would be promoted. This feature may also persist in the solution state.

In order to further explore this concept, bimetallic complexes bridged by 1,4-diethynylbenzene ([**94a**]), 1,4-diethynyl-2,5-dimethylbenzene ([**94a-Me**]) and 1,4-diethynyl-2,5-diisopropylbenzene ([**94a-^{i}Pr**]) with trimethylsilyl binding groups (Figure 4.5) have been prepared here and their optoelectronic properties investigated by electrochemical and spectroelectrochemical methods.

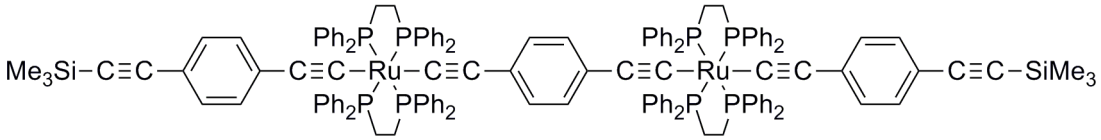

[**94a**]

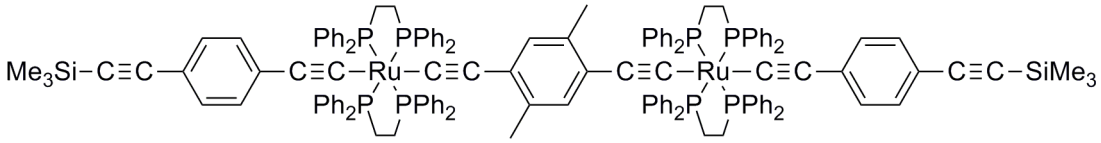

[**94a-Me**]

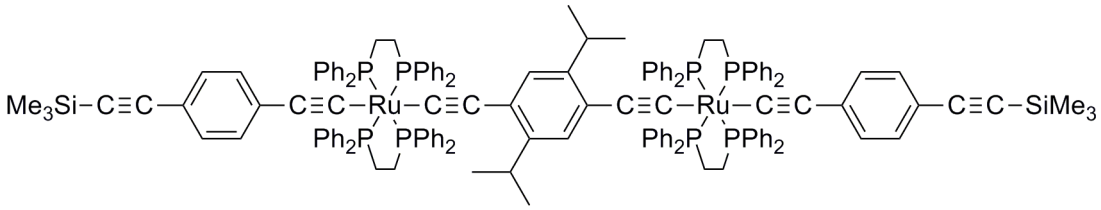

[**94a-^{i}Pr**]

Figure 4.5: Series 2: complexes explored in this Chapter to elucidate the steric role of bridging moiety on the underlying electronic structure.

Having explored the synthesis and electronic characterisations of multi-metallic 'wire-like' molecules, our attention turns to consideration of how such complexes might be integrated into device-like structures. As a soft, top-contact electrode fabrication technique, TIDOC has only emerged recently (2014) and so far has only been used for organic molecular wires.[30] In this technique, the preliminary step is formation of SAMs of gold-containing complexes onto gold surfaces *via* the Langmuir-Blodgett technique (left, Figure 4.6). Following this, complexes are annealed in order to simultaneously cleave Au-P (or Au-C)[30] bonds and reduce Au^{I} to Au^{0}, leading to the formation of

metallic gold nano-particles (GNPs) and gold nano-islands (GNIs) on the film surface (right, Figure 4.6). Electrical properties of these Au|monolayer|Au-nano-particle arrays are measured by recording I-V curves using conducting-probe atomic force microscopy (CP-AFM).

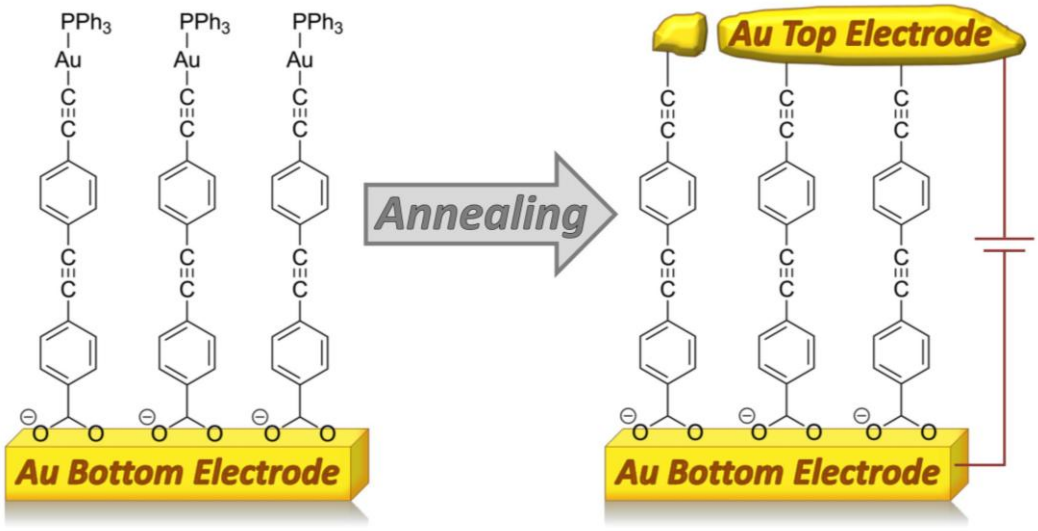

Figure 4.6: Illustrative diagram of the TIDOC method, where the preliminary step involves SAM assembly (left) followed by the formation of gold nano-particles and islands as the top-contact electrode (right) through annealing of a gold-containing complex.[30]

Some advantages of the TIDOC method over other traditional molecular junction forming methods include being facile and of low cost in addition to circumventing the top-contact electrode problem[xvi] without damaging or de-functionalising the wire sub-structure. As a future outlook, gold nano-particles generated in this way may even function as seeds in the deposition of a thicker, more uniform top-contact electrode. To these ends, the mixed metal Ru / Au complex, *trans*-[{(*th*-3-C≡C)(dppe)$_2$Ru}(μ-C≡CC_6H_4-4-C≡C){$AuPPh_3$}], [**100**] (Figure 4.7) has been prepared as the first organometallic complex to form Au|monolayer|Au junctions *via* the TIDOC method.

[xvi] Often, the top-contact electrode penetrates the organic film establishing shorter source-drain pathways leading to short-circuiting and an invalid device.

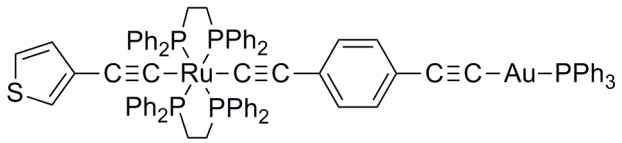

[**100**]

Figure 4.7: Target complex for exploring the capacity for the conductance of organometallic complexes to be measured using the TIDOC method.

4.3. Results and discussion

The syntheses of multi-metallic complexes discussed in this Chapter are based on a common synthetic strategy (Scheme 4.1). The strategy relies on the use of smaller *mono*-metallic complexes, *trans*-[RuCl(C≡CR)(dppe)$_2$] and *trans*-[Ru(C≡CR)$_2$(dppe)$_2$], and organic building blocks.

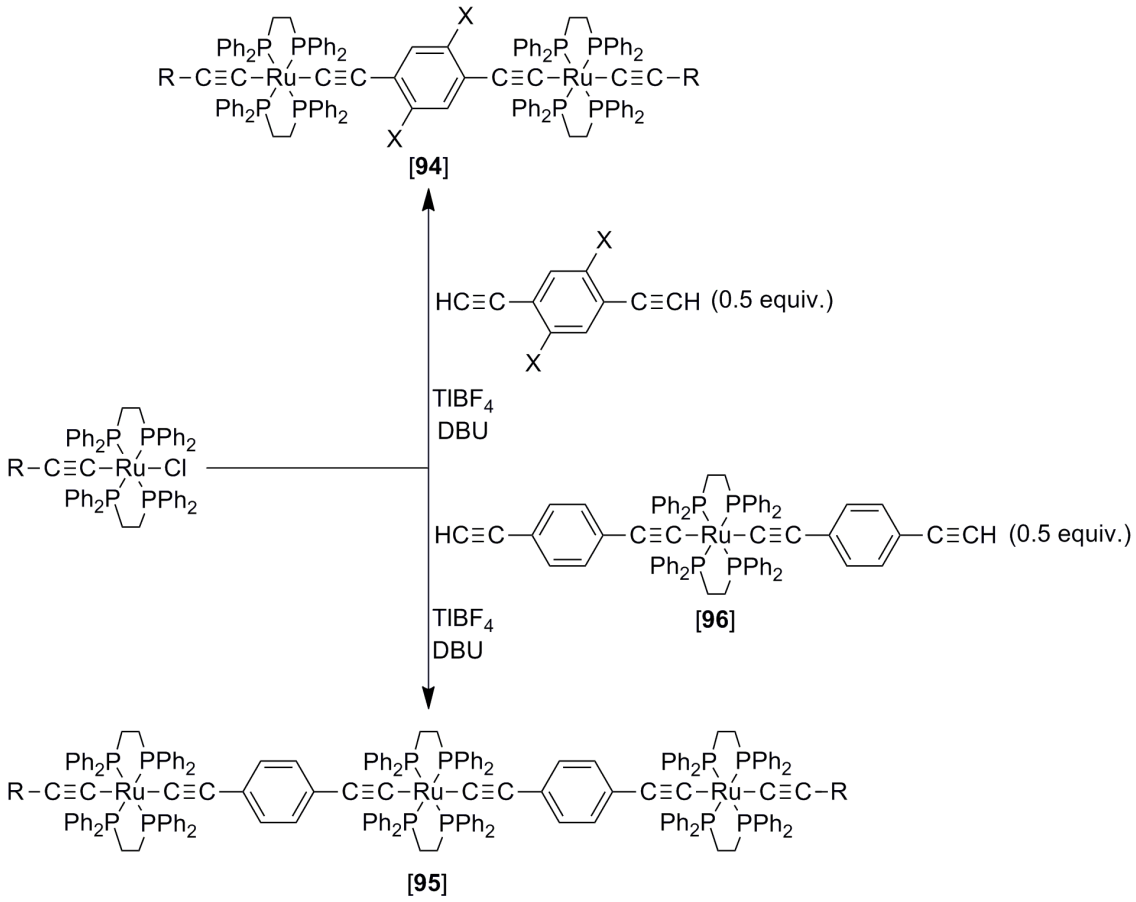

Scheme 4.1: The syntheses of bimetallic, [**94**], and trimetallic, [**95**], complexes described in this Chapter are based on a common synthetic strategy.

4.3.1. Synthesis of *mono*-metallic {Ru(dppe)$_2$} complexes: building blocks for higher molecular architectures

4.3.1.1. Mono-alkynyl complexes: RC≡C-[Ru]-Cl

In order to access the target multi-metallic complexes outlined for this Chapter (Figures 4.3 and 4.5), the *mono*-alkynyl complexes, *trans*-[RuCl(C≡CC$_6$H$_4$-4-C≡CSiMe$_3$)(dppe)$_2$],[31] [**38a**], *trans*-[RuCl(C≡C-3-*th*)(dppe)$_2$], [xvii] [**38b**], *trans*-[RuCl(C≡CSiMe$_3$)(dppe)$_2$], [**38c**], were prepared. Although [**38c**] has been

[xvii] The synthesis of [**38b**], from the reaction of [**36**]OTf with HC≡C-3-*th* (1.1 equiv.) and DBU (excess) in methanol, is presented with thanks to S. Bock of the PJL group. Electrochemical data of [**38b**], conducted in a [N^{n}Bu$_4$]PF$_6$ CH$_2$Cl$_2$ solution in an acetone / dry ice bath and referenced to ferrocene using a decamethylferrocene internal standard, includes: $E_{1/2}(1) = 0.04$ V *rev*; $\Delta E_p(1) = 0.09$ V; $E_{1/2}(2) = 0.81$ V *irrev*; $\Delta E_p(2) = 0.16$ V; ΔE_p(DMFC) = 0.05 V.

synthesised previously (in a 70 % yield from the reaction between *cis*-[$RuCl_2(dppe)_2$] (*cis*-[**35**]), MeLi (1.6 equiv.) and $Me_3SiC{\equiv}CSiMe_3$ (3 equiv.) in THF),[32] an alternative method is reported here which circumvents the use of alkynyl-lithium reagents. Addition of $HC{\equiv}CSiMe_3$ (1 equiv.) to a CH_2Cl_2 solution of [$RuCl(dppe)_2$]OTf ([**36**]OTf) and DBU (excess) resulted in the rapid (one hour) formation of [**38c**] (61 %), with spectroscopic data consistent with that previously published.[32] Crystallisation by layer diffusion ($CDCl_3$ / MeOH) gave single crystals of [**38c**] suitable for X-ray diffraction (Figure 4.8).

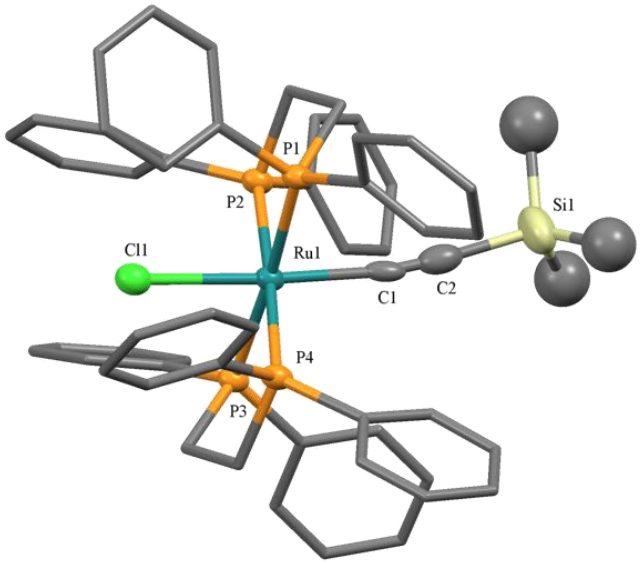

Figure 4.8: Solid state structure of [**38c**], with solvents of crystallisation (0.5 × $CDCl_3$, 0.5 × MeOH) and hydrogen atoms removed for clarity. Ellipsoids of key atoms are drawn at the 50 % probability level. Selected bond lengths / Å: Ru(1)-Cl 2.479(1), Ru(1)-C(1) 2.100(6), Ru(1)-P(1) 2.357(1), Ru(1)-P(2) 2.351(1), Ru(1)-P(3) 2.376(1), Ru(1)-P(4) 2.375(1), C(1)-C(2) 1.033(9). Selected bond angles / °: C(1)-Ru(1)-Cl 176.4(1), Ru-C(1)-C(2) 171.6(5), P(1)-Ru(1)-P(2) 82.53(4), P(3)-Ru(1)-P(4) 82.42(4), P(1)-Ru(1)-P(3) 176.05(4), P(2)-Ru(1)-P(4) 177.61(4).

The complex [**38c**] crystallizes in the monoclinic space group $P2_1/n$. The octahedral geometry about the metal centre is defined by two chelating *bis*-phosphine ligands, chloride and alkynyl ligands in a mutual *trans*-position. The Cl-Ru-C(1)≡C(2) bond angles and those between *trans*-phosphines, P(1)-Ru(1)-P(3) and P(2)-Ru(1)-P(4) are close to 180 ° (~ 175 °), while *cis*-phosphine bond angles, P(1)-Ru(1)-P(2) and

P(3)-Ru(1)-P(4), are close to 80 ° (~ 82 °) constrained by the chelate ring. Selected bond lengths of [**38c**] (this work), in addition with the previously reported structure *trans*-[RuCl(C≡CH)(dppe)$_2$][33] for comparison, are summarised in Table 4.1.

Table 4.1: Selected bond lengths (Å) for *trans*-[RuCl(C≡CSiMe$_3$)(dppe)$_2$], [**38c**], (this work) and *trans*-[RuCl(C≡CH)(dppe)$_2$].[33]

Complex	**Ru-Cl**	**Ru-C(1)**	**C(1)≡C(2)**	**Ru-P$_{avg}$**
[**38c**]	2.479(1)	2.100(6)	1.033(9)	2.365
trans-[RuCl(C≡CH)(dppe)$_2$]	2.584(2)	1.936(5)	1.190(5)	2.367

The very short C(1)≡C(2) bond length of [**38c**] is taken to be an artifact of the data collection method,[27] and will not be discussed further. The Ru-C(1) distance is significantly longer in [**38c**] than in the desilylated analogue *trans*-[RuCl(C≡CH)(dppe)$_2$], which is inconsistent with 'hyper-conjugation' effects to the silicon centre.[34] Rather, the longer Ru-C(1) distance in [**38c**] is accompanied by a shorter Ru-Cl distance, and *vice-versa*, which may be due to the electron withdrawing influence of the silyl moiety. The Ru-Cl bond lengths seem to be more responsive than the average Ru-P distances.

4.3.1.2. 'Symmetric' trans-bis(alkynyl) complexes: RC≡C-[Ru]-C≡CR

The 'symmetric' [xviii] *trans*-bis(alkynyl) complexes, *trans*-[Ru(C≡CC$_6$H$_4$-4-C≡CSiMe$_3$)$_2$(dppe)$_2$], [**43a**],[31] and *trans*-[Ru(C≡C-3-*th*)$_2$(dppe)$_2$], [**43b**],[xix] serve as the first members of Series 1 (Figure 4.3). Treatment of [**43a**] with TBAF.3H$_2$O (2 equiv.) gave *trans*-[Ru(C≡CC$_6$H$_4$-4-C≡CH)$_2$(dppe)$_2$], [**96**],[31] featuring unsubstituted terminal alkyne fragments, which serves as the central linker unit in the formation of trimetallic complexes, [**95**] (Scheme 4.1).

[xviii] The term 'symmetric' is adopted here to distinguish complexes *trans*-[Ru(C≡CR)$_2$(dppe)$_2$] from 'asymmetric' examples *trans*-[Ru(C≡CR)(C≡CR′)(dppe)$_2$].

[xix] The synthesis of *trans*-[Ru(C≡C-3-*th*)$_2$(dppe)$_2$], from reactions of [**36**]OTf and HC≡C-3-*th* (excess) with either TlBF$_4$ (1 equiv.) and DBU (excess) or KO^{t}Bu (2.5 equiv.) in CH$_2$Cl$_2$ solutions, is attributed with thanks to S. Bock within the PJL group

4.3.1.3. 'Asymmetric' trans-bis(alkynyl) complexes; RC≡C-[Ru]-C≡CR′

'Asymmetric' *trans*-bis(alkynyl) complexes *trans*-[Ru(C≡CR)(C≡CR′)(dppe)$_2$] present as complementary building blocks in the sequential assembly of multi-metallic complexes. The complexes *trans*-[Ru(C≡C-3-*th*)(C≡CC_6H_4-4-C≡C$SiMe_3$)(dppe)$_2$], [**97**], which offers both a surface binding thienyl group and a protected alkyne for further elaboration, and *trans*-[Ru(C≡C$SiMe_3$)(C≡CC_6H_4-4-C≡C$SiMe_3$)(dppe)$_2$], [**98**], were prepared in 75 and 91 % yields (respectively) through the room temperature reactions (5 − 16 hours) of [**38b**] or [**38a**] with $TlBF_4$ (1 equiv.), HC≡CC_6H_4-4-C≡C$SiMe_3$ (1 − 3 equiv.) and DBU (excess) in CH_2Cl_2 solutions, based on an earlier procedure reported by Low and co-workers.[31] Selective deprotection of the extended alkyne fragment in [**98**] can be achieved upon reaction of [**98**] with TBAF.3H_2O (1.3 equiv.), forming *trans*-[Ru(C≡C$SiMe_3$)(C≡CC_6H_4-4-C≡CH)(dppe)$_2$] (92 %), [**99**]. The strongly bound trimethylsilyl group on the shorter alkyne fragment has been noted previously.[32, 34]

Complexes [**97 − 99**] gave characteristic ^{1}H NMR spectra with two apparent doublet resonances for the two different environments of protons on the 1,4-phenylene fragment observed at δ 6.60 and 7.25 ppm ([**97**]), δ 6.41 and 7.21 ppm ([**98**]) and δ 6.43 and 7.21 ppm ([**99**]), with a mutual splittings of 8 Hz. In the $^{13}C\{^1H\}$ NMR spectra, the presence of the two different metal-alkynyl groups in complexes [**97 − 99**] were confirmed by two singlet resonances (in each case) between δ 111.3 – 124.3 ppm (Ru-C≡*C*) in addition to two quintet resonances (in each case) between δ 127.8 − 153.5 ppm ($^2J_{CP}$ = 15 Hz; Ru-*C*≡C) coupling to four mutually *cis*-phosphines. In the IR spectra, broad ν(RuC≡C) bands within the range 2058 – 2067 cm^{-1} further supported metal-alkynyl functionality, while ν(C≡C$SiMe_3$) bands at 2147 cm^{-1} in [**97, 98**] and a ν(C≡CH) band at 1994 cm^{-1} in addition with a ν(≡C-H) band at 3045 cm^{-1} in [**99**] confirmed the presence of the terminal alkynes. In the mass spectra, molecular ion peaks ([**97**], 1202; [**98**], 1192; [**99**], 1120 *m/z*) were observed. The purities of complexes [**97 − 99**] have been confirmed by elemental analyses. The structures of [**97**] (Figure 4.9), [**98**] (Figure 4.10) and [**99**] (Figure 4.11) have also been determined by single crystal X-ray diffraction, supporting structural assignments based on spectroscopy.

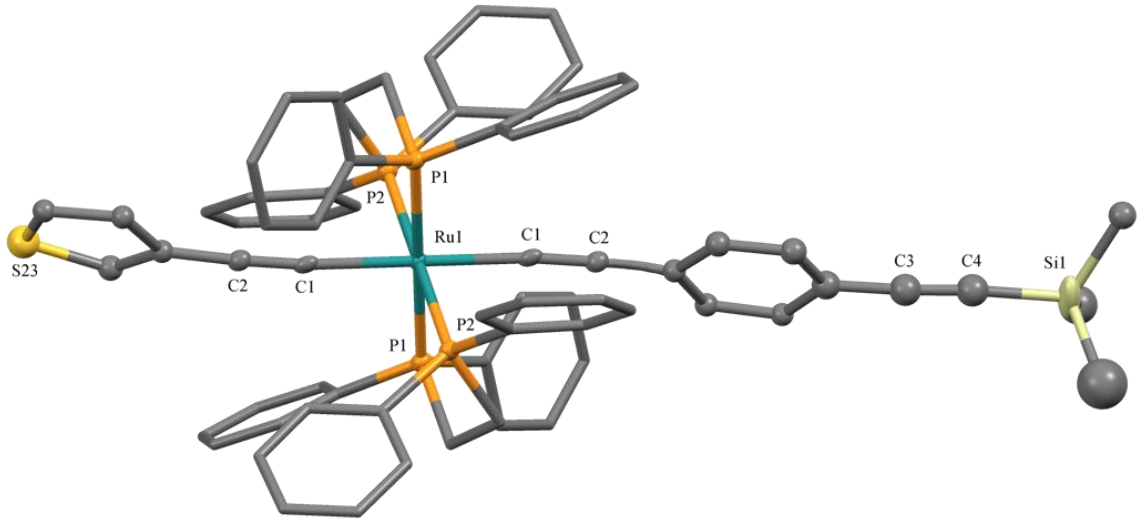

Figure 4.9: Solid state structure of [**97**] with solvent of crystallisation (1 × $CDCl_3$) and hydrogen atoms removed for clarity. Only one component of the disordered atoms is shown. Ellipsoids of key atoms are drawn at the 50 % probability level. Selected bond lengths / Å: Ru(1)-C(1) 2.049(5), Ru(1)-P(1) 2.3488(12), Ru(1)-P(2) 2.3554(12), C(1)-C(2) 1.220(7), C(3)-C(4) 1.238(17). Selected bond angles / °: C(1)-Ru(1)-C(1) 180.0, Ru-C(1)-C(2) 174.7(4), C(3)-C(4)-Si(1) 175.8(1), P(1)-Ru(1)-P(1) 180.00(6), P(1)-Ru(1)-P(2) 97.05(4), P(1)-Ru(1)-P(2) 82.95(4).

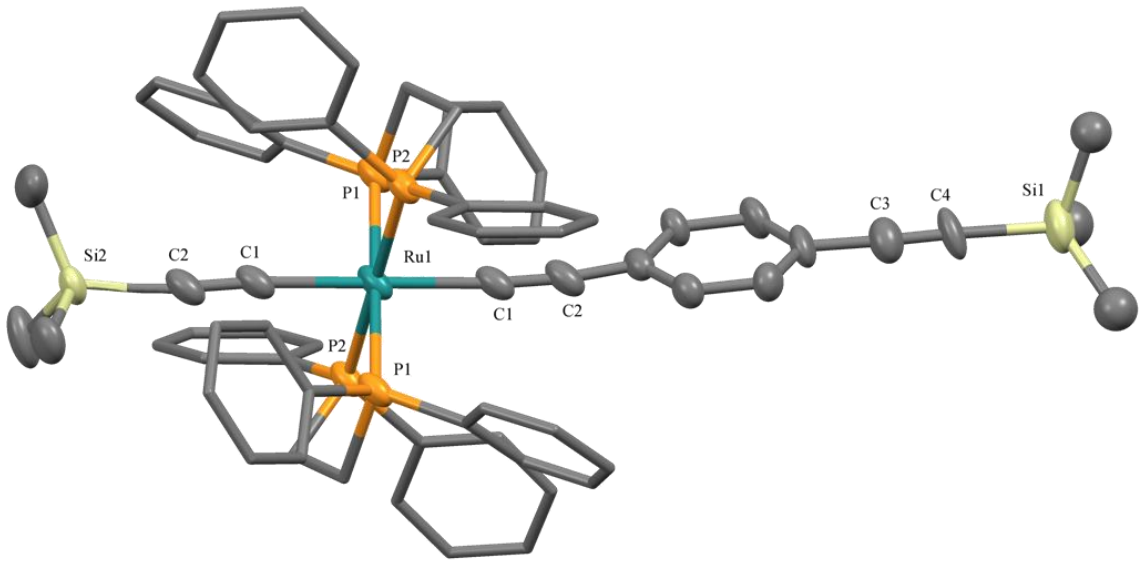

Figure 4.10: Solid state structure of [**98**] with solvent of crystallisation (1 × CH_2Cl_2) and hydrogen atoms removed for clarity. Only one component of the disordered atoms is shown. Ellipsoids of key atoms are drawn at the 50 % probability level. Selected bond lengths / Å: Ru(1)-C(1) 2.067(3), Ru(1)-P(1) 2.3534(8), Ru(1)-P(2) 2.3595(7), C(1)-C(2) 1.207(5), C(3)-C(4) 1.151(10). Selected bond angles / °: C(1)-Ru(1)-C(1) 180.0, C(3)-C(4)-Si(1) 176.0(8), Ru-C(1)-C(2) 175.6(3), Si(2)-C(2)-C(1) 174.0(3), P(1)-Ru(1)-P(1) 180.00(3), P(1)-Ru(1)-P(2) 97.30(3), P(1)-Ru(1)-P(2) 82.70(3).

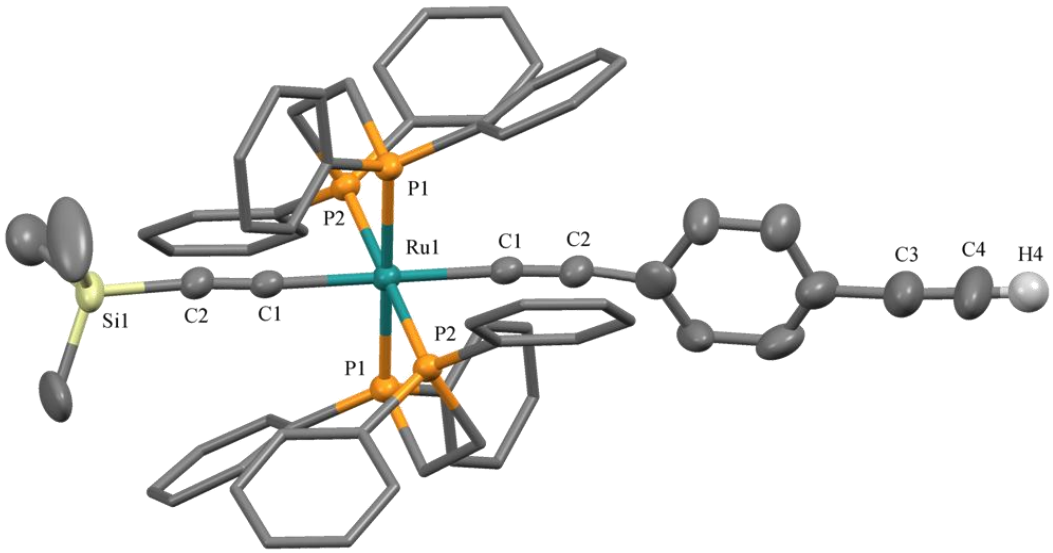

Figure 4.11: Solid state structure of [**99**] with selected hydrogen atoms removed for clarity. Only one component of the disordered atoms is shown. Ellipsoids of key atoms are drawn at the 50 % probability level. Selected bond lengths / Å: Ru(1)-C(1) 2.070(3), Ru(1)-P(1) 2.3512(7), Ru(1)-P(2) 2.3513(7), C(1)-C(2) 1.205(4), C(3)-C(4) 1.205(12). Selected bond angles / °: C(1)-Ru(1)-C(1) 180.0, Ru-C(1)-C(2) 175.7(2), Si(1)-C(2)-C(1) 171.8(3), C(24)-C(3)-C(4) 174.8(1), P(1)-Ru(1)-P(1) 180.00(4), P(1)-Ru(1)-P(2) 97.18(2), P(1)-Ru(1)-P(2) 82.82(2).

Complexes [**97 – 99**] are all found in triclinic crystal systems with $P\bar{1}$ space groups. The molecules [**97**] and [**98**] are situated on a crystallographic inversion centre. The structures suffer from some disorder in the position of the alkynyl ligands, and were refined with a 50 : 50 population of each alkynyl ligand at each site. Disordered solvents of crystallisation ([**97**]: $CDCl_3$; [**98**]: CH_2Cl_2) were also present in the crystal. The structure of [**97**] is isomorphous with [**98**].

Disorder with respect to the position of the alkyne fragments has been noted previously for 'asymmetric' *trans*-bis(alkynyl) complexes, *trans*-[Ru(C≡CR)(C≡CR′)(dppe)$_2$].[31] This disorder, combined with the fact that the aryl ring π-systems of the 1,4-diethynyl benzene fragments in complexes [**97 − 99**] are not well aligned with Ru-P bonds (*i.e.* the Ar(π) systems are not strongly conjugated with the Ru(*d*) orbitals, with positive C_{ortho}-C_{ipso}-Ru-(P*C*H$_2$*C*H$_2$P)$_{centroid}$ angles determined between 39.2 – 63.4 °) meaning

limited structural correlations with the electronic character of the substituent,[31] impedes detailed structural analysis of complexes [**97** − **99**].

4.3.2. Synthesis of bimetallic {Ru(dppe)$_2$} complexes

4.3.2.1. Symmetric bimetallic complexes: RC≡C-[Ru]-C≡CC$_6$H$_2$-2,5-X$_2$-4-C≡C-[Ru]-C≡CR

Homo-bimetallic *trans*-bis(alkynyl) ruthenium complexes are not uncommon having been prepared by a number of different synthetic strategies.[11, 13, 26, 35-37] The choice of strategy depends on the specific ancillary ligands, terminal alkynyl substituents and bridging motifs. Bearing strongest similarities with the work presented here is the synthetic account given by Rigaut and Frisbie in their formation of bimetallic *trans*-bis(alkynyl) complexes based on the {Ru(dppe)$_2$} moiety featuring thioacetate-protected thiol binding groups.[13] The complexes *trans*-[{(RC$_6$H$_4$-4-C≡C)(dppe)$_2$Ru}$_2$(μ-C≡CC$_6$H$_4$-4-C≡C)] (R = CH$_2$SAc, [**57**]; O(CH$_2$)$_6$SAc, [**60**]; 67 − 97 %) were synthesised through the initial reaction (24 hours, r.t.) of [**36**]OTf with HC≡CC$_6$H$_4$-4-C≡CH (0.5 equiv.) in a CH$_2$Cl$_2$ solution, generating the bimetallic vinylidene complex, *trans*-[{Cl(dppe)$_2$Ru}$_2${μ-(=C=CHC$_6$H$_4$-4-CH=C=)}][OTf]$_2$ (71 %), followed by subsequent reaction (4 days, r.t.) with HC≡CC$_6$H$_4$-4-R (R = CH$_2$SAc, O(CH$_2$)$_6$SAc; 3 equiv.), NaPF$_6$ (4 equiv.) and NEt$_3$ (excess) in CH$_2$Cl$_2$ (Scheme 4.2). The extended duration of the latter reaction is presumably as a consequence of the strongly bound *trans*-chloride and the choice of NaPF$_6$ as a halide abstracting agent.

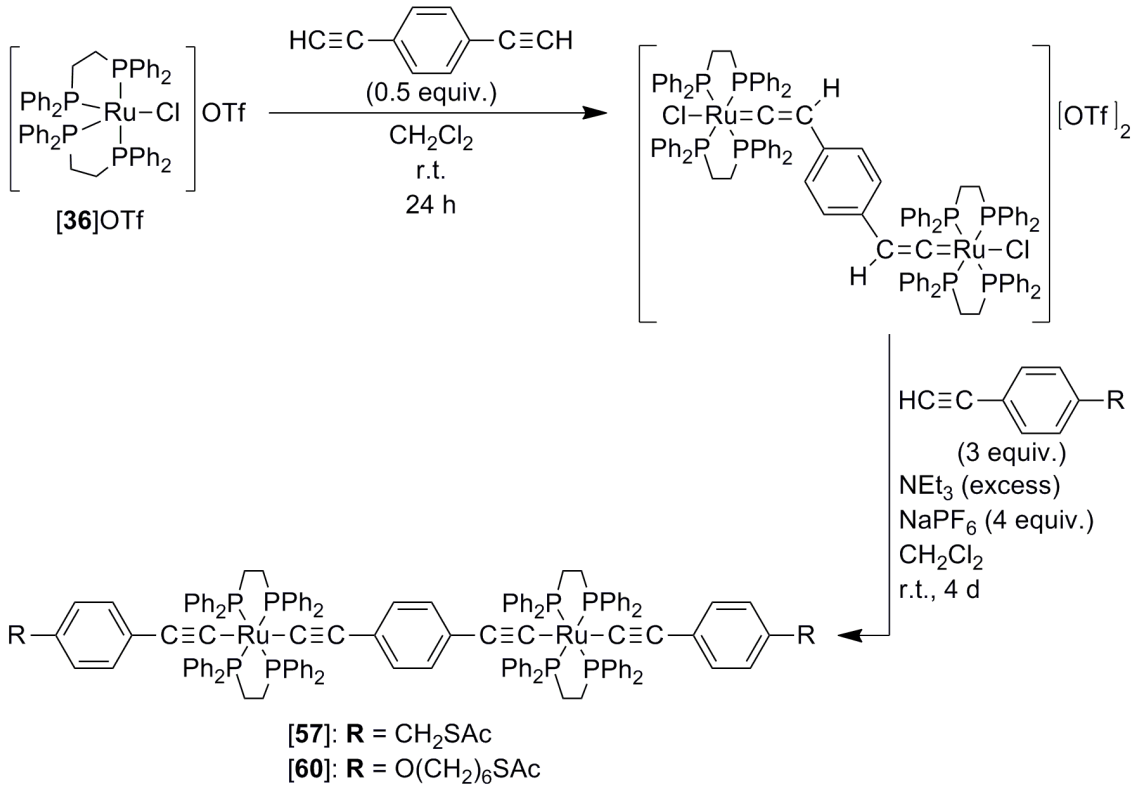

Scheme 4.2: Synthesis of bimetallic complexes [**57, 60**].[13]

Alternatively, bimetallic ruthenium *trans-bis*(alkynyl) complexes can be built up in a step-wise manner by initial formation of a *mono*-metallic vinylidene, addition of the bridging unit (in a basic medium) followed by reaction with a further *mono*-metallic vinylidene (in a basic medium) to produce the target bimetallic compound, as has been reported for the preparation of *trans*-[{(HC(=O)NHC$_6$H$_4$-4-C≡C)(dppe)$_2$Ru}$_2$(μ-C≡CC$_6$H$_4$-4-C≡C)] (Scheme 4.3).[11] In this case, the bimetallic complex was obtained in a similarly high yield (70 %) but in a much reduced reaction time (20 hours) compared with the preparations of [**57, 60**]. The bimetallic complex [**54**], bearing the isocyanide surface contacting groups, was subsequently prepared by reaction of *trans*-[{(HC(=O)NHC$_6$H$_4$-4-C≡C)(dppe)$_2$Ru}$_2$(μ-C≡CC$_6$H$_4$-4-C≡C)] with POCl$_3$ (1.2 equiv.) and NH^{i}Pr$_2$ (3 equiv.) in a CH$_2$Cl$_2$ solution (Scheme 4.3)

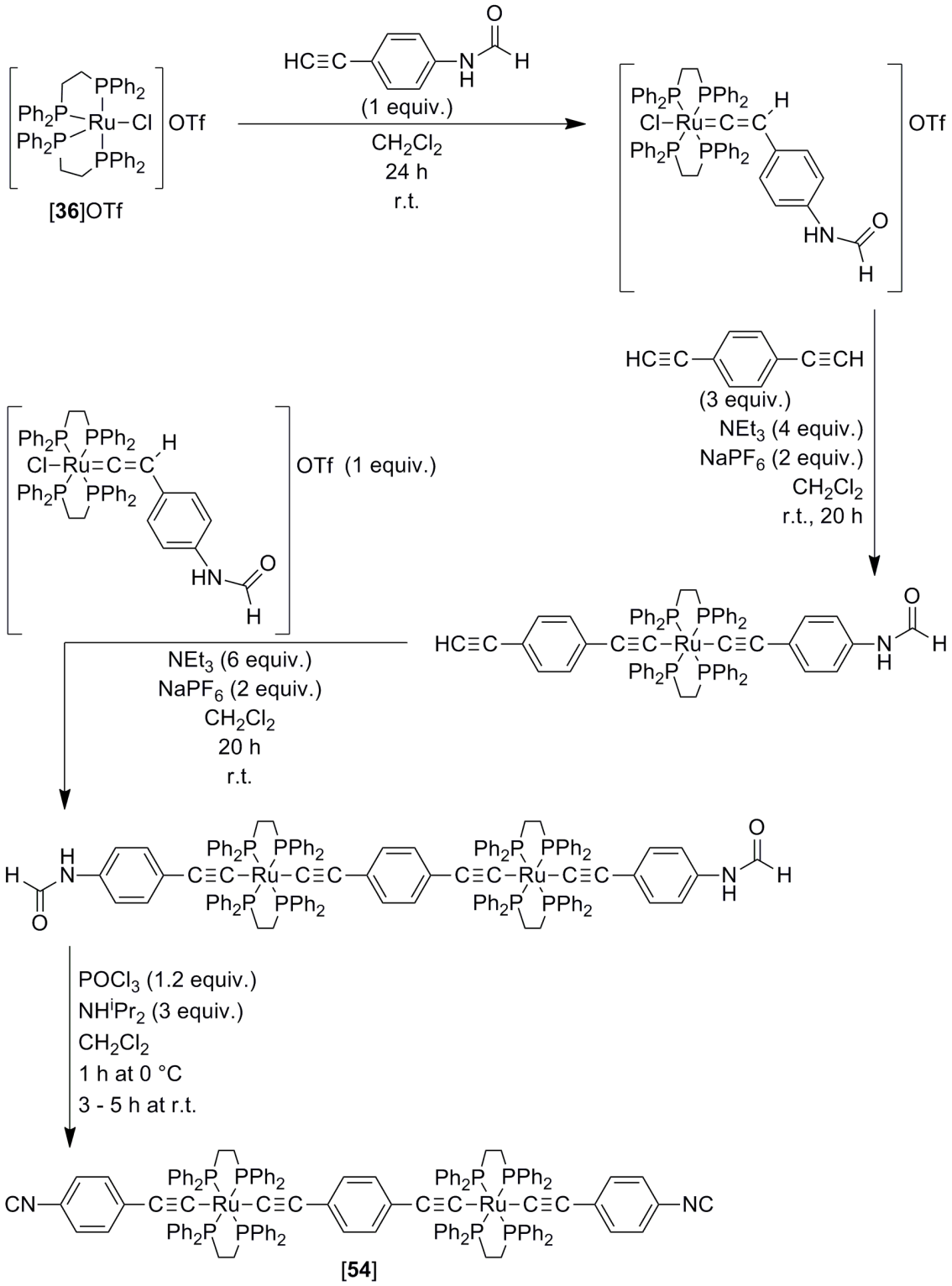

Scheme 4.3: Synthesis of bimetallic complexes, *trans*-[{(HC(=O)NHC$_6$H$_4$-4-C≡C)(dppe)$_2$Ru}$_2$(μ-C≡CC$_6$H$_4$-4-C≡C)] and [**54**].[11]

Given that 'asymmetric', *mono*-metallic *trans*-bis(alkynyl) complexes can be prepared on the {Ru(dppe)$_2$} scaffold in rapid (30 minute) reactions involving Tl^I salts as strong, non-oxidising halide abstracting agents, we elected to explore the synthesis of novel bimetallic complexes using this protocol.[31] The slow addition (dropwise over 30 minutes – one hour) of dilute CH_2Cl_2 solutions of terminal alkyne, HC≡CC_6H_2-2,5-X_2-4-C≡CH (0.5 equiv.; X = H, Me, ^{i}Pr), to dilute CH_2Cl_2 room temperature solutions of *trans*-[RuCl(C≡CR)(dppe)$_2$] (R = C_6H_4-4-C≡C$SiMe_3$, [**38a**]; 3-*th*, [**38b**]; $SiMe_3$, [**38c**]), $TlBF_4$ (1 – 1.5 equiv.) and DBU (excess), followed by further reaction (ten minutes − overnight), resulted in the formation of bimetallic complexes, *trans*-[{(RC≡C)(dppe)$_2$Ru}$_2$(μ-C≡CC_6H_2-2,5-X_2-4-C≡C)], [**94**], in 44 to 84 % yields (Scheme 4.4).

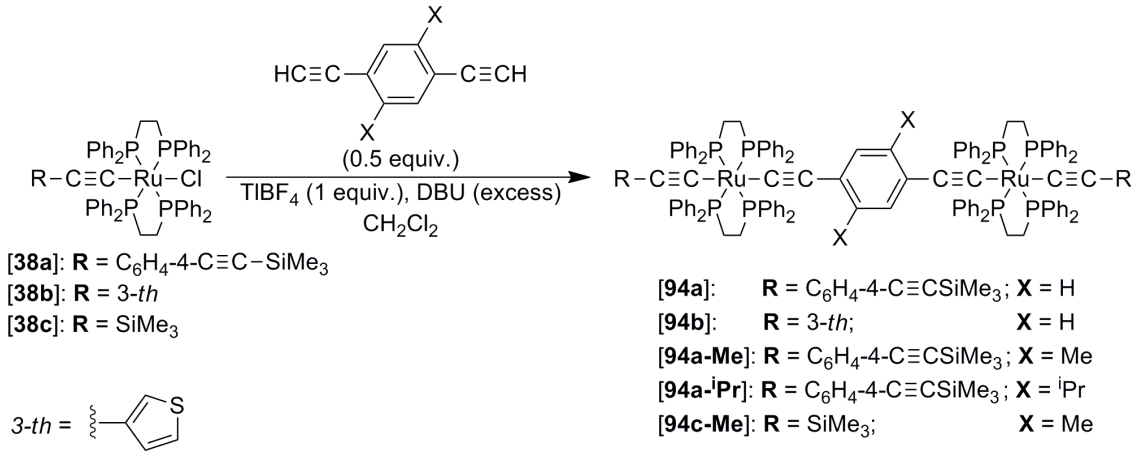

Scheme 4.4: Synthetic route to bimetallic complexes, [**94**], outlined in this Chapter.

Evidence for the formation of [**94**] arises from the ^{1}H NMR spectra, where the four equivalent phenylene protons of the bridging ligand in [**94a**] and [**94b**] are observed as singlet resonances at δ 6.72 and 6.68 ppm, respectively. For [**94a-Me**] and [**94c-Me**], the two equivalent arylene protons are observed as singlets at δ 6.40 ([**94a-Me**]) and 6.07 ppm ([**94c-Me**]), while the two equivalent methyl groups of the same central fragment are observed as singlets at δ 1.86 ([**94a-Me**]) and 1.75 ppm ([**94c-Me**]). In the case of [**94a-^{i}Pr**], the arylene protons are similarly observed as a singlet resonance (δ 6.70 ppm) while the two methyl groups of the isopropyl fragments are observed as a doublet at 0.93 ppm ($^3J_{HH}$ = 6 Hz) showing coupling to the proton of the isopropyl fragment.

For all complexes of [**94**], singlet resonances in the $^{31}P\{^{1}H\}$ NMR spectra are observed within the range δ 53.4 – 55.5 ppm, confirming the equivalent *trans*-arrangement of four phosphine ligands in each bimetallic complex. As a result of the low intensity of quaternary carbons, combined with the relatively low solubility of these bimetallic complexes, the characteristic quintet resonances corresponding to the Ru-*C* carbon nuclei were not observed in the $^{13}C\{^{1}H\}$ NMR spectra. However, singlet resonances corresponding to the Ru-C≡*C* carbon nuclei were found between δ 115.2 – 120.4 ppm. In the IR spectra, broad ν(RuC≡C) bands were observed between 2038 – 2066 cm^{-1} (and at 1992 cm^{-1} for ν(C≡CSiMe_3) in [**94c-Me**]). The purities of [**94a**], [**94a-Me**] and [**94b**] have been confirmed by elemental analyses. Satisfactory analyses of [**94a-^{i}Pr**] and [**94c-Me**] have not yet been obtained, but spectroscopic information points to the absence of significant organic or organometallic impurities.

In contrast to the other complexes of [**94**], [**94c-Me**] is oxygen and / or moisture sensitive, as the yellow solid of [**94c-Me**] can be observed turning red in air (over ~ 10 − 15 minutes) whilst yellow solutions of [**94c-Me**] rapidly (~ 2 minutes) turn deep red in reagent grade CH_2Cl_2 (neither dried or degassed). As the IR spectrum of the deep red / CH_2Cl_2 solution showed formation of an intense NIR band, oxidation of [**94c-Me**] (forming [**94c-Me**]$^{+}$) is thought to occur. An identical NIR spectrum was observed during the spectroelectrochemical investigation of [**94c-Me**] (see section 4.6), confirming aerial oxidation and discounting vinylidene formation by protonation, which are also typically prepared as red solutions. Similar rapid oxidation pathways were also observed for crude samples of *trans*-[{(Me_3SiC≡C)(dppe)$_2$Ru}$_2$(μ-C≡CC_6H_4-4-C≡C)], [**94c**], which could not be isolated and fully characterised due to time constraints. Nevertheless, the studies of [**94c-Me**] and the preliminary evidence from [**94c**] evinces the additional stabilising effects of terminal aryl ethynyl ligands, as in [**94a**], [**94a-Me**], [**94a-^{i}Pr**] and [**94b**].

4.3.2.2. 'Mixed-valence' 'symmetric' bimetallic complexes: [RC≡C-[Ru]-C≡CC_6H_2-2,5-X_2-4-C≡C-[Ru]-C≡CR]$^{+}$

Following formation of neutral bimetallic complexes, [**94**], and evidence of facile oxidation of [**94c-Me**], *mono*-oxidised complexes [**94a, a-Me, b**]PF_6 were prepared in

high yields (91 – 93 %) from reactions (one hour, r.t.) of [**94a, a-Me, b**] with $FcPF_6$ (1 equiv.) in CH_2Cl_2 solutions (Scheme 4.5).

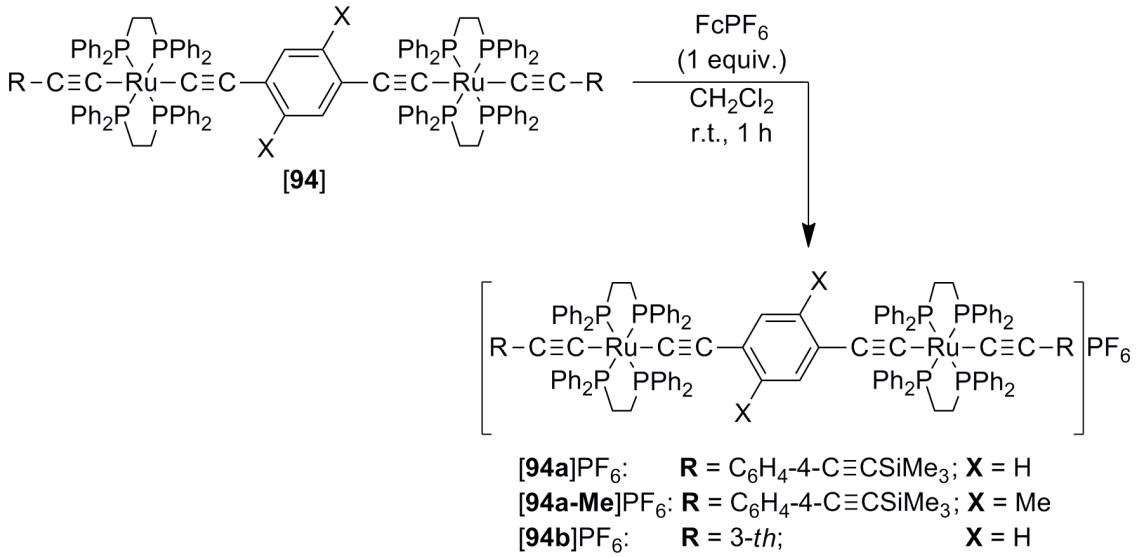

Scheme 4.5: Synthetic route to *mono*-oxidised bimetallic complexes, [**94a, a-Me, b**]PF_6.

Evidence for the formations of [**94a, a-Me, b**]PF_6 principally arises from the observation of intense, broad NIR (IVCT) bands within the range 5468 – 5715 cm^{-1} and intense $\nu([C\equiv C]^+)$ bands some 80 – 100 cm^{-1} lower in frequency than $\nu(C\equiv C)$ bands observed in the precursors ([**94a, a-Me, b**]: $\nu(C\equiv C)$ 2036 – 2067 cm^{-1}; [**94a, a-Me, b**]PF_6: 1953 – 1966 cm^{-1}). In CH_2Cl_2 solutions in air, [**94a, a-Me, b**]PF_6 were found to decompose completely over 10 – 13 hours (monitored by IR spectroscopy). In contrast, the solid 'mixed-valence' form is stable in air for ~ two weeks.

4.3.2.3. 'Asymmetric', mixed-metal (Ru / Au) bimetallic complexes

The Ru / Au mixed-metal bimetallic complex, *trans*-[{(*th*-3-C≡C)$(dppe)_2$Ru}(μ-C≡CC_6H_4-4-C≡C){$AuPPh_3$}], [**100**], was obtained in a high yield (84 %) from the initial reaction (15 minutes, r.t.) of [**97**] with TBAF.$3H_2O$ (1 equiv.) in a mixed MeOH / THF solution (generating [**99**] *in situ*) followed by the addition of NaOH (1 equiv.) and [$AuCl(PPh_3)$] (1 equiv.) in a reaction that completed

over 42 hours at room temperature (Scheme 4.6). The related complex [{(η^5-C_5H_5)(PPh_3)$_2$Ru}(μ-C≡CC_6H_4-4-C≡C){$AuPPh_3$}] has been previously prepared in a 49 % yield from the reaction of [Ru(C≡CC_6H_4-4-C≡CH)(PPh_3)$_2$(η^5-C_5H_5)], [**93a**], with [Au(Cl)(PPh_3)] (1 equiv.) in a $NHEt_2$ solution in the presence of catalytic copper iodide.[38]

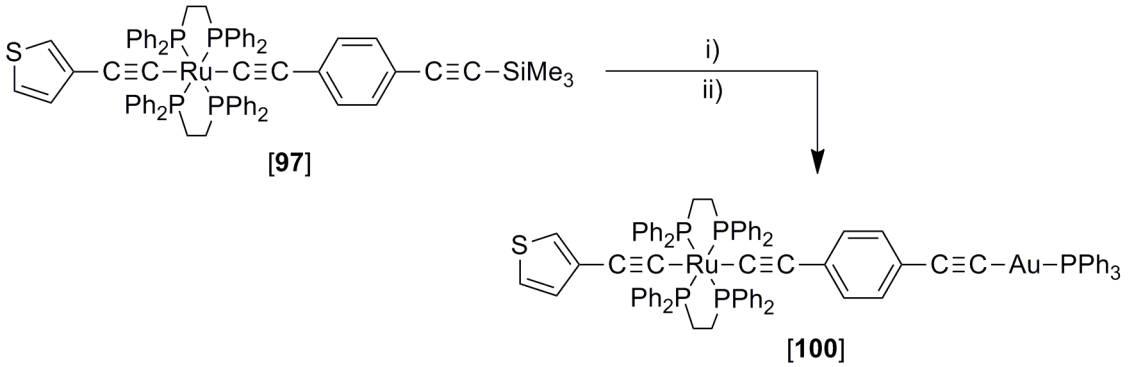

i) TBAF.3H_2O (1 equiv.), MeOH / THF, r.t., 15 m
ii) NaOH (1 equiv.), [Au(Cl)(PPh_3)] (1 equiv.), r.t., 42 h

Scheme 4.6: Synthetic route to the Ru / Au mixed-metal bimetallic complex, [**100**].

Evidence for the formation of [**100**] includes two apparent doublet resonances in the ^{1}H NMR spectrum (δ 6.60 and 7.28 ppm), with a mutual splitting of 8 Hz, corresponding to the two environments of the four protons comprising the 1,4-diethynylbenzene bridge. In the $^{31}P\{^1H\}$ NMR spectrum, two singlets corresponding to the two different phosphine ligands are observed at δ 43.6 and 54.6 ppm (*c.f.* [Au(Cl)(PPh_3)]: δ_P 30.1 ppm;[39] [**97**]: δ_P 54.5 ppm). Although resonances corresponding to the alkynyl quaternary carbons (Ru-*C*) were of too low intensity to be observed in the $^{13}C\{^1H\}$ NMR spectrum, multiple alkynyl functionality was evinced by IR spectroscopy, where two principal ν(MC≡C) bands were observed in the spectrum at 2060 and 2053 cm^{-1}. The purity of [**100**] has been confirmed by elemental analysis, which provides further evidence to support the identity of the complex.

4.3.3. Synthesis of trimetallic *trans*-bis(alkynyl) {Ru(dppe)$_2$} complexes: RC≡C-[Ru]-C≡CC$_6$H$_4$-4-C≡C-[Ru]-C≡CC$_6$H$_4$-4-C≡C-[Ru]-C≡CR

The synthesis of linear, trimetallic complexes follows that of the bimetallic complexes where one equivalent of a *mono*-alkynyl complex is reacted with half an equivalent of the (now metal-containing) linker unit (Scheme 4.1). The slow addition (dropwise, over 30 – 40 minutes) of dilute CH_2Cl_2 solutions of [**96**] (0.5 equiv.) to dilute CH_2Cl_2, room temperature solutions of *trans*-[RuCl(C≡CR)(dppe)$_2$] (R = C$_6$H$_4$-4-C≡CSiMe$_3$, [**38a**]; 3-*th*, [**38b**]), $TlBF_4$ (1 – 1.5 equiv.) and DBU (excess), followed by a further overnight reaction, resulted in the formation of trimetallic complexes; *trans-trans*-[{(dppe)$_2$Ru}{μ-(C≡CC$_6$H$_4$-4-C≡C)Ru(dppe)$_2$(C≡CR)}$_2$], [**95**], ([**95a**]: R = C$_6$H$_4$-4-C≡CSiMe$_3$; [**95b**]: R = 3-*th*), in 43 − 66 % yields (Scheme 4.7).

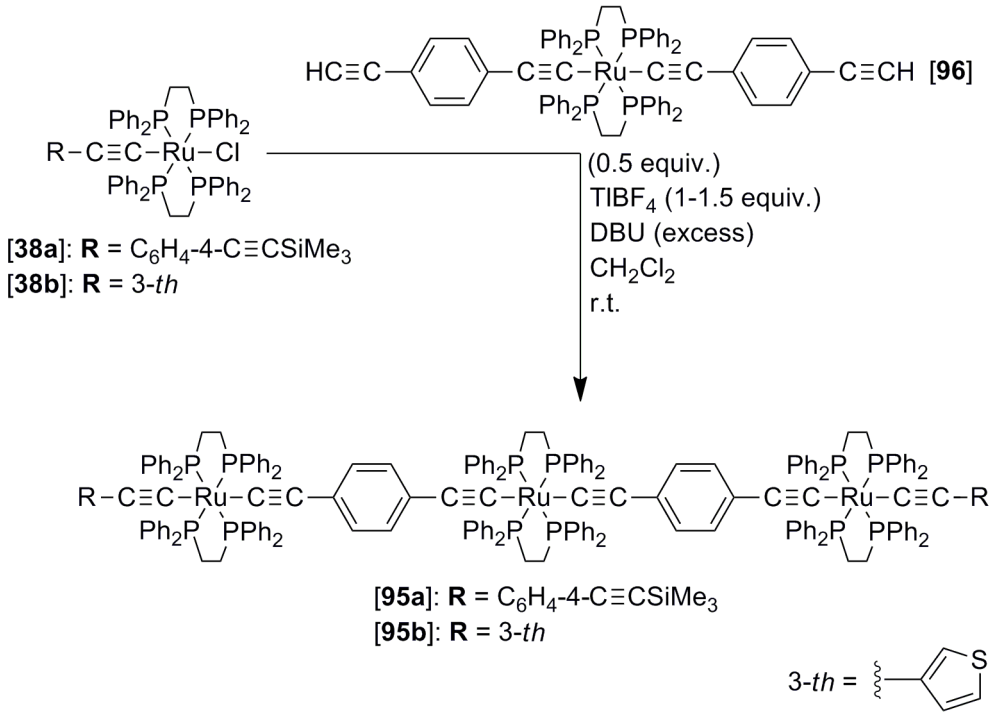

Scheme 4.7: Synthetic route to trimetallic complexes, [**95**], outlined in this Chapter.

Notably, the trimetallic complexes *trans-trans*-[{(dppe)$_2$Ru}{μ-(C≡CC$_6$H$_4$-4-C≡C)Ru(dppe)$_2$(C≡CC$_6$H$_4$-4-R)}$_2$] (R = CH_2SAc, [**58**]; $O(CH_2)_6SAc$, [**61**]; 63 − 95 %) have previously been prepared from room temperature reactions of *trans*-[RuCl(=C=CHC$_6$H$_4$-4-R)(dppe)$_2$][OTf] with [**96**] (0.5 equiv.), $NaPF_6$ (2 equiv.)

and NEt_3 (excess) in CH_2Cl_2 solutions lasting over four days[13] while *trans-trans*-[{(dppe)$_2$Ru}{μ-(C≡CC_6H_4-4-C≡C)Ru(dppe)$_2$(C≡CC_6H_4-4-C≡CNH(C=O)H)}$_2$] (60 %) has been obtained from the reaction (20 hours, r.t.) of *trans*-[Ru(C≡CC_6H_4-4-C≡CH)(C≡CC_6H_4-4-NH(C=O)H)(dppe)$_2$] with *cis*-[**35**] (0.5 equiv.), $NaPF_6$ (2 equiv.) and NEt_3 (excess) in a CH_2Cl_2 solution.[11]

Evidence for the formation of the trimetallic complexes [**95**] is given by the ^{1}H NMR spectra, where C*H*$_2$ protons corresponding to the phosphine backbones of the three {Ru(dppe)$_2$} motifs are, in each case, observed as two multiplets in a 2 : 1 ratio within the ranges of δ 2.57 − 2.82 ppm ([**95a**]) and δ 2.50 − 2.76 ppm ([**95b**]), inferring the different {Ru(dppe)$_2$} environment of the central metal fragment to the two terminal {Ru(dppe)$_2$} fragments. Low spectral resolution, as a result of the increasing insolubility of these higher molecular weight molecules in NMR solvents, precluded absolute assignments of the eight bridge protons, with them instead being observed as a collection of resonances (reported as multiplets) within the ranges of δ 6.62 − 6.72 ppm ([**95a**]) and δ 6.62 − 6.76 ppm ([**95b**]). In the ^{31}P{^{1}H} NMR spectra, two singlets are observed in a 2 : 1 ratio at δ 54.6 and 54.7 ppm ([**95a**]) and δ 54.72 and 54.74 ppm ([**95b**]), again implicating the relative proportions of the two different phosphine environments. Although multiplet and singlet resonances corresponding to the quaternary carbons of the alkynyl fragments (Ru-*C* and Ru-C≡*C*) were of too low intensity to be observed in the ^{13}C{^{1}H} NMR spectra (with the exception of [**95a**] where Ru-C≡*C* resonances are observed at ~ 117 ppm), metal-alkynyl functionality was supported by IR spectroscopy, where a principal ν(RuC≡C) band was observed at 2057 cm^{-1} for [**95a**], whilst a collection of ν(RuC≡C) bands, of similar intensities, were observed for [**95b**] (between 2024 – 2084 cm^{-1}). In the mass spectra, although molecular ions were not observed, significant fragment ions that supported the structural identity of [**95**] were observed. For [**95a**], these included [{(Me$_3$SiC≡CC_6H_4-4-C≡C)(dppe)$_2$Ru}(μ-C≡CC_6H_4-4-C≡C){Ru(dppe)$_2$} + MeCN + H]$^+$ (2158 *m/z*) and [Ru(C≡CC_6H_4-4-C≡CSiMe$_3$)(dppe)$_2$ + MeCN]$^+$ (1136 *m/z*) whereas for [**95b**] these included: [{(*th*-3-C≡C)(dppe)$_2$Ru}(μ-C≡CC_6H_4-4-C≡C){Ru(dppe)$_2$(C≡CC_6H_4-4-C≡CH)} + H]$^+$ (2153 *m/z*), [Ru(C≡C-3-*th*)(C≡CC_6H_4-4-C≡CH)(dppe)$_2$ + H]$^+$ (1131 *m/z*) and [Ru(C≡C-3-*th*)(dppe)$_2$ + MeCN]$^+$ (1046 *m/z*). Although the purity of [**95a**] has been

confirmed by elemental analysis, a satisfactory analysis of [**95b**] has not yet been achieved.

4.4. Electrochemistry

The electrochemical responses of complexes [**43**], [**94**] and [**95**] were examined by cyclic voltammetry (CV) in 0.1 M tetra-butylammonium hexafluorophosphate ($[N^nBu_4]PF_6$) CH_2Cl_2 solutions in an acetone / dry ice bath, unless otherwise stated (Table 4.2). All potentials are quoted against the ferrocene / ferrocenium couple ($[Fe\{\eta^5\text{-}C_5H_5\}_2]$ / $[Fe\{\eta^5\text{-}C_5H_5\}_2]^+$) = 0 V) using an internal decamethylferrocene / decamethylferrocenium reference ($[Fe\{\eta^5\text{-}C_5Me_5\}_2]$ / $[Fe\{\eta^5\text{-}C_5Me_5\}_2]^+ = -0.48$ V).[40] Notably, the electrochemical profile of [**43a**] has been previously studied,[31] although in an alternative electrolyte solution ($[N^nBu_4]BF_4$ / CH_2Cl_2), hence has been re-measured here for consistency and completeness. In all cases, the number of *reversible*[xx] oxidation processes parallels the number of integrated metal centres (although these redox processes are not necessarily metal-centred), where i_{pa} / i_{pc} and ΔE_p (E_{pc} - E_{pa}) values are comparable with those of the (by definition) reversible internal standard decamethylferrocene upon increasing scan rates, which is consistent with the analogous series of $\{Ru(dppe)_2\}$ molecular wires described by Rigaut and co-workers.[12, 13] At room temperature there was some minor evidence of electrochemical-chemical (EC) behavior, with i_{pc} values marginally larger than i_{pa} values, but with improvement to the chemical reversibility evident at reduced temperatures (dry ice / acetone bath), where current ratios approach unity.

[xx] Defining electrochemical reversibility as the case when $i_{pa} / i_{pc} \approx 1$, $\Delta E_p \approx 60$ mV and $i_p \propto \nu^{1/2}$, where the rate of electron transfer is mass transport limited.

Table 4.2: Selected electrochemical data (V) of *mono*-metallic, [**43**], bimetallic, [**94**], and trimetallic, [**95**], {Ru(dppe)$_2$} complexes.[xxi]

Complex	$E_{1/2}(1)$	$E_{1/2}(2)$	$E_{1/2}(3)$	$E_{1/2}(4)$	ΔE_{1-2}	ΔE_{2-3}	ΔE_{3-4}
[**43a**]	0.10[a]	0.91[c]	-	-	0.81	-	-
[**43b**]	0.00[a]	0.81[c]	-	-	0.82	-	-
[**94a**]	− 0.18[a]	0.13[a]	0.84[b]	1.03[c]	0.31	0.71	0.19
[**94a-Me**]	− 0.20[a]	0.12[a]	0.86[b]	1.09[c]	0.32	0.74	0.23
[**94a-^{i}Pr**]	− 0.19[a]	0.13[a]	0.88[b]	1.09[c]	0.32	0.75	0.21
[**94b**]	− 0.19[a]	0.12[a]	0.80[b]	1.05[c]	0.31	0.68	0.25
[**94c-Me**]	− 0.30[a]	0.08[a]	0.93[c]	1.08[c]	0.38	0.85	0.15
[**95a**][d]	− 0.27[a]	− 0.06[a]	0.15[a]	0.61[b]	0.21	0.21	0.46
[**95b**]	− 0.19[a]	− 0.04[a]	0.14[a]	0.66[b]	0.15	0.18	0.52
[**95b**][d]	− 0.26[a]	− 0.08[a]	0.13[b]	0.63[c]	0.18	0.21	0.50

[a]reversible; [b]quasi-reversible; [c]irreversible; [d]0.2 M [N^nBu_4]PF_6 $CHCl_3$ solution, acetone / dry ice bath

The 'symmetric' *trans*-bis(alkynyl) complexes [**43**] display a single, reversible oxidation and a single, irreversible oxidation at higher potentials, consistent with previously published data for similar complexes.[31] The two oxidations of [**43**] exhibit a degree of alkynyl character, where both $E_{1/2}$(1, 2) of [**43b**] bearing electron releasing thienyl fragments are more facile than [**43a**] (by 0.10 V) bearing modestly electron accepting trimethylsilyl substituents.

Bimetallic complexes, [**94**], generally display four oxidations in the CH_2Cl_2 solvent window (Figure 4.12). The first two are reversible while the third is *quasi*-reversible and the fourth irreversible with the exception of [**94c-Me**] where both the third and fourth oxidations are irreversible. Interestingly, the corresponding oxidation events between the four extended complexes of [**94**] ([**94a**], [**94a-Me**], [**94a-^{i}Pr**] and [**94b**]) occur at very similar potentials, only differing in each individual case by 0.01 – 0.08 V. Consequently, changing the terminal fragment ([**94a**] *vs.* [**94b**]) or bridging fragment ([**94a**] *vs.* [**94a-Me**] *vs.* [**94a-^{i}Pr**]) has little effect on the underlying electronic structure of these complexes. This collectively indicates a highly delocalised structure for [**94**]$^{n+}$, especially given that the oxidation potentials of [**43**] were notably different as a result of

[xxi] Additional characterisation for [**95b**] includes: $E_{1/2}$(5), 0.82 V[b]; $E_{1/2}$(6), 0.95 V[c]; $E_{1/2}$(7), 1.09 V[c]. Electrochemical data for the mixed-metal complex [**100**] has been included in the experimental section.

the electronic character of the terminal fragment. In keeping with these observations, the oxidation potential values for [**54**] ($E_{1/2}(1) = -0.20$; $E_{1/2}(2) = 0.11$; $E_{1/2}(3) = 0.94$ V) collected under analogous conditions are comparable with the data reported here.[11] Between [**43**] and [**94**], $E_{1/2}(1)$ values are lower in [**94**] (by 0.18 – 0.30 V) as a result of increased conjugation.[11, 13] The low $E_{1/2}(1, 2)$ values of [**94**] may lead to further application of these complexes as convenient redox switches, but such studies are beyond the scope of this work.

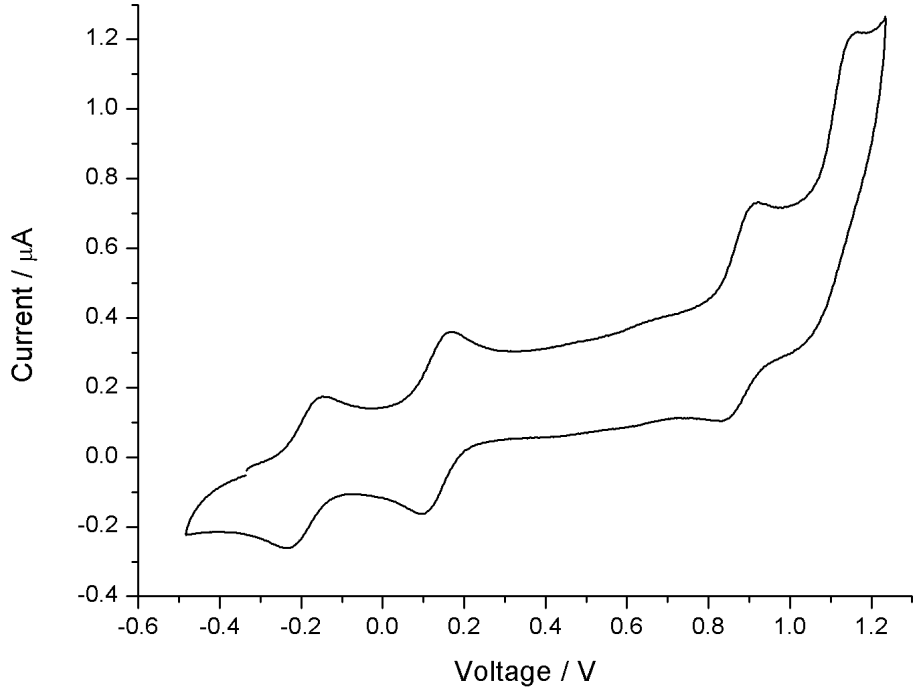

Figure 4.12: Cyclic voltammogram of [**94a-^{i}Pr**] as a representative bimetallic complex, showing four redox waves within the solvent window. The voltammogram was obtained from a 0.1 M $[N^{n}Bu_4]PF_6$ CH_2Cl_2 solution cooled with a dry ice / acetone bath at a scan rate of 100 mVs^{-1} and has been referenced against internal decamethylferrocene (not shown).

Complex [**95a**] proved to be too insoluble in 0.1 M $[N^{n}Bu_4]PF_6$ / CH_2Cl_2 for accurate measurement. In contrast, the more soluble complex [**95b**] exhibited several one-electron redox waves (the first three reversible, the fourth *quasi*-reversible) in this medium (Figure 4.13).

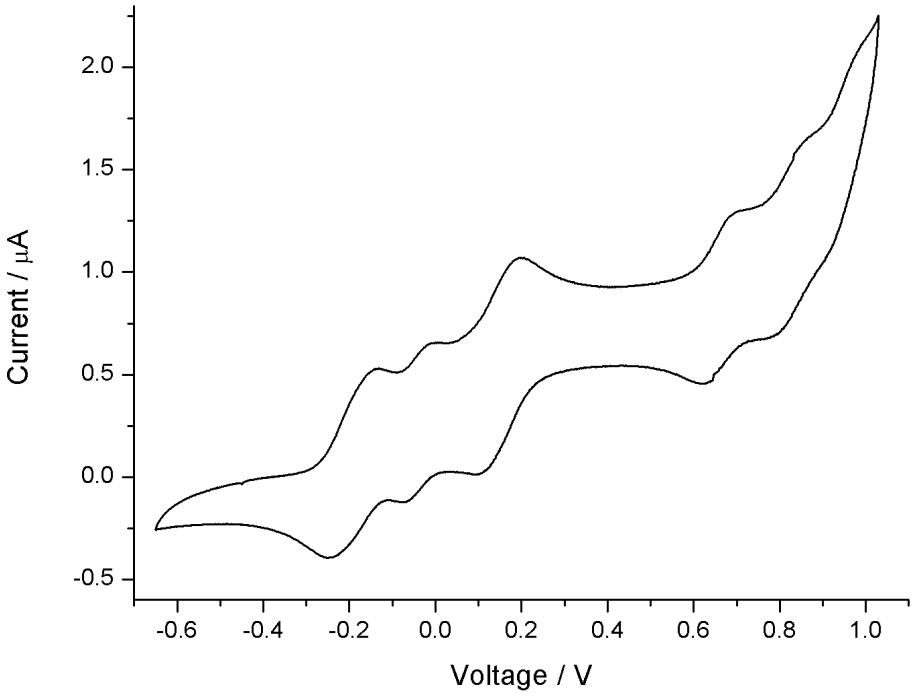

Figure 4.13: Cyclic voltammogram of [**95b**] showing several redox waves within the solvent window. The voltammogram was obtained from a 0.1 M $[N^nBu_4]PF_6$ CH_2Cl_2 solution cooled with a dry ice / acetone bath at a scan rate of 100 mVs^{-1} and has been referenced against internal decamethylferrocene (not shown).

Both [**95a**] and [**95b**] were soluble in the alternative electrolyte solution 0.2 M $[N^nBu_4]PF_6$ / $CHCl_3$, hence the electrochemical responses were also examined in this medium. In each case, only four redox waves were observed (Figure 4.14), with the additional processes noted above (Figure 4.13) assumed to occur outside the solvent window. Between the two structures of [**95**], redox potentials $E_{1/2}(1-4)$ differ by only 0.01 – 0.02 V indicating that, as with the bimetallic series, changing the terminal fragments from –C≡C-3-*th* to –C≡CC_6H_4-4-C≡C$SiMe_3$ does not significantly affect the redox chemistry.

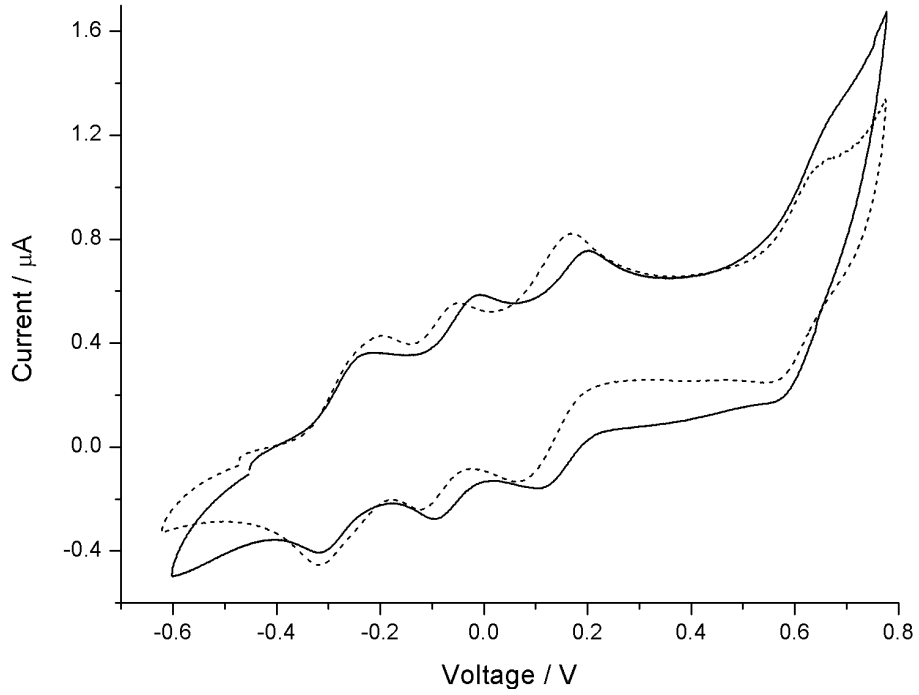

Figure 4.14: Cyclic voltammograms of [**95a**] (black solid line) and [**95b**] (black dashed line) displaying four oxidations at similar potentials within the solvent window. Scans were conducted in 0.2 M $[N^nBu_4]PF_6$ $CHCl_3$ solutions, cooled with dry ice / acetone baths, at rates of 100 mVs^{-1} and have been referenced against internal decamethylferrocene (not shown).

4.5. Spectroelectrochemistry

Although variation of the electronic properties of phosphine ligands in order to optimise through-charge transport has already been explored,[41-43] the importance of both steric and symmetry effects are somewhat lacking. Recently, the Low and Kaupp groups subjected a series of *trans*-$[Ru(C{\equiv}CC_6H_4\text{-}4\text{-}R)_2(dppe)_2]$ complexes (R = Me, C_5H_{11}, OMe, COOMe, NO_2, $C{\equiv}CSiMe_3$ [**43a**], $C{\equiv}C^tBu$, NH_2) to electrochemical, spectroelectrochemical and computational investigation.[31] The convoluted NIR band envelope produced upon *mono*-oxidation of *trans*-$[Ru(C{\equiv}CC_6H_4\text{-}4\text{-}R)_2(dppe)_2]$, forming *trans*-$[Ru(C{\equiv}CC_6H_4\text{-}4\text{-}R)_2(dppe)_2]^+$, could be explained by considering populations of rotamers in solution rather than only a single, lowest energy structure. From potential energy surface calculations, three closely lying minima were identified (Figure 4.15). Such structures differ in the orientation of the aromatic rings of the aryl-alkynyl fragments with respect to the RuP_4 plane and the five membered rings formed by the

Ru(dppe) coordination motif. Low intramolecular barriers permit each of these distinct conformers to be thermally populated in solution.

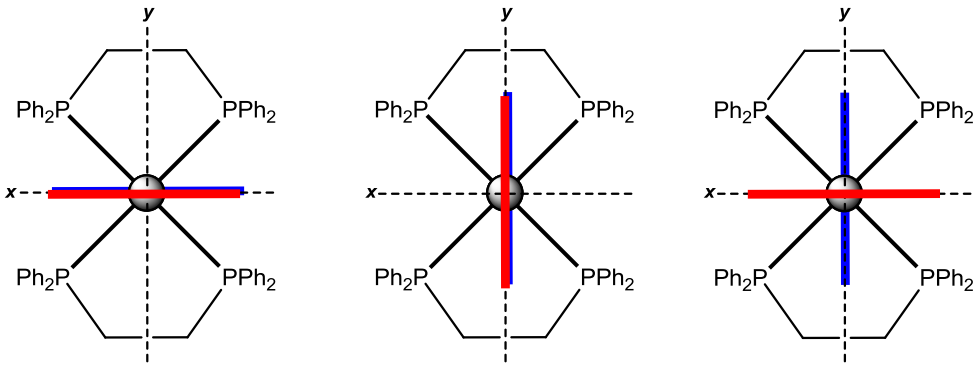

Figure 4.15: Schematic representations of the three lowest energy rotamers found for *trans*-[Ru(C≡CC_6H_4-4-R)$_2$(dppe)$_2$]$^+$ complexes, where red and blue lines represent the aromatic rings of the two aryl-alkynyl fragments (-C≡C*C_6H_4*-4-R).[31]

Whilst calculations with no single conformation could adequately model the experimentally observed spectra, it was found that the superposition of computationally determined absorption spectra for the various conformations of *trans*-[Ru(C≡CC_6H_4-4-R)$_2$(dppe)$_2$]$^+$ (Figure 4.15) better described the experimentally observed NIR band envelopes. The lowest energy NIR transitions were found to represent IVCT (LMCT) transitions within the most delocalised, planar conformations whereas the higher energy NIR transitions (often appearing as band shoulders) reflect MLCT / IL (π to π^*) transitions occurring within complexes exhibiting a partial loss of conjugation following rotations of the phenyl fragment about the C≡C-Ru-C≡C axis. In addition to this, the collaboration of Paul, Rigaut and Humphrey found that the differences in energy between the two conformations, where the aromatic ring of the aryl-alkynyl fragment is either perpendicular to or bisects the diphosphinoethane (dpe) fragment (Figure 4.16) in a series of *trans*-[RuCl(C≡CC_6H_4-4-R)(dpe)$_2$]$^+$ (R = H, NO_2, OMe, NMe_2) complexes, is largest for complexes bearing electron releasing groups, evincing a conformational population bias based on the electronics of the R substituent, with the bisecting conformation (right, Figure 4.16) being the lowest energy form in all cases.[44]

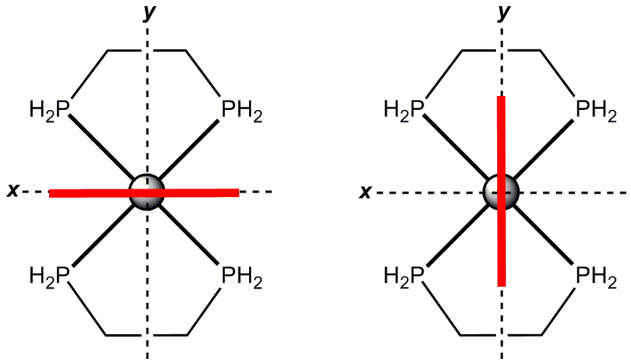

Figure 4.16: Schematic representations of *trans*-[RuCl(C≡CC_6H_4-4-R)(dpe)$_2$]$^+$ complexes, where red lines represent the aromatic ring of the aryl-alkynyl fragment (-C≡C*C_6H_4*-4-R), showing the aryl ring perpendicular to (left) or bisecting (right) the *bis*-diphosphinoethane (dpe) motif.

4.5.1. IR spectroelectrochemistry

Using the work described above as a foundation, the two reversible, one-electron oxidations of bimetallic complexes [**94**] (forming [**94**]$^+$ and [**94**]$^{2+}$) in 0.1 M [N^{n}Bu$_4$]PF$_6$ CH_2Cl_2 solutions (Figure 4.17) and the three reversible, one-electron oxidations of the trimetallic complex [**95a**] (forming [**95a**]$^+$, [**95a**]$^{2+}$ and [**95a**]$^{3+}$) in a 0.2M [N^{n}Bu$_4$]PF$_6$ $CHCl_3$ solution (Figure 4.25), were explored by IR spectroelectrochemistry. During the spectroelectrochemical experiment, oxidised products were generated systematically *in situ* by increasing the applied potential step-wise. Following the formation of a new, oxidised species ([X]$^{n+}$), the potential is always reversed so as to re-generate the neutral starting material ([X]). This is to ensure that the spectrum of the oxidised species is true and does not instead represent decomposition. The progress of the individual oxidations was monitored by the intensity of the characteristic NIR bands, which were observed in the spectra of all oxidised complexes. Key vibrational modes, such as ν([C≡C]$^{n+}$) and ν([C=C]$^{n+}$) (n = 0 – 2) are summarised in Table 4.3.

Table 4.3: Selected IR spectroelectrochemical data (cm^{-1}) for neutral and oxidised bimetallic, $[\mathbf{94}]^{n+}$, and trimetallic, $[\mathbf{95}]^{n+}$, complexes (n = 0, 1, 2).[xxii]

Complex	ν(C≡C)	ν(C≡C]$^{+}$)	ν(C≡C]$^{2+}$)	ν(C≡CSiMe$_3$)	ν(C≡CSiMe$_3$]$^{+}$)	ν(C≡CSiMe$_3$]$^{2+}$)	ν(C=C)	ν(C=C]$^{+}$)	ν(C=C]$^{2+}$)
[94a]	2112 w,	2057w, 1981 s,	2052 w, 2044 w,	2148 w	2148 w	2177 w,	1594 w	1594w,	1594w,
	2057 m,	1963 s, 1910 w	2027 w,			2148 w		1564 w	1564 w
	2040 w,		1979 m, 1958 m,						
	2014w		1904 w						
[94a-Me]	2067 w,	2067w, 2054 m,	2054 w, 2042 w,	2148 w	2148 w	2155 w,	1593 w	1593 w,	1593 w,
	2054 m,	2044 m, 1953 s,	2032 w, 1953 w,			2148 w		1574 w	1574 w
	2044 m	1923 w	1890 w, 1837 w						
[94a-^{i}Pr]	2066 m,	2066 w, 2036 w,	2061 w, 2025 w,	2148 w	2148 w	2155 w,	1592 w	1592 w,	*
	2036 m	1942 s, 1894 w	1984 w, 1942 w,			2148 w		1567 w	
			1882 w						
[94b]	2085 w,	2060 w, 1986 s,	2060 w, 2046 w,	-	-	-	1586 w	1586 w,	1586 w,
	2060 m,	1966 s,	1986 m, 1966 m,					1560 m	1560 m
	2051 w,	1917 w	1912 w						
	2038 w								
[94c-Me]	2060 w,	2060 w, 2048 w,	2060 w, 1986 w,	1992 m	1992 m	2099 m	1574 w	1584 w,	1574 w,
	2048 w	1947 s, 1923 m	1947 w, 1903 w					1574 w	1570 w
[95a]	2056 m,	2056 w, 2010 s,	2056 w , 1958 s,	2147 w	2147 w	2148 w	1593 w	1593 w,	1593 w,
	2035 w	1990 s, 1971 s,	1899 s					1530 s	1550 s
		1848 s, 1754 w							

*where s-strong; m-medium; w-weak, *too low intensity for absolute characterisations / peaks are lost in the baseline.*

[xxii] Additional characterisations include $[\mathbf{95a}]^{3+}$: 2152 w ν($[C{\equiv}CSiMe_3]^{3+}$), 2056 w ν($[C{\equiv}C]^{3+}$), 2025 w ν($[C{\equiv}C]^{3+}$), 1958 w ν($[C{\equiv}C]^{3+}$), 1899 w ν($[C{\equiv}C]^{3+}$), 1593 w ν($[C{=}C]^{3+}$), 1550 s ν($[C{=}C]^{3+}$) cm^{-1}.

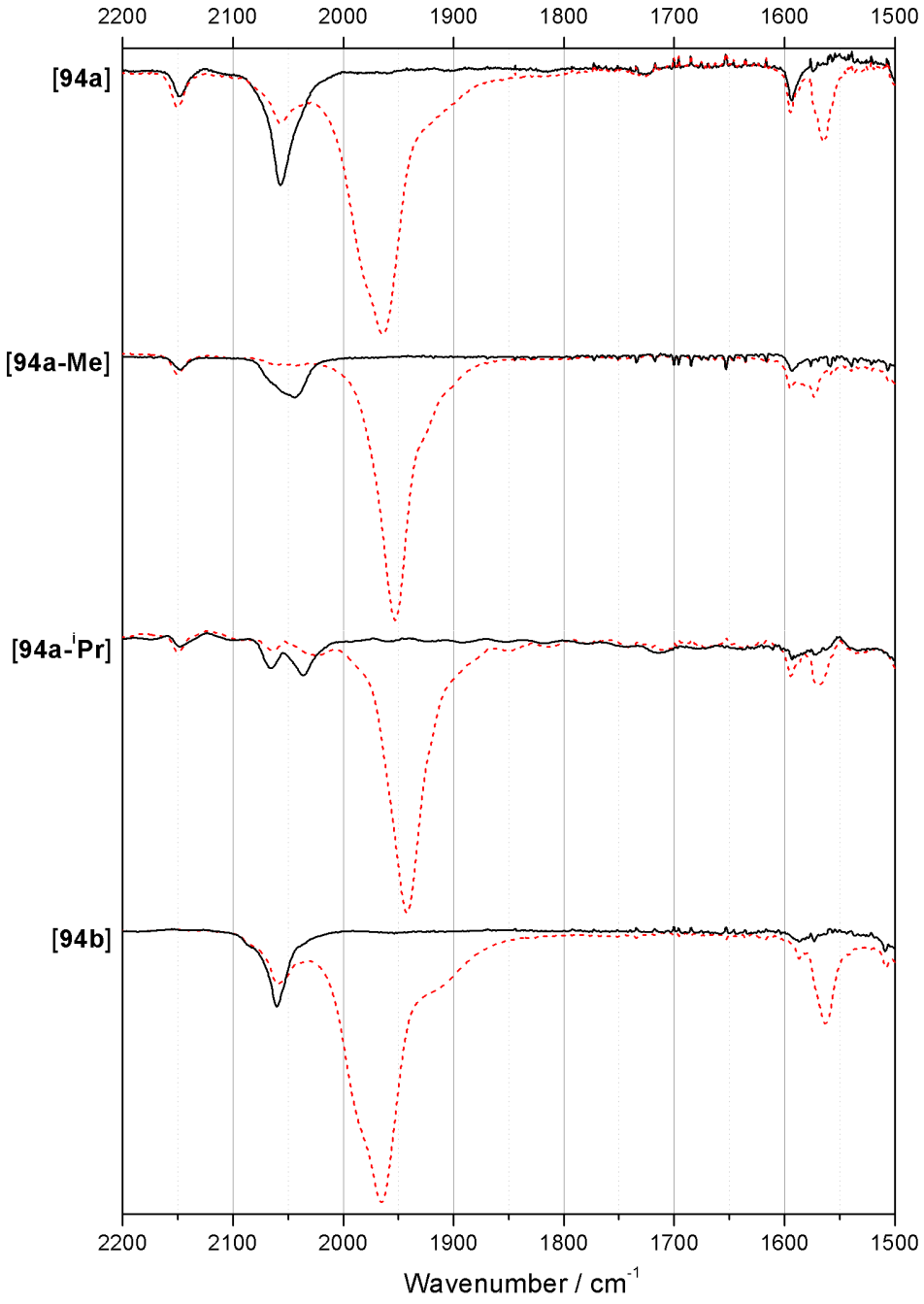

Figure 4.17: IR spectra, recorded from 0.1 M $[N^nBu_4]PF_6$ CH_2Cl_2 solutions, of *trans*-$[\{(RC{\equiv}C)(dppe)_2Ru\}_2(\mu\text{-}C{\equiv}CC_6H_2\text{-}2,5\text{-}X_2\text{-}4\text{-}C{\equiv}C)]^{n+}$ complexes (n = 0, black solid line; n = 1, red dotted line), where [**94a**]: R = C_6H_4-4-C≡CSiMe_3, X = H; [**94a-Me**]: R = C_6H_4-4-C≡CSiMe_3, X = Me; [**94a-^{i}Pr**]: R = C_6H_4-4-C≡CSiMe_3, X = ^{i}Pr and [**94b**]: R = 3-*th*, X = H. The *mono*-oxidised forms (n = 1) were formed *in situ* at potentials of 0.55, 0.44, 0.34 and 0.43 V respectively.

The IR spectrum of [**94a**] serves as a convenient point to begin discussion of the infrared spectroelectrochemical results. The compound contains three chemically distinct alkyne moeities, labelled **A** − **C** in Figure 4.18. The outermost alkyne ν(C≡C) (**A**) is observed as a weak band at 2148 cm^{-1}. The ν(C≡C) (**B**) and ν(C≡C) (**C**) vibrations are overlapped and observed as a stronger band near 2057 cm^{-1}. The aryl ring breathing modes, ν(C=C) (**α**, **β**), which are also overlapped, are observed at 1594 cm^{-1}. Closer inspection of the ν(C≡C) (**B**, **C**) envelope reveals a number of small shoulders that are not clearly resolved, but which cause a broadening and assymetric appearance to the band (marked by asterisks in Figure 4.18). These likely arise from the presence of rotamers in the sample. The IR spectrum of [**94b**] is similar to [**94a**], although obviously missing an '**A**-type' alkyne stretch (Figure 4.17). The spectra of [**94a-Me**] and [**94a-^{i}Pr**] display the '**A**-type' alkyne stretch as a weak band at 2148 cm^{-1}. The introduction of the additional steric bulk to the central ring in these two complexes causes substantial broadening ([**94a-Me**]) or splitting ([**94a-^{i}Pr**]) (Figure 4.17) of the ν(C≡C) (**B**, **C**) envelope. This further supports the notion of a conformational influence on the appearance of ν(C≡C) profiles.

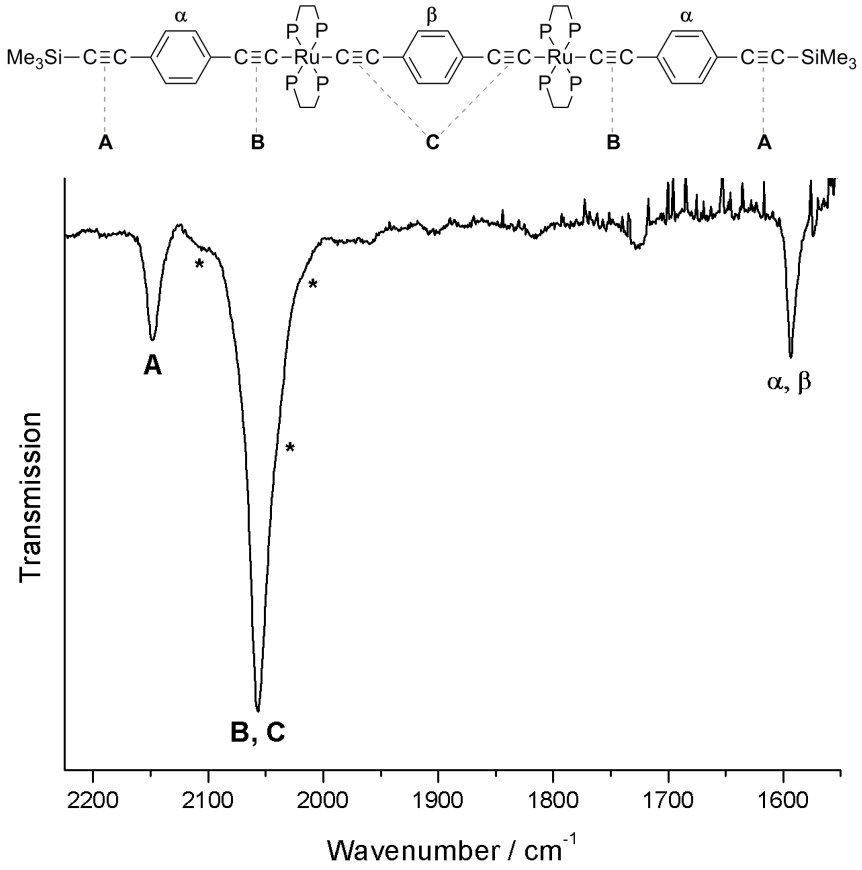

Figure 4.18: The IR spectrum of [**94a**] (extracted from Figure 4.17) as a representative example of complexes [**94**] showing the assignment of ν(C≡C) and ν(C=C) stretches and the anticipated contribution of rotamers (marked by asterisks) (P = PPh_2).

Compound [**94a**] again serves as a convenient point for which to commence discussion of the spectra of complexes [**94**] upon oxidation. On oxidation of [**94a**] to [**94a**]$^+$ (Figure 4.17), the ν(C≡C) (**A**) band is essentially unchanged, indicating that oxidation is not substantially affecting the electron density at the outermost parts of the molecular framework. In contrast, the ν(C≡C) (**B**, **C**) band envelope at 2057 cm^{-1} (shown in Figure 4.18) splits into two band envelopes at 2057 cm^{-1} (weak) and ~ 1970 cm^{-1} (broad, strong; Figure 4.17), with the latter exhibiting unresolved additional features. The aryl ring ν(C=C) (**α**, **β**) band envelope at ~ 1594 cm^{-1} (Figure 4.18) also splits into two separate envelopes at 1594 cm^{-1} and 1564 cm^{-1} (Figure 4.17).

The new band envelope at ~ 1970 cm^{-1} observed in the spectrum of [**94a**]$^+$ is similar to the primary feature observed at 1966 cm^{-1} for both *trans*-[{Cl(dppe)Ru}$_2$(μ-C≡CC_6H_4-

4-C≡C)]$^+$, [**44**]$^+$, and [{(η^5-C_5Me_5)(dppe)Ru}$_2$(μ-C≡CC_6H_4-4-C≡C)]$^+$,[35, 45] [**101**]$^+$, which in turn are much higher than the principal (strongest) ν(C≡C) band observed in *trans*-[Ru(C≡CC_6H_4-4-C≡C$SiMe_3$)$_2$(dppe)$_2$]$^+$, [**43a**]$^+$, (1899 cm^{-1}).[31] This clearly supports assignment of the oxidation process to the inner most diethynyl phenylene fragment and the band envelope at 1970 cm^{-1} to ν(C≡C) ([**C**]$^+$) (Figure 4.19). The ν(C≡C) band at 2057 cm^{-1} in [**94a**]$^+$ can therefore be clearly assigned to unoxidised ν(C≡C) (**B**) (Figure 4.19).

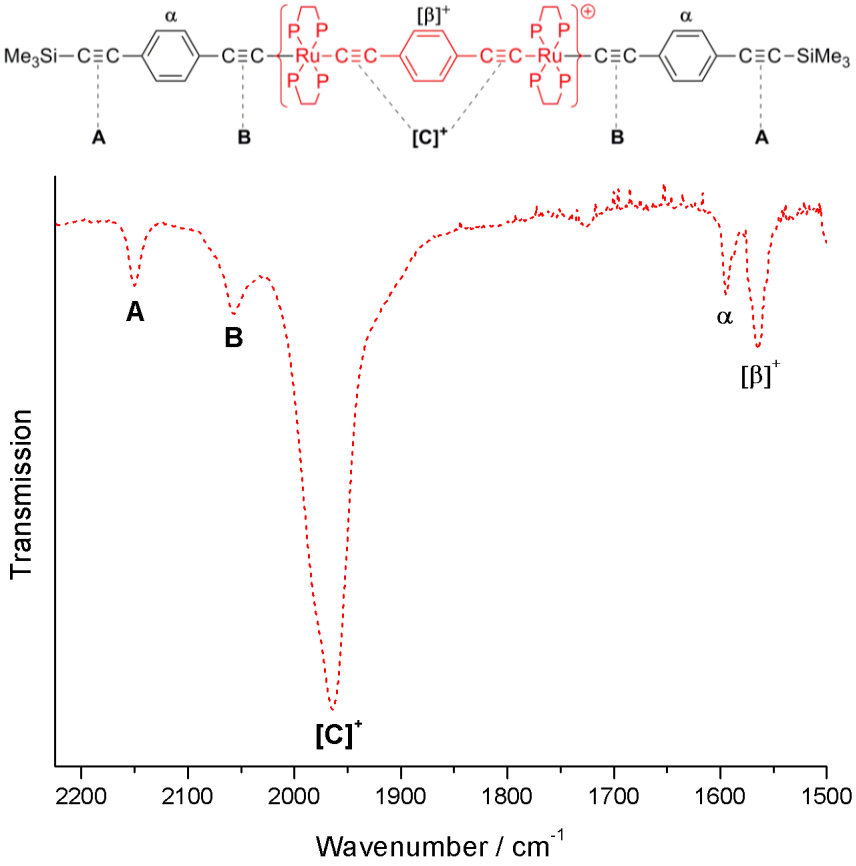

Figure 4.19: The IR spectrum of [**94a**]$^+$ (extracted from Figure 4.17) is used as a representative example of complexes [**94**]$^+$ to show the assignment ν(C≡C) and ν(C=C) bands (P = PPh_2).

The new ν(C=C) feature at 1564 cm^{-1} (in [**94a**]$^+$) is consistent with the oxidised diethynyl phenylene ligand between ruthenium centres.[35, 45] Thus, the observation of bands at 1594 cm^{-1} (unoxidised **α** phenylene, Figure 4.19) and 1564 cm^{-1} (oxidised **β** phenylene, Figure 4.19) is also consistent with this structural interpretation of [**94a**]$^+$. The ~ 100 cm^{-1} shift in the primary band envelope from ν(C≡C) (**C**) in [**94a**]

(Figure 4.18) to ν(C≡C) ([**C**]$^+$) in [**94a**]$^+$ (Figure 4.19) is somewhat smaller than the ~ 150 cm^{-1} shift which accompanies oxidation of *mono*-metallic model systems[46, 47] indicating an extensively delocalised electronic structure within this *mono*-oxidised central fragment of [**94a**]$^+$.

Closer inspection of the IR spectrum of [**94a**]$^+$ reveals shoulders to each of the primary band envelopes (Figure 4.20). Such features have also been observed in the spectra of [**44**]$^+$ and [**101**]$^+$.[35, 45] These smaller features can be attributed to the presence of conformational isomers, with rotation of the central **β** phenylene ring with repect to the metal fragments giving rise to less conjugated structures with more pronounced electron localisation (Figure 4.20).

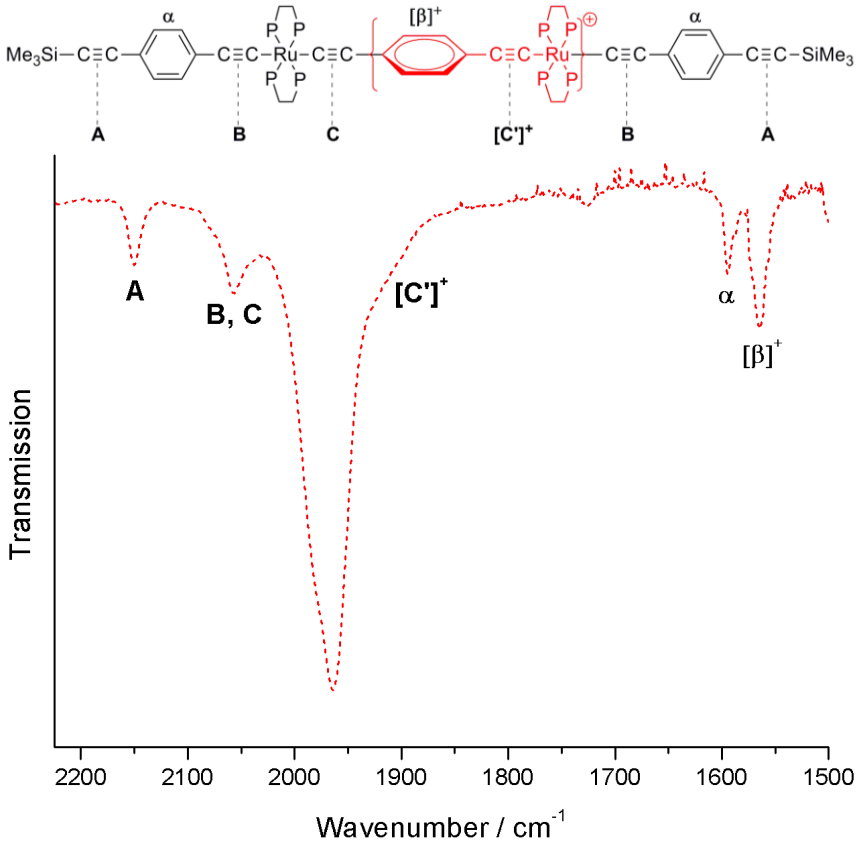

Figure 4.20: The IR spectrum of [**94a**]$^+$ (extracted from Figure 4.17) showing the assignment of ν(C≡C) and ν(C=C) bands in a conformation isomer of [**94a**]$^+$ (P = PPh_2).

Trends observed in the oxidation of [**94a**] to [**94a**]$^+$ are similarly observed in the *mono*-oxidation of [**94b**]. In the cases of [**94a-Me**]$^+$ and [**94a-^{i}Pr**]$^+$, the same general features

are also apparent, where the limited shift in the ν(C≡C) (**A**) band on oxidation and the observation of distinct ν(C=C) bands for the **α** and **β** rings together with small band envelopes for ν(C≡C) (**B**) all support oxidation of the **β** ring, with the breadth of ν(C≡C) ([**C**]$^+$) bands (and often the present of additional features) owing to the presence of thermodynamically accessible rotamers. However the ν(C≡C) ([**C**]$^+$) band at ~ 1970 cm^{-1} is significantly narrower in the case of [**94a-Me**]$^+$ and [**94a-^{i}Pr**]$^+$ than in [**94a**]$^+$ or [**94b**]$^+$ (Figure 4.17) suggesting that the population of rotamers is biased as a result of restricted rotation of the aryl-ethynyl fragment about the C≡CRuC≡C axis.

In turning to doubly oxidised dications [**94**]$^{2+}$, we again use [**94a**] as an initial example. Oxidation of [**94a**]$^+$ to [**94a**]$^{2+}$ results not in a further low frequency shift of the ν(C≡C) ([**C**]$^+$) band (Figure 4.19), as is the case for [**44**]$^+$ and [**101**]$^+$,[35, 45] but rather a splitting of the ν(C≡C) (**A**) bands and formation of a new '**B** type' band at 2027 cm^{-1} (Figure 4.21). We cautiously attribute these factors to oxidation of one of the outer **α** phenylene rings, aligning with previous assignments.[13]

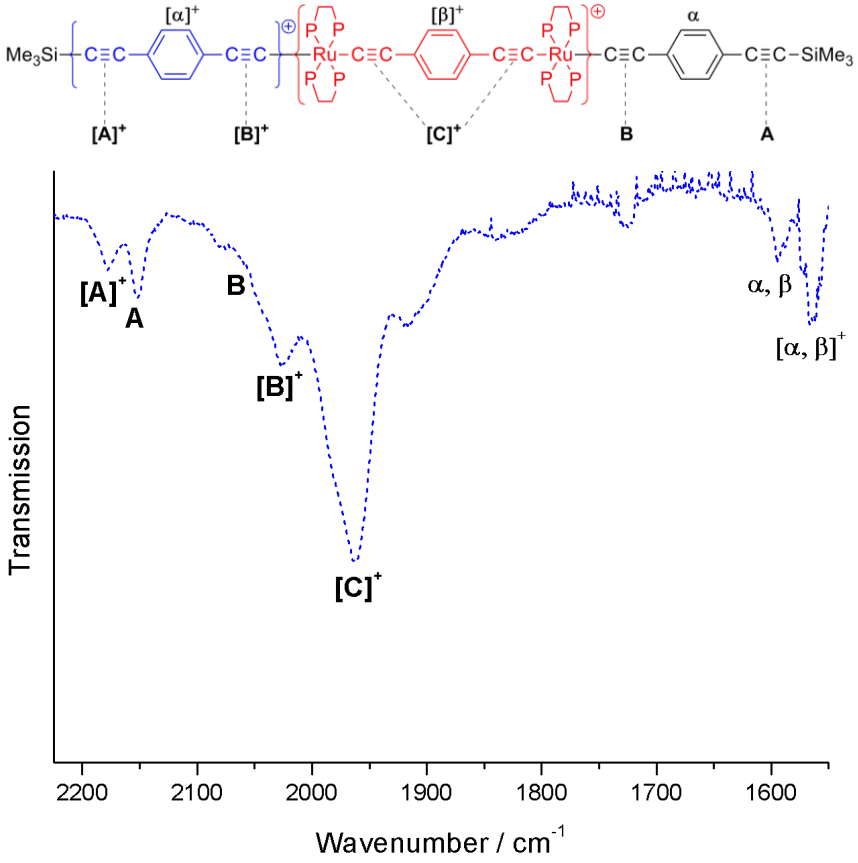

Figure 4.21: IR spectrum of [**94a**]$^{2+}$ (generated at 1.55 V, recorded from a 0.1 M [N^{n}Bu$_4$]PF$_6$ CH_2Cl_2 solution) as a representative example of [**94**]$^{2+}$ to show the assignment of ν(C≡C) and ν(C=C) bands (P = PPh_2).

As the IR spectra of *trans*-[Ru(C≡CC_6H_4-4-R)$_2$(dppe)$_2$]$^+$ *mono*-metallic complexes display a ν(C≡C) band around 1900 cm^{-1},[31] the feature at 1904 cm^{-1} in [**94a**]$^{2+}$ is attributed to presence of redox isomers in solution (Figure 4.22).

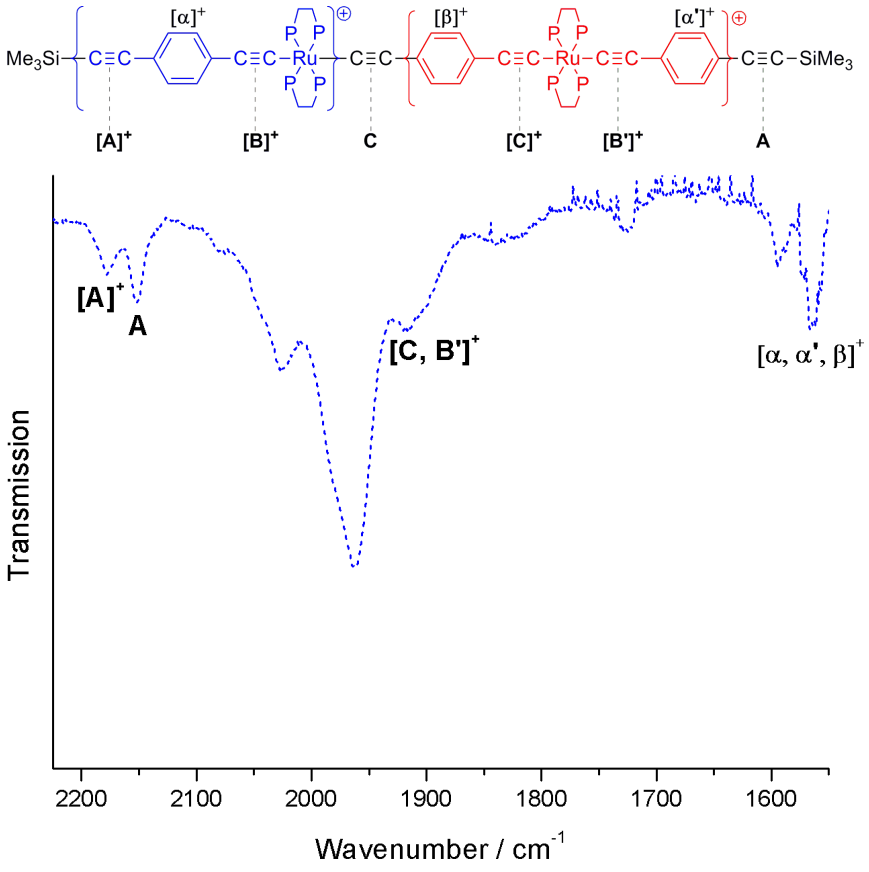

Figure 4.22: The IR spectrum of [**94a**]$^{2+}$ (taken from Figure 4.21) showing the alternative assignment of ν(C≡C) and ν(C=C) bands for a redox isomer of [**94a**]$^{2+}$ (P = PPh_2).

To test these proposals, the simpler complex [**94c-Me**] (Scheme 4.4; $E_{1/2}(1) = -0.30$ V *rev*; $E_{1/2}(2) = 0.08$ V *rev*; $E_{1/2}(3) = 0.93$ V *irrev*; $E_{1/2}(4) = 1.08$ V *irrev*, in a 0.1 M [N^nBu_4]PF_6 / CH_2Cl_2 solution *vs.* internal decamethylferrocene) was also investigated by IR-spectroelectrochemistry (Figure 4.23). The IR spectrum of [**94c-Me**] is characterised by a ν(C≡C) band envelope near 2050 cm^{-1}, which is assigned to a '**C**-type' alkyne with the splitting due to the usual distribution of rotamers enhanced by the methyl substituents on the bridging phenylene. The '**B**-type' ν(C≡C) band [in this case: ν(C≡C$SiMe_3$)] is observed as a sharp feature at 1992 cm^{-1}. On oxidation to [**94c-Me**]$^+$, the ν(C≡C) (**C**) band envelope undergoes the anticipated shift of ~ − 100 cm^{-1} to give a strong, broad band envelope centered at 1970 cm^{-1}. The ν(C≡C) (**B**) band is largely unaffected by the oxidation and is observed as a higher energy shoulder to the [**C**]$^+$ band (Figure 4.23). These observations are consistent with those in [**94a**]$^+$ where the cation radical is stablised by a diruthenium diethynylbenzene

electrophore. Rotation of the central (**β**) aryl fragment, giving rise to a more localised valence description, is thought to account for the lower energy shoulder of the ν(C≡C) ([**C**]$^{+}$) band (labelled [**C′**]$^{+}$; Figure 4.23).

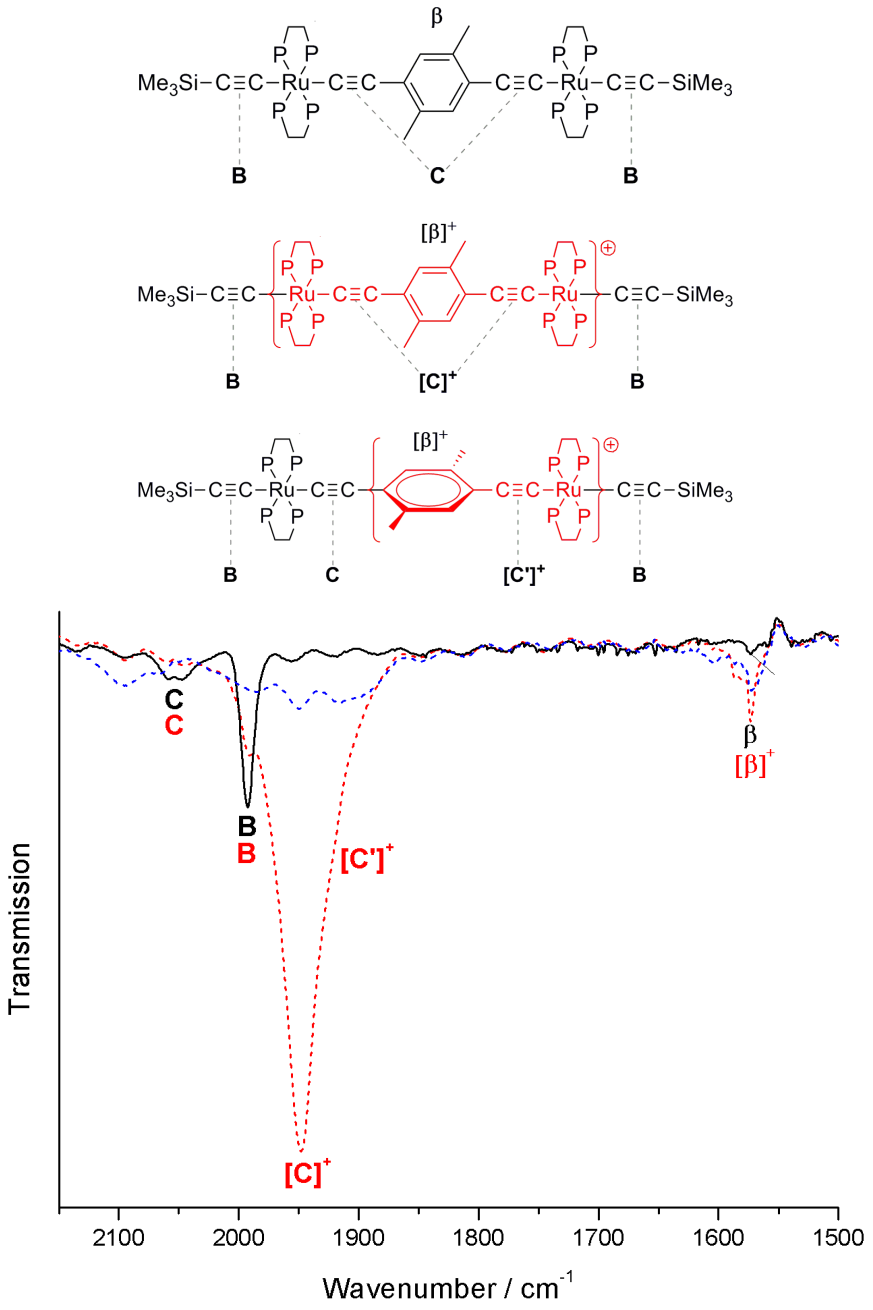

Figure 4.23: IR spectra of [**94c-Me**]$^{n+}$, recorded from a 0.1 M [N^{n}Bu$_4$]PF$_6$ CH_2Cl_2 solution, where n = 0 (black solid line, black labels), 1 (red dashed line, red labels, generated at 0.16 V), 2 (blue dashed line, generated at 0.47 V) and P = PPh_2, showing the assignment of ν(C≡C) and ν(C=C) bands.

The further oxidation of [**94c-Me**]$^{+}$ to [**94c-Me**]$^{2+}$ (Figure 4.23) causes a collapse of the ν(C≡C) features. Although resolution of the spectrum with the dication is poor, the weak feature at 1903 cm^{-1} is consistent with other examples of {Ru}-C≡CC$_6$H$_4$-4-C≡C-{Ru} systems reported elsewhere[45] and is tentatively assigned here to ν(C≡C) ([**C**]$^{2+}$) while the weak band at ~ 2100 cm^{-1} is then assigned to ν(C≡CSiMe$_3$) ([**B**]$^{2+}$) (Figure 4.24).

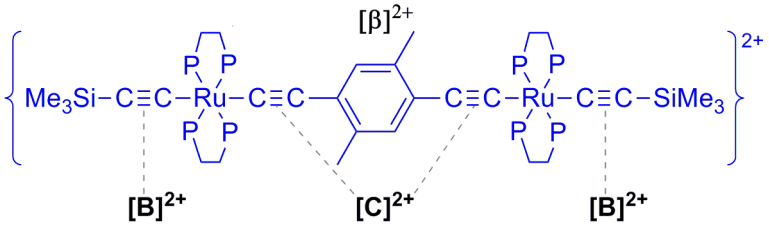

Figure 4.24: Proposed structure for [**94c-Me**]$^{2+}$ where P = PPh$_2$.

The IR spectrum of the more extended trimetallic complex [**95a**], in addition with the spectra of the oxidised forms, [**95a**]$^{n+}$ (n = 1 – 3), is given in Figure 4.25. Notably, the IR profiles of [**95a**]$^{0/1+/2+/3+}$ parallel those previously reported for [**58**]$^{0/1+/2+/3+}$.[13]

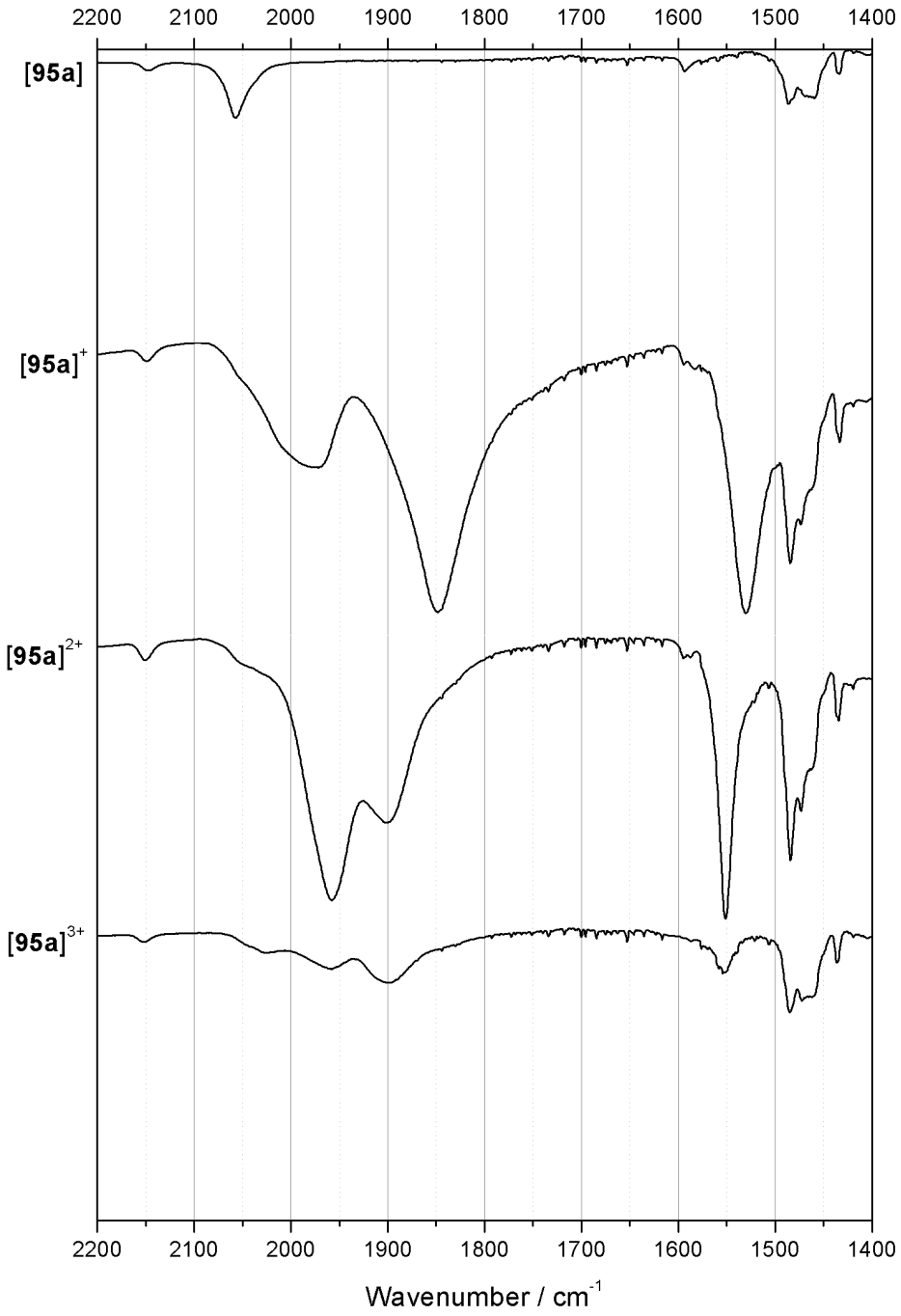

Figure 4.25: IR spectra of [**95a**], recorded from a 0.2 M $[N^nBu_4]PF_6$ $CHCl_3$ solution, and after three consecutive oxidations (forming $[\mathbf{95a}]^+$, $[\mathbf{95a}]^{2+}$ and $[\mathbf{95a}]^{3+}$ *in situ* at potentials of 0.13, 0.39 and 0.64 V respectively), where band intensities are comparable.

The IR spectrum of the trimetallic complex [**95a**] (Figure 4.25) is similar that of [**94a**] (Figure 4.17), exhibiting a weak, single '**A** type' ν(C≡C) band at 2147 cm^{-1} and ν(C≡C) band envelope, comprising **B**, **C** and **D** alkyne fragments, at 2056 cm^{-1} (Figure 4.26). Furthermore, ν(C≡C) (**α**, **β**, **γ**, **δ**) bands are observed at ~ 1590 cm^{-1} (Figure 4.26).

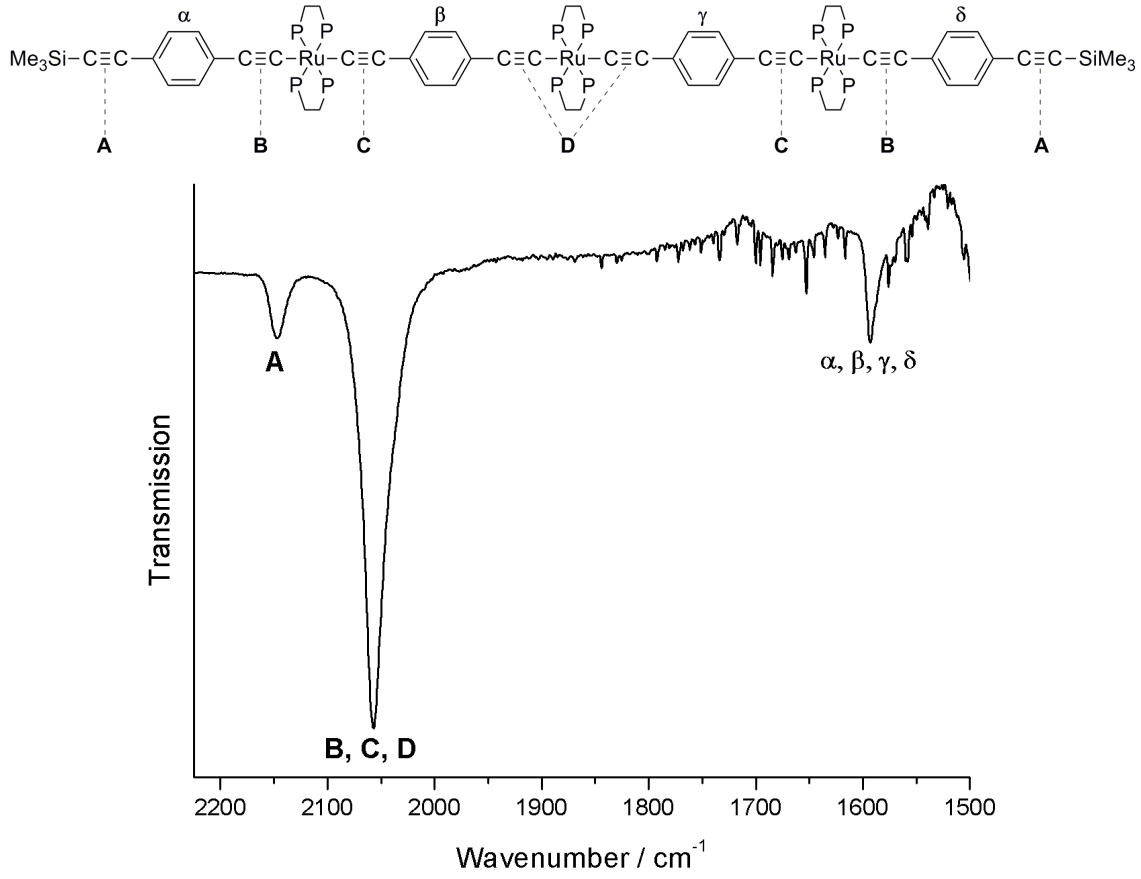

Figure 4.26: IR spectrum of [**95a**] (extracted from Figure 4.25) showing the assignments of ν(C≡C) and ν(C=C) bands (P = PPh_2).

We now turn to discuss the spectrum of the dication, $[\mathbf{95a}]^{2+}$, which provides a basis from which to interpret the spectra of the various redox states. The dication exhibits a weak ν(C≡C) (**A**) band at 2148 cm^{-1} in addition with two strong, broad band profiles centered at 1958 and 1899 cm^{-1} (Figures 4.25 and 4.27). Furthermore, two ν(C=C) bands are observed at 1550 and 1593 cm^{-1}. Given that both $[\mathbf{44}]^{+}$ [35] and $[\mathbf{101}]^{+}$ [45] exhibit strong transitions at 1966 cm^{-1} combined with the fact that $[\mathbf{43a}]^{+}$ displays a strong transition at 1899 cm^{-1},[31] as was noted earlier in the discussions of bimetallic complexes, the spectral profile of $[\mathbf{95a}]^{2+}$ is thought to reflect 'individual' oxidations of the -{Ru}-C≡CC_6H_4-4-C≡C-{Ru}- and -C≡CC_6H_4-4-C≡C-{Ru}-C≡CC_6H_4-4-C≡C- electrophores (Figure 4.27).

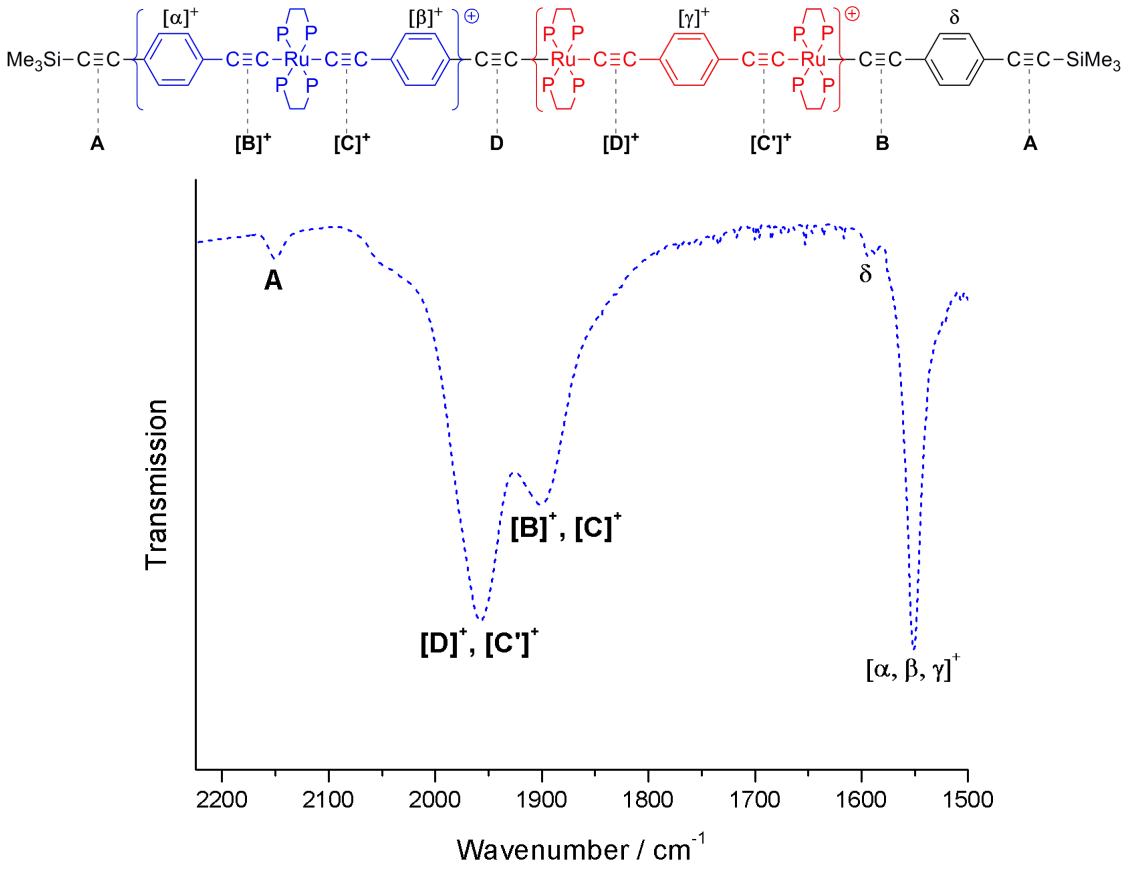

Figure 4.27: IR spectrum of [**95a**]$^{2+}$ (extracted from Figure 4.25) showing the assignments of ν(C≡C) and ν(C=C) bands (P = PPh_2).

Given this description of [**95a**]$^{2+}$, the spectra of the *mono*-cation [**95a**]$^{+}$, which similarly exhibits two strong, broad ν(C≡C) bands centred at 1848 and ~ 1980 cm^{-1} (Figure 4.25), is thought to reflect a distribution of redox isomers of the bimetallic diethynylbenzene and *mono*-metallic *bis*-aryl-ethynyl electrophores (Figure 4.28). The spectrum of [**95a**]$^{+}$ also shows the weak ν(C≡C) (**A**) band at 2147 cm^{-1}, implicating that the outer most portions of the molecule are not strongly contributing to the spectral profile of [**95a**]$^{+}$. The substantial widths of the ν([C≡C]$^{n+}$) band envelopes (n = 1, 2) indicates that multiple conformers are likely to be present in these samples.

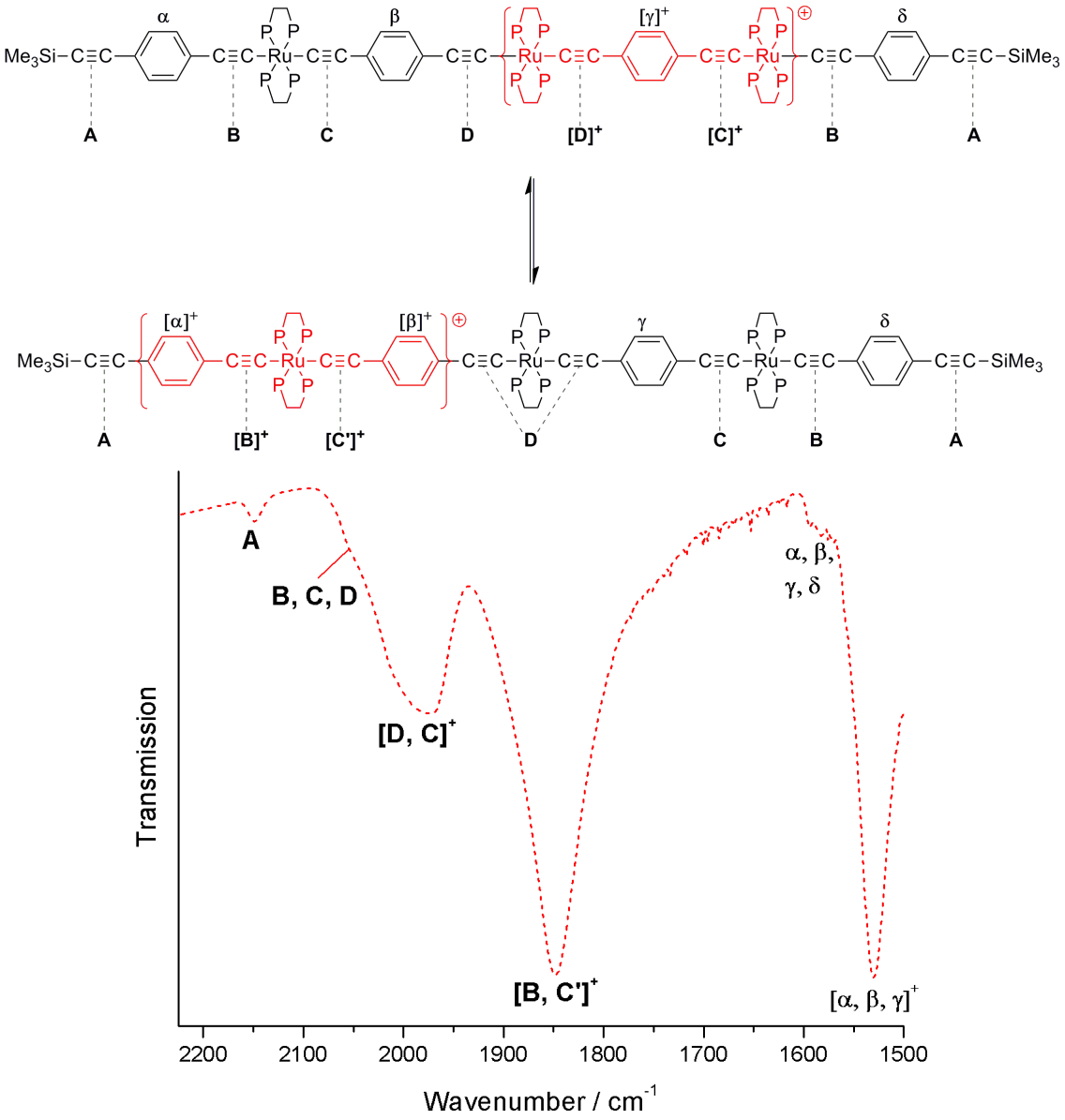

Figure 4.28: IR spectrum of [**95a**]$^{+}$ (extracted from Figure 4.25) showing the assignments of ν(C≡C) and ν(C=C) bands (P = PPh_2).

Upon oxidation of [**95a**]$^{2+}$ to form [**95a**]$^{3+}$, all vibrational bands lose intensity (Figure 4.25). Although poorly resolved, the energies of ν(C≡C) bands in [**95a**]$^{3+}$ are similar to those observed in [**95a**]$^{2+}$. This would imply that the location of the third oxidation is the remaining, unoxidised terminal portion of [**95a**]$^{2+}$ (Figure 4.27), establishing a highly delocalised complex (Figure 4.29), with the reduction in band intensities being consistent with a loss of polarity across the molecule. The '**A**-type' ν(C≡C) band in [**95a**]$^{3+}$ is observed at 2152 cm^{-1}. This slight shift from analogous bands

in [**95a**]$^{2+}$ (of 4 cm^{-1}) indicates that the oxidation event still does not largely affect the terminal C≡CSiMe$_3$ fragments.

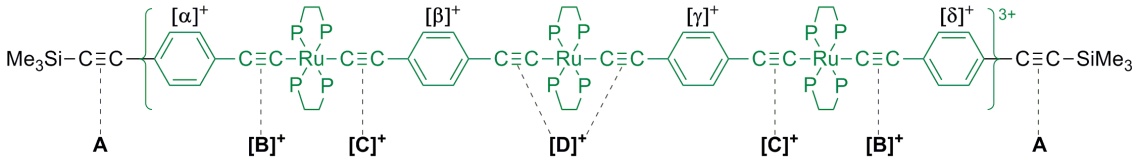

Figure 4.29: Anticipated structure of [**95a**]$^{3+}$, where P = PPh$_2$.

4.5.2. UV-Vis-NIR spectroelectrochemistry

Complexes [**94**] in 0.1 M [N^{n}Bu$_4$]PF$_6$ CH$_2$Cl$_2$ solutions and [**95a**] in a 0.2 M [N^{n}Bu$_4$]PF$_6$ CHCl$_3$ solution were also subjected to UV-Vis-NIR spectroelectrochemical investigations, with results summarised in Table 4.4 ([**94**]) and Table 4.5 ([**95a**]). The NIR-Vis region (between 4000 – 23 000 cm^{-1}) of neutral complexes, [**94**] and [**95a**], are featureless. Upon oxidation to generate [**94**]$^{n+}$ (n = 1, 2) and [**95a**]$^{n+}$ (n = 1 – 3) several bands are observed.

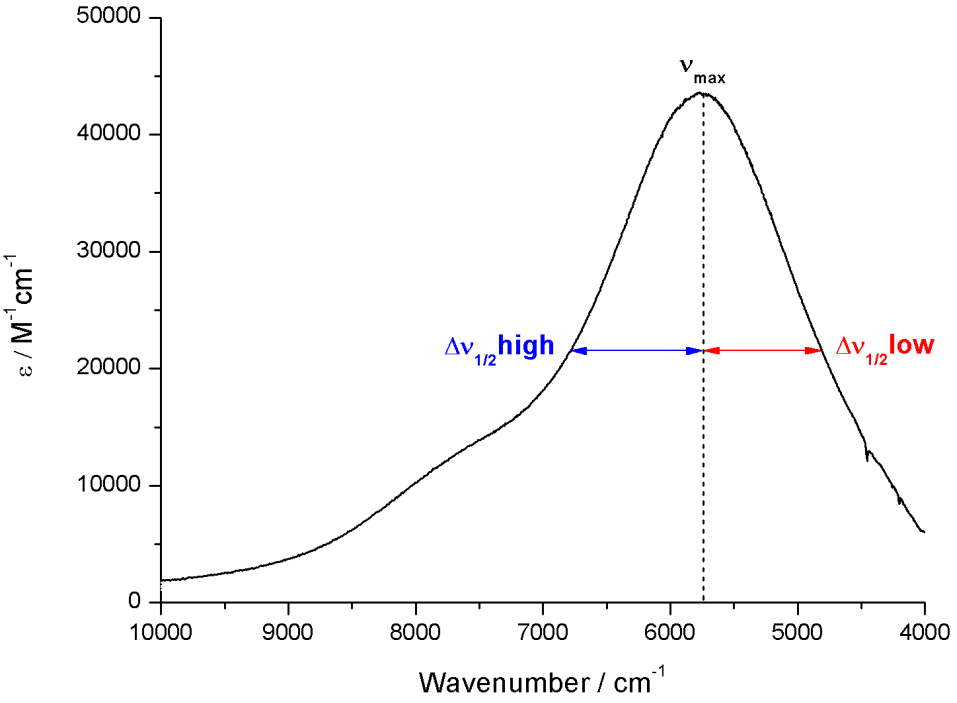

Figure 4.30: Definition of ν_{max}, $\Delta\nu_{1/2}$low and $\Delta\nu_{1/2}$high values used in Tables 4.4 and 4.5 for oxidised complexes [**94**]$^{n+}$ and [**95a**]$^{n+}$ (where appropriate), using the NIR profile of [**94a-Me**]$^{+}$ as a representative example, where the addition of $\Delta\nu_{1/2}$low and $\Delta\nu_{1/2}$high values equals the full width at half height (FWHH).

Table 4.4: Selected UV-Vis-NIR spectroelectrochemical data for the oxidised bimetallic, [**94**]$^{n+}$, complexes (n = 1, 2) between 4000 – 30 000 cm^{-1}, where ν_{max}, FWHH and $\Delta\nu_{1/2}$ values are reported in cm^{-1} while ε is reported in M^{-1}cm^{-1}.

Complex	ν_{max}	ε	FWHH	$\Delta\nu_{1/2}$low	$\Delta\nu_{1/2}$high
[**94a**]$^{+}$	5590	11 014	1996	990	1006
	7375	3417	-	-	-
	19 685	7900	-	-	-
[**94a**]$^{2+}$	5307	1530	-	-	-
	8292	9736	2676	746	1930
	10 582	4388	-	-	-
	15 408	2840	-	-	-
	26 882	7770	-	-	-
[**94a-Me**]$^{+}$	5721	43 318	2003	949	1054

	7485	13 978	-	-	-
	19 569	25 426	-	-	-
[**94a-Me**]$^{2+}$	5534	6048	-	-	-
	8453	48 345	2806	810	1996
	10 823	21 282	-	-	-
	14 992	11 199	-	-	-
	27 855	21 028	-	-	-
[**94a-^{i}Pr**]$^{+}$	5597	30 920	2051	1054	997
	7384	9651	-	-	-
	19 687	23 273	-	-	-
[**94a-^{i}Pr**]$^{2+}$	5390	2451	-	-	-
	8194	19 286	2250	710	1540
	10 245	8482	-	-	-
	15 660	6823	-	-	-
	26 838	22 748	-	-	-
[**94b**]$^{+}$	5504	24 470	1850	817	1033
	7622	6112	-	-	-
	19 881	14 331	-	-	-
[**94b**]$^{2+}$	5525	13 739	-	-	-
	8217	27 025	2409	793	1616
	10 776	10 509	-	-	-
	15 314	5946	-	-	-
[**94c-Me**]$^{+}$	6006	57 928	841	1021	1862
	7710	20 620	-	-	-
	20 243	36 668	-	-	-
[**94c-Me**]$^{2+}$	6993	18 717	-	-	-
	9728	33 292	-	-	-
	11 136	23 947	-	-	-
	15 773	9930	-	-	-
	20 040	17 293	-	-	-

Table 4.5: UV-Vis-NIR spectroelectrochemical data for the oxidised trimetallic complex, [**95a**]$^{n+}$, (n = 1 – 3) between 4000 – 30 000 cm^{-1}, where ν_{max}, FWHH and $\Delta\nu_{1/2}$ values are reported in cm^{-1} while ε is reported in M^{-1}cm^{-1}.

Complex	ν_{max}	ε	FWHH	$\Delta\nu_{1/2}$low	$\Delta\nu_{1/2}$high
[**95a**]$^{+}$	4487	3820	-	-	-
	10298	2055	-	-	-
	11084	2163	-	-	-
	12111	1257	-	-	-
	19 439	5973	-	-	-
[**95a**]$^{2+}$	5268	8322	2638	1264	1374
	10 441	2787	-	-	-
	12 631	18 069	2255	982	1273
	15 617	6985	-	-	-
	19 242	12 897	-	-	-
[**95a**]$^{3+}$	4554	3065	-	-	-
	10 411	2277	-	-	-
	13 654	6138	-	-	-
	23 344	8375	-	-	-

UV-Vis-NIR spectroelectrochemical experiments of the complexes [**94**] follow expectations based on previous studies of [**44**] and [**101**] and the conclusions drawn from the IR studies conducted here (see section 4.5.1.). On oxidation of [**94a**] to [**94a**]$^{+}$, an intense asymmetric band at 5590 cm^{-1} with a higher energy shoulder (at 7375 cm^{-1}) is observed, together with an absorption envelope near 20 000 cm^{-1} that displays evidence of additional vibronic structure (Figure 4.31).

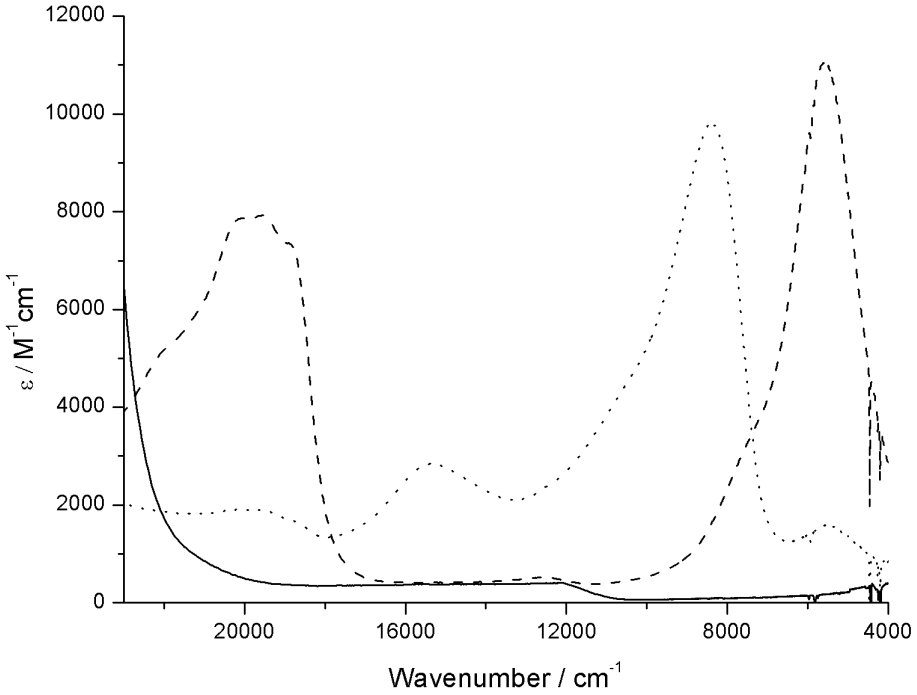

Figure 4.31: The UV-Vis-NIR spectra of [**94a**] (solid line), [**94a**]$^{+}$ (dashed line, generated at 0.65 V) and [**94a**]$^{2+}$ (dotted line, generated at 1.35 V) between 4000 − 23 000 cm^{-1} as representative examples for the series of complexes [**94**]. Spectra were collected *via* spectroelectrochemical methods from a 0.1 M [N^{n}Bu$_4$]PF$_6$ CH_2Cl_2 solution.

The structured band at ~ 20 000 cm^{-1}, similarly observed in the spectrum of [**44**]$^{+}$,[35] is assigned to transitions arising from a phenylene cation and is in keeping with the largely ligand centered nature of this oxidation process.[45] The principal NIR band (5590 cm^{-1}) is attributed to a transition with appreciable π-π* (intra-ligand, IL) character on the central diethynyl benzene-bridged bimetallic fragment. This might also be termed the 'charge-resonance' band if this fragment is considered as a Class III (fully delocalised) Robin and Day[48] 'mixed-valence' species (Figure 4.32).

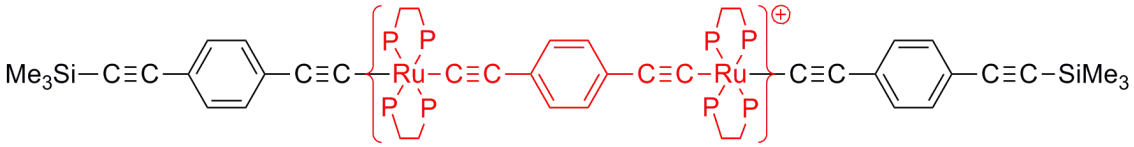

Figure 4.32: Class III (fully delocalised) description of [**94a**]$^{+}$, where P = PPh_2.

After an analysis by Parthey and colleagues on *mono*-metallic *trans*-[Ru(C≡CC_6H_4-4-R)$_2$(dppe)$_2$]$^+$ model complexes, the shoulder transition (7375 cm^{-1}) is attributed to an MLCT process which gains intensity for the conformers in which the central phenylene ring is rotated out of conjugation,[31, 45] leading to a more localised (Class II) Robin and Day description (Figure 4.33).

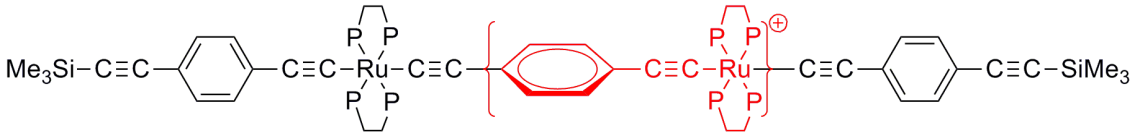

Figure 4.33: Class II (localised) description of [**94a**]$^+$, where P = PPh$_2$.

General trends observed in the generation of [**94a**]$^+$ from [**94a**] are similarly observed for all other members of the series of [**94**] (forming [**94**]$^+$). Although between extended complexes of [**94**]$^+$ ([**94a**]$^+$, [**94a-Me**]$^+$, [**94a-^{i}Pr**]$^+$ and [**94b**]$^+$), the intensities of the principal (low energy) NIR bands are notably different, where benzene-bridged complexes ([**94a**]$^+$ and [**94b**]$^+$) are less intense (11 014 and 24 470 M^{-1}cm^{-1}, respectively) than the methyl-xylene ([**94a-Me**]$^+$: 43 318 M^{-1}cm^{-1}) and diisopropyl-xylene-bridged complexes ([**94a-^{i}Pr**]$^+$; 30 920 M^{-1}cm^{-1}), indicating more Class III-like (more delocalised) complexes for the more hindered complexes. This might suggest that for the bulkier analogous, a higher proportion of the more conjugated, lower energy, rotamers are present as a consequence of hindered aryl rotation. The increased symmetry of the principal NIR band in [**94a**]$^+$ (*vs.* [**94a-Me**]$^+$ and [**94a-^{i}Pr**]$^+$) supports this argument although the equivalent band in [**94b**]$^+$, bearing strong structural and electronic resemblance to [**94a**]$^+$, is the most asymmetric (Δνlow (817) ≈ Δνhigh (1033)) and does not correlate with this trend.

On further oxidation of [**94a**]$^+$ to [**94a**]$^{2+}$, the characteristic absorption bands of [**94a**]$^+$ are simply blue shifted by ~ 3000 – 9000 cm^{-1} (Figure 4.31) suggesting the character of these transitions is retained. New bands at 5307 cm^{-1} and 15 408 cm^{-1} are also observed. These are assigned as *dπ*-*dπ* and LMCT-type transitions (respectively) on the *mono*-nuclear like external fragments by analogy with spectra of *trans*-[RuCl(C≡CC_6H_4-4-R)(dppe)$_2$]$^+$ and *trans*-[Ru(C≡CC_6H_4-4-R)(C≡CC_6H_4-4-R′)(dppe)$_2$]$^+$ complexes.[31, 44, 49] Hence, the spectra of [**94a**]$^{2+}$ is likely reflective of redox

isomers in solution (Figure 4.34). General trends observed in the generation of [**94a**]$^{2+}$ from [**94a**]$^{+}$ are again closely followed by the other members of the series of [**94**].

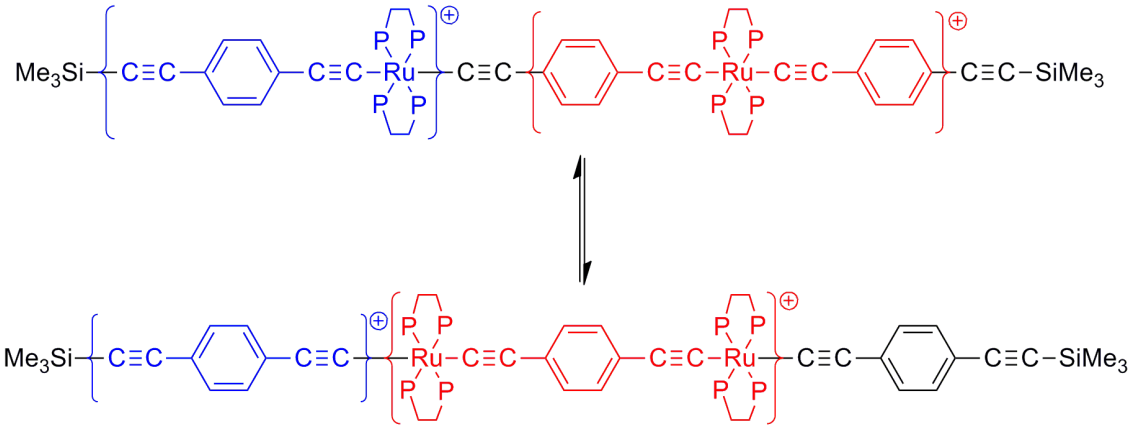

Figure 4.34: Redox isomers of [**94a**]$^{2+}$ are proposed to account for the optical bands observed in the UV-Vis-NIR spectra of [**94**]$^{2+}$, where P = PPh_2.

The UV-Vis-NIR oxidation profiles of the extended trimetallic complex [**95a**]$^{n+}$ (n = 0 − 3) are given in Figure 4.35. Upon oxidation of [**95a**] to [**95a**]$^{+}$, three broad, low intensity (~ 2500 $M^{-1}cm^{-1}$) bands are generated at ~ 5000, 11 000 and 20 000 cm^{-1} (Figure 4.35).

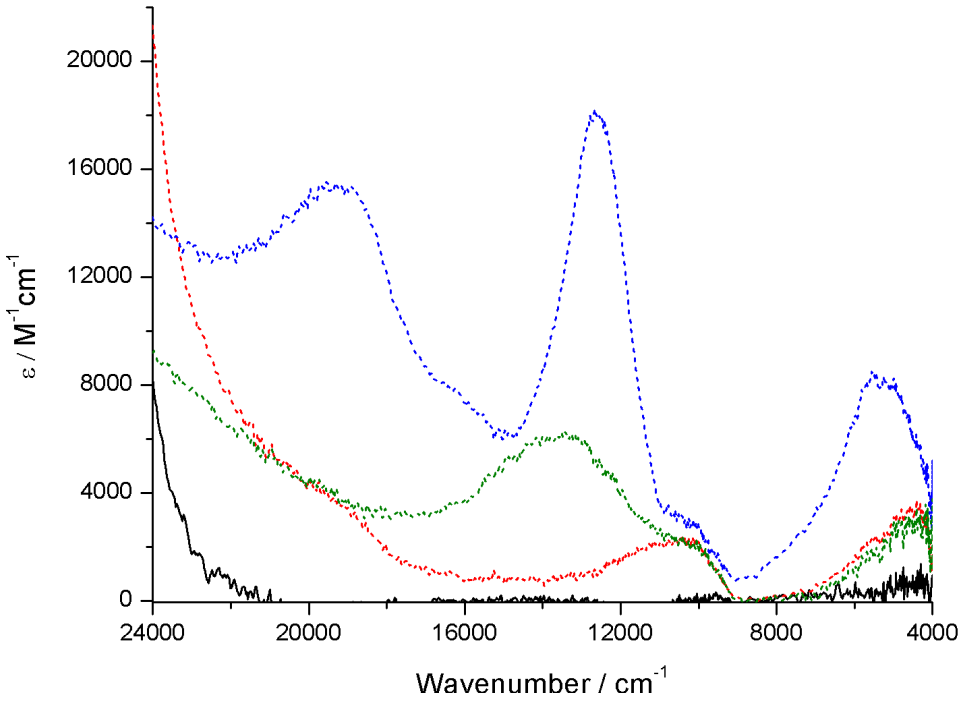

Figure 4.35: The UV-Vis-NIR spectra of [**95a**] (black solid line), [**95a**]$^{+}$ (red dashed line, generated at – 0.80 V), [**95a**]$^{2+}$ (blue dashed line, generated at 0.55 V) and [**95a**]$^{3+}$ (green dashed line, generated at 1.26 V) between 4000 – 24 000 cm^{-1}. Spectra were collected *via* spectroelectrochemical methods from a 0.2 M [N^{n}Bu$_4$]PF$_6$ CHCl$_3$ solution.

Given that bands near 5000 and 20 000 cm^{-1} were assigned to the formation of the bimetallic diethynyl benzene cation in the bimetallic series ([**94**]$^{+}$) and bands near 5000 and 10 000 cm^{-1} are consistent with those observed in the *mono*-oxidised *bis*-aryl ethynyl *mono*-metallic complexes, the spectra of [**95a**]$^{+}$ is thought to reflect admixtures of redox isomers (Figure 4.36), which is consistent with results obtained (and valence descriptions derived) through IR spectroelectrochemistry. The low intensity and width of the optical bands produced in [**95a**]$^{+}$ are no doubt a consequence of the heightened number of rotamer conformations and redox isomers possible in this extended complex.

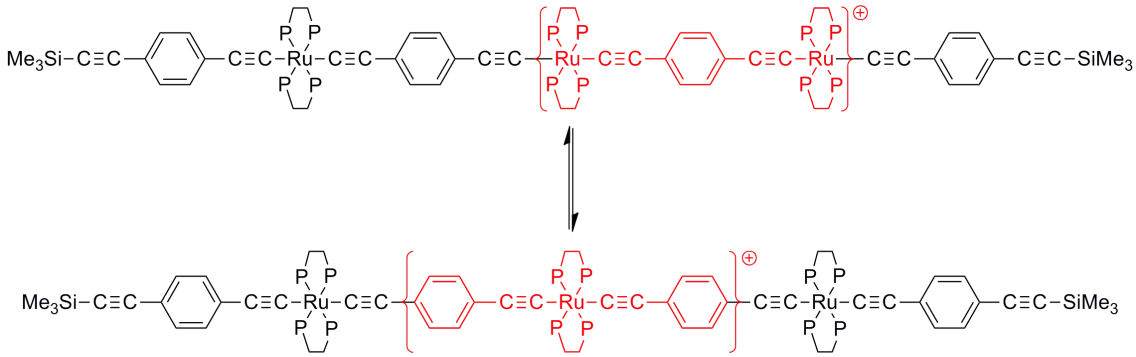

Figure 4.36: Redox isomers of [**95a**]$^{+}$ to account for the main optical bands observed in the corresponding UV-Vis-NIR spectrum (P = PPh_2).

The spectrum of [**95a**]$^{2+}$ is similar to [**95a**]$^{+}$, exhibiting bands near 5500, 12 500 and 20 000 cm^{-1} (Figure 4.35), therefore is consistent with the redox description given earlier to account for the IR spectroelectrochemical profile of [**95a**]$^{2+}$ (Figure 4.27). To this end, the dication is described as two 'individual' cations. The first, accounting for the bands at ~ 5500 (π-π*, IL) and 20 000 cm^{-1} (π-π*, aromatic radical bands), is located on the bimetallic diethynylbenzene motif while the second, accounting for the bands at ~ 5500 (*dπ*-*dπ*) and 12 500 cm^{-1} (LMCT), is located on a *bis*-aryl ethynyl *mono*-metallic motif (Figure 4.37). The broadness of these optical bands observed for [**95a**]$^{2+}$ again eludes to the presence of rotamers in solution (giving rise to 'charge trapping' and more localised valence descriptions).

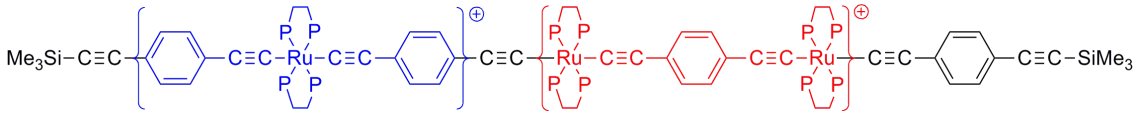

Figure 4.37: Redox description of [**95a**]$^{2+}$ to account for the optical bands observed in the corresponding UV-Vis-NIR spectrum (P = PPh_2).

Consistent with IR spectroelectrochemical observations, upon further oxidation of [**95a**]$^{2+}$ (forming [**95a**]$^{3+}$) optical bands lose intensity and are significantly broadened, increasing the difficultly in the interpretation. As the energies of band maxima in [**95a**]$^{3+}$ look to correspond with those in *both* [**95a**]$^{+}$ and [**95a**]$^{2+}$, the structure of [**95a**]$^{3+}$ is tentatively assigned as a composition of both [**95a**]$^{+}$ and [**95a**]$^{2+}$ redox descriptions and is presumably again complicated by the presence of rotamers.

A deeper analysis of the data obtained from IR and UV-Vis-NIR spectroelectrochemical studies than that given here for the trimetallic complex [**95**] is difficult. This is in part due to these extended compounds containing six near-equivalent Ru-C≡C fragments and seven rotational axes (Figure 4.38).

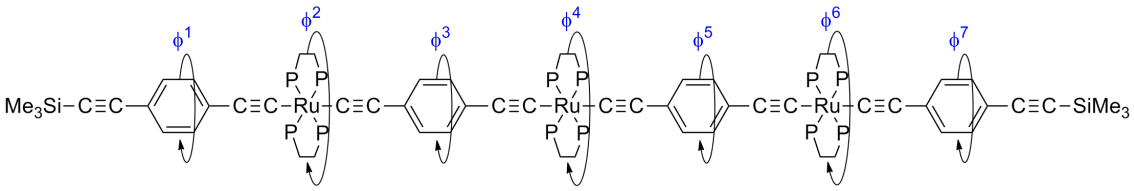

Figure 4.38: Depiction of the seven rotational axes (ϕ^n) present in trimetallic complexes of this type, using [**95a**] as an example, where P = PPh_2.

Each individual rotation in Figure 4.38 about an individual rotational axis (ϕ^n) will give rise to an alternate conformer (where structures with the highest amount of Ru(*d*) / Ar(π) overlap are most favoured),[31] that will exhibit novel vibrational and electronic transitions. As a result, spectral profiles are very highly convoluted. Even if the lowest energy (most conjugated) conformation is considered, these molecules contain ~ 400 atoms, therefore it is, at present, extremely difficult to model accurately by quantum chemical calculations, where computational power scales exponentially with the number of atoms. In order to simplify this problem in the short term, higher symmetry complexes are sought. As a result, the number of independent rotamer conformations will be decreased; hence the complexity of spectral profiles, currently prohibiting clear assignments, will be reduced. The design of future complexes for understanding charge transport in long multi-metallic wires should foremost work towards replacing the dppe ancillary ligands.

4.6. TIDOC studies

The fabrication of the top electrode in an electrode|monolayer|electrode device is a key area of research in the assembly of functional device structures,[50-53] as opposed to single molecule test junctions (electrode|molecule|electrode).[54] As mentioned in the introduction, one of the main problems associated with top-electrode formation is the

degree of damage caused to the monolayer during deposition, as the metal of the top electrode quite often penetrates the organic film, resulting in short-circuits and an invalid device. As a means to circumvent such issues, Cea and co-workers have devised a novel, 'soft', method for the fabrication of the top metallic electrode[30] based on the earlier work of Coco and Espinet who demonstrated that metallic gold nano-particles (GNPs) could be formed by annealing a metal organic compound (MOC) in solution.[55]

In the Cea method, a gold(I) complex is initially 'tagged' to the end of a nascent molecule wire, to give complexes such as [(Ph_3P)Au(C≡CC_6H_4C≡C-4-C_6H_4-4-COOH)] and [($MeOC_6H_4$-4-N≡C)Au(C≡CC_6H_4-4-NH_2)]. The Au^I complex is immobilised on a substrate *via* the Langmuir-Blodgett technique, forming a well-packed, directionally orientated monolayer. The substrate is then annealed in order to simultaneously break the Au-C or Au-P bonds to the ancillary ligand, and reduce Au^I to Au^0 presumably in concert with oxidation of the liberated ancillary ligand, resulting in the formation of gold nano-particles (GNPs) or gold nano-islands (GNIs) on the surface of the monolayer, establishing the Au|monolayer|Au junction. This Thermally Induced Decomposition of an Organometallic Compound (TIDOC) method was found to be effective at moderate temperatures (150 – 200 °C for two hours), with the electrical properties of the resulting Au|molecule|GNI junctions being characterised by the usual sigmoidal I-V curve that signifies a molecular junction, as opposed to metallic contact.

In this section, the first results for the application of the TIDOC method to a multiple-metal organic compound (MMOC), forming an organometallic monolayer, are reported. The experiments described below were conducted by Dr. S. Martín at the University of Zaragoza. A quartz crystal microbalance (QCM) substrate was incubated in a 10^{-4} M solution of *trans*-[{(*th*-3-C≡C)(dppe)$_2$Ru}(μ-C≡CC_6H_4-4-C≡C){AuPPh_3}], [**100**], in chloroform. The surface coverage of the organometallic monolayer formed, [**100**]-SAM of 1.7×10^{-10} molcm^{-2}, as determined by the Sauerbrey equation[xxiii]

[xxiii] $\Delta f = -\frac{2 \cdot f_0^2 \cdot \Delta m}{A \cdot \rho_q^{1/2} \cdot \mu_q^{1/2}}$

Where: Δf = frequency variation before and after deposition of the monolayer; f_0 = fundamental resonant frequency of 5 MHz; Δm = mass change; A = electrode area; ρ_q = density of the quartz (2.65 gcm^{-3}) and μ_q = the shear module (2.95×10^{11} dyncm^{-2}).

with an observed frequency variation of -30 Hz, is in good agreement with the theoretical surface coverage of 2.4×10^{-10} molcm^{-2}, confirming monolayer deposition. After the annealing process (150 °C for two hours) and subsequent rinsing with chloroform, a further frequency variation of 6 Hz was observed, which is in good agreement with a loss of a material of 262 amu, *i.e.* triphenyl phosphine (PPh_3); if it is assumed that the surface coverage of the organic monolayer is maintained after the annealing, washing and drying process. The loss of PPh_3 after thermal treatment of [**100**]-SAM (Figure 4.39), in addition with the subsequent formal reduction of Au^I to Au^0 (Figure 4.40), was confirmed by XPS spectroscopy, where spectra were recorded on a silver substrate to avoid any possible misinterpretation of the results from using a gold substrate and a gold-containing sample. Spectral bands were deconvoluted using the CasaXPS program.

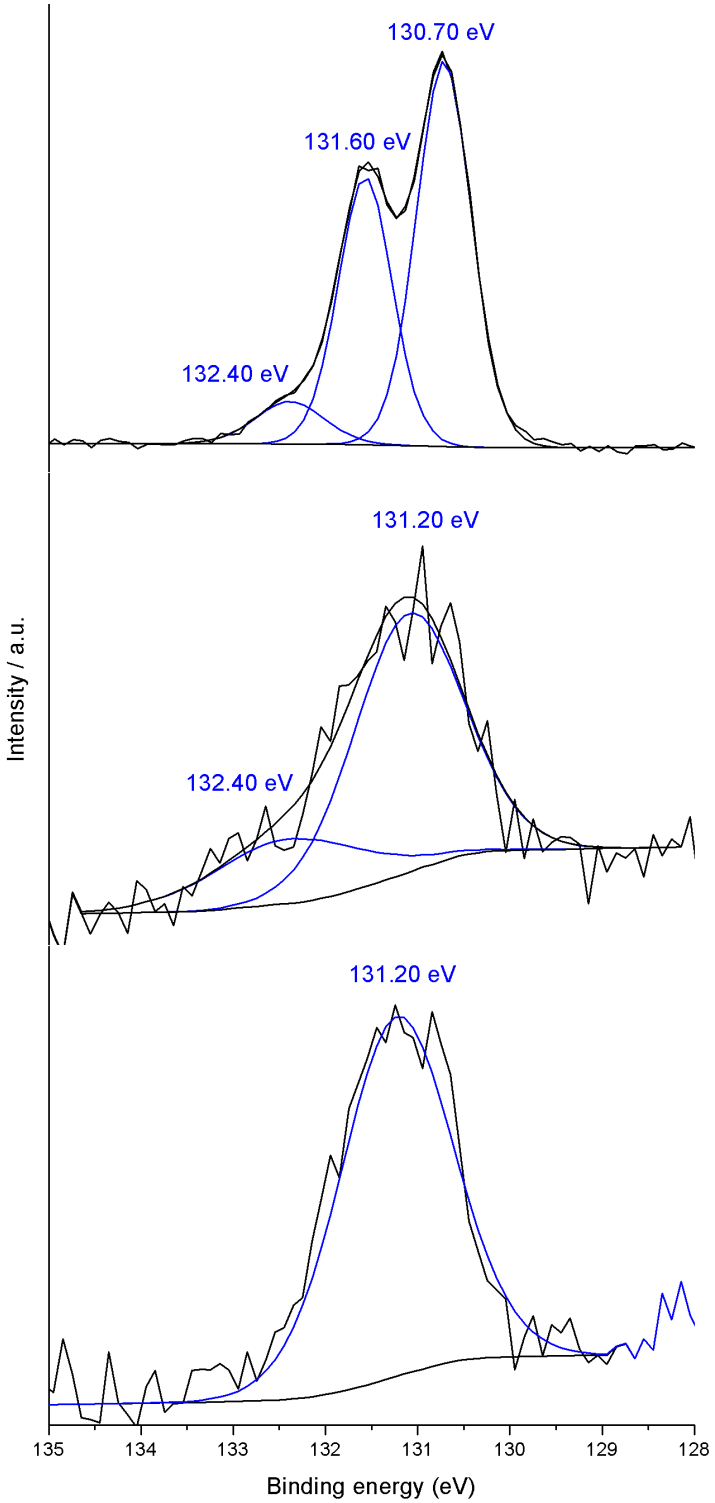

Figure 4.39: XPS spectra of the P(2*p*) region of i) [**100**] as a powder (top); ii) [**100**]-SAM (middle), still showing the characteristic P(2*p*) energy band of PPh_3 at 132.40 eV (FWHH values for the two bands at 131.20 and 132.40 eV are comparable), and iii) after annealing [**100**]-SAM for two hours at 150 °C (bottom), where the P(2*p*) energy band of PPh_3 could not be calculated.

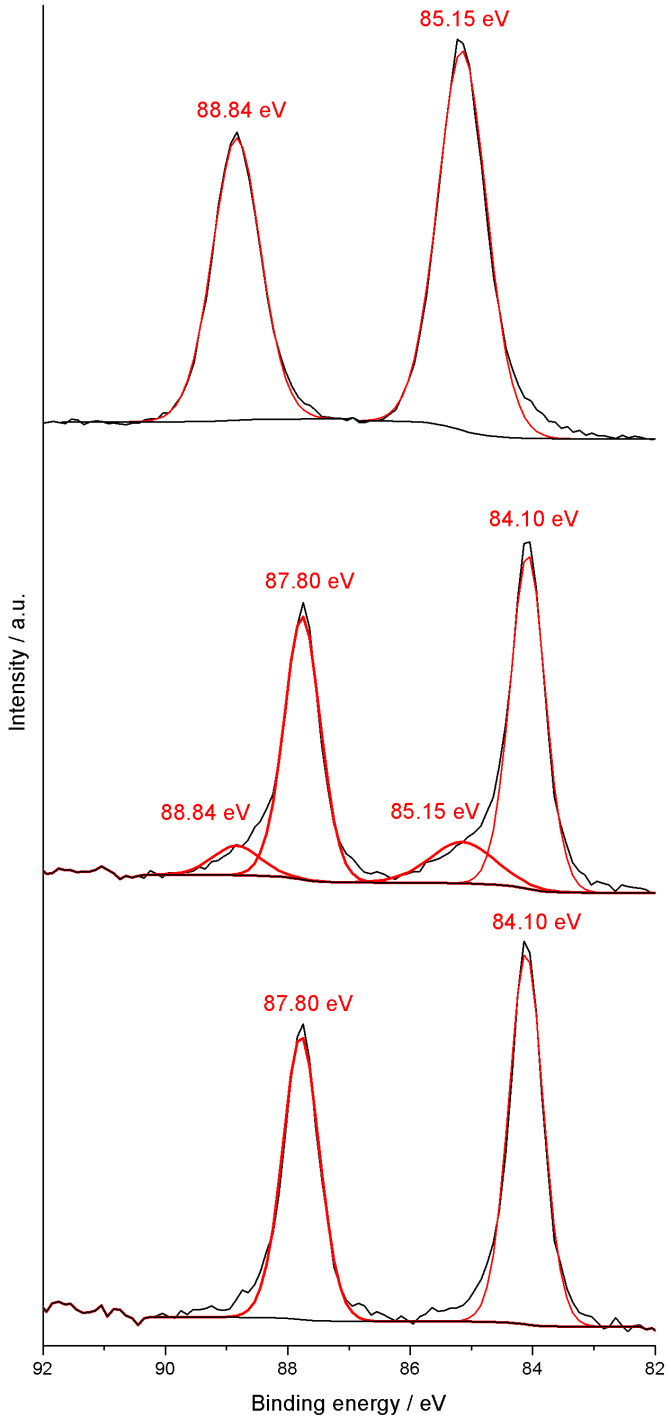

Figure 4.40: XPS spectra of the Au(4*f*) region of i) [**100**] as a powder (top), showing two intense Au^{I} peaks at 88.84 and 85.15 eV; ii) [**100**]-SAM (middle), indicating the preservation of Au^{I} at 88.84 and 85.15 eV whilst revealing two new, intense peaks at 87.80 and 84.10 eV, which correspond to Au^{0} that is likely formed during the irradiation process necessary for the recording of the spectrum,[30] and iii) after annealing [**100**]-SAM for two hours at 150 °C (bottom), showing two intense Au^{0} peaks at 87.80 and 84.10 eV.

With reference to Figures 4.39 and 4.40, a higher spectral resolution is obtained for the powder samples, where a large amount of compound is studied, whereas a lower spectral resolution is obtained from experiments on SAMs, where only a single monolayer is studied. To this end, the baseline corrections and levels of noise are inconsistent between spectra within these figures. Similarly, higher signal intensity is achieved in the powder experiments (with particular reference to Figure 4.39, revealing doublet peaks due to spin-orbit splitting effects) compared with the SAM experiments (where only a single, broad, averaged peak in Figure 4.39 was observed).

The differences in appearance, physical characteristics and compositions of [**100**]-SAM, before and after thermal treatment, was monitored by AFM (Figure 4.41). In the first instance, the images show that [**100**]-SAM before thermal treatment (left, Figure 4.41) does not form a complete monolayer. After annealing (right, Figure 4.41), bright spots of varying sizes can be observed, indicating the formations of GNPs or GNIs, where the amount of annealing time is known to influence the size of the resulting metallic structures.[30]

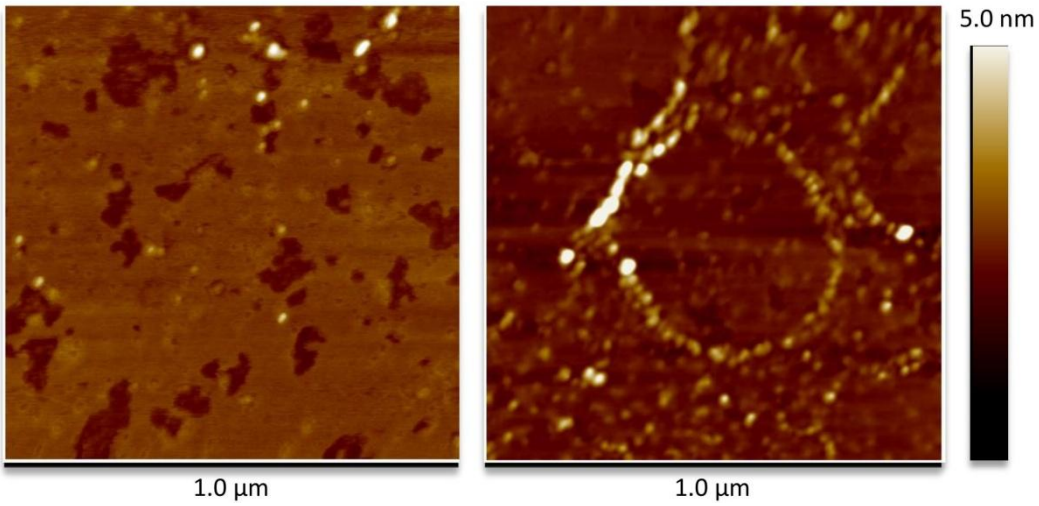

Figure 4.41: AFM images of [**100**]-SAM (left) and after annealing [**100**]-SAM for two hours at 150 °C onto a mica substrate (right).

Following annealing of [**100**]-SAM on a Au(111) surface, current-voltage (I-V) curves were recorded using conductive-AFM (Figure 4.42). The sigmoidal character of the trace, indicating molecular conductance, is in keeping with previous I-V curves

recorded for related complexes bearing the {Ru(dppe)$_2$} motif within gold junctions.[12, 14, 56, 57]

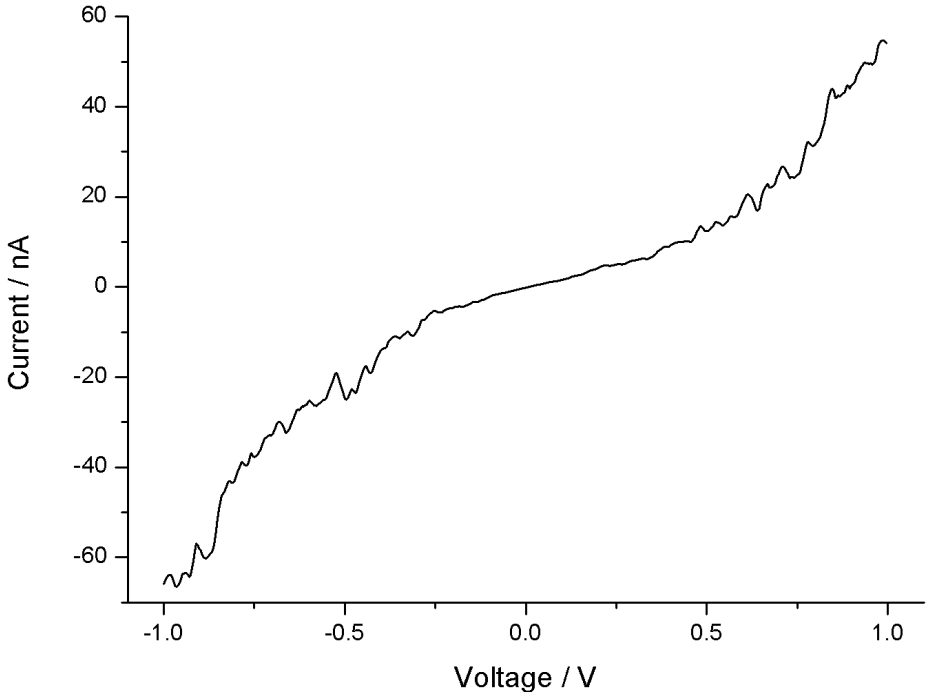

Figure 4.42: I-V curve recorded of [**100**]-SAM after annealing onto a Au(111) surface using CP-AFM positioned on top of the GNIs with a set point force of 10 nN.

4.7. Conclusions

In this Chapter, an array of multi-metallic *trans*-bis(alkynyl) complexes bearing the {Ru(dppe)$_2$} motif have been prepared, differing in i) the number of metals present; ii) the nature of the terminal binding groups; iii) the nature of the bridging ligands and iv) oxidation state. Bimetallic ([**94**]) and trimetallic ([**95**]) complexes display two and three reversible oxidations, respectively. Changing the nature of the end group (C≡CSiMe$_3$, C≡C-3-*th*, C≡CC$_6$H$_4$-4-C≡CSiMe$_3$) or central bridging fragment (C$_6$H$_4$-4-, C$_6$H$_2$-2,5-Me$_2$-4-, C$_6$H$_2$-2,5-^{i}Pr$_2$-4-) was not shown to significantly affect the underlying electronic structure of these highly conjugated complexes. The oxidation events show an appreciable amount of alkyne character.

The *mono*-oxidation complexes [**94**]$^+$ and [**95a**]$^+$ exhibit a principal, low energy NIR absorption band (π-π*, IL), several further higher energy NIR absorption bands (LMCT)

in addition with an aromatic radical band (π-π*). The structures of [**94**]$^+$ and [**95a**]$^+$ are consistent with the cation radical being stabilised on both a diruthenium diethynylbenzene bridged electrophore and a *mono*-metallic aryl ethynyl fragment, evincing the presence of redox isomers in solution as a result of thermally populated rotamer conformers. For [**94**]$^+$, upon increasing the steric bulk of the bridge (from [**94a**]$^+$ to [**94a-Me**]$^+$ to [**94a-^{i}Pr**]$^+$), complexes tend more towards Class III 'mixed-valence' systems (more intense, asymmetric bands), implicating a conformational bias of rotamers in solutions.

Ultimately, this work suggests that the redesign of molecules tailored for molecular electronics studies towards higher symmetry complexes, where the number of spectroscopically distinct rotamers will be reduced (leading to less convoluted spectra and more convincing data interpretations), is key. This work has also demonstrated the generality of the TIDOC method for top contact electrode fabrication, with the first reports of the method being applied to a multiple-metal organic complex (MMOC), forming an organometallic wire within fabricated Au|monolayer|Au junctions.

4.8. Experimental section

4.8.1. General conditions

All reactions were carried out under dry, high-purity nitrogen environments using oven-dried (119 °C) glassware and standard Schlenk techniques, although no special precautions were taken in order to exclude air or moisture during work-up. The reaction solvents CH_2Cl_2, THF, hexane and diethyl ether were used directly from the in-house solvent purification system, while MeOH was dried over dry magnesium turnings and iodine. All other solvents were reagent grade and used without further purification. The compounds: $HC{\equiv}CC_6H_4$-4-$C{\equiv}CH$,[58] $Me_3SiC{\equiv}CC_6H_2$-2,5-Me_2-4-$C{\equiv}CSiMe_3$,[58] $Me_3SiC{\equiv}CC_6H_2$-2,5-$^i Pr_2$-4-$C{\equiv}CSiMe_3$,[59] $HC{\equiv}CC_6H_2$-2,5-$^i Pr_2$-4-$C{\equiv}CH$,[60] $HC{\equiv}CC_6H_4$-4-$C{\equiv}CSiMe_3$,[61] $FcPF_6$,[40] $TlBF_4$,[62] $[AuCl(PPh_3)]$,[63] $[RuCl(dppe)_2]OTf$ ([**36**]OTf),[64] *trans*-$[RuCl(C{\equiv}CC_6H_4$-4-$C{\equiv}CSiMe_3)(dppe)_2]$ ([**38a**]),[31] *trans*-$[RuCl(C{\equiv}C$-3-*th*$)(dppe)_2]$ ([**38b**]),[65] *trans*-$[Ru(C{\equiv}CC_6H_4$-4-$C{\equiv}CSiMe_3)_2(dppe)_2]$,[31] [**43a**], *trans*-$[Ru(C{\equiv}C$-3-*th*$)_2(dppe)_2]$,[65] [**43b**] and

trans-[Ru(C≡CC_6H_4-4-C≡CH)$_2$(dppe)$_2$] ([**96**])[31] were synthesised by literature methods. All other reagents were commercially available and used as received.

Safety spectacles and gloves were worn at all times, and all experiments conducted in an efficient fume hood, following completion of appropriate COSHH assessments. Relatively non-toxic solvents were disposed of in the appropriate waste solvent container (chlorinated / non-chlorinated). Given the extremely toxicity of $TlBF_4$, the reagent was separately weighed in a sealed container in a fume hood. The solid was transferred to the reaction flask using a disposable paper funnel. The paper funnel was discarded immediately after use into a thallium-containing solid waste receptacle. For larger scale reactions, a secondary containment flask was utilised during the reaction period. Reactions reported below involving $TlBF_4$, (generally) produce equimolar amounts of TlCl, which is similarly extremely toxic. After completion of the reaction, following isolation of TlCl / residual $TlBF_4$ by the work-up procedures reported, the salts were either disposed of by i) dissolving in HNO_3 (aq.) and transferring into a thallium-containing solvent waste container or ii) in a thallium-containing solid waste container (along with the chromatographic medium, celite *etc.*).

NMR spectra were recorded at 25 °C on Varian Inova 300 (^{1}H, 300.2 MHz; ^{31}P, 121.5 MHz) or Bruker Avance 600 (^{1}H, 600.1 MHz; ^{13}C, 150.9 MHz; ^{31}P, 242.9 MHz) spectrometers. Chemical shifts were determined relative to internal residual solvent signals ($CDCl_3$: ^{1}H, δ = 7.26 ppm, ^{13}C, δ = 77.2 ppm; CD_2Cl_2: ^{1}H, δ = 5.32 ppm, ^{13}C, δ = 53.8 ppm) or external 85% H_3PO_4 (^{31}P, δ = 0.0 ppm).[66] FT-IR spectra were measured on a Nicolet Avatar 6700 or an Agilent Technologies Cary 660 spectrophotometer in a thin-layer cell fitted with CaF_2 windows. ESI-MS were recorded on a Waters LCT Premier XE mass spectrometer in positive ion mode from solutions in methanol. Cyclic voltammetry was carried out using a Versastat 3 potentiostat with a platinum disc working electrode, a platinum wire counter electrode, and a platinum wire pseudo-reference electrode, from 0.1 M $[N^nBu_4]PF_6$ CH_2Cl_2 solutions or 0.2 M $[N^nBu_4]PF_6$ $CHCl_3$ solutions. Potentials are reported *vs.* the ferrocene / ferrocenium couple ($[Fe(\eta^5\text{-}C_5H_5)_2]$ / $[Fe(\eta^5\text{-}C_5H_5)_2]^+$ = 0 V) using a decamethylferrocene / decamethylferrocenium internal standard ($[Fe(\eta^5\text{-}C_5Me_5)_2]$ / $[Fe(\eta^5\text{-}C_5Me_5)_2]^+$ = − 0.48 V).[40] Spectroelectrochemical measurements were made in an

OTTLE cell of Hartl design,[67] from 0.1 M $[N^nBu_4]PF_6$ CH_2Cl_2 solutions or 0.2 M $[Bu_4N]PF_6$ $CHCl_3$ solutions. The cell was fitted into the sample compartment of an Agilent Technologies Cary 5000 FT-IR spectrometer, Agilent Technologies Cary-5000 UV-Vis-NIR spectrometer or an Avantes diode array UV-Vis-NIR spectrometer system comprising two light sources (UV-Vis: AvaLight-DH-S-Bal, Vis-NIR: AvaLight-Hal-S) and two spectrometers (UV-Vis: AvaSpec-ULS204-8L-USB2, NIR: AvaSpec-NIR256-2.5TEC) connected to a custom-built sample holder by bifurcated fibre optic cables. The Vis-NIR light source was attenuated with a band-pass filter transparent between 900 – 4700 nm. Electrolysis in the cell was performed with a Palm Instruments EmStat 2 or EmStat 3 potentiostat.

4.8.2. Syntheses and characterisations of organic compounds

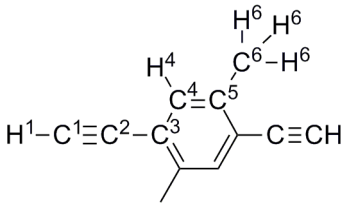

Synthesis of HC≡CC$_6$H$_2$-2,5-Me$_2$-4-C≡CH

A mixture of $Me_3SiC{\equiv}CC_6H_2$-2,5-Me_2-4-C≡C$SiMe_3$ (1.39 g, 4.7 mmol) and K_2CO_3 (2.05 g, 14.9 mmol) in MeOH (30 ml) and H_2O (4 ml) was stirred overnight. The reaction was quenched by addition of water (30 ml) and CH_2Cl_2 (30 ml), forming two layers. The organic layer was washed three times with water and twice with brine before being dried over magnesium sulphate. The pale yellow solution was filtered through filter paper and filtrate concentrated to dryness, where a white precipitate formed and was collected (0.67 g, 93 %).

IR (CH_2Cl_2, cm^{-1}): 2104s ν(C≡C). ^{1}H NMR ($CDCl_3$, 600 MHz) δ / ppm: 2.38 (s, 6H, H^6), 3.32 (s, 2H, H^1), 7.30 (s, 2H, H^4). ^{13}C NMR ($CDCl_3$, 300MHz) δ / ppm: 20.0 (s, C^6), 82.26 (s, C^1), 82.31 (s, C^2), 122.5 (s, C^3), 133.4 (s, C^4), 138.0 (s, C^5). ESI(+)-MS (*m/z*): 154 $[HC{\equiv}CC_6H_2$-2,5-Me_2-4-C≡$CH]^+$.

4.8.3. Syntheses and characterisations of *mono*-metallic complexes

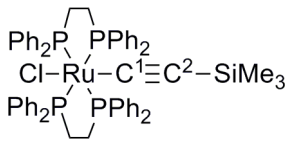

*Synthesis of trans-[RuCl(C≡CSiMe$_3$)(dppe)$_2$], [**38c**]*

A mixture of [**36**]OTf (0.12 g, 0.11 mmol), HC≡CSiMe$_3$ (16 µL, 0.11 mmol) and DBU (~ 5 drops, excess) in CH_2Cl_2 (8 ml) was stirred under N_2 for one hour. The solution colour changed from red / brown to yellow over the reaction period and a fine white solid precipitated. The yellow solution was concentrated under high vacuum to ~ 1 ml and excess MeOH added, resulting in the instant precipitation of a bright yellow solid. The yellow solid was collected by filtration, washed with MeOH (3 × 10ml) and hexanes (2 × 10 ml) then air dried (0.067 g, 61 %). A crystal suitable for X-ray crystallography was grown from a $CDCl_3$ / MeOH layer diffusion.

IR (CH_2Cl_2, cm^{-1}): 1990 ν(RuC≡C), 1606 ν(C=C). ^{1}H NMR ($CDCl_3$, 600 MHz) δ / ppm: − 0.01 (s, 9H, $SiMe_3$), 2.53 – 2.65 (m, 4H, CH_2, dppe), 2.70 – 2.84 (m, 4H, CH_2, dppe), 6.78 – 6.85 (m, 8H, H_o, dppe), 6.89 (t, J = 7 Hz, 8H, H_m, dppe), 7.12 (t, J = 7 Hz, 8H, H_m, dppe), 7.12 (t, J = 7 Hz, 4H, H_p, dppe), 7.27 (t, J = 7 Hz, 4H, H_p, dppe), 7.05 – 7.12 (m, 8H, H_o, dppe). ^{31}P{^{1}H} ($CDCl_3$, 300 MHz) δ / ppm: 52.3 (s, Ru(dppe)$_2$). ^{13}C{^{1}H} NMR ($CDCl_3$, 600 MHz) δ / ppm: 1.3 (s, $SiMe_3$), 31.0 (t, J = 12 Hz, CH_2, dppe), 120.6 (s, C^2), 126.8 (s, C_m, dppe), 127.2 (s, C_m, dppe), 128.5 (s, C_p, dppe), 129.4 (s, C_p, dppe), 134.1 (s, C_o, dppe), 135.4 (s, C_o, dppe), 136.0 (quin., J = 10 Hz, C_i, dppe), 137.7 (quin., J = 10 Hz, C_i, dppe), 146.8 (quin., J = 15 Hz, C^1). ESI(+)-MS (*m/z*): 1030 [RuCl(C≡CSiMe$_3$)(dppe)$_2$]$^+$, 995 [Ru(C≡CSiMe$_3$)(dppe)$_2$]$^+$. *The experimental data reported here are in agreement with that published previously.*[32]

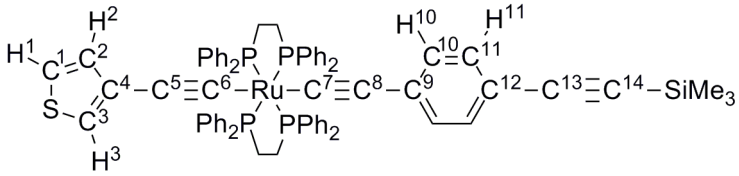

*Synthesis of trans-[Ru(C≡C-3-th)(C≡CC$_6$H$_4$-4-C≡CSiMe$_3$)(dppe)$_2$], [**97**]*

A mixture of [**38b**] (0.066 g, 0.063 mmol), HC≡CC$_6$H$_4$-4-C≡CSiMe$_3$ (0.013 g, 0.068 mmol), TlBF$_4$ (0.022 g, 0.076 mmol) and DBU (~ 4 drops, excess) in CH_2Cl_2 (7 ml) was stirred under N_2 for 16 hours. The yellow solution colour lightened over the reaction period and a white solid (TlCl) precipitated. The yellow solution was filtered through alumina (oven-dried, basic) to remove TlCl and reaction salts and yellow filtrate concentrated to dryness by rotary evaporation, yielding a bright yellow precipitate. The precipitate was washed with diethyl ether (3 × 10 ml) and hexanes (3 × 10 ml) then air dried (0.057 g, 75 %). Crystals suitable for single crystal X-ray crystallography were grown from a $CDCl_3$ / MeOH layer diffusion at reduced temperature (− 18 °C).

IR (CH_2Cl_2, cm^{-1}): 2147 ν(C≡CSiMe$_3$), 2058 ν(RuC≡C). ^{1}H NMR ($CDCl_3$, 600 MHz) δ / ppm: 0.27 (s, 9H, SiMe$_3$), 2.51 – 2.74 (m, 8H, CH_2, dppe), 6.55 (d, J = 2 Hz, 1H, H^3), 6.60 (apparent doublet, splitting = 8 Hz, 2H, H^{10}), 6.65 (d, J = 5 Hz, 1H, H^2), 6.93 (t, J = 7 Hz, 8H, H$_m$, dppe), 6.98 (t, J = 7 Hz, 8H, H$_m$, dppe), 7.11 (dd, J = 5, 2 Hz, 1H, H^1), 7.15 (t, J = 7 Hz, 4H, H$_p$, dppe), 7.19 (t, J = 7 Hz, 4H, H$_p$, dppe), 7.25 (apparent doublet, splitting = 8 Hz, 2H, H^{11}), 7.42 – 7.51 (m, 8H, H$_o$, dppe), 7.52 – 7.61 (m, 8H, H$_o$, dppe). ^{31}P{^{1}H} ($CDCl_3$, 300 MHz) δ / ppm: 54.5 (s, Ru(dppe)$_2$). ^{13}C{^{1}H} NMR ($CDCl_3$, 600 MHz) δ / ppm: 0.33 (s, SiMe$_3$), 31.6 (t, J = 12 Hz, CH_2, dppe), 93.7 (s, C^{14}), 106.3 (s, C^{13}), 111.3 (s, C^5), 116.6 (s, C^8), 117.3 (s, C^9), 120.5 (s, C^3), 122.9 (s, C^1), 127.1 (s, C$_m$, dppe), 127.2 (s, C$_m$, dppe), 127.8 (quin., J = 15 Hz, C^6 or C^7), 128.7 (s, C$_p$, dppe), 128.8 (s, C$_p$, dppe), 129.87 (s, C^{10}), 129.92 (s, C^2), 130.3 (s, C^4), 131.1 (s, C^{12}), 131.4 (s, C^{11}), 134.3 (s, C$_o$, dppe), 134.5 (s, C$_o$, dppe), 136.7 – 137.1 (m, C$_i$, dppe), 137.1 – 137.4 (m, C$_i$, dppe), 138.9 (quin., J = 15 Hz, C^6 or C^7). ESI(+)-MS (*m/z*): 1202 [Ru(C≡C-3-*th*)(C≡CC$_6$H$_4$-4-C≡CSiMe$_3$)(dppe)$_2$]$^+$, 1136 [Ru(C≡CC$_6$H$_4$-4-C≡CSiMe$_3$)(dppe)$_2$ + MeCN]$^+$, 1046 [Ru(C≡C-3-*th*)(dppe)$_2$ + MeCN]$^+$, 1004 [Ru(C≡C-3-*th*)(dppe)$_2$ – H]$^+$, 898 [Ru(dppe)$_2$]$^+$. Anal. found: C, 70.42; H, 5.09. Calc. for C$_{71}$H$_{64}$P$_4$RuSSi: C, 70.87; H, 5.37 %. Complex [**97**] exhibits two redox events (E$_{1/2}$(1):

0.05 V *rev*; ΔE_p(DMFC): 0.05 V; ΔE_p(1): 0.09 V; $E_{1/2}$(2): 0.88 V *irrev vs.* ferrocene using decamethylferrocene as an internal standard) in a $[N^nBu_4]PF_6$ CH_2Cl_2 medium.

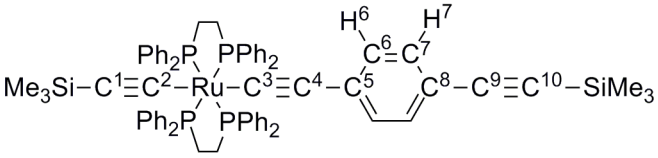

*Synthesis of trans-[Ru(C≡CSiMe$_3$)(C≡CC$_6$H$_4$-4-C≡CSiMe$_3$)(dppe)$_2$], [**98**]*

A mixture of [**38c**] (0.046 g, 0.045 mmol), HC≡CC$_6$H$_4$-4-C≡CSiMe$_3$ (0.025 g, 0.13 mmol), $TlBF_4$ (0.014 g, 0.049 mmol) and DBU (~ 7 drops, excess) in CH_2Cl_2 (7 ml) was stirred under N_2 for five hours. A white solid (TlCl) precipitated from the pale yellow solution over the reaction period. The yellow solution was concentrated to ~ 2 ml under high vacuum and filtered through a HPLC Teflon filter (20 μm pores) to remove TlCl and reaction salts. An excess of MeOH was then added to the yellow filtrate, resulting in the instant precipitation of a pale yellow solid. The solid was collected by filtration, washed with MeOH (3 × 15 ml) and air dried (0.049 g, 91 %). Crystals suitable for single crystal X-ray crystallography were grown from a CH_2Cl_2 / MeOH layer diffusion.

IR (CH_2Cl_2, cm^{-1}): 2147 ν(C≡CSiMe$_3$), 2065 ν(RuC≡C), 2061 ν(RuC≡C), 1593 ν(C=C). ^{1}H NMR ($CDCl_3$, 600 MHz) δ / ppm: − 0.03 (s, 9H, C^1-Si*Me*$_3$), 0.27 (s, 9H, C^{10}-Si*Me*$_3$), 2.55 – 2.66 (m, 4H, CH_2, dppe), 2.66 – 2.78 (m, 4H, CH_2, dppe), 6.41 (apparent doublet, splitting = 8 Hz, 2H, H^6), 6.82 (t, J = 8 Hz, 8H, H$_m$, dppe), 6.98 – 7.03 (m, 8H, H$_o$, dppe), 7.08 (t, J = 7 Hz, 4H, H$_p$, dppe), 7.10 (t, J = 7 Hz, 8H, H$_m$, dppe), 7.21 (apparent doublet, splitting = 8 Hz, 2H, H^7), 7.25 (t, J = 8 Hz, 4H, H$_p$, dppe), 8.00 – 8.07 (m, 8H, H$_o$, dppe). ^{31}P{^{1}H} ($CDCl_3$, 300 MHz) δ / ppm: 55.0 (s, Ru(dppe)$_2$). ^{13}C{^{1}H} NMR ($CDCl_3$, 600 MHz) δ / ppm: 0.35 (s, C^{10}-Si*Me*$_3$), 1.21 (s, C^1-Si*Me*$_3$), 31.6 (t, J = 12 Hz, CH_2, dppe), 93.6 (s, C^{10}), 106.7 (s, C^9), 115.5 (s, C^5), 116.3 (s, C^4), 124.3 (s, C^1), 126.97 – 127.10 (m, C$_m$, dppe), 128.3 (s, C$_p$, dppe), 129.2 (s, C$_p$, dppe), 130.1 (s, C^6), 131.1 (s, C^8), 131.2 (s, C^7), 133.8 (s, C$_o$, dppe), 135.2 (s, C$_o$, dppe), 136.7 (quin., J = 10 Hz, C$_i$, dppe), 137.8 (quin., J = 10 Hz, C$_i$, dppe), 140.5 (quin., J = 15 Hz, C^2 or C^3), 153.5 (quin., J = 15 Hz, C^2 or C^3). ESI(+)-MS (*m/z*): 1192 [Ru(C≡CSiMe$_3$)(C≡CC$_6$H$_4$-4-C≡CSiMe$_3$)(dppe)$_2$]$^+$, 995 [Ru(C≡CSiMe$_3$)(dppe)$_2$]$^+$, 898

$[Ru(dppe)_2]^+$. Anal. found: C, 66.58; H, 5.56. Calc. for $C_{70}H_{70}P_4RuSi_2 \times CH_2Cl_2$: C, 66.76; H, 5.69 %.

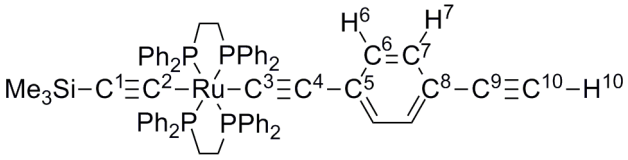

*Synthesis of trans-[Ru(C≡CSiMe$_3$)(C≡CC$_6$H$_4$-4-C≡CH)(dppe)$_2$], [**99**]*

A mixture of [**98**] (0.0216 g, 0.018 mmol) and TBAF.3H$_2$O (0.1M THF solution, 0.23 ml, 0.023 mmol) in CH_2Cl_2 (7 ml) was stirred under N_2 overnight. The yellow solution colour darkened over the reaction period. To the reaction mixture was added MeOH (~ 5 ml) and solvent slowly concentrated by rotary evaporation. Upon formation of a yellow / brown solid in a brown solution, the suspension was filtered, yielding a brown / yellow precipitate. The solid was washed with MeOH (3 × 10 ml) and hexanes (2 × 10 ml), then air dried (0.019 g, 92 %). Crystals suitable for single crystal X-ray crystallography were grown from a CH_2Cl_2 / hexanes layer diffusion at reduced temperature (− 18 °C).

IR (CH_2Cl_2, cm^{-1}): 3045 ν(≡C-H) 2067 ν(RuC≡C), 2062 ν(RuC≡C), 1994 ν(C≡CH), 1593 ν(C=C). ^{1}H NMR ($CDCl_3$, 600 MHz) δ / ppm: − 0.04 (s, 9H, $SiMe_3$), 2.55 – 2.66 (m, 4H, CH_2, dppe), 2.66 – 2.78 (m, 4H, CH_2, dppe), 3.10 (s, 1H, H^{10}), 6.43 (apparent doublet, splitting = 8 Hz, 2H, H^6), 6.84 (t, J = 8 Hz, 8H, H_m, dppe), 6.98 – 7.06 (m, 8H, H_o, dppe), 7.10 (t, J = 8 Hz, 8H, H_m, dppe), 7.21 (apparent doublet, splitting = 8 Hz, 2H, H^7), 7.24 (t, J = 8 Hz, 8H, H_p, dppe), 7.99 – 8.06 (m, 8H, H_o, dppe). ^{31}P{^{1}H} ($CDCl_3$, 300 MHz) δ / ppm: 55.0 (s, $Ru(dppe)_2$). ^{13}C{^{1}H} NMR ($CDCl_3$, 600 MHz) δ / ppm: 1.20 (s, $SiMe_3$), 31.6 (t, J = 12 Hz, CH_2, dppe), 76.9 (s, C^{10}), 85.1 (s, C^9), 115.3 (s, C^8), 115.4 (s, C^4), 124.3 (s, C^1), 127.1 (s, C_m, dppe), 128.4 (s, C_p, dppe), 129.2 (s, C_p, dppe), 130.1 (s, C^6), 131.3 (s, C^7), 131.4 (s, C^5), 133.8 (s, C_o, dppe), 135.2 (s, C_o, dppe), 136.7 (quin., J = 10 Hz, C_i, dppe), 137.8 (quin., J = 10 Hz, C_i, dppe), 140.6 (quin., J = 15 Hz, C^2 or C^3), 153.5 (quin., J = 15 Hz, C^2 or C^3). ESI(+)-MS (*m/z*): 1120 $[Ru(C{\equiv}CSiMe_3)(C{\equiv}CC_6H_4\text{-}4\text{-}C{\equiv}CH)(dppe)_2]^+$, 1023 $[Ru(C{\equiv}CC_6H_4\text{-}4\text{-}C{\equiv}CH)(dppe)_2]^+$, 995 $[Ru(C{\equiv}CSiMe_3)(dppe)_2]^+$, 898 $[Ru(dppe)_2]^+$. Anal. found: C, 71.63; H, 5.48. Calc. for $C_{67}H_{62}P_4RuSi$: C, 71.77; H, 5.18 %.

4.8.4. Syntheses and characterisations of bimetallic complexes

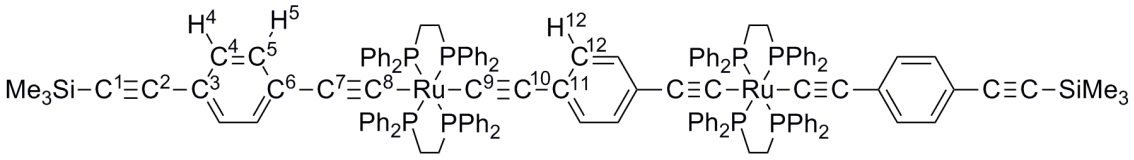

*Synthesis of trans-[{(Me$_3$SiC≡CC$_6$H$_4$-4-C≡C)(dppe)$_2$Ru}$_2$(μ-C≡CC$_6$H$_4$-4-C≡C)], [**94a**]*

The reagents [**38a**] (0.10 g, 0.092 mmol), $TlBF_4$ (0.030 g, 0.10 mmol) and DBU (~ 3 drops, excess) were added to a flask containing CH_2Cl_2 (20 ml) fitted with a pressure equalising dropping funnel. A solution of HC≡CC$_6$H$_4$-4-C≡CH (0.0059 g, 0.047 mmol) in CH_2Cl_2 (10 ml) was added to the dropping funnel. The colourless alkyne solution was added to the yellow ruthenium solution slowly dropwise (over ~ 30 minutes), and the complete solution then stirred for a further ten minutes under N_2. The yellow solution remained constant throughout the reaction period but a white solid (TlCl) precipitated. The yellow solution was concentrated carefully under high vacuum to ~ 2 ml and then filtered through alumina (basic, oven-dried) to remove TlCl and reaction salts, eluting with minimum CH_2Cl_2. The yellow filtrate was then concentrated again to ~ 2 ml and excess hexanes added, yielding a bright yellow solid. The solid was collected by filtration, washed with hexanes (2 × 20 ml) and cold MeOH (2 × 20 ml), then vacuum dried (0.090 g, 84 %).

IR (CH_2Cl_2, cm^{-1}): 2148 ν(C≡CSiMe$_3$), 2056 ν(RuC≡C). ^{1}H NMR ($CDCl_3$, 600 MHz) δ / ppm: 0.27 (s, 18H, SiMe$_3$), 2.61 – 2.75 (m, 16H, CH_2, dppe), 6.56 (apparent doublet, splitting = 8 Hz, 4H, H^5), 6.72 (s, 4H, H^{12}), 6.92 (t, J = 8 Hz, 16H, H$_m$, dppe), 7.02 (t, J = 8 Hz, 16H, H$_m$, dppe), 7.15 (t, J = 8 Hz, 8H, H$_p$, dppe), 7.22 (t, J = 8 Hz, 8H, H$_p$, dppe), 7.24 (apparent doublet, splitting = 8 Hz, 4H, H^4), 7.35 – 7.42 (m, 16H, H$_o$, dppe), 7.66 – 7.75 (m, 16H, H$_o$, dppe). ^{31}P{^{1}H} NMR ($CDCl_3$, 600 MHz) δ / ppm: 53.4 (s, Ru(dppe)$_2$). ^{13}C{^{1}H} NMR ($CDCl_3$, 600 MHz) δ / ppm: 1.21 (s, SiMe$_3$), 31.7 (t, J = 12 Hz, CH_2, dppe), 93.7 (s, C^1), 106.8 (s, C^2), 116.5 (s, C^7), 117.1 (s, C^6), 118.5 (s, C^{10}), 125.8 (s s, C^{11}), 127.2 (s, C$_m$, dppe), 127.3 (s, C$_m$, dppe), 128.7 (s, C$_p$, dppe), 128.8 (s, C$_p$, dppe), 129.4 (s, C^{12}), 129.9 (s, C^5), 131.2 (s, C^3), 131.4 (s, C^4), 134.3 (s, C$_o$, dppe), 134.7 (s, C$_o$, dppe), 136.7 − 137.3 (m, C$_i$, dppe), 137.4 – 137.9 (m, C$_i$, dppe). ESI(+)-MS (*m/z*): 2316 [(Me$_3$SiC≡CC$_6$H$_4$-4-C≡C)(dppe)$_2$Ru}$_2$(μ-C≡CC$_6$H$_4$-4-C≡C) + 2H]$^+$, 1123 [Ru(C≡CC$_6$H$_4$-4-C≡CSiMe$_3$)(dppe)$_2$ + C$_2$H$_4$]$^+$, 940 [Ru(dppe)$_2$ + MeCN +

H]$^+$, 897 [Ru(dppe)$_2$ – H]$^+$. Anal. found: C, 71.62; H, 4.64. Calc. for $C_{140}H_{126}P_8Ru_2Si_2$: C, 72.58; H, 5.49 %.

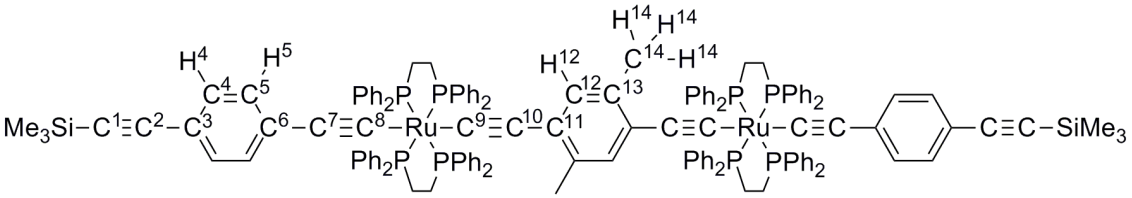

*Synthesis of trans-[{(Me$_3$SiC≡CC$_6$H$_4$-4-C≡C)(dppe)$_2$Ru}$_2$(μ-C≡CC$_6$H$_2$-2,5-Me$_2$-4-C≡C)], [**94a-Me**]*

The reagents [**38a**] (0.096 g, 0.085 mmol), $TlBF_4$ (0.029 g, 0.10 mmol) and DBU (~ 4 drops, excess) were added to a flask containing CH_2Cl_2 (20 ml) fitted with a pressure equalising dropping funnel. A solution of HC≡CC$_6$H$_2$-2,5-Me$_2$-4-C≡CH (0.0065 g, 0.042 mmol) in CH_2Cl_2 (10 ml) was added to the dropping funnel. The colourless alkyne solution was added to the dilute yellow ruthenium solution slowly dropwise (over ~ one hour), and the complete solution then left to stir under N_2 overnight. The yellow solution remained constant throughout the reaction period but a white solid (TlCl) precipitated. The yellow solution was concentrated carefully under high vacuum to ~ 10 ml and filtered through alumina (basic, oven-dried) to remove TlCl and reaction salts, eluting with CH_2Cl_2. The yellow filtrate was again concentrated to ~ 2 ml and an excess of diethyl ether added, yielding a bright yellow precipitate. The precipitate was collected by filtration, washed with diethyl ether (2 × 20 ml) and hexanes (2 × 20 ml), then vacuum dried (0.067 g, 67 %).

IR (CH_2Cl_2, cm^{-1}): 2149 ν(C≡CSiMe$_3$), 2059 ν(RuC≡C), 2044 ν(RuC≡C). ^{1}H NMR (CD_2Cl_2, 600 MHz) δ / ppm: 0.26 (s, 18H, SiMe$_3$), 1.86 (s, br., 6H, H^{14}), 2.57 – 2.70 (m, 8H, CH$_2$, dppe), 2.72 – 2.84 (m, 8H, CH$_2$, dppe), 6.40 (s, br., 2H, H^{12}), 6.49 (apparent doublet, splitting = 7 Hz, 4H, H^5), 6.87 (t, J = 8 Hz, 16H, H$_m$, dppe), 7.05 − 7.11 (m, 32H, H$_o$ and H$_m$, dppe), 7.13 (t, J = 8 Hz, 8H, H$_p$, dppe), 7.20 (apparent doublet, splitting = 7 Hz, 4H, H^4), 7.26 (t, J = 8 Hz, 8H, H$_p$, dppe), 7.94 – 8.04 (m, H$_o$, dppe). ^{31}P{^{1}H} NMR (CD_2Cl_2, 600 MHz) δ / ppm: 53.9 (s, Ru(dppe)$_2$). ^{13}C{^{1}H} NMR (CD_2Cl_2, 600 MHz) δ / ppm: 0.6 (s, SiMe$_3$), 20.8 (s, C^{14}), 31.4 – 31.8 (m, CH$_2$, dppe), 94.3 (s, C^1), 115.9 (s, C^7 or C^{10}), 119.5 (s, C^7 or C^{10}), 127.7 (s, C$_m$, dppe), 128.0 (s, C$_m$, dppe), 129.0 (s, C$_p$, dppe), 129.8 (s, C$_p$, dppe), 130.9 (s, C^5), 131.7 (s, C^4), 131.8 (s, C^{12}), 134.4 (s, C$_o$, dppe), 135.9 (s, C$_o$, dppe), 137.6 – 138.6 (m, C$_i$, dppe). ESI(+)-MS

(*m/z*): 2342 $[\{(Me_3SiC{\equiv}CC_6H_4\text{-}4\text{-}C{\equiv}C)(dppe)_2Ru\}_2(\mu\text{-}C{\equiv}CC_6H_2\text{-}2,5\text{-}Me_2\text{-}4\text{-}C{\equiv}C)]^+$, 1136 $[Ru(C{\equiv}CC_6H_4\text{-}4\text{-}C{\equiv}CSiMe_3)(dppe)_2 + MeCN]^+$, 897 $[Ru(dppe)_2 - H]^+$. Anal. found: C, 72.84; H, 5.52. Calc. for $C_{142}H_{130}P_8Ru_2Si_2$: C, 72.74; H, 5.59 %.

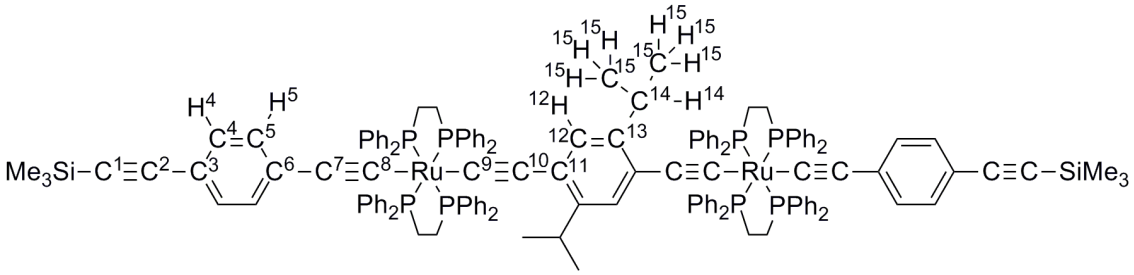

*Synthesis of trans-[{(Me$_3$SiC≡CC$_6$H$_4$-4-C≡C)(dppe)$_2$Ru}$_2$(μ-C≡CC$_6$H$_2$-2,5-^{i}Pr$_2$-4-C≡C)], [**94a-^{i}Pr**]*

The reagents [**38a**] (0.084 g, 0.074 mmol), $TlBF_4$ (0.034 g, 0.11 mmol) and DBU (~ 6 drops, excess) were added to a flask containing CH_2Cl_2 (20 ml) fitted with a pressure equalising dropping funnel and solution stirred under N_2 for 30 minutes. Over this period, the yellow solution colour lightened and a white solid (TlCl) precipitated. A solution of $HC{\equiv}CC_6H_2$-2,5-^{i}Pr$_2$-4-C≡CH (0.0078 g, 0.037 mmol) in CH_2Cl_2 (7 ml) was added to the dropping funnel. The colourless alkyne solution was added to the dilute yellow ruthenium solution slowly dropwise (over ~ one hour), and the complete solution then left to stir under N_2 overnight. The yellow solution was concentrated carefully under high vacuum to ~ 1 ml, filtered through a HPLC Teflon filter (20 μm pores) to remove TlCl and reaction salts, and MeOH added (6 ml) to the filtrate, where a yellow solid formed in a yellow solution. The solution was left in the fridge for several hours to aid precipitation before being filtered (care* filtrate may contain unreacted $TlBF_4$) and washed with minimum cold MeOH (3 × 2 ml) [Note: $TlBF_4$ is soluble is MeOH]. The solid was further washed with cold diethyl ether (3 × 5 ml) and hexanes (1 × 5 ml), then vacuum dried (0.039 g, 44 %).

IR ($CHCl_3$, cm^{-1}): 2149 ν(C≡CSiMe$_3$), 2066 ν(RuC≡C), 2038 ν(RuC≡C), 1593 (C=C). ^{1}H NMR ($CDCl_3$, 600 MHz) δ / ppm: 0.26 (s, 18H, SiMe$_3$), 0.93 (d, J = 6 Hz, 12H, H^{15}), 2.48 – 2.60 (m, 8H, CH$_2$, dppe), 2.75 – 2.87 (m, 8H, CH$_2$, dppe), 3.27 – 3.35 (m, 2H, H^{14}), 6.33 (apparent doublet, splitting = 8 Hz, 4H, H^5), 6.70 (s, 2H, H^{12}), 6.79 (t, J = 7 Hz, 16H, H$_m$, dppe), 6.82 – 6.87 (m, 16H, H$_o$, dppe), 7.07 (t, J = 7 Hz, 8H, H$_p$, dppe), 7.11 (t, J = 7 Hz, 16H, H$_m$, dppe), 7.18 (apparent doublet, splitting = 8 Hz, 4H,

H^4), 7.23 (t, J = 7 Hz, 8H, H_p, dppe), 8.15 – 8.22 (m, 16H, H_o, dppe). $^{31}P\{^1H\}$ NMR ($CDCl_3$, 600 MHz) δ / ppm: 55.5 (s, $Ru(dppe)_2$). $^{13}C\{^1H\}$ NMR ($CDCl_3$, 600 MHz) δ / ppm: 0.35 (s, $SiMe_3$), 24.6 (s, C^{15}), 32.1 (t, J = 14 Hz, CH_2, dppe), 30.5 (s, C^{14}), 93.6 (s, C^1), 106.9 (s, C^2), 116.0 (s, C^7), 120.4 (s, C^{10}), 124.9 (s, C^{11}), 127.0 (s, C_m, dppe), 127.5 (s, C_m, dppe), 127.7 (s, C^{12}), 128.1 (s, C_p, dppe), 129.4 (s, C_p, dppe), 130.3 (s, C^5), 131.1 (s, C^4), 133.6 (s, C_o, dppe), 135.5 (s, C_o, dppe), 136.8 – 137.3 (m, C_i, dppe), 138.0 – 138.3 (m, C_i, dppe), 144.7 (s, C^{13}). ESI(+)-MS (*m/z*): 2399 $[\{(Me_3SiC{\equiv}CC_6H_4\text{-}4\text{-}C{\equiv}C)(dppe)_2Ru\}_2(\mu\text{-}C{\equiv}CC_6H_2\text{-}2,5\text{-}^iPr_2\text{-}4\text{-}C{\equiv}C)]^+$, 2327 $[\{(Me_3SiC{\equiv}CC_6H_4\text{-}4\text{-}C{\equiv}C)(dppe)_2Ru\}(\mu\text{-}C{\equiv}CC_6H_2\text{-}2,5\text{-}^iPr_2\text{-}4\text{-}C{\equiv}C)\{Ru(dppe)_2(C{\equiv}CC_6H_4\text{-}4\text{-}C{\equiv}CH)\}]^+$, 1136 $[Ru(C{\equiv}CC_6H_4\text{-}4\text{-}C{\equiv}CSiMe_3)(dppe)_2 + MeCN]^+$, 1124 $[Ru(C{\equiv}CC_6H_4\text{-}4\text{-}C{\equiv}CSiMe_3)(dppe)_2 + C_2H_4]^+$, 930 $[Ru(dppe)_2 + MeOH]^+$.

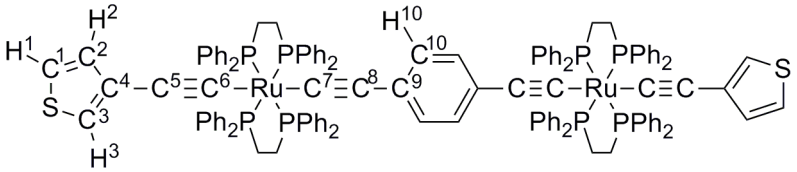

*Synthesis of trans-[{(th-3-C≡C)(dppe)$_2$Ru}$_2$(μ-C≡CC$_6$H$_4$-4-C≡C)], [**94b**]*

The reagents [**38b**] (0.11 g, 0.10 mmol), $TlBF_4$ (0.032 g, 0.11 mmol) and DBU (~ 6 drops, excess) were added to a flask containing CH_2Cl_2 (15 ml) fitted with a pressure equalising dropping funnel. A solution of $HC{\equiv}CC_6H_4$-4-C≡CH (0.0064 g, 0.051 mmol) in CH_2Cl_2 (7 ml) was added to the dropping funnel. The colourless alkyne solution was added to the dilute yellow ruthenium solution slowly dropwise (over ~ 40 minutes), then the complete solution stirred under N_2 for a further 90 minutes. Over this period, the yellow solution colour lightened and a white solid (TlCl) precipitated. The yellow solution was concentrated carefully under high vacuum to ~ 2 ml and then filtered through alumina (basic, oven-dried) to remove TlCl and reaction salts, eluting with minimum CH_2Cl_2. The yellow filtrate was concentrated again to ~ 2 ml and excess hexane added, yielding a bright yellow solid. The solid was collected by filtration, washed with hexanes (3 × 20 ml) and vacuum dried (0.089 g, 82 %).

IR (CH_2Cl_2, cm^{-1}): 2060 ν(RuC≡C). ^1H NMR ($CDCl_3$, 600 MHz) δ / ppm: 2.62 – 2.72 (m, 16H, CH_2, dppe), 6.48 (dd, J = 3, 1 Hz, 2H, H^3), 6.59 (dd, J = 5, 1 Hz, 2H, H^2), 6.68

(s, 4H, H^{10}), 6.97 (t, J = 8 Hz, 16H, H_m, dppe), 7.00 (t, J = 8 Hz, 16H, H_m, dppe), 7.08 (dd, J = 5, 3 Hz, 2H, H^1), 7.18 (t, J = 8 Hz, 4H, H_p, dppe), 7.22 (t, J = 8 Hz, 4H, H_p, dppe), 7.43 – 7.49 (m, 16H, H_o, dppe), 7.65 – 7.70 (m, 16H, H_o, dppe). $^{31}P\{^1H\}$ NMR ($CDCl_3$, 300 MHz) δ / ppm: 54.7 (s, $Ru(dppe)_2$). $^{13}C\{^1H\}$ NMR ($CDCl_3$, 600 MHz) δ / ppm: 31.8 (t, J = 12 Hz, CH_2, dppe), 110.5 (s, C^5), 118.0 (s, C^8), 120.3 (s, C^3), 122.7 (s, C^2), 125.8 (s, C^9), 127.1 (s, C_m, dppe), 127.2 (s, C_m, dppe), 128.6 (s, C_p, dppe), 128.7 (s, C_p, dppe) 128.7 (s, C^{10}), 130.2 (s, C^1), 130.5 (s, C^4), 134.4 (s, C_o, dppe), 134.7 (s, C_o, dppe), 137.2- 138.2 (m, C_i, dppe). ESI(+)-MS (*m/z*): 2134 [(*th*-3-C≡C)$(dppe)_2Ru\}_2(\mu$-C≡CC_6H_4-4-C≡C)]$^+$, 1130 [Ru(C≡C-3-*th*)(C≡CC_6H_4-4-C≡CH)$(dppe)_2]^+$, 898 $[Ru(dppe)_2]^+$. Anal. found: C, 70.86; H, 5.03. Calc. for $C_{126}H_{106}P_8Ru_2S_2$: C, 70.84; H, 5.01 %.

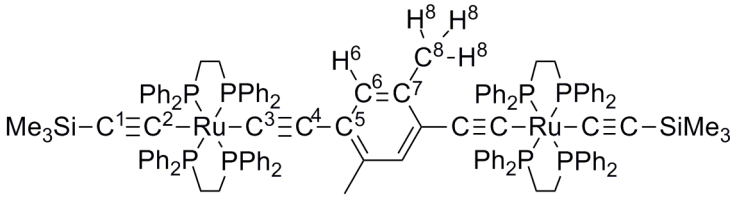

*Synthesis of trans-[{(Me₃SiC≡C)(dppe)₂Ru}₂(μ-C≡CC_6H_2-2,5-Me_2-4-C≡C)], [**94c-Me**]*

The reagents [**38c**] (0.070 g, 0.068 mmol), $TlBF_4$ (0.021 g, 0.072 mmol) and DBU (~ 6 drops, excess) were added to a flask containing CH_2Cl_2 (20 ml) fitted with a pressure equalising dropping funnel. A solution of HC≡CC_6H_2-2,5-Me_2-4-C≡CH (0.0052 g, 0.034 mmol) in CH_2Cl_2 (5 ml) was added to the dropping funnel. The colourless alkyne solution was added to the dilute yellow ruthenium solution slowly dropwise (over ~ 30 minutes), then the complete solution stirred under N_2 for a further three hours. Over this period, the yellow solution colour lightened and a white solid (TlCl) precipitated. The yellow solution was concentrated carefully to dryness and transferred into a glovebox. The solution was re-extracted with CH_2Cl_2 (10 ml) and filtered through a small basic alumina plug to remove TlCl and reaction salts, eluting with CH_2Cl_2. The bright yellow filtrate was concentrated to dryness, yielding a bright yellow, air-sensitive solid (0.049 g, 67 %).

IR (CH_2Cl_2, cm^{-1}): 2055 ν(RuC≡C), 2046 ν(RuC≡C), 1992 ν(C≡C$SiMe_3$), 1482 ν(C=C). ^1H NMR ($CDCl_3$, 600 MHz) δ / ppm: − 0.10 (s, 18H, $SiMe_3$), 1.75 (s, 6H, H^8), 2.64 − 2.82 (m, 16H, CH_2, dppe), 6.07 (s, 2H, H^6), 6.96 (t, J = 8 Hz, 16H, H_m, dppe), 6.99 (t, J = 8 Hz, 16H, H_m, dppe), 7.16 (t, J = 8 Hz, 16H, H_p, dppe), 7.46 – 7.52 (m,

16H, H_o, dppe), 7.61 – 7.68 (m, 16H, H_o, dppe). $^{31}P\{^1H\}$ NMR ($CDCl_3$, 600 MHz) δ / ppm: 54.0 (s, $Ru(dppe)_2$). $^{13}C\{^1H\}$ NMR ($CDCl_3$, 600 MHz) δ / ppm: 1.5 (s, $SiMe_3$), 20.0 (s, C^8), 31.4 – 31.9 (m, CH_2, dppe), 115.2 (s, C^4), 118.6 (s, C^1), 127.0 (s, C_m, dppe), 127.2 (s, C_m, dppe), 128.5 (s, C_p, dppe), 128.7 (s, C_p, dppe), 132.7 (s, C^6), 133.5 (s, C^7), 134.6 (s, C_o, dppe), 134.7 (s, C^5), 135.0 (s, C_o, dppe), 137.3 – 138.2 (m, C_i, dppe). ESI(+)-MS (*m/z*): 2174 $[(Me_3SiC{\equiv}C)(dppe)_2Ru\}_2(\mu\text{-}C{\equiv}CC_6H_2\text{-}2,5\text{-}Me_2\text{-}4\text{-}C{\equiv}C) + MeOH]^+$, 1036 $[Ru(C{\equiv}CC_6H_2\text{-}2,5\text{-}Me_2\text{-}C{\equiv}CH)(dppe)_2]^+$, 898 $[Ru(dppe)_2]^+$.

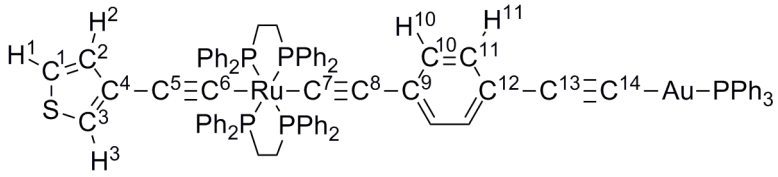

*Synthesis of trans-[{(th-3-C≡C)(dppe)$_2$Ru}(μ-C≡CC_6H_4-4-C≡C){AuPPh$_3$}], **[100]***

A mixture of [**97**] (0.054 g, 0.045 mmol) and TBAF.$3H_2O$ (0.013 g, 0.048 mmol) in MeOH (5 ml), THF (10 ml) and CH_2Cl_2 (4 ml) was stirred under N_2 for 15 minutes. The yellow solution darkened over the reaction period. Following this, NaOH (0.017 g, 0.42 mmol) was added and solution stirred for a further 10 minutes. Finally, [$AuCl(PPh_3)$] (0.023 g, 0.45 mmol) was added to the yellow solution and solution stirred under N_2 for a further 42 hours. The solvent was removed under high vacuum, yielding a yellow residue. The residue was extracted with CH_2Cl_2 and filtered through alumina (basic, oven-dried) to remove reaction salts. The pale yellow filtrate was concentrated to dryness by rotary evaporation, yielding a pale yellow solid. The solid was washed with MeOH (3 × 10 ml) and hexanes (3 × 10 ml), then air dried (0.060 g, 84 %).

IR (CH_2Cl_2, cm^{-1}): 2060 ν(C≡C), 2053 ν(C≡C). ^1H NMR ($CDCl_3$, 300 MHz) δ / ppm: 2.47 – 2.72 (m, 8H, CH_2, dppe), 6.50 (d, J = 3 Hz, 1H, H^3), 6.60 (apparent doublet, splitting = 8 Hz, 2H, H^{10}), 6.61 (d, J = 4 Hz, 1H, H^2), 6.89 – 7.63 (m, 55H, Ph, dppe and PPh_3), 7.09 (dd, J = 4, 3 Hz, 1H, H^1), 7.28 (apparent doublet, splitting = 8 Hz, 2H, H^{11}). $^{31}P\{^1H\}$ ($CDCl_3$, 300 MHz) δ / ppm: 43.6 (s, $AuPPh_3$), 54.6 (s, $Ru(dppe)_2$). $^{13}C\{^1H\}$ NMR ($CDCl_3$, 600 MHz) δ / ppm: 31.4 – 32.0 (m, CH_2, dppe), 111.2 (s, C^5 or C^8), 111.3 (s, C^5 or C^8), 120.4 (s, C^3), 122.8 (s, C^1), 127.1 (s, C_m, Ph), 127.2 (s, C_m, Ph), 128.7 (s, C_p, Ph), 128.8 (s, C_p, Ph), 129.27 (s, C_p, Ph), 129.33 (s, C_p, Ph), 130.0 (s, C^2), 131.7 (s, C^{10} or C^{11}), 131.8 (s, C^{10} or C^{11}), 134.2 − 134.8 (m, C_o, Ph), 136 – 137.8 (m,

C_i, Ph). ESI(+)-MS (*m/z*): 1155 [Ru(C≡C-3-*th*)(C≡CC_6H_4-4-C≡C)(dppe)$_2$ + C_2H_4]$^+$, 898 [Ru(dppe)$_2$]$^+$. Anal. found: C, 64.89; H, 4.26. Calc. for $C_{86}H_{70}AuP_5RuS$: C, 64.98; H, 4.44 %. Complex [**100**] exhibits three redox events ($E_{1/2}$(1): 0.03 V *rev*; ΔE_p(DMFC): 0.06 V; ΔE_p(1): 0.06 V; $E_{1/2}$(2): 0.77 V *irrev*; $E_{1/2}$(3): 0.89 V *irrev vs.* ferrocene using decamethylferrocene as an internal standard) in a [N^{n}Bu$_4$]PF_6 CH_2Cl_2 medium.

4.8.5. Syntheses and characterisations of 'mixed-valence' bimetallic complexes

*Synthesis of trans-[{(Me$_3$SiC≡CC_6H_4-4-C≡C)(dppe)$_2$Ru}$_2$(μ-C≡CC_6H_4-4-C≡C)]PF_6, [**94a**]PF_6*

A mixture of [**94a**] (0.055 g, 0.024 mmol) and FcPF_6 (0.0079 g, 0.024 mmol) in CH_2Cl_2 (5 ml) was stirred under N_2 for one hour. The solution instantaneously changed colour from yellow to red. The solvent was concentrated to ~ 0.5 ml under high vacuum, yielding a deep red solution. The solution was cooled in an acetone / dry ice bath. Pre-cooled (acetone / dry ice bath), dry hexane (~ 5 ml) was transferred *via* cannular into the cooled reaction mixture causing the precipitation of a deep red solid. The mixture was filtered *via* cannular filtration (to remove Fc contained in the orange filtrate) and the remaining red solid washed continuously with cold, dry hexane in this way until the extracts were colourless. The solid was vacuum dried (0.054 g, 93 %).

IR (CH_2Cl_2, cm^{-1}): 5468 (NIR), 2148 ν([RuC≡C]$^+$), 1965 ν([RuC≡C]$^+$), 1982 ν([RuC≡C]$^+$). ESI(+)-MS (*m/z*): 2314 [{(Me$_3$SiC≡CC_6H_4-4-C≡C)(dppe)$_2$Ru}$_2$(μ-C≡CC_6H_4-4-C≡C)]$^+$, 1136 [Ru(dppe)$_2$(C≡CC_6H_4-4-C≡CSiMe$_3$) + MeCN]$^+$.

*Synthesis of trans-[{(Me$_3$SiC≡CC_6H_4-4-C≡C)(dppe)$_2$Ru}$_2$(μ-C≡CC_6H_2-2,5-Me$_2$-4-C≡C)]PF_6, [**94a-Me**]PF_6*

A mixture of [**94a-Me**] (0.019 g, 0.008 mmol) and FcPF_6 (0.0026 g, 0.008 mmol) in CH_2Cl_2 (4 ml) was stirred under N_2 for one hour. The solution instantaneously changed colour from yellow to red. The solvent was concentrated to ~ 0.5 ml under high vacuum, yielding a deep red solution. The solution was then cooled in an acetone / dry ice bath. Pre-cooled (acetone / dry ice bath), dry hexane (~ 5 ml) was transferred *via* cannular into the cooled reaction mixture, causing the precipitation of a deep red solid. The mixture was filtered *via* cannular filtration (to remove Fc contained in the orange

filtrate) and the remaining red solid washed continuously with cold, dry hexane in this way until the extracts were colourless. The solid was vacuum dried (0.0019 g, 93 %).
IR (CH_2Cl_2, cm^{-1}): 5715 (NIR), 2151 ν([RuC≡C]$^+$), 1953 ν([RuC≡C]$^+$), 1926 ν([RuC≡C]$^+$).

*Synthesis of trans-[{(th-3-C≡C)(dppe)$_2$Ru}$_2$(μ-C≡CC$_6$H$_4$-4-C≡C)]PF$_6$, **[94b]PF$_6$***
A mixture of [**94b**] (0.048 g, 0.023 mmol) and $FcPF_6$ (0.0076 g, 0.023 mmol) in CH_2Cl_2 (4 ml) was stirred under N_2 for one hour. The solution instantaneously changed colour from yellow to red. The solvent was concentrated to ~ 0.5 ml under high vacuum, yielding a deep red solution. The solution was cooled in an acetone / dry ice bath. Pre-cooled (acetone / dry ice bath), dry diethyl ether (~ 5 ml) was then transferred *via* cannular into the cooled reaction mixture, causing the precipitation of a deep red solid. The mixture was filtered *via* cannular filtration (to remove Fc contained in the orange filtrate) and the remaining red solid washed continuously with cold, dry diethyl ether in this way until the extracts were colourless. The solid was vacuum dried (0.046 g, 91 %).
IR (CH_2Cl_2, cm^{-1}): 5537 (NIR), 2060m ν([RuC≡C]$^+$), 1966 ν([RuC≡C]$^+$), 1986 ν([RuC≡C]$^+$).

4.8.6. Syntheses and characterisations of trimetallic complexes

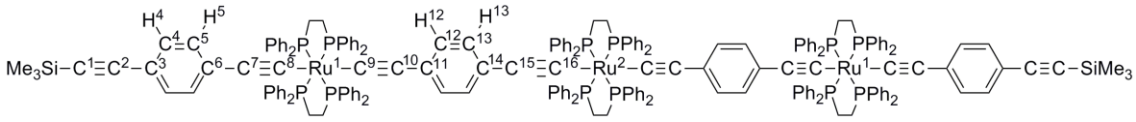

*Synthesis of trans-trans-[{(dppe)$_2$Ru}{μ-(C≡CC$_6$H$_4$-4-C≡C)Ru(dppe)$_2$(C≡CC$_6$H$_4$-4-C≡CSiMe$_3$)}$_2$], **[95a]***
The reagents [**38a**] (0.093 g, 0.082 mmol), $TlBF_4$ (0.035 g, 0.12 mmol) and DBU (~ 6 drops, excess) were added to a flask containing CH_2Cl_2 (25 ml) fitted with a pressure equalising dropping funnel. A solution of [**96**] (0.047 g, 0.041 mmol) in CH_2Cl_2 (10 ml) was added to the dropping funnel. The latter yellow ruthenium solution (of [**96**]) was added to the main yellow ruthenium solution (containing [**38a**]) slowly dropwise (over ~ 40 minutes), then the complete solution left to stir under N_2 overnight. Over this period, the yellow solution colour lightened and a white solid (TlCl) precipitated. The yellow solution was filtered *via* cannular filtration to remove TlCl and

reaction salts and the yellow filtrate concentrated to 2 ml carefully under high vacuum (*care required as may still contain unreacted $TlBF_4$). The yellow solution was left in the fridge for ~ 30 minutes to aid precipitation of a yellow solid. The solid was then filtered and washed with minimum, cold CH_2Cl_2 (3 × 10 ml), MeOH (3 × 10 ml) [Note: $TlBF_4$ is soluble is MeOH] and hexanes (3 × 10 ml). This yellow solid was then re-extracted with $CHCl_3$, filtered, and excess diethyl ether added to the yellow filtrate, resulting in the instantaneous precipitation of a yellow solid. The yellow solid was collected by filtration and vacuum dried (0.059 g, 43 %).

IR (CH_2Cl_2, cm^{-1}): 2146 ν(C≡CSiMe$_3$), 2057 ν(RuC≡C). ^{1}H NMR ($CDCl_3$, 600 MHz) δ / ppm: 0.27 (s, 18H, SiMe$_3$), 2.57 – 2.70 (m, 16H, CH_2, dppe, Ru^1), 2.70 – 2.82 (m, 8H, CH_2, dppe, Ru^2), 6.54 (apparent doublet, splitting = 8 Hz, 4H, H^5), 6.62 – 6.72 (m, 8H, H^{12} and H^{13}), 6.92 (t, J = 8 Hz, 16H, H$_m$, dppe), 7.02 (t, J = 8 Hz, 16H, H$_m$, dppe), 7.03 (t, J = 8 Hz, 16H, H$_m$, dppe), 7.15 (t, J = 8 Hz, 8H, H$_p$, dppe), 7.22 (t, J = 8 Hz, 8H, H$_p$, dppe), 7.23 (t, J = 8 Hz, 8H, H$_p$, dppe), 7.25 (apparent doublet, splitting = 8 Hz, 4H, H^4), 7.35 – 7.40 (m, 16H, H$_o$, dppe), 7.60 – 7.64 (m, 16H, H$_o$, dppe), 7.70 – 7.74 (m, 16H, H$_o$, dppe). ^{31}P{^{1}H} NMR ($CDCl_3$, 300 MHz) δ / ppm: 54.6 (s, Ru(dppe)$_2$), 54.7 (s, Ru(dppe)$_2$). ^{13}C{^{1}H} NMR ($CDCl_3$, 600 MHz) δ / ppm: 0.36 (s, SiMe$_3$), 31.7 (t, J = 12 Hz, CH_2, dppe), 31.8 (t, J = 12 Hz, CH_2, dppe), 93.7 (s, C^1), 106.8 (s, C^2), 116.5 (s, C^7), 117.1 (s, C^6), 118.6 (s, C^{10} or C^{15}), 127.18 (s, C$_m$, dppe), 127.20 (s, C$_m$, dppe), 127.3 (s, C$_m$, dppe), 128.6 (s, C$_p$, dppe), 128.7 (s, C$_p$, dppe), 128.8 (s, C$_p$, dppe), 130.0 (s, C^5), 131.2 (s, C^3), 131.4 (s, C^4), 134.3 (s, C$_o$, dppe), 134.6 (s, C$_o$, dppe), 134.7 (s, C$_o$, dppe), 136.8 – 137.2 (m, C$_i$, dppe), 137.5 – 137.8 (m, C$_i$, dppe). ESI(+)-MS (*m/z*): 2158 [{(Me$_3$SiC≡CC$_6$H$_4$-4-C≡C)(dppe)$_2$Ru}(μ-C≡CC$_6$H$_4$-4-C≡C){Ru(dppe)$_2$} + MeCN + H]$^+$, 2173 [{(HC≡CC$_6$H$_4$-4-C≡C)(dppe)$_2$Ru}(μ-C≡CC$_6$H$_4$-4-C≡C){Ru(dppe)$_2$} + C_2H_4]$^+$, 1136 [Ru(C≡CC$_6$H$_4$-4-C≡CSiMe$_3$)(dppe)$_2$ + MeCN]$^+$, 1123 [Ru(C≡CC$_6$H$_4$-4-C≡CSiMe$_3$)(dppe)$_2$ + C_2H_4]$^+$. Anal. found: C, 72.04; H, 5.33. Calc. for $C_{202}H_{178}P_{12}Ru_3Si_2$: C, 72.65; H, 5.38 %.

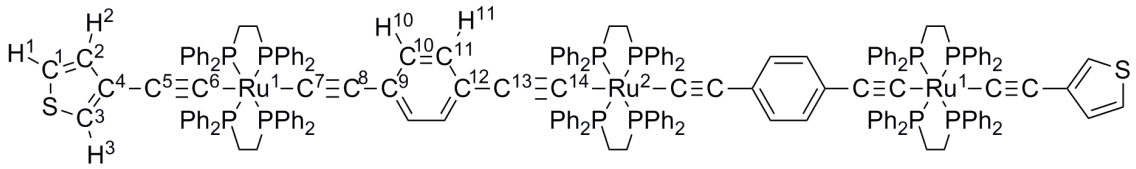

*Synthesis of trans-trans-[{(dppe)$_2$Ru}{μ-(C≡CC$_6$H$_4$-4-C≡C)Ru(dppe)$_2$(C≡C-3-th)}$_2$], **[95b]***

The reagents [**38b**] (0.059 g, 0.057 mmol), $TlBF_4$ (0.019 g, 0.063 mmol) and DBU (~ 7 drops, excess) were added to a flask containing CH_2Cl_2 (50 ml) fitted with a pressure equalising dropping funnel and stirred under N_2 for 30 minutes. Over the reaction period, a white solid (TlCl) precipitated from the yellow solution. A solution of [**96**] (0.033 g, 0.028 mmol) in CH_2Cl_2 (10 ml) was added to the dropping funnel. The latter yellow ruthenium solution (of [**96**]) was added to the main yellow ruthenium solution (containing [**38b**]) slowly dropwise (over ~ 30 minutes), then the complete solution left to stir under N_2 overnight. The yellow solution colour darkened over this period. The yellow solution was filtered *via* cannular filtration to remove TlCl and reaction salts then the yellow filtrate concentrated to dryness carefully under high vacuum (*care required as may still contain unreacted $TlBF_4$), yielding a yellow residue. Excess MeOH (~ 20 ml) [Note: $TlBF_4$ is soluble is MeOH] was added to the residue, where a yellow solid was observed in a yellow solution. The yellow solid was collected by filtration (*care required as filtrate may contain unreacted $TlBF_4$), washed with MeOH (3 × 15 ml), hexanes (3 × 10 ml) and diethyl ether until extracts were colourless, then air dried (0.059 g, 66 %).

IR ($CHCl_3$, cm^{-1}): 2024 ν(RuC≡C), 2054 ν(RuC≡C), 2059 ν(RuC≡C), 2084 ν(RuC≡C). ^{1}H NMR ($CDCl_3$, 600 MHz) δ / ppm: 2.50 – 2.70 (m, 16H, CH_2, dppe, Ru^1), 2.70 – 2.82 (m, 8H, CH_2, dppe, Ru^2), 6.42 – 6.50 (m, 2H, H^3), 6.54 – 6.62 (m, 2H, H^2), 6.62 − 6.76 (m, 8H, H^{10} and H^{11}), 6.86 – 7.14 (m, 50H, H$_m$, dppe and H^1), 7.14 − 7.35 (m, 24H, H$_p$, dppe), 7.35 – 7.54 (m, 24H, H$_o$, dppe), 7.56 – 7.78 (m, 24H, H$_o$, dppe). ^{31}P{^{1}H} NMR ($CDCl_3$, 300 MHz) δ / ppm: 54.72 (s, Ru(dppe)$_2$), 54.74 (s, Ru(dppe)$_2$). ^{13}C{^{1}H} NMR ($CDCl_3$, 600 MHz) δ / ppm: 31.4 – 32.3 (m, CH_2, dppe), 120.4 (s, C^3), 122.7 (s, C^1), 126.9 – 127.6 (m, C$_m$, dppe), 128.5 – 129.0 (s, C$_p$, dppe), 129.2 – 129.5 (m, C^{10} and C^{11}), 130.0 (s, C^2), 134.2 – 134.9 (s, C$_o$, dppe), 136.7 – 138.0 (s, C$_i$, dppe). ESI(+)-MS (*m/z*): 2153 [{(*th*-3-C≡C)(dppe)$_2$Ru}(μ-C≡CC$_6$H$_4$-4-C≡C){Ru(dppe)$_2$(C≡CC$_6$H$_4$-4-C≡CH)} + H]$^+$, 2086 [{(dppe)$_2$Ru}(μ-C≡CC$_6$H$_4$-4-

C≡C){Ru(dppe)$_2$(C≡CC_6H_4-4-C≡CH)} + MeCN]$^+$, 1131 [Ru(C≡C-3-*th*)(C≡CC_6H_4-4-C≡CH)(dppe)$_2$ + H]$^+$, 1064 [Ru(C≡CC_6H_4-4-C≡CH)(dppe)$_2$ + MeCN]$^+$, 1046 [Ru(C≡C-3-*th*)(dppe)$_2$ + MeCN]$^+$, 931 [Ru(dppe)$_2$ + MeOH + H]$^+$.

4.9. References

1. G. J. Ashwell, B. Urasinska, C. Wang, M. R. Bryce, I. Grace and C. J. Lambert, *Chem. Commun.*, **2006**, 4706.
2. W. A. Chalifoux and R. R. Tykwinski, *Nat. Chem.*, **2010**, *2*, 967.
3. Q. Zheng, J. C. Bohling, T. B. Peters, A. C. Frisch, F. Hampel and J. A. Gladysz, *Chem. Eur. J.*, **2006**, *12*, 6486.
4. W. Mohr, J. Stahl, F. Hampel and J. A. Gladysz, *Chem. Eur. J.*, **2003**, *9*, 3324.
5. M. I. Bruce, B. K. Nicholson and N. N. Zaitseva, *C. R. Chim.*, **2009**, *12*, 1280.
6. G. Sedghi, K. Sawada, L. J. Esdaile, M. Hoffmann, H. L. Anderson, D. Bethell, W. Haiss, S. J. Higgins and R. J. Nichols, *J. Am. Chem. Soc.*, **2008**, *130*, 8582.
7. N. Tuccitto, V. Ferri, M. Cavazzini, S. Quici, G. Zhavnerko, A. Licciardello and M. A. Rampi, *Nat. Mater.*, **2009**, *8*, 41.
8. M. P. Eng and B. Albinsson, *Angew. Chem. Int. Ed. Engl.*, **2006**, *45*, 5626.
9. H. L. Anderson, *Chem. Commun.*, **1999**, 2323.
10. A. Tsuda and A. Osuka, *Science*, **2001**, *293*, 79.
11. C. Olivier, B. Kim, D. Touchard and S. Rigaut, *Organometallics*, **2008**, *27*, 509.
12. B. Kim, J. M. Beebe, C. Olivier, S. Rigaut, D. Touchard, J. G. Kushmerick, X. Y. Zhu and C. D. Frisbie, *J. Phys. Chem. C*, **2007**, *111*, 7521.
13. A. Benameur, P. Brignou, E. Di Piazza, Y.-M. Hervault, L. Norel and S. Rigaut, *New J. Chem.*, **2011**, *35*, 2105.
14. L. Luo, A. Benameur, P. Brignou, S. H. Choi, S. Rigaut and C. D. Frisbie, *J. Phys. Chem. C*, **2011**, *115*, 19955.
15. E. A. Weiss, J. K. Kriebel, M. A. Rampi and G. M. Whitesides, *Philos. T. R. Soc. A*, **2007**, *365*, 1509.
16. P. J. Low, *Dalton Trans.*, **2005**, 2821.
17. G. Kastlunger and R. Stadler, *Phys. Rev. B*, **2015**, *91*, 125410.
18. Q. Lu, K. Liu, H. Zhang, Z. Du, X. Wang and F. Wang, *ACS Nano*, **2009**, *3*, 3861.
19. M. I. Bruce, P. J. Low, K. Costuas, J.-F. Halet, S. P. Best and G. A. Heath, *J. Am. Chem. Soc.*, **2000**, *122*, 1949.
20. J. B. G. Gluyas, A. J. Boden, S. G. Eaves, H. Yu and P. J. Low, *Dalton Trans.*, **2014**, *43*, 6291.
21. N. S. Hush, *Trans.Faraday Soc.*, **1961**, *57*, 557.
22. R. A. Marcus, *J. Chem. Phys.*, **1956**, *24*, 966.
23. E. Laborda, M. C. Henstridge and R. G. Compton, *J. Electroanal.Chem.*, **2012**, *667*, 48.
24. C. E. D. Chidsey, *Science*, **1991**, *251*, 919.
25. C. Lambert, G. Noll and J. Schelter, *Nat. Mater.*, **2002**, *1*, 69.
26. M. C. B. Colbert, J. Lewis, N. J. Long, P. R. Raithby, M. Younus, A. J. P. White, D. J. Williams, N. N. Payne, L. Yellowlees, D. Beljonne, N. Chawdhury and R. H. Friend, *Organometallics*, **1998**, *17*, 3034.

27. R. L. Cordiner, M. E. Smith, A. S. Batsanov, D. Albesa-Jove, F. Hartl, J. A. K. Howard and P. J. Low, *Inorg. Chim. Acta*, **2006**, *359*, 946.
28. F. Barigelletti, L. Flamigni, J.-P. Collin and J.-P. Sauvage, *Chem. Commun.*, **1997**, 333.
29. M. Younus, N. J. Long, P. R. Raithby, J. Lewis, N. A. Page, A. J. P. White, D. J. Williams, M. C. B. Colbert, A. J. Hodge, M. S. Khan and D. G. Parker, *J. Organomet. Chem.*, **1999**, *578*, 198.
30. L. M. Ballesteros, S. Martín, J. Cortés, S. Marqués-González, F. Pérez-Murano, R. J. Nichols, P. J. Low and P. Cea, *Adv. Mater. Inter.*, **2014**, *1*, 1400128.
31. S. Marqués-González, M. Parthey, D. S. Yufit, J. A. K. Howard, M. Kaupp and P. J. Low, *Organometallics*, **2014**, *33*, 4947.
32. S. Rigaut, J. Perruchon, L. Le Pichon, D. Touchard and P. H. Dixneuf, *J. Organomet. Chem.*, **2003**, *670*, 37.
33. A. Trujillo, M. Fuentealba, R. Arratia-Perez and J. A. K. Howard, *Acta Crystallogr., Sect. E*, **2012**, *68*, m1445.
34. Y. Sun, N. J. Taylor and A. J. Carty, *Organometallics*, **1992**, *11*, 4293.
35. A. Klein, O. Lavastre and J. Fiedler, *Organometallics*, **2006**, *25*, 635.
36. O. Lavastre, J. Plass, P. Bachmann, S. Guesmi, C. Moinet and P. H. Dixneuf, *Organometallics*, **1997**, *16*, 184.
37. E. Wuttke, F. Pevny, Y.-M. Hervault, L. Norel, M. Drescher, R. F. Winter and S. Rigaut, *Inorg. Chem.*, **2012**, *51*, 1902.
38. M. I. Bruce, B. C. Hall, P. J. Low, B. W. Skelton and A. H. White, *J. Organomet. Chem.*, **1999**, *592*, 74.
39. N. Mezailles, L. Ricard and F. Gagosz, *Org. Lett.*, **2005**, *7*, 4133.
40. N. G. Connelly and W. E. Geiger, *Chem. Rev.*, **1996**, *96*, 877.
41. Y. B. Zhu, O. Clot, M. O. Wolf and G. P. A. Yap, *J. Am. Chem. Soc.*, **1998**, *120*, 1812.
42. D. Han, J. Liu, R. Miao, L. Zhao and G. Zhang, *Polyhedron*, **2015**, *85*, 506.
43. L.-B. Gao, J. Kan, Y. Fan, L.-Y. Zhang, S.-H. Liu and Z.-N. Chen, *Inorg. Chem.*, **2007**, *46*, 5651.
44. N. Gauthier, N. Tchouar, F. Justaud, G. Argouarch, M. P. Cifuentes, L. Toupet, D. Touchard, J.-F. Halet, S. Rigaut, M. G. Humphrey, K. Costuas and F. Paul, *Organometallics*, **2009**, *28*, 2253.
45. M. Parthey, J. B. G. Gluyas, M. A. Fox, P. J. Low and M. Kaupp, *Chem. Eur. J.*, **2014**, *20*, 6895.
46. F. Paul, B. G. Ellis, M. I. Bruce, L. Toupet, T. Roisnel, K. Costuas, J.-F. Halet and C. Lapinte, *Organometallics*, **2006**, *25*, 649.
47. M. A. Fox, R. L. Roberts, W. M. Khairul, F. Hartl and P. J. Low, *J. Organomet. Chem.*, **2007**, *692*, 3277.
48. M. B. Robin and P. Day, *Adv. Inorg. Chem. Radiochem.*, **1968**, *10*, 422.
49. C. E. Powell, M. P. Cifuentes, J. P. Morrall, R. Stranger, M. G. Humphrey, M. Samoc, B. Luther-Davies and G. A. Heath, *J. Am. Chem. Soc.*, **2003**, *125*, 602.
50. S. Martín, G. Pera, L. M. Ballesteros, A. J. Hope, S. Marqués-González, P. J. Low, F. Pérez-Murano, R. J. Nichols and P. Cea, *Chem. Eur. J.*, **2014**, *20*, 3421.
51. H. Haick and D. Cahen, *Acc. Chem. Res.*, **2008**, *41*, 359.
52. H. B. Akkerman and B. De Boer, *J. Phys.: Condens. Mat.*, **2008**, *20*, 013001.
53. R. L. McCreery and A. J. Bergren, *Adv. Mater.*, **2009**, *21*, 4303.
54. R. J. Nichols, W. Haiss, S. J. Higgins, E. Leary, S. Martín and D. Bethell, *Phys. Chem. Chem. Phys.*, **2010**, *12*, 2801.

55. R. Chico, E. Castillejos, P. Serp, S. Coco and P. Espinet, *Inorg. Chem.*, **2011**, *50*, 8654.
56. F. Meng, Y.-M. Hervault, Q. Shao, B. Hu, L. Norel, S. Rigaut and X. Chen, *Nat. Commun.*, **2014**, *5*, 1.
57. F. Meng, Y.-M. Hervault, L. Norel, K. Costuas, C. Van Dyck, V. Geskin, J. Cornil, H. H. Hng, S. Rigaut and X. Chen, *J. Chem. Sci.*, **2012**, *3*, 3113.
58. S. Takahashi, Y. Kuroyama, K. Sonogashira and N. Hagihara, *Synthesis*, **1980**, 627.
59. J. B. G. Gluyas, *Personal Communication*, **2015**.
60. J. Kim, D. T. McQuade, S. K. McHugh and T. M. Swager, *Angew. Chem. Int. Edit.*, **2000**, *39*, 3868.
61. S. Marqués-González, D. S. Yufit, J. A. K. Howard, S. Martín, H. M. Osorio, V. M. García-Suárez, R. J. Nichols, S. J. Higgins, P. Cea and P. J. Low, *Dalton Trans.*, **2013**, *42*, 338.
62. F. J. Arnaiz, *J. Chem. Educ.*, **1997**, *74*, 1332.
63. M. I. Bruce, B. K. Nicholson, O. Binshawkataly, J. R. Shapley and T. Henly, *Inorg. Synth.*, **1989**, *26*, 324.
64. M. A. Fox, J. E. Harris, S. Heider, V. Pérez-Gregorio, M. E. Zakrzewska, J. D. Farmer, D. S. Yufit, J. A. K. Howard and P. J. Low, *J. Organomet. Chem.*, **2009**, *694*, 2350.
65. S. Bock, *Personal Communication*, **2015**.
66. H. E. Gottlieb, V. Kotlyar and A. Nudelman, *J. Org. Chem.*, **1997**, *62*, 7512.
67. M. Krejčik, M. Daněk and F. Hartl, *J. Electroanal. Chem. Interfac. Electrochem*, **1991**, *317*, 179.

CHAPTER 5

Synthesis, electrochemical and electronic properties of *trans*-[Ru(C≡CR)$_2${P(OEt)$_3$}$_4$] complexes

5.1. Abstract

In this Chapter, *trans*-[Ru(C≡CR)$_2${P(OEt)$_3$}$_4$] complexes are explored as higher symmetry (*pseudo*-D_{4h}) alternatives to the more common *trans*-[Ru(C≡CR)$_2$(dppe)$_2$] (*pseudo*-D_{2h}) architecture. Enhancing the symmetry was intended to reduce the spectral complexity by minimising the number of distinct rotamer conformations leading to a fuller understanding of charge transport in *trans*-bis(alkynyl) ruthenium complexes, furthering their use in molecular electronics. A reliable synthesis of *trans*-bis(alkynyl) *tetrakis*-triethylphosphite complexes, *trans*-[Ru(C≡CR)$_2${P(OEt)$_3$}$_4$], [**18**], ([**18a**]: R = C_4H_9; [**18b**]: 3-thiophene (3-*th*); [**18c**]: C_6H_5; [**18d**]: C_6H_4-4-NO_2; [**18e**]: C_6H_4-4-C≡N; [**18f**]; C_6H_4-4-C≡CSiMe$_3$; [**18g**]: C_6H_4-4-C_5H_{11}; [**18h**]: C_6H_4-4-COOMe; [**18i**]: C_6H_4-4-OMe) from reactions of *trans*-[RuCl$_2${P(OEt)$_3$}$_4$], [**19**], with terminal alkyne, HC≡CR, and KPF_6 in solutions of EtOH and NH^iPr_2, is described. The molecular structures of [**18b – i**] are reported, with comparisons to closely related structures found in the literature made where appropriate. Electrochemical studies reveal that complexes [**18**] undergo one reversible (ligand-centred) and one irreversible (metal-centred) oxidation process. Spectroelectrochemical studies have shown that the *mono*-oxidation products, [**18**]$^+$, exhibit simple electronic spectra, confirming that the higher local symmetry around the RuP_4 plane reduces the number of electronically distinct conformations relative to *trans*-[Ru(C≡CR)$_2$(dppe)$_2$]$^+$ (Chapter 4). The primary NIR bands of [**18**]$^+$ bearing electron donating fragments are intense and asymmetric, in accordance with traditional descriptions of strongly coupled Class II (or Class III) 'mixed-valence' complexes [here being ligand based 'mixed-valence' (RC≡C-{Ru}-C≡CR)$^+$, {Ru} = *trans*-Ru{P(OEt)$_3$}$_4$] complexes. In comparison, for

complexes containing electron withdrawing fragments, NIR bands are less intense and more symmetric, indicating more weakly coupled Class II 'mixed-valence' complexes. The single molecule conductance of *trans*-[Ru(C≡C-3-*th*)$_2${P(OEt)$_3$}$_4$], [**18b**], measured within an STM junction, is comparable with *trans*-[Ru(C≡C-3-*th*)$_2$(dppe)$_2$], [**43b**], although the high conduction band in the conductance histogram is much narrower. This has been interpreted in terms of additional junctions being formed through the phenyl rings of the dppe ligands in [**43b**]. The axial trialkylphosphite ligands may therefore be considered a more effective 'insulating sheath' around the conductive 'wire-like', linear *trans*-bis(alkynyl) backbone.

5.2. Introduction

As mentioned in Chapter 1, a variety of ancillary ligands supporting *trans*-bis(alkynyl) ruthenium complexes exist, such as macrocyclic amines,[1] terpyridines[2] and carbonyl (CO).[3, 4] However, by far the most commonly reported are those based on phosphine ligands,[5-10] which is presumably due to their structural variety and availability of both *mono*- and *bi*-dentate phosphines.[11]

In addition to finding extensive application as building blocks and donors for the construction of NLO active materials,[8, 12-14] including redox-switchable examples;[15, 16] donor molecules within solar cells[17-19] and applications as sensors,[20] *trans*-[Ru(C≡CR)$_2$(dppe)$_2$] complexes and closely related *trans*-[Ru(C≡CR)$_2$(dppm)$_2$] systems commonly feature as prototypical metal-containing molecular wires. Scanning tunnelling microscopy (STM) serves as a convenient, and therefore popular, method to investigate the applicability of complexes to perform at the molecular level as active components in prototypical devices.[21] As mentioned in Chapter 1, the organometallic complex, *trans*-[Ru(C≡CC$_6$H$_4$-4-SAc)$_2$(dppm)$_2$], [**51**], (Figure 5.1), in addition to the organic compound, AcSC$_6$H$_4$-4-C≡CC$_6$H$_4$-4-C≡CC$_6$H$_4$-4-SAc, [**52**], have been successfully fabricated as Au|molecule|Au junctions *via* the STM break junction.[22, 23] Between the two, [**51**] (Figure 5.1) exhibited a higher single molecule conductance value ($2.45 \pm 0.90 \times 10^{-4}$ G_0 *vs.* $0.46 \pm 0.26 \times 10^{-4}$ G_0), although the molecular length is notably shorter (1.88 nm *vs.* 2.01 nm), and a smaller molecular surface density was obtained due to the steric demands of the bulky dppe ancillary ligands. The β decay

constants (calculated using the STM apparent height method)[24] of the two wires are comparable (1.01 ± 0.25 $Å^{-1}$ *vs.* 1.11 ± 0.18 $Å^{-1}$).

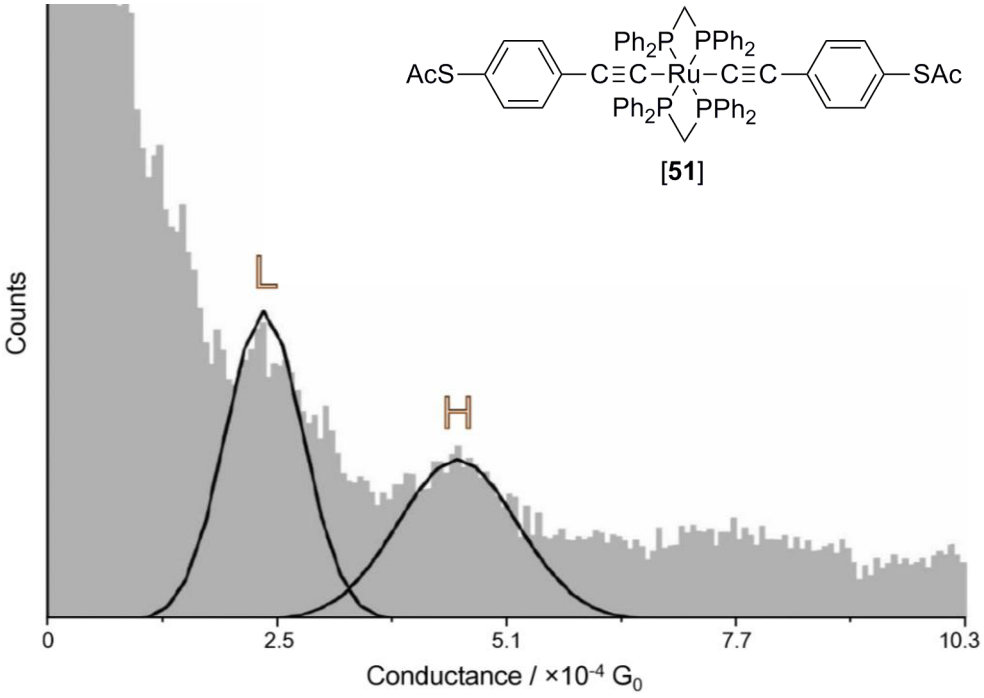

Figure 5.1.: Conductance histogram of [**51**] obtained by the STM break junction method, where L and H refer to low and high conductance respectively. (Adapted with permission from ref[22]. Copyright 2008 American Chemical Society).

The distribution of data obtained from STM experiments (such as in Figure 5.1), represents a range of conductance measurements and arises from several factors such as the molecular tilt-angle,[25] the number of molecules confined within a junction[26] and the nature of molecule-surface site binding mode, such as on flat terraces (type A, Figure 5.2), near step edges or adjacent adatoms on one (type B, Figure 5.2) or both (type C, Figure 5.2) contacts.[27, 28] The second (higher, H) conductance peak in the histogram of [**51**] (Figure 5.1) is thought to arise due to either a more conductive B or C (Figure 5.2) binding conformation within the junction, or from junctions that have trapped two molecules. The conductance traces generated from *trans*-[$Ru(C{\equiv}CC_6H_4\text{-}4\text{-}C{\equiv}CSiMe_3)_2(dppe)_2$], [**43a**], and $Me_3SiC{\equiv}CC_6H_4\text{-}4\text{-}C{\equiv}CC_6H_4\text{-}4\text{-}C{\equiv}CC_6H_4\text{-}4\text{-}C{\equiv}CSiMe_3$, [**67**], by the I(s) method[23] were simplified with trimethylsilylethynyl binding groups, with only a single, narrow (A-type; Figure 5.2) conductance peak being obtained as the steric bulk of the termini restricts the range of

available, conductive contacts (*i.e.* B and C-type contacts; Figure 5.2).[29] A higher conductance value was again obtained for the organometallic complex [**43a**] ($5.10 \pm 0.99\ 10^{-5}\ G_0$) compared with the organic analogue [**67**] ($2.75 \pm 0.56\ 10^{-5}\ G_0$).

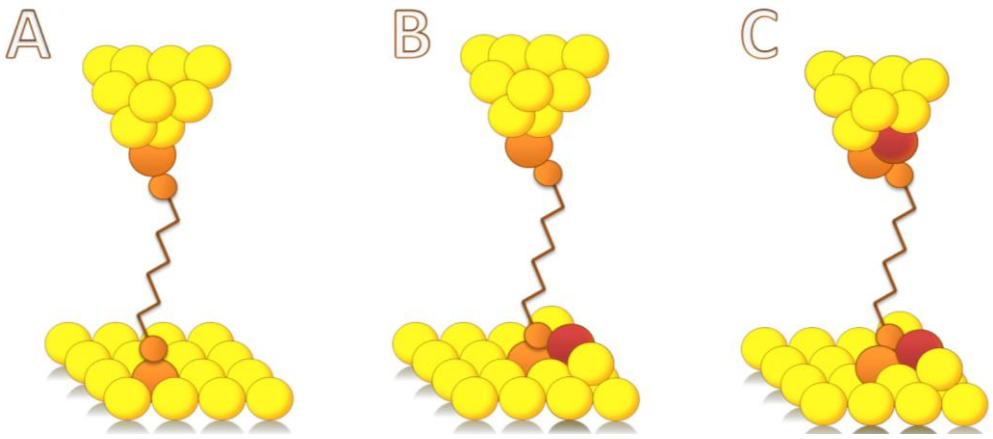

Figure 5.2: Contact modes A, B and C observed in Au|molecule|Au junctions are expected to contribute to the number of bands observed in resultant conductance profiles. Conductance is increased with increasing surface roughness (*i.e.* from A → B → C). Orange and red colour coding represents molecule-metal contact.

In a preliminary investigation, in collaboration with Prof. R. J. Nichols at the University of Liverpool, the single molecule conductance of *trans*-[Ru(C≡C-3-*th*)$_2$(dppe)$_2$], [**43b**],[30] (Figure 5.3), which features the 3-thienyl surface contacting group, has been measured.

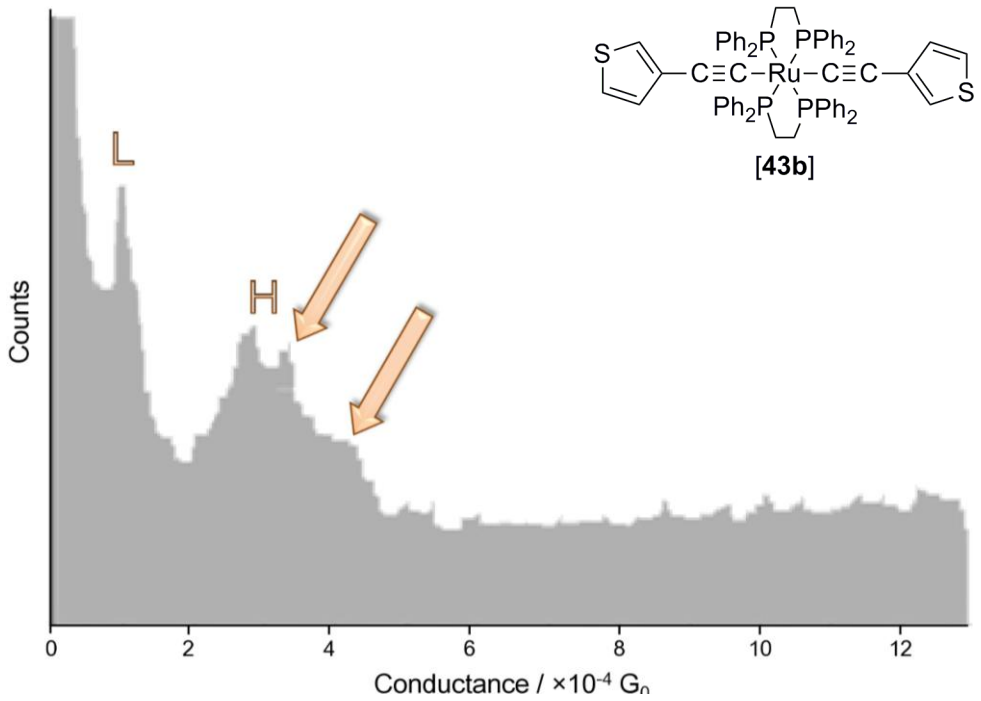

Figure 5.3: Conductance histogram of [**43b**], obtained by the I(s) method, showing additional features in the H peak (as indicated by the arrows), where L and H refer to low and high conductance values respectively.

The conductance histograms of [**51**] (Figure 5.1) and [**43b**] (Figure 5.3) reveal additional features in the broad higher (H) conductance peaks (as indicted by the arrows in Figure 5.3). Whilst the presence of high (H) and low (L) conductance peaks are attributed to the mode of metal-molecule contact (where the molecule binds to various defect sites on the gold surface and tip, Figure 5.2),[29] these additional features on the H peak are more difficult to rationalise based solely on this explanation. Instead, the additional conduction pathways of [**43b**] and [**51**] might be a result of the ancillary ligands, where electron density of the phenyl rings comprising the sterically demanding {Ru(dppe)$_2$} and {Ru(dppm)$_2$} motifs may be sufficient to form supplementary Au|molecule|Au junctions (Figure 5.4). In this context the use of diphenylphosphine as a contacting group by Venkataraman should be noted.[31, 32]

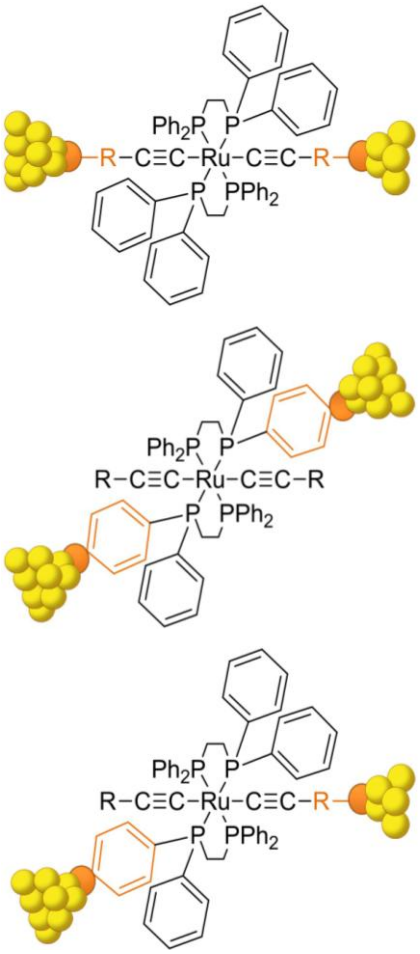

Figure 5.4: Possible binding modes of *trans*-[Ru(C≡CR)$_2$(dppe)$_2$] complexes to gold surfaces forming supplementary Au|molecule|Au junctions, where R represents a nascent binding group.

Consequently, STM data obtained for shorter *trans*-[Ru(C≡CR)$_2$(dppe)$_2$] complexes, and related complexes bearing aromatic ancillary ligands, such as dppm, may not reflect conduction through the ideal linear junction in isolation (top, Figure 5.4). Thus, despite the prevalence of {Ru(dppe)$_2$} fragments in molecular electronics studies of *trans*-bis(alkynyl) complexes, the potential for competing conductance pathways (especially for shorter, less anisotropically structured derivatives) suggests that redesign to complexes with minimal additional (conductive) contacting points, such as *trans*-[Ru(C≡CR)$_2$(PX$_3$)$_4$], is prudent.

In contrast to the popularity of *trans*-bis(alkynyl) ruthenium complexes featuring chelating *bis*-phosphines, *i.e.* *trans*-[Ru(C≡CR)$_2$(dppe)$_2$] and

trans-[Ru(C≡CR)$_2$(dppm)$_2$], related complexes bearing *mono*-dentate trialkylphosphine ligands, *trans*-[Ru(C≡CR)$_2$(PX$_3$)$_4$], are relatively rare. As mentioned in Chapter 1, the study of such complexes bearing the {Ru(PMe$_3$)$_4$} motif, *trans*-[Ru(C≡CR)$_2$(PMe$_3$)$_4$], is limited by their generally low to moderate stability in air and acid sensitivity, forming η^3-butenynyl complexes (*c.f.* Chapter 2),[33, 34] in addition to the complexity of syntheses involving highly toxic tin, or reactive sodium, magnesium and lithium reagents.[33-38] Moreover, *trans*-[Ru(C≡CR)$_2$(PMe$_3$)$_4$] complexes are commonly obtained as isomeric (*cis*- / *trans*-) mixtures, which are arduous to separate.[35] The synthesis of *trans*-bis(alkynyl) complexes bearing *tetrakis*-trialkylphosphite fragments, *trans*-[Ru(C≡CR)$_2${P(OX)$_3$}$_4$] (where X = Me, Et), although rapid (15 minutes) with a simple work-up procedure (trituration from either methanol or ethanol), similarly relies on alkynyl-lithium reagents (Scheme 5.1) and is low yielding (~ 35 %).[39] Despite being air-stable and obtained in high isomeric purity, final products are sensitive to reactions with electrophiles, forming alkynyl-vinylidene complexes, which may then undergo further rearrangement to form η^3-butenynyl complexes.[39, 40] Moreover, the phosphite ligand is prone to dissociate in a polar medium,[41] necessitating a degree of care in their preparation and subsequent use.

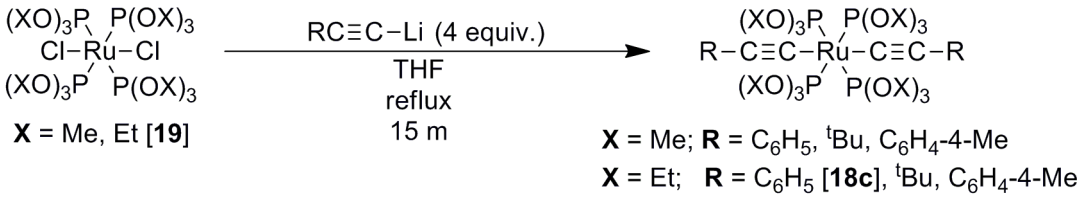

Scheme 5.1: Formation of *trans*-*bis*(alkynyl) *tetrakis*-trialkylphosphite ruthenium complexes, as described by Albertin.[39]

In this Chapter, a facile, high-yielding and reproducible route to complexes of the type, *trans*-[Ru(C≡CR)$_2${P(OEt)$_3$}$_4$] is described. These complexes have been studied by electrochemical, spectroelectrochemical and DFT-based methods to explore their optoelectronic properties. Furthermore, the notion of 'insulating' the 'wire-like' *trans*-bis(alkynyl) core with trialkylphosphite ligands has been explored through single molecule conductance studies, in collaboration with the University of Liverpool. Throughout the Chapter, comparisons of the {Ru{P(OEt)$_3$}$_4$} fragment with the widely

reported {Ru(dppe)$_2$} motif are made where necessary to better understand the structural, spectroscopic and electronic influence of the ancillary ligands.

5.3. Results and discussion

5.3.1. Synthesis of *trans*-bis(alkynyl) *tetrakis*-triethylphosphite ruthenium complexes

The preparation of *trans-bis*(alkynyl) *tetrakis*-triethylphosphite ruthenium complexes *via* lithiated alkynyl reagents is shown in Scheme 5.1. Here, an EtOH solution of *trans*-[RuCl$_2${P(OEt)$_3$}$_4$], [**19**],[42] treated with KPF_6 (4 equiv.) and the appropriate terminal alkyne HC≡CR (excess) in the presence of NH^iPr_2 (excess) resulted in the slow formation (5 days – 4 weeks) of complexes [**18a** – **i**] (Scheme 5.2).

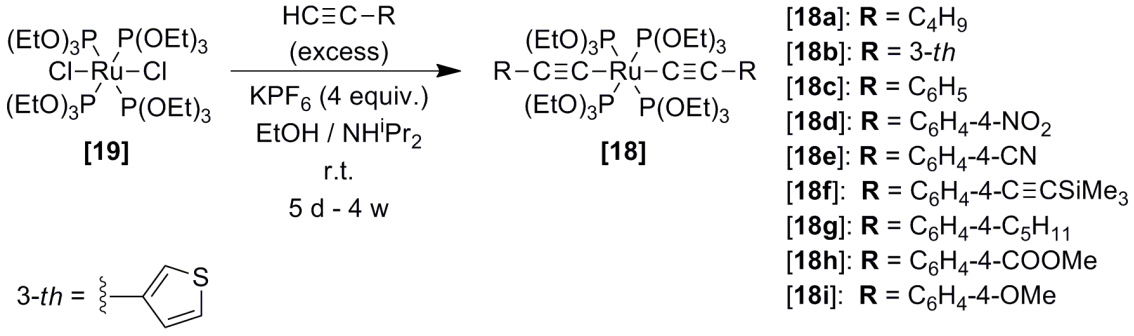

Scheme 5.2: Formation of *trans*-bis(alkynyl) *tetrakis*-triethylphosphite ruthenium complexes [**18a** – **i**].

The extensive reaction length is compensated by the ease of purification where precipitation from either methanol or ethanol at completion of the reaction is sufficient to obtain [**18**] in high purity (confirmed by elemental analyses for complexes [**18b − d, f – i**]) and in moderate to good yields (34 − 85 %), with the exception of [**18e**]. The yield of [**18e**] (19 %) is lower due to the formation of additional side products during the reaction; presumably a consequence of competing coordination from the nucleophillic nitrile group.[43] Evidence for the formation of [**18**] includes triplet and quartet resonances in the ^{1}H NMR spectra corresponding to the -C*H*$_3$ and -C*H*$_2$-ethyl fragments (respectively) on the four equivalent phosphite groups about the

ruthenium centre. Resonances occur between δ 1.18 – 1.21 ppm (C*H*$_3$) and δ 4.25 − 4.32 ppm (C*H*$_2$) with mutual $^3J_{HH}$ couplings of 7 Hz. Singlet resonances in the $^{31}P\{^1H\}$ NMR spectra, between δ 136.2 – 139.5 ppm, support the *trans*-arrangement of the alkynyl ligands. In the $^{13}C\{^1H\}$ NMR spectra, quintet (or unresolved multiplet) resonances observed between δ 89.9 – 131.6 ppm for the Ru-*C* carbon nuclei, coupling to the four *cis*-phosphines ($^2J_{CP}$ = 19 – 21 Hz), and singlet resonances observed between δ 104.9 – 116.9 ppm for the Ru-C≡*C* carbon nuclei confirmed the presence of the alkynyl ligand. In the IR spectra, ν(RuC≡C) bands observed between 2055 – 2147 cm^{-1} further support alkynyl functionality. Finally, the structures [**18b – i**] have been determined by single crystal X-ray diffraction studies (see section 5.3.2.), which confirmed the structural assignments based on spectroscopy.

Evidence from reaction monitoring using *in situ* $^{31}P\{^1H\}$ NMR spectra suggests that the formation of [**18**] from [**19**] proceeds *via* the intermediate *mono*-alkynyl complex, *trans*-[RuCl(C≡CR){P(OEt)$_3$}$_4$], as transient signals comparable with the previously reported *mono*-alkynyl *tetrakis*-triethylphosphite complex, *trans*-[RuCl(C≡CC$_6$H$_5$){P(OEt)$_3$}$_4$], [**102**], ($^{31}P\{^1H\}$ NMR (CD_2Cl_2): δ 132.3 ppm),[41] were observed.

In an attempt to optimise the synthetic route of [**18**], reactions of [**19**] with the simple terminal alkyne phenylacetylene, HC≡CC$_6$H$_5$ (5 equiv.), and NH^{i}Pr$_2$ (excess) in EtOH solutions were conducted in the presence of 2.2 equivalents of various halide abstracting agents: a) KPF_6 (Figure 5.5), b) $NaPF_6$, c) AgOTf and d) $TlBF_4$.

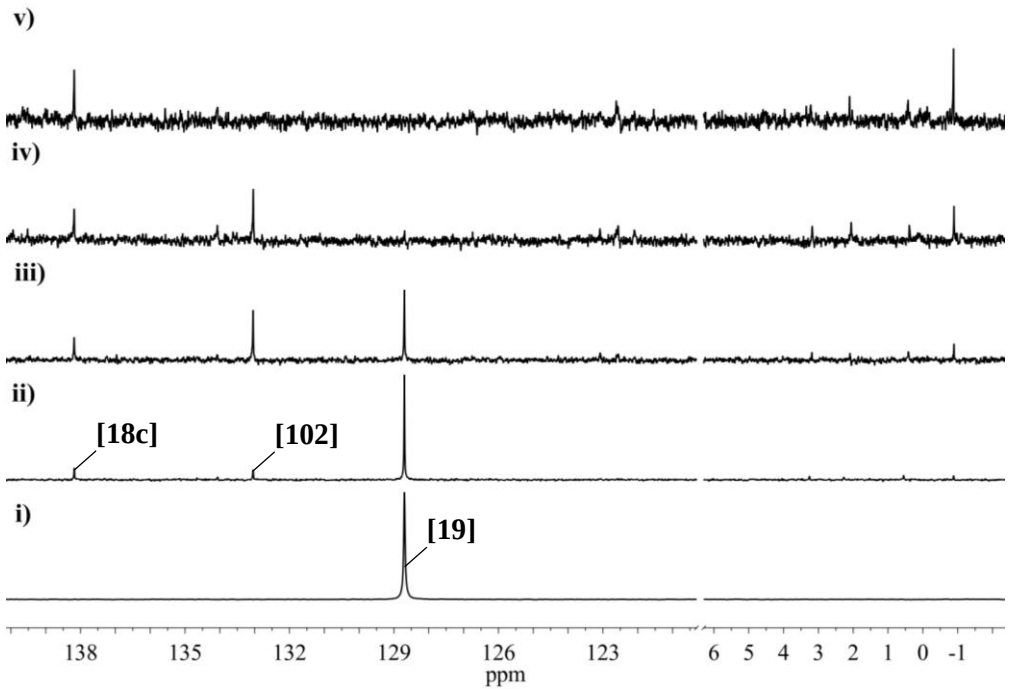

Figure 5.5: *In situ*, unlocked $^{31}P\{^{1}H\}$ NMR (300 MHz) solution spectroscopy monitoring of [**19**], (i), with $HC{\equiv}CC_6H_5$ (5 equiv.), KPF_6 (2.2 equiv) and $NH^{i}Pr_2$ (excess) at room temperature in dry ethanol after ii) 7 hours; iii) 26 hours; iv) 47 hours and v) 9 days.

Over the course of the reaction shown in Figure 5.5, using KPF_6, [**19**] (s, δ 128.7 ppm) is slowly transformed into the *trans*-bis(alkynyl) complex [**18c**], (s, δ 138.2 ppm) *via* the intermediate *mono*-alkynyl complex [**102**] (s, δ 133.1 ppm). Presumably as a consequence of the extensive reaction length required for the full conversion from *mono*- to *trans*-bis(alkynyl) (9 days in this case), ^{31}P-containing decomposition products are also evident (observed as multiple singlets within the range δ − 1.12 to 2.24 ppm). Under these conditions, [**18c**] is obtained in a 59 % yield following the work-up procedure described in the experimental section.

The analogous reaction sequence with $NaPF_6$ is very similar to that shown in Figure 5.5 with KPF_6 except that only a single ^{31}P-containing decomposition peak is exhibited (at δ − 0.89 ppm), albeit in much greater quantities. In this case, [**18c**] is obtained in a comparable yield (56 %) after a 13 day reaction.

With $TlBF_4$ as the halide abstracting agent, the reaction sequence is again similar, where a slow generation of [**18c**] from [**19**] *via* the *mono*-alkynyl intermediate [**102**] is observed with some ^{31}P-containing impurities. However, in this case, the conversion from the intermediate *mono*-[**102**] to the product *trans*-bis(alkynyl), [**18c**], could not be driven to completion, even after the addition of excess $TlBF_4$ and alkyne and a reaction length of 14 days. Given the extreme toxicity of Tl^I salts, and subsequent increased difficulty of work-up procedures, this route is not considered optimal.

In contrast to using KPF_6, $NaPF_6$ and $TlBF_4$, the course of the reaction using AgOTf was notably different. After two days in solution, the reaction mixture contained mostly [**19**] with minor quantities of the *mono*-[**102**] and *trans*-bis(alkynyl), [**18c**], complexes, in addition to some ^{31}P-containing decomposition products (consistent with previous reactions). However, shortly after this period, resonances attributed to these intermediate and product complexes are replaced with a plethora of other, unassigned resonances, evincing a complex mixture of products in solution. The propensity of Ag^I salts to coordinate to other species in the reaction mixture (such as chlorides and alkynes) has been previously demonstrated,[44-46] and similar processes are proposed to account for observations here. The results of these four reactions indicate that either KPF_6 or $NaPF_6$ should foremost be used as halide abstracting agents over $TlBF_4$ and AgOTf in the optimised transformation of [**19**] to [**18**].

As the synthesis of [**102**] is known,[41] this prompted exploration of novel, 'asymmetric' *trans*-bis(alkynyl) *tetrakis*-triethylphosphite ruthenium complexes of the type; *trans*-[Ru(C≡CR)(C≡CC_6H_5){P(OEt)$_3$}$_4$]. A mixture of [**102**], HC≡CC_6H_4-4-NO_2 (3 equiv.), KPF_6 (2 equiv.) and NH^iPr_2 (excess) in an EtOH solution was stirred under N_2. After ten days in solution, the *in situ* $^{31}P\{^1H\}$ NMR spectrum showed three main resonances, each of approximately equal intensity (Figure 5.6).

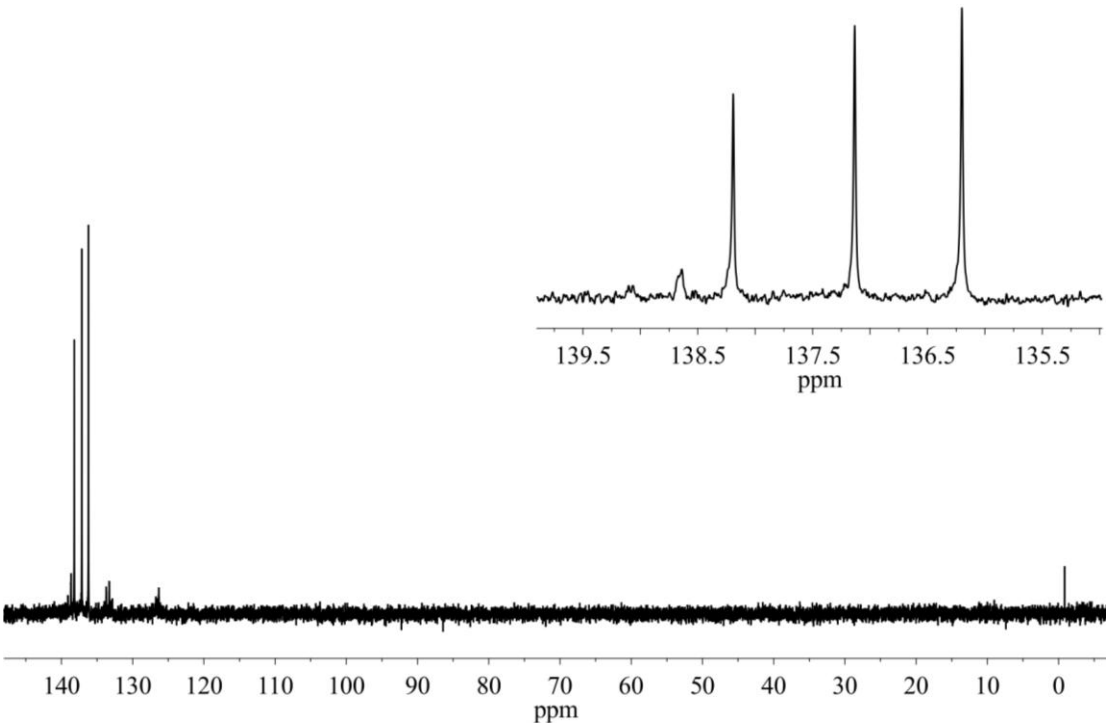

Figure 5.6: *In situ*, unlocked, $^{31}P\{^{1}H\}$ (300 MHz) NMR solution spectroscopy monitoring of [**102**], $HC{\equiv}CC_6H_4$-4-NO_2 (3 equiv.), KPF_6 (2 equiv.) and $NH^{i}Pr_2$ (excess) in an EtOH solution after stirring at room temperature for ten days.

The spectral region in Figure 5.6 where these three principal $^{31}P\{^{1}H\}$ resonances appear (δ 136.2 – 138.2 ppm), suggests formation of three unique *trans*-bis(alkynyl) complexes. The solution was left for a further seven days to determine whether product distribution is weighted, however no changes were observed to the *in situ* $^{31}P\{^{1}H\}$ NMR profile (shown in Figure 5.6) after this period. After removing reaction salts by filtration, the mixture was purified by preparative TLC (silica, 100 % CH_2Cl_2). Of the several chromatographic bands that arose, only the second dark red band could be characterised (33 % yield) as [**18d**] (see experimental section). Formation of [**18d**] is only possible as a result of ligand scrambling effects (Scheme 5.3), which arise as a consequence of a reversible reaction scheme and are especially anticipated in this case given the extended reaction lengths and the acid-base relationship that exists between alkynyl and vinylidene complexes.

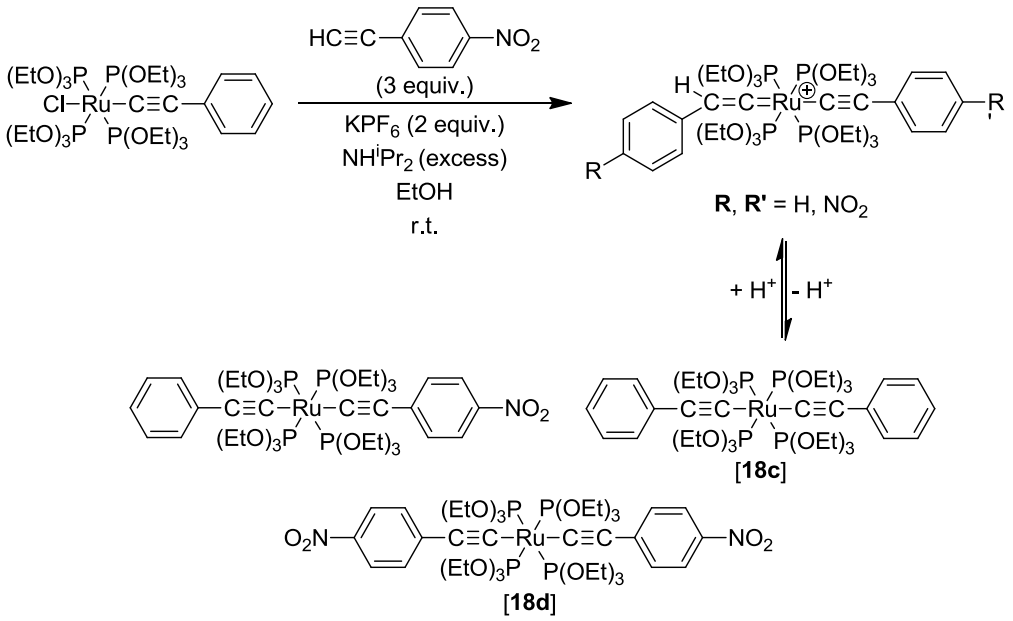

Scheme 5.3: Ligand scrambling observed in the reaction of [**102**], $HC{\equiv}CC_6H_4$-4-NO_2 (3 equiv.), KPF_6 (2 equiv.) and NH^iPr_2 (excess) in an EtOH, forming a mixture of 'symmetric' and 'asymmetric' *trans*-bis(alkynyl) Ru{$P(OEt)_3$}$_4$ complexes.

5.3.2. Single crystal X-ray diffraction studies

Single crystal X-ray structure determinations have been made for *trans*-[Ru(C≡C-3-*th*)$_2${$P(OEt)_3$}$_4$], [**18b**] (Figure 5.7); *trans*-[Ru($C{\equiv}CC_6H_5$)$_2${$P(OEt)_3$}$_4$], [**18c**]; *trans*-[Ru($C{\equiv}CC_6H_4$-4-NO_2)$_2${$P(OEt)_3$}$_4$], [**18d**]; *trans*-[Ru($C{\equiv}CC_6H_4$-4-C≡N)$_2${$P(OEt)_3$}$_4$], [**18e**] (Figure 5.8); *trans*-[Ru($C{\equiv}CC_6H_4$-4-C≡C$SiMe_3$)$_2${$P(OEt)_3$}$_4$], [**18f**] as a $CHCl_3$ solvate; *trans*-[Ru($C{\equiv}CC_6H_4$-4-C_5H_{11})$_2${$P(OEt)_3$}$_4$], [**18g**]; *trans*-[Ru($C{\equiv}CC_6H_4$-4-COOMe)$_2${$P(OEt)_3$}$_4$], [**18h**] as a CH_2Cl_2 solvate and *trans*-[Ru($C{\equiv}CC_6H_4$-4-OMe)$_2${$P(OEt)_3$}$_4$], [**18i**], with important bond lengths and bond angles summarised in Tables 5.1 and 5.2.

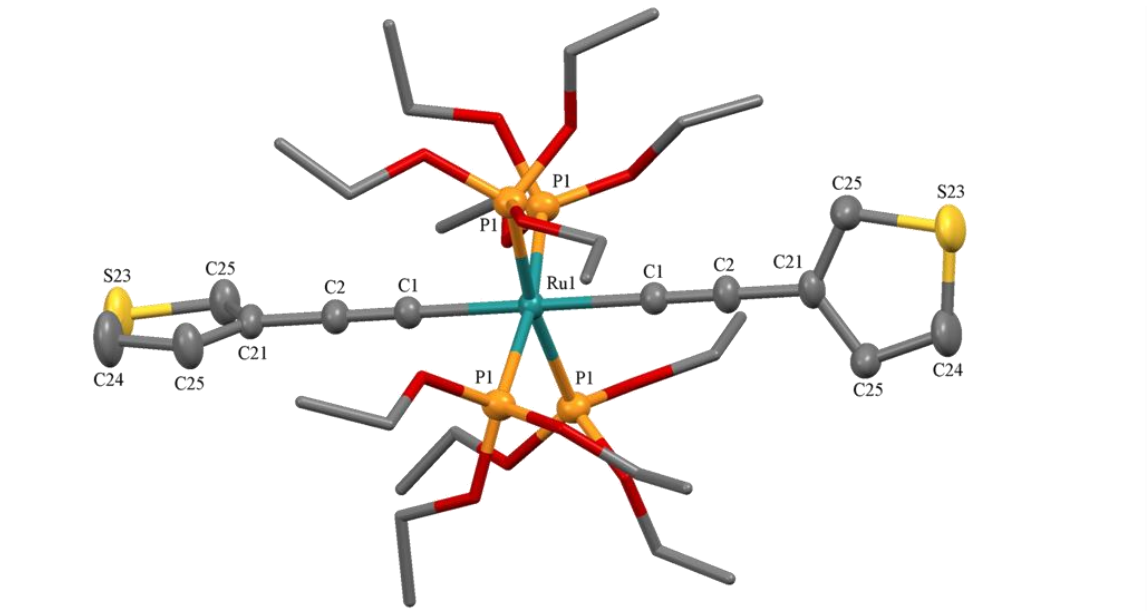

Figure 5.7: Projection of a single molecule of [**18b**] with hydrogen atoms omitted for clarity. Ellipsoids for key atoms are drawn at the 50 % probability level.

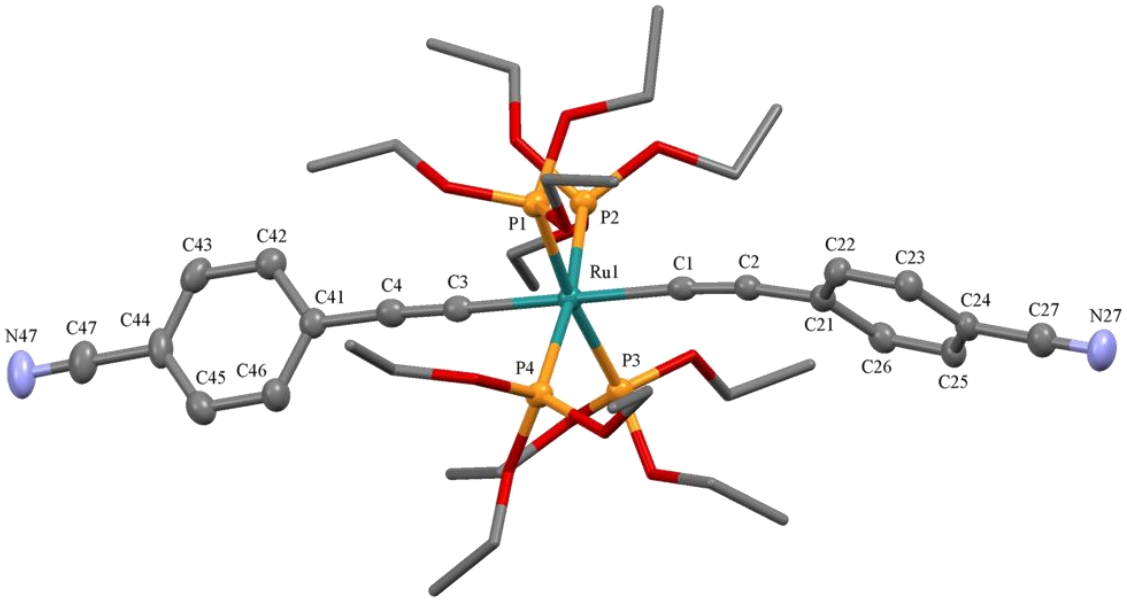

Figure 5.8: Projection of a single molecule of [**18e**] with hydrogen atoms omitted for clarity. Ellipsoids for key atoms are drawn at the 50 % probability level.

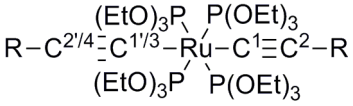

Figure 5.9: The atom labeling scheme used in Tables 5.1 and 5.2.

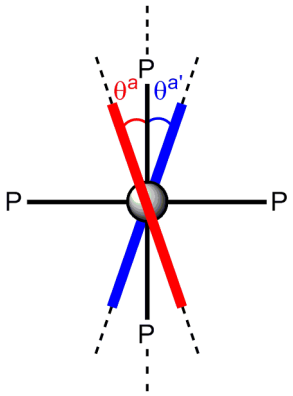

Figure 5.10: Representation of angles θ^{a} and $\theta^{a'}$ in *trans*-[Ru(C≡CR)$_2${P(OEt)$_3$}$_4$] complexes ([**18b – i**]), as being the smallest C_{ortho}-C_{ipso}-Ru-P(any) torsion angles (irrespective of sign) calculated for each of the two aryl rings (depicted as red and blue lines) on the *trans*-bis(aryl)alkynyl fragments.

Table 5.1: Selected bond distances (Å), C_{ortho}-C_{ipso}-Ru-P(any) torsion angles (θ^a, $\theta^{a'}$ / °) and angles between planes containing the aryl-ring fragments (θ^p / °) for *trans*-[Ru(C≡CR)$_2${P(OEt)$_3$}$_4$] complexes [**18b** – **i**].

Complex	R	Space group	Ru-C^1	Ru-C^3	C^1≡C^2	C^3≡C^4	Ru-P	Ru-P$_{avg}$	θ^a / $\theta^{a'}$	θ^p
[**18b**]	3-*th*	$P\bar{4}2_1c$	2.059(2)	-	1.221(2)	-	2.3149(3)	2.3149(3)	– 27.5, 27.5	87.6
[**18c**]	C_6H_5	$I4_1/acd$	2.066(3)	-	1.207(4)	-	2.3166(9), 2.3245(9)	2.323	– 12.2, 40.8	61.2
[**18d**]	C_6H_4-4-NO_2	$P2_1/c$	2.059(2)	2.063(2)	1.214(3)	1.214(3)	2.3161(6), 2.3167(6), 2.3176(6), 2.3199(6)	2.318	– 39.1, 22.9	26.0
[**18e**]	C_6H_4-4-C≡N	$C2/c$	2.053(3)	2.052(3)	1.213(4)	1.213(4)	2.3155(7), 2.3156(7), 2.3161(7), 2.3170(7)	2.316	9.4, – 27.2	79.7
[**18f**]	C_6H_4-4-C≡CSiMe_3	$P2_1/n$	2.056(3)	2.062(4)	1.218(5)	1.214(5)	2.327(1), 2.328(1), 2.316(1), 2.309(1)	2.320	23.8, 42.0	22.2
[**18g**]	C_6H_4-4-C_5H_{11}	$P\bar{1}$	2.072(2)	2.075(2)	1.210(3)	1.218(3)	2.3129(6), 2.3133(6), 2.3175(6), 2.3178(5)	2.315	16.4, 22.6	69.7
[**18h**]	C_6H_4-4-COOMe	$P3_121$	2.050(5)	-	1.217(7)	-	2.292(3), 2.300(3), 2.322(3), 2.331(3)	2.311	16.3, – 22.6	83.6
[**18i**]	C_6H_4-4-OMe	$Pna2_1$	2.078(2)	2.066(2)	1.207(3)	1.204(3)	2.3041(6), 2.3061(6), 2.3123(6), 2.3138(6)	2.309	29.3, – 18.2	13.9

Table 5.2: Selected bond angles (°) for *trans*-[Ru(C≡CR)$_2${P(OEt)$_3$}$_4$], [**18b – i**].

Complex	R	C^3-Ru-C^1	Ru-C^1-C^2	Ru-C^3-C^4	P-Ru-P (*cis*)	P-Ru-P (*trans*)
[**18b**]	3-*th*	180.0	180.0	180.0	90.33(1)	171.19(2)
[**18c**]	C_6H_5	180.0	180.0	180.0	90.27(4), 89.74(4)	179.93(6), 171.46(5)
[**18d**]	C_6H_4-4-NO_2	178.7(1)	176.3(2)	178.7(2)	88.87(2), 89.89(2), 91.33(2), 90.70(2)	173.39(2), 172.87(2)
[**18e**]	C_6H_4-4-C≡N	179.5(1)	175.2(2)	178.6(2)	89.76 (3), 90.29(3), 89.80(3), 91.09(3)	173.03(3), 172.13(3)
[**18f**]	C_6H_4-4-C≡C$SiMe_3$	178.8(1)	178.5(3)	179.6(3)	89.99(3), 91.56(4), 89.97(4), 89.23(4)	172.17(4), 174.39(4)
[**18g**]	C_6H_4-4-C_5H_{11}	178.3(1)	177.7(2)	176.5(2)	89.31(2), 91.91(2), 90.68(2), 88.83(2)	174.43(2), 172.44(2)
[**18h**]	C_6H_4-4-COOMe	179.8(4)	178.8(6)	179.8(4)	90.36(12), 89.69(10), 89.37(11), 92.17(11)	172.25(10), 167.90(10)
[**18i**]	C_6H_4-4-OMe	177.7(2)	178.8(2)	175.7(2)	89.25(2), 89.34(2), 90.75(2), 92.44(2)	168.56(2), 170.81(2)

Although the mixed alkynyl-vinylidene complex, *trans*-[Ru(C≡CC_6H_5)(=C=CMeC_6H_5){P$(OEt)_3$}$_4$]OTf, has been structurally characterised,[39] the series of complexes [**18**] represents the first structurally characterised *trans*-bis(alkynyl) derivatives of the type *trans*-[Ru(C≡C$R)_2${P$(OR)_3$}$_4$]. Complexes [**18b**] and [**18c**] display tetragonal crystal systems, whilst [**18d**], [**18e**] and [**18f**] are found in monoclinic crystal systems. The crystal system of [**18g**] is triclinic, [**18h**] is trigonal and [**18i**] is orthorhombic. In the crystal, [**18b**] is situated on a crystallographic $\bar{4}$ axis so there is only one unique phosphite group. The dihedral angle between the two thiophene groups (which are disordered about the crystallographic 2-fold axis) is therefore 90 °. In a further instance, [**18c**] lies on a crystallographic 4_1 axis, on a site of 222 symmetry. In this case, the 2-fold axis establishes two unique phosphite groups and relates the two halves of the phenyl ring. The phosphite groups are disordered about the other two 2-fold axes. For all cases, [**18b − i**], the P-Ru-P bond angles between *cis*-phosphines (~ 90 °) and those between *trans*-phosphines (~ 180 °) in addition to ≡C-Ru-C≡ angles (~ 180 °), indicate the octahedral geometry about the ruthenium centre, in agreement with the previously published alkynyl-vinylidene complex.[39]

Orpen and Connelly have summarised geometric variations in a series of metal-phosphine and phosphite complexes.[47] The M-PX_3 (X = R, OR; R = alkyl, aryl) bond length increases upon oxidation of the metal centre, evincing M-PX_3 π-backbonding. The P-X bonds are correspondingly shortened on oxidation, implicating P(σ*), the predominantly antibonding combinations of P($3p_{x,y}$) with X(σ), as the acceptor orbital in the backbonding model. The P(σ*) orbital is lowered in energy when X is more electronegative and the PX_3 fragment is made more pyramidal. This is due to the reduction in destabilising overlap between P($3p_{x,y}$) and X(σ) when the X atoms move out of the *xy* plane. As a result, the π-accepting character of P$(OEt)_3$ (Tolman cone angle 109 °)[11] is expected to be far superior than PPh_3 (Tolman cone angle 145 °)[11] and other related ligands bearing aromatic fragments, such as dppe and dppm. Hence for the crystallographically determined complexes [**18b – i**], variations in Ru-P bond lengths are anticipated to reflect the degree of Ru-P π-backbonding.

The angles θ^{a} and $\theta^{a'}$ (Figure 5.10, Table 5.1) provide a convenient proxy measure for the alignment of the aryl π-systems, Ar(π), with Ru(*d*) on geometric grounds. Given the difficulty in defining a unique value for θ, with two indistinguishable aryl rings and four indistinguishable phosphite groups, θ^{a} and $\theta^{a'}$ values reported here represent the smallest C_{ortho}-C_{ipso}-Ru-P(any) torsion angles (irrespective of sign) measured for each of the two ring fragments (Figure 5.10). Therefore, in this case, angles close to 0 ° represent the most effective M(*d*)-Ar(π) overlaps and hence greatest correlation of structural and electronic properties.[48] As an indication of the extent of delocalisation, θ^{p} values, representing the angle between planes containing the aryl ring fragments, are given. Angles with a higher deviation from 0 ° (perfectly 'aligned' ring systems) reflect more twisted conformations.

With the exception of [**18i**] (θ^{p} = 13.9 °), and perhaps [**18f**] (θ^{p} = 22.2 °) and [**18d**] (θ^{p} = 26.0 °), the phenylene rings in these *bis*-aryl acetylide complexes [**18**] do not lie in the same plane (with θ^{p} values within the range 61.2 – 87.6 °). In addition, complexes [**18**] generally display θ^{a} and $\theta^{a'}$ values between ~ 20 – 40 °, evincing that the Ar(π) systems and Ru(*d*) are not optimally aligned. Whilst [**18e**] does show alignment of one Ar(π) with Ru(*d*) (θ^{a} / $\theta^{a'}$ = 9.4 °), the second ring is not aligned, (θ^{a} / $\theta^{a'}$ = − 27.2 °). For these reasons, it is unsurprising to find that a definitive trend between Ru-P_{avg} and the electronic character of the aryl substituent does not exist. For example, the unsubstituted complex [**18c**] has the longest Ru-P_{avg} bond length (2.321 Å) of the series. For all structures [**18b − i**], the Ru-$C^{1/3}$ bond lengths are consistent with single bond character, although complexes containing electron withdrawing *para*-substituents on the aromatic ring ([**18d**], [**18e**], [**18f**] and [**18h**]) are found to have generally shorter lengths (2.050(5) – 2.063(2) Å) than those bearing electron donating *para*-substituents ([**18g**] and [**18i**]; between 2.066(2) – 2.078(2) Å), evincing an electronic substituent effect, possibly propagated through the σ-framework. In this case, the unsubstituted complex, [**18c**], has a Ru-C^{1} bond length between these two ranges (2.066(3) Å). For all cases, the $C^{1/3}$≡$C^{2/4}$ bond lengths are consistent with triple bond character. Differences in $C^{1/3}$≡$C^{2/4}$ bond lengths as a result of the R substituent are found to be within statistical error.

5.4. Electrochemistry

The electrochemical responses of *trans*-bis(alkynyl) *tetrakis*-triethylphosphite complexes [**18a − i**] in low temperature (acetone / ice bath) CH_2Cl_2 solutions containing 0.1 M *tetra*-butylammonium hexafluorophosphate ($[N^nBu_4]PF_6$) were examined by cyclic voltammetry (Table 5.3). All potentials are quoted against the ferrocene / ferrocenium couple ($[Fe\{\eta^5\text{-}C_5H_5\}_2]$ / $[Fe\{\eta^5\text{-}C_5H_5\}_2]^+$ = 0 V) using an internal decamethylferrocene / decamethylferrocenium reference ($[Fe\{\eta^5\text{-}C_5Me_5\}_2]$ / $[Fe\{\eta^5\text{-}C_5Me_5\}_2]^+$ = − 0.48 V).[49] This data represents the first electrochemical exploration of *trans*-bis(alkynyl) complexes containing the *trans*-$[Ru(C{\equiv}CR)_2\{P(OEt)_3\}_4]$ motif.

Electrochemical reversibility describes the experiment where the rate of electron transfer is mass transport limited, and characterised by $i_{pa} / i_{pc} \approx 1$, $\Delta E_p \approx 60$ mV and $i_p \propto \nu^{1/2}$.[xxiv] The *trans*-bis(alkynyl) complexes [**18**] generally exhibit two oxidation events, with the exceptions of [**18d**] exhibiting an additional single reduction event, and [**18b, i**], which contain the most electron donating substituents, exhibiting three oxidation events. The unique reduction event observed in [**18d**] is assigned to the closely occurring independent reductions of the two nitro groups on the basis of the higher peak current, and large ΔE_p value (220 mV) in comparison with the internal standard (60 mV). For the first oxidation of [**18**], there was evidence of electrochemical-chemical (EC) behaviour, with $i_{pc} > i_{pa}$ and additional signals observed on the reverse scan when conducting the experiment at room temperature. However at reduced temperatures (acetone / dry ice bath), current ratios approached unity, indicating improvements to the chemical reversibility. The second oxidation processes (and third for [**18b, i**]) are irreversible at all temperatures.

[xxiv] Where i_{pa} = anodic peak height; i_{pc} = cathodic peak height; ΔE_p = maximum current – minimum current and ν = scan rate.

Table 5.3: Selected electrochemical data (V) of [**18a** – **i**] complexes obtained from low temperature (acetone / dry ice bath), 0.1 M $[N^nBu_4]PF_6$, CH_2Cl_2 solutions.

Complex	R	$E_{1/2}(1)$	$E_{1/2}(2)$	$E_{1/2}(3)$	$E_{1/2}$(red)	ΔE_{1-2}	ΔE_{2-3}
[**18a**]	C_4H_9	− 0.09[b]	0.83[c]	-	-	0.92	-
[**18b**]	3-*th*	0.05[a]	0.63[c]	0.96[c]	-	0.58	0.33
[**18c**]	C_6H_5	0.09[a]	0.85[c]	-	-	0.76	-
[**18d**]	C_6H_4-4-NO_2	0.38[a]	0.93[c]	-	− 1.73[d]	0.55	-
[**18e**]	C_6H_4-4-C≡N	0.30[a]	0.83[c]	-	-	0.53	-
[**18f**]	C_6H_4-4-C≡C$SiMe_3$	0.14[a]	0.89[c]	-	-	0.75	-
[**18g**]	C_6H_4-4-C_5H_{11}	0.02[a]	0.74[c]	-	-	0.72	-
[**18h**]	C_6H_4-4-COOMe	0.19[a]	0.88[c]	-	-	0.69	-
[**18i**]	C_6H_4-4-OMe	− 0.11[a]	0.39[c]	0.81[c]	-	0.50	0.42

[a]*reversible;* [b]*quasi-reversible;* [c]*irreversible;* [d]*two-electron redox event*

Electronic effects of the R group on molecular properties are expected to be more apparent in the solution state over the solid state, as a result of greater conformational freedom, which permits better overlap and conjugation through the molecular backbone. As the first oxidation potentials ($E_{1/2}(1)$) span a 500 mV range (Table 5.3), and display a clear dependence on the electronic characteristics of the R substituent (Figure 5.11), oxidations are presumably largely centred on the alkynyl ligand(s). Alkynyl ligand-based oxidation in ruthenium complexes are common[50] as illustrated by the trends in redox potentials in a similar series of *trans*-bis(alkynyl) complexes containing the {$Ru(dppe)_2$} motif.[48] There are few *trans*-bis(ethynylthiophene) metal complexes reported in the literature to date.[51, 52] As $E_{1/2}(1)$ of [**18b**] is found at the lower (less positive) range of oxidation potentials in the series, the ligand fragment can be superficially categorised similarly to those containing electron donating groups.

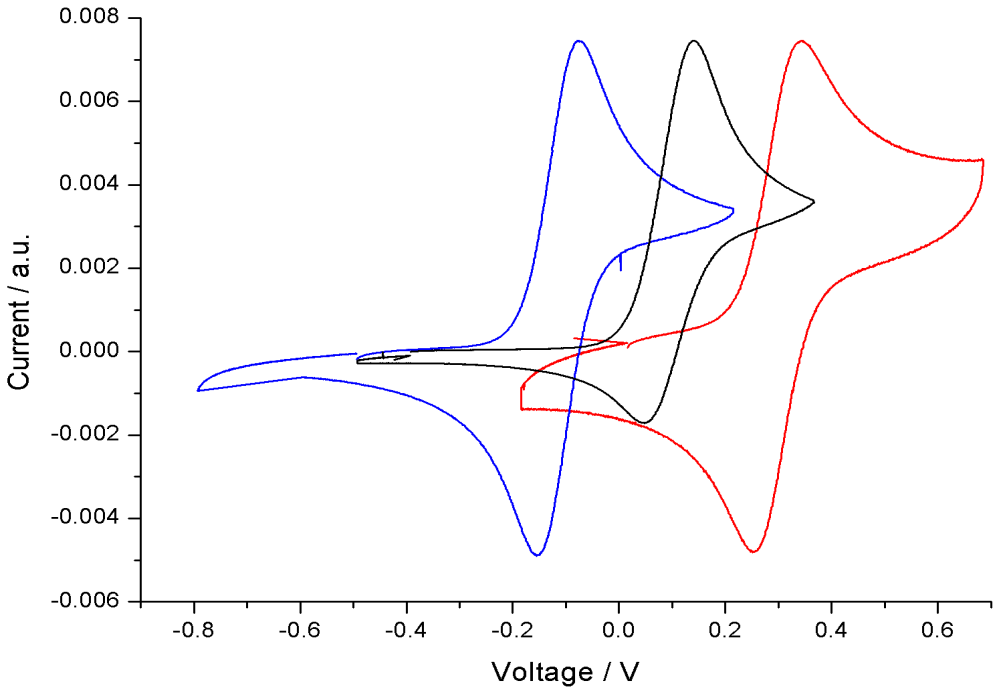

Figure 5.11: Cyclic voltammograms of representative *trans*-[Ru(C≡CR)$_2${P(OEt)$_3$}$_4$] complexes (R = C_6H_5, [**18c**], black line; C_6H_4-4-C≡N, [**18e**], red line; C_6H_4-4-OMe, [**18i**], blue line) showing the dependence of $E_{1/2}(1)$ on the electronic character of the R substituent. Scans were conducted at room temperature in 0.1 M [N^{n}Bu$_4$]PF_6 CH_2Cl_2 solutions at 100 mVs^{-1} and have been referenced to internal decamethylferrocene (not shown). Scan have been normalised to the same anodic maximum.

In contrast, $E_{1/2}(2)$ is less sensitive to the nature of the R group, where values fall within a narrower 150 mV range, therefore the second oxidation (or third in the cases of [**18b, i**]) can be assigned to more metal-centred [Ru^{II}] / [Ru^{III}] processes. The additional redox events observed within complexes [**18b**] and [**18i**] are thought to arise as a result of the strongly electron donating alkynyl fragments and {Ru{P(OEt)$_3$}$_4$} motif.

Comparison between *trans*-bis(alkynyl) complexes of the type *trans*-[Ru(C≡CC_6H_4-4-R′)$_2$(PP′)] (R′ = NO_2, COOMe, C≡CSiMe_3; PP′ = (dppm)$_2$ (see Chapter 2), (dppe)$_2$,[48] {P(OEt)$_3$}$_4$), reveals that electrochemical responses of complexes containing {Ru(dppe)$_2$} and {Ru(dppm)$_2$} fragments are similar, albeit determined under different experimental conditions (where 0.1 M [N^{n}Bu$_4$]BF_4 / CH_2Cl_2 and 0.1 M [N^{n}Bu$_4$]PF_6 / CH_2Cl_2 electrolyte solutions were respectively employed). In contrast, {Ru{P(OEt)$_3$}$_4$} containing complexes have higher (more positive) oxidation potentials (by ~ + 0.10 V),

reflecting the increased π-accepting character of the phosphite ancillary ligands, compared to the dppm and dppe alternatives.[47]

5.5. Spectroelectrochemistry

As discussed elsewhere in this Thesis (see section 4.5 of Chapter 4), the appearance of both vibrational and electronic spectra of complexes *trans*-[Ru(C≡CC_6H_4-4-R′)$_2$(dppe)$_2$]$^{n+}$ (n = 0, 1) are best accounted for in terms of a distribution of conformers, which could be approximated by three low energy structures differing in terms of the relative orientation of the C_6H_4-4-R′ rings with respect to the {Ru(dppe)$_2$} fragment.[48] The higher *pseudo*-symmetry of complexes bearing *mono*-dentate *tetrakis*-triethylphosphite ligands, *trans*-[Ru(C≡CR)$_2${P(OEt)$_3$}$_4$] (*pseudo*-D_{4h}), than *trans*-[Ru(C≡CR)$_2$(dppe)$_2$] (*pseudo*-D_{2h}) makes the phosphite complexes [**18**] a convenient series through which to explore conformational effects. Moreover, this work represents the first spectroelectrochemical study of complexes bearing the {Ru{P(OEt)$_3$}$_4$} motif.

The one-electron oxidations of complexes [**18**] to [**18**]$^+$ in 0.1 M [N^{n}Bu$_4$]PF_6 CH_2Cl_2 solutions have been monitored by IR spectroelectrochemistry (Figure 5.12) with the key vibrational modes, ν(C≡C) and ν(C=C), summarised in Table 5.4.

Table 5.4: Selected infrared spectroelectrochemical data (cm^{-1}) for neutral, *trans*-[Ru(C≡CR)$_2${P(OEt$_3$}$_4$], [**18**], and *mono*-oxidised, *trans*-[Ru(C≡CR)$_2${P(OEt$_3$}$_4$]$^+$, [**18**]$^+$, complexes, obtained from 0.1 M [N^{n}Bu$_4$]PF$_6$ CH_2Cl_2 solutions.[xxv]

Complex	R	ν(C≡C)	ν([C≡C]$^+$)	ν(C=C)	ν([C=C]$^+$)
[**18a**]	C_4H_9	2098 m	1960 s	-	-
[**18b**]	3-*th*	2070 m , 2087 m	1893 w	*	*
[**18c**]	C_6H_5	2073 m	1898 w	1590 w	1662 w, 1631 w
[**18d**]	C_6H_4-4-NO_2	2054 m	1929 w	1580 w	1583 w
[**18e**]	C_6H_4-4-C≡N	2063 m	1922 w	1590 w	1592 w
[**18f**]	C_6H_4-4-C≡C$SiMe_3$	2066 m	1898 w	1592 w	1572 w
[**18g**]	C_6H_4-4-C_5H_{11}	2075 m	1889 m	1497 w	1582 w
[**18h**]	C_6H_4-4-COOMe	2066 m	1919 m	1592 w	1595 w
[**18i**]	C_6H_4-4-OMe	2077 m	1878 s	1501 w	1576 w

*s-strong; m-medium; w-weak; *too low intensity for absolute characterisations / peaks are lost in the baseline*

[xxv] Further characterisations include / cm^{-1}: [**18d**]: 1498 w, ν(N=O); 1322 w, ν(N-O); [**18d**]$^+$: 1517 w, ν([N=O]$^+$); 1338 w, ν([N-O]$^+$); [**18e**]: 2234 w, ν(C≡N); 2218 w, ν(C≡N); [**18e**]$^+$: 2227 w, ν([C≡N]$^+$); [**18f**]: 2147 w, ν(C≡C$SiMe_3$); [**18f**]$^+$: 2149 w, ν([C≡C$SiMe_3$]$^+$); [**18h**]: 1704 m, ν(C=O) and [**18h**]$^+$: 1716 m ν([C=O]$^+$).

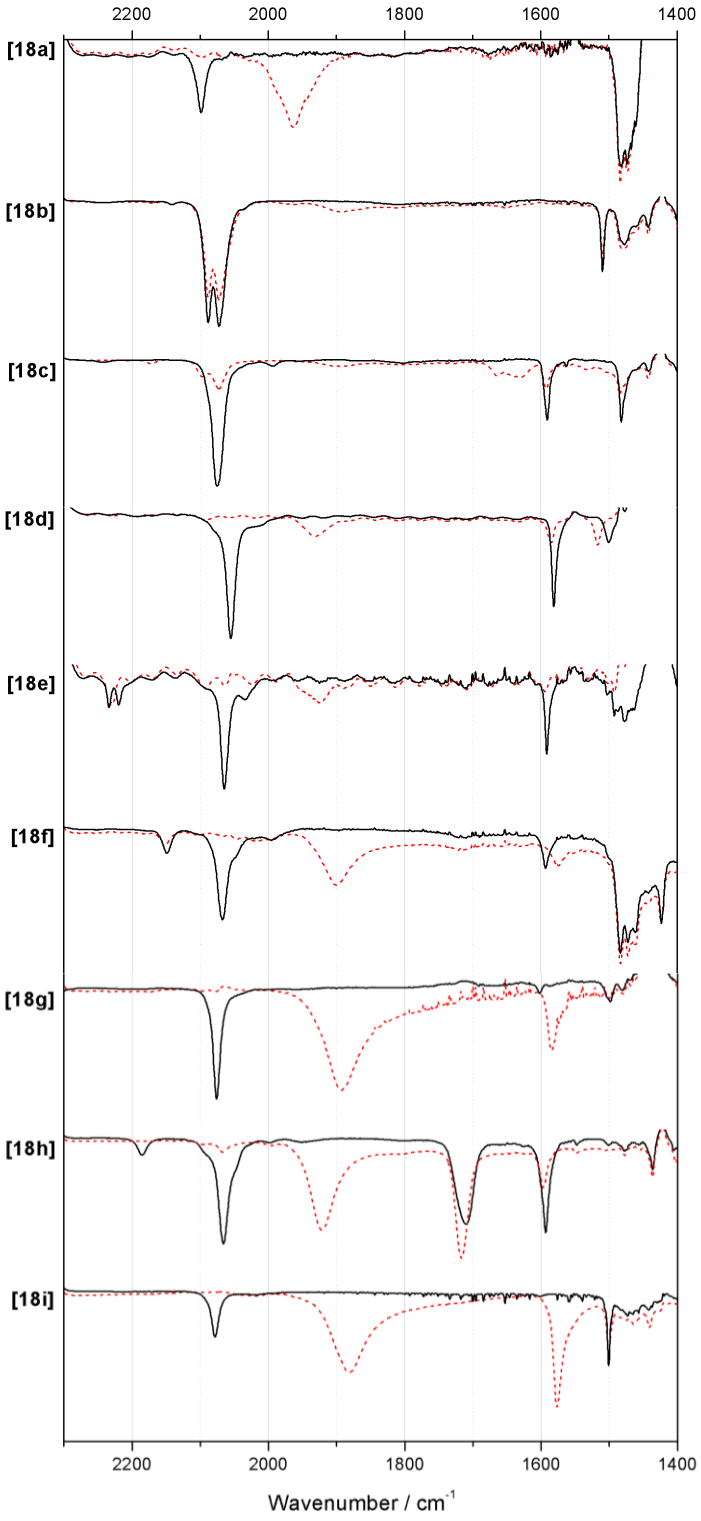

Figure 5.12: IR spectra of *trans*-[Ru(C≡CR)$_2${P(OEt)$_3$}$_4$], [**18**], (neutral form, black solid line) and *trans*-[Ru(C≡CR)$_2${P(OEt)$_3$}$_4$]$^+$, [**18**]$^+$, (*mono*-oxidised form, red dashed line), from 0.1 M [N^{n}Bu$_4$]PF$_6$ CH_2Cl_2 solutions, where: R = C_4H_9, [**18a**]; 3-*th*, [**18b**]; C_6H_5, [**18c**]; C_6H_4-4-NO_2, [**18d**]; C_6H_4-4-C≡N, [**18e**]; C_6H_4-4-C≡C$SiMe_3$, [**18f**]; C_6H_4-4-C_5H_{11}, [**18g**]; C_6H_4-4-COOMe, [**18h**] and C_6H_4-4-OMe, [**18i**]. The *mono*-oxidised forms, [**18**]$^+$, were generated at potentials of: 0.49 (**a**), 0.57 (**b**), 0.59 (**c**), 0.90 (**d**), 0.87 (**e**), 0.75 (**f**), 0.62 (**g**), 0.74 (**h**) and 0.58 V (**i**).

Each of the *trans*-bis(alkynyl) *tetrakis*-triethylphosphite ruthenium complexes show the same general spectral patterns upon oxidation, with the exceptions of [**18b**] and [**18c**], which are discussed separately at the end of this section (see section 5.5.2.). The strong, well resolved ν(C≡C) bands, which characterise complexes [**18**], collapse completely with new, strong, broad ν([C≡C]$^+$) bands observed at lower (~ − 125 to − 199 cm^{-1}) energy in [**18**]$^+$, the precise magnitude (Figure 5.13) and relative intensity (Table 5.5) of which is sensitive to the electronic character of the R group. Together, these observations indicate a ligand-centred oxidation and a delocalised structure (at least on the IR timescale), whilst the significant broadening of the ν([C≡C]$^+$) band envelope is consistent with a distribution of conformers. The shifts of the ring breathing modes of the aryl fragments upon oxidation (from ν(C=C) to ν([C=C]$^+$)), follow the same general trend, except for derivative [**18a**], which lacks a phenyl substituent.

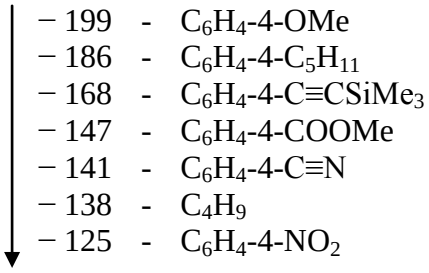

Figure 5.13: Variations in Δν(C≡C) ([**18**] → [**18**]$^+$) values (cm^{-1}) as a function of R substituent.

Table 5.5: Intensities of ν([C≡C]$^+$) as a percentage of ν(C≡C) and corresponding R substituent.

Complex	**R**	$\frac{\lvert \textbf{intensity } \nu([\mathbf{C{\equiv}C}]^+) \rvert}{\lvert \textbf{intensity } \nu(\mathbf{C{\equiv}C}) \rvert} \times \mathbf{100\ (\%)}$
[**18a**]	C_4H_9	125
[**18d**]	C_6H_4-4-NO_2	16
[**18e**]	C_6H_4-4-C≡N	21
[**18f**]	C_6H_4-4-C≡C$SiMe_3$	62
[**18g**]	C_6H_4-4-C_5H_{11}	92
[**18h**]	C_6H_4-4-COOMe	80
[**18i**]	C_6H_4-4-OMe	180

The intensity of $\nu([C\equiv C]^+)$ (*vs.* $\nu(C\equiv C)$) is known to reflect the increasing electron-releasing strength of the R substituent, as has been previously noted for *mono*-alkynyl complexes of the type *trans*-[RuCl(C≡CC_6H_4-4-R′)$(dppe)_2$] (R′ = H, F, NO_2, COH, COMe, OMe, NMe_2).[53] Similar effects are observed here (Table 5.5). A positive linear free energy relationship (LFER) has also been found between the positive Hammett parameter (σ_p^+) and the isotropic *g*-value (g_{iso}) demonstrating that increasing the electron releasing strength of the R′ substituent tends the *mono*-oxidation products more towards organic radicals, as g_{iso} is moved towards the free electron value (g_e = 2.00232)[54] with such subsitutuents, which is consistent with conclusions drawn here for the {Ru{$P(OEt)_3$}$_4$} series. Furthermore, for the *mono*-oxidised, computationally less demanding complexes, *trans*-[RuCl(C≡CC_6H_4-4-R′)$(dpe)_2]^+$ (R′ = H, NO_2, OMe, NMe_2), the Mulliken spin density on ruthenium was calculated to be more positive (by ~ 0.14) with electron withdrawing R′ groups (*i.e.* a more metal-centred cation radical) than electron donating R′ groups (*i.e.* a more ligand-centred cation radical). The trend in intensity of $\nu([C\equiv C]^+)$ (*vs.* $\nu(C\equiv C)$) with electron-releasing strength of the R′ substituent can also be seen for the recently published (2014) series of *trans*-bis(alkynyl) complexes, *trans*-[Ru(C≡CC_6H_4-4-R′$)_2(dppe)_2$] (R′ = OMe, C≡C$SiMe_3$ [**43a**], NH_2), though was not acknowledged in the paper.[48]

Complexes [**18**] in 0.1 M [N^nBu_4]PF_6 / CH_2Cl_2 solutions were also subjected to UV-Vis-NIR spectroelectrochemical investigations (Table 5.6). For convenience, the spectroelectrochemical responses of [**18b**] and [**18c**] will again be discussed at the end of this section.

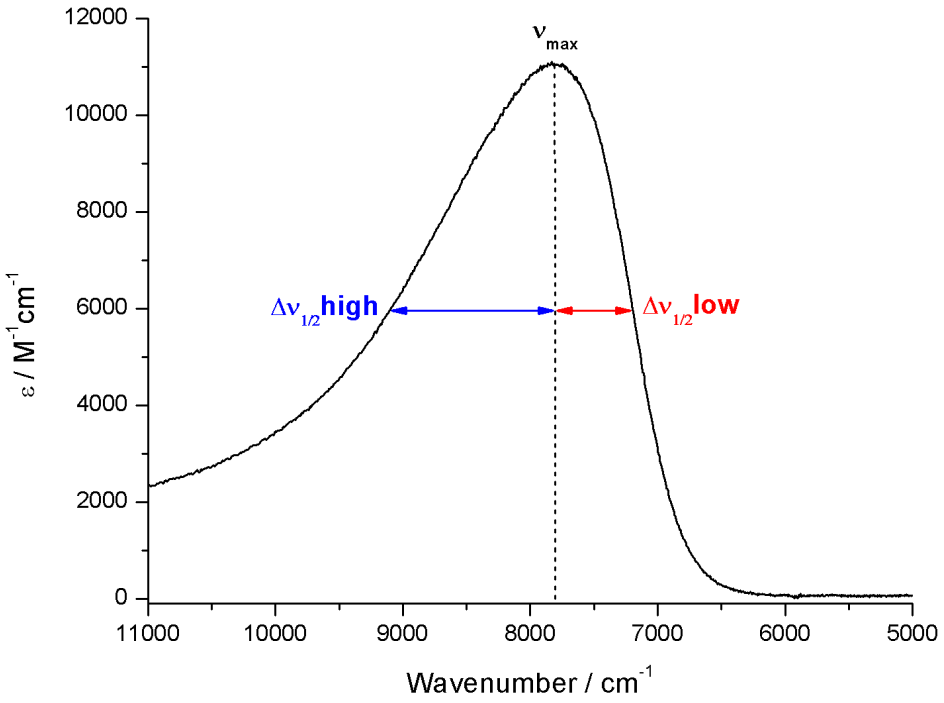

Figure 5.14: Definitions of ν_{max}, $\Delta\nu_{1/2}$low and $\Delta\nu_{1/2}$high values used in Table 5.6 for *mono*-oxidised complexes *trans*-$[Ru(C{\equiv}CR)_2\{P(OEt)_3\}_4]^+$, [**18**]$^+$, using the NIR profile of [**18i**]$^+$ as a representative example, where the addition of $\Delta\nu_{1/2}$low and $\Delta\nu_{1/2}$high values equals the full width at half height (FWHH).

Table 5.6: UV-Vis-NIR spectroelectrochemical data obtained for *mono*-oxidised complexes *trans*-[Ru(C≡CR)$_2${P(OEt)$_3$}$_4$]$^+$, [**18**]$^+$, between 5000 – 16 000 cm^{-1}, where ν_{max}, FWHH and $\Delta\nu_{1/2}$ are reported in cm^{-1} while ε is reported in M^{-1}cm^{-1}.

Complex	R	ν_{max}(1)	ε(1)	FWHH(1)	$\Delta\nu_{1/2}$(1)low	$\Delta\nu_{1/2}$(1)high	ν_{max}(2)	ε(2)	ν_{max}(3)	ε(3)
[**18a**]$^+$	C_4H_9	10 460	888	2117	854	1263	12 804	328	-	-
[**18b**]$^+$	3-*th*	8217	1421	2058	715	1343	11 876	312	-	-
[**18d**]$^+$	C_6H_4-4-NO_2	8897	7867	*	707	*	11 038	4685	11 862	4065
[**18e**]$^+$	C_6H_4-4-C≡N	8772	1729	*	688	*	11 261	918	-	-
[**18f**]$^+$	C_6H_4-4-C≡CSiMe$_3$	8026	4433	2142	635	1507	11 455	1381	-	-
[**18g**]$^+$	C_6H_4-4-C_5H_{11}	8197	10 262	1823	621	1202	11 521	2140	-	-
[**18h**]$^+$	C_6H_4-4-COOMe	8650	9314	*	676	*	11 161	3993	-	-
[**18i**]$^+$	C_6H_4-4-OMe	7831	11 103	2703	660	1368	12 063	2144	-	-

* *shoulder is too intense to calculate this value*

In the NIR region (between 5000 – 16 000 cm^{-1}), multiple bands have been observed for *mono*-oxidised *trans*-[RuCl(C≡CC_6H_4-4-R′)$(dppe)_2]^+$ complexes[53] and *trans*-[Ru(C≡CC_6H_4-4-R′$)_2(dppe)_2]^+$ complexes,[48] which have been assigned to the various distinct rotamer conformers based on supporting quantum chemical calculations. In contrast, complexes [**18**]$^+$ generally exhibit one principal asymmetric band within the range 7819 − 10 460 cm^{-1} and a shoulder of varying relative intensity between 11 038 − 12 804 cm^{-1} (Figure 5.15). This simplification is presumed to arise from the higher symmetry of complexes [**18**] (*vs.* chelating *bis*-phosphine derivatives) and the smaller number of spectroscopically distinct rotamer conformations that can form.

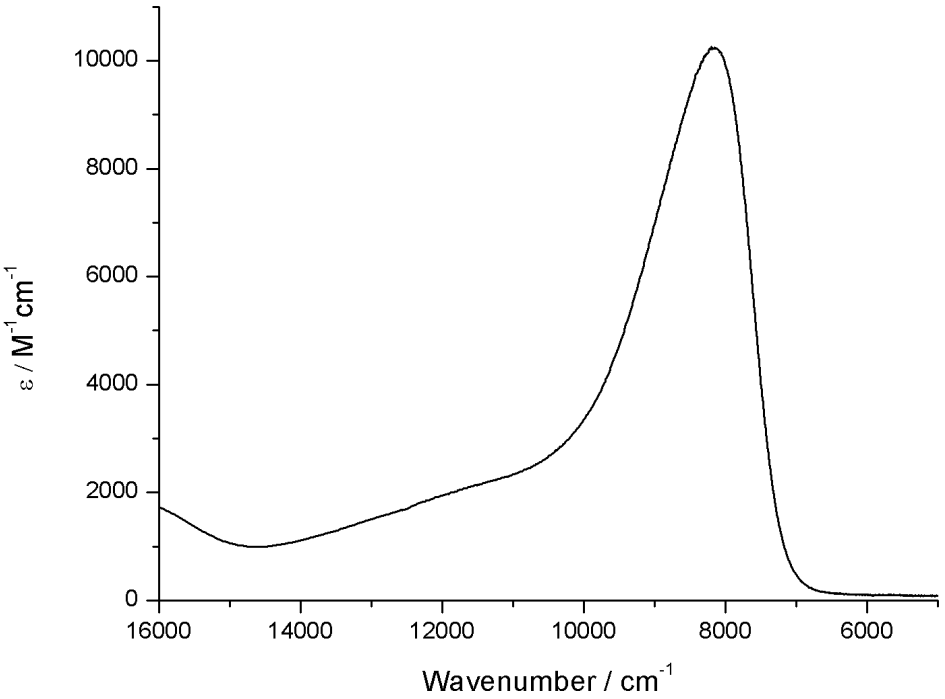

Figure 5.15: UV-Vis-NIR spectrum of [**18g**]$^+$ (recorded in a 0.1 M [N^nBu_4]PF_6 CH_2Cl_2 solution, generated at 0.52 V), between 5000 – 16 000 cm^{-1} as a representative example of [**18**]$^+$, displaying one asymmetric, intense band at lower energy and a further, less intense, band at higher energy.

The asymmetry of the lowest energy, principal bands (where $\nu_{1/2}(1)low \neq \nu_{1/2}(1)high$) of [**18**]$^+$, which are of appreciable intensity for complexes bearing *bis*-aryl ethynyl fragments (4433 – 11 103 $M^{-1}cm^{-1}$) indicate that these systems tend towards Class III 'mixed-valence' systems, according to the traditional Robin and Day classification system, consistent with IR spectroelectrochemistry.[55] For [**18**]$^+$ bearing electron

releasing substituents, the peak asymmetry and band intensities are heightened compared with those bearing electron accepting groups, revealing more strongly coupled (organic) 'mixed-valence' systems (and vice-versa).[56] As a result of the Hush-type characteristics exhibited, the lower energy band may be considered as an IVCT for the organic 'mixed-valence' state.

The higher energy NIR band / shoulder presumably reflects a more MLCT-type transition arising as a consequence of free rotation of the (aryl-containing) R group about the C≡C-Ru-C≡C axis, leading to a loss in conjugation, as is reported for similar complexes.[48] Given that complexes bearing electron withdrawing substituents exhibit broader NIR band envelopes than those bearing electron donating substituents (Figure 5.16), an electronically-controlled population bias of rotamers may exist. This is not an uncommon phenomenon, having been previously noted for *trans*-[RuCl(C≡CC_6H_4-4-R′)$(dpe)_2$]$^+$ complexes (R = H, NO_2, OMe, NMe_2) through quantum calculations.[53] Alternatively, the redistribution of charge in *trans*-bis(alkynyl) complexes with electron withdrawing R groups (as being more metal-centred) might be invoking additional optical (presumably LMCT-type) transitions.

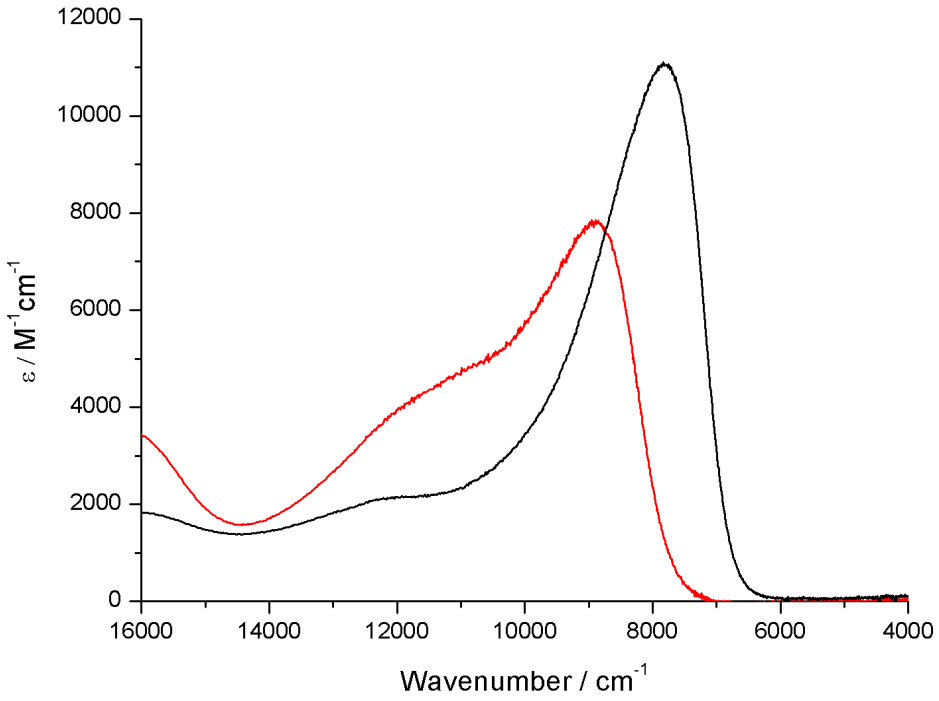

Figure 5.16: The UV-Vis-NIR spectra of [**18d**]$^+$ (red line, generated at 0.68 V) bearing electron withdrawing nitro substituents has a broader band envelope between 4000 − 16 000 cm^{-1} than [**18i**]$^+$ (black line, generated at 0.54 V) with electron donating OMe groups. Spectra were recorded from 0.1 M [N^{n}Bu$_4$]PF$_6$ CH_2Cl_2 solutions.

In summary, the observation of a single ν([C≡C]$^+$) band means complexes [**18**]$^+$ are delocalised on the IR timescale. The intensity and asymmetry of the principal NIR band also points to strongly coupled Class II (or Class III) character. These characteristics are most pronounced for electron donating groups, consistent with the better stabilisation of the radical cation on the alkynyl ligand(s). The observation of fewer NIR bands, compared with *trans*-bis(alkynyl) {Ru(dppe)$_2$} analogous, point to fewer spectroscopically distinct species in solution, consistent with the higher *pseudo*-symmetry.

5.5.1. Quantum chemical calculations

Density functional theory (DFT) and time-dependent DFT (TD-DFT) calculations, summarised in Table 5.7, have been performed by W / Prof. P. J. Low (at the University of Western Australia) on the 'flat' and 'twisted' optimised structures of

trans-[Ru(C≡CC_6H_4-4-OMe)$_2${P(OMe)$_3$}$_4$], [**18i′**]$^{n+}$ (n = 0, 1; Figure 5.17), as a less computationally demanding derivative of [**18i**] through which to better understand the optical and vibrational spectra of complexes [**18**]$^{n+}$.

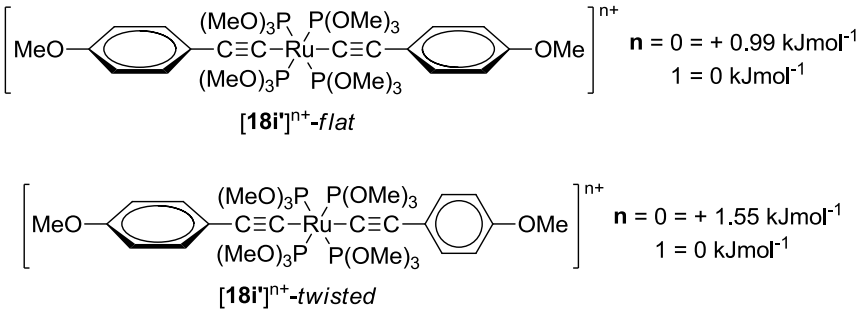

Figure 5.17: 'Flat' ([**18i′**]$^{n+}$-*flat*) and 'twisted' ([**18i′**]$^{n+}$-*twisted*) conformations, and respective energy calculations, of *trans*-[Ru(C≡CC_6H_4-4-OMe)$_2${P(OMe)$_3$}$_4$]$^{n+}$ ([**18i′**]$^{n+}$), as a representative *tetrakis*-trialkylphosphite *trans*-bis(alkynyl) ruthenium complex for the following quantum chemical investigation.

Table 5.7: Selected vibrational frequencies (cm^{-1}), optical transition energies (ν_{max} / cm^{-1}) and respective orbital contributions for *trans*-[Ru(C≡CC_6H_4-4-OMe)$_2${P(OMe)$_3$}$_4$], [**18i′**], and *trans*-[Ru(C≡CC_6H_4-4-OMe)$_2${P(OMe)$_3$}$_4$]$^+$, [**18i′**]$^+$, in both 'flat' and 'twisted' conformations (Figure 5.17), where oscillator strengths are given in brackets unless otherwise stated.

Complex	**ν(C≡C)**	**ν([C≡C]$^+$)**	**ν(C=C)**	**ν([C=C]$^+$)**	**ν_{max}(1)**	**Transition (% contribution)**	**ν_{max}(2)**	**Transition (% contribution)**
[**18i′**]-*flat*	2126 (764.7)	-	1493 (755.2)	-	-	-	-	-
[**18i′**]$^+$-*flat*	-	1963 (6934.7)	-	1565 (4760.6)	9524 (0.4754)	β-HOMO → β-LUMO (80 %)	17 123 (0.1190)	β-HOMO-2 → β-LUMO (45 %) β-HOMO-3 → β-LUMO (21 %)
[**18i′**]-*twisted*	2126 (785.1)	-	1493 (765.6)	-	-	-	-	-
[**18i′**]$^+$-*twisted*	-	1993 (1444.4)	-	1571 (4483.2)	12 160 (0.5046)	β-HOMO-1 → β-LUMO (73 %)	19 267 (0.0571)	β-HOMO-3 → β-LUMO (65 %)

The energy differences between the 'flat' ([**18i′**]-*flat*) and 'twisted' ([**18i′**]-*twisted*) complexes in their neutral and *mono*-oxidised states ($0 - 1.55$ kJmol^{-1}) are not significant, strongly indicating that both conformational forms are present at room temperature.

For both the neutral, 'flat' complex ([**18i′**]-*flat*) and neutral, 'twisted' complex ([**18i′**]-*twisted*) a medium intensity ν(C≡C) band was calculated at 2126 cm^{-1} while a medium intensity ν(C=C) band was determined at 1493 cm^{-1}, which are in close agreement with values obtained experimentally for [**18i**] (ν(C≡C): 2077 m cm^{-1}; ν(C=C): 1501 w cm^{-1}), inferring the accuracy of the calculations. Upon oxidation, ν([C≡C]$^{+}$) bands are formed at lower energy by ~ − 160 cm^{-1} both experimentally and computationally, consistent with increased cumulenic character and a high degree of alkynyl character in the initial oxidation. For [**18i**]$^{+}$, a single, very intense but broad, ν([C≡C]$^{+}$) band is found at 1878 cm^{-1}. The broadness of this band is ascribed to the presence of rotamers in solution, which is supported by the fact that ν([C≡C]$^{+}$) bands of [**18i′**]$^{+}$-*flat* and [**18i′**]$^{+}$-*twisted* differ by some 30 cm^{-1} (1963 cm^{-1} and 1993 cm^{-1} respectively). Alternatively for [**18i**]$^{+}$, the ν([C=C]$^{+}$) band (1576 w cm^{-1}) is fairly narrow. For [**18i′**]$^{+}$, ν([C=C]$^{+}$) bands for the 'flat' and 'twisted' geometries differ by only 6 cm^{-1} (1565 cm^{-1} and 1571 cm^{-1} respectively), consistent with the narrower experimental band envelope.

For [**18i′**]$^{+}$-*flat*, optical transition energies are calculated at 1050 nm (9524 cm^{-1}; β-HOMO → β-LUMO) and 584 nm (17 123 cm^{-1}; β-HOMO-2 and β-HOMO-3 → β-LUMO**)**, which are in agreement with bands observed experimentally in the UV-Vis-NIR spectrum of [**18i**]$^{+}$ (7831 cm^{-1} and 16 026 cm^{-1}). Considering the contributions of molecular orbitals to these transitions (Table 5.7) and distributions of the individual orbitals (Figure 5.18), the lower energy band represents an IVCT transition for the organic 'mixed-valence' state, with the C_6H_4-4-OMe fragment as the redox centre. Alternatively, the transition may be described as LL′CT, an analogous concept to MM′CT transitions often encountered in more traditional 'mixed-valence' complexes.[57] The higher energy band has predominantly more MLCT character, but is better described as a mixed MLCT / IL transition. In this example, the β-HOMO-1 to β-LUMO transition (Figure 5.18) is forbidden by symmetry.

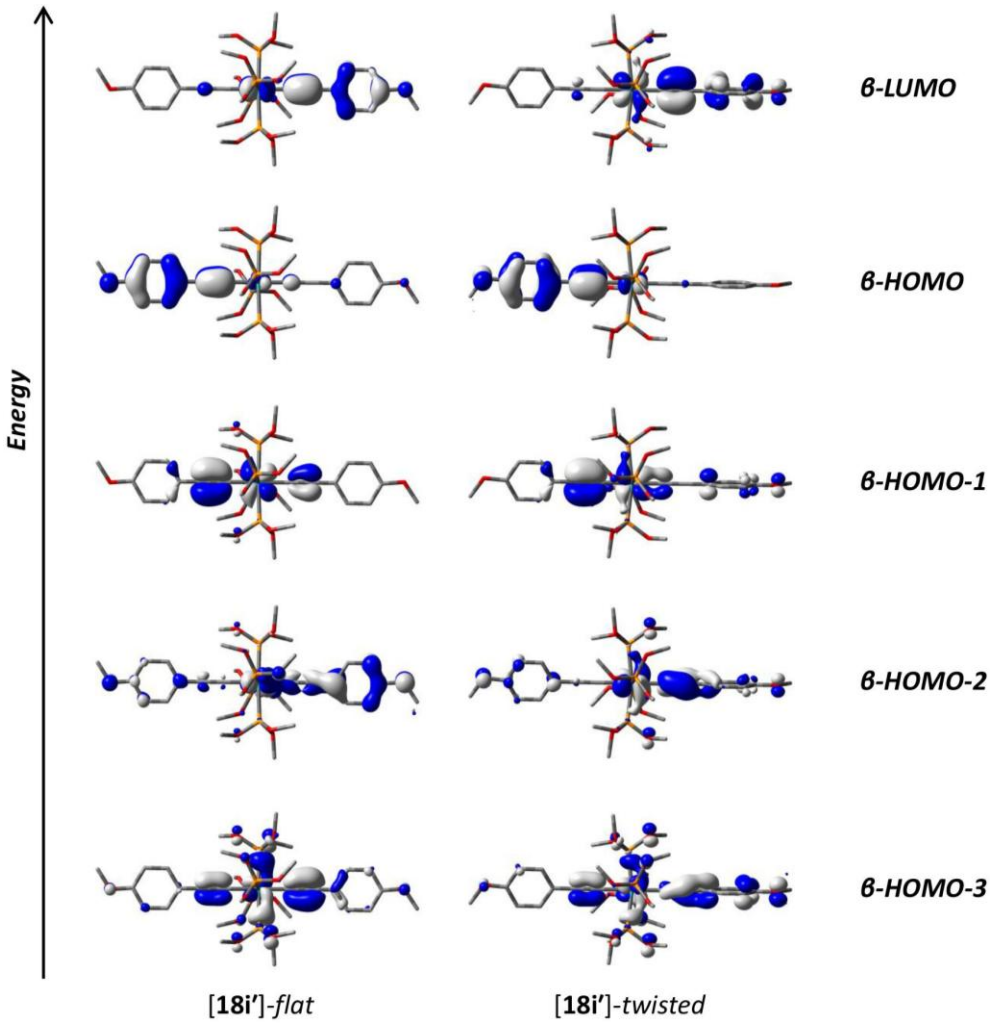

Figure 5.18: Frontier orbital plots and energy diagram (not to scale) of [**18i′**]$^+$ with the aryl rings planar ([**18i′**]$^+$-*flat*) and twisted ([**18i′**]$^+$-*twisted*), where orbitals have been plotted with contour values ± 0.04 $(e / b^3)^{1/2}$.

For [**18i′**]$^+$-*twisted*, optical transition energies were calculated at 822 nm (12 160 cm^{-1}; β-HOMO-1 → β-LUMO) and 519 nm (19 267 cm^{-1}; β-HOMO-3 → β-LUMO), which are also in agreement with bands observed experimentally in the UV-Vis-NIR spectrum of [**18i**]$^+$ (12 063 cm^{-1} and 19 157 cm^{-1}). Considering the contributions (Table 5.7) and distributions (Figure 5.18) of the molecular orbitals, the lower energy band is best ascribed as a mixture of MLCT / IL transitions while the higher energy band has predominantly more IL character. Notably, the β-HOMO-1 to β-LUMO transition is now permitted, as a consequence of the reduced symmetry. Optical transitions of

[**18i′**]$^+$-*twisted* are blue-shifted compared with [**18i′**]$^+$-*flat*, consistent with reduced conjugation in the former as a result of aryl ring rotation out of the plane.

The best agreement of the computational with the experimental data is not solely the 'flat' or 'twisted' orientations, rather a superposition of the two (Figure 5.19).

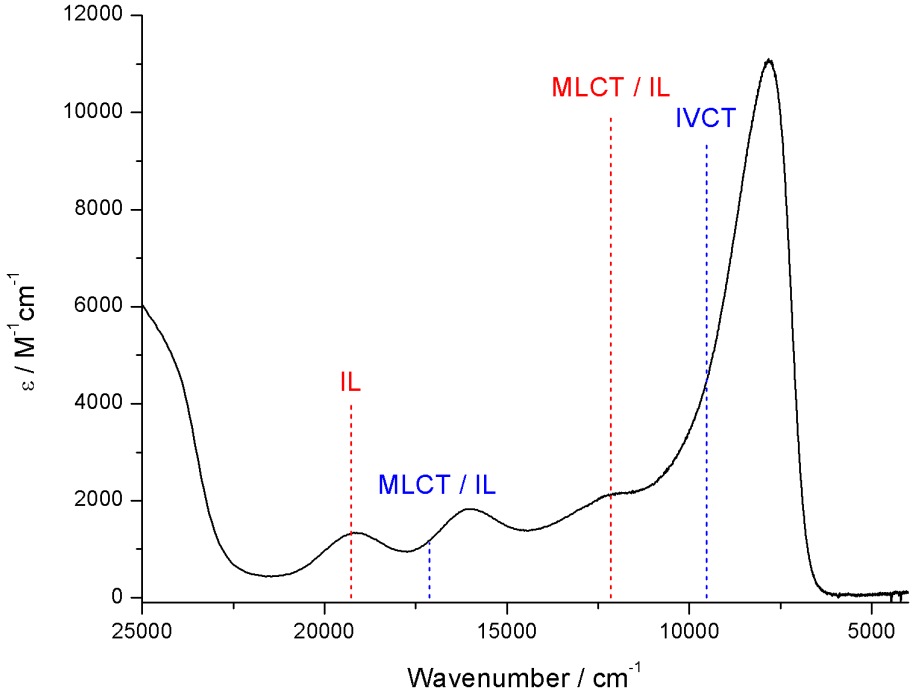

Figure 5.19: UV-Vis-NIR spectrum of [**18i**]$^+$ between 4000 – 25 000 cm^{-1} determined experimentally (black line) from a 0.1 M [N^{n}Bu$_4$]PF$_6$ CH_2Cl_2 solution (generated at 0.54 V) along with computed transition energies of [**18i′**]$^+$-*flat* (blue dashed line) and [**18i′**]$^+$-*twisted* (red dashed line), evincing the contribution of rotameric forms to the appearance of the spectrum. The intensities of the computed absorption energies are scaled based on respective oscillator strengths.

5.5.2. Spectroelectrochemical profiles of [18b] and [18c]

During standard CV experiments, complexes [**18b**], *trans*-[Ru(C≡C-3-*th*)$_2${P(OEt)$_3$}$_4$], and [**18c**], *trans*-[Ru(C≡CC_6H_5)$_2${P(OEt)$_3$}$_4$], behave similarly to the other members of the series [**18**] (see section 5.4.). However, on longer timescales, such as during IR and UV-Vis-NIR spectroelectrochemistry experiments conducted by step-wise changes in

the potential and allowing the system to equilibrate before collecting spectra, [**18b**] and [**18c**] display strong evidence of electrochemical-chemical (EC) behaviour.

During IR spectroelectrochemical investigations of [**18b**], generating [**18b**]$^{+}$, on the initial oxidation cycle (denoted 0 to +1(1)) the two ν(C≡C) bands (perhaps observed as a result of Fermi coupling)[58] decrease to approximately four-fifths the original intensity with a new, low intensity, broad ν([C≡C]$^{+}$) band appearing at lower wavenumbers (1893 cm^{-1}) (Table 5.4, Figure 5.12). In addition to this, an asymmetric NIR band is observed at 8217 cm^{-1}. Upon reduction, the original spectrum of [**18b**] is obtained, albeit with less intense, slightly broadened ν(C≡C) bands. Upon a second oxidation cycle (denoted 0 to +1(2)), the same spectral profile of [**18b**]$^{+}$ is recovered, though again with reduced ν([C≡C]$^{+}$) band intensities (*vs.* 0 to +1(1)). However, upon decreasing the potential for the second reduction cycle (+1 to 0(2)) en route to [**18b**], a new species, [**18b′**]$^{n+}$, is generated, signified by a new NIR band (5609 cm^{-1}) (Figure 5.20), and new, low intensity, broad ν([C≡C]$^{n+}$) bands at 1927 cm^{-1} and 1944 cm^{-1}. If the potential is reduced further, the spectral profile of [**18b**] is largely recovered (Figure 5.20). For the final cycle (0 to +1(3)), [**18b**]$^{+}$ and [**18b′**]$^{n+}$ are formed simultaneously, as determined by the joint formations of the two diagnostic NIR bands (at 8217 cm^{-1} and 5609 cm^{-1}) in addition to the corresponding ν([C≡C]$^{+}$) bands. The data indicates slow electrochemical generation of the secondary species [**18b′**]$^{n+}$ from [**18b**]$^{+}$.

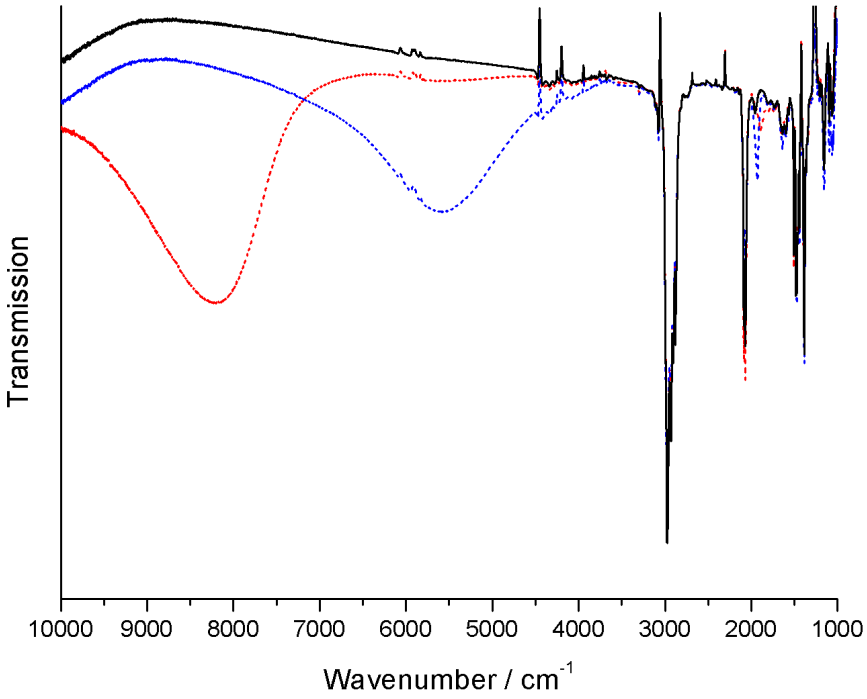

Figure 5.20: IR spectroelectrochemical investigation of [**18b**] (from a 0.1 M $[N^nBu_4]PF_6$ CH_2Cl_2 solution) showing i) $[\mathbf{18b}]^+$ formed (at 0.57 V) after the completed second oxidation cycle (0 to +1(2)), red dashed line; ii) [**18b**] re-formed (at – 0.7 V) after the completed second reduction cycle (+1 to 0(2)), black solid line and iii) the intermediate $[\mathbf{18b'}]^{n+}$ formed (at 0.20 V) *during* the second reduction cycle (+1 to 0(2)), blue dashed line.

Repeating the IR and UV-Vis-NIR spectroelectrochemistry experiments on a faster timescale (continuously recording spectra whilst the potential is swept between – 0.83 to 0.17 V at scan rates of 10 mVs^{-1}) successfully avoided the generation of $[\mathbf{18b'}]^{n+}$ for the first several cycles. However if the sample is continuously cycled (> 8 cycles), the formation of $[\mathbf{18b'}]^{n+}$ is evident in the corresponding thin-layer cyclic voltammograms (Figure 5.21), which are run in parallel with these fast IR and UV-Vis-NIR spectroelectrochemistry experiments, where the current of the [**18b**] / $[\mathbf{18b}]^+$ redox couple (occurring at 0.05 V), is progressively reduced with the generation of two new 1 : 1 oxidation events at lower potentials (at ~ − 0.38 and − 0.20 V).

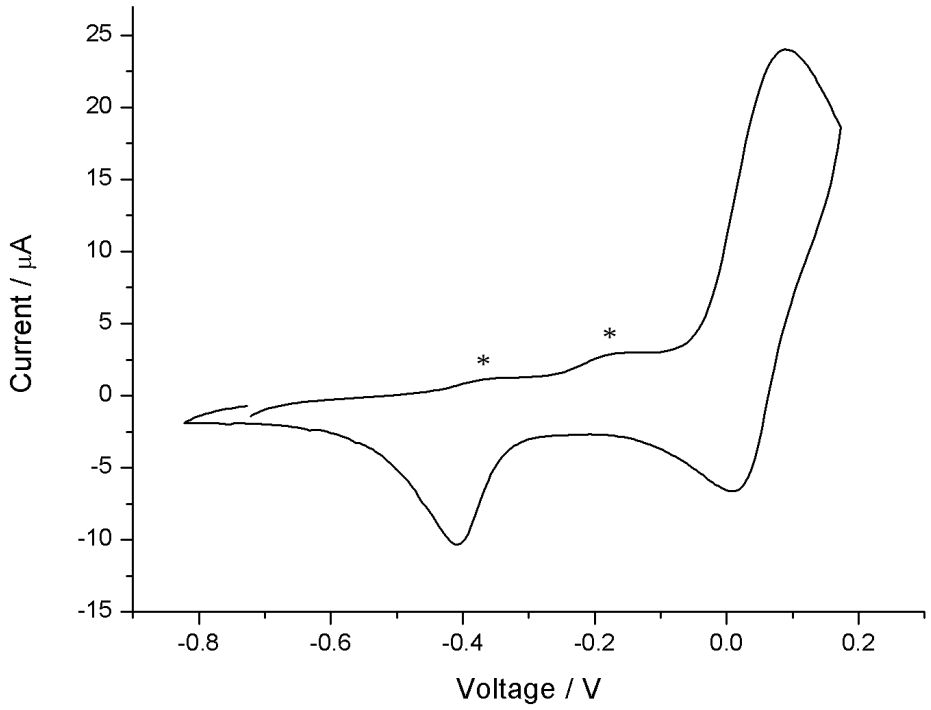

Figure 5.21: Thin-layer cyclic voltammogram recorded during the fast (10 mVs^{-1}) UV-Vis-NIR spectroelectrochemistry experiment of [**18b**] (in a 0.1 M $[N^nBu_4]PF_6$ / CH_2Cl_2 solution) following ten repeated single oxidation / reduction cycles implicating formation of a more conjugated, bimetallic species (marked by asterisks). The scan is referenced to $E_{1/2}(1)$ of [**18b**] (0.05 V *vs.* $[Fe(\eta^5\text{-}C_5H_5)_2]$ / $[Fe(\eta^5\text{-}C_5H_5)_2]^+$ = 0 V) assuming that the large oxidation event shown here at 0.05 V corresponds to [**18b**] / [**18b**]$^+$.

Given that [**18**]$^+$ exhibit significant ligand radical character, especially in the presence of an electron donating group, the formation of [**18b′**]$^{n+}$ as a dimeric species could be reasonably proposed (Figure 5.22). Similar ligand coupling reactions have been noted previously.[50]

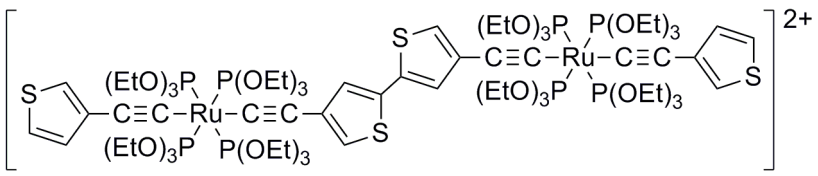

Figure 5.22: Proposed complex for [**18b′**]$^{n+}$, formed in the spectroelectrochemical investigation of [**18b**].

As [**18b′**]$^{n+}$ is formed slowly, it is fair to assume that the first cycle (0 to +1(1)) of the IR and UV-Vis-NIR spectrochemical experiments will reflect the true *mono*-oxidation of [**18b**] and so these values have been included in Tables 5.4 and 5.6. It is however curious that ν(C≡C) does not collapse completely in the oxidation of [**18b**], which is in contrast to the other compounds in the series. This might suggest a more localised oxidation (L-M-L^{+}) in this case, or instead partial oxidation. The NIR band of [**18b**]$^{+}$ is unexpectedly broader and more symmetric (*i.e.* more weakly coupled Class II-type character) than [**18i**]$^{+}$, the complex of most structural and electronic resemblance to [**18b**]$^{+}$, which warrants further investigation but is beyond the time available for this Thesis.

During IR spectroelectrochemical investigations of [**18c**], en route to generating [**18c**]$^{+}$, a single, low intensity NIR band begins to form at 8303 cm^{-1}. Correspondingly, a broad, low intensity ν([C≡C]$^{+}$) band is propagated at lower wavenumbers (1898 cm^{-1}) *vs.* ν(C≡C) (2073 cm^{-1}) (Table 5.4, Figure 5.12). However, as the intensity of the NIR band continues to increase, the maximum shifts from 8303 cm^{-1} to 7612 cm^{-1}, even if the potential is held after formation of the first electrochemically generated species has begun. Correspondingly in the IR region, new, broad, low intensity bands are observed at 2171 and 1895 cm^{-1} in addition with a sharp, low intensity band at 2094 cm^{-1}. In the spectral profiles of following cycles (0 to +1(2); +1 to 0(2); 0 to +1(3) *etc.*), the initial NIR band (8303 cm^{-1}) is absent, yet the second NIR band (7612 cm^{-1}) remains (for oxidised complexes). This implicates [**18c**]$^{+}$ as the first electrochemically generated complex, as opposed to an intermediate species, and an unknown (rapidly) electrochemically generated complex, [**18c′**]$^{n+}$, as the second. Similar observations were made in the UV-Vis-NIR spectroelectrochemical investigations of [**18c**].

In light of previous work, IR and UV-Vis-NIR spectroelectrochemistry experiments of [**18c**] were repeated on a faster timescale (10 mVs^{-1}), with spectra recorded continuously whilst the potential was ramped between – 0.6 to 0.16 V. Although the generation of [**18c′**]$^{n+}$ was avoided, neither the anomalously low maximum NIR band intensity nor the intensities of ν([C≡C]$^{+}$) bands of [**18c**]$^{+}$ were improved, precluding electronic characterisation. Notably, corresponding thin-layer cyclic voltammograms of

these fast scan experiments showed irreversible electrochemical behaviour, which will certainly be contributing to the results obtained here.

As [**18**]$^{+}$ exhibit organic 'mixed-valence' behaviour and [**18c**]$^{+}$ is without a charge-directing (stabilising) *para*-substituent on the *trans*-disposed arylethynyl fragments, the formation of [**18c′**]$^{n+}$ as a dimer is anticipated *via* radical dimerisation (Figure 5.23).

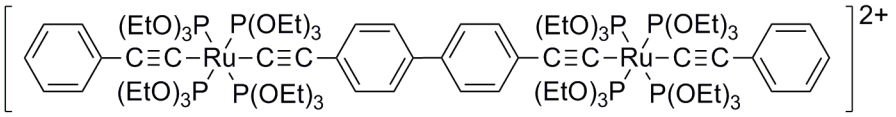

Figure 5.23: Proposed structure for [**18c′**]$^{n+}$, formed as an electrochemically generated species in the spectroelectrochemical investigation of [**18c**].

In support of the proposed biaryl bridging species (Figure 5.23), the intensity of the principal NIR band of [**18c′**]$^{n+}$ (461 $M^{-1}cm^{-1}$) is significantly lower than [**18**]$^{+}$ (between 4433 − 11 103 $M^{-1}cm^{-1}$ for *bis*-arylethynyl complexes, Table 5.6) and is more Gaussian shaped *vs.* [**18**]$^{+}$ (*i.e.* a more weakly coupled Class II complex). The NIR band of [**18c**]$^{+}$ is however more asymmetric than [**18c′**]$^{n+}$ (*i.e.* a more strongly coupled Class II system) which is consistent with the bulk series. Given that [**18c′**]$^{n+}$ is formed coincidentally during the electrochemical generation of [**18c**]$^{+}$, values for the UV-Vis-NIR spectroelectrochemical experiments of [**18c**] have not been included in Table 5.6.

5.6. Single molecule conductance measurements

As discussed in the introduction, in collaboration with Prof. R. J. Nichols (University of Liverpool), the conductance histogram of *trans*-[Ru(C≡C-3-*th*)$_2$(dppe)$_2$], [**43b**],[30] (reproduced in Figure 5.24) displayed additional features in the high (H) conductance peak. Such features are thought to reflect the formation of supplementary Au|molecule|Au junctions through the electron rich phenyl rings comprising the sterically demanding {Ru(dppe)$_2$} motif, especially for shorter systems with low axial anisoptropy. The analogous *tetrakis*-triethylphosphite complex, *trans*-[Ru(C≡C-3-*th*)$_2${P(OEt)$_3$}$_4$], [**18b**] serves as convenient complex through which to explore this hypothesis (Figure 5.24).

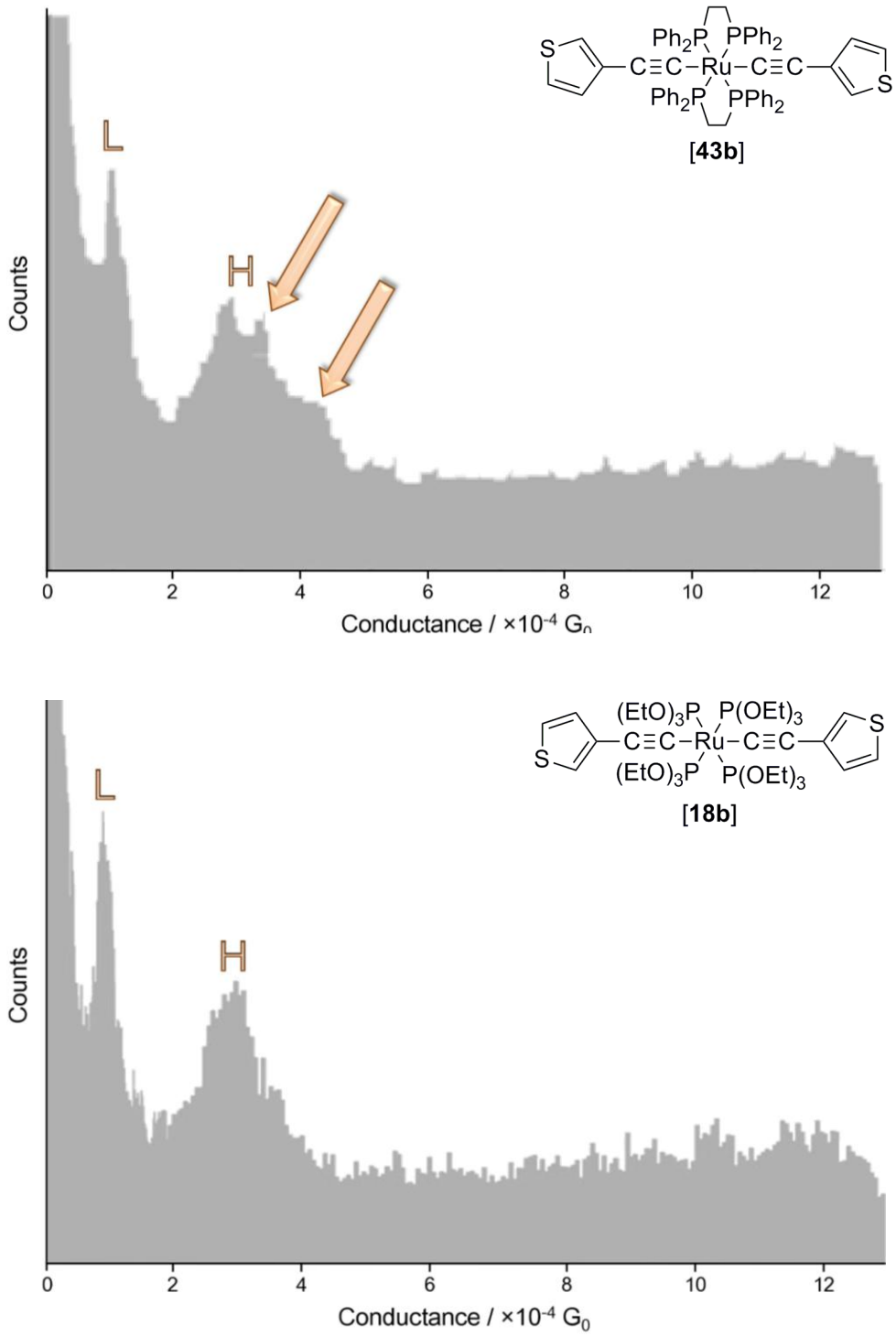

Figure 5.24: Conductance histograms obtained by the I(s) method, of [**43b**] (top), showing additional features in the broad H peak (as indicated by the arrows), and [**18b**] (bottom), exhibiting a narrower H peak, where L and H refer to low and high conductance values, respectively.

The histogram of [**18b**] (bottom, Figure 5.24) displays a narrower H peak, evincing the formation of a narrower distribution of Au|molecule|Au junctions compared with [**43b**] (top, Figure 5.24). As both [**18b**] and [**43b**] contain identical thienyl binding groups, disparities between the appearance of the H profiles are unlikely to be a result of different molecule-gold molecular binding modes.[29] Instead, differences are more likely attributable to ancillary ligand selection, where additional conduction pathways (Figure 5.4) are circumvented in [**18b**] with the omission of phenyl substituents. The conductance values of [**43b**] and [**18b**] are similar (Table 5.8).

Table 5.8: Conductance values (10^{-4} G_0) for [**43b**] and [**18b**], recorded using the I(s) method where L and H refer to low and high conductance values respectively.

Complex	**L**	**H**
[**43b**]	0.80 ± 0.12	3.21 ± 1.04
[**18b**]	0.98 ± 0.14	3.06 ± 0.49

At present, work in our group is underway to further confirm that phenyl moieties (in particular comprising the {Ru(dppe)$_2$} motif) can form sufficient contacts with Au. For this purpose, complexes *trans*-[Ru(C≡CC_4H_9)$_2$(dppe)$_2$] and *trans*-[Ru(C≡CC_6H_5)$_2$(dppe)$_2$], [**13**], without conventional binding groups, have been synthesised (see experimental section). The resulting conductance plots can then be compared with those of analogous complexes, *trans*-[Ru(C≡CC_4H_9)$_2${P(OEt)$_3$}$_4$], [**18a**], and *trans*-[Ru(C≡CC_6H_5)$_2${P(OEt)$_3$}$_4$], [**18c**].

At present there is considerable interest in the preparation and study of 'insulated' molecular wires. This has been achieved through inclusion of 'wire-like' fragments within the cavity of cyclodextrins[59-61] through the formation of rotaxane-based structures,[61-63] and the use of α,ω-*bis*-phosphinoalkanes to wrap around an extended polyyne chain.[64] This work contributes an additional design feature for 'insulated' single molecule 'wires' in which auxiliary ligands placed at the equatorial position of metal fragments decorated along the 'wire-like' chain serve to prevent additional conductive contacts (short-circuits) whilst still permitting the useful electronic features of the metal fragment to be realised.

5.7. Conclusions

In the presence of a simple halide abstracting agent, KPF_6, in a basic polar reaction medium, NH^iPr_2 in EtOH, conversion of *trans*-[$RuCl_2${$P(OEt_3)_4$}] ([**19**]) to *trans*-bis(alkynyl) complexes, *trans*-[$Ru(C{\equiv}CR)_2${$P(OEt)_3$}$_4$] ([**18**]) can be achieved in moderate to high yields and in high purity. The first electrochemical studies of these complexes bearing the *tetrakis*-triethylphosphite motif, reveal a single (one-electron) reversible oxidation event.

Through spectroelectrochemical studies, the redox event is found to have appreciable (alkynyl) ligand character, generating fully delocalised ([$RC{\equiv}C\text{-}Ru\text{-}C{\equiv}CR]^+$) complexes on the IR timescale. Valence descriptions of *mono*-oxidised *bis*-aryl ethynyl complexes *trans*-[$Ru(C{\equiv}CC_6H_4\text{-}4\text{-}R')_2${$P(OEt)_3$}$_4]^+$ follow the electronic nature of the R substituent, with the cation radical located more on the molecular termini with 'charge-stabilising' electron donating substituents. These 'mixed-valence' complexes, *trans*-[$Ru(C{\equiv}CC_6H_4\text{-}4\text{-}R')_2${$P(OEt)_3$}$_4]^+$, generally exhibit one principal NIR (IVCT) band and several higher energy (MLCT / IL) bands in the UV-Vis-NIR spectra. Complexes bearing electron donating R′ groups exhibit intense, asymmetric principal bands therefore are described as strongly coupled Class II (or Class III) complexes. In contrast, complexes with electron withdrawing R′ fragments display broader, less intense principal bands, and are therefore instead described as weakly-coupled Class II systems.

Between the various *trans*-[$Ru(C{\equiv}CC_6H_4\text{-}4\text{-}R')_2${$P(OEt)_3$}$_4$] complexes reported here and the more widely studied *trans*-[$Ru(C{\equiv}CC_6H_4\text{-}4\text{-}R')_2(dppe)_2$] complexes, the higher symmetry (*pseudo* D_{4h}) *trans*-[$Ru(C{\equiv}CC_6H_4\text{-}4\text{-}R')_2${$P(OEt)_3$}$_4]^+$ complexes display fewer vibrational and optical bands as a result of less symmetrically distinct rotamer conformations, advantageously reducing the complexity of data interpretations. Furthermore, preliminary single molecule conductance measurements of *trans*-[$Ru(C{\equiv}C\text{-}3\text{-}th)_2${$P(OEt)_3$}$_4$] ([**18b**]) and *trans*-[$Ru(C{\equiv}C\text{-}3\text{-}th)_2(dppe)_2$] ([**43b**]) revealed that the {$Ru(dppe)_2$} derivative with a much broader conductance profile is contacting through the aromatic rings comprising the dppe ancillary ligands, evincing

the advantage of *trans*-bis(alkynyl) complexes bearing a non-aromatic 'insulating sheath'.

Conclusively, redesign of model complexes tailored for molecular electronics applications towards higher symmetry complexes bearing non-aromatic ancillary ligands, such as the *trans*-bis(alkynyl) *tetrakis*-triethylphosphite complexes studied in this Chapter, is strongly advantageous for the generation of 'simpler' band profiles allowing rapid data interpretation and to favour the formation of the ideal linear junction arrays.

5.8. Experimental section

5.8.1. General considerations

All reactions were carried out under a dry, high-purity, nitrogen environment using oven-dried (119 °C) glassware and standard Schlenk techniques, although no special precautions were taken in order to exclude air or moisture during work-up. The reaction solvent EtOH was dried over dry magnesium turnings and iodine, whilst NH^iPr_2 was dried over KOH and CH_2Cl_2 was dried over CaH_2. All other solvents were reagent grade and used without further purification. The compounds: $HC{\equiv}CC_6H_4$-4-NO_2,[65] HC≡C-3-*th*,[66,67] $HC{\equiv}CC_6H_4$-4-C≡N,[68] $HC{\equiv}CC_6H_4$-4-COOMe;[65] $HC{\equiv}CC_6H_4$-4-C≡$CSiMe_3$,[29] $TlBF_4$,[69] *trans*-$[RuCl_2\{P(OEt)_3\}_4]$ ([**19**])[42] and $[RuCl(dppe)_2]OTf$ ([**36**]OTf)[43] were synthesised by literature methods. All other reagents were commercially available and used as received.

Safety spectacles and gloves were worn at all times, and all experiments conducted in an efficient fume hood, following completion of appropriate COSHH assessments. Relatively non-toxic solvents were disposed of in the appropriate waste solvent container (chlorinated / non-chlorinated). Given the extremely toxicity of $TlBF_4$, the reagent was separately weighed in a sealed container in a fume hood. The solid was transferred to the reaction flask using a disposable paper funnel. The paper funnel was discarded immediately after use into a thallium-containing solid waste receptacle. For larger scale reactions, a secondary containment flask was utilised during the reaction

period. Reactions reported below involving $TlBF_4$, (generally) produce equimolar amounts of TlCl, which is similarly extremely toxic. After completion of the reaction, following isolation of TlCl / residual $TlBF_4$ by the work-up procedures reported, the salts were either disposed of by i) dissolving in HNO_3 (aq.) and transferring into a thallium-containing solvent waste container or ii) in a thallium-containing solid waste container (along with the chromatographic medium, celite *etc.*).

NMR spectra were recorded at 25 °C on Varian Inova 300 (^{1}H, 300.2 MHz; ^{31}P, 121.5 MHz) or Bruker Avance 600 (^{1}H, 600.1 MHz; ^{13}C, 150.9 MHz; ^{31}P, 242.9 MHz) spectrometers. Chemical shifts were determined relative to internal residual solvent signals ($CDCl_3$: ^{1}H, δ = 7.26 ppm; ^{13}C, δ = 77.2 ppm) or external 85% H_3PO_4 (^{31}P, δ = 0.0 ppm).[70] FT-IR spectra were measured on a Nicolet Avatar 6700 or an Agilent Technologies Cary 660 spectrophotometer from solutions in CH_2Cl_2 in a thin-layer cell fitted with CaF_2 windows. ESI-MS and APCI-MS were recorded on a Waters LCT Premier XE mass spectrometer in positive ion mode from solutions in methanol. Cyclic voltammetry was carried out using a Versastat 3 potentiostat with a platinum disc working electrode, a platinum wire counter electrode, and a platinum wire *pseudo*-reference electrode, from solutions in CH_2Cl_2 containing 0.1 M $[N^nBu_4]PF_6$ as the electrolyte. Potentials are reported *vs.* the ferrocene / ferrocenium couple ($[Fe(\eta^5\text{-}C_5H_5)_2]$ / $[Fe(\eta^5\text{-}C_5H_5)_2]^+$ = 0 V) using a decamethylferrocene / decamethylferrocenium internal standard ($[Fe(\eta^5\text{-}C_5Me_5)_2]$ / $[Fe(\eta^5\text{-}C_5Me_5)_2]^+$ = − 0.48 V).[49] Spectroelectrochemical measurements were made in an OTTLE cell of Hartl design,[71] from CH_2Cl_2 solutions containing 0.1 M $[N^nBu_4]PF_6$ as the electrolyte. The cell was fitted into the sample compartment of an Agilent Technologies Cary 660 FT-IR, Agilent Technologies Cary-5000 UV-Vis-NIR or an Avantes diode array UV-Vis-NIR system comprising two light sources (UV-Vis: AvaLight-DH-S-Bal, Vis-NIR: AvaLight-Hal-S) and two spectrometers (UV-Vis: AvaSpec-ULS204-8L-USB2, NIR: AvaSpec-NIR256-2.5TEC) connected to a custom-built sample holder by bifurcated fibre optic cables. The Vis-NIR light source was attenuated with a band-pass filter transparent between 900 – 4700 nm. Electrolysis in the cell was performed with a Palm Instruments EmStat 2 or EmStat 3 potentiostat.

5.8.2. Syntheses and characterisations of {Ru{P(OEt)$_3$}$_4$} complexes

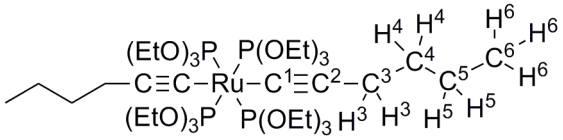

*Synthesis of trans-[Ru(C≡CC$_4$H$_9$)$_2${P(OEt)$_3$}$_4$], [**18a**]*

A mixture of [**19**] (0.21 g, 0.25 mmol), KPF_6 (0.25 g, 1.3 mmol) and $HC{\equiv}CC_4H_9$ (0.18 ml, 1.6 mmol) in EtOH (5 ml) and NH^iPr_2 (2.5 ml) was stirred under N_2 for 15 days (or until all *mono*-alkynyl was converted to the *trans*-bis(alkynyl) complex in solution, monitored by unlocked $^{31}P\{^1H\}$ NMR spectroscopy). The solution colour changed from yellow to orange / brown over the reaction period and a white solid precipitated. The reaction solvents were removed under high vacuum, yielding a brown oily residue. A minimum amount of MeOH (~ 3 ml) was added to the residue and solution stirred until a white solid separated out (~ 5 minutes). The solution was left in an ice bath for ~ 20 minutes, to complete precipitation, before filtering. The collected white solid was washed with minimum cold MeOH (3 × 8 ml) and vacuum dried (0.10 g, 45 %).

IR (CH_2Cl_2, cm^{-1}): 2098 ν(RuC≡C). ^1H NMR ($CDCl_3$, 300 MHz) δ / ppm: 0.83 (t, J = 7 Hz, 6H, H^6), 1.19 (t, J = 7 Hz, 36H, C*H*$_3$, P(OEt)$_3$), 1.26 (quin., J = 7 Hz, 4H, H^4), 1.36 (sex., J = 7 Hz, 4H, H^5), 2.10 (t, J = 7 Hz, 4H, H^3), 4.27 (quar., J = 7 Hz, 24H, C*H*$_2$, P(OEt)$_3$). $^{31}P\{^1H\}$ NMR ($CDCl_3$, 300 MHz) δ / ppm: 139.5 (s, Ru{P(OEt)$_3$}$_4$). $^{13}C\{^1H\}$ NMR ($CDCl_3$, 600 MHz) δ / ppm: 14.2 (s, C^6), 16.5 (s, *C*H$_3$, P(OEt)$_3$), 22.3 (s, C^5), 22.4 (s, C^3), 33.4 (s, C^4), 60.8 (s, *C*H$_2$, P(OEt)$_3$), 89.9 (quin., J = 20 Hz, C^1), 109.3 (s, C^2). ESI(+)-MS (*m/z*): 929 [Ru(C≡CC$_4$H$_9$)$_2${P(OEt)$_3$}$_4$ + H]$^+$, 888 [Ru(C≡CC$_4$H$_9$){P(OEt)$_3$}$_4$ + MeCN]$^+$, 879 [Ru(C≡CC$_4$H$_9$){P(OEt)$_3$}$_4$ + MeOH]$^+$, 847 [Ru(C≡CC$_4$H$_9$){P(OEt)$_3$}$_4$]$^+$.

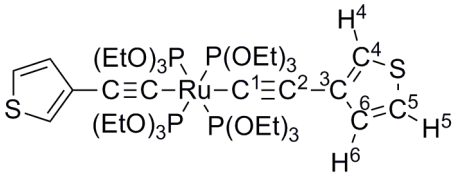

*Synthesis of trans-[Ru(C≡C-3-th)$_2${P(OEt)$_3$}$_4$], [**18b**]*

A mixture of [**19**] (0.19 g, 0.23 mmol), KPF_6 (0.14 g, 0.77 mmol) and 3-ethynylthiophene (0.4 ml, excess) in EtOH (4 ml) and NH^iPr_2 (1.5 ml) were stirred under N_2 for 12 days (or until all *mono*-alkynyl converted to the *trans*-bis(alkynyl) complex in solution, monitored by *in situ* unlocked $^{31}P\{^1H\}$ NMR spectroscopy). The solution colour changed from yellow to brown over the reaction period and a white solid precipitated. The reaction was filtered to remove reaction salts and filtrate concentrated to dryness, yielding a brown oily residue. A minimum amount of MeOH (3 ml) was added to the oily substance and solution left in the fridge for ~ two hours to aid precipitation of an off-white solid. The solid was collected by filtration, washed with cold MeOH (3 × 10 ml) and air dried (0.099 g, 45 %). The precipitate may be further purified by recrystallisation from a CH_2Cl_2 / EtOH layer diffusion, yielding large pale brown crystals suitable for X-ray crystallography.

IR (CH_2Cl_2, cm^{-1}): 2088 ν(RuC≡C), 2072 ν(RuC≡C). ^1H NMR ($CDCl_3$, 600 MHz) δ / ppm: 1.21 (t, J = 7 Hz, 36H, C*H*$_3$, P(OEt)$_3$), 4.31 (quar., J = 7 Hz, 24H, C*H*$_2$, P(OEt)$_3$), 6.64 (d, J = 2 Hz, 2H, H^4), 6.76 (d, J = 4 Hz, 2H, H^6), 7.05 (dd, J = 4, 2 Hz, 2H, H^5). $^{31}P\{^1H\}$ NMR ($CDCl_3$, 600 MHz) δ / ppm: 137.0 (s, Ru{P(OEt)$_3$}$_4$). $^{13}C\{^1H\}$ NMR ($CDCl_3$, 600 MHz) δ / ppm: 16.6 (s, *C*H$_3$, P(OEt)$_3$), 61.0 (s, *C*H$_2$, P(OEt)$_3$), 107.4 (s, C^2), 113.5 (quin., J = 20 Hz, C^1), 119.4 (s, C^4), 122.9 (s, C^5), 130.2 (s, C^6), 130.8 (s, C^3). ESI(+)-MS (*m/z*): 980 [Ru(C≡C-3-*th*)$_2${P(OEt)$_3$}$_4$]$^+$, 873 [Ru(C≡C-3-*th*){P(OEt)$_3$}$_4$]$^+$. Anal. Found: C, 43.98; H, 6.73. Calc for $C_{36}H_{66}O_{12}P_4RuS_2$: C, 44.07; H, 6.79 %.

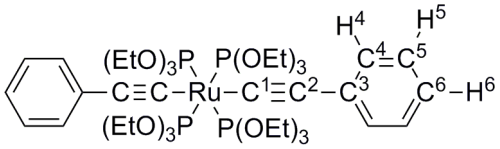

*Synthesis of trans-[Ru(C≡CC_6H_5)$_2${P(OEt)$_3$}$_4$], [**18c**]*

A mixture of [**19**] (0.15 g, 0.18 mmol), KPF_6 (0.13 g, 0.73 mmol) and HC≡CC_6H_5 (0.2 ml, excess) in EtOH (5 ml) and NH^iPr_2 (2 ml) was stirred under N_2 for 11 days (or until all *mono*-alkynyl converted to the *trans*-bis(alkynyl) complex in solution, monitored by *in situ* unlocked $^{31}P\{^1H\}$ NMR spectroscopy). The solution colour changed from yellow to orange over the reaction period and a white solid precipitated. The reaction solvents were removed under high vacuum, yielding an orange / brown residue. The residue was extracted with minimum CH_2Cl_2, filtered through celite to remove reaction salts and concentrated to dryness by rotary evaporation, yielding an orange / brown residue. A minimum amount of MeOH (3 ml) was added to the residue and solution left in the fridge for ~ two hours to aid precipitation of a white solid. The solid was collected by filtration, washed with cold MeOH (3 × 10 ml) and air dried (0.15 g, 85 %). The precipitate may be further purified by recrystallisation from CH_2Cl_2 / MeOH layer diffusion, yielding large white crystals suitable for X-ray crystallography.

IR (CH_2Cl_2, cm^{-1}): 2076 ν(RuC≡C). ^1H NMR ($CDCl_3$, 600 MHz) δ / ppm: 1.21 (t, J = 7 Hz, 36H, C*H*$_3$, P(OEt)$_3$), 4.31 (quar., J = 7 Hz, 24H, C*H*$_2$, P(OEt)$_3$), 6.94 (t, J = 7 Hz, 2H, H^6), 7.03 (d, J = 8 Hz, 4H, H^4), 7.11 (t, J = 7 Hz, 4H, H^5). $^{31}P\{^1H\}$ NMR ($CDCl_3$, 300 MHz) δ / ppm: 138.2 (s, Ru{P(OEt)$_3$}$_4$). $^{13}C\{^1H\}$ NMR ($CDCl_3$, 600 MHz) δ / ppm: 16.6 (s, *C*H$_3$, P(OEt)$_3$), 61.0 (s, *C*H$_2$, P(OEt)$_3$), 113.8 (s, C^2), 116.7 (quin., J = 20 Hz, C^1), 122.5 (s, C^6), 130.1 (s, C^4), 131.5 (s, C^3). ESI(+)-MS (*m/z*): 969 [Ru(C≡CC_6H_5)$_2${P(OEt)$_3$}$_4$]$^+$, 867 [Ru(C≡CC_6H_5){P(OEt)$_3$}$_4$]$^+$. Anal. Found: C, 49.37; H, 7.16. Calc for $C_{40}H_{70}O_{12}P_4Ru$: C, 49.57; H, 7.29 %.

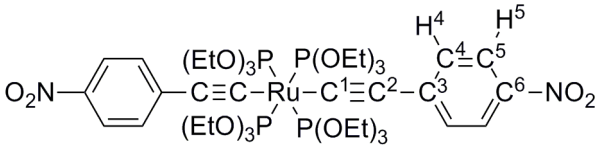

*Synthesis of trans-[Ru(C≡CC$_6$H$_4$-4-NO$_2$)$_2${P(OEt)$_3$}$_4$], **[18d]***

A mixture of [**19**] (0.10 g, 0.12 mmol), KPF_6 (0.086 g, 0.47 mmol) and HC≡CC$_6$H$_4$-4-NO$_2$ (0.044 g, 0.30 mmol) in EtOH (5 ml) and NH^{i}Pr$_2$ (2 ml) was stirred under N_2 for 24 days. The solution colour changed from orange to brown over the reaction period and a white solid precipitated. The reaction solvents were removed under high vacuum, yielding a dark red oily residue, which was purified by column chromatography (silica, 90 : 10, hexanes : acetone). The first bright red / orange band was collected and solvent removed to yield the product as a bright red precipitate (0.075 g, 59 %). Crystals suitable for single crystal X-ray crystallography were obtained by slow evaporation from CH_2Cl_2 at reduced temperature (− 18 °C).

IR (CH_2Cl_2, cm^{-1}): 2054 ν(RuC≡C), 1584 ν(N=O), 1324 ν(N-O). ^{1}H NMR ($CDCl_3$, 600 MHz) δ / ppm: 1.21 (t, J = 7 Hz, 36H, C*H*$_3$, P(OEt)$_3$), 4.25 (quar., J = 7 Hz, 24H, C*H*$_2$, P(OEt)$_3$), 7.03 (apparent doublet, splitting = 9 Hz, 4H, H^4), 8.02 (apparent doublet, splitting = 9 Hz, 4H, H^5). ^{31}P{^{1}H} NMR ($CDCl_3$, 600 MHz) δ / ppm: 136.2 (s, Ru{P(OEt)$_3$}$_4$). ^{13}C{^{1}H} NMR ($CDCl_3$, 600 MHz) δ / ppm: 16.5 (s, *C*H$_3$, P(OEt)$_3$), 61.1 (s, *C*H$_2$, P(OEt)$_3$), 102.2 (quin., J = 21 Hz, C^1), 116.9 (s, C^2), 124.0 (s, C^5), 129.9 (s, C^4), 137.9 (s, C^3), 142.8 (s, C^6). ESI(+)-MS (*m/z*): 1058 [Ru(C≡CC$_6$H$_4$-4-NO$_2$)$_2${P(OEt)$_3$}$_4$]$^+$, 953 [Ru(C≡CC$_6$H$_4$-4-NO$_2$){P(OEt)$_3$}$_4$ + MeCN]$^+$, 912 [Ru(C≡CC$_6$H$_4$-4-NO$_2$){P(OEt)$_3$}$_4$]$^+$. Anal. Found: C, 45.46; H, 6.50; N, 2.67. Calc. for $C_{40}H_{68}N_2O_{16}P_4Ru$: C, 45.36; H, 6.48; N, 2.65 %.

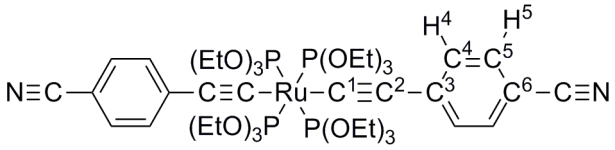

*Synthesis of trans-[Ru(C≡CC$_6$H$_4$-4-C≡N)$_2${P(OEt)$_3$}$_4$], **[18e]***

A mixture of [**19**] (0.21 g, 0.25 mmol), KPF_6 (0.11 g, 0.59 mmol) and HC≡CC$_6$H$_4$-4-C≡N (0.076 g, 0.60 mmol) in EtOH (4 ml) and NH^{i}Pr$_2$ (2 ml) was stirred under N_2 for four weeks. The solution colour changed from yellow to orange / brown

over the reaction period and a white solid precipitated. The reaction solvents were removed under high vacuum, yielding a brown oily residue. The residue was extracted with minimum CH_2Cl_2, filtered through a cotton wool plug to remove reaction salts and concentrated to dryness by rotary evaporation, yielding an orange / brown oily residue. A minimum amount of MeOH (~ 3 ml) was added to the residue and solution left in the fridge for 24 hours to aid precipitation of an orange solid. The orange solid was collected by filtration, washed with minimum cold MeOH (3 × 3 ml) and air dried (0.040 g, 19 %). The precipitate may be further purified by recrystallisation from a $CHCl_3$ / MeOH layer diffusion, yielding yellow needles suitable for X-ray crystallography.

IR (CH_2Cl_2, cm^{-1}): 2234 ν(C≡N), 2219 ν(C≡N), 2065 ν(RuC≡C), 1606 ν(C=C), 1591 ν(C=C). ^{1}H NMR ($CDCl_3$, 300 MHz) δ / ppm: 1.19 (t, J = 7 Hz, 36H, C*H*$_3$, P(OEt)$_3$), 4.25 (quar., J = 7 Hz, 24H, C*H*$_2$, P(OEt)$_3$), 7.01 (apparent doublet, splitting = 8 Hz, 4H, H^4), 7.37 (apparent doublet, splitting = 8 Hz, 4H, H^5). ^{31}P{^{1}H} NMR ($CDCl_3$, 300 MHz) δ / ppm: 136.8 (s, Ru{P(OEt)$_3$}$_4$). ^{13}C{^{1}H} NMR ($CDCl_3$, 600 MHz) δ / ppm: 16.5 (s, *C*H$_3$, P(OEt)$_3$), 61.1 (s, *C*H$_2$, P(OEt)$_3$), 104.9 (s, C^2), 115.1 (s, C^3), 120.4 (s, CN), 130.2 (s, C^4), 131.6 (quin., J = 20 Hz, C^1), 131.9 (s, C^5), 135.5 (s, C^6). ESI(+)-MS (*m/z*): 1019 [Ru(C≡CC$_6$H$_4$-4-C≡N)$_2${P(OEt)$_3$}$_4$ + H]$^+$.

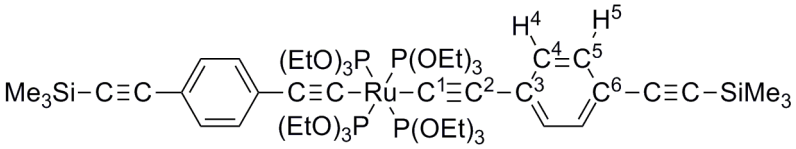

*Synthesis of trans-[Ru(C≡CC$_6$H$_4$-4-C≡CSiMe$_3$)$_2${P(OEt)$_3$}$_4$], **[18f]***

A mixture of [**19**] (0.12 g, 0.15 mmol), KPF_6 (0.12 g, 0.65 mmol) and HC≡CC$_6$H$_4$-4-C≡CSiMe$_3$ (0.089 g, 0.45 mmol) in EtOH (4 ml) and NH^{i}Pr$_2$ (1.5 ml) was stirred under N_2 for 17 days (or until all *mono*-alkynyl converted to the *trans*-bis(alkynyl) complex in solution, monitored by *in situ* unlocked ^{31}P{^{1}H} NMR spectroscopy). The solution colour changed from yellow to orange over the reaction period and a white solid precipitated. The reaction solvents were removed under high vacuum, yielding a brown oily residue. The residue was extracted with minimum CH_2Cl_2, filtered through celite to remove reaction salts and concentrated to dryness by rotary evaporation, yielding a brown oily residue. The residue was re-extracted with

hexanes and filtered until extracts ran clear. The extracts were concentrated to dryness, yielding an orange solid. The orange solid was extracted a final time with minimum CH_2Cl_2 and filtered through a small alumina plug (basic, oven-dried). The first orange / yellow fraction was collected, concentrated to dryness yielding an orange solid, washed with minimum cold MeOH (3 × 3 ml) and air dried (0.072 g, 43 %). Crystals suitable for single crystal X-ray crystallography were grown from a $CHCl_3$ / MeOH layer diffusion at reduced temperature (− 18 °C).

IR (CH_2Cl_2, cm^{-1}): 2147 ν(C≡CSiMe$_3$), 2068 ν(RuC≡C). ^{1}H NMR ($CDCl_3$, 600 MHz) δ / ppm: 0.22 (s, 18H, $SiMe_3$), 1.18 (t, J = 7 Hz, 36H, C*H*$_3$, P(OEt)$_3$), 4.27 (quar., J = 7 Hz, 24H, C*H*$_2$, P(OEt)$_3$), 6.91 (apparent doublet, splitting = 8 Hz, 4H, H^4), 7.21 (apparent doublet, splitting = 8 Hz, 4H, H^5). ^{31}P{^{1}H} NMR ($CDCl_3$, 300 MHz) δ / ppm: 137.6 (s, Ru{P(OEt)$_3$}$_4$). ^{13}C{^{1}H} NMR ($CDCl_3$, 600 MHz) δ / ppm: 0.3 (s, $SiMe_3$), 16.6 (s, *C*H$_3$, P(OEt)$_3$), 61.0 (s, *C*H$_2$, P(OEt)$_3$), 93.5 (s, C^8), 106.5 (s, C^7), 114.8 (s, C^3), 116.4 (s, C^2), 123.3 (quin., J = 20 Hz, C^1), 129.8 (s, C^4), 131.7 (s, C^5). APCI(+)-MS (*m/z*): 1161 [Ru(C≡CC$_6$H$_4$-4-C≡CSiMe$_3$)$_2${P(OEt)$_3$}$_4$ + H]$^+$, 963 [Ru(C≡CC$_6$H$_4$-4-C≡CSiMe$_3$){P(OEt)$_3$}$_4$]$^+$. Anal. Found: C, 51.90; H, 7.46. Calc. for $C_{50}H_{86}O_{12}P_4RuSi_2$: C, 51.71; H, 7.47.

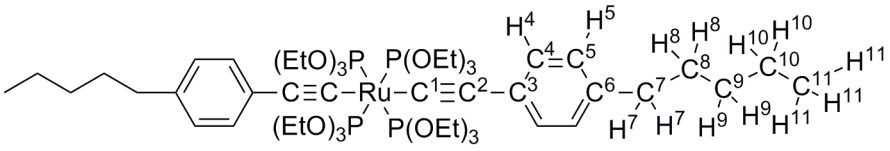

*Synthesis of trans-[Ru(C≡CC$_6$H$_4$-4-C$_5$H$_{11}$)$_2${P(OEt)$_3$}$_4$], [**18g**]*

A mixture of [**19**] (0.19 g, 0.22 mmol), KPF_6 (0.14 g, 0.75 mmol) and HC≡CC$_6$H$_4$-4-C$_5$H$_{11}$ (0.22 ml, 1.13 mmol) in EtOH (5 ml) and NH^{i}Pr$_2$ (2 ml) was stirred under N_2 for 17 days (or until all *mono*-alkynyl converted to the *trans*-bis(alkynyl) complex in solution, monitored by *in situ* unlocked ^{31}P{^{1}H} NMR spectroscopy). The solution colour changed from yellow to orange over the reaction period and a white solid precipitated. The reaction solvents were removed under high vacuum, yielding a brown residue. The residue was extracted with minimum CH_2Cl_2, filtered through celite to remove reaction salts and concentrated to dryness by rotary evaporation, yielding a brown residue. A minimum amount of EtOH (2.5 ml) was added to the residue and solution stirred in an ice bath until a yellow solid separated out

(~ 30 minutes). The solid was collected by filtration, washed with minimum cold EtOH (3 × 5 ml) and vacuum dried (0.083 g, 34 %). Large white crystals, suitable for X-ray crystallography, were grown from a $CDCl_3$ / EtOH layer diffusion.

IR (CH_2Cl_2, cm^{-1}): 2076 ν(RuC≡C), 1602 ν(C=C). ^1H NMR ($CDCl_3$, 600 MHz) δ / ppm: 0.89 (t, J = 7 Hz, 6H, H^{11}), 1.20 (t, J = 7 Hz, 36H, C*H*$_3$, P(OEt)$_3$), 1.29 − 1.37 (m, 8H, H^8 and H^{10}), 1.58 (quin., J = 7 Hz, 4H, H^9), 2.51 (t, J = 7 Hz, 4H, H^7), 4.32 (quar., J = 7 Hz, 24H, C*H*$_2$, P(OEt)$_3$), 6.92 (apparent doublet, splitting = 8 Hz, 4H, H^5), 6.94 (apparent doublet, splitting = 8 Hz, 4H, H^4). $^{31}P\{^1H\}$ NMR ($CDCl_3$, 300 MHz) δ / ppm: 138.4 (s, Ru{P(OEt)$_3$}$_4$). $^{13}C\{^1H\}$ NMR ($CDCl_3$, 600 MHz) δ / ppm: 14.2 (s, C^{11}), 16.6 (s, *C*H$_3$, P(OEt)$_3$), 23.0 (s, C^8 or C^{10}), 31.3 (s, C^9), 31.9 (s, C^8 or C^{10}), 35.9 (s, C^7), 61.0 (s, *C*H$_2$, P(OEt)$_3$), 113.5 (s, C^2), 114.2 (quin. J = 21 Hz, C^1) 127.8 (s, C^5), 128.9 (s, C^3), 129.9 (s, C^4), 136.9 (s, C^6). APCI(+)-MS (*m/z*): 1109 [Ru(C≡CC_6H_4-4-C_5H_{11})$_2${P(OEt)$_3$}$_4$ + H]$^+$, 937 [Ru(C≡CC_6H_4-4-C_5H_{11}){P(OEt)$_3$}$_4$]$^+$, 771 [Ru(C≡CC_6H_4-4-C_5H_{11}){P(OEt)$_3$}$_3$]$^+$, 605 [Ru(C≡CC_6H_4-4-C_5H_{11}){P(OEt)$_3$}$_2$ + H]$^+$. Anal. Found: C, 54.23; H, 8.09. Calc. for $C_{50}H_{90}O_{12}P_4Ru$: C, 54.13; H, 8.18 %.

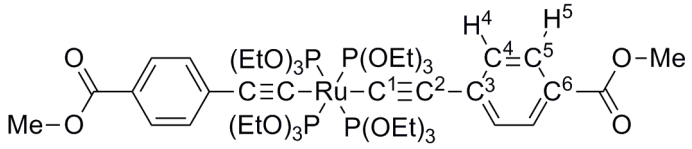

*Synthesis of trans-[Ru(C≡CC_6H_4-4-COOMe)$_2${P(OEt)$_3$}$_4$], [**18h**]*

A mixture of [**19**] (0.17 g, 0.20 mmol), KPF_6 (0.23 g, 1.2 mmol) and HC≡CC_6H_4-4-COOMe (0.21 g, 1.3 mmol) in EtOH (5 ml) and NH^iPr_2 (2 ml) was stirred under N_2 for 20 days (or until all *mono*-alkynyl was converted to the *trans*-bis(alkynyl) complex in solution, monitored by *in situ* unlocked $^{31}P\{^1H\}$ NMR spectroscopy). The solution colour changed from yellow to orange / brown over the reaction period and a white solid precipitated. The reaction solvents were removed under high vacuum, yielding a brown oily residue. The residue was extracted with minimum CH_2Cl_2, filtered through celite to remove reaction salts and concentrated to dryness by rotary evaporation, yielding an orange / brown oily residue. A minimum amount of MeOH (2.5 ml) was added to the residue and solution left in an ice bath (~ 30 minutes) to aid precipitation of a yellow solid. The solid was collected by filtration, washed with minimum cold MeOH (3 × 10 ml) and air dried (0.12 g, 56 %).

Large, yellow, needle-like crystals, suitable for X-ray crystallography, were grown from a CH_2Cl_2 / MeOH layer diffusion.

IR (CH_2Cl_2, cm^{-1}): 2066 ν(RuC≡C), 1706 ν(C=O), 1594 ν(C=C). ^1H NMR ($CDCl_3$, 300 MHz) δ / ppm: 1.19 (t, J = 7 Hz, 36H, C*H*$_3$, P(OEt)$_3$), 3.86 (s, 6H, OC*H*$_3$), 4.28 (quar., J = 7 Hz, 24H, C*H*$_2$, P(OEt)$_3$), 7.02 (apparent doublet, splitting = 8 Hz, 4H, H^4), 7.80 (apparent doublet, splitting = 8 Hz, 4H, H^5). $^{31}P\{^1H\}$ NMR ($CDCl_3$, 300 MHz) δ / ppm: 137.3 (s, Ru{P(OEt)$_3$}$_4$). $^{13}C\{^1H\}$ NMR ($CDCl_3$, 600 MHz) δ / ppm: 16.5 (s, *C*H$_3$, P(OEt)$_3$), 51.9 (s, O*C*H$_3$), 61.1 (s, *C*H$_2$, P(OEt)$_3$), 115.4 (s, C^2), 123.7 (s, C^3), 127.9 (quin., J = 20 Hz, C^1), 129.4 (s, C^5), 130.0 (s, C^4), 136.0 (s, C^6), 167.7 (s, C=O). APCI(+)-MS (*m/z*): 1085 $[Ru(C{\equiv}CC_6H_4\text{-}4\text{-}COOMe)_2\{P(OEt)_3\}_4 + H]^+$, 925 $[Ru(C{\equiv}CC_6H_4\text{-}4\text{-}COOMe)\{P(OEt)_3\}_4]^+$. Anal. Found: C, 48.64; H, 6.86. Calc. for $C_{44}H_{74}O_{16}P_4Ru$: C, 48.70; H, 6.88 %.

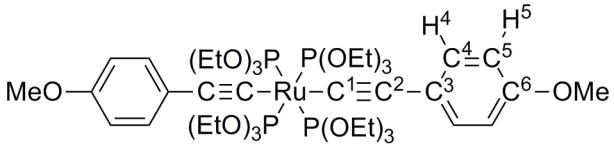

*Synthesis of trans-[Ru(C≡CC$_6$H$_4$-4-OMe)$_2${P(OEt)$_3$}$_4$], [**18i**]*

A mixture of [**19**] (0.11 g, 0.13 mmol), KPF_6 (0.087 g, 0.47 mmol) and HC≡CC$_6$H$_4$-4-OMe (0.3 ml, excess) in EtOH (5 ml) and NH^iPr_2 (2 ml) was stirred under N_2 for 14 days (or until all *mono*-alkynyl was converted to the *trans*-bis(alkynyl) complex in solution, monitored by *in situ* unlocked $^{31}P\{^1H\}$ NMR spectroscopy). The solution colour changed from yellow to orange over the reaction period and a white solid precipitated. The reaction solvents were removed under high vacuum, yielding a brown oily residue. The residue was extracted with minimum CH_2Cl_2, filtered through celite to remove reaction salts and concentrated to dryness by rotary evaporation, yielding a brown oily residue. A minimum amount of MeOH (3 ml) was added to the oily residue, solution stirred for ~ two minutes and left in the fridge for ~ one hour, where a white solid was formed. The solid was collected by filtration, washed with cold MeOH (3 × 10 ml) and air dried (0.095 g, 72 %). Crystals suitable for single crystal X-ray crystallography were grown *via* slow evaporation of a CH_2Cl_2 / hexanes solution.

IR (CH_2Cl_2, cm^{-1}): 2077 ν(RuC≡C), 1501 ν(C-O). ^1H NMR ($CDCl_3$, 600 MHz) δ / ppm: 1.20 (t, J = 7 Hz, 36H, C*H*$_3$, P(OEt)$_3$), 3.75 (s, 6H, OC*H*$_3$), 4.32 (quar., J = 7 Hz, 24H,

C*H*$_2$, P(OEt)$_3$), 6.68 (apparent doublet, splitting = 8 Hz, 4H, H^4), 6.96 (apparent doublet, splitting = 8 Hz, 4H, H^5). ^{31}P{^{1}H} NMR (CDCl$_3$, 300 MHz) δ / ppm: 138.4 (s, Ru{P(OEt)$_3$}$_4$). ^{13}C{^{1}H} NMR (CDCl$_3$, 600 MHz) δ / ppm: 16.6 (s, *C*H$_3$, P(OEt)$_3$), 55.3 (s, O*C*H$_3$), 61.0 (s, *C*H$_2$, P(OEt)$_3$), 112.1 (quin., J = 19 Hz, C^1), 112.5 (s, C^2), 113.4 (s, C^4), 124.6 (s, C^3), 130.8 (s, C^5), 155.5 (s, C^6). ESI(+)-MS (*m/z*): 1028 [Ru(C≡CC_6H_4-4-OMe)$_2${P(OEt)$_3$}$_4$]$^+$, 938 [Ru(C≡CC_6H_4-4-OMe){P(OEt)$_3$}$_4$ + MeCN]$^+$, 897 [Ru(C≡CC_6H_4-4-OMe){P(OEt)$_3$}$_4$]$^+$. Anal. Found: C, 48.94; H, 7.32. Calc. for $C_{42}H_{74}O_{14}P_4Ru$: C, 49.01; H, 7.25 %.

5.8.3. Syntheses and characterisations of {Ru(dppe)$_2$} complexes

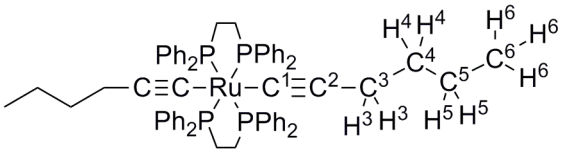

Synthesis of trans-[Ru(C≡CC_4H_9)$_2$(dppe)$_2$]

A mixture of [**36**]OTf (0.22 g, 0.20 mmol), HC≡CC_4H_9 (58 µL, 0.50 mmol) and DBU (~ 7 drops, excess) in CH_2Cl_2 (6 ml) was stirred under N_2 for 15 minutes. The solution colour changed from red / brown to yellow over the reaction period. To the mixture was then added $TlBF_4$ (0.034 g, 0.11 mmol), and solution stirred under N_2 overnight. Over this period, the solution colour remained the same but a white solid (TlCl) precipitated. The yellow solution was concentrated carefully under high vacuum to ~ 3 ml and filtered through alumina (basic, oven-dried) to remove TlCl and reaction salts. The yellow filtrate was concentrated to ~ 2 ml by rotary evaporation and excess MeOH added causing the instant precipitation of a bright yellow solid. The yellow solid was collected by filtration, washed with MeOH (3 × 10 ml) and hexanes (3 × 10 ml), then dried in air (0.14 g, 67 %). Crystals suitable for single crystal X-ray crystallography were grown from a $CDCl_3$ / MeOH layer diffusion at reduced temperature (− 18 °C).

IR (CH_2Cl_2, cm^{-1}): 2086s ν(RuC≡C). ^{1}H NMR ($CDCl_3$, 300 MHz) δ / ppm: 0.88 (t, J = 6 Hz, 6H, H^6), 1.15 – 1.38 (m, 8H, H^4 and H^5), 1.92 (t, J = 6 Hz, 4H, H^3), 2.38 − 2.71 (m, 8H, CH_2, dppe), 6.95 (t, J = 8 Hz, 16H, H$_m$, dppe), 7.15 (t, J = 8 Hz, 8H, H$_p$, dppe), 7.39 – 7.57 (m, 16H, H$_o$, dppe). ^{31}P{^{1}H} ($CDCl_3$, 300 MHz) δ / ppm: 56.0 (s, Ru(dppe)$_2$). ^{13}C{^{1}H} NMR ($CDCl_3$, 600 MHz) δ / ppm: 14.3 (s, C^6), 22.9 (s, C^5), 23.5

(s, C^3), 31.9 (t, J = 12 Hz, CH_2, dppe), 32.7 (s, C^4), 108.0 (quin., J = 15 Hz, C^1), 112.9 (s, C^2), 126.7 (s, C_m, dppm), 128.3 (s, C_p, dppm), 134.6 (s, C_o, dppm), 138.1 (quin., J = 10 Hz, C_i, dppm). ESI(+)-MS (*m/z*): 1061 $[Ru(C{\equiv}CC_4H_9)_2(dppe)_2 + H]^+$, 1060 $[Ru(C{\equiv}CC_4H_9)_2(dppe)_2]^+$, 899 $[Ru(dppe)_2 + H]^+$. Anal. Found: C, 68.98; H, 5.99. Calc. for $C_{64}H_{66}P_4Ru$: C, 72.43; H, 6.27.

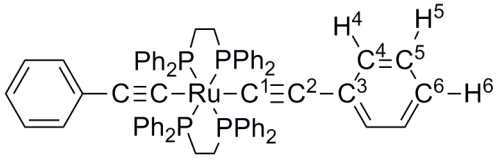

[**13**]

*Synthesis of trans-[Ru(C≡CC$_6$H$_5$)$_2$(dppe)$_2$], [**13**]*

A mixture of [**36**]OTf (0.20 g, 0.19 mmol), HC≡CC_6H_5 (47 µL, 0.43 mmol) and DBU (~ 6 drops, excess) in CH_2Cl_2 (7 ml) was stirred under N_2 for 15 minutes. The solution colour changed from red / brown to yellow over the reaction period. To the mixture was then added $TlBF_4$ (0.063 g, 0.22 mmol), and solution stirred under N_2 overnight. Over this period, the solution colour remained the same, but a white solid (TlCl) precipitated. The yellow solution was concentrated carefully under high vacuum to ~ 3 ml and filtered through alumina (basic, oven-dried) to remove TlCl and reaction salts. The yellow filtrate was concentrated to ~ 1 ml by rotary evaporation and excess diethyl ether added, resulting in the instantaneous precipitation of a bright yellow solid. The yellow solid was collected by filtration, washed with diethyl ether (3 × 10 ml) and hexanes (3 × 10 ml), then dried in air (0.15 g, 73 %).

IR (CH_2Cl_2, cm^{-1}): 2060 ν(RuC≡C). ^{1}H NMR ($CDCl_3$, 600 MHz) δ / ppm: 2.54 – 2.75 (m, 8H, CH_2, dppe), 6.78 (d, J = 8 Hz, 4H, H^4), 6.96 (t, J = 8 Hz, 16H, H_m, dppe), 7.01 (t, J = 8 Hz, 2H, H^6), 7.13 (t, J = 8 Hz, 4H, H^5), 7.17 (t, J = 8 Hz, 8H, H_p, dppe), 7.50 − 7.59 (m, 16H, H_o, dppe). $^{31}P\{^1H\}$ ($CDCl_3$, 600 MHz) δ / ppm: 53.9 (s, $Ru(dppe)_2$). $^{13}C\{^1H\}$ NMR ($CDCl_3$, 600 MHz) δ / ppm: 31.7 (t, J = 12 Hz, CH_2, dppe), 116.8 (s, C^2), 123.0 (s, C^6), 127.2 (s, C_m, dppe), 127.6 (s, C^5), 128.7 (s, C_p, dppe), 130.2 (s, C^4), 130.9 (s, C^3), 134.5 (s, C_o, dppe), 137.1 – 137.6 (m, C_i, dppe). ESI(+)-MS (*m/z*): 1101 $[Ru(C{\equiv}CC_6H_5)_2(dppe)_2 + H]^+$, 1100 $[Ru(C{\equiv}CC_6H_5)_2(dppe)_2]^+$. Anal. Found: C, 74.25; H, 5.34. Calc. for $C_{68}H_{58}P_4Ru$: C, 74.16; H, 5.31 %. *The experimental data reported here are in agreement with, and is an extension of, that published previously.*[6]

5.9. References

1. C.-Y. Wong, C.-M. Che, M. C. W. Chan, J. Han, K.-H. Leung, D. L. Phillips, K.-Y. Wong and N. Zhu, *J. Am. Chem. Soc.*, **2005**, *127*, 13997.
2. H.-M. Wen, Y. Yang, X.-S. Zhou, J.-Y. Liu, D.-B. Zhang, Z.-B. Chen, J.-Y. Wang, Z.-N. Chen and Z.-Q. Tian, *J. Chem. Sci.*, **2013**, *4*, 2471.
3. Y. Sun, N. J. Taylor and A. J. Carty, *Organometallics*, **1992**, *11*, 4293.
4. Y. Sun, N. J. Taylor and A. J. Carty, *J. Organomet. Chem.*, **1992**, *423*, C43.
5. D. Touchard, P. Haquette, N. Pirio, L. Toupet and P. H. Dixneuf, *Organometallics*, **1993**, *12*, 3132.
6. D. Touchard, P. Haquette, S. Guesmi, L. Le Pichon, A. Daridor, L. Toupet and P. H. Dixneuf, *Organometallics*, **1997**, *16*, 3640.
7. L. D. Field, A. V. George, G. R. Purches and A. H. White, *J. Chem. Soc., Dalton Trans.*, **1996**, 2011.
8. A. M. McDonagh, I. R. Whittall, M. G. Humphrey, B. W. Skelton and A. H. White, *J. Organomet. Chem.*, **1996**, *519*, 229.
9. J. B. G. Gluyas, A. J. Boden, S. G. Eaves, H. Yu and P. J. Low, *Dalton Trans.*, **2014**, *43*, 6291.
10. C. Lebreton, D. Touchard, L. Le Pichon, A. Daridor, L. Toupet and P. H. Dixneuf, *Inorg. Chim. Acta*, **1998**, *272*, 188.
11. C. A. Tolman, *Chem. Rev.*, **1977**, *77*, 313.
12. A. Colombo, F. Nisic, C. Dragonetti, D. Marinotto, I. P. Oliveri, S. Righetto, M. G. Lobello and F. De Angelis, *Chem. Commun.*, **2014**, *50*, 7986.
13. A. Barlow, B. Babgi, M. Samoc, T. C. Corkery, S. van Cleuvenbergen, I. Asselberghs, K. Clays, M. P. Cifuentes and M. G. Humphrey, *Aust. J. Chem.*, **2012**, *65*, 834.
14. A. M. McDonagh, I. R. Whittall, M. G. Humphrey, D. C. R. Hockless, B. W. Skelton and A. H. White, *J. Organomet. Chem.*, **1996**, *523*, 33.
15. C. E. Powell, M. P. Cifuentes, J. P. Morrall, R. Stranger, M. G. Humphrey, M. Samoc, B. Luther-Davies and G. A. Heath, *J. Am. Chem. Soc.*, **2002**, *125*, 602.
16. N. Gauthier, G. Argouarch, F. Paul, L. Toupet, A. Ladjarafi, K. Costuas, J.-F. Halet, M. Samoc, M. P. Cifuentes, T. C. Corkery and M. G. Humphrey, *Chem. Eur. J.*, **2011**, *17*, 5561.
17. A. Colombo, C. Dragonetti, D. Roberto, R. Ugo, L. Falciola, S. Luzzati and D. Kotowski, *Organometallics*, **2011**, *30*, 1279.
18. F. Nisic, A. Colombo, C. Dragonetti, E. Garoni, D. Marinotto, S. Righetto, F. De Angelis, M. G. Lobello, P. Salvatori, P. Biagini and F. Melchiorre, *Organometallics*, **2015**, *34*, 94.
19. S. De Sousa, L. Ducasse, B. Kauffmann, T. Toupance and C. Olivier, *Chem. Eur. J.*, **2014**, *20*, 7017.
20. R. Gatri, I. Ouerfelli, M. L. Efrit, F. Serein-Spirau, J. P. Lere-Porte, P. Valvin, T. Roisnel, S. Bivaud, H. Akdas-Kilig and J. L. Fillaut, *Organometallics*, **2014**, *33*, 665.
21. F. Chen, J. Hihath, Z. Huang, X. Li and N. J. Tao, *Annu. Rev. Phys. Chem.*, **2007**, *58*, 535.
22. K. Liu, X. Wang and F. Wang, *ACS Nano*, **2008**, *2*, 2315.
23. R. J. Nichols, W. Haiss, S. J. Higgins, E. Leary, S. Martín and D. Bethell, *Phys. Chem. Chem. Phys.*, **2010**, *12*, 2801.

24. L. A. Bumm, J. J. Arnold, T. D. Dunbar, D. L. Allara and P. S. Weiss, *J. Phys. Chem. A,* **1999**, *103*, 8122.
25. W. Haiss, C. S. Wang, I. Grace, A. S. Batsanov, D. J. Schiffrin, S. J. Higgins, M. R. Bryce, C. J. Lambert and R. J. Nichols, *Nat. Mater.*, **2006**, *5*, 995.
26. B. Xu and N. J. Tao, *Science*, **2003**, *301*, 1221.
27. W. Haiss, S. Martin, E. Leary, H. van Zalinge, S. J. Higgins, L. Bouffier and R. J. Nichols, *J. Phys. Chem. C*, **2009**, *113*, 5823.
28. C. Wang, A. S. Batsanov, M. R. Bryce, S. Martín, R. J. Nichols, S. J. Higgins, V. M. García-Suárez and C. J. Lambert, *J. Am. Chem. Soc.*, **2009**, *131*, 15647.
29. S. Marqués-González, D. S. Yufit, J. A. K. Howard, S. Martín, H. M. Osorio, V. M. García-Suárez, R. J. Nichols, S. J. Higgins, P. Cea and P. J. Low, *Dalton Trans.*, **2013**, *42*, 338.
30. S. Bock, *Personal Communication*, **2015**.
31. R. Parameswaran, J. R. Widawsky, H. Vázquez, Y. S. Park, B. M. Boardman, C. Nuckolls, M. L. Steigerwald, M. S. Hybertsen and L. Venkataraman, *J. Phys. Chem. Lett.*, **2010**, *1*, 2114.
32. M. Frei, S. V. Aradhya, M. S. Hybertsen and L. Venkataraman, *J. Am. Chem. Soc.*, **2012**, *134*, 4003.
33. L. D. Field, A. M. Magill and P. Jensen, *Organometallics*, **2008**, *27*, 6539.
34. L. D. Field, A. M. Magill, M. M. Bhadbhade and S. J. Dalgarno, *Organometallics*, **2009**, *28*, 5514.
35. L. D. Field, A. M. Magill, S. J. Dalgarno and P. Jensen, *Eur. J. Inorg. Chem.*, **2008**, 4248.
36. T. Rappert and A. Yamamoto, *Organometallics*, **1994**, *13*, 4984.
37. J. Gotzig, R. Werner and H. Werner, *J. Organomet. Chem.*, **1985**, *290*, 99.
38. S. J. Davies, B. F. G. Johnson, J. Lewis and P. R. Raithby, *J. Organomet. Chem.*, **1991**, *414*, C51.
39. G. Albertin, S. Autoniutti, E. Bordignon, F. Cazzaro, S. Ianelli and G. Pelizzi, *Organometallics*, **1995**, *14*, 4114.
40. G. Albertin, P. Amendola, S. Antoniutti, S. Ianelli, G. Pelizzi and E. Bordignon, *Organometallics*, **1991**, *10*, 2876.
41. G. Albertin, S. Antoniutti, E. Bordignon and M. Granzotto, *J. Organomet. Chem.*, **1999**, *585*, 83.
42. W. G. Peet, D. H. Gerlach and D. D. Titus, *Inorg. Synth.*, **2007**, *15*, 38.
43. M. A. Fox, J. E. Harris, S. Heider, V. Pérez-Gregorio, M. E. Zakrzewska, J. D. Farmer, D. S. Yufit, J. A. K. Howard and P. J. Low, *J. Organomet. Chem.*, **2009**, *694*, 2350.
44. S. J. Higgins, A. La Pensée, C. A. Stuart and J. M. Charnock, *J. Chem. Soc., Dalton Trans.*, **2001**, 902.
45. S. J. Higgins, C. A. Stuart and A. Mills, *Inorg. Chem. Commun.*, **2000**, *3*, 208.
46. E. Bustelo, M. Jiménez-Tenorio, K. Mereiter, M. C. Puerta and P. Valerga, *Organometallics*, **2002**, *21*, 1903.
47. A. G. Orpen and N. G. Connelly, *Organometallics*, **1990**, *9*, 1206.
48. S. Marqués-González, M. Parthey, D. S. Yufit, J. A. K. Howard, M. Kaupp and P. J. Low, *Organometallics*, **2014**, *33*, 4947.
49. N. G. Connelly and W. E. Geiger, *Chem. Rev.*, **1996**, *96*, 877.
50. P. A. Schauer and P. J. Low, *Eur. J. Inorg. Chem.*, **2012**, 390.
51. Y. B. Zhu, D. B. Millet, M. O. Wolf and S. J. Rettig, *Organometallics*, **1999**, *18*, 1930.
52. J. Nishijo, K. Judai, S. Numao and N. Nishi, *Inorg. Chem.*, **2009**, *48*, 9402.

53. N. Gauthier, N. Tchouar, F. Justaud, G. Argouarch, M. P. Cifuentes, L. Toupet, D. Touchard, J.-F. Halet, S. Rigaut, M. G. Humphrey, K. Costuas and F. Paul, *Organometallics*, **2009**, *28*, 2253.
54. W. Kaim, S. Ernst and V. Kasack, *J. Am. Chem. Soc.*, **1990**, *112*, 173.
55. M. B. Robin and P. Day, *Adv. Inorg. Chem. Radiochem.*, **1968**, *10*, 422.
56. B. S. Brunschwig, C. Creutz and N. Sutin, *Chem. Soc. Rev.*, **2002**, *31*, 168.
57. C. Creutz, *Prog. Inorg. Chem.*, **1983**, *30*, 1.
58. G. A. Koutsantonis, P. J. Low, C. F. R. Mackenzie, B. W. Skelton and D. S. Yufit, *Organometallics*, **2014**, *33*, 4911.
59. J. Terao, *Polym. Chem.*, **2011**, *2*, 2444.
60. M. Kiguchi, S. Nakashima, T. Tada, S. Watanabe, S. Tsuda, Y. Tsuji and J. Terao, *Small*, **2012**, *8*, 726.
61. F. Cacialli, J. S. Wilson, J. J. Michels, C. Daniel, C. Silva, R. H. Friend, N. Severin, P. Samori, J. P. Rabe, M. J. O'Connell, P. N. Taylor and H. L. Anderson, *Nat. Mater.*, **2002**, *1*, 160.
62. S. Anderson, R. T. Aplin, T. D. W. Claridge, T. Goodson, A. C. Maciel, G. Rumbles, J. F. Ryan and H. L. Anderson, *J. Chem. Soc., Perkin Trans. 1*, **1998**, 2383.
63. N. Weisbach, Z. Baranova, S. Gauthier, J. H. Reibenspies and J. A. Gladysz, *Chem. Commun.*, **2012**, *48*, 7562.
64. L. de Quadras, F. Hampel and J. A. Gladysz, *Dalton Trans.*, **2006**, 2929.
65. S. Takahashi, Y. Kuroyama, K. Sonogashira and N. Hagihara, *Synthesis-Stuttgart*, **1980**, 627.
66. D. Solooki, J. D. Bradshaw, C. A. Tessier and W. J. Youngs, *Organometallics*, **1994**, *13*, 451.
67. D. Solooki, V. O. Kennedy, C. A. Tessier and W. J. Youngs, *Synlett*, **1990**, 427.
68. S. Takahashi, Y. Kuroyama, K. Sonogashira and N. Hagihara, *Synthesis*, **1980**, 627.
69. F. J. Arnaiz, *J. Chem. Educ.*, **1997**, *74*, 1332.
70. H. E. Gottlieb, V. Kotlyar and A. Nudelman, *J. Org. Chem.*, **1997**, *62*, 7512.
71. M. Krejčik, M. Daněk and F. Hartl, *J. Electroanal. Chem. Interfac. Electrochem.*, **1991**, *317*, 179.

CONCLUSIONS

This Thesis has explored several series of *trans*-bis(alkynyl), 'wire-like', ruthenium complexes, *trans*-[Ru(C≡CR)$_2$(L)$_4$], and related oligomeric systems as models through which to understand the effects that varying i) the nature of the ancillary ligands (L), ii) the *pseudo*-symmetry at the metal centre and iii) the number of metal centres along the 'wire-like' molecular backbone have on the underlying electronic structures and hence spectroscopic and charge transfer properties. Within this work a novel design strategy for the 'insulating sheath' component of molecules tailored for applications within the area of molecular electronics has been identified.

Reactions of *cis*-[RuCl$_2$(dppm)$_2$] with terminal alkynes, HC≡CC$_6$H$_4$-4-R, bearing electron withdrawing R groups in the presence of the halide abstracting agent TlBF$_4$ and base cleanly afforded *trans*-bis(alkynyl) complexes, *trans*-[Ru(C≡CC$_6$H$_4$-4-R)$_2$(dppm)$_2$]. In contrast, analogous reactions with alkynes bearing electron donating R groups were intercepted with the formation of cationic η^3-butenynyl complexes, *E*-[Ru(η^3-{HC(C$_6$H$_4$-4-R)=CC≡C(C$_6$H$_4$-4-R)})(dppm)$_2$]$^+$. Such transformations of alkynes at the {Ru(dppm)$_2$} centre are thought to arise as a result of the strained phosphine bite angle (especially when compared with {Ru(dppe)$_2$} systems, where analogous reactions were not observed). These synthetic difficulties are likely to have contributed to the declining prevalence of *trans*-[Ru(C≡CC$_6$H$_4$-4-R)$_2$(dppm)$_2$] (*vs.* *trans*-[Ru(C≡CC$_6$H$_4$-4-R)$_2$(dppe)$_2$]) complexes within the literature. Furthermore, reactions of *cis*-[RuCl$_2$(dppm)$_2$] with di-alkynes, HC≡CC$_6$H$_2$-2,5-X$_2$-4-C≡CH, and nucleophillic chloride ([N^{n}Bu$_4$]Cl) generated the Markovnikov addition product, *trans*-[RuCl(C≡CC$_6$H$_2$-2,5-R$_2$-4-CCl=CH$_2$)(dppm)$_2$], inferring the presence of a quinoidal cumulene intermediate.

The importance of molecular *pseudo*-symmetry, which is in turn governed by the ancillary ligands, on spectral profiles has been highlighted following synthetic and spectroscopic investigation of multi-metallic, *trans*-alkynyl {Ru(dppe)$_2$} complexes bridged by 1,4-diethynylbenzenes. Complexes derived from the {Ru(dppe)$_2$} motif

bearing *bis*-aryl ethynyl fragments and the two chelating phosphine ligands, exhibit a number of thermally accessible conformers, which are spectroscopically distinct. As a result, the spectra of both neutral and oxidised complexes are complicated, making superficial interpretations of the data difficult. Increasing the steric bulk of the bridging aryl ethynyl fragment between metal centres, therefore hindering rotation of the linker, resulted in cleaner band shapes in the resultant spectra as a consequence of fewer accessible rotamer conformations. Through careful consideration of the spectra of these multi-metallic systems with those from model *mono*- and *bi*-nuclear fragments, an interpretation of the spectroscopic profiles in terms of localisation of the charge at various 'redox sinks' along the backbone and intramolecular redox isomers can be offered. The aromatic fragments comprising the {$Ru(dppe)_2$} motif were also shown to contact to gold surfaces, establishing additional undesirable conductance pathways for *trans*-[$Ru(C{\equiv}CR)_2(dppe)_2$] complexes, resulting in broader conductance profiles.

As superior model molecular wires, higher symmetry (*pseudo* D_{4h}) *trans*-[$Ru(C{\equiv}CR)_2\{P(OEt)_3\}_4$] complexes, bearing non-aromatic ancillary ligands, were synthesised. The lower number of spectroscopically distinct rotamer conformations, *vs.* chelating *bis*-phosphines (*pseudo* D_{2h}), translated to cleaner spectral profiles allowing for more facile data interpretations, whilst the non-aromatic triethylphosphite groups allowed formation of predominantly linear Au|molecule|Au junctions, noted by the sharper conductance histograms obtained. Given their relatively low first oxidation potentials, *trans*-[$Ru(C{\equiv}CR)_2\{P(OEt)_3\}_4$] complexes also present as superior (by way of power efficiency) redox switches and perhaps transistors, adding another dimension to their already brimming capacity.

In summary, the design of molecules as electrical components should look towards using higher symmetry *trans*-bis(alkynyl) complexes bearing non-aromatic ancillary ligands in order to accelerate the field of molecular electronics by simplifying spectral profiles, leading to more consistent and accurate results, and establishing cleaner molecular junctions.

"It's five-o-clock somewhere…"

Alan Jackson

LIST OF COMPOUNDS

[**1**] 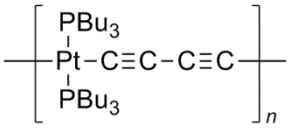

[**2**] 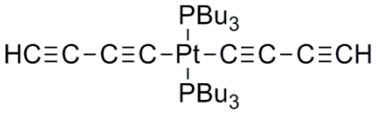

[**3**] 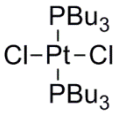

[**4**] 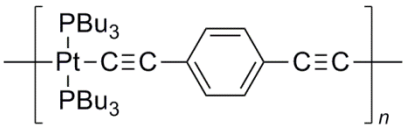

[**5**] 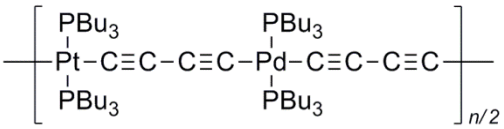

[**6**] 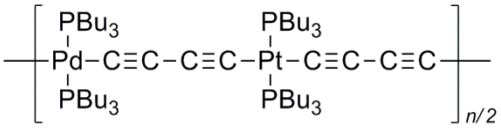

[**7**] 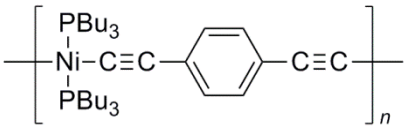

[**8**] 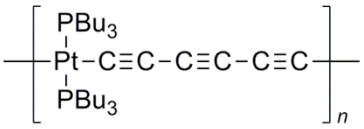

[**9**] 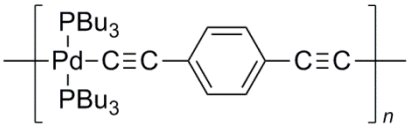

[**10**] 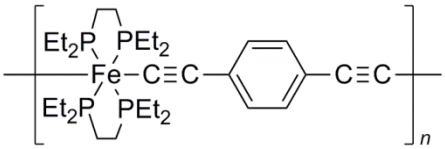

[**11**] 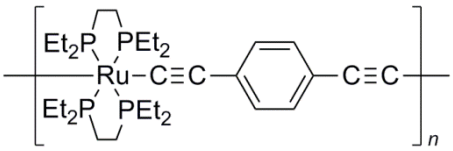

[**12**] 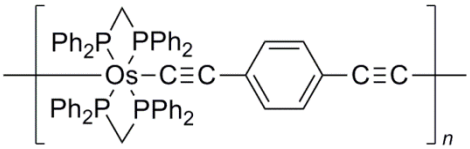

[**13**] 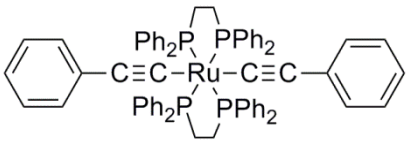

[**14**] 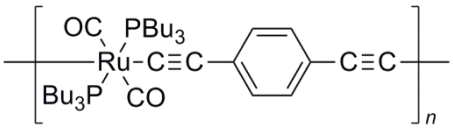

[**15**] 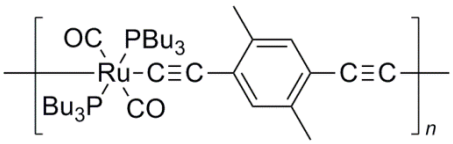

[**16**] 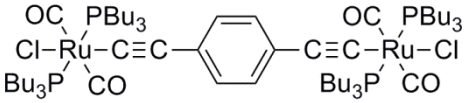

[**17**] 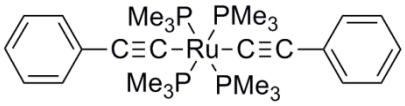

[**18**] 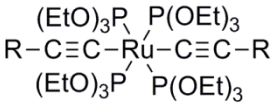

a: **R** = C_4H_9
b: **R** = 3-*th*
c: **R** = C_6H_5
d: **R** = C_6H_4-4-NO_2
e: **R** = C_6H_4-4-CN
f: **R** = C_6H_4-4-C≡CSiMe_3
g: **R** = C_6H_4-4-C_5H_{11}
h: **R** = C_6H_4-4-COOMe
i: **R** = C_6H_4-4-OMe

3-*th* = 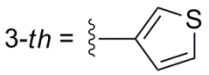

[**19**] 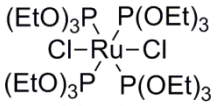

cis-[**20**] 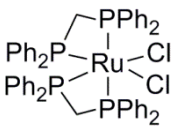

trans-[**20**] 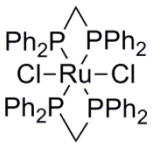

[**21**] $[RuCl_2(DMSO)_4]$

[**22**]$^+$ 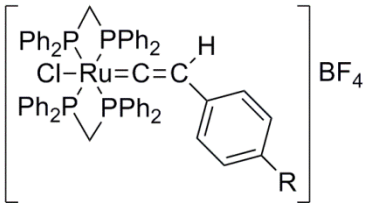

a: **R** = NO_2
b: **R** = COOMe
c: **R** = C≡CSiMe$_3$
d: **R** = H
e: **R** = Me
f: **R** = OMe

[**23**] 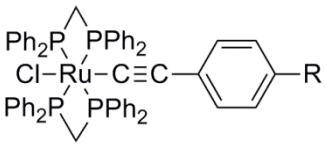

a: **R** = NO_2
b: **R** = COOMe
c: **R** = C≡CSiMe$_3$
d: **R** = H
e: **R** = Me
f: **R** = OMe

[**24**] 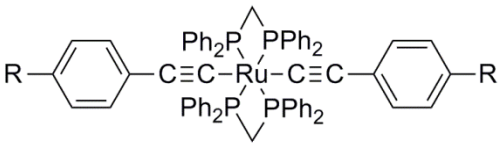

a: **R** = NO_2
b: **R** = COOMe
c: **R** = C≡CSiMe$_3$
d: **R** = H
e: **R** = Me
f: **R** = OMe

[**25**] 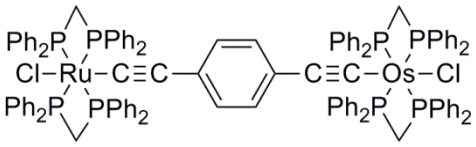

[**26**] 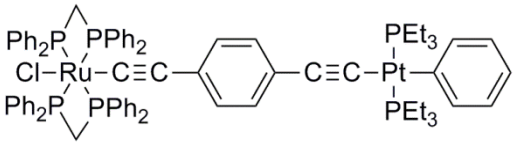

[**27**] 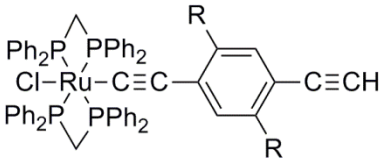

a: **R** = H
b: **R** = Me

[**28**]$^+$ 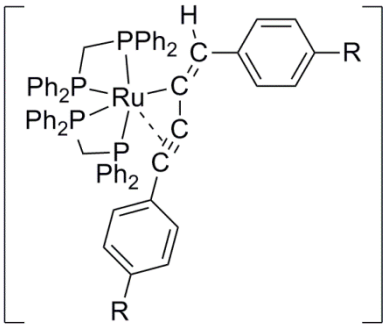

a: **R** = NO_2
b: **R** = COOMe
c: **R** = $C{\equiv}CSiMe_3$
d: **R** = H
e: **R** = Me
f: **R** = OMe

[**29**]$^+$ 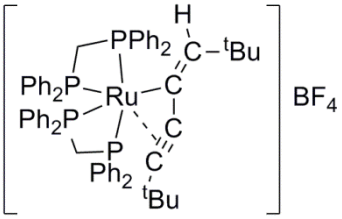

[**30**]$^+$ 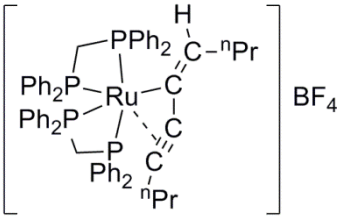

[**31**]$^+$ 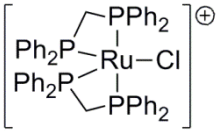

cis-[**32**]$^+$ 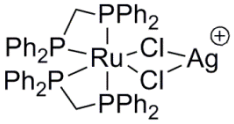

trans-[**32**]$^+$ 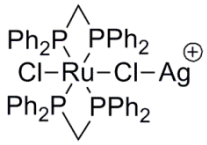

cis-[**33**]$^+$ 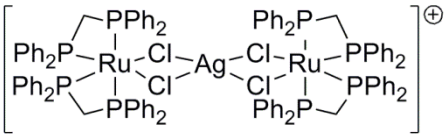

[**34**]$^+$ 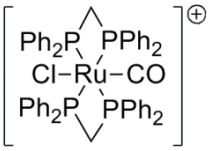

cis-[**35**] 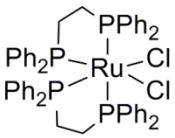

trans-[**35**] 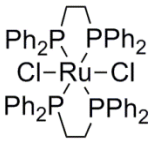

[**36**]$^{+}$ 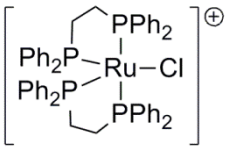

[**37**] 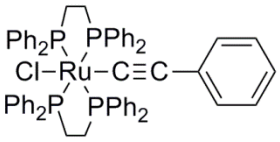

[**38**] 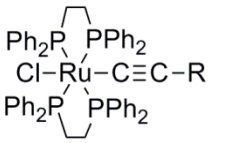
a: **R** = C_6H_4-4-C≡C−$SiMe_3$
b: **R** = 3-*th*
c: **R** = $SiMe_3$
3-*th* = 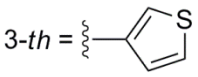

[**39**] 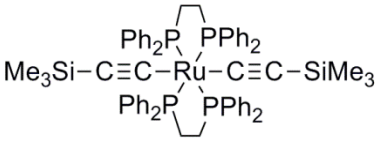

[**40**] 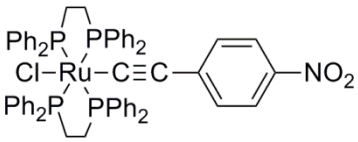

[**41**] 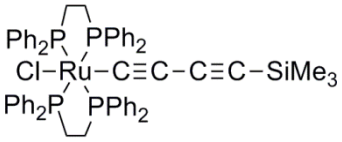

[**42**] 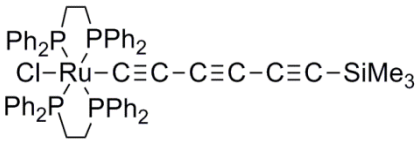

[**43**] 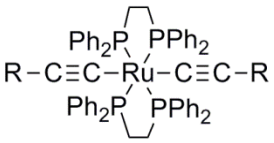
a: **R** = C_6H_4-4-C≡C−$SiMe_3$
b: **R** = 3-*th*
3-*th* = 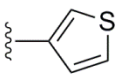

[**44**] 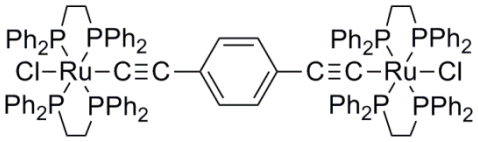

[**45**] 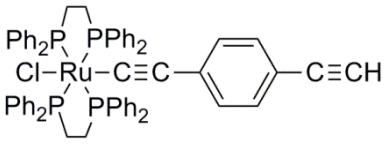

[**46**]$^{+}$ 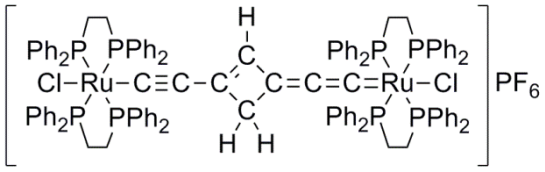

[**47**]$^{+}$ 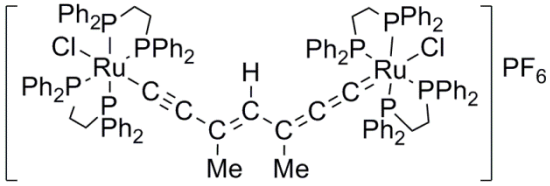

[**48**]$^{+}$ 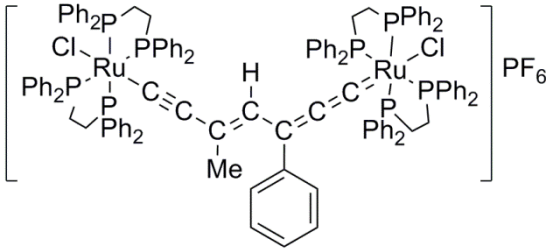

[**49**]$^{+}$ 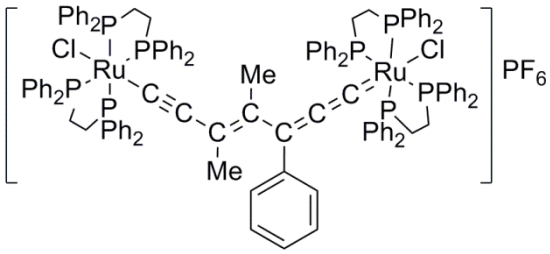

[**50**]$^{2+}$ 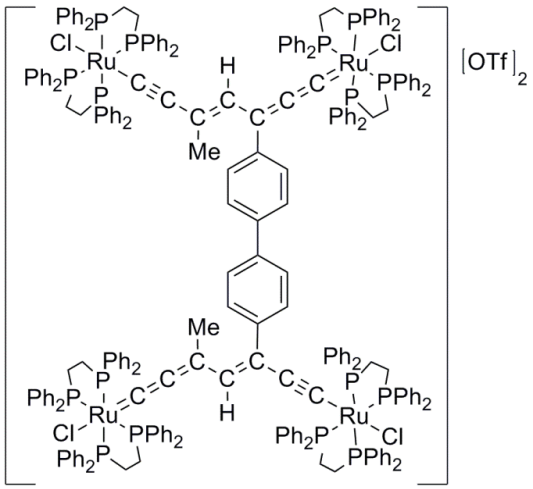

[**51**] 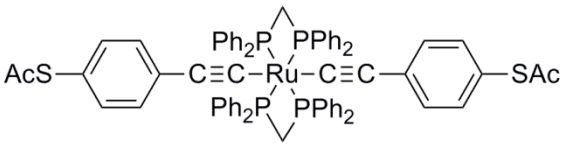

[**52**] 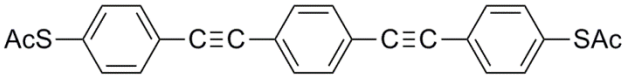

[**53**] 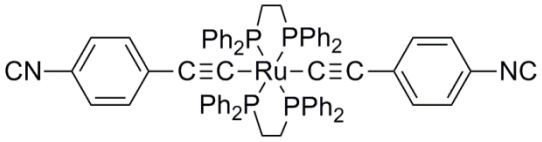

[**54**] 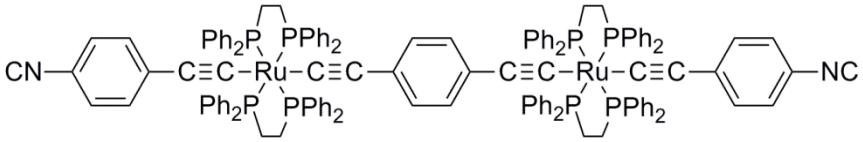

[**55**] 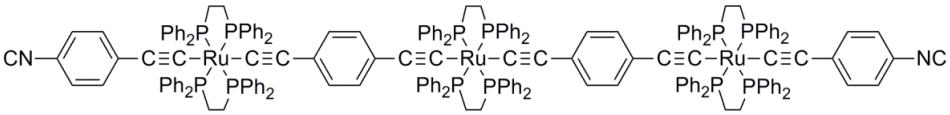

[**56**] 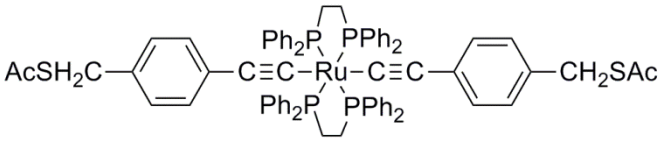

[**57**] 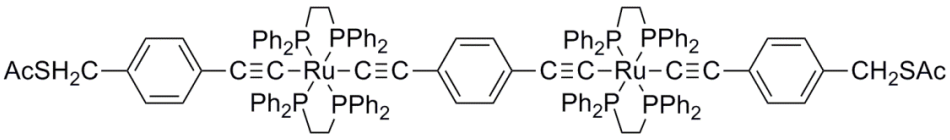

[**58**] 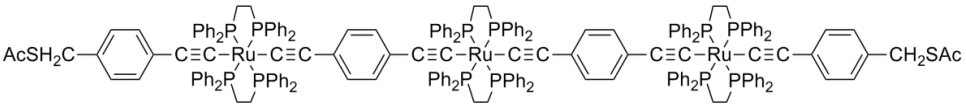

[**59**] 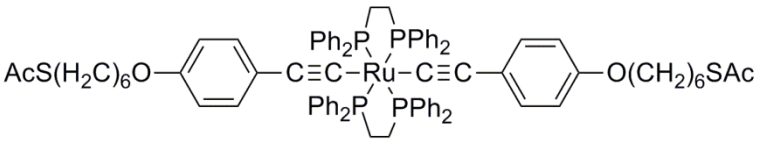

[**60**] 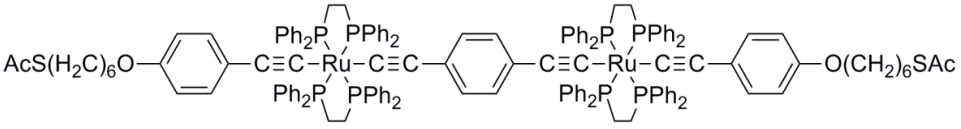

[**61**] 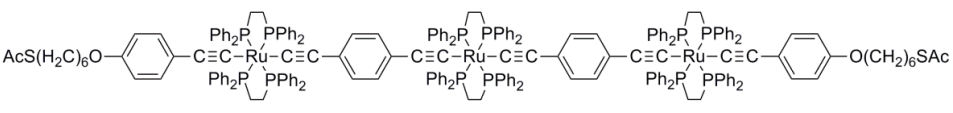

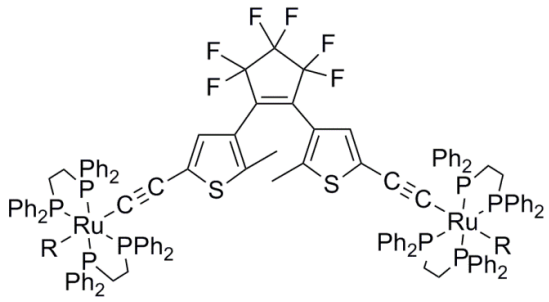

open-[**62-66**]

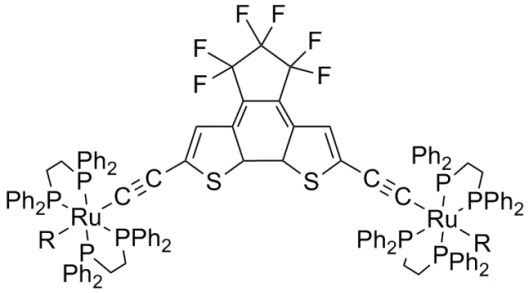

closed-[**62-66**]

[**62**]: **R** = Cl
[**63**]: **R** = C≡C–C$_6$H$_4$–
[**64**]: **R** = C≡C–C$_6$H$_4$–NO$_2$
[**65**]: **R** = C≡C–C$_6$H$_4$–NH$_2$
[**66**]: **R** = C≡C–C$_6$H$_4$–SAc

[**67**] 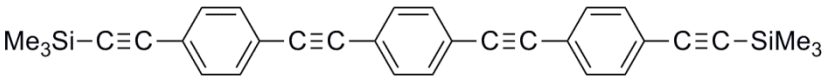

[**68**] 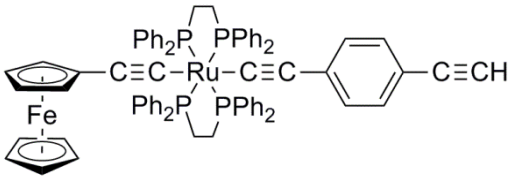

[**69**] 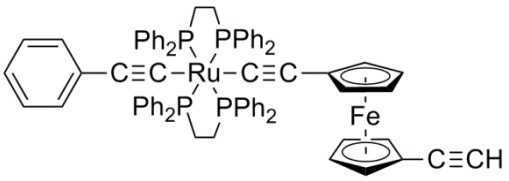

[**70**] 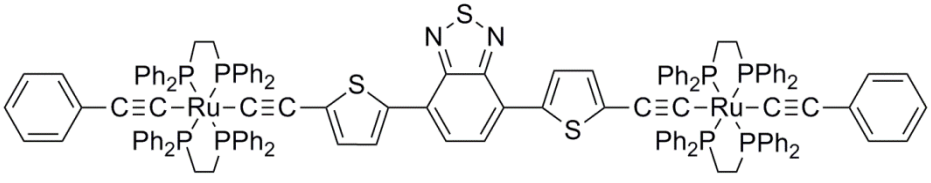

[**71**] 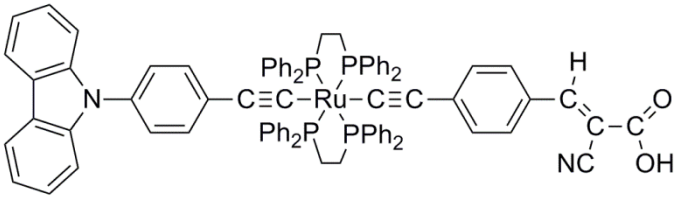

[**72**]

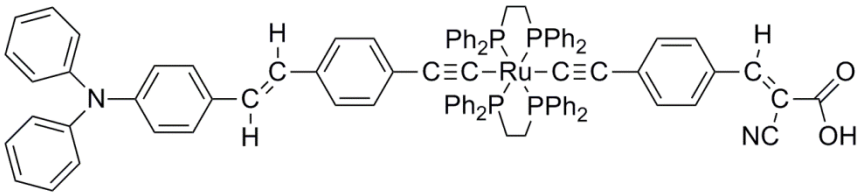

[**73**]

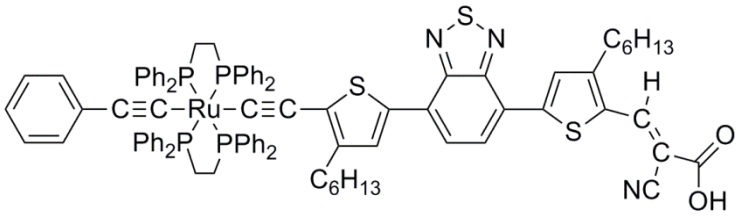

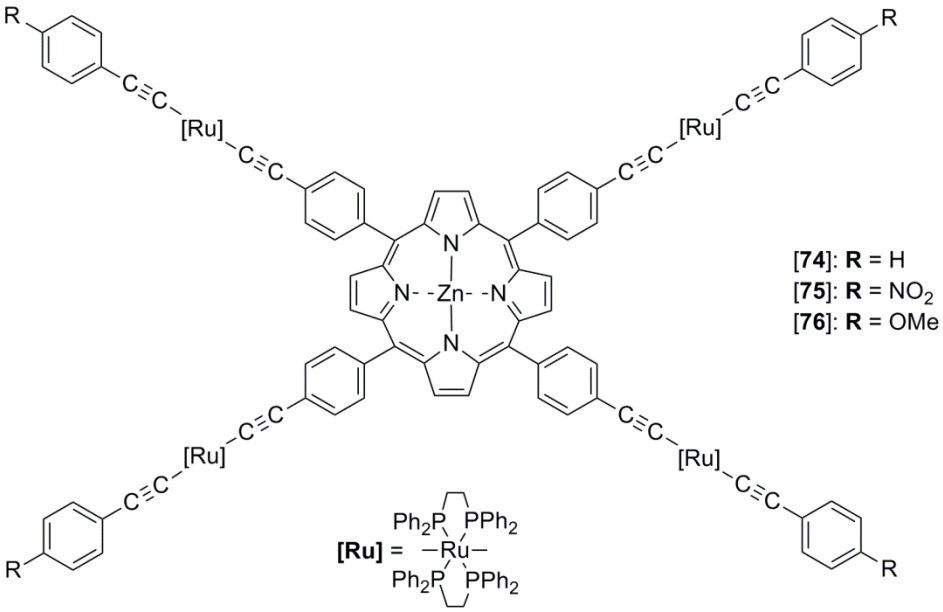

[**77**]

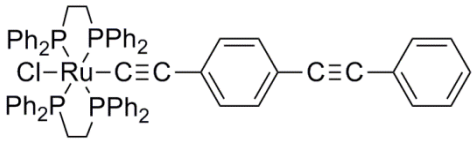

[**78**]

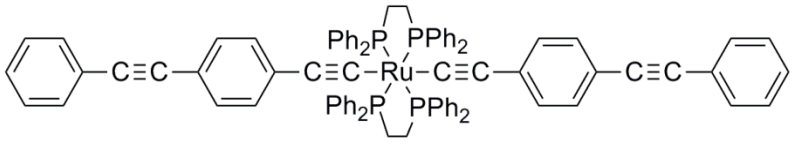

[**79**]

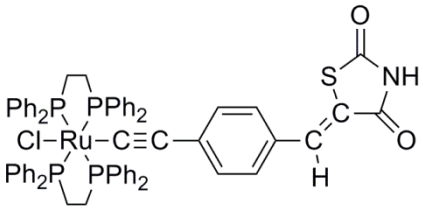

[**80**]

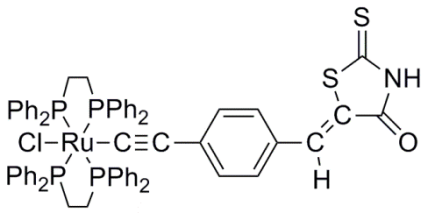

[**81**]

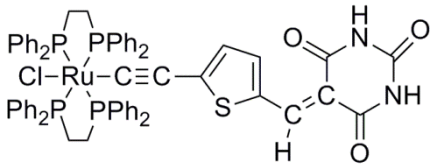

[**82**]$^{+}$

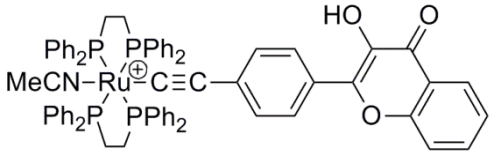

[**83**]

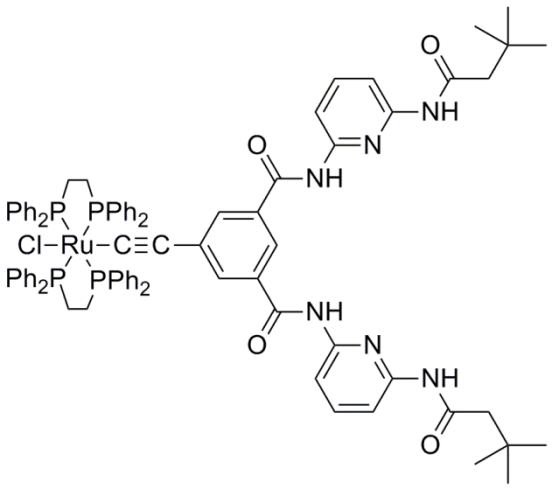

[**84**]

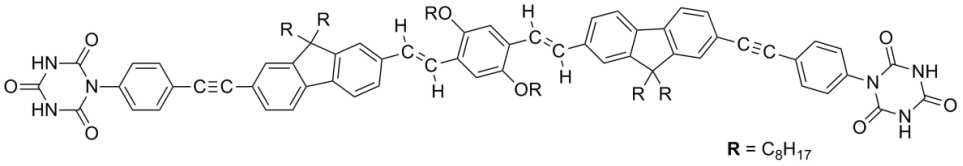

[**85**]

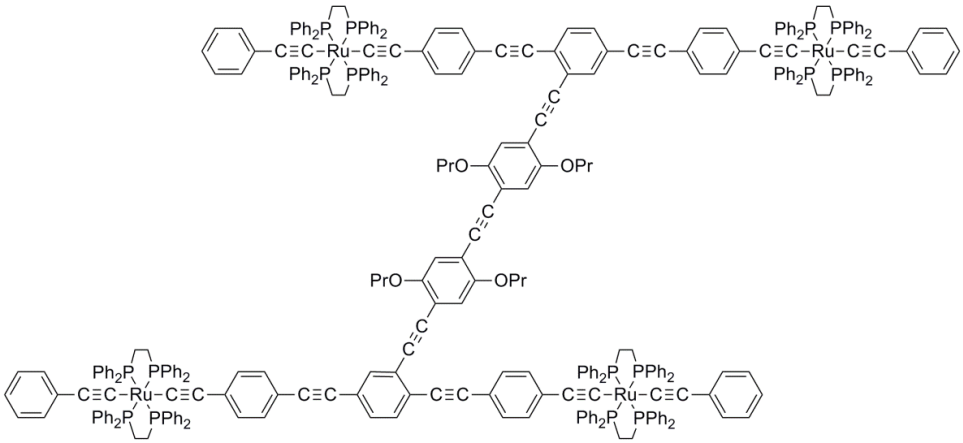

[**86**]

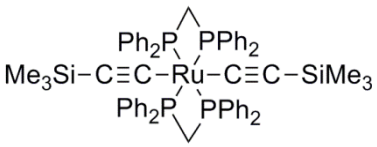

[**87**]$^{+}$

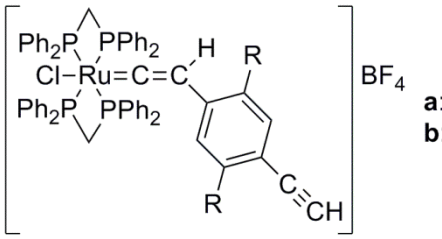

a: **R** = H
b: **R** = Me

[**88**]$^{+}$

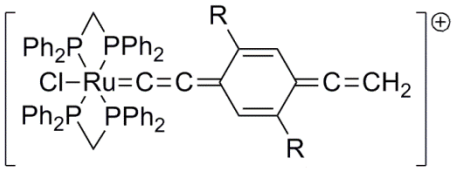

a: **R** = H
b: **R** = Me

[**89**]

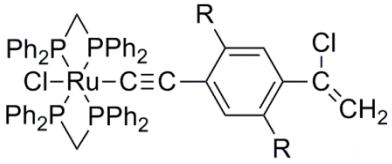

a: **R** = H
b: **R** = Me

[**90**]

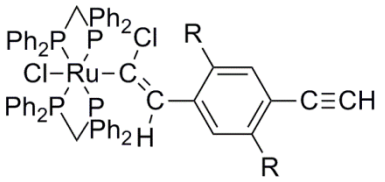

a: **R** = H
b: **R** = Me

[**91**]$^{+}$

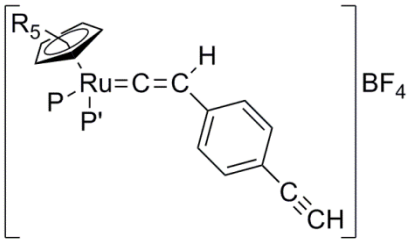

a: **R** = H; **PP'** = $(PPh_3)_2$
b: **R** = Me; **PP'** = dppe

[**92**]

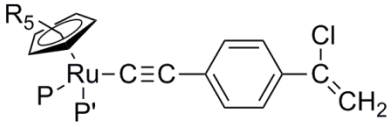

a: **R** = H; **PP'** = $(PPh_3)_2$
b: **R** = Me; **PP'** = dppe

[**93**]

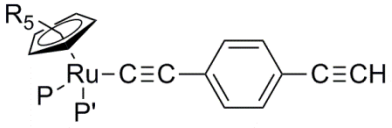

a: **R** = H; **PP'** = $(PPh_3)_2$
b: **R** = Me; **PP'** = dppe

[**94**]

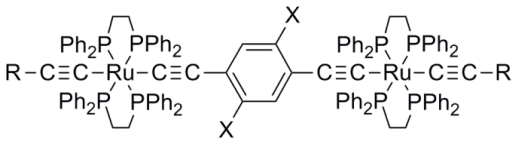

[**94a**]: **R** = C_6H_4-4-C≡CSiMe$_3$; **X** = H
[**94b**]: **R** = 3-*th*; **X** = H
[**94a-Me**]: **R** = C_6H_4-4-C≡CSiMe$_3$; **X** = Me
[**94a-^{i}Pr**]: **R** = C_6H_4-4-C≡CSiMe$_3$; **X** = ^{i}Pr
[**94c**]: **R** = SiMe$_3$; **X** = Me
[**94c-Me**]: **R** = SiMe$_3$; **X** = Me

3-th = 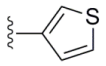

[**95**]

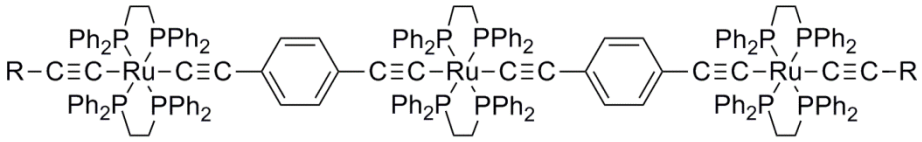

[**95a**]: **R** = C_6H_4-4-C≡CSiMe$_3$
[**95b**]: **R** = 3-*th*

3-*th* = 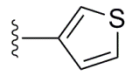

[**96**]

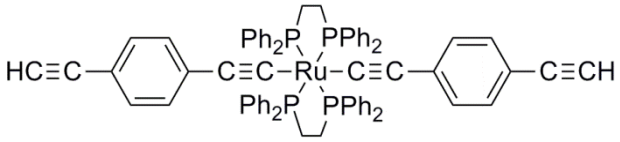

[**97**]

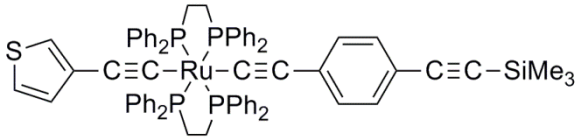

[**98**]

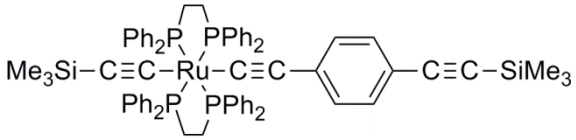

[**99**]

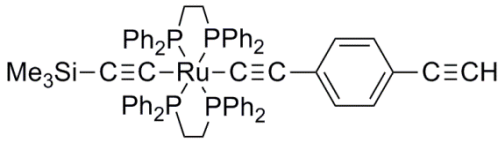

[**100**]

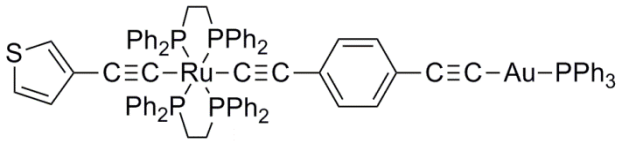

[**101**]

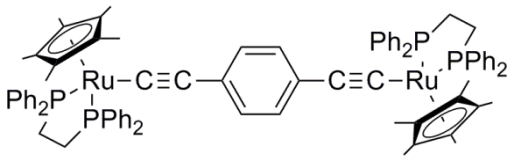

[**102**]